ÇUKUROVA UNIVERSITY
INSTITUTE OF NATURAL AND APPLIED SCIENCES

PhD THESIS

Hasan DANIŞMAN

INVESTIGATION OF GAS LIQUID TWO PHASE FLOWS IN HORIZONTAL CIRCULAR PIPES WITH ECCENTRICALLY INSERTED RODS

DEPARTMENT OF MECHANICAL ENGINEERING

ADANA, 2002

ÇUKUROVA ÜNİVERSİTESİ
FEN BİLİMLERİ ENSTİTÜSÜ

INVESTIGATION OF GAS LIQUID TWO PHASE FLOWS IN HORIZONTAL CIRCULAR PIPES WITH ECCENTRICALLY INSERTED RODS

HASAN DANIŞMAN

DOKTORA TEZİ

MAKİNA MÜHENDİSLİĞİ ANABİLİM DALI

Bu Tez 08/04/2002 Tarihinde Aşağıdaki Jüri Üyeleri Tarafından Oybirliği İle KABUL Edilmiştir.

İmza:	İmza:	İmza:
Prof. Dr. Tuncay YILMAZ	Doç. Dr. Orhan BÜYÜKALACA	Doç. Dr. Yasin VAROL
DANIŞMAN	ÜYE	ÜYE

Bu Tez Enstitümüz Makina Mühendisliği Anabilim Dalında Hazırlanmıştır.

Kod No: 660

Prof. Dr. Fikri AKDENİZ
Enstitü Müdürü

T.C. ÇUKUROVA ÜNİVERSİTESİ FEN BİLİMLERİ ENSTİTÜSÜ MÜDÜRLÜĞÜ 1973

Bu çalışma Çukurova Üniversitesi Araştırma Fonu tarafından desteklenmiştir.
Proje No: FBE.97D.106

ABSTRACT

PhD THESIS

INVESTIGATION OF GAS LIQUID TWO PHASE FLOWS IN HORIZONTAL CIRCULAR PIPES WITH ECCENTRICALLY INSERTED RODS

HASAN DANIŞMAN

DEPARTMENT OF MECHANICAL ENGINEERING
INSTITUTE OF NATURAL AND APPLIED SCIENCES
UNIVERSITY OF ÇUKUROVA

Supervisor : Prof.Dr. Tuncay YILMAZ
Year: 2002, Pages: 288
Jury : Prof.Dr. Tuncay YILMAZ
: Assoc.Prof.Dr. Orhan BÜYÜKALACA
: Assoc.Prof.Dr. Yasin VAROL

The objective of the investigation reported in this thesis was to experimentally study the gas-liquid two-phase flow regimes, to measure void fraction (or liquid hold-up) and pressure drop in horizontal tubes with eccentrically inserted rods. Initially, two horizontal circular transparent pipes with different diameters have been tested to become familiar with the experimental procedure, comparing the results obtained from our measurements with the data given in the literature. Afterwards, two-phase co-current flow in an upwardly inclined pipe has been investigated. This pipe which was mounted on an adjustable metal bridge was one of the circular transparent pipes used for the horizontal experiments.

The flow regimes in two-phase flow depend on many different parameters, such as pipe angle, flow direction, fluid properties, pressure, heat flux, mass flow rates, and channel geometry. In designing industrial equipments, the tubes, gaps, bundles, separators, and junctions could be used depending on the requirements of the process. Investigations on the gas liquid flows have been mostly focused on the regular geometries for a long time. It is clearly expressed that, the channel settlement could be not only vertical, horizontal, or inclined, but also different combinations of them. The usage of irregular channel geometries is the another complexity of gas liquid flows in compact devices. This study is an approach to the more complex channel geometries.

In this study, gas-liquid flows in horizontal eccentric pipes have been examined to fill up the deficiency in the literature. Slug flows have been investigated in a detailed manner using both measurement devices and camera. Therefore, differences between eccentric and circular pipe flow parameters have been examined. Particularly, variations of flow regimes with respect to gas, liquid flow rates, diameters and eccentricity of two pipes have been determined. The results of this investigation will shed light on the developments of new equipment.

Keywords: Two-phase flow; Pressure drop; Void fraction; Slug flow; Flow regimes.

ÖZ

DOKTORA TEZİ

YATAY İÇ İÇE EKSANTRİK BORULAR ARASINDA GAZ SIVI AKIŞININ İNCELENMESİ

HASAN DANIŞMAN

ÇUKUROVA ÜNİVERSİTESİ
FEN BİLİMLERİ ENSTİTÜSÜ
MAKİNA MÜHENDİSLİĞİ ANABİLİM DALI

Danışman : Prof.Dr. Tuncay YILMAZ
Yıl: 2002, Sayfa: 288
Jüri : Prof.Dr. Tuncay YILMAZ
: Doç.Dr. Orhan BÜYÜKALACA
: Doç.Dr. Yasin VAROL

İki fazlı gaz-sıvı akışları bir çok bilim adamı tarafından yoğun bir şekilde araştırılmaktadır. Fakat; gelişigüzel kanal geometrisine sahip borular içerisinde oluşan, iki fazlı gaz-sıvı akışları ile ilgili araştırmalara pek sık rastlanılmaz. Bu alandaki bilgi eksikliği en kısa zamanda giderilerek, endüstride kullanılan cihazların tasarımı için güvenilir yöntemlerin geliştirilmesi gerekmektedir. Çok fazlı gaz-sıvı akışları üzerine yayınlanmış çalışmaların çoğunluğu dairesel borular içerisinde oluşan akışlarla ilgili olmakla beraber, dairesel olmayan kanallardaki akış karakteristiklerinin belirlenmesiyle ilgili az sayıda çalışmaya da rastlanmaktadır.

Değişik kesit alanlı kanallarda meydana gelen iki fazlı gaz-sıvı akışlarının incelenmesinin diğer bir önemli nedeni de, akış sırasında oluşan basınç düşümünün doğru bir şekilde hesaplanmasıdır. Yatay eksantrik borularda basınç düşümünün hesaplanması ve akış karakteristiklerinin belirlenmesi için yapılmış herhangi bir çalışma bulunmamaktadır. Bu nedenle yatay iç içe eksantrik borular arasında iki fazlı akış rejimlerinin belirlenmesi ve basınç kaybının hesaplanması için sistematik ve hassas yöntemlerin araştırılması gerekmektedir.

Tarafımızdan yapılan bu çalışmada, yatay eksantrik borular içindeki iki fazlı gaz-sıvı akışları incelenmiş ve literatürdeki bir eksikliğin giderilmesine çalışılmıştır. Özellikle uygulamalarda büyük öneme sahip olan heyelanlı akış tipi üzerinde çalışmalar yoğunlaştırılmıştır. Ölçüme ve gözleme dayalı yapılmış olan deneysel çalışmalarda, çeşitli ölçüm cihazları ve kamera kullanılarak, eşmerkezli veya eksantrik yatay bir boru içindeki çift fazlı gaz-sıvı akışı ile dairesel yatay bir boru içindeki gaz-sıvı akışı arasındaki farklar araştırılmıştır. Gaz ve sıvı debileri, boru çapları ve iç içe iki boru arasındaki eksantrisite değiştirilerek, akış rejimlerinde meydana gelen değişmeler incelenmiştir.

Anahtar Kelimeler: İki fazlı akış, Basınç kaybı, Heyelanlı akış, Akış tipleri, Eksantrik borular.

ACKNOWLEDGEMENTS

I am truly grateful to my research supervisor, Prof. Dr.-Ing. Tuncay YILMAZ, for his invaluable guidance and support throughout this thesis and during my undergraduate and graduate education.

I would like to express my sincere appreciation to Assoc. Prof. Dr. Orhan BÜYÜKALACA, for his technical support, guidance throughout the preparation of this thesis.

I wish to express my gratitude to The German Academic Exchange Service for scholarship in Germany.

I also would like to thank to Prof. Dr. Dieter MEWES and Research Assistants of the Institute of Process Engineering at University of Hanover enabled to do most of my experiments.

In addition, I would like to thank my entire Research Assistant friends and all staff of the Mechanical Engineering Department.

And thanks to my wife for her patience and encouragement.

TABLE OF CONTENTS

LIST OF TABLES

LIST OF FIGURES

LIST OF SYMBOLS AND ABBREVIATIONS

A	Cross-sectional area of the empty tube.	(m^2)
ρ_G	Gas density.	(kg/m^3)
ρ_L	Liquid density.	(kg/m^3)
ρ_{air}	Air density.	(kg/m^3)
ρ_{water}	Water density.	(kg/m^3)
$\dot{M}_T$	Total mass flow rate of gas liquid mixture.	(kg/s)
$\dot{M}_G$	Gas mass flow rate.	(kg/s)
$\dot{M}_L$	Liquid mass flow rate.	(kg/s)
$\dot{m}_T$	Total mass velocity of gas liquid mixture.	(kg/m^2s)
$\dot{m}_G$	Gas mass velocity.	(kg/m^2s)
$\dot{m}_L$	Liquid mass velocity.	(kg/m^2s)
u_G	Actual gas velocity.	(m/s)
u_L	Actual liquid velocity.	(m/s)
u_{Gs}	Superficial gas velocity.	(m/s)
u_{Ls}	Superficial liquid velocity.	(m/s)
A	Cross-sectional flow area of the empty tube.	(m^2)
A_G	Cross-sectional flow area of the gas phase in the empty tube.	(m^2)
A_L	Cross-sectional flow area of the liquid phase in the empty tube.	(m^2)
R	Resistance due to gas liquid flow in pipe	(Pa/m)
α	Void fraction	(-)
β	Liquid hold-up	(-)
$\dot{x}$	Mass quality	(-)
Fr_G	Froud number	(-)
Re_G	Reynolds number of gas	(-)

Ku	Kutdelaze number	(-)
T_D	Function defined by Taitel and Dukler (1976)	(-)
$R(d)$	The cross-correlation coefficient	(-)
$f1(t)$	The time-varying fluctuation of the first sensor	(-)
$f1_m$	Mean value of $f1(t)$ over a sufficiently long period.	(-)
$f2(t+d)$	The time-varying fluctuation of the last sensor	(-)
$f2_m$	Mean value of $f2(t+d)$ over a sufficiently long period.	(-)
d	Delay time between the time-varying fluctuations sensors	(s)
t	Sufficiently long measuring time.	(s)
PT_{Big}	Big pressure transducer used in experiments.	(-)
PT_{Small}	Small pressure transducer used in experiments.	(-)
LED1	Light emitting diode upflow.	(-)
LED2	Light emitting diode downflow.	(-)
$[Volt(t)]_{LED1}$	Instant volt value of LED1	(volt)
$[Volt_m]_{LED1}$	Mean volt value of LED1 over a sufficiently long period.	(volt)
$[Volt(t)]_{LED2}$	Instant volt value of LED2	(volt)
$[Volt_m]_{LED2}$	Mean volt value of LED2 over a sufficiently long period.	(volt)
$L_{LED1-LED2}$	The distance between LED1 and LED2.	(m)
t_d	Delay time calculated via the cross-correlation technique.	(s)
V_{slug}	Mean slug velocity	(m/s)
L_{act}	Actual length	(m)
L_{pre}	Predicted length	(m)
PT1	Pressure transducer 1.	(-)
PT2	Pressure transducer 2.	(-)
CONC	Concentrically inserted rod.	(-)
ECC	Eccentrically inserted rod.	(-)

1. INTRODUCTION

The objective of the investigation reported in this thesis was to experimentally study the gas-liquid two-phase flow regimes, to measure void fraction (or liquid hold-up) and pressure drop in horizontal tubes with eccentrically inserted rods. Initially, two horizontal circular transparent pipes with different diameters have been tested to become familiar with the experimental procedure, comparing the results obtained from our measurements with the data given in the literature. Afterwards, two-phase co-current flow in an upwardly inclined pipe has been investigated. This pipe which was mounted on an adjustable metal bridge was one of the circular transparent pipes used for the horizontal experiments.

Two-phase flows occur in an extremely wide range of environmental situations and industrial plants. The interacting flow of two phases of gas and liquid is termed as two-phase flow which takes place in boilers, condensers, heat exchangers, air-conditioning and refrigeration equipment, distillation columns, nuclear reactors, chemical reactors, rocket motors, oil wells and pipelines. These are some examples in which two-phase flow is important. All of these systems and equipment require economical designs, optimised operating conditions, and well assessed safety factors which need quantitative information. For example, a pipeline designer tries to minimise the total cost of construction and operation of a pipeline over a period of time. To serve this aim, engineer has to calculate an optimum pipe diameter regarding the pressure loss, so that he could decrease all material and pumping station costs.

Increases in rating, competition in capital and operating costs and the importance of reliability and safety have accentuated the need of quantitative information in the last quarter of 20th century. In the 19th and early 20th century, boilers and condensers for power-generating plant were designed on the basis of empirical relationships derived from experience, and the problems were mainly associated with materials, which set severe limits to their capabilities. Efficiency was not a predominating factor and fuel consumptions were very high compared with modern figures.

In recent decades the pressure to achieve increased efficiency has resulted in very much increased thermal ratings. Combining with new developments in metallurgy, the performances of new devices have been brought into the area where the heat transfer and fluid dynamic problems become limiting factors. Therefore, one of the purposes of studying two-phase flow is to understand the physical phenomena which could limit the performances of equipment, for example "flooding" in packed columns, hydrodynamic instability in steam generators or burn-out in liquid-cooled nuclear reactors.

The greatest incentive to the study of two-phase flow has been the development of water-cooled nuclear reactors whose heat fluxes in excess of those previously experienced in industry are required. In order to achieve good performance and to guarantee safe and efficient operation, it has been necessary to investigate two-phase phenomena in much greater than up to now. The contribution of the development of water-cooled nuclear reactors on the study of two-phase flow is also evident from the rapid growth of literature on the subject during the last decades.

Another major area of development is in the chemical and processing industries where the demand for new products has necessitated new types of plant involving two-phase flow. Thus, understanding of the basic mechanisms of two-phase flow has been a prerequisite of new-generation developments. In recent years the growth of computer-based design methods has led to the need for more accurate data covering a wide range of two-phase flow and heat transfer conditions. Thereafter, the purpose of studying two-phase flow has been the derivation of accurate equations which predicts the engineering parameters describing performance such as pressure drop, void fraction, heat and mass transfer coefficients. However, in spite of the large amount of work which has been done in this field, for the present, nobody has been able to find a general solution which covers all the possible flow and geometric conditions. This situation is a consequence of the extreme complexity of two-phase fluid flows.

The main complicating feature of two-phase flows, as distinct from single phase flows, is the existence of gas liquid interfaces within the flow. In principle, there are an infinite range of possibilities for the instantaneous distribution of the interfaces within a given channel for given phase flow rates. Despite the complexity being inherent in gas-liquid flows, the aim has been to investigate the whole subject dividing into some sub-divisions such as those related to system geometry and flow regimes. System geometry is directly related to the special needs of plant. But, in general, all of the designs in which two-phase flow mechanism appears can be classified as vertical, horizontal or inclined. The knowledge of flow regimes which is also called as flow patterns is one of the most important prerequisites in the study of any two-phase flow system.

Two-phase flow phenomena is composed of four combinations which are gas-liquid, liquid-solid, liquid-liquid, and gas-solid flows. Gas-liquid flow, which is the most comprehensive part of the subject because of the both phases are in motion and interface between the phases is influenced by this movement, embraces the whole subject of boiling, evaporation and condensation.

There are several reasons to be interested in the operations related with the gas-liquid flows of the process industries. The amount of interfacial area produced by various mixing schemes, the interfacial transport rates, and possibly pressure drop for pumping are the key questions of this area. Heat transfer rates and physical properties of gas-liquid flows become different as applied to heating, air conditioning, and refrigeration. Especially, the circumferential variation of the heat transfer coefficient in these equipment is affected by gas-liquid flow patterns. Also, the technological importance of two-phase gas-liquid flows are immeasurable when the amount of capital invested in equipment, in which gas-liquid flow takes place, is considered.

Gas-liquid flows in conduits may take on a variety of geometrical configurations related to the spatial distribution of the two phases in the pipe. Determination of flow patterns is important and useful in the study of gas-liquid flows. It is essential to ensure correct identification and definition of regimes to rationalise the situation. For example, the design of a two-phase transportation piping system would firstly require the information about the flow regimes in order the predict the hydrodynamic properties of the flow. A change of pattern means a change in the mode of transport of momentum or heat.

Gas-liquid flows in devices such as evaporators, condensers, petroleum transportation lines, separators and nuclear reactors should be distinguished precisely in view of their reliability and effectiveness. For example, different flow regimes occur in an evaporator of an air-conditioning device. Refrigerant cycled in air conditioner is exposed to different thermodynamic processes. Heat is absorbed from ambient in evaporator and released to ambient in condenser. During the heat transfer mechanism between heat exchangers and ambient, heat transfer coefficient is the most important phenomena for efficiency. For instance, when the coolant comes from expansion valve in to evaporator, it is single phase subcooled liquid. Figure 1.1. shows a horizontal tube heated uniformly over its length with moderate heat flux and fed subcooled liquid from the left end. During the first part, the liquid is being heated up to the saturation temperature and the wall temperature remains below that necessary for nucleation. The heat is being transferred to single phase liquid, and the normal correlations for convection apply here. At some point along the tube, the conditions are such that vapour bubbles begin to form on the wall from some nucleation sites. Initially the bulk of the fluid is subcooled while vapour bubbles form on the wall, and the heat transfer region is referred to as subcooled nucleate boiling. In this region, the wall temperature remains essentially constant a few degrees above the saturation temperature. The mean bulk temperature of the fluid increases all the time linearly, until saturation temperature is reached. Important points to note from a heat transfer viewpoint are the possibility of intermittent drying and rewetting of the upper surfaces of the tube in slug and wavy flow. At lower inlet liquid velocities the influence of gravity is more obvious. The liquid phase accumulates at the lower half of horizontal pipe and the wall temperature distribution throughout the periphery becomes asymmetrical. This is the result of non-uniformly formed film thickness. Because of the lower part accumulated liquid phase, film thickness of upper half of the pipe gets thinner or fully disappeared and the heat transfer coefficient of this region decreases. The major factors which affect the heat transfer coefficient of a horizontal pipe are the superficial velocity, slug length, velocity, and frequency. Thus, the circumferential variation of the heat transfer coefficient in horizontal devices is influenced by the non-uniformity of two-phase flow patterns.

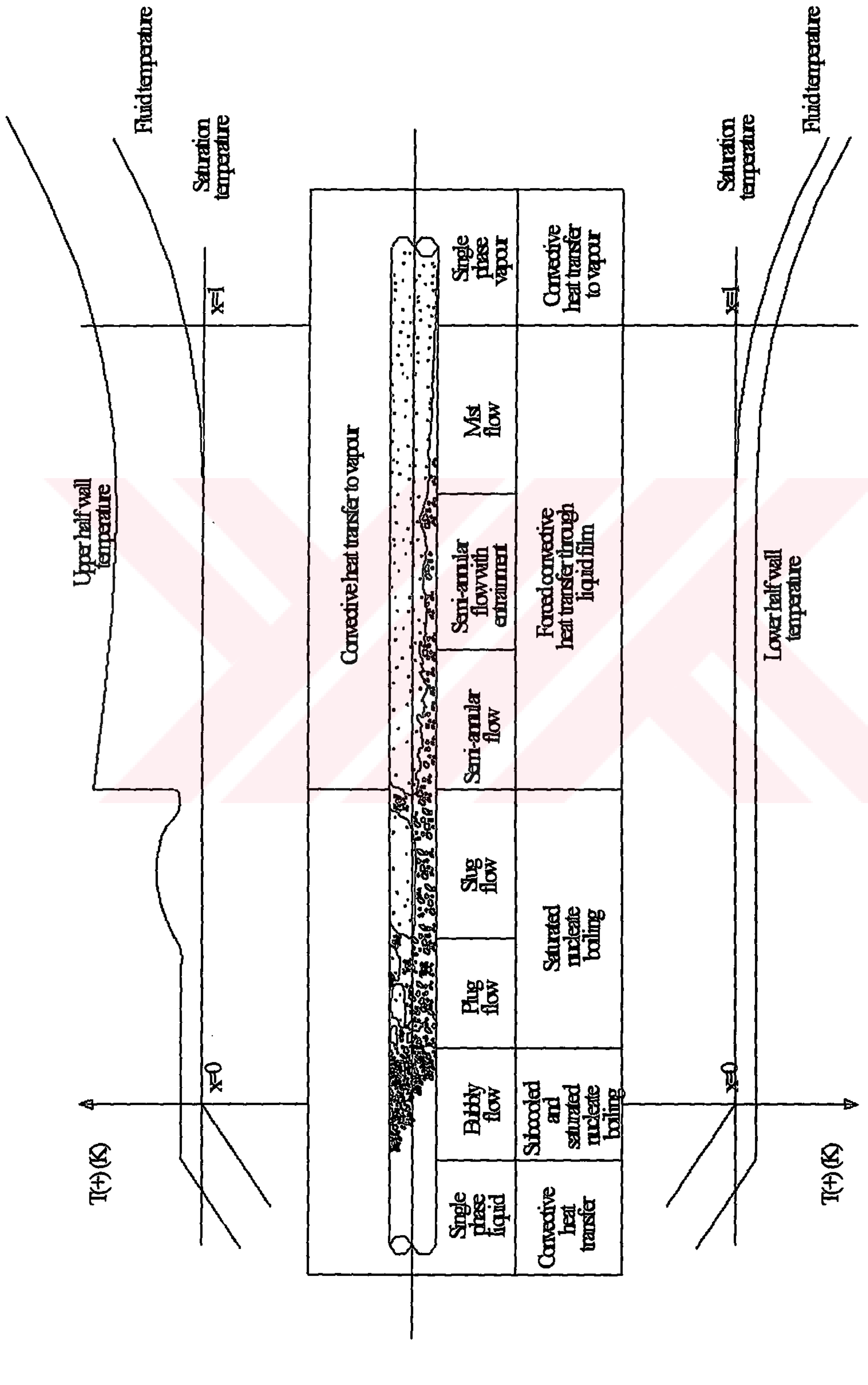

Figure 1.1. Flow patterns and wall temperature variations in a horizontal evaporator tube.

1.1. Importance of This Study

The flow regimes in two-phase flow depend on the many different parameters, such as pipe angle, flow direction, fluid properties, pressure, heat flux, mass flow rates, and channel geometry. In the designing of industrial equipment, the tubes, gaps, bundles, separators, junctions and so on could be used depending on the requirements of the process. Investigations on the gas liquid flows have been mostly focused on the regular geometries for a long time. It is clearly expressed that, the channel settlement could be not only vertical, horizontal, or inclined, but also different combinations of them. The usage of irregular channel geometries is the another complexity of gas liquid flows in compact devices. This study is an approach to the more complex channel geometries.

In this study, gas-liquid flows in horizontal eccentric pipes have been examined to fill up the deficiency in the literature. Especially slug flows have been investigated in a detailed manner using both measurement devices and camera. Therefore, differences between eccentric and circular pipe flow parameters have been examined. Particularly, variations of flow regimes with respect to gas, liquid flow rates, diameters and eccentricity of two pipes have been determined. The results of this investigation will shed light on the developments of new equipment.

2. PREVIOUS STUDIES

The gas-liquid flow processes are spreading out to various applications of technology. The importance of reliability and safety of this processes and immense amount of capital invested in plants have directed the people to find out new design methods which have been the driving force behind a very large research effort in two-phase gas-liquid flow over the past 50 years. As a result of this importance, many works have been carried out at universities, in different laboratories, and at industrial research and design organizations in many countries of the world. Because of the complexity of gas-liquid flows, most proposed predictive correlations have been based largely on experiment and are valid only under conditions near that of the experiment. Each time a new condition is to be investigated, new experiments are necessary.

The investigations on gas liquid flows can be classified in many different respects. In this section, the studies about the gas liquid flows will be arranged from the viewpoint of flow direction. The common literature will be firstly outlined and then, the studies associated with the vertical, horizontal, and inclined flow will be given.

Owen *et al.* (1976) published a critical review associated with the transient and statistical measurement techniques for two phase flows. They reviewed recent developments that fluctuating characteristics of two phase flows were studied in detail. The authors explained a broad range of measurement techniques for two phase flows such as optical probes, hot-film anemometry, electrical probes, and photon attenuation. At that time, they reported that instrumental methods were capable of providing flow pattern transitions, interfacial area densities, void and velocity profiles.

Cheremisinoff and Cheremisinoff (1988) described the techniques for studying the flow structure of two phase systems. They explained the usage of some pressure transducers and electro resistivity sensors. The authors described the probes, their electrical circuits, and the analysing of their outputs. For example, different types of conductivity probes and the meanings of their recorded traces were explained in detail.

Bachalo (1994) outlined the experimental methods in multiphase flows. The research in the field of multiphase flows has been advanced as a result of the availability of optical diagnostics that allow the simultaneous measurement of the particle size and velocity of the dispersed phase. This capability also allows the measurement of the continuous phase turbulence parameters in the presence of the dispersed phase. The phase Doppler method has been a key method in providing this information. This study represented the well known laser Doppler velocimeter (LDV) to be applied to the experimentation in multiphase flows. The phase Doppler method was described and the measurement characteristics were discussed along with the limitations of the method. The work concluded with some representative examples of the measurements in two-phase turbulent flows. These measurements were used to verify the drag coefficient and evaluate the particle response in turbulent flows. The particle interaction with large scale turbulent eddies was also studied and some examples of these data were provided.

2.1. Literature Review of Vertical Gas Liquid Flows

Özgü *et al.* (1973) used a capacitance method to measure the film thickness of two phase flow. They described a new capacitance method for measurement of the local, time-varying or steady-state film thickness in two phase flow. Their method is suitable for use in simple and complex geometries, and works for either electrically nonconducting or slightly conducting fluids. The concept utilised in this development was to locate both electrodes of a capacitance circuit in the surface over which the liquid film flows. Test data were obtained on bubbles of different lengths rising in a circular vertical tube filled with water. Their results for film thicknesses and bubble residence times have showed a good self-consistency and agreement with other available data.

Jagota *et al.* (1973) studied the measurement of residence times, as well as film and droplet velocities in two phase annular flow. The development of tracer pulse techniques for the measurement of the mean film and droplet velocities in vertical two phase annular flow was described. The experiments were carried out by injecting a sodium chloride solution into the water-air stream flowing in the test section, which was made of 25.4 mm ID acrylic tube. Tracer concentrations were monitored by conductivity probes located downstream from the point of injection. The conductivity values were transmitted to a recording oscillograph. They discussed the results of experiments and compared with a computer simulation. The authors reported that the experiments showed the mean film velocity could be determined accurately, but not the droplet velocity. The computer simulation supported the experimental results. The effect of interchange was also shown to be sufficiently large in much of the annular flow region to give average film and droplet residence times. Finally, the authors concluded that the use of the tracer pulse technique could be used to measure the liquid holdup in annular flow.

Taitel *et al.* (1980) proposed physically based mechanisms for predicting flow pattern transitions during steady gas liquid flow in vertical tubes. These models incorporated the effect of fluid properties and pipe size and thus were largely free of the limitations of empirically based transition maps or correlations. In the study, theoretically predicted transitions for upflow were compared with the recommendations of many earlier investigators whose results were primarily based on experimental measurements. There was considerable disagreement between the results of these various investigators. However, the authors notified that the theory presented in this paper was in satisfactory agreement with the most of the earlier experimental results. The authors claimed that the results of their mechanisms were applicable for wider range of properties and conduit sizes than would be expected from empirically determined transitions.

Iida (1980) suggested a prediction method for flow patterns in vertical gas liquid flow. The author's aim was to find a quantitative indication method of gas liquid interface structure and its transient feature in an existing two phase flow. He discussed the relation between flow pattern and statistical feature of local void fraction fluctuation. Iida (1980) demonstrated that his method was useful to indicate, compare, and predict the flow pattern.

McQuillan and Whalley (1985) studied flow patterns in upwards vertical two phase flow. They described basic flow patterns and discussed the use of flow pattern maps. The transition between plug flow and churn flow was modelled under assumption that flooding of the falling liquid film limited the stability of plug flow.

The resulted equation was combined with other flow pattern transition equations to produce theoretical flow pattern maps. They proposed some further works to improve the predictive methods of flow patterns and their transitions.

Spedding and Spence (1987) wrote the Chapter 2 of the Handbook of Heat and Mass Transfer. This section was related with the predicting holdup in vertical two phase gas liquid flow. They explained some relations, correlations, and models in detail. They concluded that holdup in vertical cocurrent upward flow in bubble and slug regimes could be predicted by the Nicklin *et al.* (1962)'s relation. The authors illustrated clearly how the holdup depended on flow regimes for vertical cocurrent flow.

Kelessidis and Dukler (1989) investigated the modelling of flow pattern transitions for upward gas liquid flow in vertical concentric and eccentric annuli. Two phase flow in concentric and eccentric annuli occurs in a variety of important practical situations. The influx of the gas into the wellbore of an oil well creates two phase flow in an annulus. During the measurements in oil wells, the presence of the instrument creates annular passages. The authors stated that better understanding of two phase flow in an annulus would provide more reliable design methods for many types of industrial equipment, such as double pipe heat exchangers, water cooled nuclear reactors, and serpentine boilers. The test section of this study consisted of two acrylic tubes, which are electrically non conducting. The inner tube had an outside diameter of 50.8mm and the outer tube with an inner diameter of 76.2 mm. The length of the system was approximately 7 m. and eccentricity between two pipes was about 50%. They proposed a new method for flow pattern identification based on probability density function analysis of conductance probe signals. Flow pattern maps were constructed and mathematical models were proposed to predict the flow pattern transitions. Finally, the authors stated that the eccentricity had a minor effect on the flow pattern transitions. This was in agreement with the experimental data.

Barnea and Shemer (1989) used a conductance probe to detect the instantaneous void fraction at the centreline of a vertical tube. They studied various flow patterns and the transitions between them. The purpose of this investigation was to develop a reliable and simple method for the estimation of slug length, the average holdup within the liquid slug and the voidage in the near wake of the Taylor bubble.

Tools for quantitative identification of the transition from bubbly to slug flow and from slug to churn flow were suggested. The investigators suggested two different flow pattern identificators. The first was based on the behaviour of the short time averaged void fraction as a function of time, and the second one employed the histograms representing the bubble size distribution in the flow. They also obtained the quantitative hydrodynamic parameters of the slug flow, like the mean slug length, and the average voidage within the liquid slug. They concluded that the measured values of the voidage in the liquid slug were related to the boundaries of transition from the dispersed bubbles to the slug flow regime, and then to the churn flow.

Issa and Tang (1990) studied on the modelling of vertical gas liquid slug flow in pipes. They presented a one dimensional model based on the two fluid concept for the prediction of pressure drop and liquid holdup in the slug regime. The momentum and mass conservation equations were solved for each phase. The overall model made use of various wall and interface shear stress quantities that were determined from an examination of the detailed structure of a unit slug. They proposed a simplified structure model and validated against experimental data. The complete model was then applied to several cases of slug flow for which measurement of void fraction and pressure drop were available. The authors stated that the results were in remarkable agreement with all the data.

Ma *et al.* (1991) proposed two methods for determining void fractions for two-phase flow. Two simple and economical techniques to determine this quantity were developed and discussed. The improved impedance method was the first method. The differential pressure (D/P) method, in which a commercial differential pressure transmitter was used to determine the static pressure of two phase flow, was the second method. Experiments including tests in vertical and horizontal pipes for the impedance method and a vertical pipe test for the D/P method were performed. The homemade impedance probes were mounted on the inner wall of the pipe in a symmetrical configuration. A pair of shield electrodes were installed upstream and downstream of the impedance probes in order to generate a confined, two-dimensional electric field lying in the cross section of the pipe. Furthermore, theoretical models of these two techniques were developed. The authors reported that the function test showed that the output voltage of the newly designed high-frequency processing circuit could predict the variation of the capacitance. This high-frequency processing circuit made the impedance method for void fraction determination more economical and practical for use in laboratories and industries. They also stated that the D/P method was a simple and economical way to measure the void fraction for vertical pipe. The test results showed that the D/P method was as accurate as the impedance method. The most of the measured void fractions were within a 20% error band compared with the actual void fraction. Therefore, they concluded that both the impedance and D/P methods were practicable for laboratory and industry use to determine the void fraction for two-phase flow.

2.2. Literature Review of Horizontal Gas Liquid Flows

Agrawal *et al.* (1973) developed equations using a mechanistic approach to describe the stratified cocurrent flow of gas liquid mixtures in horizontal pipes. They suggested an iterative method for their solution. In the proposed model, they used a equivalent diameter, $D_G = 4A_G/(p_G + W_i)$, for gas phase in the place of the equivalent diameter for liquid phase, $D_L = 4A_L/(p_L + W_i)$ which was defined by previous workers. This modified model employed a reasonable definition of the equivalent diameter and included the effect of interfacial shear stresses. The gas phase friction factor, f_G, was evaluated directly from the Blasius equation. Experimental data were collected using air-oil mixtures in a 25.4 mm inner diameter by 30.8 m long acrylic pipe. Pressure drop and average of liquid volume fraction were presented as a function of the superficial gas velocity and were compared with the predicted results from this study and other models reported in the literature. The authors reported that pressure drop and average of liquid volume fraction data for the horizontal stratified flow of air-oil mixtures showed a good agreement with the predictions of the proposed model. They concluded that the transition from stratified to elongated bubble flow pattern was found to occur at lower liquid velocities than predicted by flow pattern maps available in the literature.

Mandhane *et al.* (1974) proposed a flow pattern map for gas liquid flows in horizontal pipes. They tested various flow pattern maps for two phase gas liquid flow in horizontal pipes against the 5935 flow pattern observations at that time contained in the UC Multiphase Pipe Flow Data Bank. The commonly used flow pattern maps have been compared using extensive data which cover a wide range of physical properties and flow parameters. The authors reported that the map presented by Hoogendorn (1959) was the most reliable of the selected maps. The terms used by the authors to designate the various flow patterns were consistent with the definitions of previous works. As a consequence of the evaluation, a modified map has been proposed which was simple to use and which was in overall better agreement with almost six thousand data points than any of the existed maps.

Russell *et al.* (1974) published a study related with the pressure drop and holdup in stratified gas liquid flow in horizontal pipes. They developed a procedure to predict the pressure drop and holdup for horizontal gas liquid pipelines in which the liquid was in laminar flow and the gas in turbulent flow. The authors solved the equations of motion for the liquid phase with the help of theoretical analysis including the interfacial stress. A mathematical model and an iterative procedure was developed to calculate the holdup and pressure drop in horizontal gas liquid flow. Their test pipes had 25.4, 38.1, and 50.8 mm inner diameter and 14 m long. They informed that the predictions of the model agreed with well over a hundred data points collected with air-water and air-glycerine solutions.

Taitel and Dukler (1976) presented a model for predicting flow regime transitions in horizontal and near horizontal gas liquid flow. The usual flow regime prediction has been to collect data for flow rates and fluid properties and to visually observe the flow pattern through transparent test section. A search was undertaken by authors to map the data in a two dimensional plot by locating transition boundaries between the regimes. The regimes considered were slug, plug, stratified smooth, stratified wavy, dispersed bubble, and annular-annular dispersed liquid flow. The authors proposed a generalised flow regime map based on physical concepts.

Taitel and Dukler (1976)'s another study dealt with the work of Lockhart and Martinelli (1949) which was one of the earliest attempts to model the functional pressure drop for two phase gas liquid flow. They used a theoretical approach to the Lockhart-Martinelli correlation for stratified flow. The authors derived equations using simple momentum balance on each phase yields. They considered equilibrium stratified flows. The authors demonstrated that the holdup and the dimesionless pressure drop for stratified flow were unique functions of X under assumption of $f_G / f_i \cong const.$ Finally, they concluded that the Lockhart-Martinelli correlation predicted considerably higher values of the dimensionless pressure drop.

Slug formation is a complex phenomena. Waves form on a growing stratified film eventually blocking the gas to form a slug. The predictions for the hydrodynamic behaviour of slug flow are not complete when the slug frequency is not included. Taitel and Dukler (1977) proposed a model for slug frequency during gas liquid flow in horizontal and near horizontal pipes. They presented a fundamental model which predicted slug frequency for entry sections in which natural slugging was permitted to take place. The agreement with experimental data was shown to be within probable limits of data uncertainty. The authors defined five dimensionless groups to control the dimensionless frequency.

Gregory *et al.* (1978) suggested a correlation for the liquid volume fraction in the slug flow for horizontal gas liquid flow. Experimental data for gas holdup in liquid slugs were reported for two different pipe sizes, 25.8 and 51.2 mm ID. The authors concluded that the form of the correlation might have to be modified including diameter, flow rate, and fluid property as appropriate data became available.

Taitel *et al.* (1978) studied the modelling of the flow pattern transitions. They developed a theory for predicting flow pattern transition under transient flow conditions and compared with experiment. Under transient conditions, flow pattern transitions can take place at flow rates substantially different than would occur under steady flow conditions. This result was demonstrated in this work both from theory and experiment. Methods were presented for predicting the flow rates at which flow pattern transitions would take place during flow transients.

Weisman *et al.* (1979) studied the effects of fluid properties and pipe diameter on two phase flow patterns in horizontal lines. Fluid properties were varied in a systematic manner to determine the effects of liquid viscosity, liquid density, interfacial tension, and gas density. The fluids chosen for the experiments were selected so as to allow large changes in one property while producing only relatively unimportant changes in the other properties. Visual observations of flow patterns were supplemented by observations of the fluctuation in pressure drop between two taps a short distance apart. The authors found these pressure drop fluctuations to be characteristic of the prevailing flow pattern. Flow pattern maps of Weisman *et al.* (1979) were described with the mass velocities of liquid and gas instead of superficial velocities. Finally, they concluded that the major factor determining the flow pattern was the relative volumetric flow rates of gas and liquid.

Hihara and Saito (1984) investigated a horizontal two phase flow from separated flow to slug flow without a phase change. The experimental apparatus used in this work had a 34 mm ID round acrylic tube and a 35 mm square acrylic tube. Both tubes were approximately 6 m long. Air and water flow supplied at room temperature and at atmospheric pressure. They presented a transition model based on the experimental results obtained in the air water system. The model was derived from the growth condition of a wave on a stratified water layer. They compared the slug flow transition with the other works.

Lin and Hanratty (1987) studied on the detection of slug flow from pressure measurements. The experiments were conducted in two horizontal pipelines of 25.4 and 95.3 mm i.d. They used strain gauge pressure transducers with a flat frequency response up to 2 kHz to measure the pressure fluctuations of slugs. Two sets of parallel wire conductance probes were used to measure the heights and velocities of waves and slugs. They analysed the output signals of the pressure transducers. They reported that large peaks in the pressure signals corresponded to the slugs moving along the pipe. The slug velocities were obtained using cross correlation method. They drew two graphs for the slug velocity for the 25.4 and 95.3 mm pipe. The graphs depicted the changing of slug velocity with the increasing of superficial gas velocity. The last graph in the paper was related with the pseudo-slug velocity versus superficial gas velocity.

Lin and Hanratty (1987)'s another work was about the effect of pipe diameter on flow patterns for air water flow in horizontal pipes. They presented new results on interfacial patterns observed for air and water flowing in horizontal 25.4 and 95.3 mm pipelines close to atmospheric conditions. They stated that the liquid flow needed to initiate slugs at low gas velocities was strongly affected by pipe diameter and appeared to depend on a linear instability. At high gas velocities, the transition was approximately independent of pipe diameter and was explained by a non-linear mechanism associated with the coalescence of roll waves. The authors determined the initiation of slugs in the annular flow regime to occur at much lower liquid flows than had been reported by previous investigators. They concluded that the transition from stratified to annular flow was different in smaller diameter pipes than in larger pipes because wave wetting played a more imported role.

Tronconi (1990) studied on the prediction of slug frequency in horizontal two phase slug flow. They explained the experimental effects of gas and liquid flow rates, pipe diameter, gas density and liquid viscosity on slug frequency. It was reported that the characteristic frequencies of liquid slugs in intermittent gas liquid horizontal pipe flow was related to the periods of the unstable waves. These waves were responsible for the generation of slugs in the inlet region of the pipe. The wave properties were estimated in accordance with the theory of finite amplitude waves. The purpose of this study was to provide simple generalized equations to estimate the slug frequency for engineering calculations.

Jepson and Taylor (1993) determined the slug flow and its transitions in large diameter horizontal pipes. They compiled a flow regime map for the air water two phase flow in a 300 mm diameter horizontal pipeline. It was stated that the transitions differed substantially from those for small diameter pipes and were not predicted accurately by any theoretical model. Data on slug frequency, length, holdup, translational velocity and pressure gradient were presented and compared with the existing data. The results showed that the pipe diameter had a large effect on all these properties. Several changes in the distribution of the phases in large-diameter pipes were reported. These were especially prominent in slug and annular flow. For instance, as the pipe diameter was increased, an increase in the superficial liquid velocity was needed to attain slug flow. Annular flow was attained at lower superficial gas velocities for large pipe diameters. The slug length increased with an increase in the pipe diameter.

2.3. Literature Review of Inclined Gas Liquid Flows

Singh and Griffith (1970) proposed a simple model of two phase slug flow in inclined pipes. The model parameters have been determined experimentally using five different size copper pipes at 5, 10, 15 degree inclinations. They used air water mixture at one atmosphere with up flow. Their model predicts the total pressure gradient due to the sum of gravity and wall shear stresses. The authors investigated the relationship between pressure gradient and pipe size. This relationship gives an optimum pipe size at which the pressure gradient is minimum. They compared their simplified predictions with the experimental results and concluded that their model could predict the pressure gradient within the ±15 percent of the experimental values.

Bonnecaze *et al.* (1971) investigated the holdup and pressure drop for two phase slug flow in inclined pipelines. They presented some results from a recent study of gas liquid flow in pipelines inclined ±10 degree from the horizontal. The authors concentrated their attentions on the slug flow regime because they found this regime to predominate in uphill and horizontal flows. This conditions can be typically encountered in pipeline applications. They reported that stratified flow tended to dominate in the downhill situation but even for this pipeline orientation, slug flow could exist the flow rate was sufficiently large. The authors accomplished to derive and verify of a holdup model for inclined slug flow. They suggested a formulation for a friction factor of a two phase slug flow. At the end of the paper, they concluded that the derivation of a two phase slug flow pressure drop for inclined pipelines was verified by field measurements.

Beggs and Brill (1973) investigated the gas liquid flows in inclined pipes to determine the effect of pipe inclination angle on liquid holdup and pressure loss. After the literature survey was completed at that time, they concluded that no correlation existed for predicting the liquid holdup and pressure drop for pipes at all angles. They developed correlations for liquid holdup and friction factor to predict the pressure gradients for two phase flow in pipes at all angles for many flow conditions. The purpose of their study was to find a correlation that would be applicable in designing for hilly terrain and tubing strings for inclined wells. The authors drew the following conclusions from this study; 1) The inclination angle of a pipe in which two phase flow is occurring definitely affects liquid holdup and pressure drop for most flow conditions. 2) In inclined two phase flow, the liquid holdup reaches a maximum at an angle of approximately +50° and minimum at approximately -50° from horizontal. The fact that holdup is approximately equal at angles of +90° and +20° explains why vertical holdup correlations can be used with some degree of success for horizontal flow. 3) Pressure recovery in the downhill section of a two phase pipeline in hilly terrain can definitely exist and should be considered in pipeline design. 4) The accuracy of a liquid holdup correlation for horizontal two phase flow can be improved by considering flow pattern. 5) Friction loss in two phase flow is greatly affected by liquid holdup. Beggs and Brill (1973) developed a correlation that could predict the liquid holdup and pressure gradients of two phase, air-water flow in 25.4 and 38.1 mm smooth, circular pipes at any angle of inclination.

Barnea *et al.* (1980) reported experimental measurements of flow patterns for gas liquid flow in inclined pipes. The results were compared with the theory of Taitel and Dukler (1976) which predicted the flow patterns in horizontal and inclined pipes. In this work the flow pattern boundaries were predicted analytically and it was shown that for each inclination angle every transition boundary can be represented by two dimensionless groups. The flow of air and water through 25.5 and 19.5 mm pipes was studied at flow angles as large as 10°. The authors explained the characteristic flow patterns for horizontal and inclined flow respectively. The agreement between experiment and theory was found to be very good up to ±10° inclination. At larger inclinations the trends predicted by theory were correct but quantitative predictions were inaccurate. The authors believed that these results ought to be considered as experimental proof of the validity of the theory until at that time was tested only for horizontal pipes. They concluded that their theory failed to predict the stratified-smooth to stratified wavy transition for inclined pipes.

Spedding *et al.* (1982) presented the two phase pressure loss data for the air water system for angle of inclination from vertical upward to vertical downward co-current flow. They summarised the investigations beginning from 1939's about the pressure loss in inclined pipes. The flow regime classification used in this work was that suggested by Spedding and Nguyen (1980). The aim of this work was to report experimental data on pressure loss for two phase flow in an inclined tube. The data were presented as frictional velocity against total velocity and in this form successfully overcame the effect of pipe diameter, liquid density except of liquid viscosity. They reported that detailed comparison with data from the literature had provided a substantial measure of agreement. Besides this, they added that all of the empirical and semi-theoretical correlations had failed to give any close agreement with the data of this study. Finally, the authors recommended that the total flow velocity ought to be kept about 15 m/s for most flow conditions in order to give a balance between flow capacity of the equipment and pressure loss.

Mukherjee and Brill (1985) proposed empirical equations to predict flow patterns in two phase inclined flow. Flow regime maps were drawn based on experimental data for different angles, including horizontal and vertical flow. The authors proposed different empirical equations for the flow regime transitions. These equations were functions of inclination angle for both upflow and downflow.

Felizola and Shoham (1995) suggested a unified model for slug flow in upward inclined pipes. The effect of pipe inclination on upward two-phase slug flow characteristics were studied both experimentally and theoretically. Experimental data were acquired for the entire range of inclination angles, from horizontal to vertical. New correlations were developed for slug length and liquid holdup in the slug body as function of inclination angle. A unified model were developed for the prediction of slug flow behavior in upward inclined pipes. Reasonable agreement was observed between the pressure drop predicted by the model and the experimental data.

Spedding *et al.* (1998) investigated two phase co current flow in inclined pipe. Data were presented on horizontal and slightly inclined flows at +5° and –5° for a 50.8 mm inner diameter pipe. The prediction capabilities of existing flow regime maps were shown to be inadequate. However, the transitions for stratified ripple to role wave, for slug to blow-through-slug, for film plus droplet to stratified, and the modified maps for stratified type to slug flows all gave good prediction performance with horizontal and slightly inclined flows. The largest liquid hold-up occurred in upward flow except at high gas rates and low liquid rates where the down flow condition gave the highest liquid hold-up. The lowest liquid hold-up occurred in downward flow allow gas flow rates and horizontal flow at high gas flow rates.

Hold-up prediction proved to be flow regime dependent. The inclined total average pressure drop data crossed over the horizontal data from higher to lower values with increasing gas rate at a gas rate of just under U_{Gs} = 10 m/s. Below this gas flow rate the horizontal pipe gave the lowest pressure drop while above this gas flow rate the upwardly inclined pipe gave the lowest pressure drop.

2.4. Conclusion of the Literature Review

The most comprehensive study found in the literature related with the objective of this thesis was the investigation of Ekberg *et al.* (1999). The authors investigated the gas liquid flows in narrow horizontal annuli. Experimental data associated with the two-phase flow regimes, void fraction and pressure drop in horizontal, narrow, concentric annuli were presented. Two transparent test sections, one with inner and outer diameters of 6.6 and 8.6 mm, and an overall length of 46.0 cm; the other with 33.2 and 35.2 mm diameters and 43.0 cm length, respectively, were used. Near-atmospheric air and water constituted the gas and liquid phases, respectively. The gas and liquid superficial velocities were varied in the 0.02—57 and 0.1 —6.1 m/s ranges, respectively. The major two-phase flow patterns observed included bubbly, slug/plug, churn, stratified, and annular. Transitional regimes, where the characteristics of two distinct flow regimes could be observed in the test sections, included bubbly-plug, stratified-slug and annular-slug. The obtained flow regime maps were different than flow regime maps typical of large horizontal channels and micro channels with circular cross-sections. They were also different from the flow regimes in rectangular thin channels. The measured average void fractions and pressure drops for the two test sections were compared with predictions of several empirical correlations.

This recently published study didn't include the eccentric conditions. The study of eccentrically inserted rod in a horizontal circular pipe will be a new and actual investigation. In this study, gas-liquid flows in horizontal eccentric pipes will be examined to fill up this deficiency in the literature.

3. MATERIAL AND METHOD

3.1. Flow Patterns

Sometimes, different subjects can be defined with the same words. The flow pattern phenomena is encountered in fluid mechanics of single phase and multiphase flow. Essentially, the words specify the visualization of flow. Streamlines, pathlines, and streaklines are visualized in single phase flow whereas bubbles, slugs, and waves in two phase flow. It is firstly necessary to decide what constitutes a flow pattern in gas liquid flow. The similar flow regimes can be seen even for different pipe sizes and fluid properties. A particular flow pattern depends on the condition of pressure, flow rates of fluids, heat flux, and channel geometry. The knowledge of the flow pattern which is depended on the operating conditions of pipe has an importance for an engineer in many respects. For instance, most oil wells deliver a mixture of gas and oil. The mixture must be collected and delivered to the refinery or customer. In the designing of such a pipe line, hilly terrain effects should be considered by specialists to predict the total pressure drop accurately.

Many well known expressions for the void fraction or for the pressure drop are limited to a certain flow pattern. A definite prediction of flow pattern is always necessary to get reliable results for the calculation of pressure loss, and other flow properties. The description of flow patterns bases mostly on visual observations in a transparent channel. When the flow is rapid, it is very hard to observe apparently what is going on. Despite the importance of subject, there is considerable disparity in the description of visual observations given by different authors. Here, we classify the flow patterns regarding the most commonly accepted terms and descriptions. It is necessary to define the flow regimes independently for vertical, horizontal, and inclined flow.

3.1.1. Gas-Liquid Flows in Vertical Pipes

Due to the subjective nature of flow regime definitions, many different flow regimes have been defined in the literature. The flow patterns encountered in vertical upwards co-current flows are shown schematically in figure 3.1. Here, we define the following six pattern for vertical flow.

In **bubbly flow**, the gas phase is distributed in discrete bubbles within the continuous liquid phase. At one extreme the bubbles may be small and spherical and at the other extreme the bubbles may be large with a spherical cap and a flat tail. In this latter state although the size of bubbles does not approach the diameter of the pipe, there may be some confusion with slug flow.

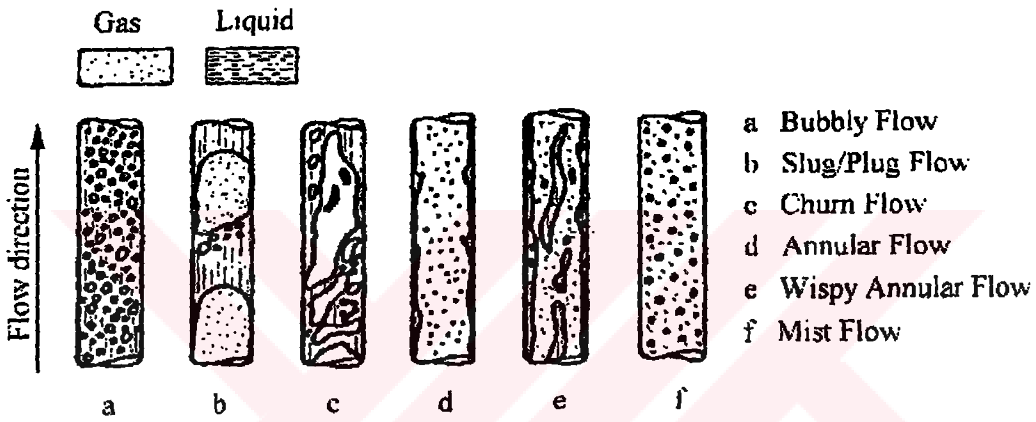

Figure 3.1. Flow patterns in vertical gas liquid flows.

When the concentration of bubbles in bubbly flow becomes high, bubble coalescence occurs, and progressively the bubble diameter approaches nearly the same diameter as that of the duct. In **slug (or plug) flow**, the bullet-shaped bubbles as illustrated in figure 3.1. result from the gravity acting parallel to the flow direction. The nose of the bubble has a characteristic spherical cap and the gas in the bubble is separated from the pipe wall by a slowly descending film of liquid. The liquid flow is contained in liquid slugs which separate successive gas bubbles. The bubbles of gas occupy most of the pipe's cross sectional area and can vary in length from the tube diameter to over a hundred diameters.

As the gas flow rate is increased, the velocity of the slug flow bubbles increases, and a break down of these bubbles occurs leading to an unstable regime. This flow regime is somewhat similar to the slug flow, but, it is much more chaotic, frothy, and disordered. This instable and oscillatory motion of flow is called as **Churn flow**. With the beginning of this flow pattern, the bullet-shaped bubbles of slug flow become narrow, and their shapes are distorted. The continuity of the liquid in the slug between bubbles is repeatedly destroyed by a high local gas concentration in the slug. The churn flow is also sometimes called as semi-annular or slug-annular flow.

Annular flow is characterized by continuity in the axial direction of the gas phase in the core. Liquid flows upward, both as a thin film and as droplets dispersed in the gas. Large amplitude waves are usually present on the liquid surface of the film. A continuous exchange between the liquid layer and the mist flow occurs by entrainment of droplets from the liquid layer and deposition of core droplets on the wall.

The flow in **wispy annular flow** takes the form of a relatively thick liquid film on the walls of the pipe together with a considerable amount of liquid entrained in a central gas core. The liquid film is aerated by small gas bubbles and the entrained liquid phase appears as large droplets which have agglomerated into long irregular filaments or wisps. This regime is characteristic of high mass velocity flows.

As the gas velocity is increased in wispy annular regime, the shear stresses between two phases reach so high values that, liquid droplets start to leave the liquid surface, then continue to their movements in gas flow. When the all liquid phase is transported in gas current as droplets, it is defined as droplet flow or **mist flow**. The transition to the gas phase flow is nearly completed with the accomplishment of this flow regime.

3.1.2. Gas-Liquid Flows in Horizontal Pipes

Flow patterns in horizontal gas-liquid flow have a tendency to be somewhat more complex than those in vertical flow. In vertical two phase flow, the gravitational force acts parallel to the flowing direction, whereas in horizontal gas-liquid flow, the gravitational force acting normal to the pipe induces an asymmetry in the flow. This irregularity of flow means that the liquid phase tend to accumulate at the bottom of the pipe. The characteristic flow patterns for the flow in a horizontal pipe are shown in figure 3.2., schematically. As the gas flow rate is increased step by step, the following flow patterns can be observed respectively; bubbly flow, plug flow, stratified flow, wavy flow, slug flow, annular flow (film flow), and mist flow.

For low gas flow rates, the buoyant force which effects on a bubble overwhelms the drag force, and gas phase moves in forms of bubbles through the upper cross-sectional area of pipe. This flow pattern is called as "Bubble Flow" or "**Bubbly Flow**". Bubbly flow occurs typically at low superficial gas velocities and high liquid velocities.

As the gas flow rate is increased, the single bubble grows and coalesces to form a **plug flow**. This flow pattern is similar to slug flow in the vertical case but the liquid layer separating the gas bubble from the wall tends to be thicker at the bottom of the pipe than at the top.

For the continual increasing of gas flow rate, the bullet-shaped plug gets so big that the surface tension is no longer enough to sustain the liquid membranes between plugs. Thus, gas and liquid begin to flow in the form of two separated layers in pipe. The gravitational separation is complete and liquid flows along the bottom of the tube, and the gas along the top part of the tube. This flow regime is named as **Stratified flow**. The separated two phases have a relatively smooth interface. Stratified flow pattern only occurs at very low liquid and gas velocities.

With the more increasing of gas flow rate, one can see an instable condition as waves on the surface. These waves develop from the stratified flow pattern and is called as **Wavy flow**.

As the gas velocity is increased in wavy flow, the shear stresses between the gas and liquid phases excite the waves on the liquid surface in a powerful manner. Then, the liquid phase begins to reach until the upper surface of tube and the pipe cross section is occupied by the excited waves intermittently. The appeared shear stresses are so big that, the gravitational force acting on a liquid bulk becomes unimportant. Accumulation of this liquid bulks create liquid pistons so called **Slug flow**. This may be described by passage along the channel of frothy slugs, in which the liquid phase is continuous, but in which a large number of gas bubbles may also be entrained. The presence of these slugs can often be troublesome in practical applications. They give rise to sudden pressure pulses, and cause vibration of tubes. The prediction of the onset of slug flow has a considerable industrial importance.

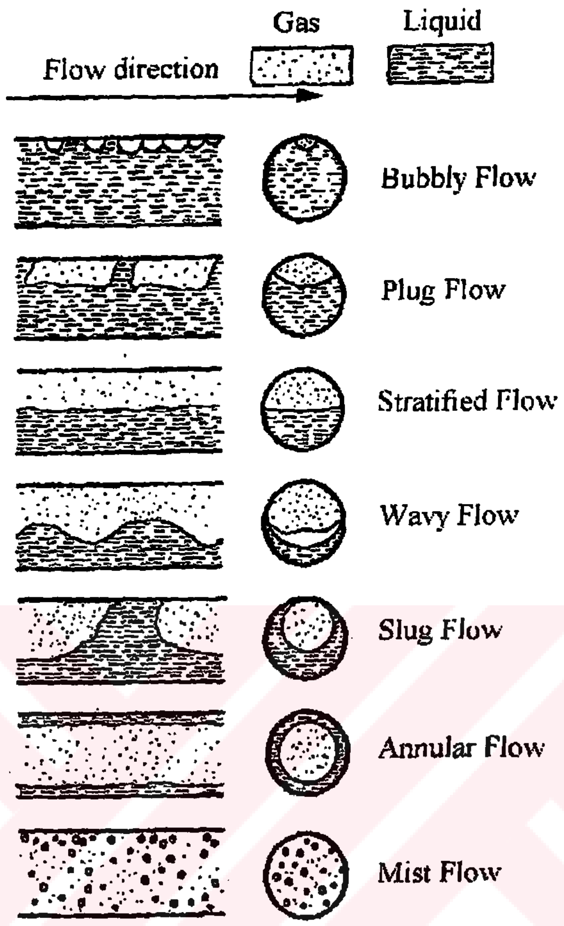

Figure 3.2. Flow patterns in horizontal gas liquid flows.

Annular flow originates from the slug flow when the gas velocity is increased. The high gas velocity causes the formation of a gas core with a liquid film around the periphery of the pipe. The film may not be continuous around the entire circumference for the low liquid flow rates. But, for the annular flow in horizontal pipes, the film thickness at the base of the pipe will always be thicker than the upper side's.

For the condition of very high gas flow rates, a foggy flow is reached. The liquid phase is transported as droplets. This flow pattern is called as **mist flow**.

3.1.3. Gas-Liquid Flows in Inclined Pipes

Most of the available flow pattern data are for normally vertical or horizontal tubes. In inclined sections of devices which are carrying gas and liquid simultaneously, liquid may accumulate when the gas velocity is insufficient to advance the liquid against the opposing action of gravity. The accumulation of liquid eventually leads to periodic pipe blockage, that is, slug or semislug flow. Semislug flow occurs when the complete circumference of the pipe is periodically wetted but the gas phase remains to some extent continuous. In gas-liquid pipe flow, slugs and semislugs are often to be avoided, for reasons of safety, increased and oscillating axial pressure gradient, oscillating liquid production, possible damage to downstream equipment, and so forth. The flow regimes in two-phase flow depend on the pipe angle and flow direction together with the other flow and fluid parameters. The present studies on the gas liquid flows in inclined pipes focus on the information of flow pattern transitions and their functional relationships with angle of inclination for either up-flow or down-flow. The purpose of investigations on inclined pipes is to develop an empirical method to predict flow patterns in pipe at all possible inclination angles.

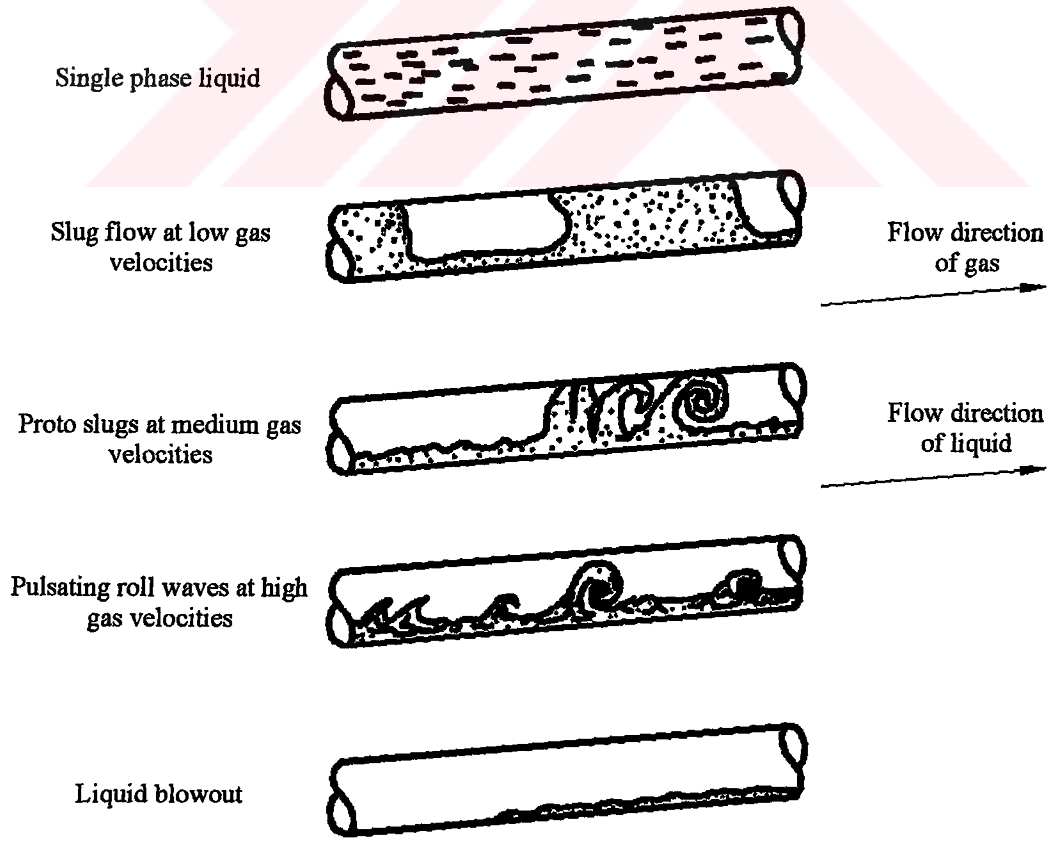

Figure 3.3. Flow patterns in inclined gas liquid flows.

When two-phase flow occurs in inclined pipes, many different varieties of patterns are developed. Liquid holdup becomes an increasingly important factor in the flow. For example, when the flow is going uphill, just 5 degrees, the liquid can flow in a rolling fashion much like a wave on a beach. If the gas is moving at a high superficial velocity the liquid holdup decreases. At higher angles (30 degrees) large slugs of liquid are created. It appears as if most of the liquid is flowing backward. The figure 3.3. reveals how the flow changes with increasing gas superficial velocity.

Flow patterns of gas liquid flows in pipes are affected from the inclination of the pipe. The studies on the inclined co-current gas liquid flows have been divided in two sections which are the upward and downward flows. The subject of this study is related with upward co-current gas liquid flows in inclined pipes.

There has been no general flow pattern map which covers the all possible inclinations and flow patterns of inclined pipes. The studies on the inclined pipes have mostly regarded the angle from the horizontal to express the inclination of the pipe. But, there has been no general agreement for the denotation of angle with positive or negative sign. This has created confusion that some authors have denoted the upward flow with negative sign, but, upward inclination angle has been mostly denoted with positive sign.

The well known studies on the inclined pipes have been summarized in the section of previous studies. These papers have mostly interested with the flow patterns, pressure drop, and void fraction in inclined pipes with different inclinations. There has been a clear agreement between the investigators that gas liquid flows in inclined pipes were different than those of the vertical or horizontal pipes.

Liquid holdup is defined as the volume fraction of the pipe which is occupied by liquid. Liquid holdup against superficial gas velocity is shown in Figures 3.4. and 3.5. for $\theta = 0^o$, and $\theta = +5^o$, respectively, for co-current air-water flow. One can see that, the variation of liquid holdup with superficial gas velocity for the horizontal flow is different than that of the inclined flow. The liquid holdup values of $\theta = +5^o$ are greater than those of the horizontal pipe.

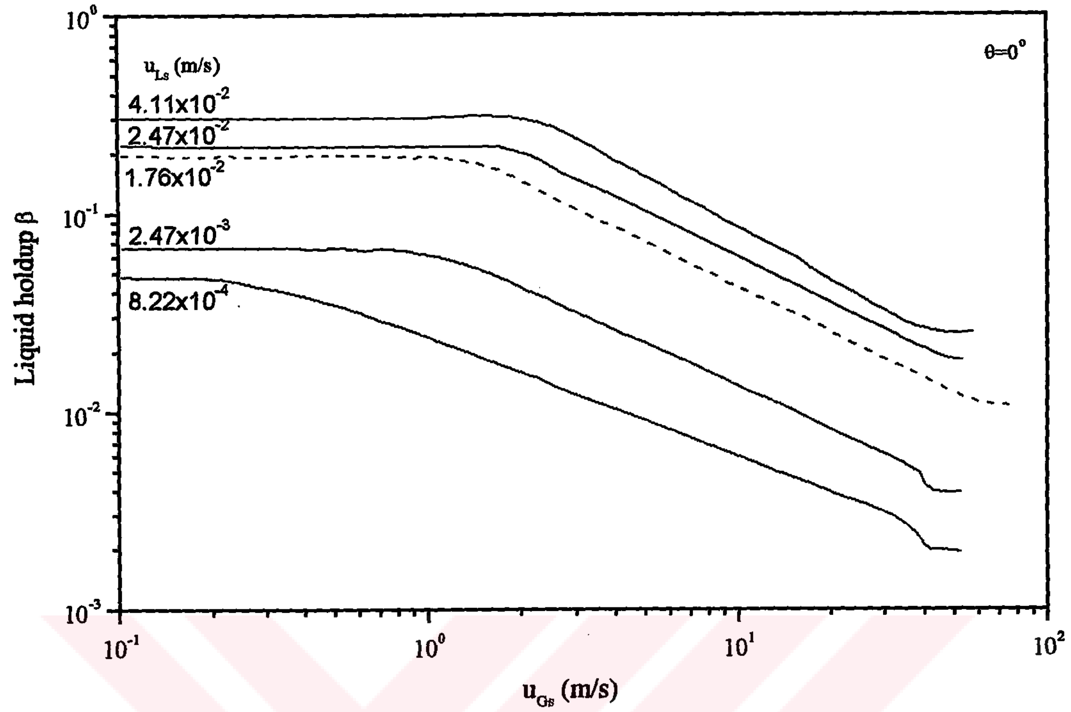

Figure 3.4. Variation of liquid holdup with superficial gas velocity in horizontal pipe

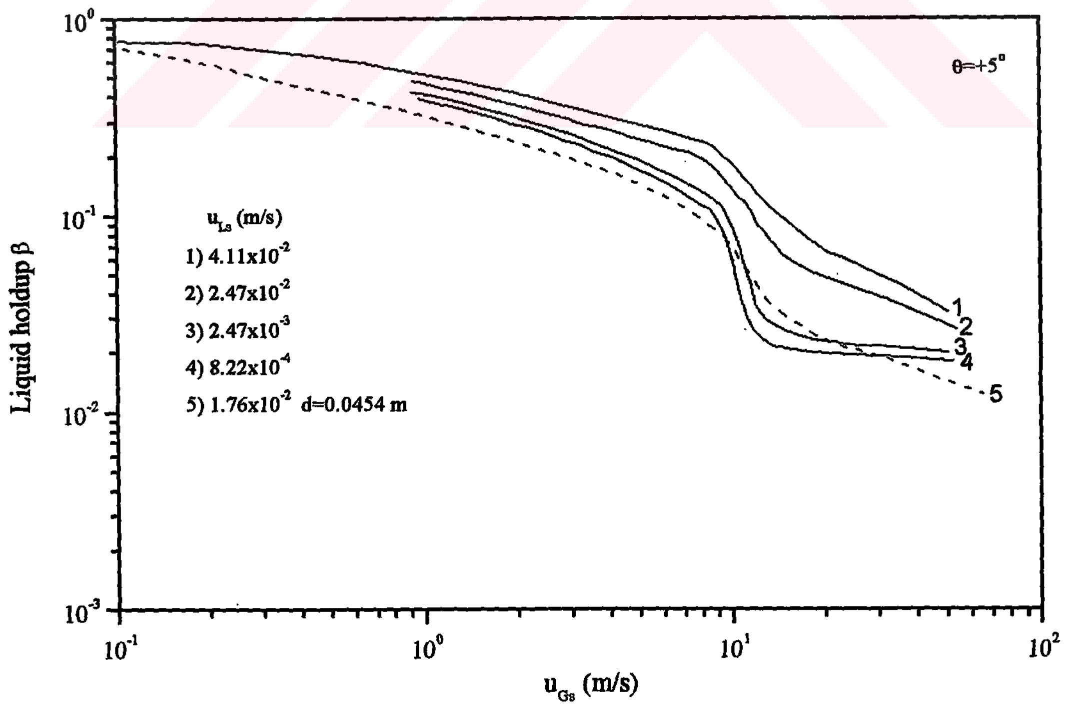

Figure 3.5. Variation of liquid holdup with superficial gas velocity in inclined pipe

Liquid holdup is greatly influenced by pipe inclination as can be seen from figure 3.6.

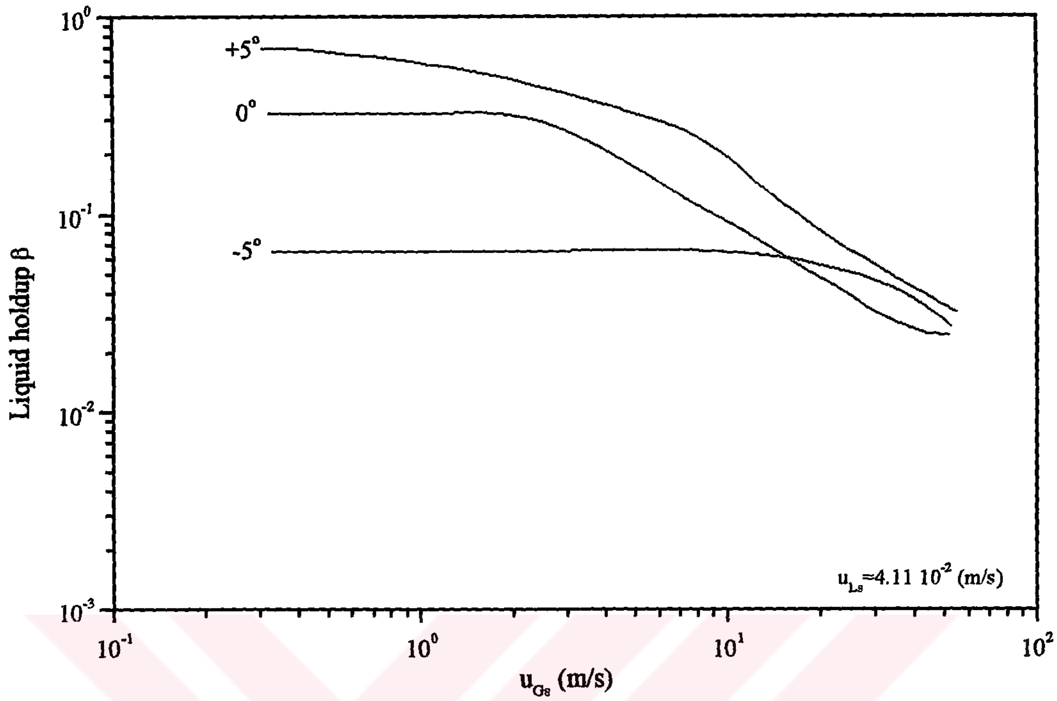

Figure 3.6. Variation of liquid holdup with superficial gas velocity for different inclinations.

Positive angles indicate uphill flow. Figure 3.6. shows the variation of liquid holdup with superficial gas velocity for constant superficial liquid velocity. These data and figure were given by Spedding et. al. (1998). They reported that, at low superficial gas velocities the slug flow regime was formed for $\theta = +5^o$ in contrast to the stratified regime for the corresponding horizontal and $\theta = -5^o$ conditions. It was not unexpected therefore, that the liquid holdup, β , for $\theta = +5^o$ angle would be greater since, in general, liquid holdup for stratified flow would be less than for the slug regime. As the superficial gas velocity was increased the liquid holdup tended to converge and run along a parallel path as similar flow regimes were developed. Spedding et. al. (1998) expressed that all the data points of the $\theta = +5^o$ lie above the data points of the $\theta = 0^o$.

Downward $\theta = -5^o$ data possessed lower liquid holdup values than the corresponding condition at other angles for $u_{Gs} < 20\,m/s$. The profile of the $\theta = -5^o$ data in this region was flat since the stratified plus inertial wave regime was present.

Total pressure loss of gas liquid flows are affected by the angle of the pipe. This is especially important for gas and oil industries. Much of the hydrocarbon production are transported from offshore fields to processing facilities in pipelines as two and three-phase mixtures. Operation of oil and gas gathering systems, compressors and pumps depend on accurate calculation of pressure drop which in turn depends on the liquid holdup and other factors. The effect of pipe angle on the total pressure loss was investigated by Spedding et. al. (1998). The variation of the total pressure loss with superficial gas velocity is shown in figure 3.7. for different pipe angles for a constant superficial liquid velocity.

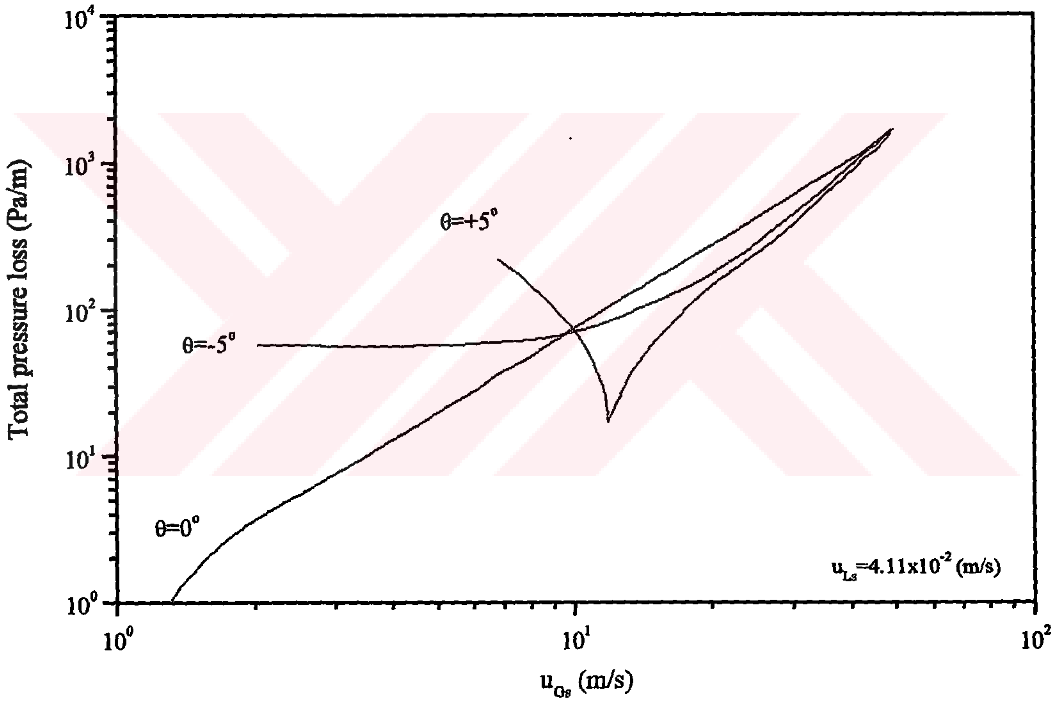

Figure 3.7. Variation of total pressure loss with superficial gas velocity for different inclinations.

Stanislav et. al.(1986) reported experimental measurements of flow patterns, pressure gradients and liquid holdup for intermittent two-phase flow in upward inclined pipes. The authors compared their experimental results with the study of Taitel and Dukler (1976). The experimental transitions of flow patterns in inclined pipes which were obtained by Stanislav et. al.(1986) are compared in figure 3.8. for the angles of 0, and +5. The figure 3.8. shows the flow pattern map of an inclined pipe with 25.8 mm inner diameter.

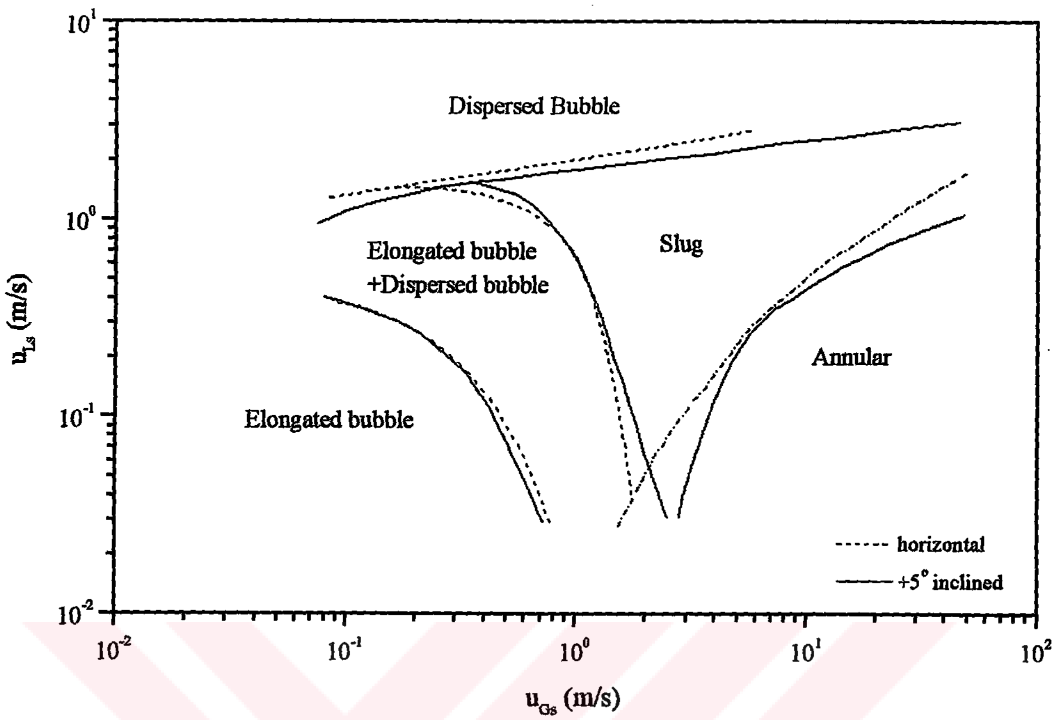

Figure 3.8. The flow pattern map of an inclined pipe with inner diameter of 25.8 mm.

The flow patterns of gas liquid flows in inclined pipes were compared by many authors with the flow patterns of the horizontal or vertical pipes regarding the same hydrodynamic and physical properties. In this study, the same method is applied for the experiments in the inclined pipe.

3.2. Flow Pattern Map

The prediction of flow patterns for the given operating parameters has been mostly accomplished with the help of empirically calculated flow pattern maps. The transitions between the flow patterns have been illustrated as lines in a two dimensional representation. Since the transitions between flow patterns which are depended on superficial velocities can a little bit vary, it is better to regard the transition lines as transition areas. Furthermore, flow pattern maps which have been restricted in a two dimensional representation can not take into account all the influences. The transitions between the patterns are affected from the superficial velocities, densities, and viscosities of the phases, as well as, the diameter, length, and inclination of the pipe to the horizontal. A detailed study of the flow pattern maps known in the literature was presented by Taitel and Dukler (1986). The authors classified the flow patterns as horizontal, vertical, and inclined. They explained the general flow patterns and the transitions between each other in detail. Taitel and Dukler (1986) explained flow pattern detection and observation methods. This useful and complete study of gas liquid flows guided to this investigation.

There are some descriptions which are mostly used in the design of two phase flow equipments, in the derivation of relationships related with the gas liquid flows, and in the representation of many flow pattern maps. The primary variables used throughout this study are briefly introduced and some simple relationships between this primary variables are derived for the case one –dimensional flow in the following.

In this study, the subscripts 'G' for gas and 'L' for liquid are used to distinguish gas and liquid phases. The subscript 's' near the subscripts 'G' for gas and 'L' for liquid refers the superficial velocity of liquid or gas phase. Velocity can be defined as the area-averaged volume flow rate. The volume or mass flow rate of phases can be individually measured before the mixing of gas and liquid. But, it is not easy to determine the actual flow area of each phases in a two phase flow condition. Therefore, a new concept that is "superficial velocity" has been used in two phase flow. Superficial velocity of a phase can be thought as if that phase is flowing in the two phase flow pipe individually. Thus, superficial velocity is the rate of volume flow rate to the cross-sectional area of two phase flow pipe. The superficial gas velocity and the superficial liquid velocity can be defined as follows, respectively.

$$u_{Gs} = \frac{\dot{M}_G}{\rho_G A} \quad ; \quad u_{Ls} = \frac{\dot{M}_L}{\rho_L A} \tag{3.1}$$

Sometimes, actual velocities u_G and u_L are used instead of the superficial velocities u_{Gs} and u_{Ls}. Definition of them are:

$$u_G = \frac{\dot{M}_G}{\rho_G A_G} \quad ; \quad u_L = \frac{\dot{M}_L}{\rho_L A_L} \tag{3.2}$$

Actual velocities can be defined in a different way as below;

$$u_G = \frac{\dot{M}_G}{\rho_G A_G} = \frac{\dot{M}_G}{\rho_G A} \cdot \frac{A}{A_G} = u_{Gs} \frac{A}{A_G} \Rightarrow u_G = \frac{u_{Gs}}{\alpha} \tag{3.3}$$

$$u_L = \frac{\dot{M}_L}{\rho_L A_L} = \frac{\dot{M}_L}{\rho_L A} \cdot \frac{A}{A_L} = u_{Ls} \frac{A}{A_L} \Rightarrow u_L = \frac{u_{Ls}}{1-\alpha} \tag{3.4}$$

The area averaged gas fraction A_G is denoted as the void fraction (α). Void fraction is always equal to or smaller than unity. Similarly, the area averaged liquid fraction A_L is called as the liquid hold-up ($1-\alpha$). The relation between the void fraction (α) and the liquid hold-up ($1-\alpha$) is demonstrated in figure 3.9. Definitions of the void fraction (α) and the liquid hold-up ($1-\alpha$) are given in eqs.(3.5) and (3.6).

$$\alpha = \frac{V_G}{V} = \frac{A_G}{A} \tag{3.5}$$

$$\beta = 1 - \alpha = \frac{V_L}{V} = \frac{A_L}{A} \tag{3.6}$$

For one component two-phase flow, the total mass flow $\dot{M}_T$ is given. For this case, one can define a mass quality.

$$\dot{x} = \frac{\dot{M}_G}{\dot{M}_T} \quad ; \quad 1 - \dot{x} = \frac{\dot{M}_L}{\dot{M}_T} \tag{3.7}$$

Superficial gas and liquid velocities can be redefined with the help of the mass quality given in eq.(3.7):

$$u_{Gs} = \frac{\dot{M}_T \dot{x}}{\rho_G A} \quad ; \quad u_{Ls} = \frac{\dot{M}_T (1-\dot{x})}{\rho_L A} \tag{3.8}$$

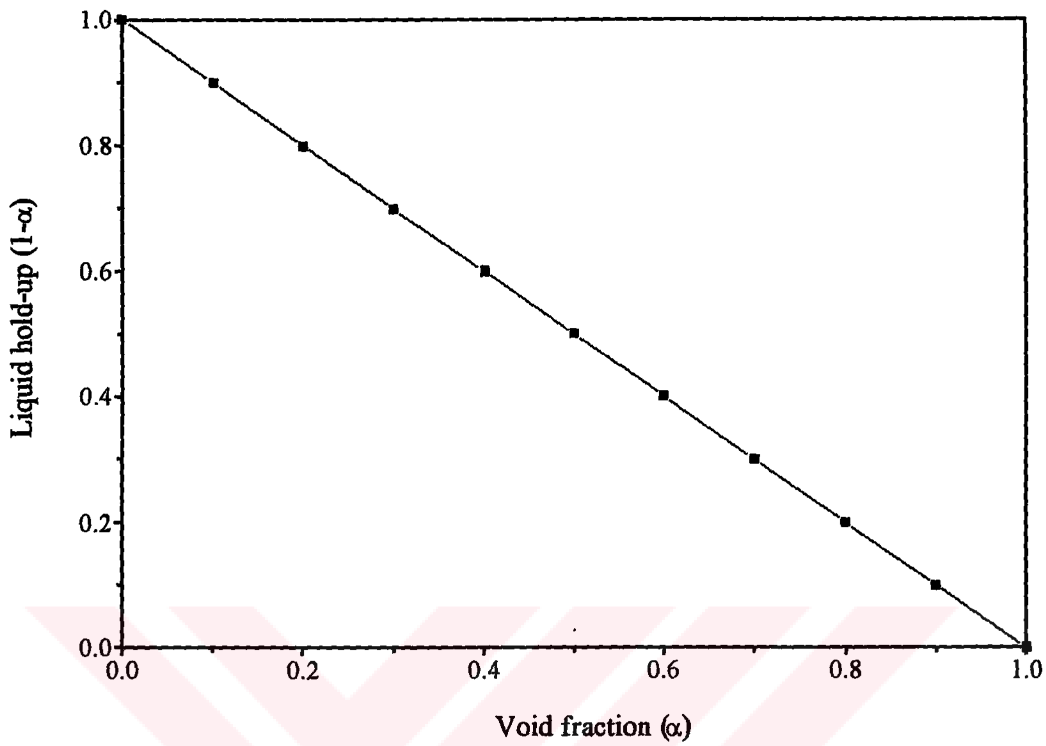

Figure 3.9. The variation of liquid hold-up with void fraction.

The rate of mass flow divided by flow area is given the name "mass velocity ($\dot{m}$)". Thus, gas mass velocity is defined in eq.(3.9).

$$\dot{m}_G = \frac{\dot{M}_G}{A} \tag{3.9}$$

Liquid mass velocity is given in eq.(3.10).

$$\dot{m}_L = \frac{\dot{M}_L}{A} \tag{3.10}$$

Total mass velocity of gas liquid mixture is as below,

$$\dot{m}_T = \frac{\dot{M}_T}{A} \tag{3.11}$$

Mass flow rate of gas phase can be redefined with the help of the total mass velocity and the mass quality:

$$\dot{M}_G = \dot{m}_T.A.\dot{x} \tag{3.12}$$

Mass flow rate of liquid phase can be determined similar to eq.(3.12):

$$\dot{M}_L = \dot{m}_T.A.(1-\dot{x}) \tag{3.13}$$

Superficial gas velocity is expressed in eq.(3.14).

$$u_{Gs} = \frac{\dot{M}_G}{\rho_G A} = \frac{\dot{m}_T.\dot{x}}{\rho_G} \tag{3.14}$$

Superficial liquid velocity can be written as:

$$u_{Ls} = \frac{\dot{M}_L}{\rho_L A} = \frac{\dot{m}_T.(1-\dot{x})}{\rho_L} \tag{3.15}$$

Actual velocities of each phases are defined using the total mass velocity and mass quality:

$$u_G = \frac{u_{Gs}}{\alpha} = \frac{\dot{m}_T.\dot{x}}{\rho_G.\alpha} \tag{3.16}$$

$$u_L = \frac{u_{Ls}}{1-\alpha} = \frac{\dot{m}_T.(1-\dot{x})}{\rho_L(1-\alpha)} \tag{3.17}$$

3.2.1. Flow Pattern Map of Horizontal Gas Liquid Flows

In a horizontal or a slightly inclined pipe, one can see many different flow patterns in a gas liquid two phase flow. An overview for the observed flow patterns of a horizontal pipe in which an air water two phase flow occurs has been presented with the help of a flow pattern map in figure 3.10. The arrangement of the flow patterns is effected from the superficial velocities of phases.

3.2.1.1. Flow Pattern Map of Baker (1954)

One of the earliest and most widely used flow pattern maps was presented by Baker (1954). Baker employed the measurement values taken from the literature and completed them with the results of his own experiments. Baker (1954) proposed a flow pattern map based on the coordinates $\Phi_B = \dot{m}_L / \lambda$ and $X_B = (\dot{m}_L / \dot{m}_G)\lambda\beta$ where $\dot{m}_G$ and $\dot{m}_L$ are superficial gas and liquid mass velocities, respectively. The boundaries of flow regimes of Baker's flow pattern map shown in figure 3.11. were indicated with the definitions of the material functions λ and β. For the determination of the searched flow pattern, firstly, the values of the coordinates, Φ_B and X_B, should be calculated with the help of material functions (λ and β) and mass flow velocities ($\dot{m}_L$ and $\dot{m}_G$).

$$X_B = x^* \lambda \beta \tag{3.18}$$

$$\Phi_B = \dot{m}_G / \lambda \tag{3.19}$$

$$x^* = \dot{m}_L / \dot{m}_G = (1 - \dot{x}) / \dot{x} \tag{3.20}$$

$$\lambda = \left[\left(\frac{\rho_G}{\rho_{air}} \right) \left(\frac{\rho_{H_2O}}{\rho_L} \right) \right]^{1/2} \quad \text{and} \quad \beta = \frac{\sigma_{H_2O-air}}{\sigma} \left[\left(\frac{\eta_L}{\eta_{H_2O}} \right) \left(\frac{\rho_{H_2O}}{\rho_L} \right)^2 \right]^{1/3} \tag{3.21}$$

The material functions λ and β includes the physical properties of the implemented two phase fluids and the reference values of air and water in standard conditions. The flow pattern expected in operating conditions can be directly read from the map or calculated on the basis of the transition equations.

Different transition equations for the flow pattern map of Baker (1954) have been proposed by many authors. These equations are useful for the determination of flow patterns using a computer. Flow regimes of many data taken from experiments can be determined using a computer program which based on these equations. The functions of transition lines of flow pattern map shown in figure 3.11. are derived in this study.

The lines separating the flow patterns on the Baker's map are numbered as follows.

Table 3.1. Definition regions of the functions

Function 1:	The line between stratified, wavy, slug, and plug region.
Function 2:	The line between wavy, slug, and annular region.
Function 3:	The line between slug, and plug region.
Function 4:	The line between slug, and annular region.
Function 5:	The line separating bubble region.
Function 6:	The line separating dispersed region.

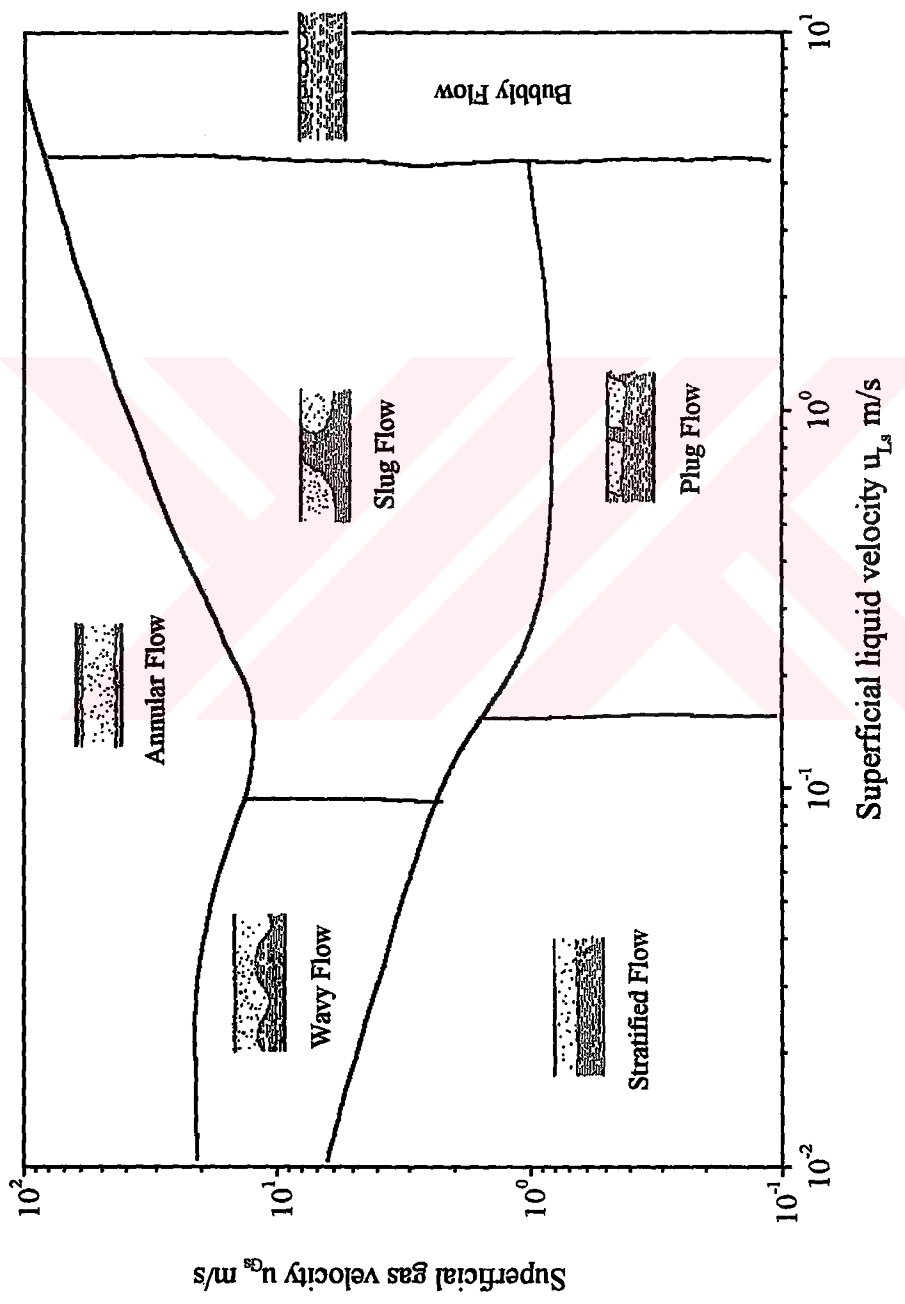

Figure 3.10. Flow patterns of cocurrent air water flow in horizontal pipe.

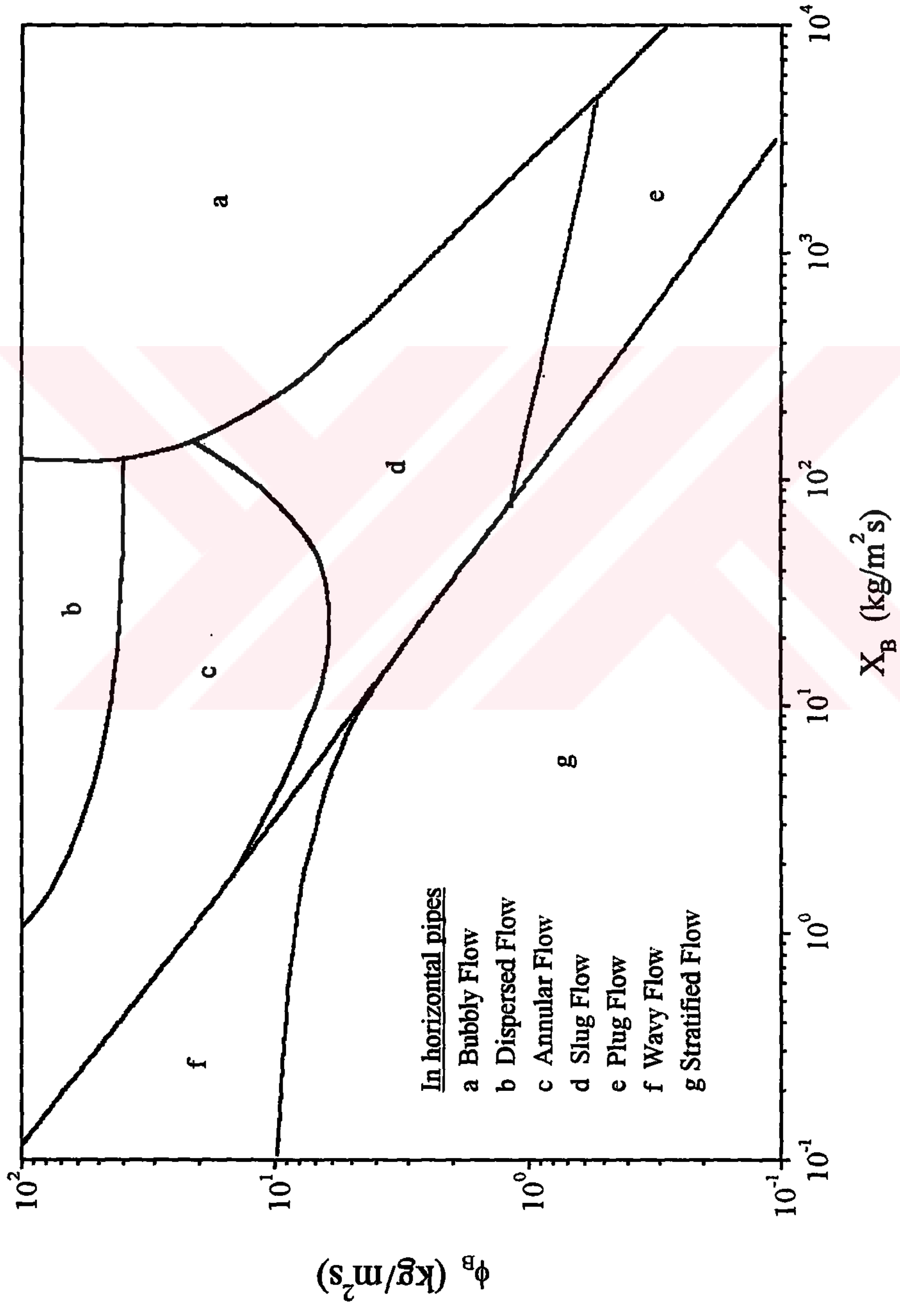

Figure 3.11. Flow Pattern Map of Baker (1954) for horizontal pipes. The functions of the axis are given in eqs.(3.18) and (3.19).

The general form of the equations fitted to all of the transition lines is same.

$$Y = \left[(a_1 X^{n1})^n + (a_2 X^{n2})^n \right]^{1/n} \tag{3.22}$$

Here Y is the dependent variable and refers the Φ_B. The independent variable X means X_B. Thus, the equation (3.22) can be written as follows:

$$\Phi_B = \left[(a_1 X_B^{n1})^n + (a_2 X_B^{n2})^n \right]^{1/n} \tag{3.23}$$

The coefficients a_1, a_2, n_1, n_2, and n were calculated for the six transition functions of Baker's map.

Table 3.2. The coefficients of the Baker's flow pattern map.

	a_1	n_1	a_2	n_2	n
Function 1 (F_1):	8.9527	-0.04079	21.5319	-0.66158	-2.52319
Function 2 (F_2):	21.2108	-0.72354	20.1759	-0.65075	11.47546
Function 3 (F_3):	2.7089	-0.19026	0	0	1
Function 4 (F_4):	19.3787	-0.48420	0.02244	1.37251	1.05191
Function 5 (F_5):	$1.8997.10^{11}$	-4.63371	1164.77	-0.90518	1.61833
Function 6 (F_6):	103.9889	-0.97255	39.4925	0.00144	1.59784

The flow pattern regions of Baker's map are defined as shown in table (3.3) in this study (Appendix 1).

Table 3.3. The flow pattern regions of the Baker's flow pattern map.

Flow Pattern	
Bubbly Flow	$\Phi_B \geq F_5$, $X_B > 150$
Stratified Flow	$\Phi_B < F_1$, $10^{-1} \leq X_B \leq 3340$
Wavy Flow	$F_1 \leq \Phi_B < F_2$, $0.01 \leq X_B \leq 16$
Plug Flow	$F_1 \leq \Phi_B < F_5 \wedge \Phi_B < F_3$, $75 \leq X_B \leq 4800$
Slug Flow	$F_1 \leq \Phi_B < F_5 \wedge F_4 < \Phi_B \leq F_3$, $1.7 \leq X_B \leq 4800$
Annular Flow	$F_2 \leq \Phi_B < F_5 \wedge F_6 < \Phi_B \leq F_4$, $0.01 \leq X_B \leq 150$
Dispersed Flow	$F_6 \leq \Phi_B < F_5$, $1 \leq X_B \leq 120$

Errors (Err(%)) between original and calculated values are given in tables (3.4), (3.5), and (3.6). The definition of Err(%) is given in eq.(3.24).

$$Err(\%) = \frac{\left[\Phi_B - (\Phi_B)_F\right]}{\Phi_B} * 100 \tag{3.24}$$

Table 3.4. Errors between original and calculated values for functions 1 and 2.

Function 1				Function 2			
X_B	Φ_B	$(\Phi_B)_{F_1}$	$Err(\%)$	X_B	Φ_B	$(\Phi_B)_{F_2}$	$Err(\%)$
0.106	9.798	9.799	-0.019	0.102	110.766	111.785	-0.920
0.141	9.639	9.677	-0.401	0.173	75.412	76.218	-1.068
0.200	9.482	9.526	-0.466	0.320	48.486	49.186	-1.445
0.284	9.328	9.368	-0.425	0.572	32.475	32.643	-0.517
0.403	9.028	9.196	-1.857	0.878	23.994	24.146	-0.633
0.607	8.882	8.962	-0.907	1.469	16.810	16.884	-0.436
0.878	8.422	8.701	-3.315	2.126	13.045	13.088	-0.329
1.271	8.151	8.362	-2.594	3.267	9.798	9.761	0.376
1.803	7.760	7.938	-2.290	4.823	7.510	7.498	0.167
2.507	7.122	7.421	-4.201	6.841	6.022	5.928	1.567
3.486	6.670	6.782	-1.668	12.458	4.083	3.975	2.649
4.727	6.222	6.099	1.981				
6.573	5.437	5.304	2.435				
8.608	5.010	4.651	7.168				
15.912	3.453	3.300	4.430				
27.702	2.390	2.346	1.841				
61.909	1.393	1.397	-0.310				
152.891	0.760	0.771	-1.462				
313.867	0.475	0.480	-0.998				
759.791	0.264	0.267	-1.439				
1349.435	0.182	0.183	-0.653				
3123.036	0.106	0.105	0.868				

Table 3.5. Errors between original and calculated values for functions 3 and 4.

Function 3				Function 4			
X_B	Φ_B	$(\Phi_B)_{F_3}$	*Err*(%)	X_B	Φ_B	$(\Phi_B)_{F_4}$	*Err*(%)
76.360	1.183	1.187	-0.401	1.767	14.688	14.744	-0.380
112.174	1.103	1.104	-0.035	2.213	13.045	13.241	-1.497
186.702	1.000	1.002	-0.158	3.016	11.445	11.431	0.119
282.614	0.918	0.926	-0.862	3.930	10.000	10.101	-1.014
530.288	0.818	0.821	-0.337	5.146	8.882	8.933	-0.578
960.830	0.718	0.733	-2.137	6.573	8.018	8.025	-0.085
1599.207	0.654	0.666	-1.846	8.438	7.510	7.244	3.550
2675.050	0.588	0.604	-2.710	10.565	6.780	6.667	1.679
4895.587	0.539	0.538	0.234	14.690	6.325	6.050	4.344
				19.142	6.121	5.781	5.556
				25.069	6.121	5.762	5.879
				33.325	6.222	6.099	1.979
				44.524	6.670	6.954	-4.258
				58.017	7.634	8.362	-9.536
				71.202	9.028	10.011	-10.892
				87.822	10.676	12.377	-15.925
				103.042	12.834	14.767	-15.068
				116.747	15.239	17.075	-12.049
				146.170	20.965	22.450	-7.086

Table 3.6. Errors between original and calculated values for functions 5 and 6.

Function 5				Function 6			
X_B	Φ_B	$(\Phi_B)_{F_3}$	*Err*(%)	X_B	Φ_B	$(\Phi_B)_{F_4}$	*Err*(%)
149.867	20.625	21.759	-5.500	0.767	134.241	146.100	-8.834
165.611	16.810	16.391	2.497	0.932	110.766	124.170	-12.102
191.424	13.315	11.954	10.218	1.127	94.050	106.764	-13.519
221.260	10.676	9.517	10.862	1.411	80.184	90.322	-12.643
266.172	8.285	7.637	7.817	1.821	70.347	76.099	-8.176
313.867	7.006	6.467	7.693	2.482	62.224	63.687	-2.350
392.971	5.828	5.236	10.155	3.646	55.265	53.663	2.899
472.738	4.598	4.422	3.819	4.945	50.510	48.653	3.677
616.010	3.641	3.477	4.509	6.979	47.504	45.044	5.180
759.791	3.017	2.876	4.689	9.705	44.677	42.930	3.911
970.476	2.429	2.304	5.147	13.630	43.239	41.611	3.765
1376.666	1.766	1.679	4.908	19.142	41.337	40.829	1.229
1952.866	1.278	1.223	4.276	29.858	41.000	40.274	1.772
2826.136	0.914	0.876	4.199	42.994	40.007	40.041	-0.085
3682.651	0.698	0.689	1.251	59.782	40.007	39.926	0.202
4727.379	0.553	0.550	0.551	78.683	39.681	39.872	-0.482
4633.867	0.553	0.560	-1.263	124.579	40.007	39.831	0.438
6160.101	0.436	0.432	0.790				
8067.231	0.344	0.339	1.475				
9704.760	0.286	0.287	-0.188				

3.2.1.2. Flow Pattern Map of Weisman (1979)

Weisman *et al.* (1979) conducted experimental studies to investigate the effects of fluid properties and pipe diameter on two phase flow patterns in horizontal pipes. Extensive data were obtained on the transitions between two phase flow patterns during co-current gas liquid flow in horizontal pipes. Fluid properties were varied in a systematic manner to determine the effects of liquid viscosity, liquid density, surface tension and gas density. Pipe diameters were varied from 1.2 to 5 cm for most of the tests. Visual observations were supplemented by an analysis of pressure drop fluctuations.

Weisman *et al.* (1979) used Froud number for the calculation of transitions between the observed flow patterns.

$$Fr_G = \frac{U_{Gs}^2}{(gd)} \tag{3.25}$$

The Reynolds number of gas,

$$\mathrm{Re}_G = \frac{\dot{m}_G d}{\eta_G} \tag{3.26}$$

The Kutdelaze number,

$$Ku = \frac{u_{Gs}\rho_G^{1/2}}{(g\Delta\rho\sigma)^{1/4}} \quad \text{, where } \Delta\rho = (\rho_L - \rho_G) \tag{3.27}$$

Function T_D defined by Taitel and Dukler (1976),

$$T_D = \left[\frac{\left(\frac{\Delta P}{L}\right)_{1L}}{(\rho_L - \rho_G)g} \right]^{1/2} \tag{3.28}$$

Weisman *et al.* (1979) calculated the flow pattern transitions shown in figure 3.12. using transition functions $u_{Gs} = f(u_{Ls}, Fr, Ku, \mathrm{Re}, T_D)$ for an air-water gas liquid flow in 20 °C, 1 bar ambient pressure and a pipe diameter of 2.54 cm.

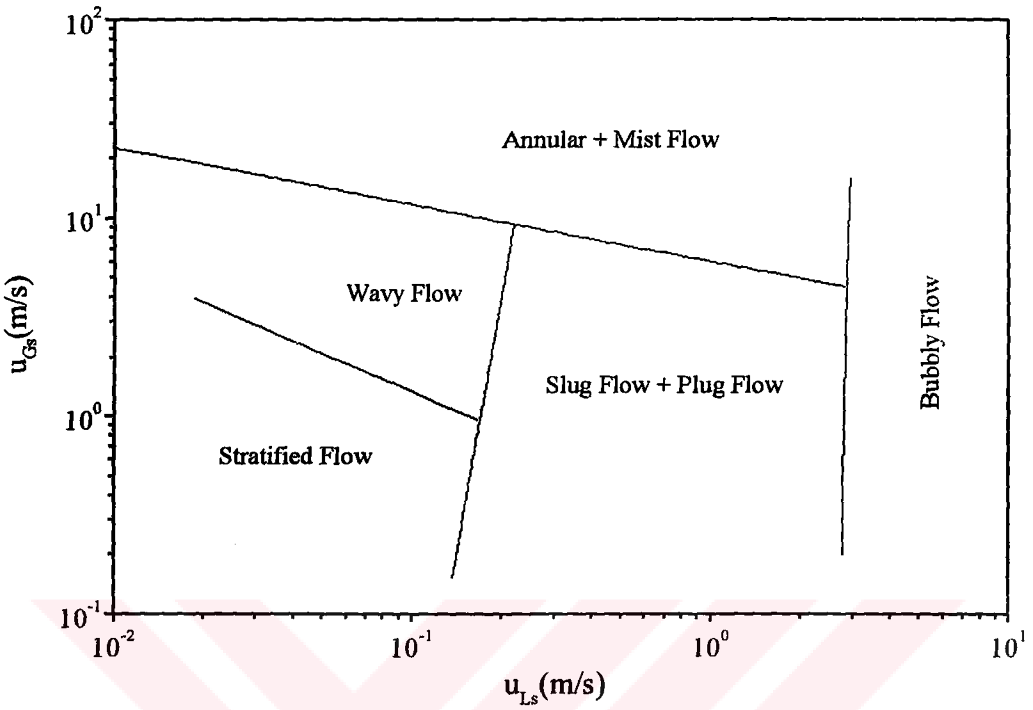

Figure 3.12. Flow Pattern Map of Weisman (1979) for horizontal pipes. Pipe diameter=25.4 mm, air/water flow, 1 atm.

The transition from wavy flow to slug or plug flow can be calculated with the help of equation (3.29),

$$u_{Gs} = \left(4\sqrt{Fr}\right)^{0.91} u_{Ls} \tag{3.29}$$

The transition to annular flow is described by the eq.(3.30),

$$u_{Gs} = 5.9 * 10^{-3}\left(Ku^{0.2} Fr\right)^{8} u_{Ls} \tag{3.30}$$

The borderline of bubbly flow is affected by the surface tension and pipe diameter. Hence, the function F_W is defined as below,

$$F_w = \frac{\sigma}{\Delta\rho d g^2} \tag{3.31}$$

The function given in eq.(3.31) includes the density difference of two phases, $\Delta\rho$, and acceleration of earth, g. Thus, the equation for the transition to bubbly flow can be written as follows;

$$T_D F_W^{1/4} = 1.7 \tag{3.32}$$

The onset of wavy flow is prescribed by the relation of shear and buoyancy forces. In this relation, the function, F_W, and the Reynolds number, Re_G, are included.

$$u_{Gs} = 2.3*10^{-6}\left(F_W^{0.2}\,\mathrm{Re}_G^{0.45}\right)^{6.25} u_{Ls} \tag{3.33}$$

The transition functions given in equations from (3.29) to (3.33) are valid for an air-water gas liquid flow in pipes with the inner diameter of 2.54 cm exclusively.

Weisman *et al.* (1979) carried out experiments for different gas liquid couples. They proposed two correction coefficients for the implementation of the equations given above. The correction coefficients, Φ_1, and Φ_2 ,which are given in tables (3.7), and (3.8) enable to calculate the dependencies of physical properties of new gas liquid couples to the pipe diameter of a new system.

Table 3.7. The correction coefficient Φ_1

Transition to	Φ_1
Wavy flow	$\left(\frac{d_S}{d}\right)^{0.17}\left(\frac{\eta_G}{\eta_{air}}\right)^{1.55}\left(\frac{\rho_{air}}{\rho_G}\right)^{1.55}\left(\frac{\Delta\rho}{\Delta\rho_S}\right)^{0.69}\left(\frac{\sigma_S}{\sigma}\right)^{0.69}$
Slug flow	1
Bubbly flow	1
Annular flow	$\left(\frac{\rho_{air}}{\rho_G}\right)^{0.23}\left(\frac{\Delta\rho}{\Delta\rho_S}\right)^{0.11}\left(\frac{\sigma}{\sigma_S}\right)^{0.11}\left(\frac{d}{d_S}\right)^{0.415}$

Table 3.8. The correction coefficient Φ_2

Transition to	Φ_2
Wavy flow	1
Slug flow	$\left(\frac{d}{d_S}\right)^{0.45}$
Bubbly flow	$\left(\frac{\rho_L}{\rho_{water}}\right)^{-0.33}\left(\frac{d}{d_S}\right)^{0.16}\left(\frac{\eta_{water}}{\eta_L}\right)^{0.09}\left(\frac{\sigma}{\sigma_S}\right)^{0.24}$
Annular flow	1

Standard conditions (index S) given by Weisman et al. (1979) for air and water:

$$d_S = 2.54\,cm \quad , \quad \rho_{air} = 1.3\,kg/m^3 \quad , \quad \rho_{water} = 1000\,kg/m^3 \qquad (3.34)$$
$$\eta_{water} = 1\,\text{Pa s} \quad , \quad \sigma_S = 0.07\,\text{N/m}$$

The correction coefficients, Φ_1, and Φ_2, for the air water gas liquid flow equal to 1. Any desired flow pattern map of any gas liquid couples can be calculated with the help of correction coefficients. The axis and ordinate of new flow pattern map become u_{Ls}/Φ_2 and u_{Gs}/Φ_1, respectively.

The transitions functions of Weisman's flow pattern map have been also derived in this study.

The indication of transitions functions separating the flow patterns on the Weisman's map are shown in table (3.9), as follows.

Table 3.9. Definition regions of the functions.

Function 1:	The line between stratified and wavy regions.
Function 2:	The line between stratified, wavy, and slug-plug regions.
Function 3:	The line between wavy, slug, and annular regions.
Function 4:	The line separating bubble region.

The general form of the equations derived for all of the transition lines is as below.

$$Y = [a.X]^n + b \qquad (3.35)$$

Here Y is the dependent variable and refers the u_{Ls}. The independent variable X means u_{Gs}. Thus, the equation (3.35) can be written as follows,

$$u_{Ls} = [a.u_{Gs}]^n + b \qquad (3.36)$$

The coefficients a, b and n were calculated for the four transition functions of Weisman's map (table 3.10).

Table 3.10. The coefficients of the Weisman's map.

	a	n	b
Function 1 (F_1):	3.322	-1.55	0
Function 2 (F_2):	$1.723.10^{-7}$	0.114	0
Function 3 (F_3):	0.1625	-3.502	0
Function 4 (F_4):	0	1	2.853

The flow pattern regions of Weisman's map are defined as shown in table (3.11) in this study (Appendix 2).

Table 3.11. The flow pattern regions of the Weisman's map.

Flow Pattern	
Bubbly Flow	$u_{Ls} \geq F_4$
Stratified Flow	$u_{Gs} < \left[\frac{1}{a}(u_{Ls} - b)^{1/n}\right]_{F_1} \wedge u_{Ls} < F_2$
Wavy Flow	$u_{Gs} < \left[\frac{1}{a}(u_{Ls} - b)^{1/n}\right]_{F_3} \wedge u_{Gs} \geq \left[\frac{1}{a}(u_{Ls} - b)^{1/n}\right]_{F_1} \wedge u_{Ls} < F_2$
Slug-Plug Flow	$u_{Gs} < \left[\frac{1}{a}(u_{Ls} - b)^{1/n}\right]_{F_3} \wedge u_{Ls} \geq F_2 \wedge u_{Ls} < F_4$
Annular-Mist Flow	$u_{Gs} \geq \left[\frac{1}{a}(u_{Ls} - b)^{1/n}\right]_{F_3} \wedge u_{Ls} < F_4$

Errors (Err(%)) between original and calculated values are given in tables (3.12), and (3.13). The definition of Err(%) is given in eq.(3.37).

$$Err(\%) = \frac{\left[u_{Ls} - (u_{Ls})_F\right]}{u_{Ls}} * 100 \tag{3.37}$$

Table 3.12. Errors between original and calculated values of functions 1 and 2.

Function 1				Function 2			
u_{Gs}	u_{Ls}	$(u_{Ls})_{F_1}$	$Err(\%)$	u_{Gs}	u_{Ls}	$(u_{Ls})_{F_1}$	$Err(\%)$
3.9378	0.01854	0.01859	-0.2489	0.15254	0.13684	0.13672	0.0853
0.9572	0.16677	0.16644	0.1952	0.95721	0.16878	0.16857	0.1265
				2.89548	0.19200	0.19124	0.3972
				9.35233	0.21840	0.21859	-0.0849

Table 3.13. Errors between original and calculated values of functions 3 and 4.

Function 3				Function 4			
u_{Gs}	u_{Ls}	$(u_{Ls})_{F_1}$	$Err(\%)$	u_{Gs}	u_{Ls}	$(u_{Ls})_{F_1}$	$Err(\%)$
22.765	0.01003	0.01003	0.0459	0.20158	2.7730	2.853	-2.885
18.021	0.02300	0.02273	1.1972	0.61227	2.7897	2.853	-2.270
13.143	0.06726	0.06864	-2.0554	1.71328	2.8233	2.853	-1.052
9.276	0.21840	0.23258	-6.4921	4.56402	2.8574	2.853	0.153
6.467	0.77823	0.82272	-5.7163	16.06700	2.9355	2.853	2.810
4.527	2.84029	2.86877	-1.0029				

3.2.1.3. Flow Pattern Map of Mandhane et al. (1974)

Mandhane et al. (1974) developed a flow pattern map with the help of some measurements taken from literature for horizontal gas liquid flows. They tested various flow pattern maps for two phase gas liquid flow against the approximately 6000 flow pattern observations, which were contained in a multiphase pipe flow data bank. The transitions between flow regimes were calculated for many different superficial velocities as a function of correction factors X_K and Y_K. The correction factors X_K and Y_K are defined in eqs. (3.38), and (3.39).

The calculation of the factors was accomplished using the density ρ_i and the viscosity η_i of each phases ($with\ \mathrm{i} = \mathrm{G,L}$) and the surface tension between phases. The physical properties of water and air at temperature of 20 °C and at pressure of 1 bar were implemented as reference values. Consequently, the authors proposed a modified flow pattern map which was simple to use and they reported that their map was overall in better agreement with almost six thousand data points than any of the existed maps. Figure 3.13. shows the flow patterns map proposed by Mandhane et al. (1974) for horizontal gas liquid flows.

$$X_K = \left(\frac{\rho_G}{\rho_{air}}\right)^{0.2} \left(\frac{\rho_L}{\rho_{water}} \frac{\sigma_{water-air}}{\sigma}\right)^{0.25} \left(\frac{\eta_G}{\eta_{air}}\right)^{0.2} \tag{3.38}$$

$$Y_K = \left(\frac{\eta_L}{\eta_{water}}\right)^{0.2} \left(\frac{\rho_L}{\rho_{water}} \frac{\sigma_{water-air}}{\sigma}\right)^{0.25} \tag{3.39}$$

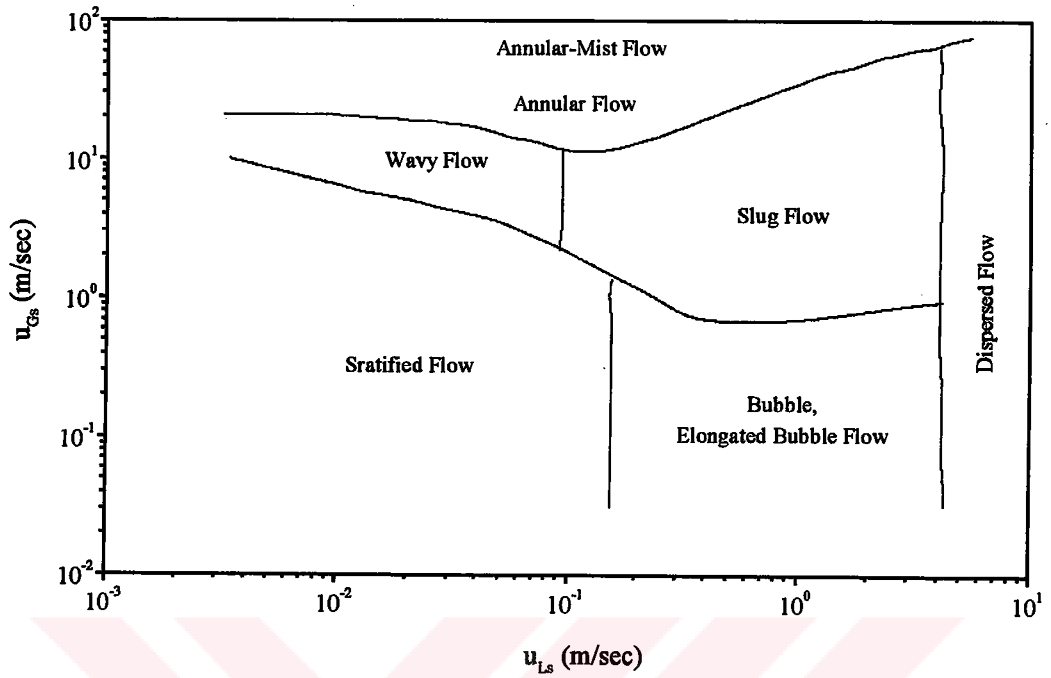

Figure 3.13. Flow pattern map proposed by Mandhane et al. (1974) for horizontal gas liquid flows.

Table 3.14. The usage of the physical property correction coefficients.

Transition region	u_{Ls} [m/s]	u_{Gs} [m/s]	Multiply the coordinates with
Stratified to elongated bubble	0.152 0.152	0.031 1.524	$1/Y_K$
Wavy to slug	0.091 0.091	2.286 12.192	Y_K
Elongated bubble and slug to dispersed flow	4.267 4.267	0.031 70.104	Y_K
Stratified and elongated bubble to wave and slug	0.003 0.031 0.061 0.351 1.453 4.267	10.668 4.267 3.200 0.762 0.762 0.991	X_K
Wave and slug to annular-mist	0.003 0.031 0.091 0.171 0.305 0.762 4.267	21.336 18.288 11.582 12.192 15.240 30.480 70.104	X_K
Dispersed bubble to annular-mist	4.267 9.144	70.104 81.991	X_K

Reference values of water and air were taken at temperature of 20 °C and at pressure of 1 bar. Mandhane et al. (1974) gave the coordinates of transition boundaries of proposed flow pattern map which have to be plotted on a log-log scale. Their table (3.14) included the usage of physical property correction defined in eqs. (3.38), and (3.39).

The transitions functions of flow pattern map of Mandhane are derived in this study. The transition functions separating the flow patterns on the Mandhane et al.'s map are explained in table (3.15).

Table 3.15. Definition regions of the functions.

Function 1:	The first section of line between stratified, wavy and slug regions ($10^{-3} \le u_{Ls} < 0.3539$).
Function 2:	The second section of function 1 between elongated bubble and slug regions ($0.3539 \le u_{Ls} < 4.1205$).
Function 3:	The first section of line between wavy, slug and annular-mist regions ($10^{-3} \le u_{Ls} < 0.1025$).
Function 4:	The second section of function 3 between slug and annular-mist regions ($0.1025 \le u_{Ls} < 0.4341$).
Function 5:	The third section of function 3 between slug, dispersed and annular-mist regions ($0.4341 \le u_{Ls} < 10$).

The general form of the equations fitted to all of the transition lines is the same.

$$Y = \left[\left(a_1 X^{n1}\right)^n + \left(a_2 X^{n2}\right)^n\right]^{1/n} \tag{3.40}$$

Here Y is the dependent variable and refers to u_{Gs}. The independent variable X means u_{Ls}. Thus, equation (3.40) can be written as follows,

$$u_{Gs} = \left[\left(a_1 u_{Ls}^{n1}\right)^n + \left(a_2 u_{Ls}^{n2}\right)^n\right]^{1/n} \tag{3.41}$$

The coefficients a_1, a_2, n_1, n_2, and n which are given in table (3.16), were calculated for the five transition functions of Mandhane's map.

Table 3.16. The coefficients of the Mandhane's map.

	a_1	n_1	a_2	n_2	n
Function 1 (F_1):	1.1074	-0.3911	0.2918	-0.87154	-9.5446
Function 2 (F_2):	0.2884	-0.8785	0.698	0.2206	3.7262
Function 3 (F_3):	22.8138	0.0162	3.1825	-0.5503	-4.0195
Function 4 (F_4):	3.3	-0.5359	37.4557	0.6867	3.5526
Function 5 (F_5):	37.9525	0.701	40.5216	0.3796	-8.9862

The flow pattern map of Mandhane et al. (1974) includes three approximately vertical lines and two curves. In this study, the curve between stratified, elongated bubble, wavy, and slug regions is named as Curve12. Curve12 has two parts which are Function 1 and Function 2.

The other curve which is between wavy, slug, dispersed, and annular-mist regions have been denoted as Curve345 because of the inclusion of Function 3, Function 4, and Function 5.

The flow pattern regions of Mandhane's map are defined as shown in table (3.17) in this study (Appendix 3).

Table 3.17. The flow pattern regions of the Mandhane's map.

Flow Pattern	
Dispersed Flow	$u_{Ls} \geq 4.1204 \wedge u_{Gs} < (u_{Gs})_{Curve345}$
Annular-Mist Flow	$u_{Gs} \geq (u_{Gs})_{Curve345}$
Slug Flow	$u_{Ls} < 4.1204 \wedge u_{Gs} < (u_{Gs})_{Curve345}$ $\wedge u_{Ls} \geq 0.09344 \wedge u_{Gs} \geq (u_{Gs})_{Curve12}$
Elongated Bubble Flow	$u_{Ls} < 4.1204 \wedge u_{Gs} < (u_{Gs})_{Curve12} \wedge u_{Ls} \geq 0.1533$
Wavy Flow	$u_{Ls} < 0.09344 \wedge u_{Gs} < (u_{Gs})_{Curve345} \wedge u_{Gs} \geq (u_{Gs})_{Curve12}$
Stratified Flow	$u_{Gs} < (u_{Gs})_{Curve12} \wedge u_{Ls} < 0.1533$

Errors (Err(%)) between the original and the calculated values are given in tables from (3.18) to (3.20). The definition of Err(%) is given in eq.(3.42).

$$Err(\%) = \frac{\left[u_{Gs} - (u_{Gs})_F\right]}{u_{Gs}} * 100 \tag{3.42}$$

Table 3.18. Errors between the original and calculated values of functions 1 and 2.

Function 1				Function 2			
u_{Ls}	u_{Gs}	$(u_{Gs})_F$	$Err(\%)$	u_{Ls}	u_{Gs}	$(u_{Gs})_F$	$Err(\%)$
4.1546	0.951	0.956	-0.524	0.3205	0.776	0.787	-1.391
3.0848	0.909	0.895	1.590	0.2799	0.870	0.885	-1.735
2.3427	0.848	0.842	0.630	0.2501	0.972	0.976	-0.454
1.7872	0.793	0.794	-0.111	0.2184	1.110	1.099	1.059
1.3211	0.742	0.745	-0.317	0.1907	1.240	1.236	0.379
1.0355	0.710	0.709	0.090	0.1536	1.454	1.491	-2.521
0.7864	0.694	0.679	2.226	0.1300	1.698	1.721	-1.343
0.6164	0.694	0.669	3.695	0.1076	1.983	2.021	-1.876
0.4831	0.694	0.689	0.819	0.0890	2.377	2.359	0.776
0.3873	0.710	0.747	-5.187	0.0753	2.656	2.679	-0.886
				0.0607	3.101	3.101	0.028
				0.0502	3.556	3.452	2.920
				0.0392	3.973	3.886	2.188
				0.0316	4.246	4.260	-0.324
				0.0261	4.538	4.600	-1.374
				0.0209	5.070	5.022	0.938
				0.0164	5.439	5.526	-1.598
				0.0125	5.813	6.152	-5.829
				0.0098	6.640	6.773	-2.011
				0.0077	7.255	7.447	-2.645
				0.0061	7.928	8.121	-2.436
				0.0051	8.505	8.754	-2.930
				0.0042	9.294	9.407	-1.220
				0.0034	10.155	10.286	-1.289

Table 3.19. Errors between the original and calculated values of functions 3 and 4.

Function 3				Function 4			
u_{Ls}	u_{Gs}	$(u_{Gs})_F$	$Err(\%)$	u_{Ls}	u_{Gs}	$(u_{Gs})_F$	$Err(\%)$
0.0032	20.798	20.757	0.196	0.1135	11.346	11.737	-3.448
0.0038	20.798	20.803	-0.027	0.1416	11.600	11.671	-0.606
0.0045	20.798	20.839	-0.199	0.1759	12.398	12.329	0.560
0.0052	20.798	20.862	-0.308	0.2069	13.598	13.261	2.475
0.0061	20.798	20.877	-0.382	0.2434	14.533	14.514	0.128
0.0070	20.798	20.877	-0.382	0.2876	16.237	16.094	0.882
0.0085	20.798	20.848	-0.242	0.3476	18.140	18.217	-0.423
0.0103	20.798	20.773	0.120	0.3980	19.896	19.948	-0.264
0.0118	20.342	20.679	-1.656				
0.0143	19.896	20.465	-2.862				
0.0169	19.896	20.194	-1.498				
0.0198	18.963	19.821	-4.525				
0.0247	18.963	19.111	-0.781				
0.0299	18.140	18.311	-0.939				
0.0361	17.743	17.340	2.269				
0.0425	16.601	16.408	1.159				
0.0489	15.533	15.546	-0.089				
0.0559	14.214	14.691	-3.354				
0.0658	13.903	13.658	1.762				
0.0774	13.008	12.640	2.834				
0.0914	11.860	11.633	1.918				

Table 3.20. Errors between the original and calculated values of function 5.

Function 5			
u_{Ls}	u_{Gs}	$(u_{Gs})_F$	$Err(\%)$
0.4702	22.228	22.211	0.076
0.5383	24.290	24.346	-0.231
0.6333	26.542	27.131	-2.221
0.7251	29.003	29.633	-2.172
0.8567	32.523	32.921	-1.223
0.9809	34.760	35.725	-2.777
1.1539	38.835	39.207	-0.956
1.3573	43.388	42.769	1.426
1.6478	45.355	47.085	-3.815
1.9916	50.859	51.359	-0.983
2.2802	55.576	54.466	1.997
2.6106	56.822	57.639	-1.439
3.0848	62.091	61.680	0.662
3.5318	63.483	65.085	-2.524
4.0436	66.361	68.628	-3.416
4.3857	70.925	70.827	0.138
5.0439	74.141	74.757	-0.831
5.6206	77.789	77.931	-0.183

Approximately vertical lines on the flow pattern map of Mandhane are accepted as vertical lines exactly. This means that the transitions from wavy flow to slug flow, from stratified flow to elongated bubble flow, and from slug flow or elongated bubble flow to dispersed flow occur in a constant superficial liquid velocity. This is impossible with regard to superficial gas velocity on a large scale. For example, the line of the transition to dispersed flow is valid for superficial gas velocities between 0.1 and 80. The exact transition lines of the original map proposed by Mandhane are defined as thick lines. The deviation from the mean value approaches to ±15 percent. In this study, the mean values of transitions on the Mandhane's map are calculated in errors with ±5 percent. The actual values of approximately vertical lines of the map are compared with their constant superficial liquid velocities. The first line is defined as Line 6, the second as Line 7, and the last one as Line 8. The notations 6, 7, and 8 come from the continuation of the Function 5. Line 6 separates the wavy flow and slug flow and the mean value of Mandhane's data is calculated as 0.09344. Line 7 lies between stratified and elongated bubble regions and its mean value is calculated as 0.1533. Finally, Line 8 is the transition to dispersed flow and its mean value is 4.1205.

Errors (Err(%)) between the original and the calculated mean values are given in tables (3.21) and (3.22). The definition of Err(%) is given in eq.(3.43).

$$Err(\%) = \frac{\left[u_{Ls} - (u_{Ls})_{constant}\right]}{u_{Ls}} * 100 \qquad (3.43)$$

Table 3.21. Errors between original and calculated values of lines 6 and 7.

Line 6			Line 7		
u_{Ls}	$(u_{Ls})_{const}$	$Err(\%)$	u_{Ls}	$(u_{Ls})_{const}$	$Err(\%)$
0.09144	0.09344	-2.187	0.15362	0.15333	0.189
0.09144	0.09344	-2.187	0.15362	0.15333	0.189
0.09394	0.09344	0.532	0.15362	0.15333	0.189
0.09394	0.09344	0.532	0.15362	0.15333	0.189
0.09394	0.09344	0.532	0.15362	0.15333	0.189
0.09394	0.09344	0.532	0.15362	0.15333	0.189
0.09394	0.09344	0.532	0.15362	0.15333	0.189
0.09394	0.09344	0.532	0.15362	0.15333	0.189
0.09394	0.09344	0.532	0.15362	0.15333	0.189
0.09394	0.09344	0.532	0.15362	0.15333	0.189
			0.15362	0.15333	0.189
			0.15362	0.15333	0.189
			0.1495	0.15333	-2.562
			0.15362	0.15333	0.189

Table 3.22. Errors between original and calculated values of lines 8.

Line 8		
u_{Ls}	$(u_{Ls})_{const}$	$Err(\%)$
4.26854	4.12045	3.469
4.26854	4.12045	3.469
4.15455	4.12045	0.821
4.15455	4.12045	0.821
4.15455	4.12045	0.821
4.15455	4.12045	0.821
4.04363	4.12045	-1.900
4.04363	4.12045	-1.900
4.04363	4.12045	-1.900
4.04363	4.12045	-1.900
4.15455	4.12045	0.821
4.15455	4.12045	0.821
4.15455	4.12045	0.821
3.93564	4.12045	-4.696
4.15455	4.12045	0.821
4.04363	4.12045	-1.900

3.3. The Cross Correlation Technique

Cross-correlation technique is a standard method of estimating the correlation of the fluctuations of any property in the flowing fluid between two points. When a probe is used to sense a local parameter such as slug velocity, void fraction or temperature, a time-varying, fluctuating curve results. The time-varying fluctuations of any property in two different points are needed to apply the cross-correlation technique. This technique involves a cross-correlation coefficient which is calculated using the fluctuations of two different points. A typical cross-correlation coefficient is defined below,

$$R(d)=\frac{\sum_{t=0}^{t=\infty}[(f1(t)-f1_m)*(f2(t+d)-f2_m)]}{\sqrt{\sum_{t=0}^{t=\infty}(f1(t)-f1_m)^2}*\sqrt{\sum_{t=0}^{t=\infty}(f2(t+d)-f2_m)^2}} \qquad (3.44)$$

In this study, the cross-correlation technique is used to calculate the slug velocities in the horizontal circular pipes with concentrically and eccentrically inserted rods, as well as in the horizontal and inclined circular pipes. Two different LEDs are installed on the outer surface of the transparent test pipe with a known distance. The distance between the LEDs is important to calculate the slug velocity. It should be sufficiently short to be able to measure the time difference without any disturbance, but also the distance between the LEDs should be sufficiently long to be able to measure a reasonable time difference which is in accurate measuring ranges of the analogue-digital inverter system. The schematic representation of the slug velocity calculation using the cross-correlation technique is shown in figure 3.15. The voltage outputs of the LED1 and LED2 shown in the figure were taken from a real experiment done in the Laboratory of Mechanical Engineering Department at Çukurova University.

The first step is the preparation of the input file for the cross correlation program. The mean voltage values of the LED1 and LED2 are calculated dividing the sum of the voltages to the measurement data number. The instantly measured voltages of both LEDs are divided to the own mean voltage values. This is expressed as follows;

$$f1(t)=\frac{[Volt(t)]_{LED1}}{[Volt_m]_{LED1}} \quad , \qquad f2(t)=\frac{[Volt(t)]_{LED2}}{[Volt_m]_{LED2}} \qquad (3.45)$$

The cross-correlation coefficients for different delays are calculated with the help of a computer program (Appendix 4). The delay value of the first maximum point of the cross-correlation coefficient is the time difference between the LED1 and LED2. Thus, the slug velocity can be expressed as follows.

$$V_{slug} = \frac{L_{LED1-LED2}}{t_d} \qquad (3.46)$$

Mean slug lengths are found using the mean slug velocity and residence times of slugs. The residence times of slugs can be obtained from the time-varying fluctuations of one of the LEDs. For example, the time-varying fluctuation of the LED1 is shown in figure 3.14.

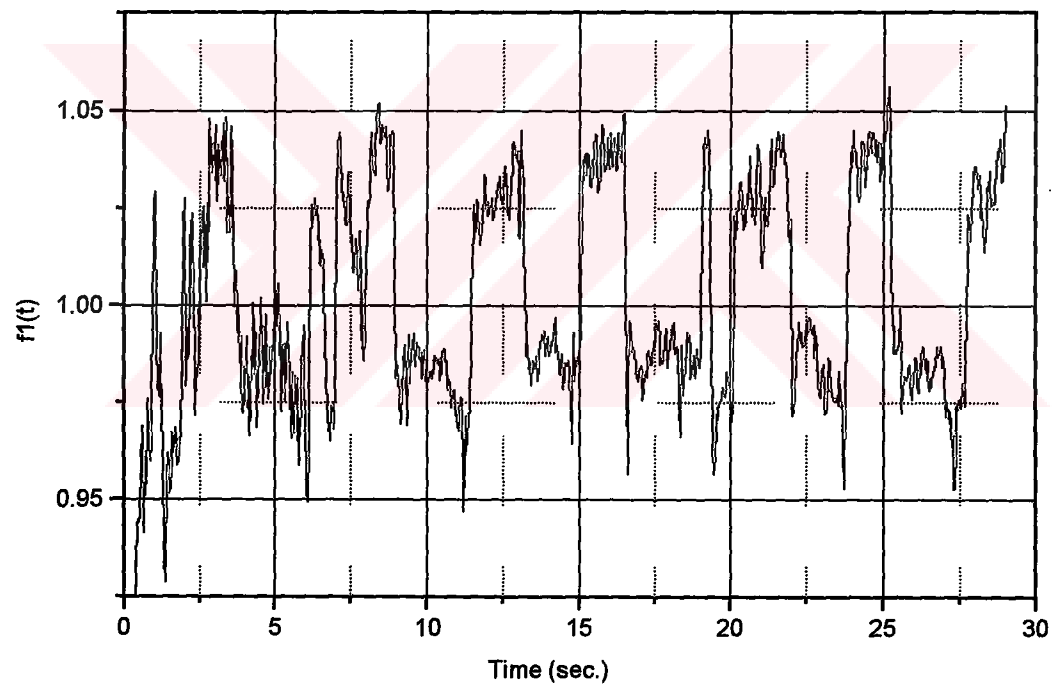

Figure 3.14. The time-varying fluctuation of the LED1.

The graph shown in figure 3.14. can be generally thought like figure 3.16. The low values of this trace is generated by the liquid bodies, namely slugs. Therefore, the residence time of any slug can be obtained from this variations. Mean slug length is calculated using the lengths of 4 or 5 slugs. If the residence times of all slugs are approximately close to each other, it can be expressed that the slug length is constant.

Slug frequency is obtained from the reverse of the time difference between the slugs. If the time difference between any two slugs is close to each other approximately, one can say that the slug frequency is constant.

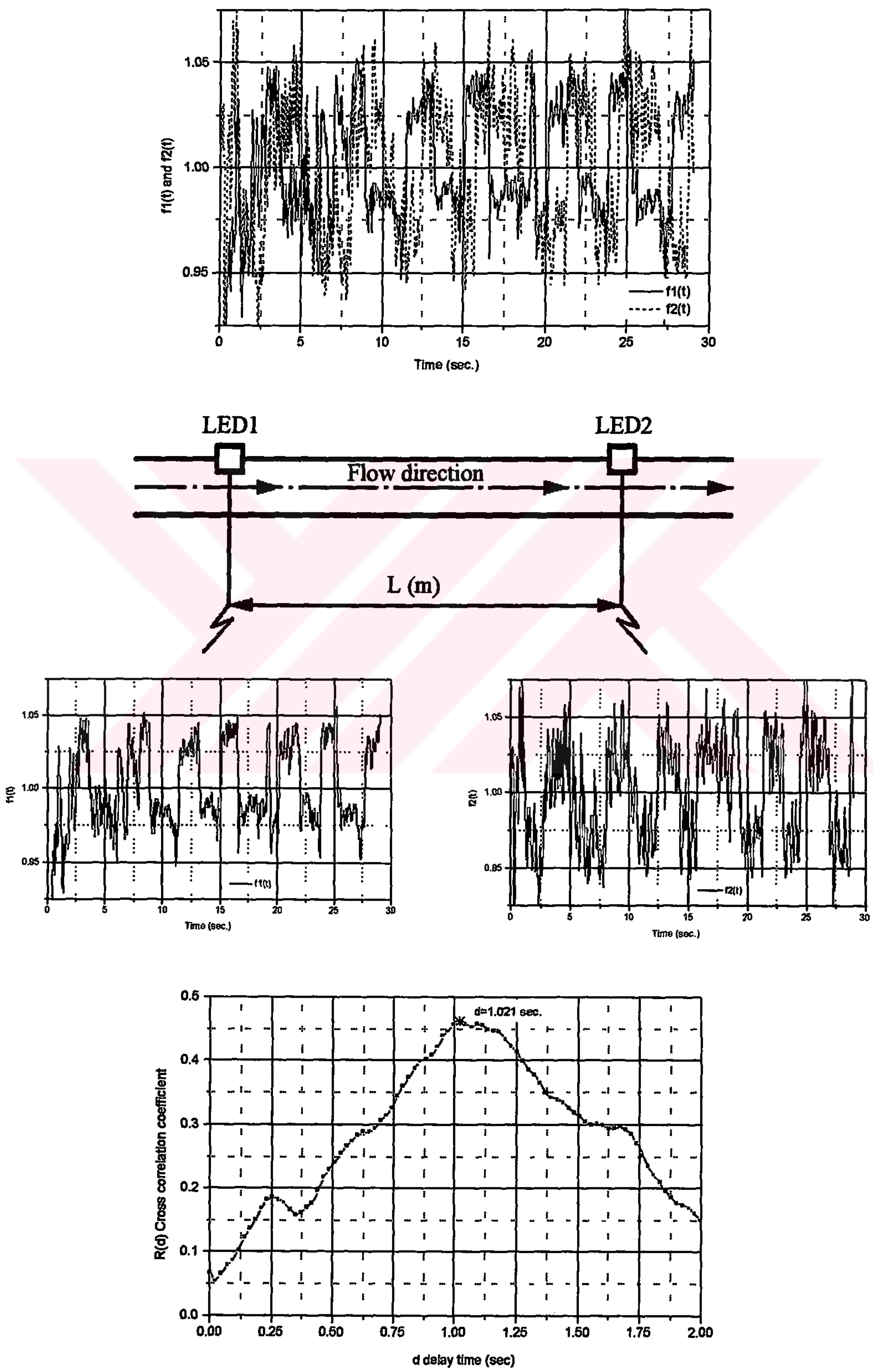

Figure 3.15. The schematic representation of the slug velocity calculation.

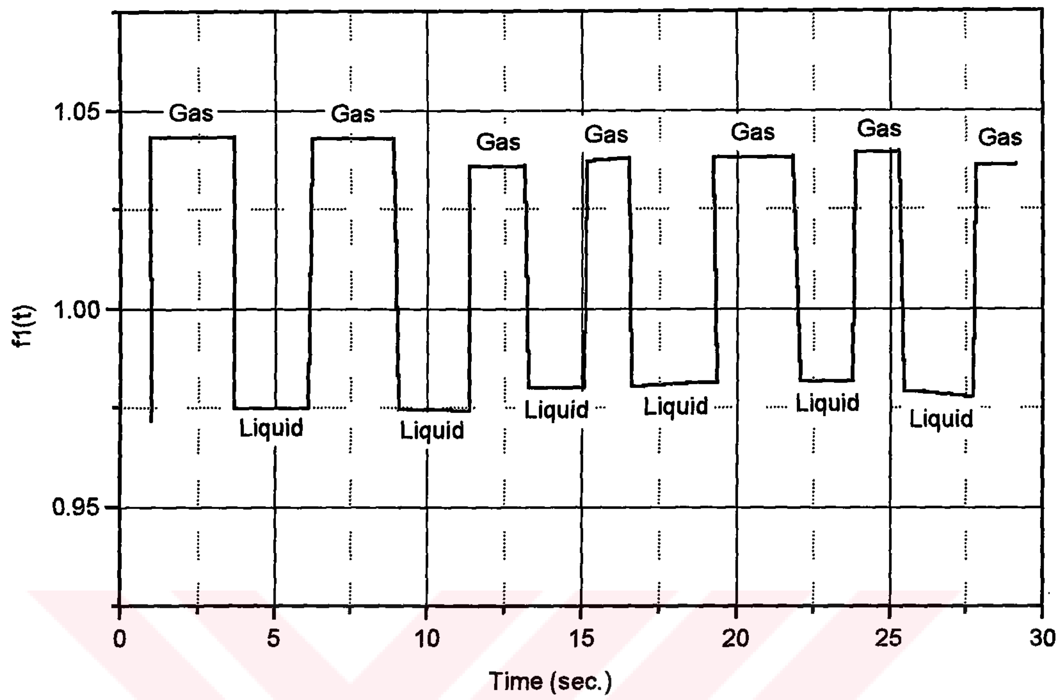

Figure 3.16. Obtaining of slug residence times from the fluctuation of the LED1.

The computer program which was written to calculate the delay between the time-varying fluctuations of the LEDs has been verified using two sine functions. While the values of the first sine function are calculated between 0 and 1440 degrees, the last sine function's values are determined between (0-d) and (1440-d) degrees. Here, **d** is the degree difference between two sine functions at the same point. Thus, when the first sine function take the any value of degree, the other sine function will take the same value of degree at **d** delay degree later. This delay degree between two sine functions can be thought as if delay time between any two time-varying fluctuations. The sine functions used to verify the cross-correlation computer program have been calculated between the degrees of 0 and 1440 but, the usage of the sine function and this interval of degree are of no importance. The same program can be run for any well known function such as a cosine function or for any interval of degree such as between 0 and 360, 0 and 720, or 0 and 946. The value of 1440 is four times greater than 360 and it is sufficiently enough to see what is going on for the very big numbers of data. A couple of sine function with 63 degree difference between them have been calculated and used as an input file for the cross-correlation computer program. These two sine functions have been shown in figure 3.17.

The variation of the cross-correlation coefficient with **d** delay degree is shown below. The first maximum point of the cross-correlation coefficient is at the value of 63

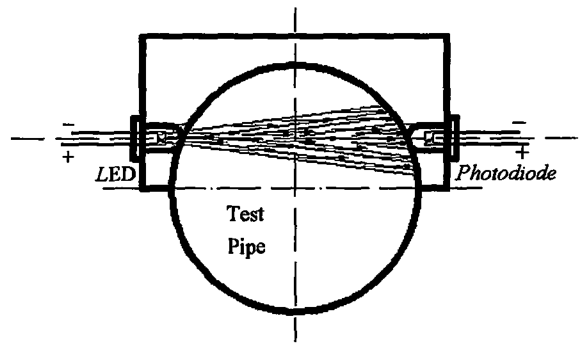

Figure 3.19. The placement of the LED-Photodiode pairs on the test section

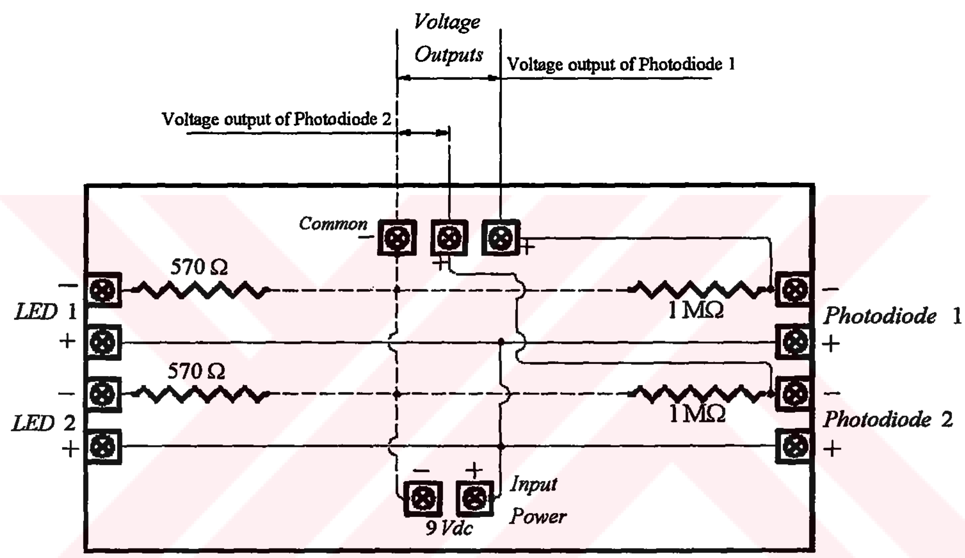

Figure 3.20. The electronic circuit of the LED-Photodiode pairs.

The LEDs connected to the circuit emit light towards the Photodiodes. The output voltages of the circuit, namely traces produced by slugs, are affected by the light sensed by the photodiodes. The intensity of light reached to the photodiode passing through the test section is affected by the refractive index of the ambient. The output voltage is maximum when the ambient is air and it is minimum when the ambient is water. The output voltages are inversely proportional to the distance between the LED-Photodiode pairs. If the top tips of the devices are oppositely touched to each other in darkness, the output voltage is approximately equal to the input voltage of the circuit.

During the experiments, the circuit shown in figure 3.20. was continuously powered with direct current of 9 V. The output voltages of the LED-Photodiode pairs were measured via an A/D converter and the measured voltages were saved on a hard disc.

3.5. Visual Prediction of Slug Length

Slug lengths are predicted visually besides the measurement of its traces with LEDs. The slowest slug seen at the beginning of the transparent test section reached to the end of the test section at most about four seconds approximately. That means, the slug length should be predicted in such a short period of time when the slug is in motion in the transparent pipe.

In this study, several slugs were observed visually and mean lengths of the slugs prevailed in an experiment were predicted. These predictions of the slug lengths were carried out in a distance of about 3 meters. The visual observations of two phase flow are important to evaluate the outputs of the LEDs and the pressure transducers. The visual observations are also useful for deciding the flow patterns in flow pattern maps.

The length predictions were performed using many materials with unknown lengths. The lengths of the materials used were predicted and written down on a paper without knowing the actual lengths. Afterwards, the real lengths of the materials have been measured. This process was repeated in three days. A calibration curve was obtained between the predicted lengths and the actual lengths. This curve is not a definite indicator of the predicted lengths in the experiments. This curve should be thought as the realization of the predictions.

The calibration equation of the predicted data are given below,

$$L_{act} = 0.128 + 0.827 * L_{pre} \tag{3.47}$$

The calibration curve for the predicted length is shown in figure 3.21.

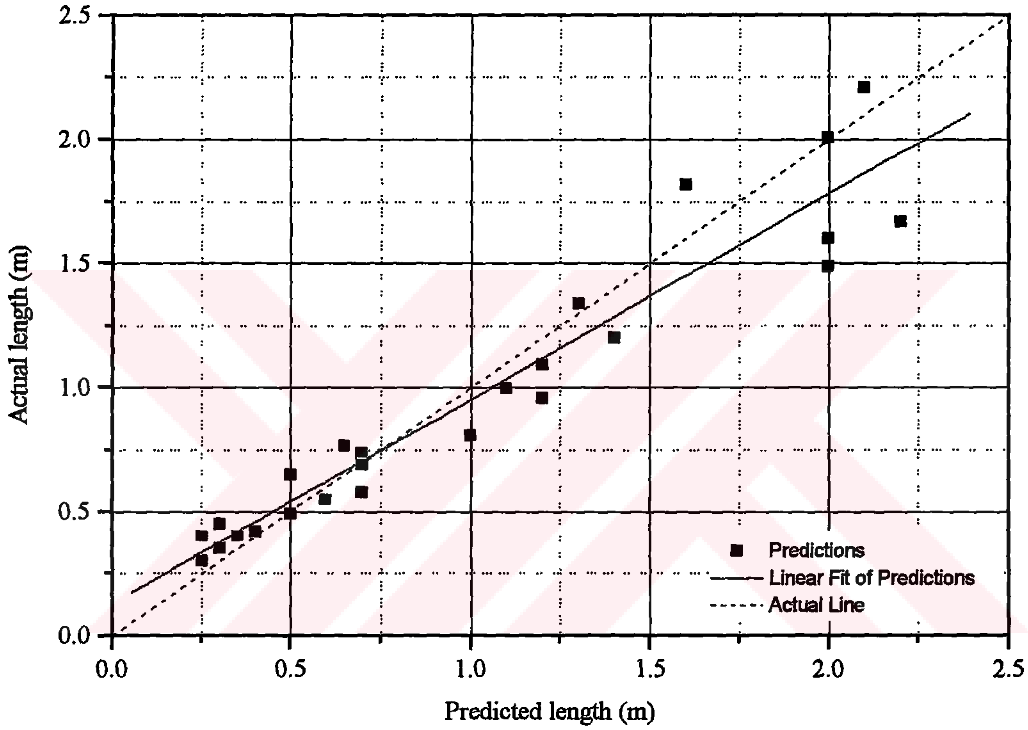

Figure 3.21. The calibration curve of length predictions

Figure 3.21. shows that, the lengths about 0.75 m are well predicted. As the lengths increased, they are over predicted. This curve is taken into consideration to interpret the slug lengths calculated using the cross-correlation technique.

4. EXPERIMENTAL SETUP

Two different experimental systems were used for the investigation of gas liquid flow in horizontal pipes. First studies were performed using a system which was built in a laboratory of Institute of Process Engineering at University of Hanover, Germany. Gas liquid flows in a horizontal and inclined circular pipe were investigated by means of the setup. Inclination of the test section from horizontal position was changed up to 15 degree with 5 degree steps upwardly. Air water gas liquid flows were investigated in this system (Experimental System 1) at four different positions which were horizontal, 5, 10, and 15 degree upwards.

Second system was constructed in the laboratory of Mechanical Engineering Department at University of Çukurova, Turkey. This experimental setup (Experimental System 2) was used to investigate the gas liquid flows in horizontal annular gaps. For the study of this geometry, a circular rod with 25 mm outer diameter was inserted in a transparent plexiglass pipe with 40 mm inner diameter. At the beginning, horizontal air water two phase flows were investigated with no insert. Afterwards, a circular rod with 25 mm outer diameter was inserted in the test section concentrically, and eccentrically. The differences between the flow patterns, pressure losses, void fractions and slug velocity-length-frequencies were investigated.

4.1. Experimental System 1

This experimental setup was previously used by another investigator (Vinage, 1996) to investigate the film thicknesses of annular flow in horizontal and inclined pipes. A transparent plexiglass pipe with 50 mm inner diameter was employed and film thicknesses of annular flow in horizontal and inclined pipes were measured using a conductance method.

For this investigation, a new transparent plexiglass pipe with 59 mm inner diameter was mounted on the system. The schematic view of the setup is shown in figure 4.1. The overall length of the test section was approximately 11.5 m. The steel bridge on which plexiglass pipe and all measurement equipment were mounted could be inclined up to 15 degree upwards. The main parts of the experimental system in which gas-liquid flows were investigated were air fan, orifice meter for the measurement of air flow rate, water pump, rotameters for water flow rate measurement, transparent test pipe, pressure transducers, sensor for void fraction measurement, and computer with an analogue digital converter for fast measurement of signals.

Air was supplied from a centrifugal fan which was driven by an electric motor. The revolution of the electric motor, namely of the air fan, could be changed with the help of an inverter. Thus, different air flow rates could be supplied to the test section. The air discharge valve was used for the regulation of air flow rate for a required value approximately. Air flow rate provided to the test section was measured using an orifice meter. The orifice plate used in the orifice meter was calibrated by the previous researcher. This calibration curve was tested against an air rotameter for small air flow rates and was agreed to use this curve. The pressure transducers measuring the pressure difference between inlet and outlet of the plate was calibrated with a precise transducer. The temperature of air sent to the test section was measured with a calibrated thermocouple.

Water was provided by a centrifugal water pump from a water reservoir whose volume was about 1 m^3. The volume flow rate of water was measured with two different rotameters. Flow rates between 0.6 and 6.3 m^3/h were measured with the help of a big rotameter, whose scale was 0.2 m^3/h. The water volume flow rates between 50 and 500 lt/h were measured using a small rotameter. The scale of this rotameter was 10 lt/h. Before starting an experiment, one of the rotameters was selected using a 3-way valve. The temperature of water was measured with a calibrated thermometer.

Air and water was met in the mixing section before entering the test pipe. Water entered to the transparent pipe parallel to the direction of two phase flow and air entrance was 45 degree inclined backwards on the upper side of mixer.

The gas and liquid mixture which actuated the pressure transducers, light emitting diodes, and the tomographic sensor flowed through the plexiglass test pipe. At end of the test section, the mixture was channelled to the water tank using a flexible hose. Finally, air and water were automatically separated with the opening of the end of the flexible hose to the atmosphere.

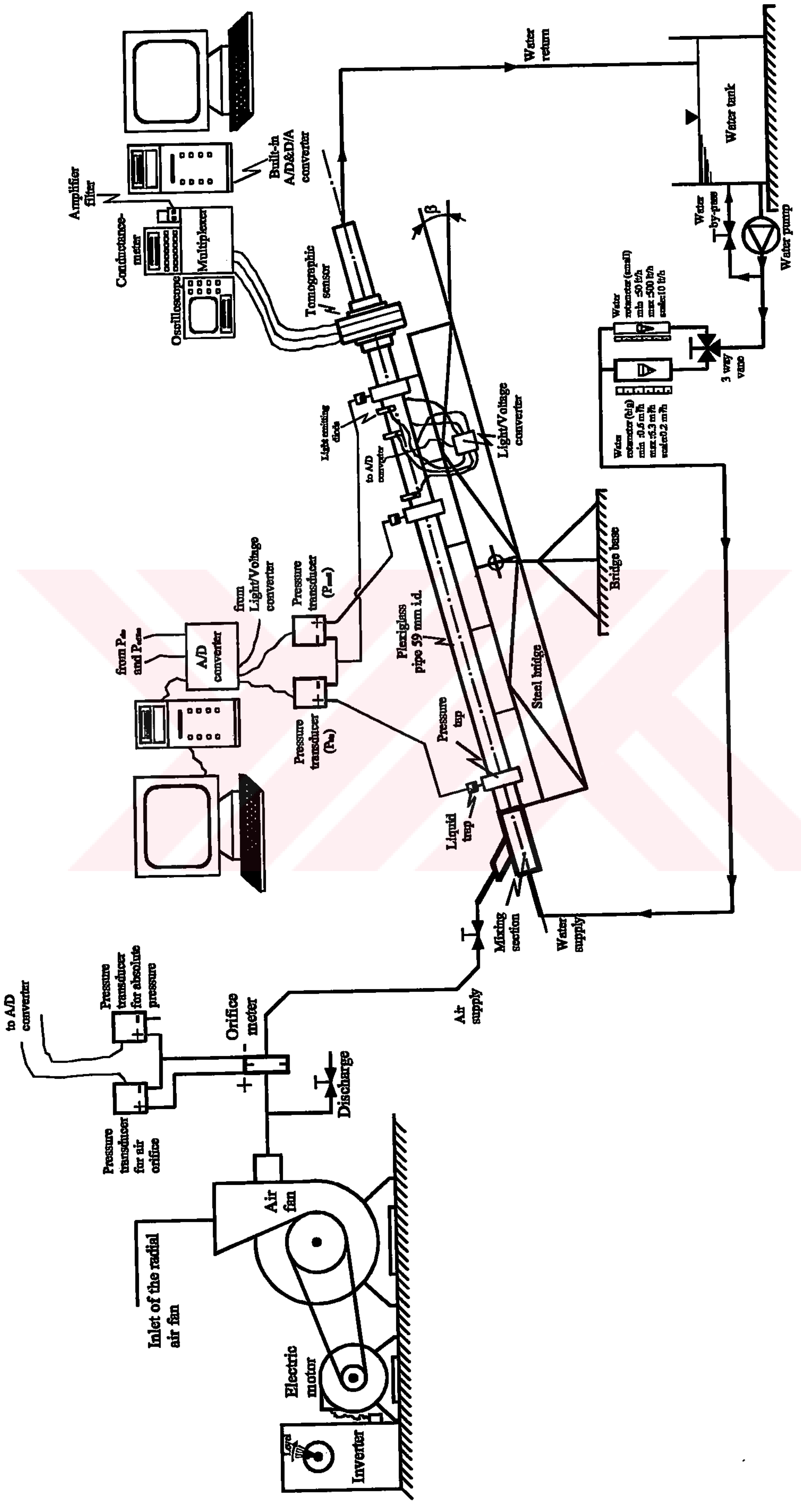

Figure 4.1. Experimental setup 1.

Pressure taps which sensed the integral static pressure overall the pipe periphery were used at three different points. First pressure tap was settled at 3285 mm distance from the connection point of mixer and transparent pipe. This was the positive end of the big pressure transducer. Second pressure tap was at 5040 mm distance from the first pressure tap. Second pressure tap was used as the positive end of the small pressure transducer. The last pressure tap was fixed at 2040 mm distance from the second tap. This pressure tap was the common negative end of the big and small pressure transducers. Thus, the measurement distance for the big pressure transducer was 7080 mm and for the small one was 2040 mm. Liquid traps were implemented on the pressure taps to prevent the liquid blockage in the plastic pressure tubes.

Between the second and the last pressure taps, three light emitting diodes were placed on the outer surface of the plexiglass pipe. Each couple of light emitting diodes included a red light emitter and a diode which were faced one another. Light emitters radiated a constant red light and diodes sensed the changing of the intensity of the light. The different light perceptions of diodes were converted to voltage by means of a light/voltage converter circuit (Section 3.4). The outputs were saved on a computer hard disc via an analogue-digital converter.

The light absorbed by a diode is affected from the flow patterns of gas liquid flows, because of the different refractive indices of air and water. For example, when a liquid slug moves between emitter-diode pair, the intensity of red light passed through the liquid body decreases and diode absorbs less light. After leaving of the liquid body, for instance, a smooth stratified layer let move below the ray of red light. Thus, the intensity of red light increases to its maximum value because of the less refractive index of air. In an experimental condition, these circuits allow to determine the velocity and frequency of slug and plug flow.

A new tomographic sensor which was developed by investigators of Institute of Process Engineering at University of Hanover was used to measure the void fraction. This new sensor for the conductive tomography is depicted in figure 4.2. schematically. Sets of parallel wires are strung across the cross-sectional area of the pipe in three close parallel planes. The planes are set 3 mm apart. In every plane, a total of 29 wires with a diameter of 100 μm are arranged. With a distance between parallel wires of 2 mm, a total free cross sectional area through the sensor of 95% is achieved.

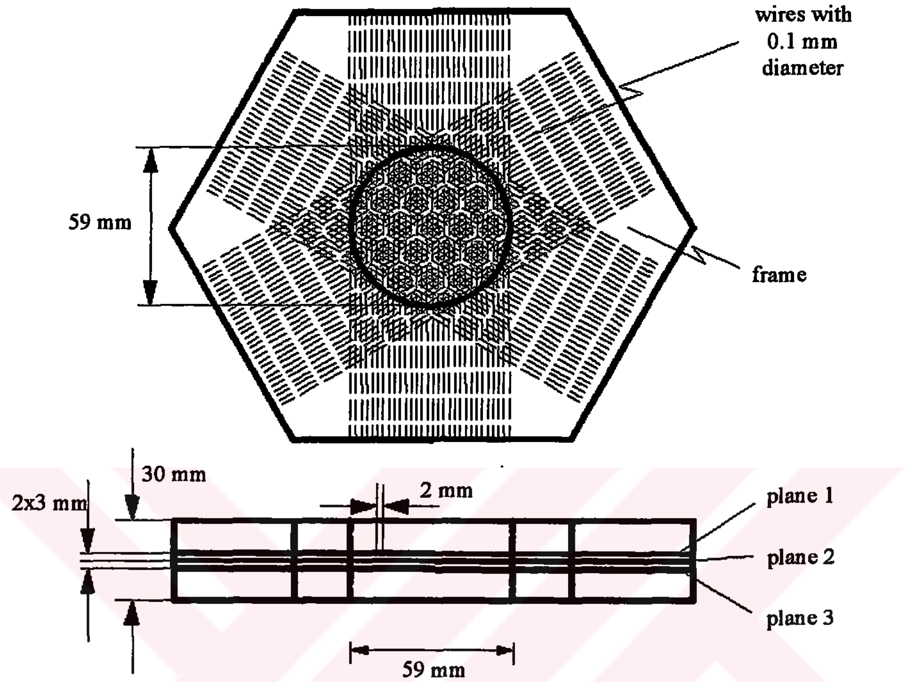

Figure 4.2. New wire-mesh sensor.

In figure 4.3., a schematic representation of the measurement chain for the new conductance tomography with the wire-mesh sensor is shown.

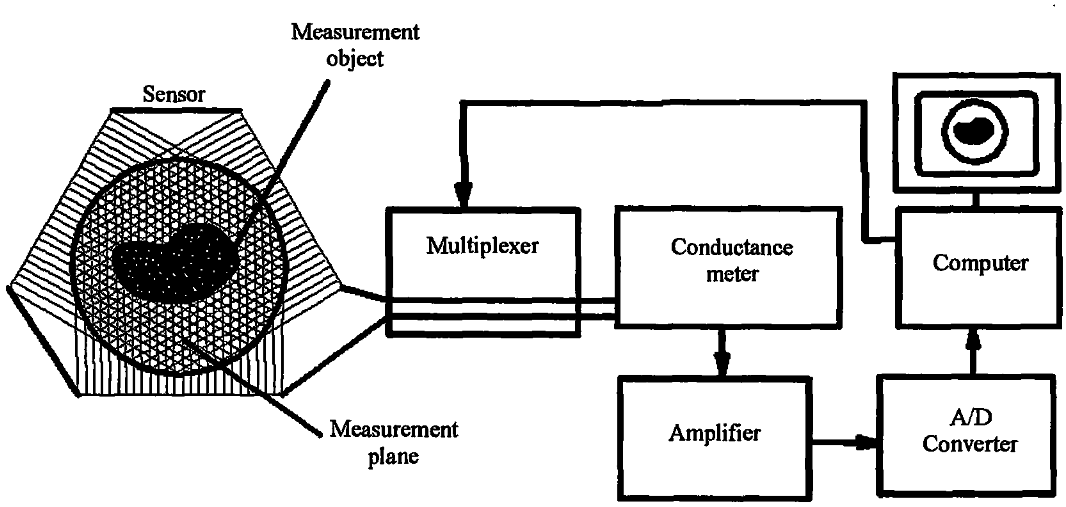

Figure 4.3. A schematic representation of the measurement chain for the new conductance tomography with the wire-mesh sensor.

4.1.1. Air Supply System

The air supply system consist of the air fan, electric motor, inverter, orifice meter, pressure transducers measuring the pressure difference of orifice meter, thermocouple for the measurement of air temperature and two different valves.

The air fan was constructed by Anton Piller KG in 1960. The air volume delivered by the fan is 45 m^3/min in 3200 rev/min. It can overcome the static pressure of 3000 mmWC. Air fan is driven with belts by an electric motor. Inverter circuit enables to change the revolution of electric motor changing the inlet voltage of the electric motor. The air volume is mainly adjusted by means of the level of the inverter. The air volume required between any two levels or below the first level is regulated by the air discharge valve.

The air flow rate provided to the test section was measured by means of an orifice meter which included three parts. Figure 4.4. shows the main parts of the air supply system. A norm orifice plate was mounted in the orifice meter. The technical information about the orifice plate has been given in table (4.1).

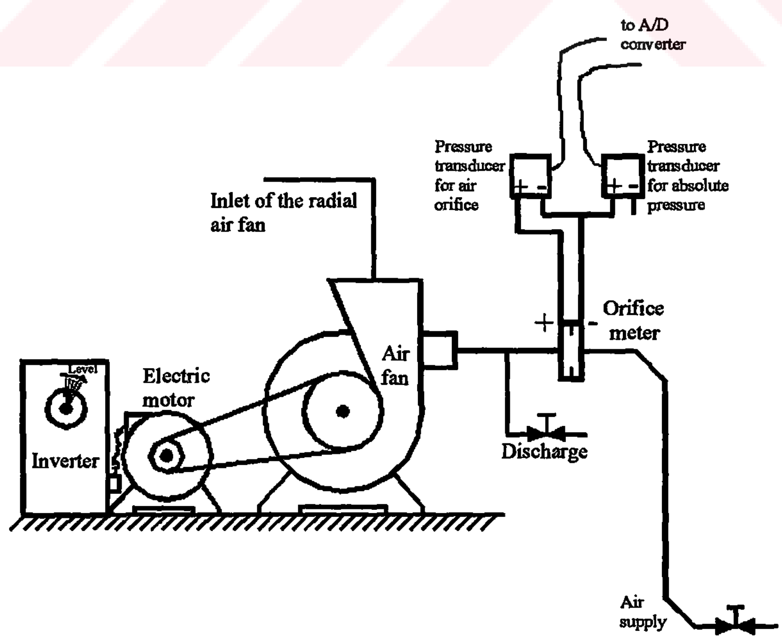

Figure 4.4. Main parts of the air supply system.

Table 4.1. Technical information of the orifice plate used.

Maximum volume flow rate	450 m^3/h
Operating pressure	1.2 bar absolute
Operating temperature	20 °C
Δp	10 mbar

This orifice meter was calibrated by Vinage (1996) who was the previous investigator used this system. The proposed calibration curve was:

$$V = \sqrt{0.9466.10^{-4} + 0.23641.10^{-4}\left\{\frac{\Delta p}{\rho_{air}}\right\}} \tag{4.1}$$

Pressure difference between inlet and outlet of the orifice plate, Δp, was measured by means of a pressure transducer (Type:G1151 DP3E12) produced by the Rosemount. The Rosemount pressure transducer was calibrated with a reference manometer and its calibration equation is given in eq.(4.2). The calibration curve of this pressure transducer is shown in figure 4.5.

$$\Delta p = 999.43601.[V_{rm} - 2.006] \tag{4.2}$$

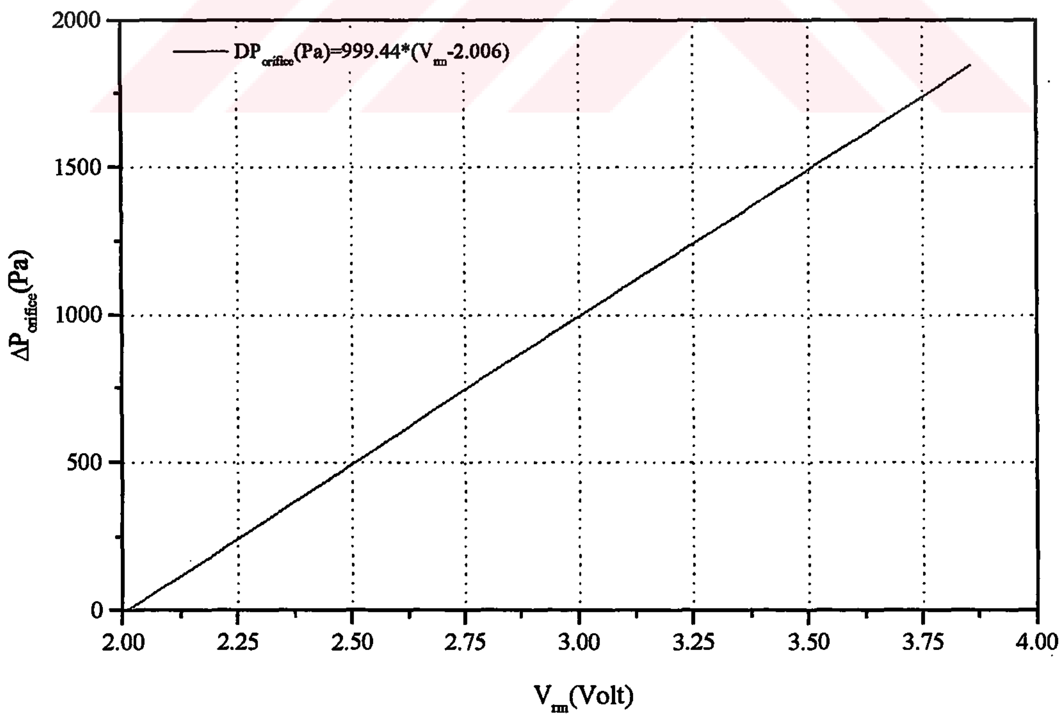

Figure 4.5. The calibration curve of the Rosemount pressure transducer.

Density of air in operating pressure and temperature, ρ_{air}, was calculated using equation (4.3).

$$\rho_{air} = \rho_{norm}\left(\frac{p_{abs}}{p_{norm}}\right)\left(\frac{T_{norm}}{T_{air}}\right) \tag{4.3}$$

Norm values of air were accepted at ambient pressure of 1 atm and at ambient temperature of 20 °C. In equation (4.3), ρ_{norm}, p and T are in dimension of kg/m^3, bar, and Kelvin, respectively. Thus, the density of air was calculated using equation (4.4):

$$\rho_{air} = 1.1881\left(\frac{p_{abs}}{1.013}\right)\left(\frac{293.15}{(273.15 + T_{orifice})}\right) \tag{4.4}$$

$T_{orifice}$ is the temperature of air sent to the test section in dimension of °C. It was measured with the help of a thermocouple system. Measuring junction of the thermocouple was inserted to the air supply pipe downward of the orifice meter as isolated from the ambient. Reference junction of the thermocouple was plunged into a pot which was full of smashed melting ice. A voltage difference depended on the temperature difference between air and smashed ice was measured in the thermocouple circuit which measured the temperature of air. The thermocouple used was calibrated using a reference thermometer as both of them were subjected to a water bath whose temperature was varied systematically. As the temperature of the water bath was changed, the voltage output of the circuit and the temperature of the reference thermometer were read. The calibration data, equation, and curve of the thermocouple are given below.

Table 4.2. The calibration data of the thermocouple.

Thermocouple output V_{tc} (Volt)	Reference Thermometer (°C)
-0.191	0.6
1.577	24.2
2.09	31
2.49	36
2.66	38.2
2.91	41.6
3.86	53.4
4.31	59.1
4.86	66

$$T_{orifice} = 3.66 + 12.9.V_{tc} \quad (4.5)$$

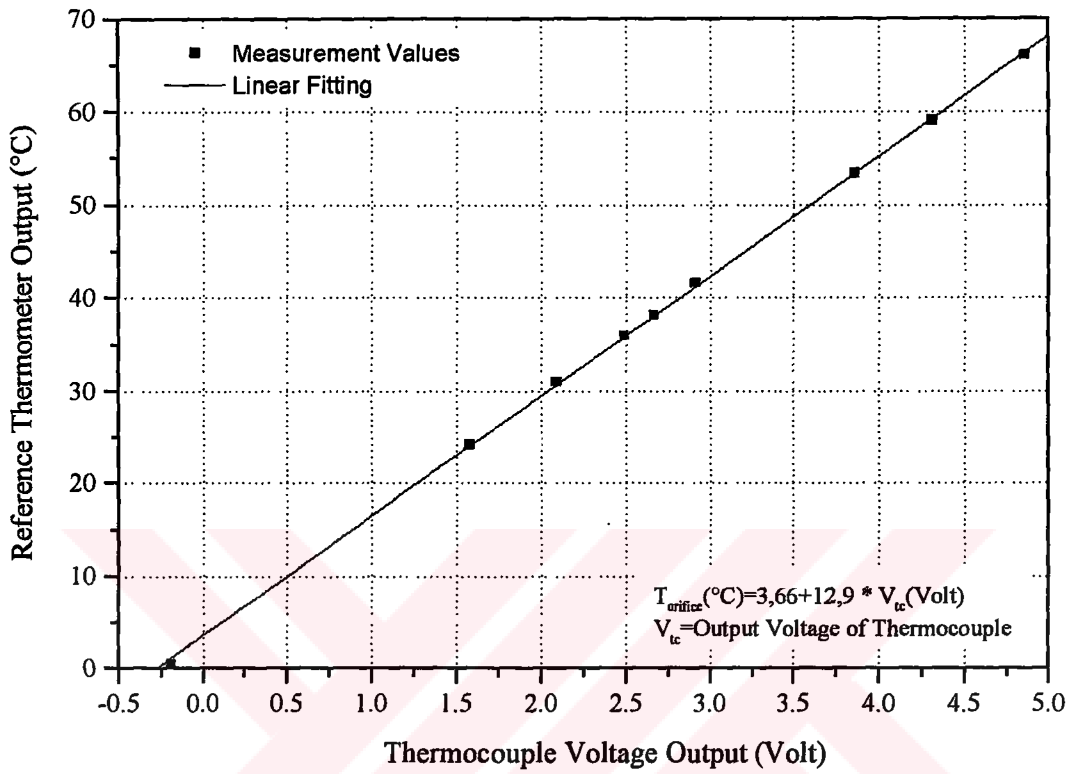

Figure 4.6. Calibration curve of air thermocouple system.

The pressure transducer measured the pressure difference between the down flow of the orifice plate and ambient was calibrated and the calibration equation is:

$$\Delta p_{d-a} = 0.42324.V_{d-a} \quad (4.6)$$

The ambient pressure was read from a mercury barometer. The absolute pressure was calculated by means of values read from the mercury barometer and calculated from equation (4.6). The top end of the mercury column in the barometer was in form of a spherical cap. The height of the barometer (mercury column) was read from two different points which were the base and the top of this spherical cap. The absolute pressure can be calculated using the heights of mercury column and the pressure difference between outlet of the orifice plate and ambient as shown in equation (4.7).

$$p_{abs} = \left\{ \frac{H_{base} + H_{top}}{2} \right\}.\rho_{mercury}.g.10^{-5} + \Delta p_{d-a} \quad (4.7)$$

4.1.2. Water Supply System

The water supply system included a water tank of 1 m^3, a centrifugal pump, a water by-pass line from the discharge of the pump to the water tank, a 3-way valve, two different scaled water rotameters, and a water supply line up to the mixer. The schematic view of the water supply system can be seen in figure 4.7.

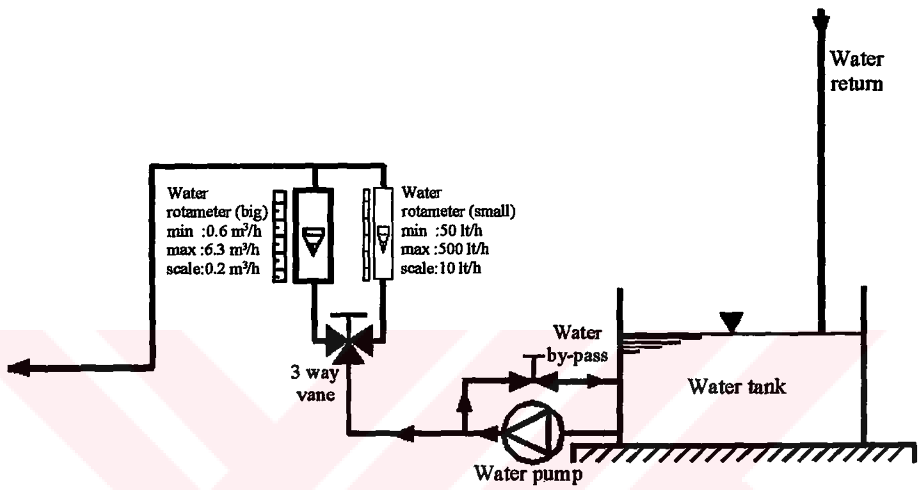

Figure 4.7. The schematic view of the water supply system

The temperature of water in the water reservoir was measured using a thermometer. This thermometer was calibrated with the reference thermometer used for calibration of the thermocouple used for the measurement of the air temperature. The calibration data is given in table (4.3).

Table 4.3. The calibration data of the water thermometer.

Water thermometer (°C)	Reference thermometer (°C)
-1	0.8
8.7	12.7
11.3	12.9
32.8	34
48.4	50.1
66.4	67.5
67.7	70

The calibration equation of the water thermometer is as follows.

$$T_{water} = 1.7 + T_{wtherm} \quad (4.8)$$

The calibration curve of the water thermometer is shown in figure 4.8.

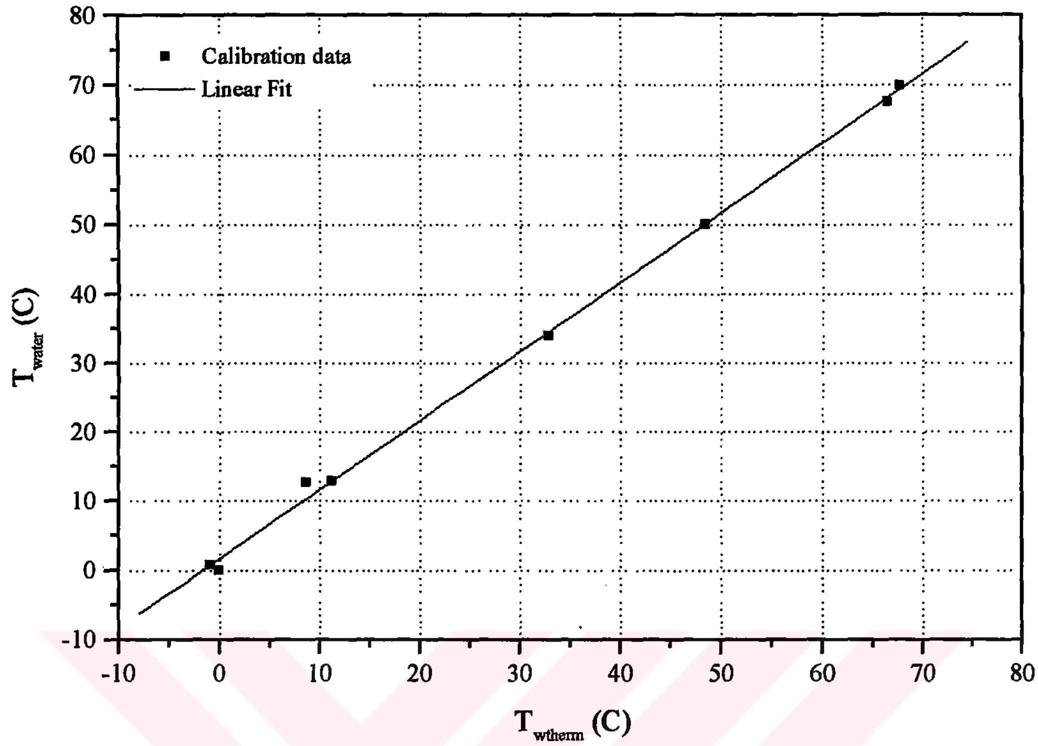

Figure 4.8. The calibration curve of the water thermometer

The water temperature which was used to calculate the density of water circulated in the test system was between 20 °C and 35 °C for all of the experiments carried out using this experimental setup. The density of water was given in table (4.4) between temperatures of 4.4 °C and 48.8 °C.

Table 4.4. The density of water.

Water temperature (°C)	Water density (kg/m^3)
4.4	999.8
10	999.2
15.5	998.6
21.1	997.4
26.6	995.8
32.2	994.9
37.7	993.0
43.3	990.6
48.8	988.8

A polynomial curve was fitted to the data given in table (4.4). The calculation of water density is easier using equation (4.9) in a data sheet or in a computer program.

$$\rho_{water} = 1000.097 - 0.0473 . T_{water} - 0.00382 . T_{water}^2 \qquad (4.9)$$

Figure 4.9. shows the graphical presentation of eq. (4.9).

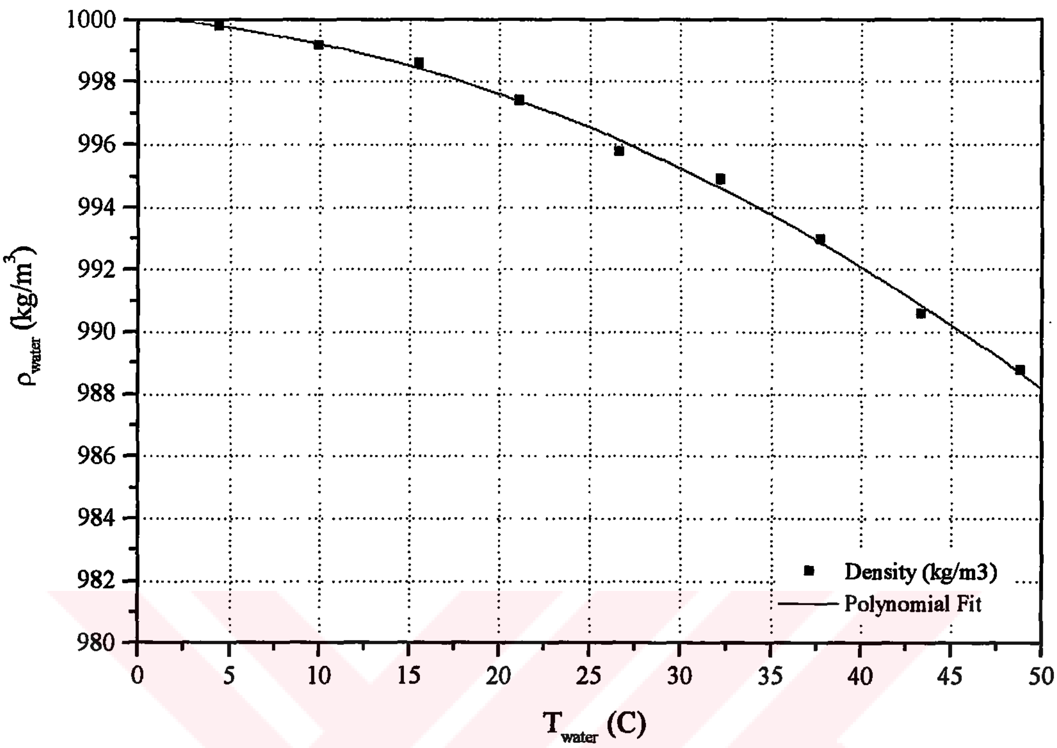

Figure 4.9. Graphical presentation of eq (4.9).

The water volume flow rates were measured with two different rotameters. Flow rates between 0.6 and 6.3 m^3/h were measured by means of the big rotameter, whose scale was 0.2 m^3/h. Figure 4.10. shows the water rotameters schematically. The water volume flow rates between 50 and 500 lt/h were measured using the small rotameter. This rotameter was capable of measuring very low water volume flow rates sensitively. The scale of the small rotameter was 10 lt/h. The selection of any rotameter was carried out by means of a 3-way valve.

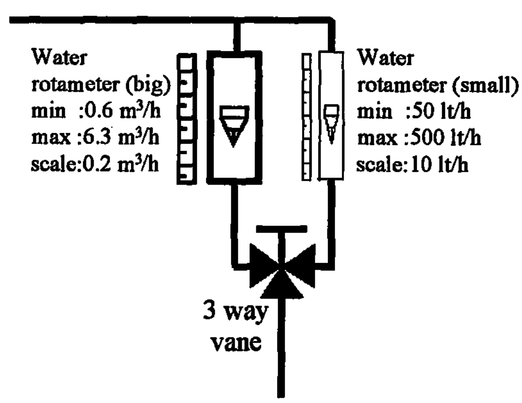

Figure 4.10. Water rotameters and 3-way valve.

4.1.3. Pressure Measurement System

Pressure differences in the experiments were measured by means of two pressure transducers having different pressure ranges. Both of the pressure transducers (DIGIMA clic pressure transducer) were manufactured by the Special Instruments. The signal outputs of the pressure transducers were between 0 and 10 Volts. The pressure difference ranges of the big and small pressure transducers were 100 mbar/D and 50 mbar/D, respectively. Both of the pressure transducers were calibrated with a reference pressure transducer.

The test section was used to calibrate the pressure transducers. The positive and negative ends of the reference transducer and of the pressure transducer which was in calibration were connected to the same pressure taps. The positive sides of transducers were attached to the pressure tap on the upflow. The negative ends were fastened to the pressure tap on the downflow. Thus, the two pressure transducers were adjusted to measure the same pressure difference. As the air volume was changed with the help of the inverter, the output voltages of the transducers were saved on a hard disc via an analogue digital converter, simultaneously. Approximately 60000 data were saved on the hard disc for each calibration process in a short period of time.

The output voltages of the calibrated pressure transducers were related to the output voltage of the reference pressure transducer using the data collected.

The final calibration equation of the big pressure transducer is given in eq. (4.10).

$$\Delta p_{PTbig} = 1480.8293 \, . V_{PTbig} \tag{4.10}$$

The calibration curve of the big pressure transducer is shown in figure 4.11.

The final calibration equation of the small pressure transducer is given in eq. (4.11).

$$\Delta p_{PTsmall} = 481.0433 \, . V_{PTsmall} \tag{4.11}$$

The last calibration curve of the small pressure transducer is shown in figure 4.12.

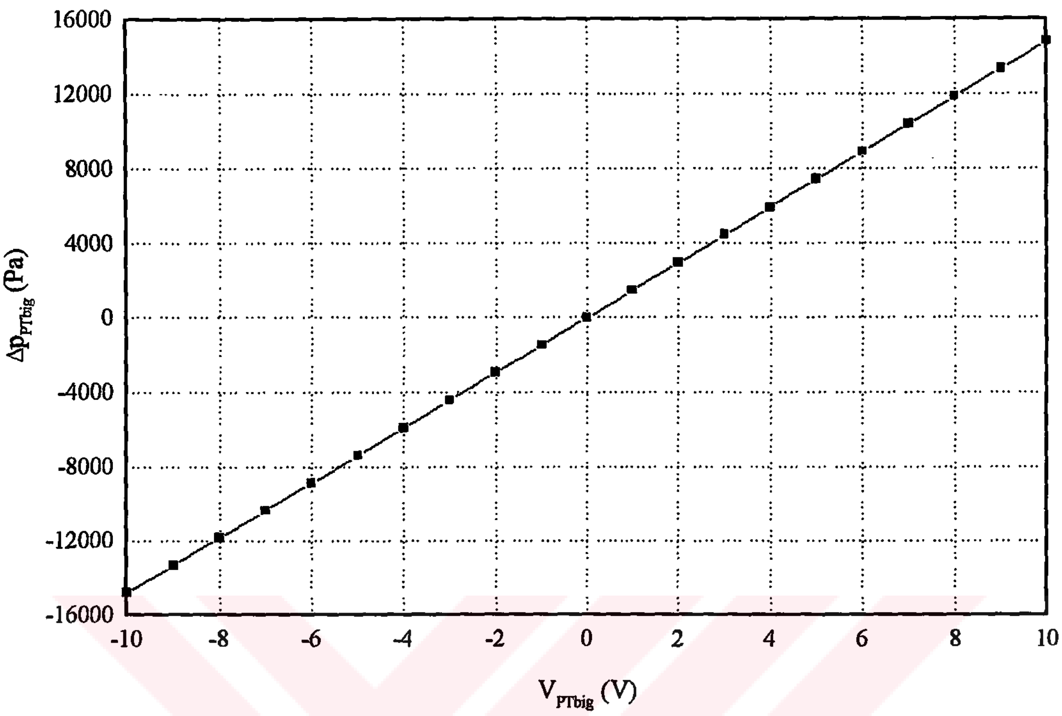

Figure 4.11. The calibration curve of the big pressure transducer

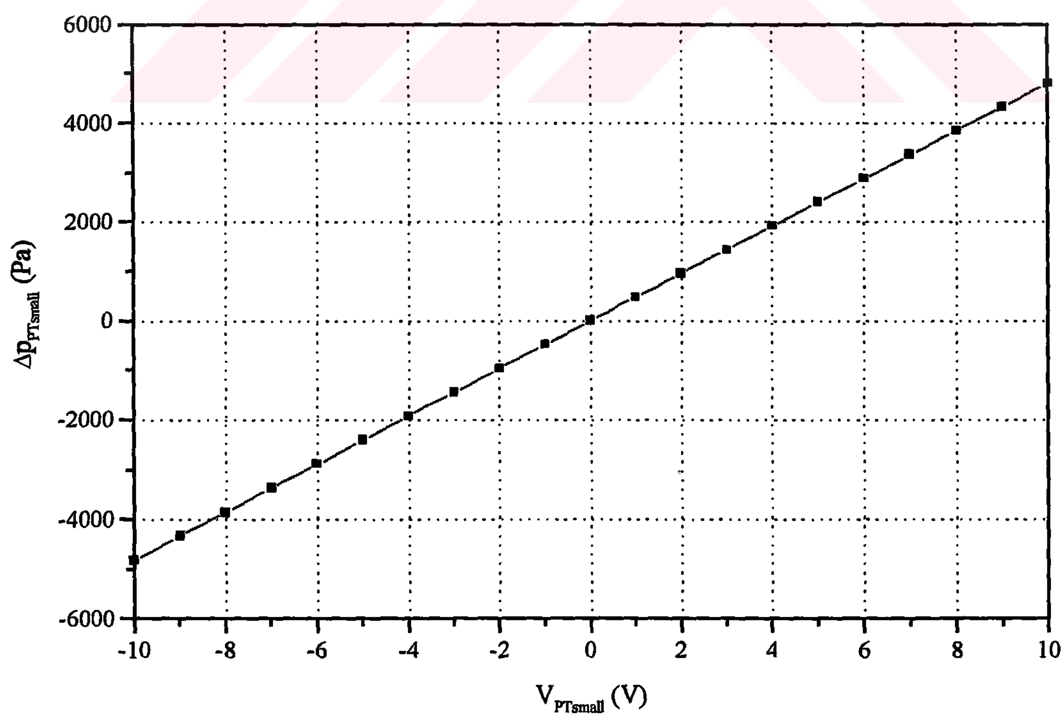

Figure 4.12. The calibration curve of the small pressure transducer

4.2. Experimental System 2

The main components of the experimental setup were constructed by BÜYÜKAKÇALI (1999) in the Laboratory of Mechanical Engineering Department at University of Çukurova, Turkey. This experimental setup was previously used to investigate the pressure losses of gas liquid flows in an horizontal tube with various inserts. Some modifications and improvements were done on the system. The last state of the whole experimental system is shown in figure 4.13.

BÜYÜKAKÇALI (1999) measured the pressure loss and observed the flow patterns visually. He did not measure the void fraction, slug velocity, slug length, and slug frequency. He had difficulty keeping the water and air flow rates constant during his experiments. Water sent to the storage tank were manually adjusted with the help of a control valve which is on the by-pass line of the water pump. This manual regulation caused the lack of water or flooding of water in the storage tank during some experiments. For the experiments of this thesis, a flooding line from the overflow end of the storage tank to the inlet tank of the water pump was added to prevent the level variations in the storage tank. The control valve of the by-pass line of the water pump was adjusted as fully closed, so that maximum water flow rate was pumped to the storage tank. This maximum water flow rate of the water pump is always greater than the maximum water flow rate used in the experiments. This means, there is always some flooding water coming from the storage tank to the inlet tank of the water pump. Therefore, the water flow rate has been kept constant in the experiments carried out within content of this study.

BÜYÜKAKÇALI (1999) measured the air and water flow rates using venturimeters. For the experiments of this thesis, two different rotameters have been installed on the experimental system to measure the air and water flow rates. Upstream of the inlet of the air flow rate rotameter, a pressure regulator has been added, so that the pressure of air sent to the test section could be adjusted and measured precisely. This is important for keeping air flow rate constant and for the calibration of the air flow rate rotameter. Because, the air flow rate rotameter was scaled with respect to the standard conditions labelled on the device, it is necessary to convert the reading value to the actual value.

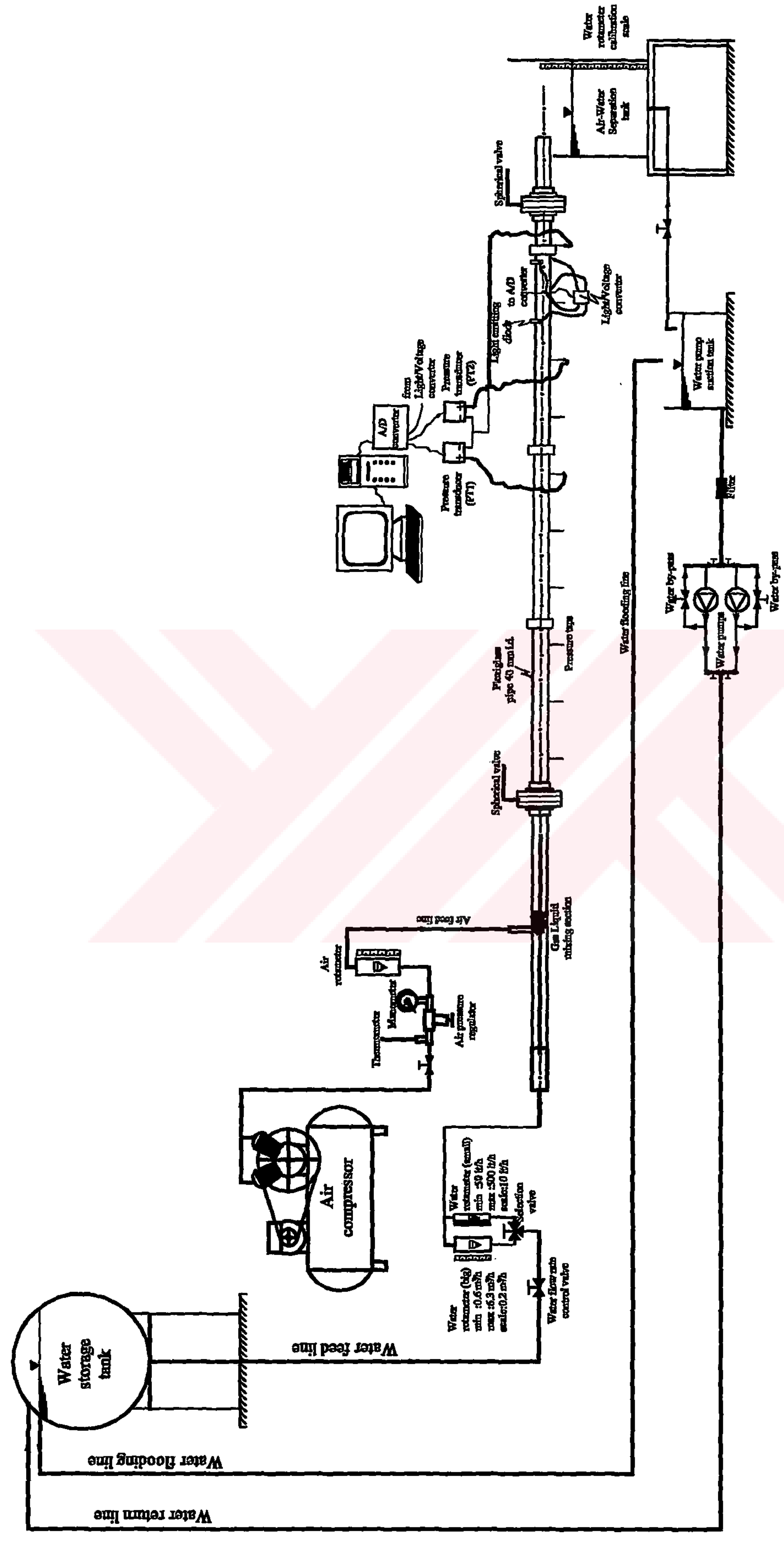

Figure 4.13. Experimental system 2.

Two spherical valves were mounted on the test section to measure the time averaged void fraction. These valves were synchronously closed at the end of each experiment. The height of the liquid layer in the transparent pipe was measured after waiting for a certain period of time until the liquid calm down. This height was used to calculate the cross sectional area occupied by the liquid layer in the test section. Thus, the liquid hold-up and the void fraction can be found.

The first experiment has been conducted in a circular pipe without any insert. Following this experiment, a circular rod with 25 mm outer diameter was inserted in the transparent plexiglas pipe. The experiments with inserted rod were conducted with the concentrically and eccentrically inserted rods. Pressure drops, void fractions, slug velocities, slug lengths, and slug frequencies were measured and flow patterns were visually observed in detail.

4.2.1. Air Supply System

The air supply system is composed of a compressor, an on-off valve, a thermometer, a pressure regulator, a manometer, an air rotameter, and a check valve.

The compressor which was constructed by SARMAK Company was located in the vicinity of the laboratory and supplied the air by means of the main air distribution system of the laboratories. The total tank volume of the compressor is 150 lt and it works between the pressures of 8 and 12 bar.

The air provided from the main air distribution circuit of the laboratory was controlled with the help of a pressure regulator. The pressure regulator consists of two manometers to measure the inlet and outlet pressures of air. The outlet pressure of the regulator is the pressure of air going through the air rotameter. The pressure measured by this manometer is important to calculate the actual air flow rate passed through the air rotameter. The value read from the air rotameter is converted to the actual value which is calculated regarding the real conditions.

The manometer located at the exit of the pressure regulator was calibrated using a water column. The calibration data is given in table (4.5), and the calibration curve in eq. (4.12).

Table 4.5. The calibration data of the air manometer on the pressure regulator.

Manometer		Water column	
bar	Pa	cm	Pa
0.050	5000	41.5	4071.2
0.065	6500	51.5	5052.2
0.070	7000	61.5	6033.2
0.080	8000	71.5	7014.2
0.090	9000	81.5	7995.2
0.100	10000	91.5	8976.2
0.110	11000	101.0	9908.1
0.125	12500	111.5	10938.2
0.135	13500	121.0	11870.1
0.140	14000	131.0	12851.1

The calibration curve of these data is shown in figure 4.14.

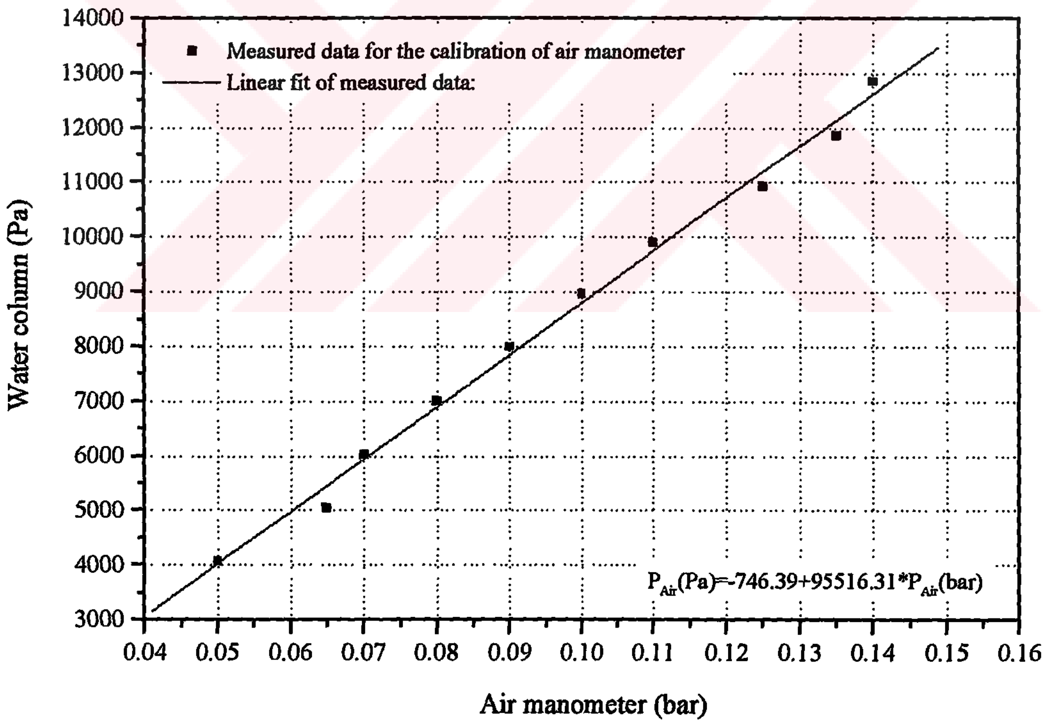

Figure 4.14. Calibration curve of the air manometer.

$$P_{Air}(Pa) = -746.39 + 95516.31 * P_{Air}(bar) \quad (4.12)$$

The air rotameter was produced by MLW Prüfgerät AG in Germany. The type of the air rotameter is LD 100. The minimum and maximum measurement ranges are 1000 and 8000 lt/h, respectively, with a scale of 100 lt/h under the ambient conditions of 15 °C and 101.3 kPa. The indicated value by this rotameter should be converted to the actual value regarding the actual conditions. The correction equation of any rotameter is given in eq. (4.13).

$$M_{act} = M_{read} * \sqrt{\frac{\rho_{act,fluid}\left(\rho_{float} - \rho_{act,fluid}\right)}{\rho_{fluid}\left(\rho_{float} - \rho_{fluid}\right)}} \tag{4.13}$$

The air rotameter was scaled for the ambient conditions of 15 °C and 101.3 kPa. The temperature and pressure of air sent to the air rotameter were measured in the experiments. These values were used to calculate the actual density of air, $\rho_{act,fluid}$. The density of fluid for the ambient conditions of 15 °C and 101.3 kPa were calculated as below.

If the air is assumed as an ideal gas, equation (4.14) can be written;

$$P.V = M.R.T \tag{4.14}$$

The substitution of ρ instead of M and V yields

$$P = \rho.R.T \tag{4.15}$$

Thus, the density can be calculated as follows,

$$\rho = \frac{P}{R.T} \tag{4.16}$$

Using the last equation, the density of the air for the ambient conditions of 15 °C and 101.3 kPa can be calculated:

$$\rho_{fluid} = \frac{101325}{287.053 * (273.15 + 15)} = 1.225 \text{ kg/m}^3 \tag{4.17}$$

The air density in experimental conditions can be similarly calculated by means of the pressure and temperature of air using equation (4.18).

$$\rho_{act,fluid} = \frac{\left[101325 + P_{Air}(Pa)\right]}{287.053 * \left[273.15 + T_{Air}(^\circ C)\right]} \text{ kg/m}^3 \tag{4.18}$$

$P_{Air}(Pa)$ is calculated from the equation (4.12) which is the calibration equation for the air manometer. This is inserted in the equation (4.18). After rearrangement of the equation, one gets;

$$\rho_{act,fluid} = \frac{[100578.61 + 95516.31 * P_{Air}(bar)]}{287.053 * [273.15 + T_{Air}(^{\circ}C)]} \quad \text{kg/m}^3 \tag{4.19}$$

There was no information about the density of the float in the air rotameter. The float was demounted and weighted using an electronic weight meter. The mass of the float is *106.9 gr*. The volume of the float was measured replacing it in a water with known volume in a scaled cup. From this experiment, the volume of the float was found to be 12.5 *mlt*. Thus, the density of the float in the air rotameter was found to be:

$$\rho_{float} = 8552 \quad \text{kg/m}^3 \tag{4.20}$$

The densities of different steels change between 7800 and 8620 kg/m^3. Since the float is made of steel, the density obtained is reasonable. Equation (4.13) can be rewritten from eq.(4.21).

$$\dot{M}_{act} = \dot{M}_{read} * \sqrt{\frac{\rho_{act,fluid}(8552 - \rho_{act,fluid})}{10474.7}} \tag{4.21}$$

The actual air flow rate is as follows;

$$\dot{M}_{act} = \dot{M}_{read} * \sqrt{\frac{\frac{[100578.61 + 95516.31 * P_{Air}(bar)]}{287.053 * [273.15 + T_{Air}(^{\circ}C)]} * \left(8552 - \frac{[100578.61 + 95516.31 * P_{Air}(bar)]}{287.053 * [273.15 + T_{Air}(^{\circ}C)]}\right)}{10474.7}} \tag{4.22}$$

$\dot{M}_{read}$, the value read on the scale of the rotameter (lt/h), is corrected using equation (4.22). $P_{Air}(bar)$, and T_{Air} are measured during the experiments and inserted into the equation above.

4.2.2. The Water Supply System

The water supply system is composed of a storage tank, a water flow rate control valve, two different scaled water rotameters, an air-water separation tank, a water pump inlet tank, a filter, two centrifugal water pumps, a water return line, and a water flooding line.

Water is supplied to the test section from a storage tank whose volume is 0.3 m^3. The water storage tank is made of galvanized plate and is replaced 6 m above the test section. Water is provided to the test section from the water storage tank with a 53 mm i.d. galvanized pipe.

The water flow rate is measured with the help of a water rotameter. Two water rotameters having different scales were installed on the experimental system, but the big one was used throughout the experiments. The water rotameter which is scaled in the unit of the gallon per minute (GPM) was produced by DWYER Company. The minimum and the maximum volume flow rate values of the big rotameter are 1 and 8 GPM, respectively. The minimum measurement scale is 0.2 GPM. This water rotameter was calibrated before starting the experiments. The calibration data is given in table (4.6).

Table 4.6. The calibration data of the water rotameter.

Volume flow rate of the rotameter (GPM)	Predefined volume in the separation tank (lt)	Time passed to fill the predefined volume (s)	Measured volume flow rate (m^3/s)
1	5	86.15	5.80E-05
2	10	90.8	1.10E-04
3	15	87.5	1.71E-04
4	20	84.5	2.37E-04
5	25	85.43	2.93E-04
6	30	82.71	3.63E-04
7	35	81.06	4.32E-04
8	40	81.57	4.90E-04

Figure 4.15. shows the calibration curve of the water rotameter.

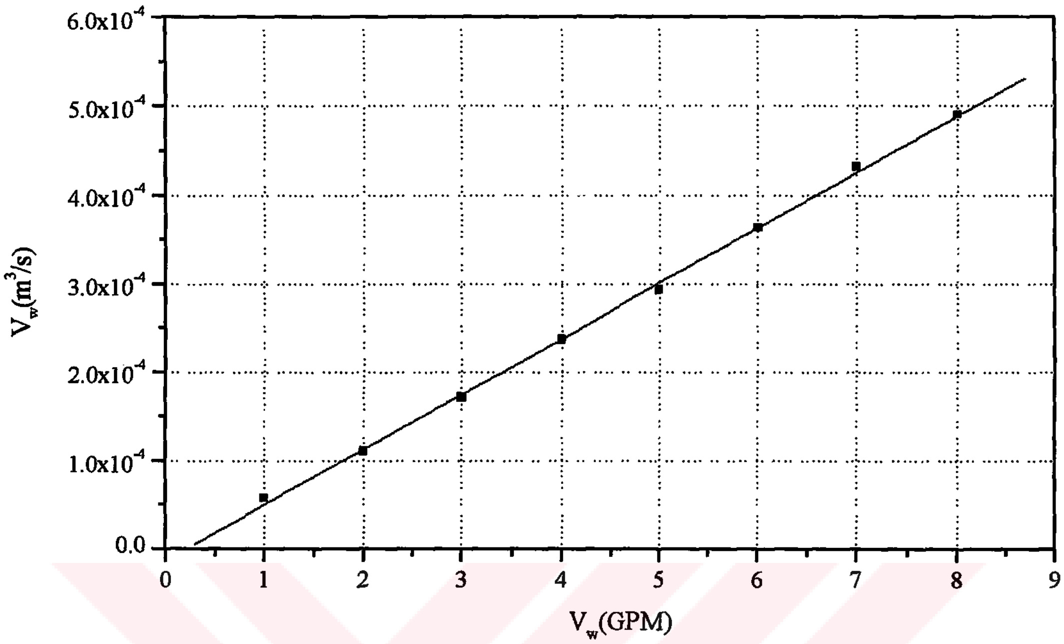

Figure 4.15. Calibration curve of the water rotameter.

The measured water volume flow rate in dimension of GPM is converted to the dimension of m^3/s using the calibration equation (4.23).

$$V_W\,(m^3/s) = -1.28\,.10^{-5} + 6.267\,.10^{-5} * V_W\,(GPM) \tag{4.23}$$

The gas liquid mixture left the plexiglas test pipe was separated in an open to atmosphere tank. While water was gathered in the air-water separation tank, air escaped to the atmosphere. The accumulated water in the air-water separation tank was flowed to the water pump inlet tank with a volume of 0.25 m^3. A filter was replaced at the downstream of the suction tank. The water from the water pump inlet tank was pumped back to the storage tank through the return line. Two pumps connected parallel were mounted on the system to pump the water from the inlet tank to the storage tank located on the roof of the laboratory. Each pump is capable of creating 20 mWG head and volume flow rate of 14 m^3/h. One of the pumps was generally enough to conduct the experiments.

4.2.3. The Pressure Measurement System

Two identical pressure transmitters were used in the experiments. They were produced by Cole Parmer Company. The measurement range of the transmitters is between 0 and 1 Psi. This can be expressed as 0 and 6895 in Pascal. The output of the pressure transmitters is current. The current output was converted to voltage using a known resistance as shown in table (4.7).

Table 4.7. The principle of adjustment of the output as current or voltage.

Current adjustment		Voltage adjustment		
Point	Connection	Point	Connection	
1	+ 24 Vdc	1	+ 24 Vdc	
2	+ 4-20 mA output	2	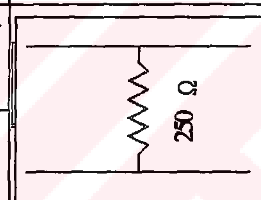	1-5 Vdc output
3	No connection	3		Common

The pressure transmitters PT1 and PT2 were calibrated using an inclined manometer. The calibration curve of the PT1 is shown in figure 4.16.

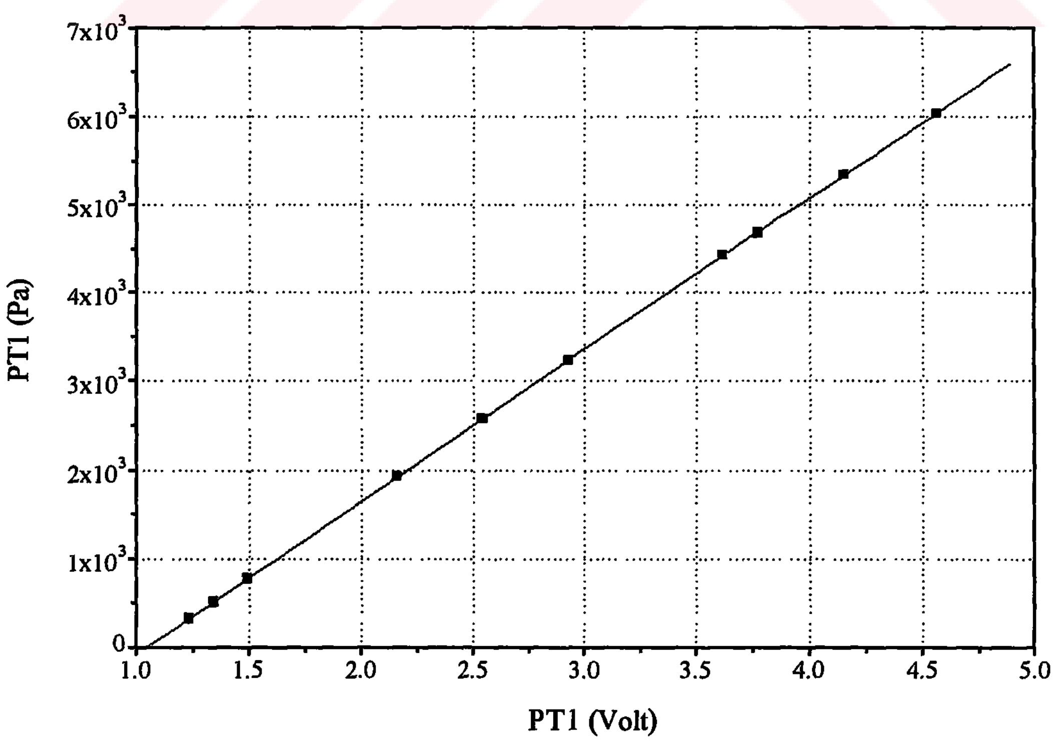

Figure 4.16. The calibration curve of the pressure transmitter PT1.

The calibration equation is given in equation (4.24).

$$\Delta P_{PT1}(Pa) = -1777.99 + 1714.56 * Volt_{PT1} \qquad (4.24)$$

A similar calibration curve and calibration equation were derived for the pressure transmitter PT2. The calibration curve of the PT2 is shown in figure 4.17.

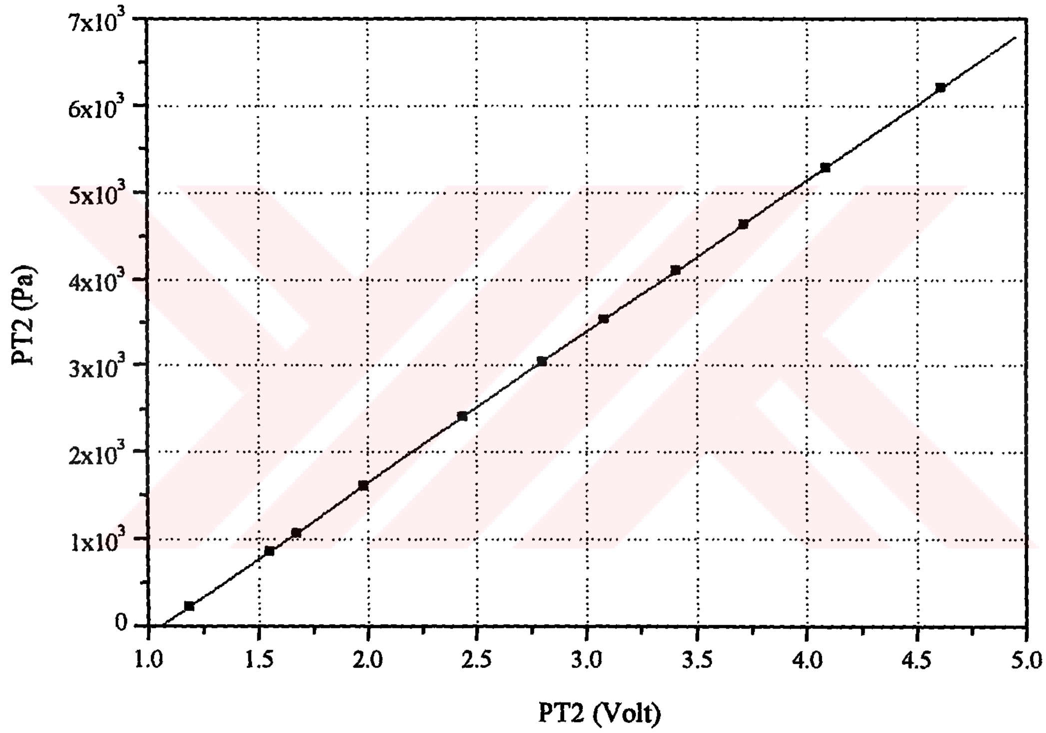

Figure 4.17. The calibration curve of the pressure transmitter PT2.

The calibration equation is given in equation (4.25).

$$\Delta P_{PT2}(Pa) = -1837.86 + 1745.35 * Volt_{PT2} \qquad (4.25)$$

The pressure differences were measured along different lengths of the test pipe not to exceed the maximum value of the transmitters. Therefore, pressure differences are given in dimension of Pa/m.

4.3. Void Fraction Calculation

The time averaged void fraction was measured with the help of two spherical valves located at the inlet and outlet of the test section. These valves were synchronously closed by two researchers at the end of each experiment. After the liquid layer is calm down, the height of the liquid in the transparent pipe was measured. The measured quantity was actually not the height of the liquid layer, but rather the periphery length, L_{read}, measured from the bottom vertical up to the outer surface projection of the liquid layer surface. A transparency scaled in millimetre between zero and the semi-circumference was attached on the outer surface of the pipe. The zero point of the scaled transparency was adjusted with the bottom vertical of the test pipe. This is shown in figure 4.18.

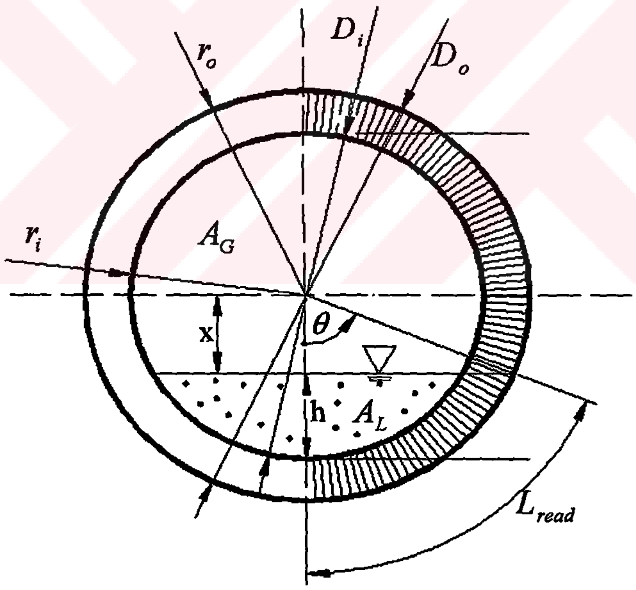

Figure 4.18. Liquid holdup calculation in the lower half of the test pipe.

The ratio of the cross-sectional area occupied by the liquid layer to the overall cross-sectional area of the test pipe is the time averaged liquid holdup. The cross-sectional area occupied by the liquid layer was calculated using equation (4.26).

$$A_L = r_i^2 . \left[\pi - Cos^{-1} . \left(\frac{h}{r_i} - 1 \right) + \left(\frac{h}{r_i} - 1 \right) . \sqrt{1 - \left(\frac{h}{r_i} - 1 \right)^2} \right] \tag{4.26}$$

The height of liquid layer, h, was calculated with the help of the periphery length, L_{read}. This calculation procedure is explained below:

For the lower half of the test pipe;

$$\theta = \frac{360 . L_{read}}{\pi . D_o} \tag{4.27}$$

$$x = Cos(\theta) . r_o \tag{4.28}$$

$$h = r_i - x \tag{4.29}$$

For the upper half of the test pipe;

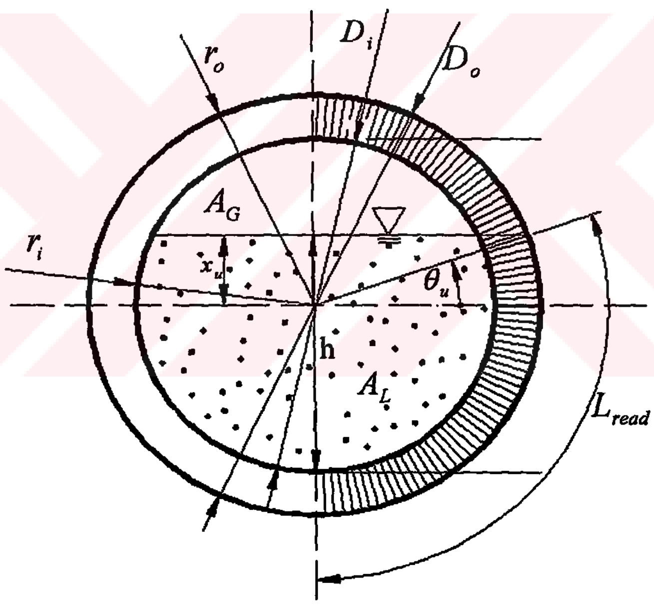

Figure 4.19. Liquid holdup calculation in the upper half of the test pipe

$$\theta_u = \frac{360 . L_{read}}{\pi . D_o} - 90 \tag{4.30}$$

$$x_u = Sin(\theta_u) . r_o \tag{4.31}$$

$$h = r_i + x_u \tag{4.32}$$

The liquid holdup is calculated using equation (4.33).

$$\beta = \frac{A_L}{A_T} \tag{4.33}$$

The void fraction is found using equation (4.34).

$$\alpha = 1 - \beta \tag{4.34}$$

A similar calculation procedure is applied to calculate the liquid holdup in the test pipe with an inserted rod. Figure 4.20. shows the test pipe with an inserted rod.

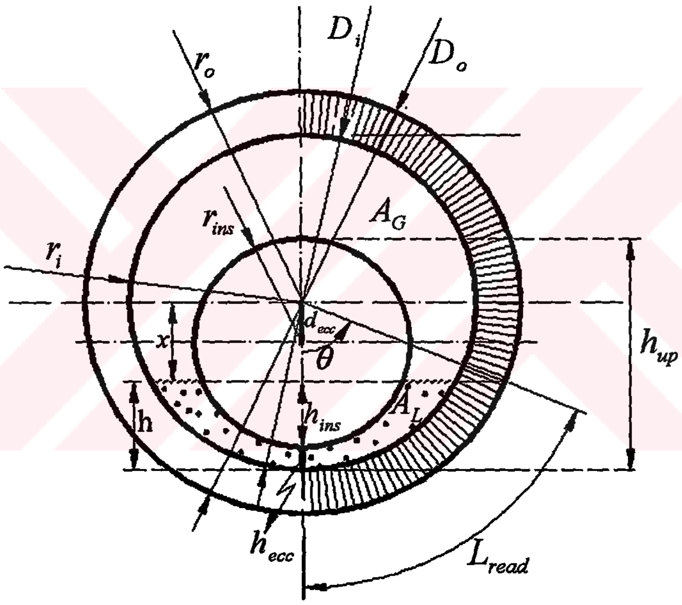

Figure 4.20. Liquid holdup calculation in the test pipe with inserted rod.

The eccentricity, ecc, changes between 0 and 1. If the eccentricity, $ecc = 0$, the inserted rod is placed concentrically. If $ecc = 1$, the rod touches to the bottom of the test tube.

$$ecc = \frac{d_{ecc}}{(r_i - r_{ins})} \tag{4.35}$$

$$d_{ecc} = ecc\,.(r_i - r_{ins}) \tag{4.36}$$

$$h_{ecc} = (r_i - r_{ins}) - d_{ecc} \tag{4.37}$$

If h is smaller than or equal to h_{ecc},

$$A_L = r_i^2.\left[\pi - Cos^{-1}.\left(\frac{h}{r_i}-1\right)+\left(\frac{h}{r_i}-1\right).\sqrt{1-\left(\frac{h}{r_i}-1\right)^2}\right] \quad (4.38)$$

$$h_{up} = h_{ecc} + 2.r_{ins} \quad (4.39)$$

If h is greater than h_{ecc} but smaller than h_{up},

$$A_L = r_i^2.\left[\pi - Cos^{-1}.\left(\frac{h}{r_i}-1\right)+\left(\frac{h}{r_i}-1\right).\sqrt{1-\left(\frac{h}{r_i}-1\right)^2}\right] - A_{ins} \quad (4.40)$$

here, A_{ins} is the buried cross-sectional area of the inserted rod under the liquid layer.

$$A_{ins} = r_{ins}^2.\left[\pi - Cos^{-1}.\left(\frac{h_{ins}}{r_{ins}}-1\right)+\left(\frac{h_{ins}}{r_{ins}}-1\right).\sqrt{1-\left(\frac{h_{ins}}{r_{ins}}-1\right)^2}\right] \quad (4.41)$$

If h is greater than or equal to h_{up},

$$A_L = r_i^2.\left[\pi - Cos^{-1}.\left(\frac{h}{r_i}-1\right)+\left(\frac{h}{r_i}-1\right).\sqrt{1-\left(\frac{h}{r_i}-1\right)^2}\right] - \left(\pi.r_{ins}^2\right) \quad (4.42)$$

The liquid holdup has been calculated using equation (4.43),

$$\beta = \frac{A_L}{A_T} \quad (4.43)$$

The void fraction has been found using equation (4.44),

$$\alpha = 1 - \beta \quad (4.44)$$

A computer program was written to calculate the void fractions using L_{read}'s read during the experiments (Appendix 5). The computer program can be used for pipes and rods in different diameters or in different eccentricity. If the diameter of the inserted rod were given zero in the computer program, the void fractions in an empty pipe would be calculated.

5. RESULTS AND DISCUSSION

5.1. Experimental System 1

5.1.1. Flow Patterns of Horizontal Pipe Experiments

The flow patterns of horizontal gas liquid flow observed in the experiments were compared with three different flow pattern maps. The flow pattern maps and transitions proposed in this study are explained in detail in the section of "Material and Method". The simple calculations of the experimental variables were carried out in Excel sheets.

The comparison of flow patterns observed in the experiments with the well-known flow pattern maps increases the reliability of the experimental setup, measurement systems and experimental method. It is not expected that all results would be in an exact agreement with the previous studies. However, the experimental data reached completely disagreement with the others are regarded suspiciously. The flow patterns observed in the experiments are compared with the three different flow pattern maps in this study.

The first flow pattern map for the comparison of the horizontal tube experiments is the flow pattern map of Baker (1954). The coordinates of the Baker's flow pattern map contains parameters that are functions of mass fluxes of gas and liquid. The abscissa is expressed with the help of the ratio of liquid mass flux and gas mass flux. The ordinate includes the mass flux of gas phase. Besides this, the coordinates of the Baker's flow pattern map includes some parameters which are equal to unity for air-water mixture. The superficial velocities of gas and liquid obtained from the experiments were converted to the mass fluxes using the cross-sectional area of the pipe and the densities of the fluids.

The second and third flow pattern maps for the comparison of the horizontal tube experiments are the flow pattern maps of Weisman (1979) and of Mandhane (1974), respectively. The coordinates of both flow pattern maps include superficial velocities of gas and liquid. The observations obtained in this study is given on the upper right corner of the maps. The experimental data given in table (5.1) were observed visually and described as "Wavy".

Table 5.1. The experimental data visually observed as "Wavy".

U_{Ls} (m/s)	U_{Gs} (m/s)	m_L (kg/m2s)	m_L/m_G (kg/m2s)	Flw Pat. Observed	Flw Pat. Baker	Flw Pat. Weisman	Flw Pat. Mandhane
0.009	11.826	7.767	0.481	Wavy Flow	Wavy Flow	Wavy Flow	Wavy Flow
0.008	16.698	7.765	0.338	Wavy Flow	Wavy Flow	Wavy Flow	Wavy Flow
0.010	8.741	10.163	0.938	Wavy Flow	Wavy Flow	Wavy Flow	Wavy Flow
0.010	9.823	10.163	0.831	Wavy Flow	Wavy Flow	Wavy Flow	Wavy Flow
0.010	12.094	10.163	0.670	Wavy Flow	Wavy Flow	Wavy Flow	Wavy Flow
0.021	10.031	20.920	1.658	Wavy Flow	Wavy Flow	Wavy Flow	Wavy Flow
0.020	13.013	20.907	1.264	Wavy Flow	Wavy Flow	Wavy Flow	Wavy Flow
0.019	13.181	20.892	1.243	Wavy Flow	Wavy Flow	Wavy Flow	Wavy Flow
0.018	17.440	20.877	0.928	Wavy Flow	Wavy Flow	Wavy Flow	Wavy Flow
0.033	9.080	29.301	2.638	Wavy Flow	Wavy Flow	Wavy Flow	Wavy Flow
0.030	8.289	30.118	2.928	Wavy Flow	Wavy Flow	Wavy Flow	Wavy Flow
0.030	9.287	30.112	2.603	Wavy Flow	Slug Flow	Wavy Flow	Wavy Flow
0.029	11.181	30.112	1.994	Wavy Flow	Annular Flow	Wavy Flow	Wavy Flow
0.030	11.868	30.107	2.017	Wavy Flow	Annular Flow	Wavy Flow	Wavy Flow
0.030	11.910	30.108	2.026	Wavy Flow	Annular Flow	Wavy Flow	Wavy Flow
0.029	11.970	30.095	1.998	Wavy Flow	Annular Flow	Wavy Flow	Wavy Flow
0.040	9.594	38.997	3.402	Wavy Flow	Annular Flow	Wavy Flow	Wavy Flow
0.040	12.056	38.977	2.661	Wavy Flow	Annular Flow	Wavy Flow	Wavy Flow
0.039	12.157	38.966	2.635	Wavy Flow	Annular Flow	Wavy Flow	Wavy Flow
0.038	16.034	38.958	1.957	Wavy Flow	Annular Flow	Annular-Wisp Fl	Wavy Flow
0.051	6.998	50.386	5.514	Wavy Flow	Annular Flow	Wavy Flow	Wavy Flow
0.051	7.336	50.381	5.260	Wavy Flow	Annular Flow	Wavy Flow	Wavy Flow
0.051	8.677	50.335	4.997	Wavy Flow	Annular Flow	Wavy Flow	Wavy Flow
0.051	8.852	50.345	4.925	Wavy Flow	Annular Flow	Wavy Flow	Wavy Flow
0.051	8.951	50.372	4.289	Wavy Flow	Annular Flow	Wavy Flow	Wavy Flow
0.050	10.423	50.396	4.078	Wavy Flow	Annular Flow	Wavy Flow	Wavy Flow
0.051	11.238	50.327	3.833	Wavy Flow	Annular Flow	Wavy Flow	Wavy Flow
0.051	11.581	50.372	3.798	Wavy Flow	Annular Flow	Wavy Flow	Wavy Flow
0.051	15.221	50.318	2.793	Wavy Flow	Annular Flow	Annular-Wisp Fl	Wavy Flow
0.073	12.126	71.284	5.100	Wavy Flow	Annular Flow	Wavy Flow	Wavy Flow
0.078	8.761	80.868	8.136	Wavy Flow	Annular Flow	Wavy Flow	Wavy Flow
0.081	9.244	80.741	6.704	Wavy Flow	Annular Flow	Wavy Flow	Wavy Flow
0.117	7.478	119.523	13.670	Wavy Flow	Annular Flow	Wavy Flow	Slug Flow
0.113	11.022	119.443	9.099	Wavy Flow	Annular Flow	Wavy Flow	Slug Flow

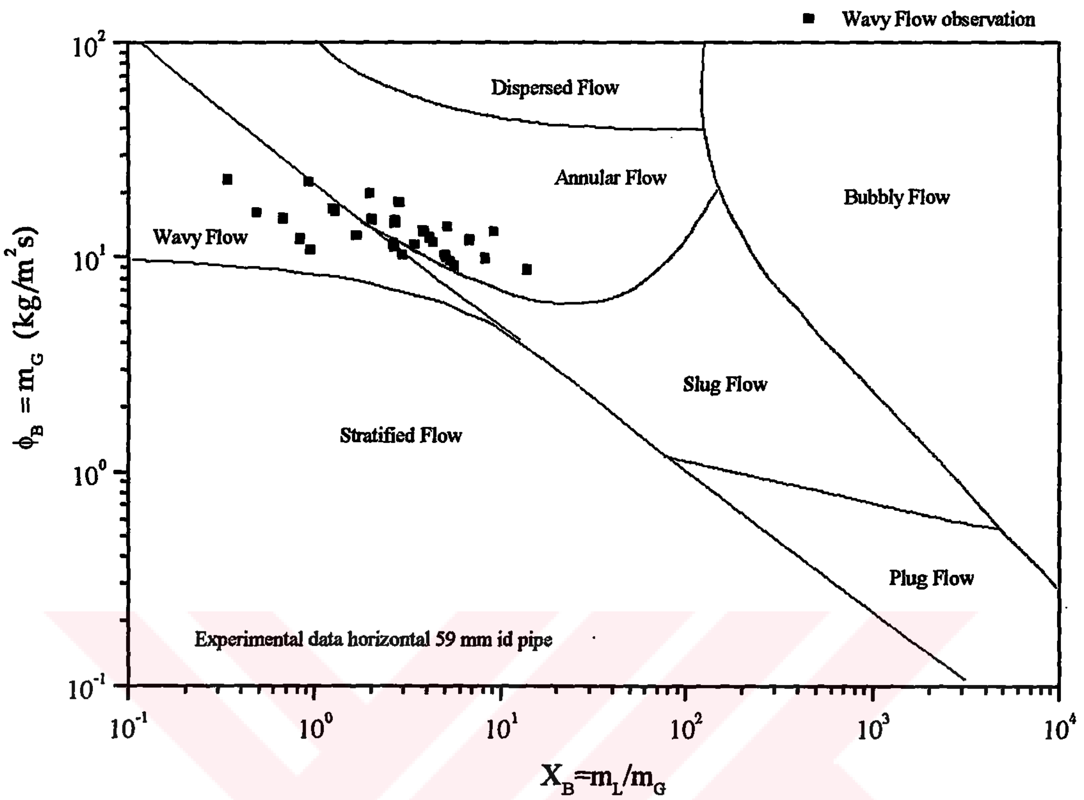

Figure 5.1. Wavy flow observations in the Baker's flow pattern map.

The wavy flow observations obtained in this study are located in the wavy and annular flow patterns of the Baker's map in figure 5.1. The agreement between the present results and the flow pattern map of Baker is not good.

The same data are compared with flow pattern map of Weisman (1979) in figure 5.2. The observed flow patterns of the experimental data are agreed approximately with the estimations of Weisman. Although a few data points are in the annular flow region, the wavy flow observation is in good agreement with the flow pattern map of Weisman.

The wavy flow observation obtained in this study are well predicted by the flow pattern map of Mandhane (1974). The comparison of the observations with the Mandhane's map is been shown in figure 5.3.

Two experimental data points sit in the region of slug flow in the flow pattern map of Mandhane (1974). For the wavy flow observation, one can say that the flow pattern maps of Weisman and Mandhane predict well the observed flow pattern.

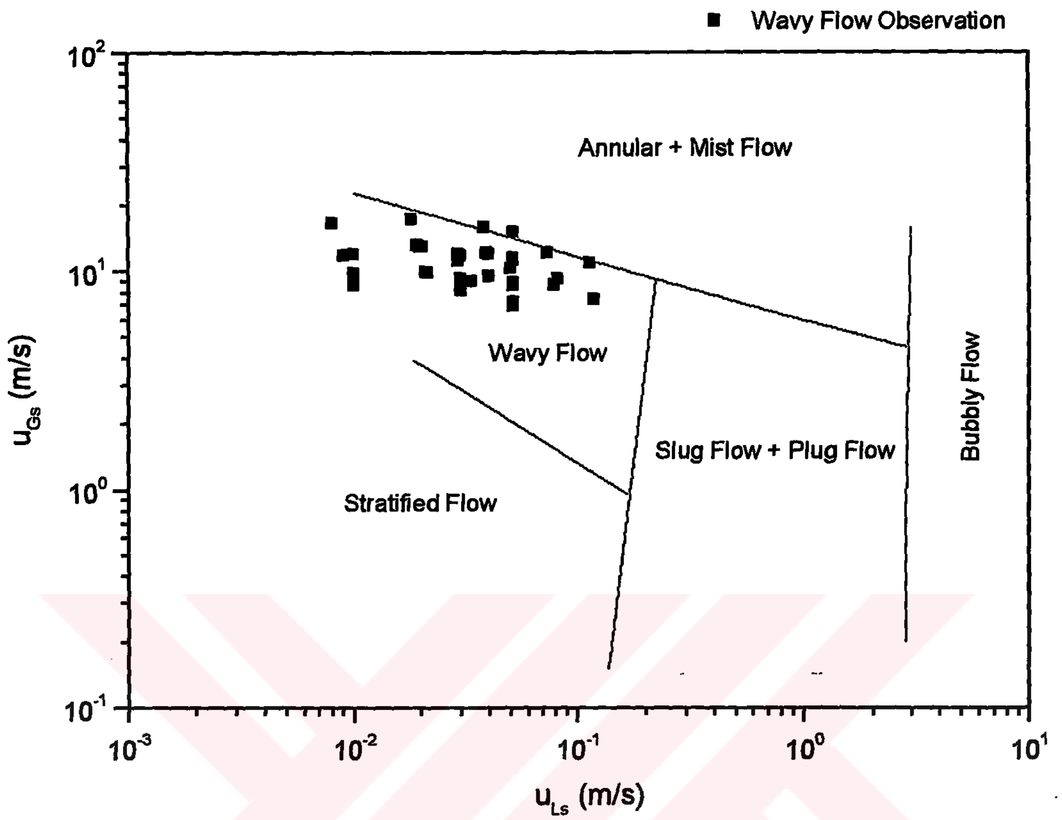

Figure 5.2. Wavy flow observations in the Weisman's flow pattern map.

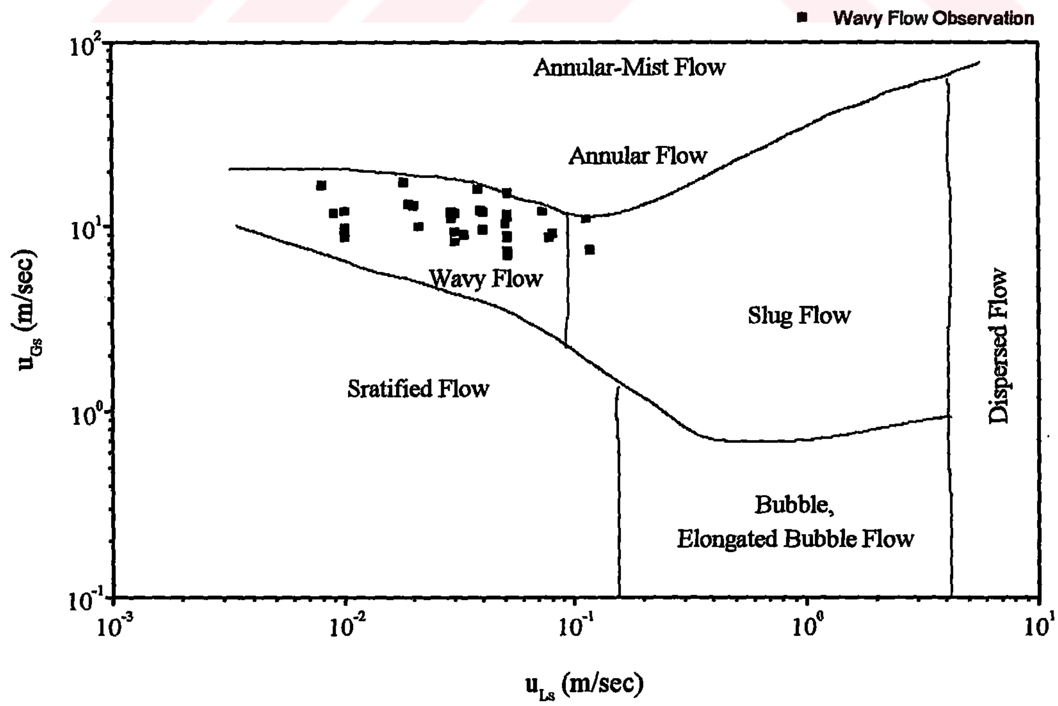

Figure 5.3. Wavy flow observations in the Mandhane's flow pattern map.

For the conditions of slug flow, while the superficial liquid velocity has a fixed value, the blow through slug flow is seen when the superficial gas velocity is increased slightly. Blow through slug flow (BTS) is a slug flow originally. One can imagine this flow type as liquid bulks attempt to touch to the upper inner surface of the test pipe, however they can not do so. This is a frothy fronted wave in the form of a semi-slug flow. In the horizontal tube experiments, some observations were similar to the definition of BTS explained above. Besides the blow through slug flow, a wavy stratified layer was seen. These flow patterns were wavy flow, but there were some blow through slugs forming periodically or non-periodically, at the same time. This observation can be described as Wavy+BTS flow.

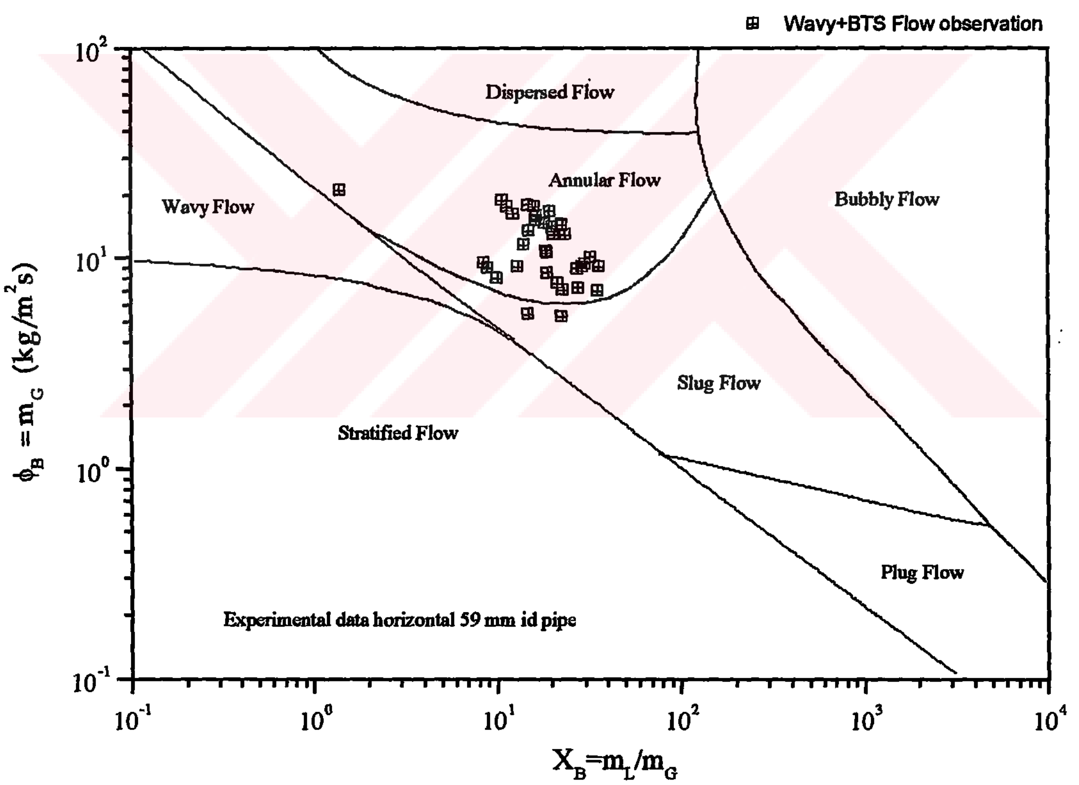

Figure 5.4. Wavy+BTS flow observations in the Baker's flow pattern map.

The "Wavy+BTS flow" observations are compared with the Baker's map in figure 5.4. The observations mostly locate in the annular flow region. Two of the observations sit in the slug flow region. It can be expressed that the flow pattern map of Baker is not capable of estimating the "Wavy+BTS flow" observations.

Table 5.2. The experimental data visually observed as "Wavy+BTS flow".

U_{Ls} (m/s)	U_{Gs} (m/s)	m_L (kg/m2s)	m_L/m_G (kg/m2s)	Flw Pat. Observed	Flw Pat. Baker	Flw Pat. Weisman	Flw Pat. Mandhane
0.028	16.583	29.257	1.381	Wavy+BTS	Annular Flow	Wavy Flow	Wavy Flow
0.081	4.897	80.916	14.786	Wavy+BTS	Slug Flow	Wavy Flow	Wavy Flow
0.081	6.313	80.770	10.004	Wavy+BTS	Annular Flow	Wavy Flow	Wavy Flow
0.081	7.030	80.755	8.906	Wavy+BTS	Annular Flow	Wavy Flow	Wavy Flow
0.080	8.456	80.892	8.480	Wavy+BTS	Annular Flow	Wavy Flow	Wavy Flow
0.120	4.562	119.573	22.528	Wavy+BTS	Slug Flow	Wavy Flow	Slug Flow
0.114	7.815	119.484	13.009	Wavy+BTS	Annular Flow	Wavy Flow	Slug Flow
0.163	5.889	161.847	21.265	Wavy+BTS	Annular Flow	Wavy Flow	Slug Flow
0.163	6.090	162.139	22.860	Wavy+BTS	Annular Flow	Wavy Flow	Slug Flow
0.163	6.119	161.532	18.809	Wavy+BTS	Annular Flow	Wavy Flow	Slug Flow
0.163	8.801	161.780	13.955	Wavy+BTS	Annular Flow	Wavy Flow	Slug Flow
0.203	5.396	200.293	27.595	Wavy+BTS	Annular Flow	Wavy Flow	Slug Flow
0.203	7.965	200.274	18.359	Wavy+BTS	Annular Flow	Wavy Flow	Slug Flow
0.201	8.831	200.751	18.791	Wavy+BTS	Annular Flow	Wavy Flow	Slug Flow
0.203	9.738	200.261	14.849	Wavy+BTS	Annular Flow	Annular-Wisp Fl	Slug Flow
0.203	12.447	200.254	11.314	Wavy+BTS	Annular Flow	Annular-Wisp Fl	Slug Flow
0.193	13.472	200.688	12.240	Wavy+BTS	Annular Flow	Annular-Wisp Fl	Ann.Mist
0.193	15.665	200.629	10.595	Wavy+BTS	Annular Flow	Annular-Wisp Fl	Ann.Mist
0.244	5.159	246.095	35.092	Wavy+BTS	Annular Flow	Slug-Plug Flow	Slug Flow
0.244	6.517	246.045	27.383	Wavy+BTS	Annular Flow	Slug-Plug Flow	Slug Flow
0.244	10.599	246.016	16.264	Wavy+BTS	Annular Flow	Annular-Wisp Fl	Slug Flow
0.265	7.235	266.257	28.874	Wavy+BTS	Annular Flow	Slug-Plug Flow	Slug Flow
0.269	10.656	266.179	20.442	Wavy+BTS	Annular Flow	Annular-Wisp Fl	Slug Flow
0.262	11.051	266.186	18.132	Wavy+BTS	Annular Flow	Annular-Wisp Fl	Slug Flow
0.269	13.359	266.098	16.583	Wavy+BTS	Annular Flow	Annular-Wisp Fl	Slug Flow
0.260	13.400	266.149	14.769	Wavy+BTS	Annular Flow	Annular-Wisp Fl	Slug Flow
0.284	6.846	284.081	29.936	Wavy+BTS	Annular Flow	Slug-Plug Flow	Slug Flow
0.284	9.938	284.034	19.960	Wavy+BTS	Annular Flow	Annular-Wisp Fl	Slug Flow
0.284	12.138	284.024	16.078	Wavy+BTS	Annular Flow	Annular-Wisp Fl	Slug Flow
0.300	10.267	303.024	23.403	Wavy+BTS	Annular Flow	Annular-Wisp Fl	Slug Flow
0.325	6.199	324.937	35.597	Wavy+BTS	Annular Flow	Slug-Plug Flow	Slug Flow
0.325	6.825	324.874	31.924	Wavy+BTS	Annular Flow	Slug-Plug Flow	Slug Flow
0.325	9.471	324.831	22.591	Wavy+BTS	Annular Flow	Annular-Wisp Fl	Slug Flow
0.325	10.934	324.810	19.318	Wavy+BTS	Annular Flow	Annular-Wisp Fl	Slug Flow

The same data are shown in the flow pattern map of Weisman in figure 5.5. The "Wavy+BTS flow" observations are intensified in the intersection region of three different flow patterns. These are wavy, annular, and slug-plug flow patterns. The predictions of the Weisman's map are more reasonable than those of the flow pattern map of Baker. The "Wavy+BTS flow" consists of wavy and slug flows, as expected. In some cases, one can additionally see an annular film on the inner surface of the test pipe. The ripples on the stratified wavy surface and the droplets travelling by means of the higher superficial air velocity cause a continually wetting on the upper inner surface. When the frequency of the BTS's is low, annular film on the surface flows as rivulets downwards. If the frequency of the BTS's is high enough to wet again the upper surface before the annular film flows completely, a continuous annular film flow is seen besides the "Wavy+BTS flow".

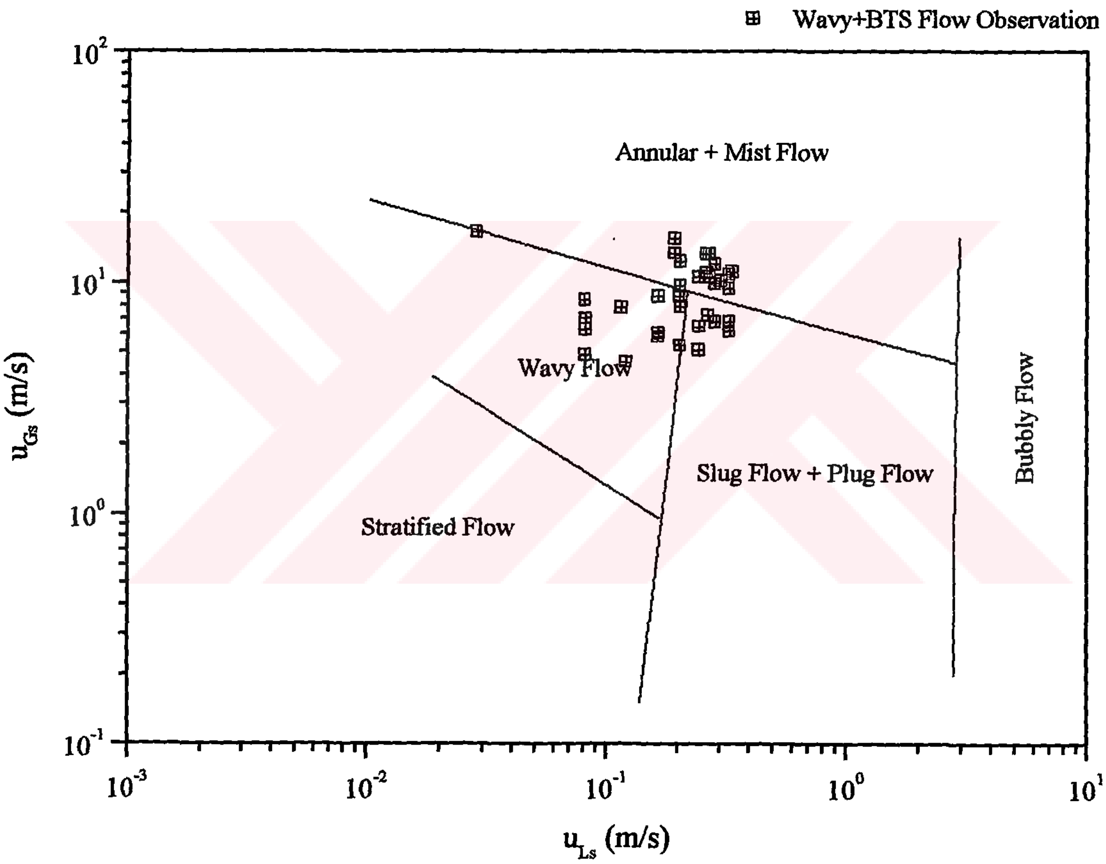

Figure 5.5. Wavy+BTS flow observations in the Weisman's flow pattern map.

The "Wavy+BTS flow" observations are compared with the flow pattern map of the Mandhane. The same data of the horizontal tube experiments are shown in the Mandhane's map in figure 5.6. The most of the experimental data sit in the slug flow region in the Mandhane's map. A few data are in the region of wavy flow and annular flow. The last two flow pattern maps show that the "Wavy+BTS flow" observation locates in the intersection region of three different flow patterns which are the wavy, annular, and slug flow. The best prediction is carried out by Weisman with respect to the real observations in this study. The predictions of the Mandhane can be accepted to be relatively enough.

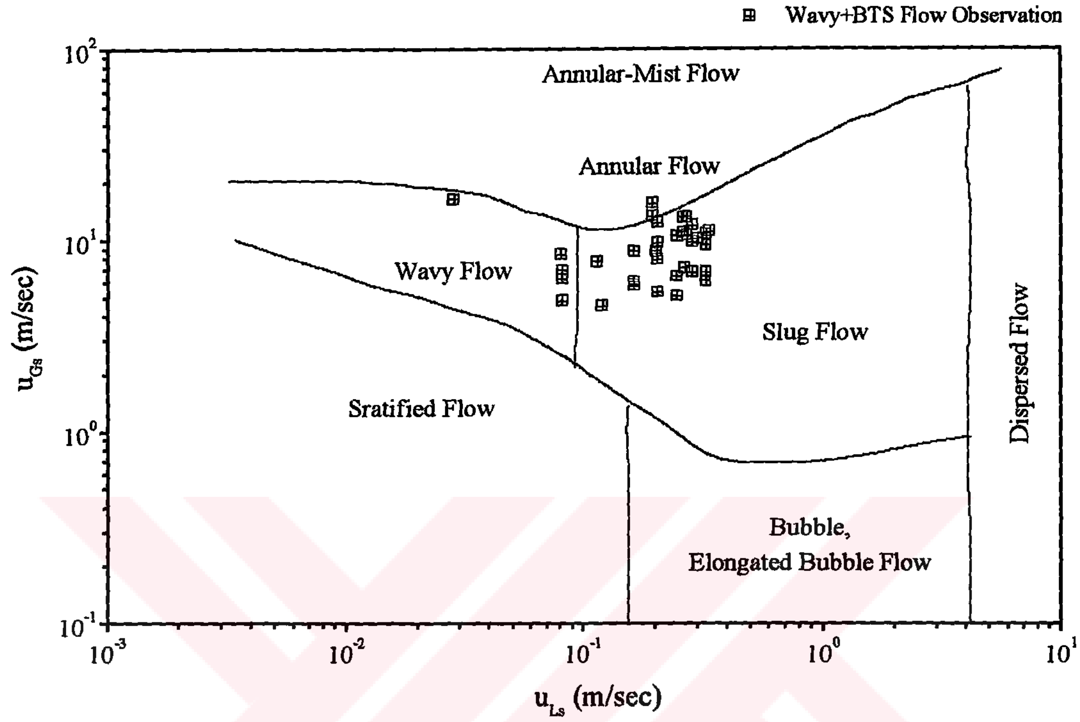

Figure 5.6. Wavy+BTS flow observations in the Mandhane's flow pattern map.

Annular+wavy flow is a stratified wavy layer with an annular film on the inner surface of the pipe. The experimental data are given in table (5.3).

The experimental data observed as "Annular+wavy flow" are shown in the flow pattern map of Baker in figure 5.7. The most of the observations sit in the annular flow region. The three of the experimental data are predicted as wavy flow by the Baker's map.

A few of the experimental data are defined as wavy+open annular flow. These observations were similar to the "Annular+wavy flow", but annular film was interrupted in the near of the inner top of the pipe. These region of the test pipe was absolutely free of water film. The "Annular+wavy flow" and "Wavy+open annular flow" observations are shown in figure 5.7. and figure 5.8. in the flow pattern map of Baker.

The same experimental data are compared with the flow pattern map of Weisman. Figure 5.9. shows the Weisman's map with the experimental data.

Table 5.3. The experimental data visually observed as "Annular+wavy flow".

U_{Ls} (m/s)	U_{Gs} (m/s)	m_L (kg/m2s)	m_L/m_G (kg/m2s)	Flw Pat. Observed	Flw Pat. Baker	Flw Pat. Weisman	Flw Pat. Mandhane
0.008	24.099	7.762	0.228	Annular+Wavy	Wavy Flow	Wavy Flow	Ann.Mist
0.008	27.227	7.761	0.201	Annular+Wavy	Wavy Flow	Annular-Wisp Fl	Ann.Mist
0.007	31.097	7.759	0.173	Annular+Wavy	Wavy Flow	Annular-Wisp Fl	Ann.Mist
0.027	15.474	29.276	1.371	Annular+Wavy	Annular Flow	Wavy Flow	Wavy Flow
0.030	16.433	30.103	1.434	Annular+Wavy	Annular Flow	Wavy Flow	Wavy Flow
0.050	14.404	50.408	2.914	Annular+Wavy	Annular Flow	Annular-Wisp Fl	Wavy Flow
0.050	21.177	50.385	1.896	Annular+Wavy	Annular Flow	Annular-Wisp Fl	Ann.Mist
0.081	12.080	80.729	5.031	Annular+Wavy	Annular Flow	Wavy Flow	Wavy Flow
0.122	11.229	119.175	7.617	Annular+Wavy	Annular Flow	Annular-Wisp Fl	Slug Flow
0.122	15.103	119.171	5.488	Annular+Wavy	Annular Flow	Annular-Wisp Fl	Ann.Mist
0.163	8.515	161.517	13.300	Annular+Wavy	Annular Flow	Wavy Flow	Slug Flow
0.163	12.939	161.512	8.488	Annular+Wavy	Annular Flow	Annular-Wisp Fl	Ann.Mist
0.188	18.271	183.527	8.164	Annular+Wavy	Annular Flow	Annular-Wisp Fl	Ann.Mist
0.264	16.572	266.052	13.439	Annular+Wavy	Annular Flow	Annular-Wisp Fl	Ann.Mist

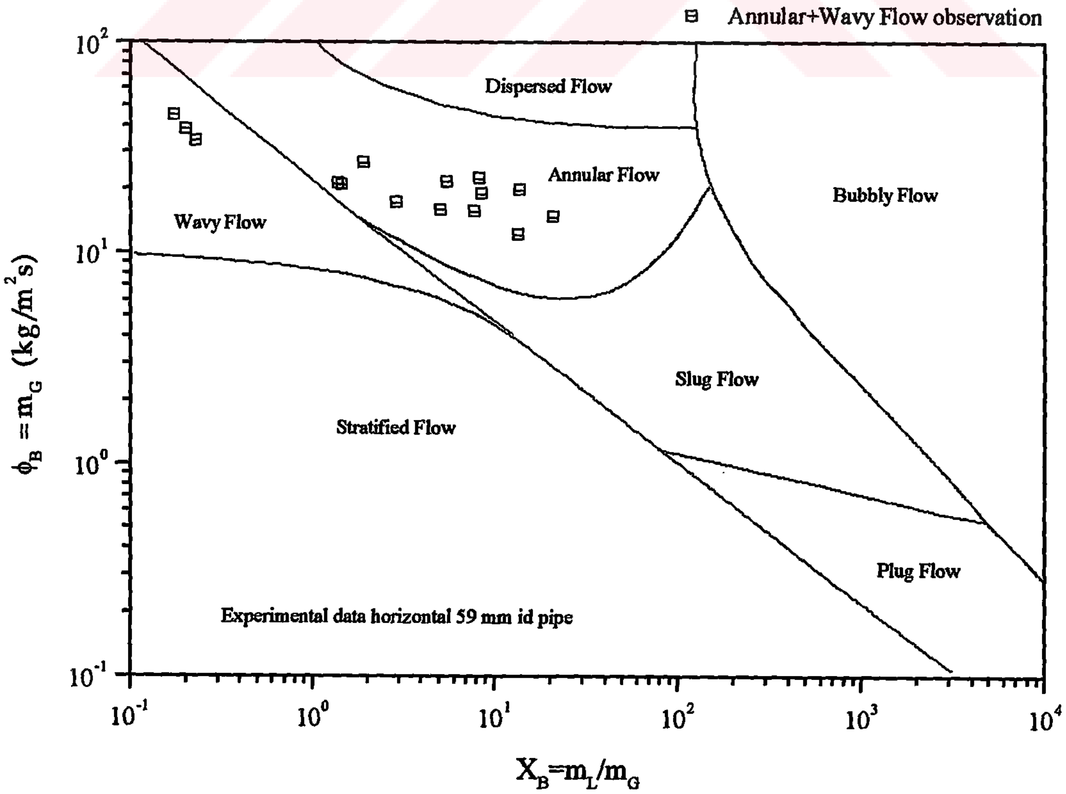

Figure 5.7. Annular+wavy flow observations in the Baker's flow pattern map.

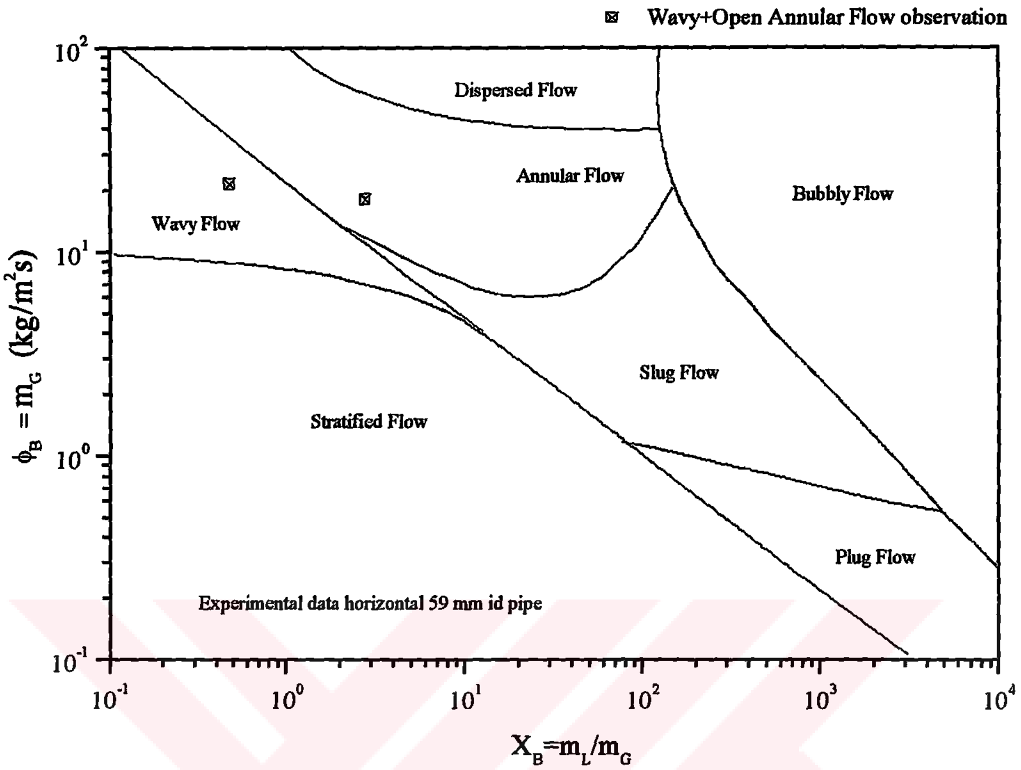

Figure 5.8. Wavy+open annular flow observations in the Baker's flow pattern map.

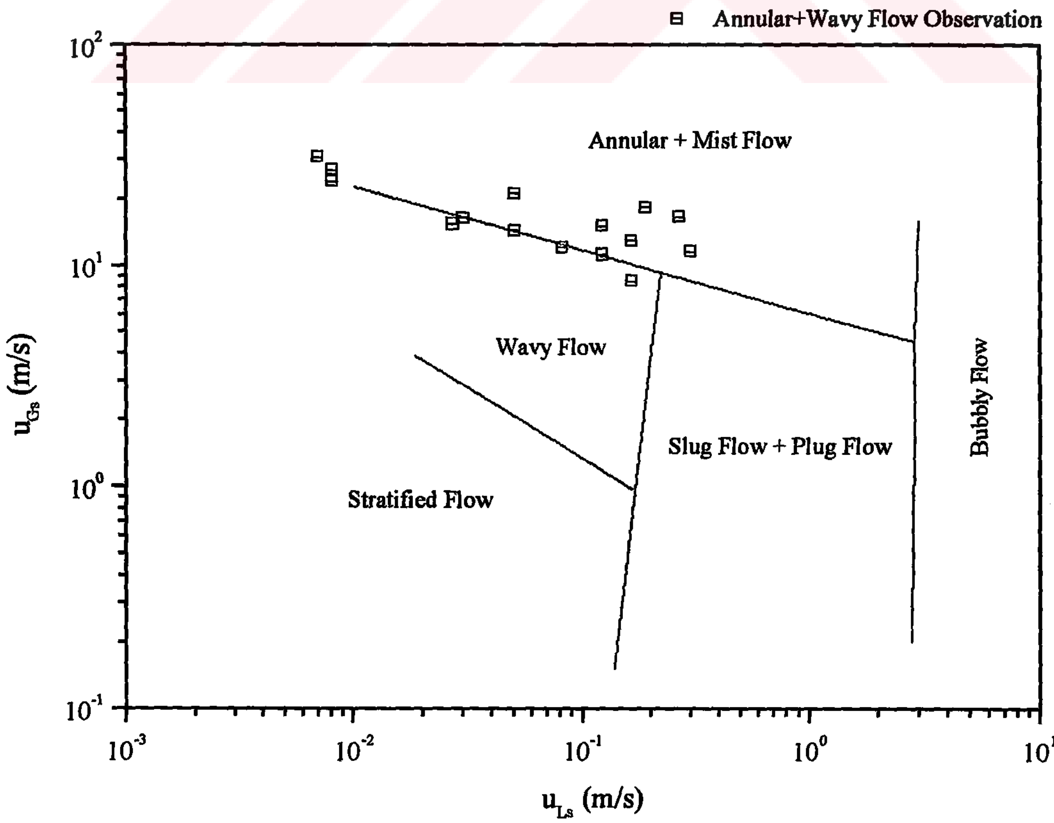

Figure 5.9. Annular+wavy flow observations in the Weisman's flow pattern map.

The flow pattern predictions of Weisman for "Annular+wavy flow" observations are better than those of the Baker's map. The "Annular+wavy flow" can be regarded as a transition flow pattern from wavy to annular flow or vice versa. This transition case is well predicted by the flow pattern map of Weisman.

The "Wavy+open annular flow" observations are also shown in the Weisman's map in figure 5.10. Both of the observations are located in the wavy flow region, but the data which is in the annular region of Baker's map is near to the annular region of Weisman's map again.

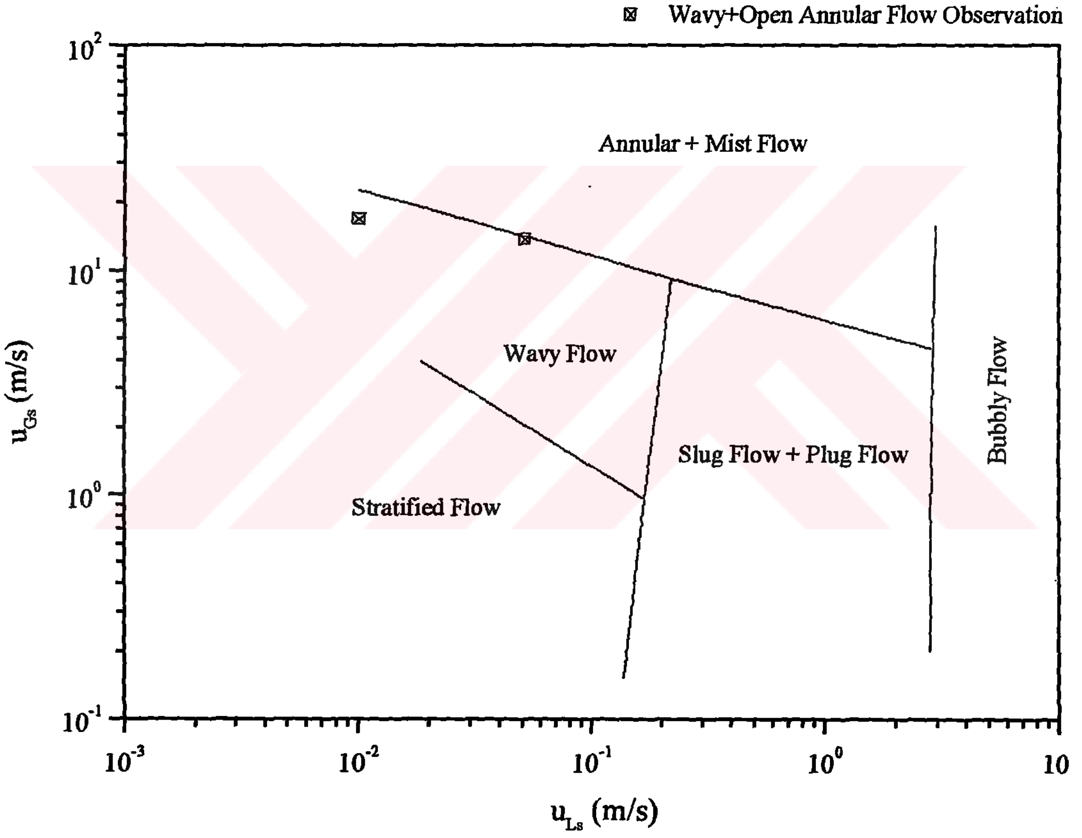

Figure 5.10. Wavy+open annular flow observations in the Weisman's flow pattern map.

Similar estimations are performed by the flow pattern map of Mandhane for the observations of the "Annular+wavy flow" and "Wavy+open annular flow".

The "Annular+wavy flow" observations are shown in figure 5.11. The experimental data observed as "Annular+wavy flow" are located in three different region in the flow pattern map of Mandhane. The approximately half the data sit between the regions of wavy and annular, the other half of the data locate in the regions of slug and annular flow. The intersection region of these three region was defined as BTS region before. The observed experimental data sometimes contained the blow through slug (BTS) flow. The flow pattern maps of Weisman and Mandhane well estimate these observations.

The "Wavy+open annular flow" observation are shown in figure 5.12. This is similar to that of the Weisman's map. The flow pattern maps of Weisman and Mandhane well predict the "Wavy+open annular flow".

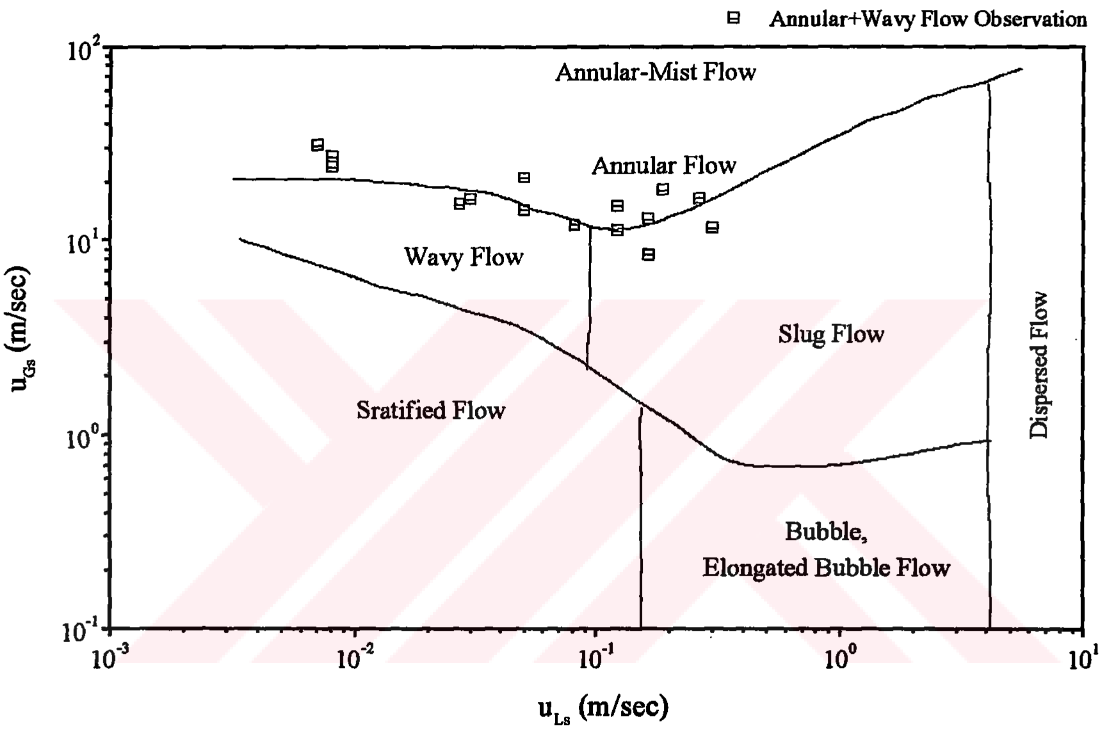

Figure 5.11. Annular+wavy flow observations in the Mandhane's flow pattern map.

Some data in the horizontal flow experiments are called as "Wavy+BTS+Annular flow". The "Wavy+BTS flow" and the "Annular+Wavy flow" observations are previously explained. The "Wavy+BTS+Annular flow" observations resemble both of the "Wavy+BTS flow" and the "Annular+Wavy flow". The data of "Wavy+BTS+Annular flow" observations are given in table (5.4).

The "Wavy+BTS+Annular flow" observations are shown in the flow pattern map of Baker (1954) in figure 5.13. All data are located in the annular flow region in the Baker's map. It would be reasonable if they were in the intersection region of annular, wavy, and slug flow. The estimations of the flow pattern map of Baker are insufficient for the "Wavy+BTS+Annular flow" observations.

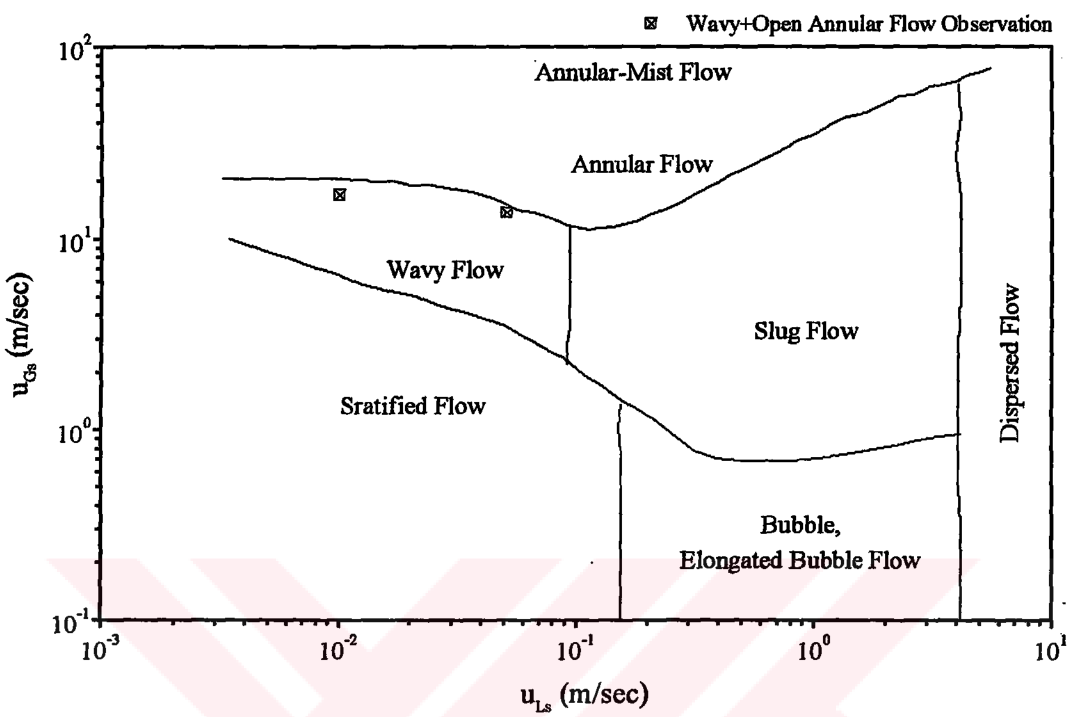

Figure 5.12. Wavy+open annular flow observations in the Mandhane's flow pattern map.

Table 5.4. The experimental data visually observed as "Wavy+BTS+Annular flow".

U_{Ls} (m/s)	U_{Gs} (m/s)	m_L (kg/m2s)	m_L/m_G (kg/m2s)	Flw Pat. Observed	Flw Pat. Baker	Flw Pat. Weisman	Flw Pat. Mandhane
0.066	22.194	62.781	2.180	Wavy+BTS+Annular	Annular Flow	Annular-Wisp Fl	Ann.Mist
0.073	11.253	71.406	5.320	Wavy+BTS+Annular	Annular Flow	Wavy Flow	Wavy Flow
0.071	17.080	71.389	3.385	Wavy+BTS+Annular	Annular Flow	Annular-Wisp Fl	Ann.Mist
0.069	19.309	71.368	2.945	Wavy+BTS+Annular	Annular Flow	Annular-Wisp Fl	Ann.Mist
0.081	6.904	81.017	9.995	Wavy+BTS+Annular	Annular Flow	Wavy Flow	Wavy Flow
0.152	19.151	146.813	5.963	Wavy+BTS+Annular	Annular Flow	Annular-Wisp Fl	Ann.Mist
0.163	9.186	162.094	14.827	Wavy+BTS+Annular	Annular Flow	Wavy Flow	Slug Flow
0.157	14.645	162.050	8.942	Wavy+BTS+Annular	Annular Flow	Annular-Wisp Fl	Ann.Mist
0.154	16.464	162.007	7.810	Wavy+BTS+Annular	Annular Flow	Annular-Wisp Fl	Ann.Mist
0.203	14.166	200.261	9.777	Wavy+BTS+Annular	Annular Flow	Annular-Wisp Fl	Ann.Mist
0.203	15.536	200.274	8.716	Wavy+BTS+Annular	Annular Flow	Annular-Wisp Fl	Ann.Mist

The same data are shown in figure 5.14. in the flow pattern map of Weisman (1979). The predictions of the Weisman's map are more reasonable than those of the Baker's map. The observations of the horizontal flow experiments sit in the regions of wavy and annular flows. There is no data point in the slug flow region.

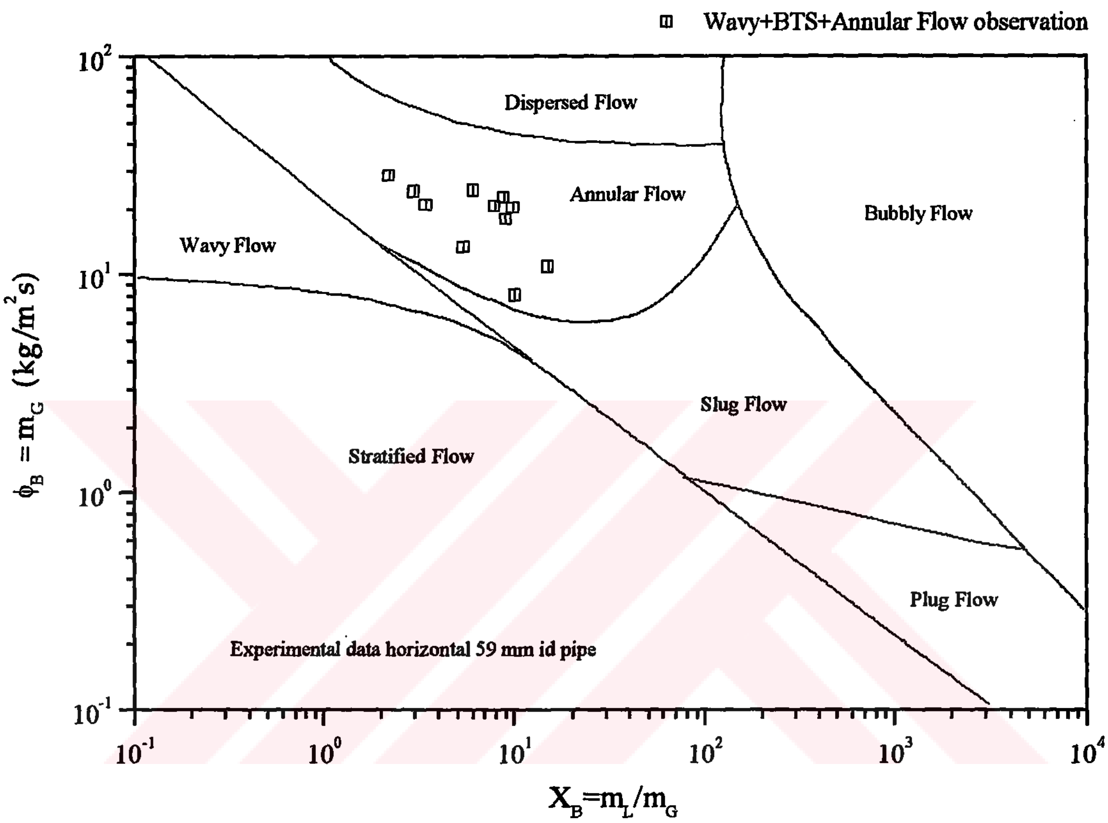

Figure 5.13. Wavy+BTS+Annular flow in the Baker's flow pattern map.

The "Wavy+BTS+Annular flow" observations have been shown in figure 5.15. in the flow pattern map of Mandhane (1974). The experimental observations have been in three different regions which are wavy, annular, and slug flow. The best estimation has been done by the flow pattern map of Mandhane.

These types of observations of the horizontal flow experiments have the properties of three different flow patterns. There have been always a wavy layer in the test pipe. This layer has been sometimes thinned as if it disappeared. There were blow through slugs seen periodically or non-periodically. Annular flow has been seen mostly in the flow as thin or thick films on the inner surface. The flow pattern map of Mandhane (1974) estimates well these observations than those of the Baker and Weisman.

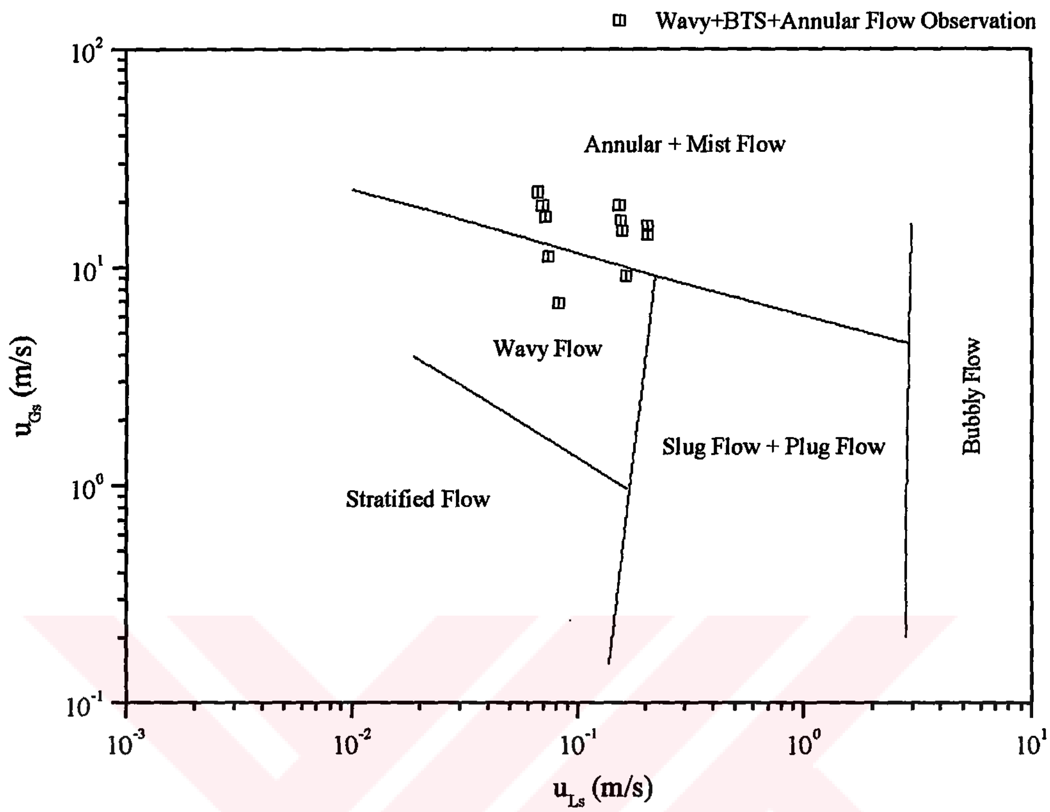

Figure 5.14. Wavy+BTS+Annular flow in the Weisman's flow pattern map.

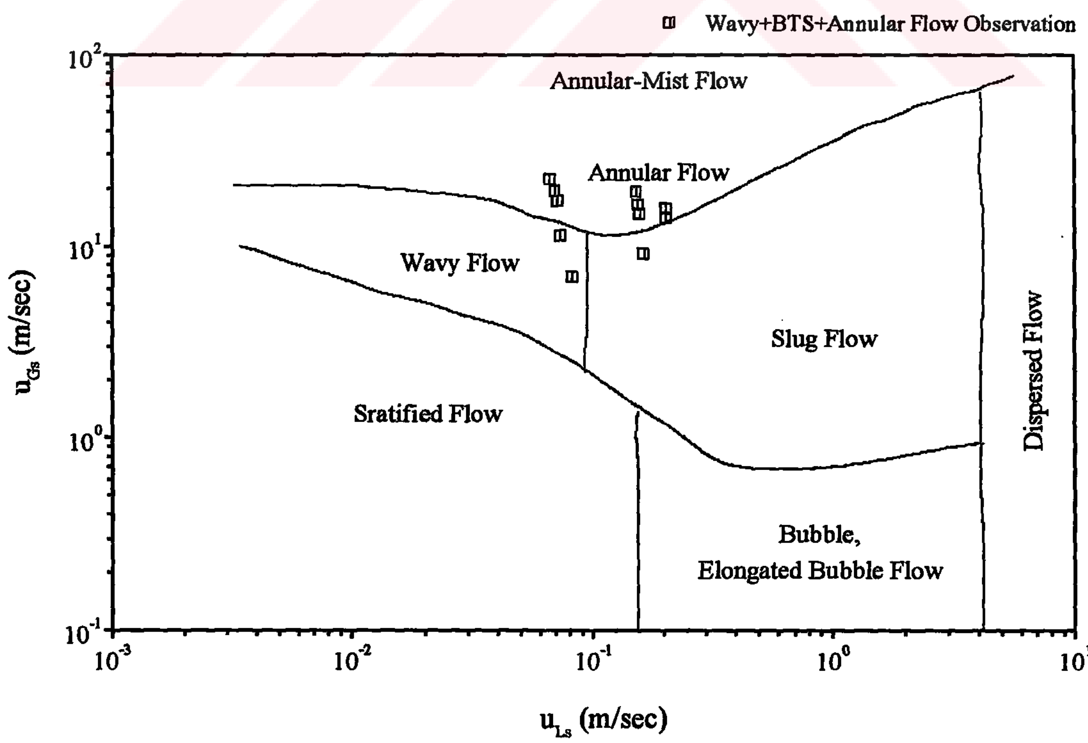

Figure 5.15. Wavy+BTS+Annular flow in the Mandhane's flow pattern map.

The slug flow observations are given in table (5.5).

Table 5.5. The experimental data visually observed as "Slug flow".

U_{Ls} (m/s)	U_{Gs} (m/s)	m_L (kg/m2s)	m_L/m_G (kg/m2s)	Flw Pat. Observed	Flw Pat. Baker	Flw Pat. Weisman	Flw Pat. Mandhane
0.244	4.168	246.286	44.011	SlugFlow	Slug Flow	Slug-Plug Flow	Slug Flow
0.303	3.903	303.279	63.075	SlugFlow	Slug Flow	Slug-Plug Flow	Slug Flow
0.305	3.904	303.822	63.524	SlugFlow	Slug Flow	Slug-Plug Flow	Slug Flow
0.341	3.891	338.803	68.170	SlugFlow	Slug Flow	Slug-Plug Flow	Slug Flow
0.345	3.906	338.481	71.042	SlugFlow	Slug Flow	Slug-Plug Flow	Slug Flow
0.203	3.912	200.965	42.924	SlugFlow	Slug Flow	Slug-Plug Flow	Slug Flow
0.244	4.168	246.213	43.961	SlugFlow	Slug Flow	Slug-Plug Flow	Slug Flow
0.244	4.436	246.144	41.023	SlugFlow	Slug Flow	Slug-Plug Flow	Slug Flow
0.271	3.908	266.688	56.260	SlugFlow	Slug Flow	Slug-Plug Flow	Slug Flow
0.284	5.157	284.138	40.463	SlugFlow	Annular Flow	Slug-Plug Flow	Slug Flow
0.305	4.227	303.770	59.114	SlugFlow	Slug Flow	Slug-Plug Flow	Slug Flow
0.325	4.645	325.259	49.339	SlugFlow	Slug Flow	Slug-Plug Flow	Slug Flow
0.325	4.864	325.112	46.509	SlugFlow	Slug Flow	Slug-Plug Flow	Slug Flow
0.325	4.873	325.171	46.783	SlugFlow	Slug Flow	Slug-Plug Flow	Slug Flow
0.341	3.907	338.878	71.348	SlugFlow	Slug Flow	Slug-Plug Flow	Slug Flow
0.341	3.913	338.870	72.500	SlugFlow	Slug Flow	Slug-Plug Flow	Slug Flow
0.163	4.667	161.586	24.962	SlugFlow	Annular Flow	Wavy Flow	Slug Flow
0.203	4.453	200.386	33.985	SlugFlow	Slug Flow	Slug-Plug Flow	Slug Flow
0.284	4.717	284.275	45.689	SlugFlow	Slug Flow	Slug-Plug Flow	Slug Flow
0.203	4.707	200.343	31.943	SlugFlow	Annular Flow	Wavy Flow	Slug Flow
0.271	4.226	266.812	51.894	SlugFlow	Slug Flow	Slug-Plug Flow	Slug Flow
0.284	4.945	284.202	42.875	SlugFlow	Slug Flow	Slug-Plug Flow	Slug Flow
0.345	4.523	338.376	61.485	SlugFlow	Slug Flow	Slug-Plug Flow	Slug Flow
0.342	6.612	338.248	41.886	SlugFlow	Annular Flow	Slug-Plug Flow	Slug Flow
0.340	8.639	339.236	32.076	SlugFlow	Annular Flow	Annular-Wisp Fl	Slug Flow
0.335	14.382	339.038	19.568	SlugFlow	Annular Flow	Annular-Wisp Fl	Slug Flow
0.325	4.855	325.010	46.184	SlugFlow	Slug Flow	Slug-Plug Flow	Slug Flow
0.305	6.227	303.698	40.281	SlugFlow	Annular Flow	Slug-Plug Flow	Slug Flow
0.201	6.243	200.811	26.777	SlugFlow	Annular Flow	Wavy Flow	Slug Flow
0.271	4.805	266.413	45.717	SlugFlow	Slug Flow	Slug-Plug Flow	Slug Flow

The slug flow observations in the horizontal flow experiments are shown in the flow pattern map of Baker (1954) in figure 5.16. A few data are very far from the transition line of slug and annular flow. Most of the experimental data are located in the region of transition of slug and annular flow. There was no an annular flow in the slug flow observations in the horizontal flow experiments. Most of the flow patterns were the slugs with different lengths and frequencies. Some of the slug flow observations consisted no bubble in the liquid body. They were developed slugs without bubbles. There were some slugs in the observations that they had some bubbles only in their noses, namely, they were bubbly fronted slugs. These bubbly fronted slugs had the developed lengths, but different frequencies. Three of the slug flow observations were slug flow with growing lengths. The growth of their lengths were not completed until the end of the test section. These observed details were not able to demonstrate in the flow pattern maps. The slug flow observations are not well predicted by the Baker's map.

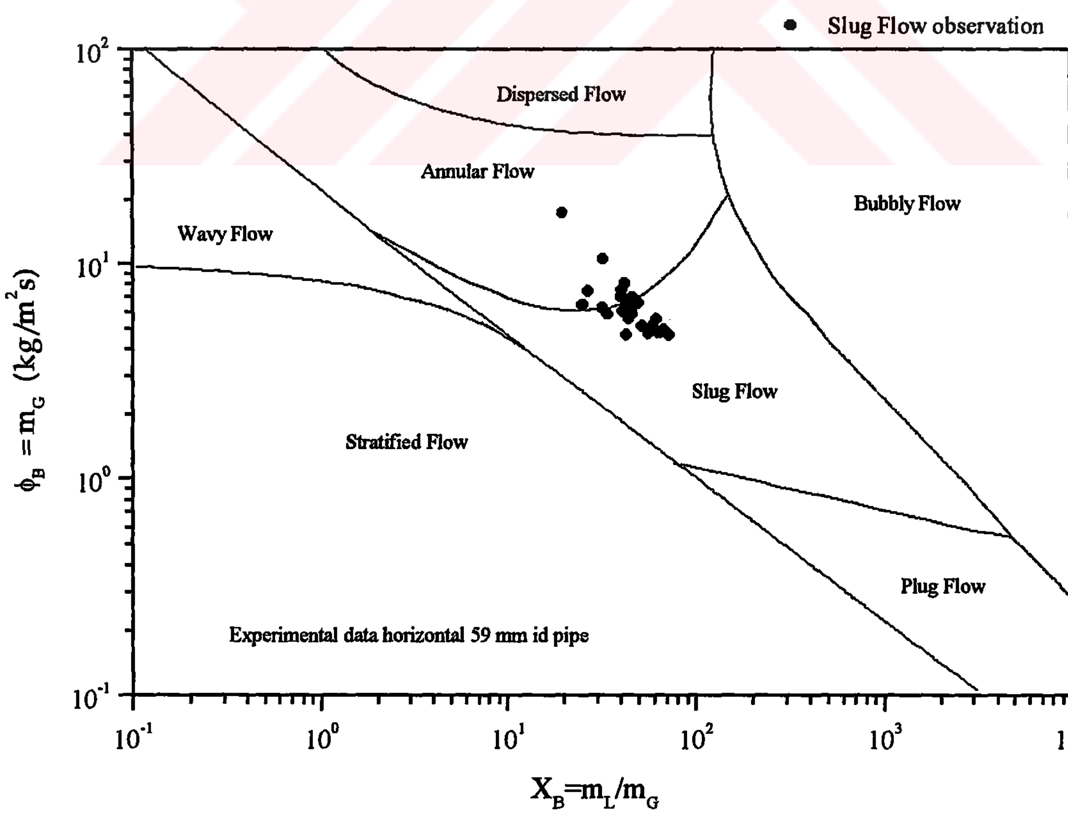

Figure 5.16. Slug flow observations in the Baker's flow pattern map.

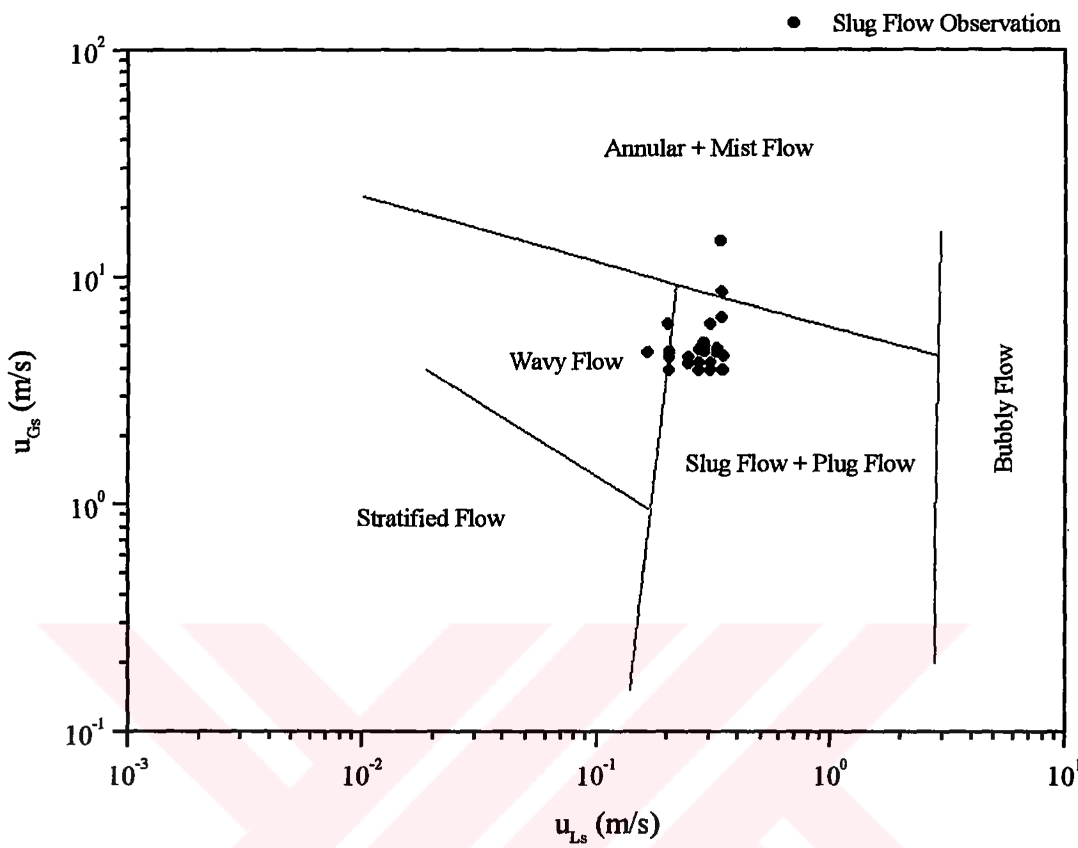

Figure 5.17. Slug flow observations in the Weisman's flow pattern map.

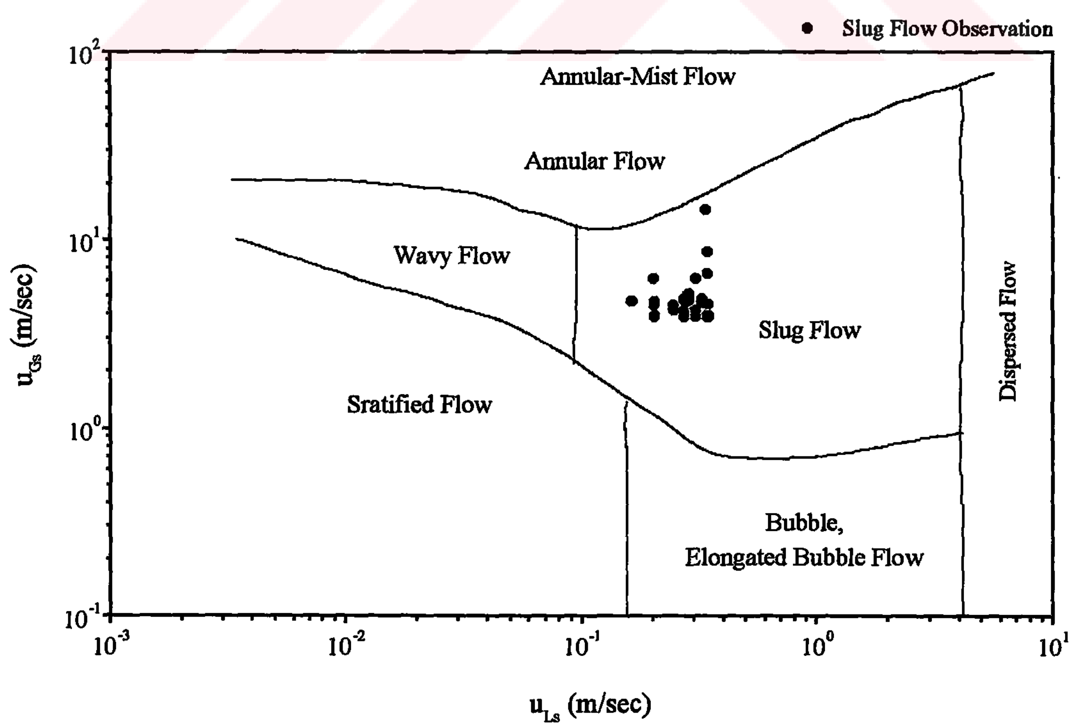

Figure 5.18. Slug flow observations in the Mandhane's flow pattern map.

The same slug flow observations are shown in figure 5.17. in the flow pattern map of Weisman (1979). The estimations of the Weisman's map are better than those of the Baker's map.

The slug flow observations of horizontal flow experiments are well predicted by the flow pattern map of Mandhane (1974) than the Weisman's map. The all data shown in figure 5.18. are located in the slug flow predictions of Mandhane's map. One can express that the slug flow observations are best predicted by the Mandhane's flow pattern map.

The annular flow observations are given in table (5.6), and shown in figure 5.19. in the flow pattern map of Baker (1954). They are well predicted except the three data in the region of wavy flow.

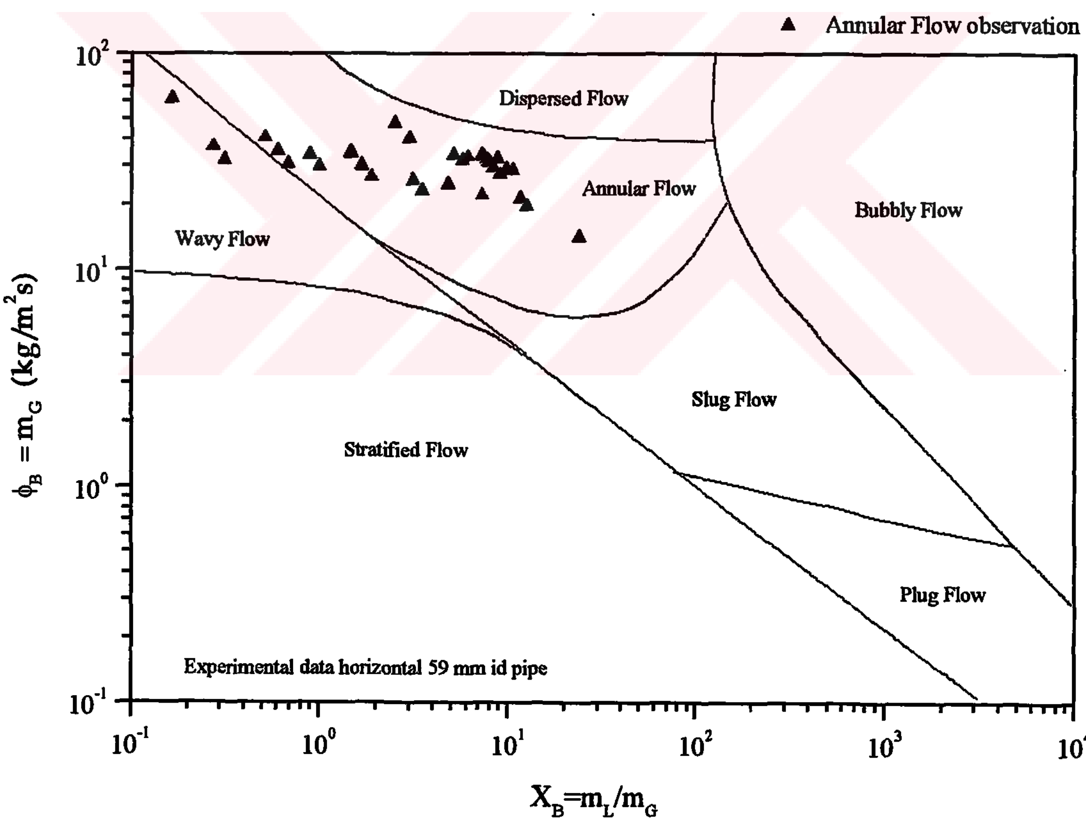

Figure 5.19. Annular flow observations in the Baker's flow pattern map.

The annular flow observations of the horizontal flow experiments are shown in figure 5.20. in the flow pattern map of Weisman (1979). The same data are shown in figure 5.21. in the flow pattern map of Mandhane (1974). A few data are sit in the slug flow region of Mandhane's map.

Table 5.6. The experimental data visually observed as "Annular flow".

U_{Ls} (m/s)	U_{Gs} (m/s)	m_L/m_G (kg/m2s)	mG (kg/m2s)	Flw Pat. Observed	Flw Pat. Baker	Flw Pat. Weisman	Flw Pat. Mandhane
0.010	42.744	0.164	61.958	Annular Flow	Wavy Flow	Annular-Wisp Fl	Ann.Mist
0.026	21.894	0.675	30.994	Annular Flow	Annular Flow	Annular-Wisp Fl	Ann.Mist
0.022	24.677	0.592	35.322	Annular Flow	Annular Flow	Annular-Wisp Fl	Ann.Mist
0.021	28.231	0.509	41.075	Annular Flow	Annular Flow	Annular-Wisp Fl	Ann.Mist
0.030	25.549	0.880	34.193	Annular Flow	Annular Flow	Annular-Wisp Fl	Ann.Mist
0.051	22.012	1.650	30.524	Annular Flow	Annular Flow	Annular-Wisp Fl	Ann.Mist
0.050	23.189	1.671	30.155	Annular Flow	Annular Flow	Annular-Wisp Fl	Ann.Mist
0.050	26.356	1.452	34.695	Annular Flow	Annular Flow	Annular-Wisp Fl	Ann.Mist
0.163	15.012	7.239	22.310	Annular Flow	Annular Flow	Annular-Wisp Fl	Ann.Mist
0.256	15.564	11.488	21.431	Annular Flow	Annular Flow	Annular-Wisp Fl	Ann.Mist
0.256	23.018	8.924	27.575	Annular Flow	Annular Flow	Annular-Wisp Fl	Ann.Mist
0.256	25.384	8.277	29.724	Annular Flow	Annular Flow	Annular-Wisp Fl	Ann.Mist
0.254	26.952	7.866	31.274	Annular Flow	Annular Flow	Annular-Wisp Fl	Ann.Mist
0.251	28.108	7.578	32.460	Annular Flow	Annular Flow	Annular-Wisp Fl	Ann.Mist
0.249	29.844	7.175	34.275	Annular Flow	Annular Flow	Annular-Wisp Fl	Ann.Mist
0.335	11.904	23.665	14.288	Annular Flow	Annular Flow	Annular-Wisp Fl	Slug Flow
0.010	24.719	0.314	32.386	Annular Flow	Wavy Flow	Annular-Wisp Fl	Ann.Mist
0.010	28.004	0.273	37.174	Annular Flow	Wavy Flow	Annular-Wisp Fl	Ann.Mist
0.030	23.058	0.992	30.335	Annular Flow	Annular Flow	Annular-Wisp Fl	Ann.Mist
0.051	24.703	1.443	34.890	Annular Flow	Annular Flow	Annular-Wisp Fl	Ann.Mist
0.081	18.743	3.118	25.894	Annular Flow	Annular Flow	Annular-Wisp Fl	Ann.Mist
0.122	17.093	4.779	24.937	Annular Flow	Annular Flow	Annular-Wisp Fl	Ann.Mist
0.122	28.997	2.493	47.814	Annular Flow	Annular Flow	Annular-Wisp Fl	Ann.Mist
0.173	27.765	5.050	34.031	Annular Flow	Annular Flow	Annular-Wisp Fl	Ann.Mist
0.181	25.816	5.676	32.328	Annular Flow	Annular Flow	Annular-Wisp Fl	Ann.Mist
0.203	21.320	5.997	33.401	Annular Flow	Annular Flow	Annular-Wisp Fl	Ann.Mist
0.244	13.695	12.423	19.802	Annular Flow	Annular Flow	Annular-Wisp Fl	Slug Flow
0.244	20.233	7.706	31.921	Annular Flow	Annular Flow	Annular-Wisp Fl	Ann.Mist
0.284	20.390	8.708	32.619	Annular Flow	Annular Flow	Annular-Wisp Fl	Ann.Mist
0.315	17.373	10.473	28.869	Annular Flow	Annular Flow	Annular-Wisp Fl	Ann.Mist

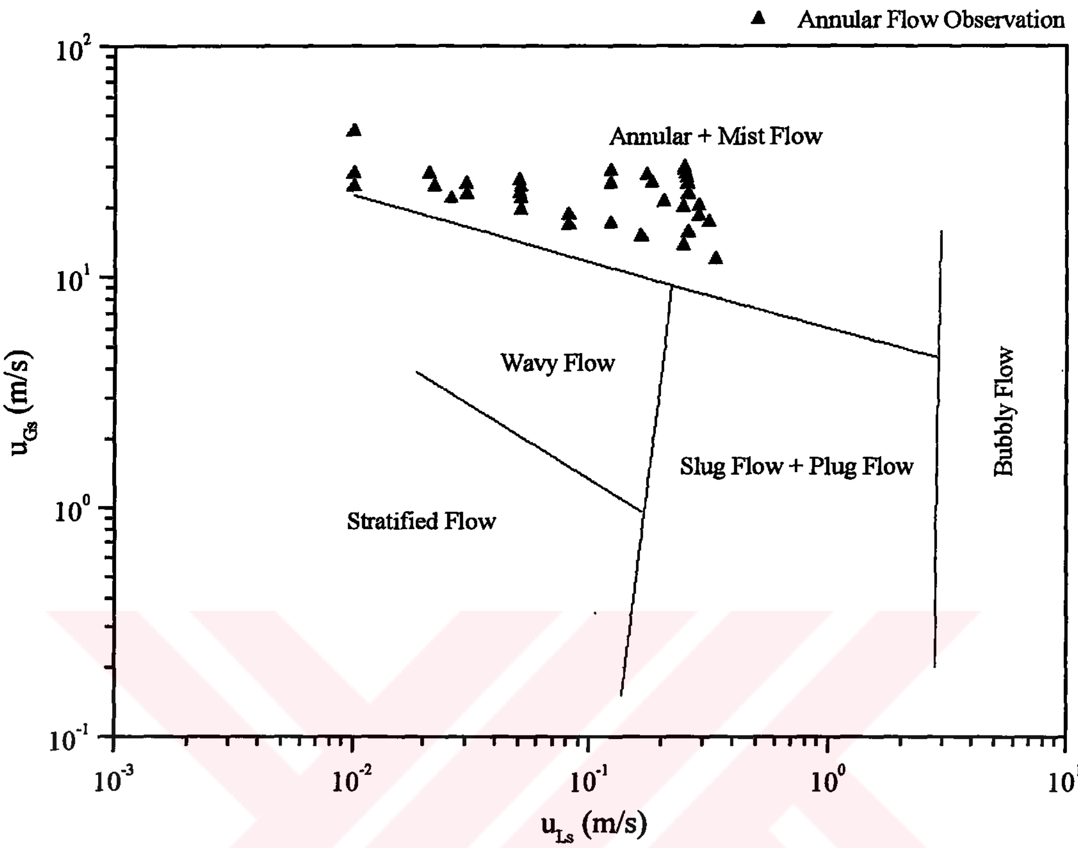

Figure 5.20. Annular flow observations in the Weisman's flow pattern map.

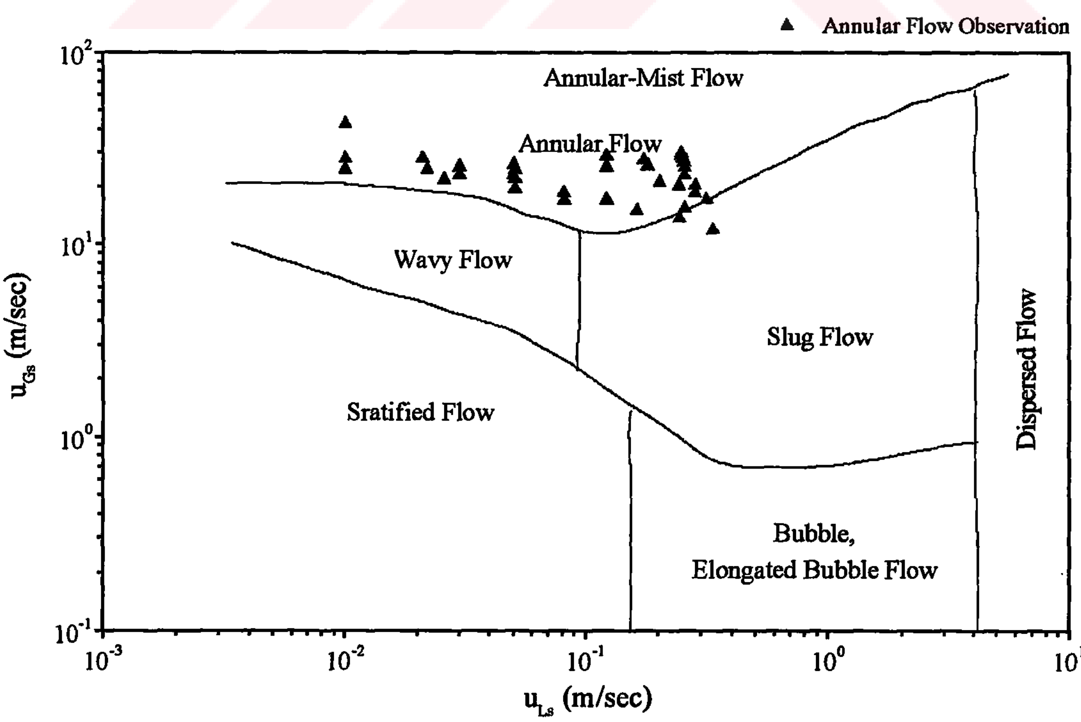

Figure 5.21. Annular flow observations in the Mandhane's flow pattern map.

The annular flow observations of the horizontal flow experiments are best predicted by the flow pattern map of Weisman (1979). The predictions of Mandhane's map are more suitable than the predictions of the Baker's map.

Some of the experimental data in horizontal flow were observed as mist flow-annular flow. These data were originally annular flow, but the flow patterns observed tended to be mist flow slightly. These flow patterns are as "Annular+Mist Flow", and their data are given in table (5.7).

The "Annular+Mist Flow" observations are shown in figure 5.22. in the flow pattern map of Baker (1954). These types of observations are located in the near of dispersed region of the Baker's map. One of the experimental data of the horizontal flow is in the region of wavy flow. The other data are well predicted by the Baker's map. The upper region of these data are not observed because of the limits of the experimental setup. The observed flow patterns in that region were very mixed, completely unordered and chaotic.

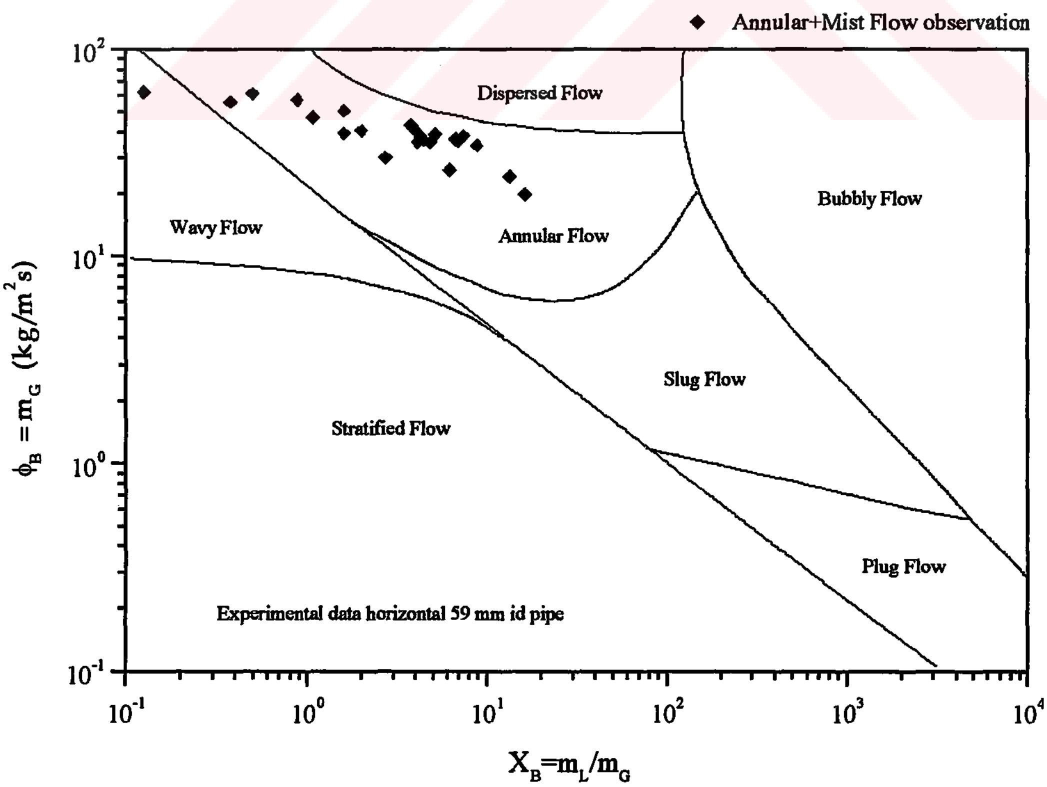

Figure 5.22. Annular+mist flow observations in the Baker's flow pattern map.

Table 5.7. The experimental data visually observed as "Annular+mist flow".

U_{Ls} (m/s)	U_{Gs} (m/s)	m_L/m_G (kg/m2s)	mG (kg/m2s)	Flw Pat. Observed	Flw Pat. Baker	Flw Pat. Weisman	Flw Pat. Mandhane
0.030	40.412	0.491	61.331	Annular+Mist Flow	Annular Flow	Annular-Wisp Fl	Ann.Mist
0.051	31.275	1.069	47.104	Annular+Mist Flow	Annular Flow	Annular-Wisp Fl	Ann.Mist
0.051	36.788	0.873	57.682	Annular+Mist Flow	Annular Flow	Annular-Wisp Fl	Ann.Mist
0.081	26.985	1.986	40.652	Annular+Mist Flow	Annular Flow	Annular-Wisp Fl	Ann.Mist
0.081	31.901	1.590	50.771	Annular+Mist Flow	Annular Flow	Annular-Wisp Fl	Ann.Mist
0.163	17.649	6.137	26.325	Annular+Mist Flow	Annular Flow	Annular-Wisp Fl	Ann.Mist
0.163	26.289	3.737	43.238	Annular+Mist Flow	Annular Flow	Annular-Wisp Fl	Ann.Mist
0.168	30.937	4.372	36.967	Annular+Mist Flow	Annular Flow	Annular-Wisp Fl	Ann.Mist
0.168	32.022	4.211	38.381	Annular+Mist Flow	Annular Flow	Annular-Wisp Fl	Ann.Mist
0.165	33.346	4.022	40.177	Annular+Mist Flow	Annular Flow	Annular-Wisp Fl	Ann.Mist
0.173	29.843	4.787	35.889	Annular+Mist Flow	Annular Flow	Annular-Wisp Fl	Ann.Mist
0.203	24.361	5.122	39.113	Annular+Mist Flow	Annular Flow	Annular-Wisp Fl	Ann.Mist
0.244	22.785	6.679	36.831	Annular+Mist Flow	Annular Flow	Annular-Wisp Fl	Ann.Mist
0.247	31.368	6.804	36.139	Annular+Mist Flow	Annular Flow	Annular-Wisp Fl	Ann.Mist
0.244	32.358	6.648	36.984	Annular+Mist Flow	Annular Flow	Annular-Wisp Fl	Ann.Mist
0.284	23.464	7.385	38.472	Annular+Mist Flow	Annular Flow	Annular-Wisp Fl	Ann.Mist
0.330	17.082	16.163	20.118	Annular+Mist Flow	Annular Flow	Annular-Wisp Fl	Slug Flow
0.330	20.479	13.299	24.511	Annular+Mist Flow	Annular Flow	Annular-Wisp Fl	Ann.Mist
0.007	41.633	0.124	62.335	Annular+Mist Flow	Wavy Flow	Annular-Wisp Fl	Ann.Mist
0.020	36.594	0.372	56.161	Annular+Mist Flow	Annular Flow	Annular-Wisp Fl	Ann.Mist
0.050	33.688	1.074	46.877	Annular+Mist Flow	Annular Flow	Annular-Wisp Fl	Ann.Mist
0.060	28.762	1.589	39.511	Annular+Mist Flow	Annular Flow	Annular-Wisp Fl	Ann.Mist
0.081	21.325	2.674	30.191	Annular+Mist Flow	Annular Flow	Annular-Wisp Fl	Ann.Mist
0.142	26.276	4.074	36.030	Annular+Mist Flow	Annular Flow	Annular-Wisp Fl	Ann.Mist
0.163	22.851	4.382	36.860	Annular+Mist Flow	Annular Flow	Annular-Wisp Fl	Ann.Mist
0.315	20.399	8.719	34.682	Annular+Mist Flow	Annular Flow	Annular-Wisp Fl	Ann.Mist

The "Annular+Mist Flow" observations are shown in figure 5.23. in the flow pattern map of Weisman (1979). All data are very far from the transition region of wavy and annular flow. The "Annular Flow" observations explained in the previous section were closer to this transition line than the "Annular+Mist Flow" observations. The same data are shown in figure 5.24. in the Mandhane's map. The observed data approach to the annular flow in the right end of the data. Moreover, one of the data is predicted as slug flow. Weisman's map is the best map to predict the "Annular+Mist Flow" observations.

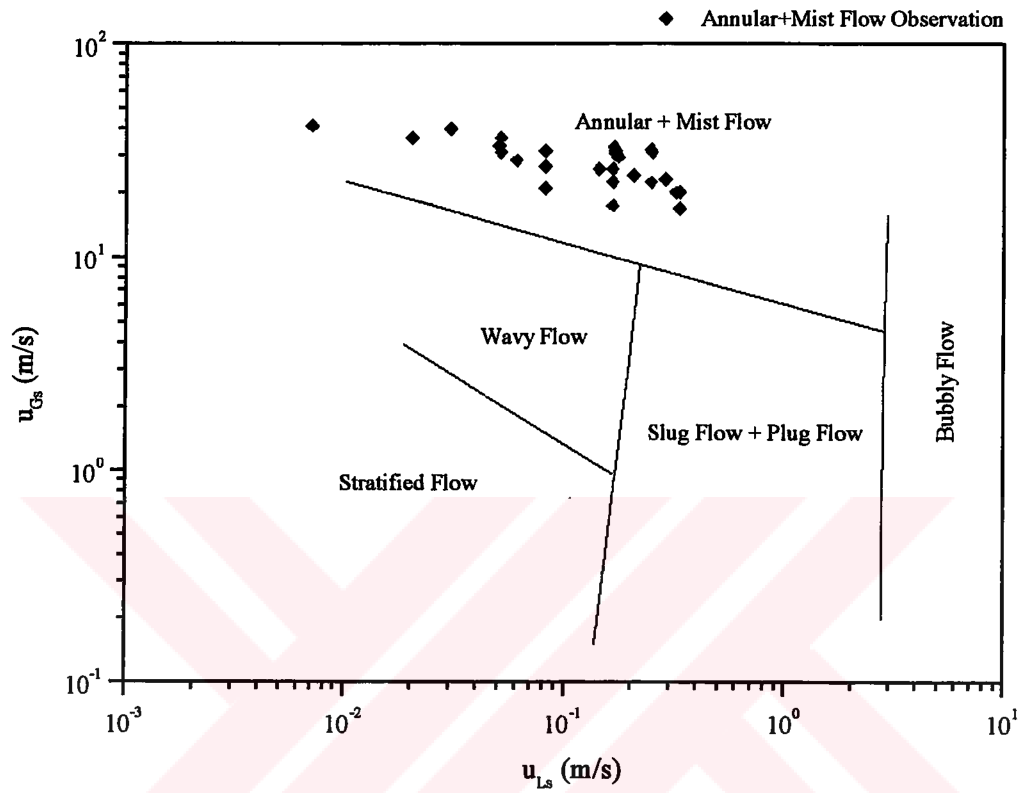

Figure 5.23. Annular+mist flow observations in the Weisman's flow pattern map.

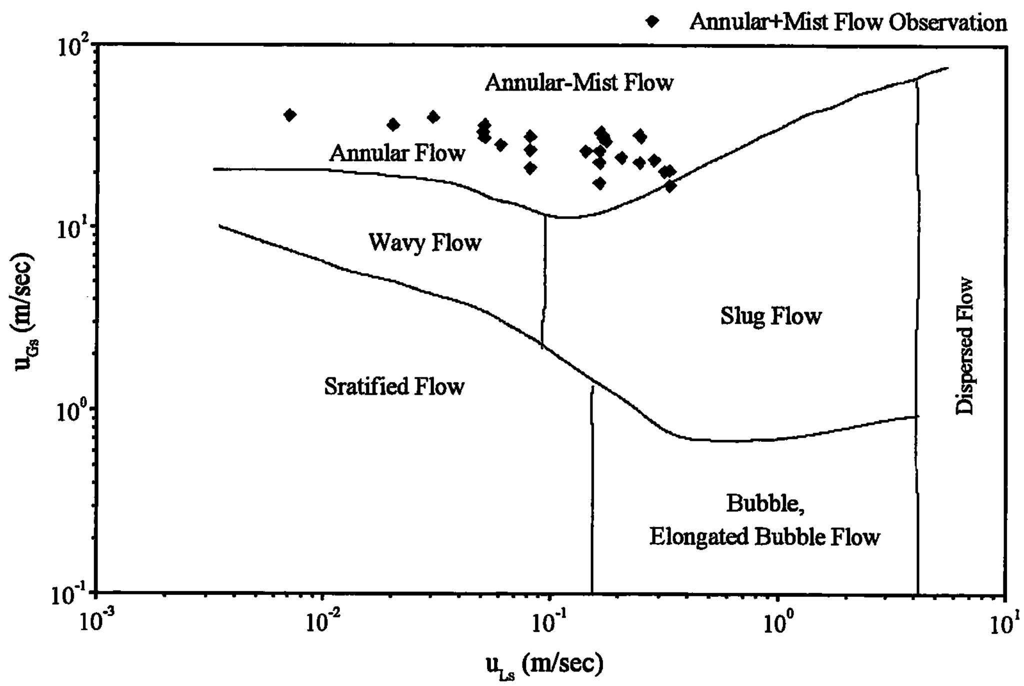

Figure 5.24. Annular+mist flow observations in the Mandhane's flow pattern map.

5.1.2. Flow Patterns of +5° Inclination Experiments

Flow patterns observed in +5° inclination experiments are compared with three different flow patterns maps. The first one is the flow pattern map of Weisman (1979) for horizontal pipes. This flow pattern map estimates the horizontal flow patterns better than the Baker's and Mandhane's maps. Therefore, the flow pattern map of Weisman is used to compare the flow patterns observations of +5° inclination experiments.

The second flow pattern map was proposed by Stanislav et al. (1986). They reported the results of experimental measurements of flow patterns, pressure gradients and liquid holdup for intermittent two phase flow in upward inclined pipes. The flow patterns observations of the investigators for the horizontal and +5° inclination experiments are shown in the same flow pattern map.

The third and last flow pattern map for the comparison of the flow patterns observed in the +5° inclination experiments was proposed by Spedding et al. (1998). They used flow rate ratio for the x-axis, and Froude number for the y-axis of the map. The flow patterns observations of Spedding et al. (1998) are found to be similar with those obtained in this study. However, there were some observations which were apparently different than those of Spedding et al. (1998). These observations are explained in this section.

The experimental observations of +5° inclination gas liquid flows are named as "Annular and rollwave (Ann+rollwave)", "Annular and droplet (Ann+droplet)", "Blow through slug (BTS)", "Blow through slug and annular (BTS+ann)", "Slug", "Slug stagnant", "Film and droplet (Film+droplet)", "Film and stratified wavy(Film+str wavy)", "Stratified wavy (str wavy)", and finally "Stratified and rollwave(Str+rollwave)".

The "Annular and rollwave" and "Annular and droplet" observations are taken into consideration in the same graph. These observations are shown in figure 5.25. in the flow pattern map of Weisman. Figure 5.26. and 5.27. show the comparisons of the experimental data with the flow patterns maps of Stanislav et al. (1986), and Spedding et al. (1998), respectively.

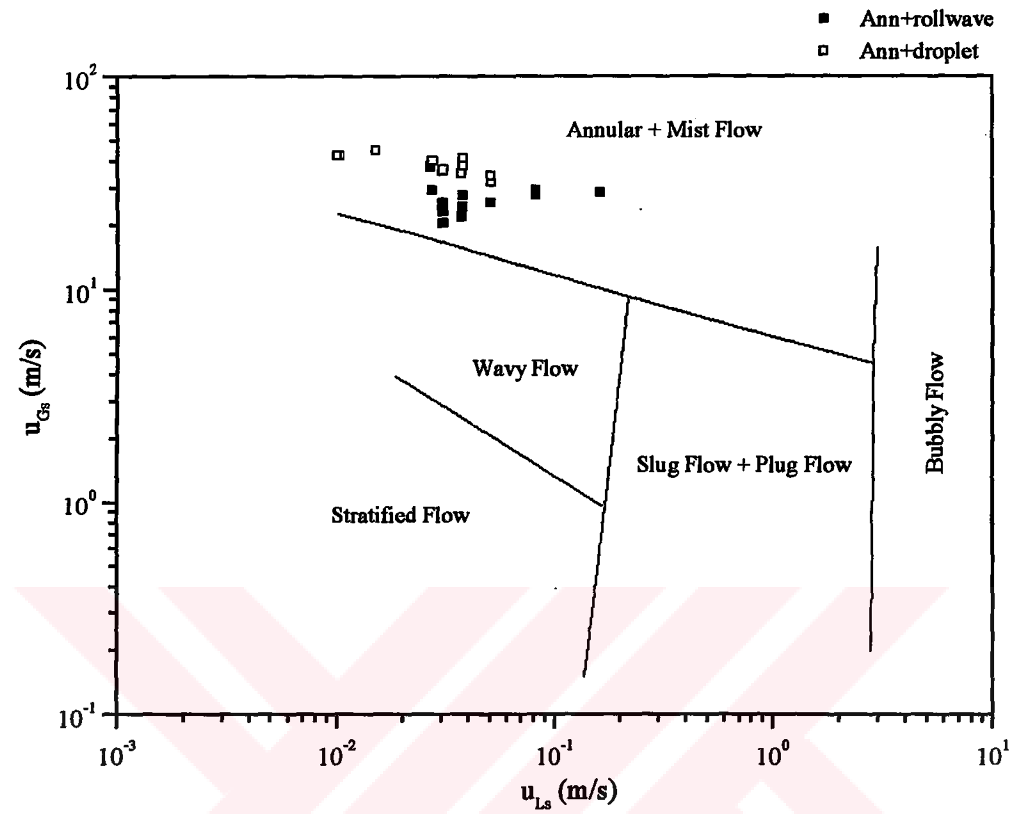

Figure 5.25. Ann+rollwave and ann+droplet flow observations in the Weisman's flow pattern map.

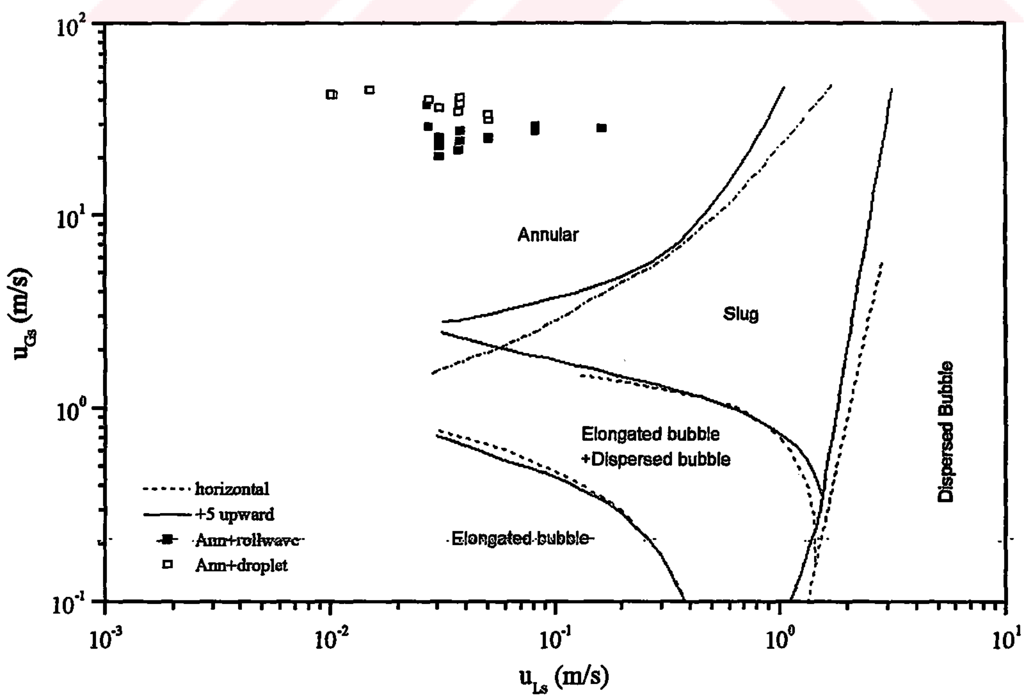

Figure 5.26. Ann+rollwave and ann+droplet flow observations in the Stanislav's flow pattern map.

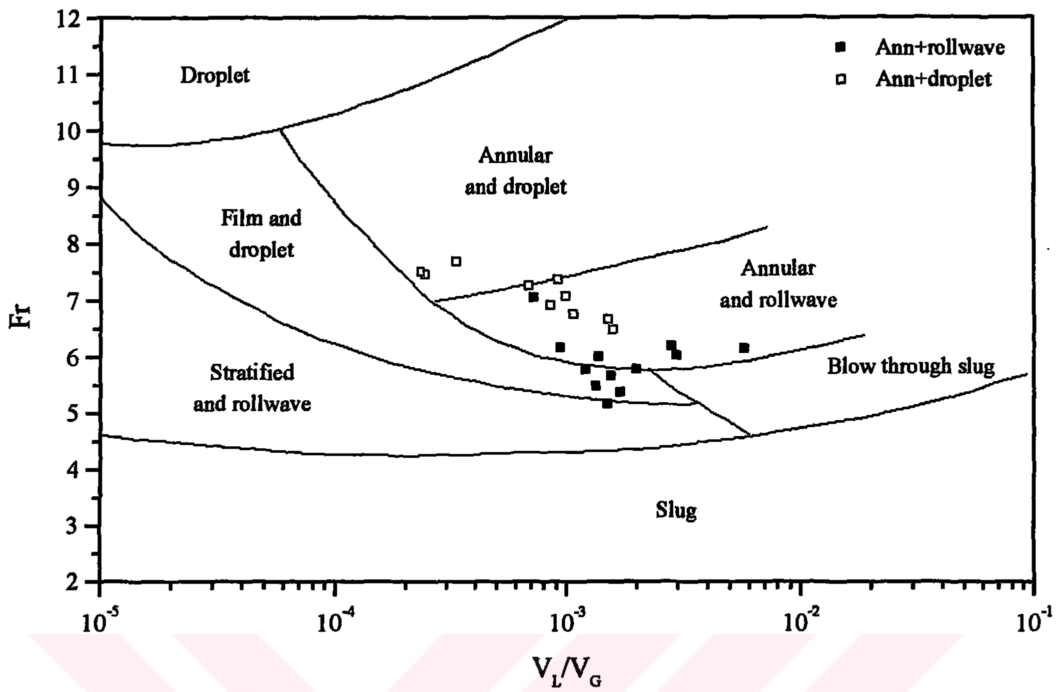

Figure 5.27. Ann+rollwave and ann+droplet flow observations in the Spedding's flow pattern map.

The flow pattern map of Weisman also estimates reasonably the +5° inclination data besides the horizontal data. The "Annular and rollwave" observations are located in the lower region of the "Annular and droplet" observations. This result is physically logic because the roll waves are dispersed as the superficial gas velocity is increased. The second flow pattern map, Stanislav's map, also shows the differences between the observations of horizontal and +5° inclination experiments. The horizontal flow pattern map of Stanislav is different than the flow pattern map of Weisman. The Stanislav's flow pattern map is important because of the comparisons of the horizontal and +5° inclination experiments. The transition between slug and annular flow in the +5° inclination experiments occurs at higher superficial gas velocities than the horizontal flow conditions. Stanislav et al. (1986) did not describe any detailed flow pattern inside the annular flow region. But, there is seemingly a transition region between "Ann+rollwave" and "Ann+droplet".

The "Annular and rollwave" and "Annular and droplet" observations are shown in figure 5.27. in the flow pattern map of Spedding et al. (1998). The number of the observations is not enough to obtain a general conclusion. However, the observed data locate in the appropriate regions. In some observations, it is not possible to define a definite flow pattern. One can see the traces of different flow patterns at the same observation.

The "BTS", "BTS+ann", "Slug", and "Slug stagnant" flow observations are shown in figure 5.28. in the Weisman's map. The "BTS" flow sit between the "Slug" flow and "BTS+ann" flow. Many data points in the +5° inclination experiments were observed as "BTS" flow. But, some of the data points locate in the annular flow region of the flow pattern map of Weisman. It is known that Weisman's map was proposed for the horizontal flow conditions, and it is evident from Stanislav's map that the transition between slug and annular flow in the +5° inclination gas liquid flows is higher than that of the horizontal flow. Therefore, the "BTS" flow observations sit in the annular flow of Weisman's map is found reasonable. The "BTS" flow region for the +5° inclination experiments have located in the upper region of "BTS" flow observed in the horizontal flow experiments.

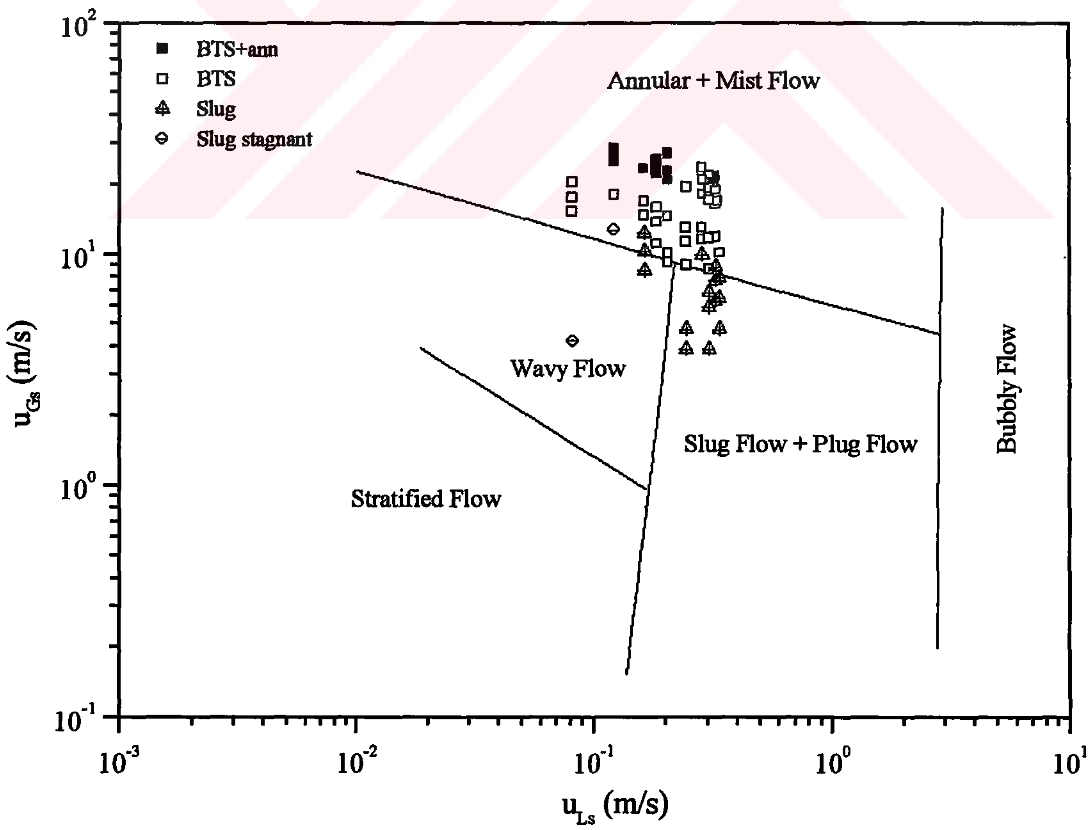

Figure 5.28. BTS+ann, BTS, Slug, and Slug stagnant flow observations in the Weisman's flow pattern map.

The same observations are shown in figures 5.29. and 5.30. in the flow pattern maps of Stanislav and Spedding, respectively.

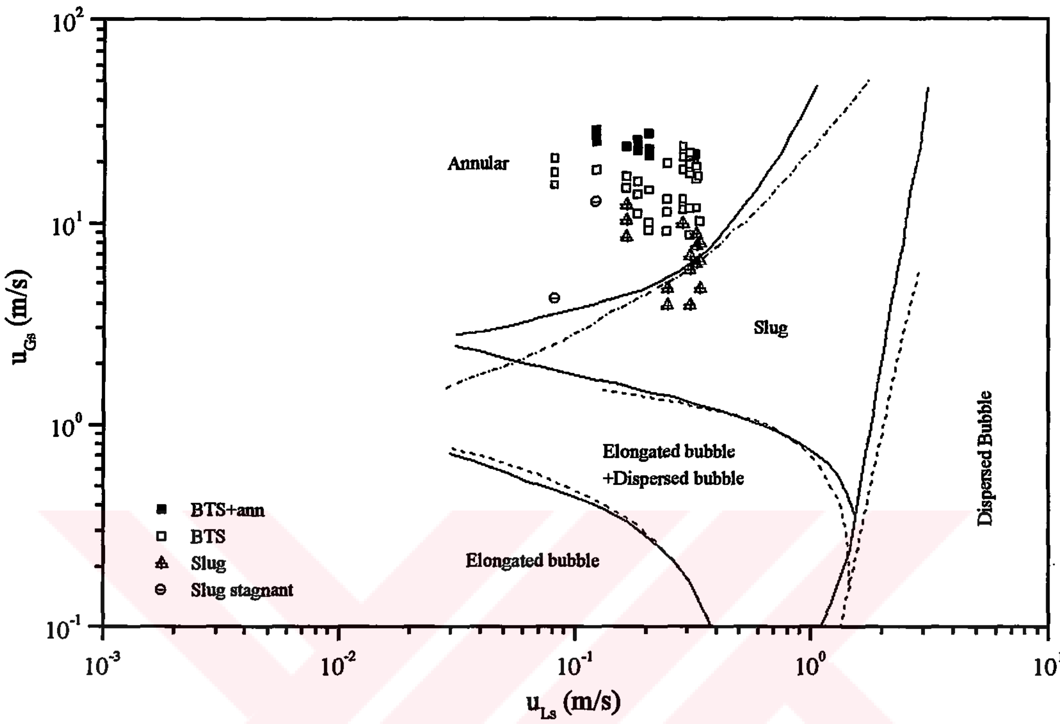

Figure 5.29. BTS+ann, BTS, Slug, and Slug stagnant flow observations in the Stanislav's flow pattern map.

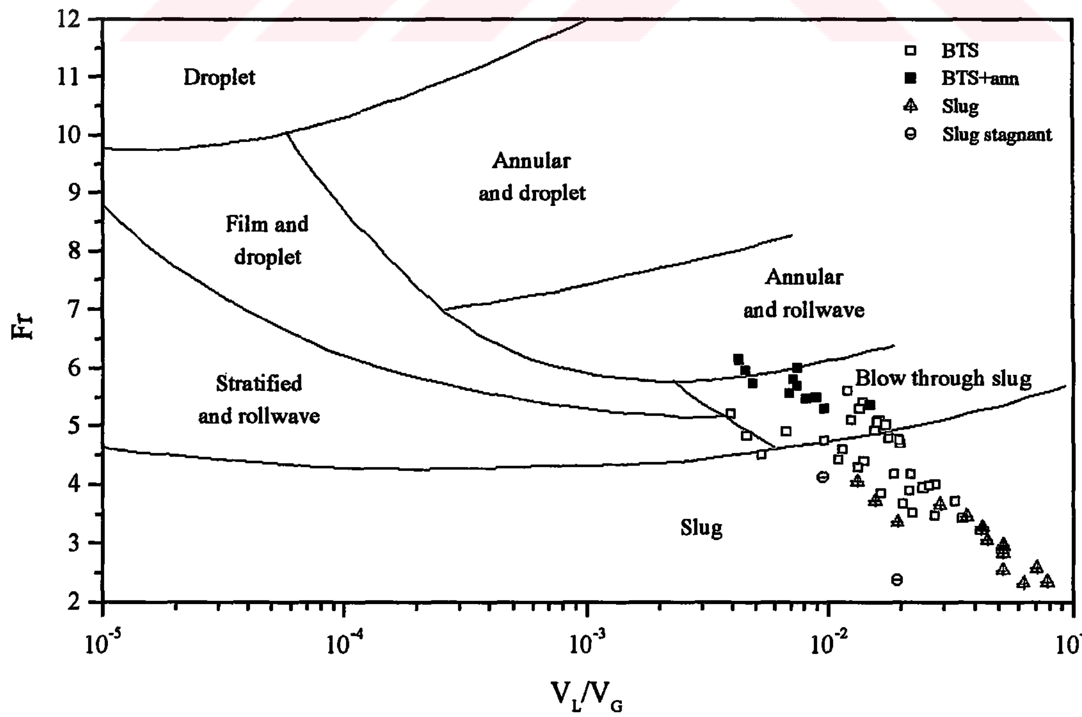

Figure 5.30. BTS+ann, BTS, Slug, and Slug stagnant flow observations in the Spedding's flow pattern map.

The flow pattern maps of Stanislav and Spedding predict approximately the observed flow patterns. The "BTS" flow region in the Stanislav's map can be clearly seen in figure 5.29. Some of the "Slug" flow observations are seen in the region of "BTS" flow observations. The "BTS" and "Slug" flow observations are approximately similar to each other in that region. The observed flow patterns consist very frothy liquid bulks. These fully frothy liquid bulks gave sometimes an impression of "BTS" or sometimes "Slug" flow.

The estimations of Spedding's map are found to be reasonable. The "BTS+ann" observations locate in the appropriate region of the map. The "BTS" observations also locate in the appropriate region, but the same confusions have arisen for the estimations of "BTS" and "Slug" flow. The fully slug flow is observed in the lower regions of this map. At the near of the blow through slug region of the map, the flow patterns more resemble to the "BTS" flow than the "Slug" flow.

The "Slug stagnant" observations are very interesting flow patterns. The formations of these flow patterns are completed in two or three steps. A frothy liquid bulk starts its movement in the test pipe. But, the gravity force and the shear stress acting on this bulk prevent reaching of the frothy liquid bulk until the end of the pipe. This bulk waits for a moment in any place in the pipe. Another liquid bulk behind this stagnant bulk are exposed to the same conditions and finally two or three liquid bulks join each other. The unified liquid bulks obstruct the pipe cross-section completely. This newly formed slug comes back a little bit in the inclined test pipe, and stops last time to start its forward movement. This flow pattern observation is been called as "Slug stagnant".

The "Film+str wavy", "Film+droplet", "Str+wavy", and "Str+rollwave" observations are shown in figures 5.31., 5.32., and 5.33. in the flow pattern maps of Weisman, Stanislav and Spedding. These observed data were similar each other in many respects. The approximately all had a stratified layer more or less. Most of the observations were wavy and some of them consisted film flow additionally. The observations are located in the appropriate region in this respect.

The flow pattern map of Spedding (1998) estimates these observations best. The "Film+droplet" observations are approximately good predicted. The "Film+str wavy" observations are located in the intersection of the "Film and droplet" and "Stratified and rollwave" regions of the map.

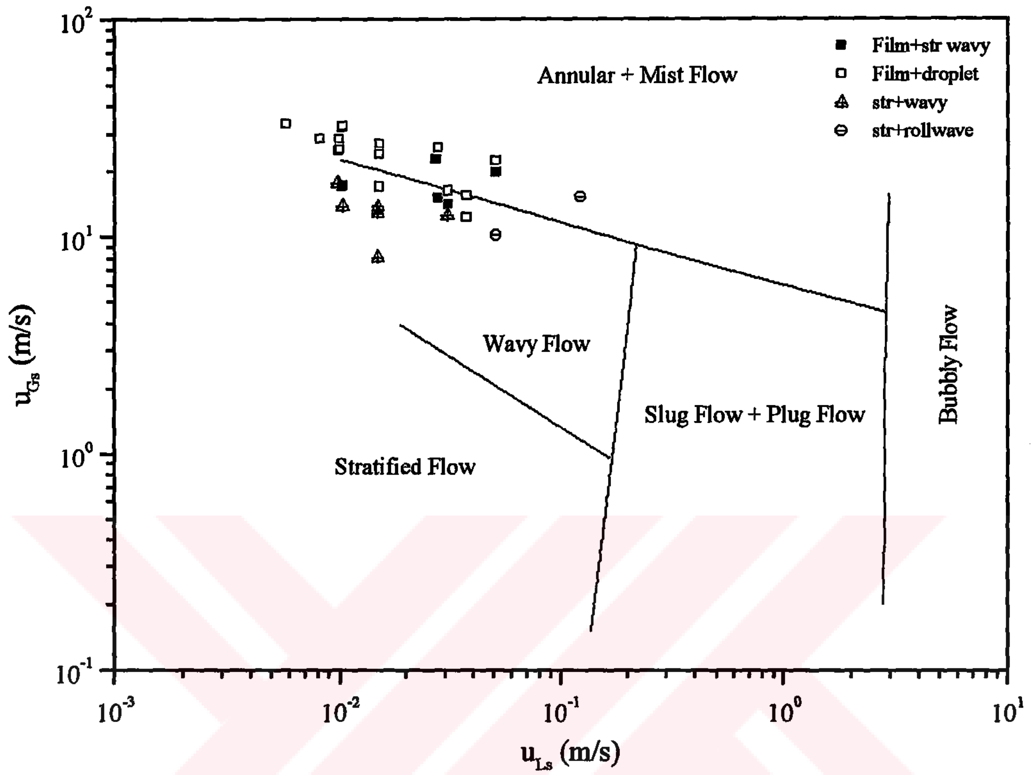

Figure 5.31. Film+str wavy, Film+droplet, str+wavy, and str+rollwave flow observations in the Weisman's flow pattern map.

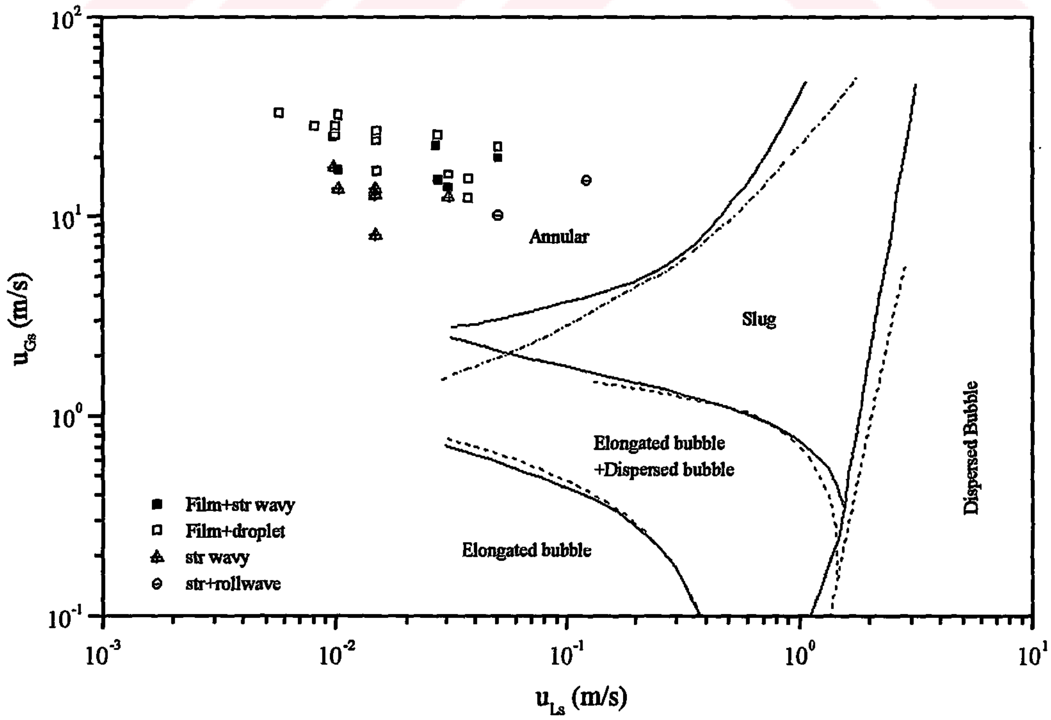

Figure 5.32. Film+str wavy, Film+droplet, str+wavy, and str+rollwave flow observations in the Stanislav's flow pattern map.

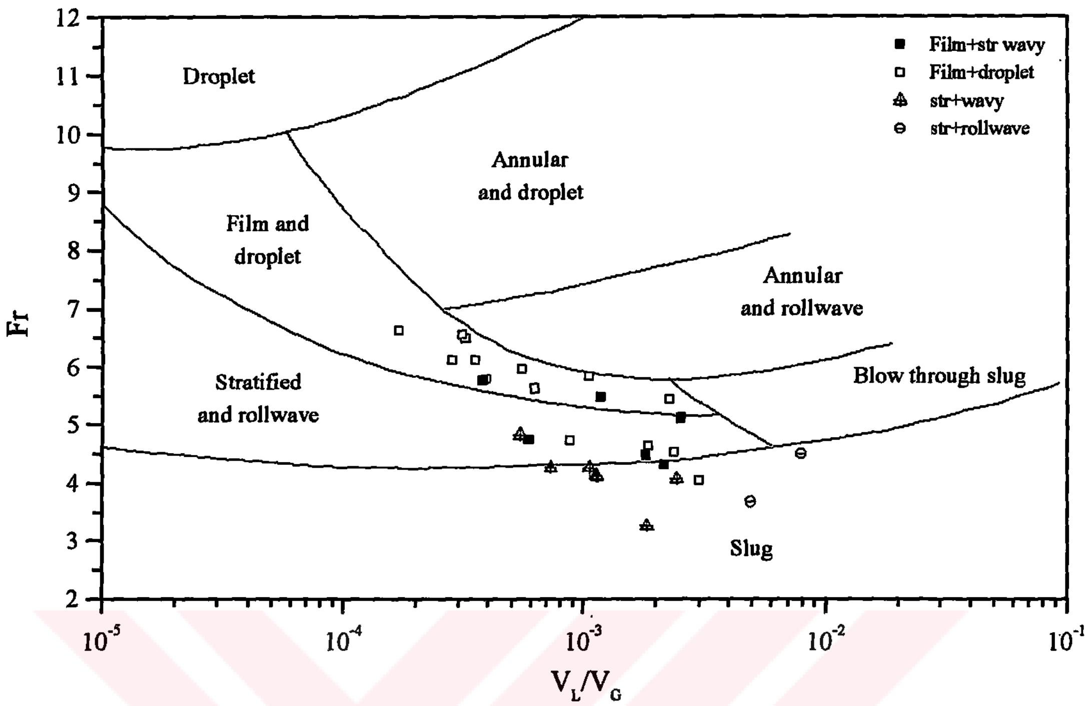

Figure 5.33. Film+str wavy, Film+droplet, str+wavy, and str+rollwave flow observations in the Spedding's flow pattern map.

5.1.3. Flow Patterns of +10° Inclination Experiments

The flow pattern observations of +10° inclination experiments are shown in figure 5.34. This flow pattern map was proposed by Shoham (1983) for 10° upward gas liquid flows. The observed flow patterns are annular, slug, elongated bubble, dispersed bubble, stratified wavy, and wavy-annular flow. The transition lines seen in the flow pattern map are drawn between the markers of the Shoham's observations. Thus, the transition lines of the flow patterns observed by Shoham are obtained.

The experimental data observed in +10° inclination experiments are shown in figure 5.35. with the flow pattern observations of Shoham (1983). The similar flow patterns of +5° inclination experiments are also defined for the +10° inclination experiments. They can be seen in the legend of the flow pattern map.

Figure 5.35. shows the same flow pattern map of Shoham in different scales. The observed data of +10° inclination experiments have taken place in the correct and reasonable regions.

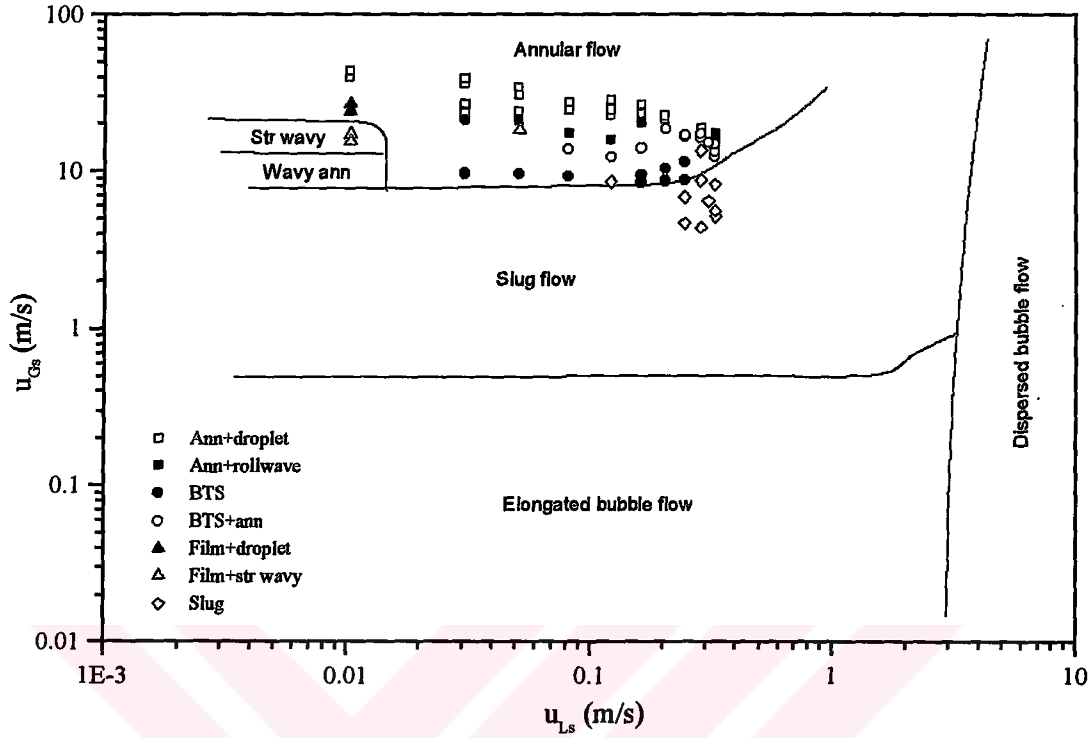

Figure 5.34. Flow pattern observations of +10° inclination experiments in the flow pattern map proposed by Shoham (1983) for 10° upward gas liquid flows.

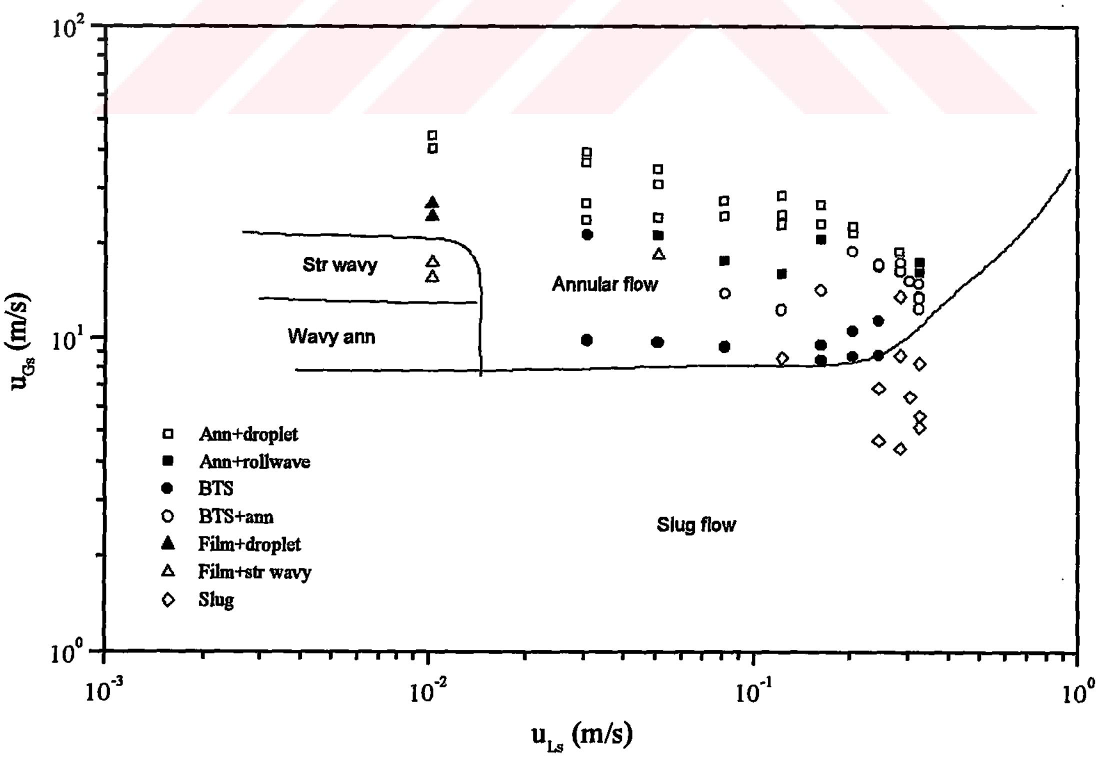

Figure 5.35. Flow pattern observations of +10° inclination experiments in the flow pattern map proposed by Shoham (1983) for 10° upward gas liquid flows.

The "Slug" and "BTS" flow observations are seen in the intersection region of slug and annular flow of the Shoham's map. The "Slug" flow observations are mostly located under the transition line of slug-annular flow. The "BTS" observations are predicted very well. They sit just over the transition line of slug-annular flow. That means slugs start deterioration to form an annular flow as the superficial gas velocity is increased. The first step of this deterioration is the "BTS" flow.

The "BTS+ann" observations are located over the "BTS" flow region. The second step of the transformation to annular flow is the "BTS+ann" flow. In this type flow pattern, the "BTS" flow can be obviously still seen, but there is a continuously annular film on the inner surface of the test pipe, at the same time.

The "Ann+rollwave" observations can be thought to be similar to the "Film+droplet" observations. The "Ann+rollwave" flow takes the form of "Film+droplet" flow, as the superficial liquid velocity is decreased.

The flow pattern map of Shoham shows the stratified wavy flow in a closed region. Two of the three observations of "Film+str wavy" flow pattern sit in that region. The third one is seen near the "Ann+rollwave" observations. These two observations are similar to each other very much. Therefore, the third data could possibly be predicted wrongly.

The "Ann+droplet" observations were obtained in the upper limits of the experimental system. These observations are well predicted by the flow pattern map of Shoham. They are very far from any transition line. The "Ann+droplet" observations can be thought as fully annular flow.

5.1.4. Flow Patterns of +15° Inclination Experiments

The +15° inclination experimental data of this investigation are shown in figure 5.36. The inclination value of 15° upwards is the maximum angle which can be reached at the experimental setup.

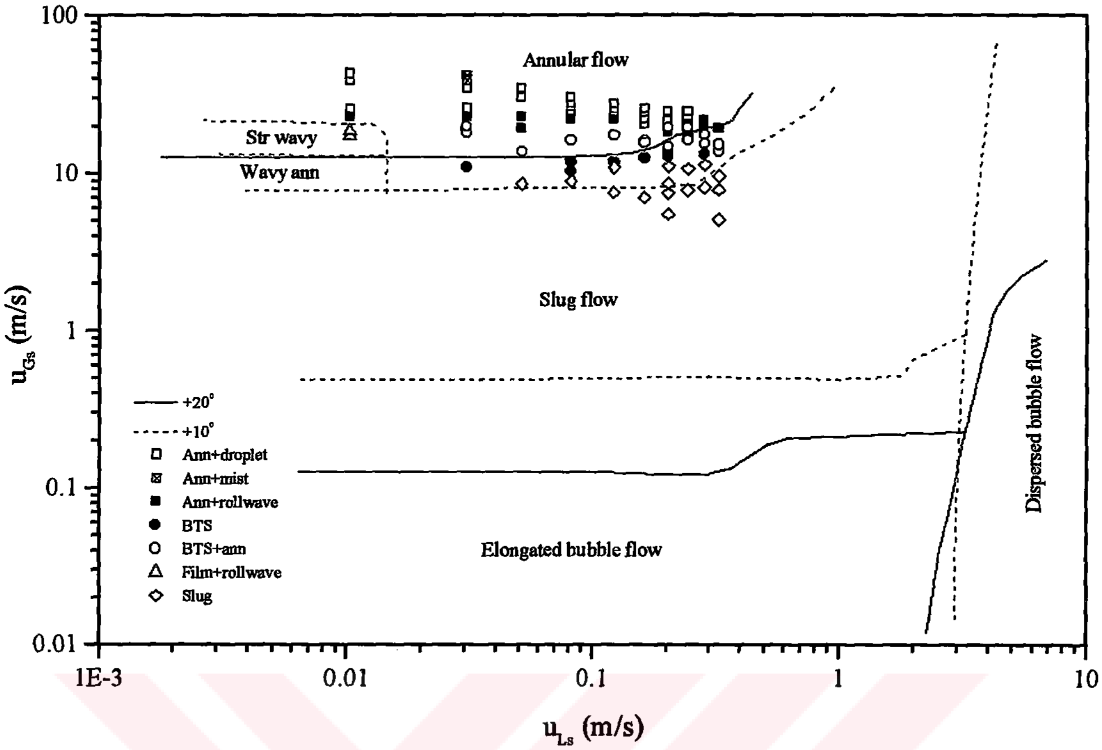

Figure 5.36. Flow pattern observations of +15° inclination experiments in the flow pattern map proposed by Shoham (1983) for 10° and 20° upward gas liquid flows.

The experimental observations of the +15° inclination experiments are compared with the experimental results of Shoham (1983). The transition lines were drawn between the observations of Shoham. The flow pattern observations of Shoham were given in two different inclinations of +10° and +20°. The 10° upwards gas liquid flow observations of Shoham are compared with the +10° experiments of this investigation. The +20° gas liquid flow observations of the same investigator are used to compare with the +15° inclination experiments of this investigation. The transition lines of Shoham's observations for the inclinations of +10° and +20° are shown in the same figure 5.36. with the experimental data of this investigation. This comparison gives reasonable results because the transitions of the experimental observed flow patterns of +15° inclination experiments are mostly located between those of the +10° and +20°.

Figure 5.37. shows the same flow pattern map of Shoham in different scales. The transition regions of the observed flow patterns of +15° inclination experiments can be clearly seen in this figure. The dashed and solid transition lines show the flow pattern transitions observed by Shoham for the inclinations of +10° and +20°, respectively.

The observed flow patterns of +15° inclination experiments have been called similar to those of the +10° inclination experiments. The transitions regions of the flow patterns of +15° inclination experiments have been seen more clear than the transitions regions of the flow patterns of +10° inclination experiments. The figure 5.38. shows the flow pattern map proposed by the author of this thesis.

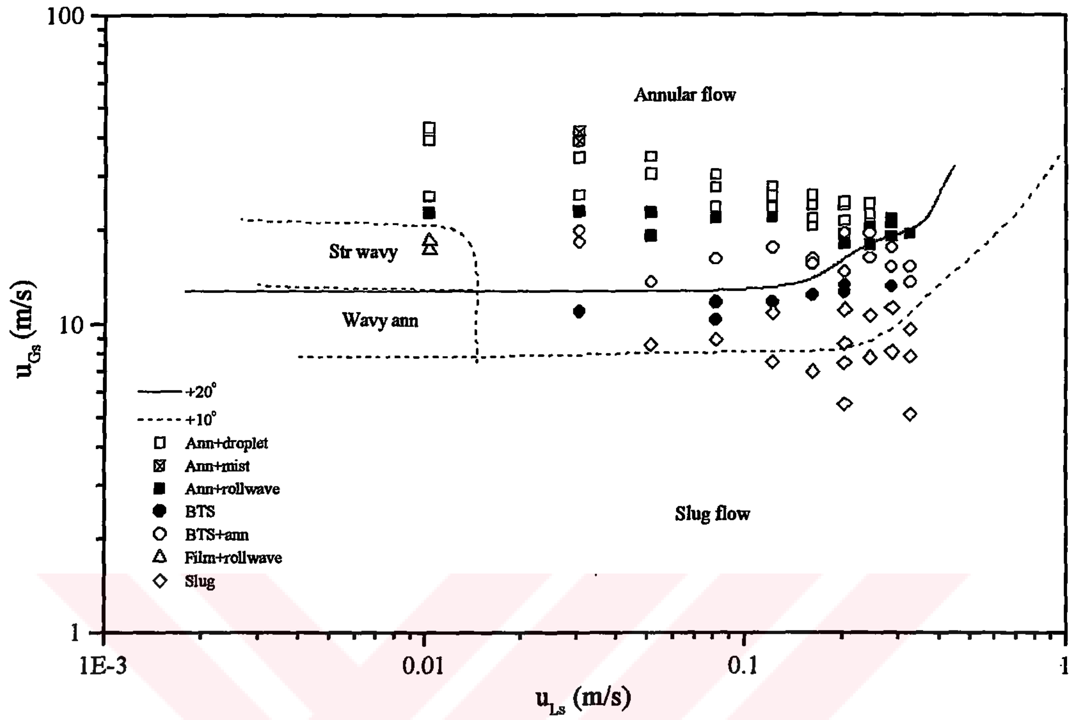

Figure 5.37. Flow pattern observations of +15° inclination experiments in the flow pattern map proposed by Shoham (1983) for 10° and 20° upward gas liquid flows.

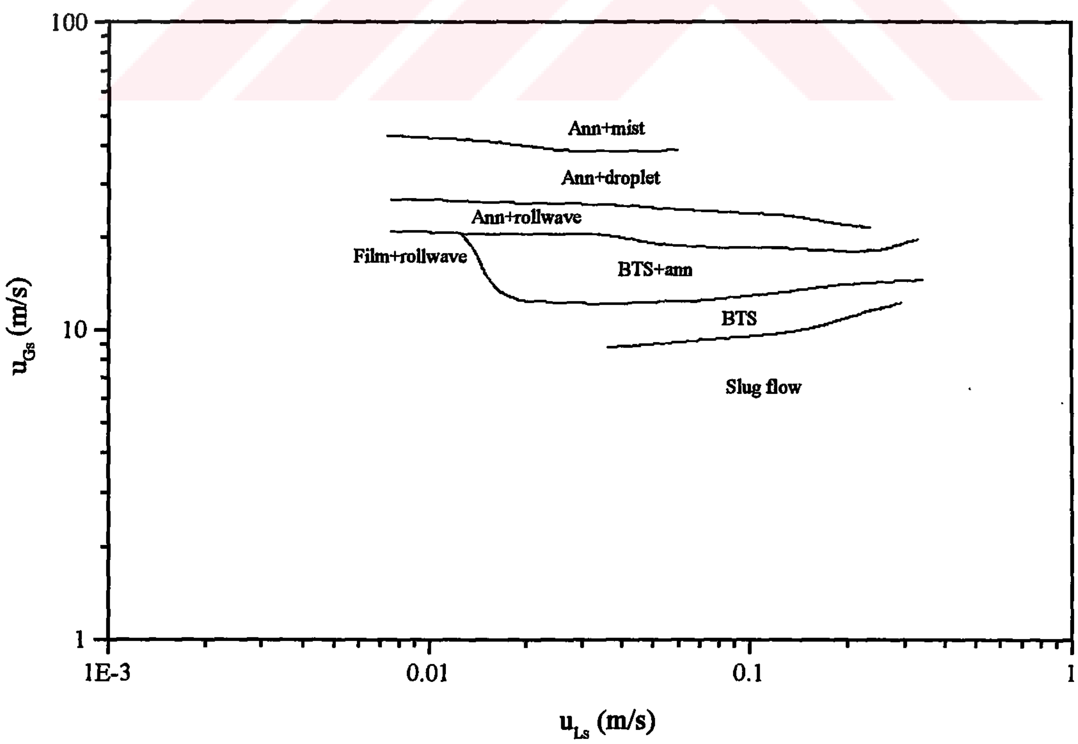

Figure 5.38. Flow pattern map proposed by the author for +15° inclination experiments.

The flow pattern transitions proposed in figure 5.38. above are valid only along the lines, because the except of these lines have not been studied in this investigation.

5.1.5. Pressure Losses of Horizontal, +5°, +10°, and +15° Inclination Experiments

Pressure losses are one of the most concerned subjects of gas liquid flows in industrial equipments. The pressure loss in any device is needed for the calculation of material strength of this device, for the selection of fan or pump which force the fluids pass through this device, for the determination of the power supplied to these devices that move fluid or gas by pressure or suction. The calculation of pressure loss for two phase flow phenomena is different than that of the single phase flow. Different empirical methods have been proposed by many investigators.

The Lockhart-Martinelli Method (LMM) is one of the well known methods to calculate pressure drop and void fraction. In this method, a definite portion of the flow area is assigned to each phase and it is assumed that conventional pressure drop equations can be applied to the flow path of each phase.

The Chisholm Method (CM) uses the equations proposed by Lockhart-Martinelli, but a new relation has been proposed by Chisholm for the calculation of constant C. The Boroczy-Chisholm Method (BCM) defines a different two-phase multiplier than that of the Lockhart-Martinelli Method. These empirical methods have been examined by Yılmaz (2001) in detail.

The pressure measurements carried out in this study are compared with the pressure losses calculated using the empirical methods of Lockhart-Martinelli, Chisholm, and Boroczy. The pressure drop per unit length is calculated using the total pressure difference and the distance between the pressure transducers for each experiment. The pressure drop per unit length (Pa/m) is represented with R, the first letter of "Resistance".

The experimentally obtained pressure losses are compared with each others for different inclinations of the experimental system. Although there are many experimental data for each inclination value, the experimental results presented here were obtained at the same superficial liquid velocities for all of the experiments with different inclinations. Therefore, the variation of pressure drop with superficial gas velocity is presented for a constant superficial liquid velocity but for different inclinations.

The variation of pressure drop with superficial gas velocity for horizontal gas liquid flow experiments is shown in figure 5.39. The values of superficial liquid velocities for all angles can be seen in the legend of this figure.

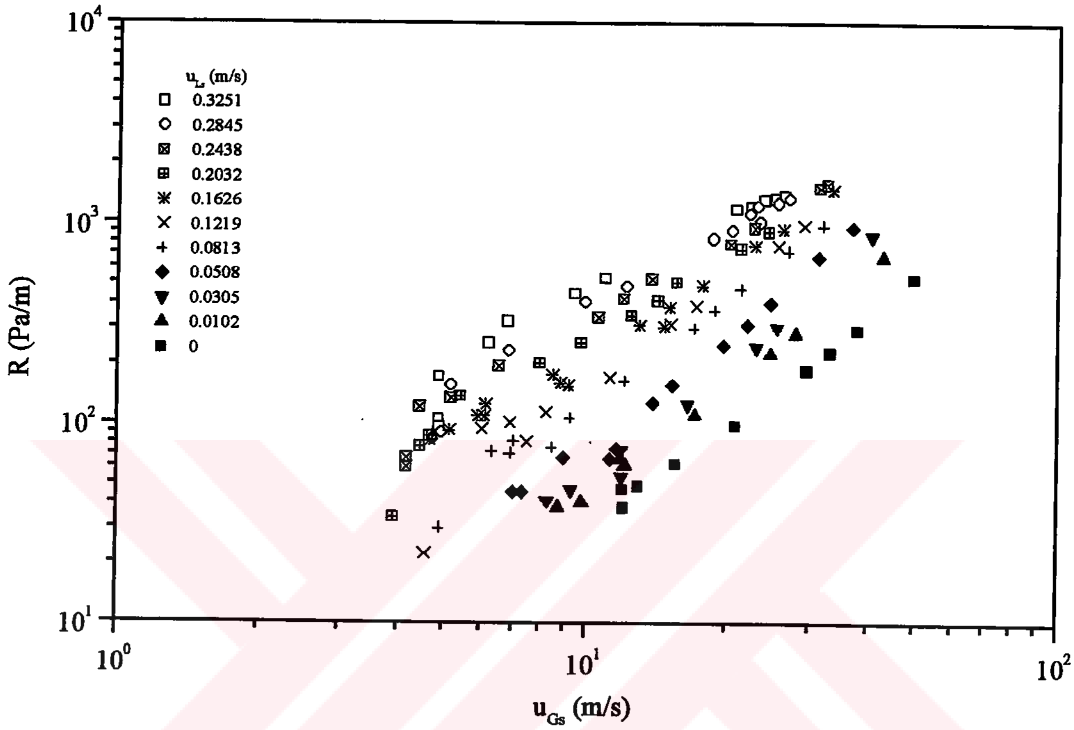

Figure 5.39. Variation of pressure drop with superficial gas velocity for horizontal gas liquid flow experiments.

The zero value for the superficial liquid velocity means that there is single phase gas flow in the pipe. The pressure losses of the single phase gas flow are the minimum values obtained in the horizontal flow experiments.

The pressure measurements of single phase gas flow are compared with the empirical methods of Lockhart-Martinelli (LMM), Chisholm (CM), Boroczy (BCM), and Theoretical Calculation Method (TCM). The empirical methods given before produce the same results for single phase flow. This is not unexpected, because these empirical methods are completely based on the calculation procedures of single phase flow. Comparison of the pressure losses obtained from the experiments with the empirical methods is shown in figure 5.40.

The measured values are close to the results calculated from the empirical methods. The relative errors between the measured values and the results of empirical methods are shown in figure 5.41. The relative error is calculated using equation (5.1).

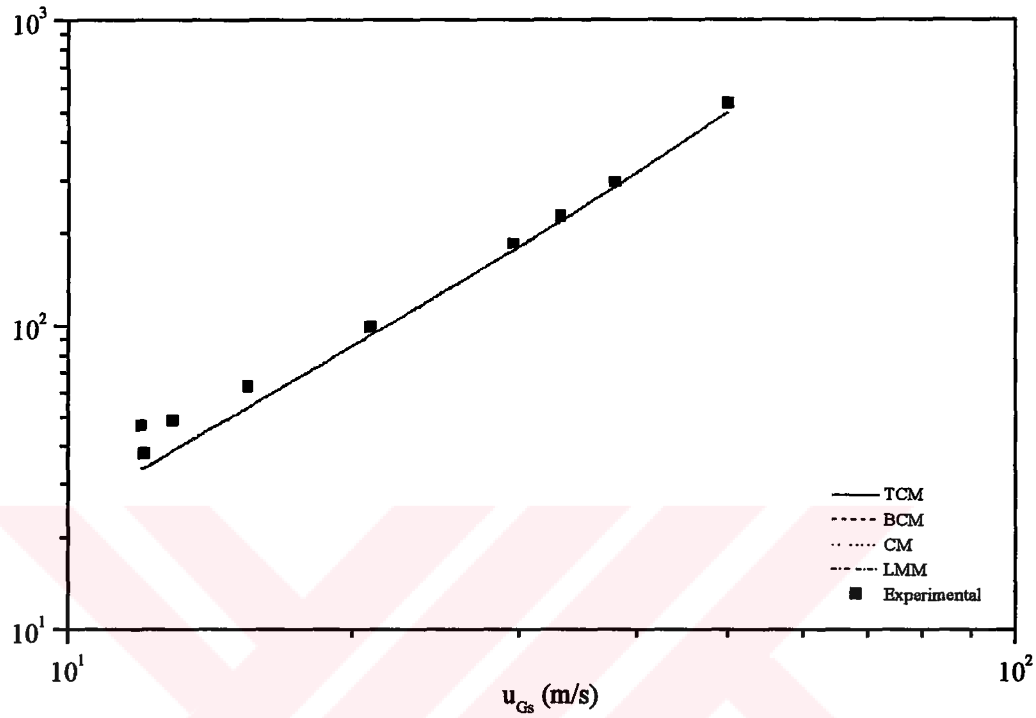

Figure 5.40. Comparison of pressure losses obtained from experiments with the empirical methods.

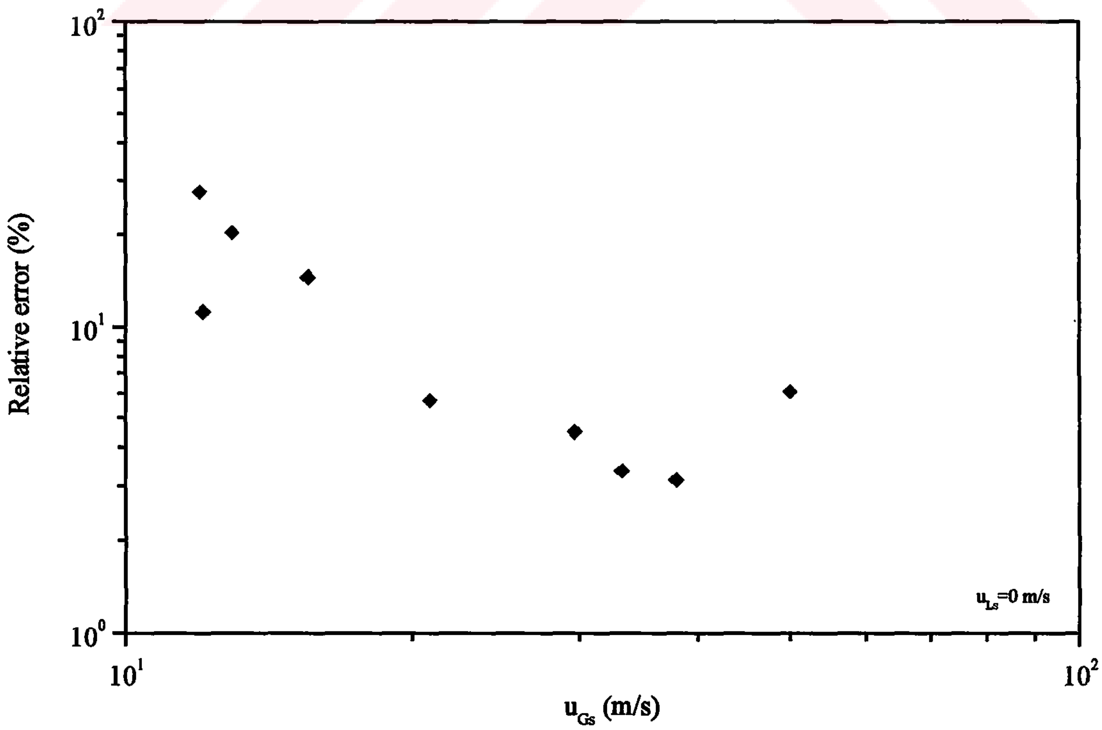

Figure 5.41. The relative errors between the measured values and results of empirical methods.

$$r_{err}(\%) = \frac{R_{Exp} - R_{Emp}}{R_{Exp}} * 100 \qquad (5.1)$$

The relative error is greater than 10%, if the superficial gas velocity is below 20 m/s. This is due to very low pressure values obtained in this region. The pressure transducers were not able to measure correctly low pressure values.

The minimum superficial liquid velocity tested was 0.0102 m/s. The pressure losses calculated from the empirical methods are different than the measured pressure losses to some extent (figure 5.42.). However, the pressure losses measured in the horizontal tube are located in the vicinity of the results of empirical methods. The results of LMM are very close to the measured values between the superficial gas velocities of 10 and 20 m/s. The CM predicts well the pressure losses between the superficial gas velocities of 20 and 40 m/s. One can conclude from figure 5.42. that the LMM predicts well the experimental pressure losses for the constant superficial liquid velocity of 0.0102 m/s. Figure 5.43. shows a similar comparison for the middle values (0.1626 m/s) of superficial liquid velocity. The results of TCM are sufficiently lower than those of the other empirical methods. One can reach a conclusion that LMM is the best for the prediction of the measured data. The results of CM and BCM are very close to each other.

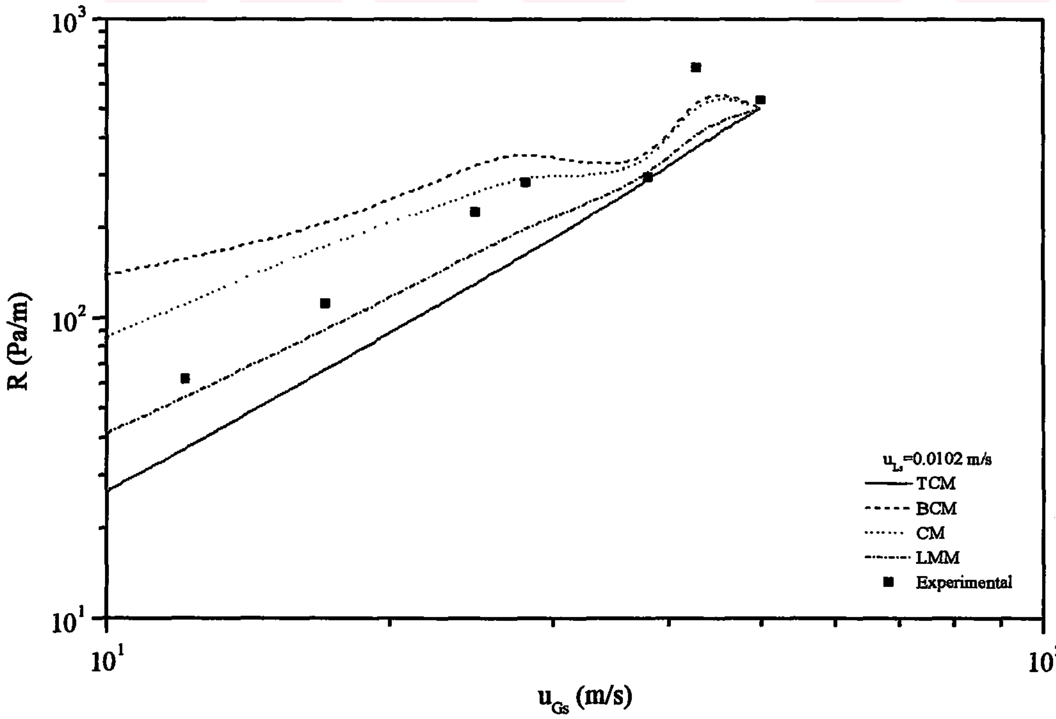

Figure 5.42. Comparison of the experimentally obtained pressure losses with the empirical methods for a constant superficial liquid velocity of 0.0102 m/s.

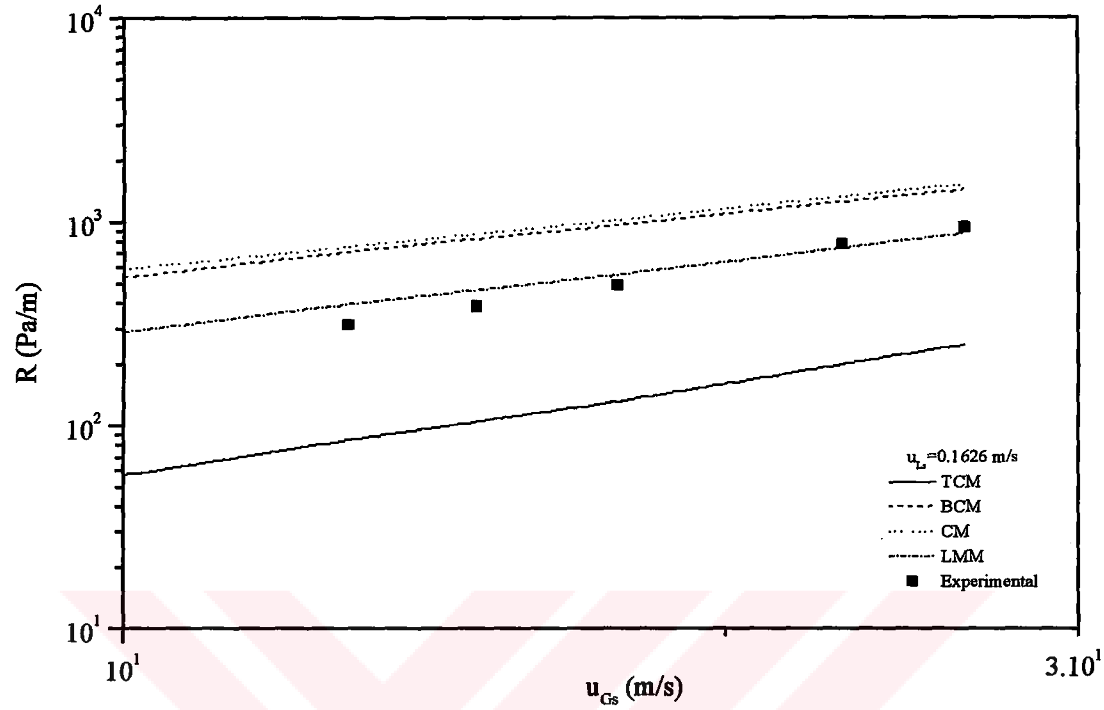

Figure 5.43. Comparison of the experimentally obtained pressure losses with the empirical methods for a constant superficial liquid velocity of 0.1626 m/s.

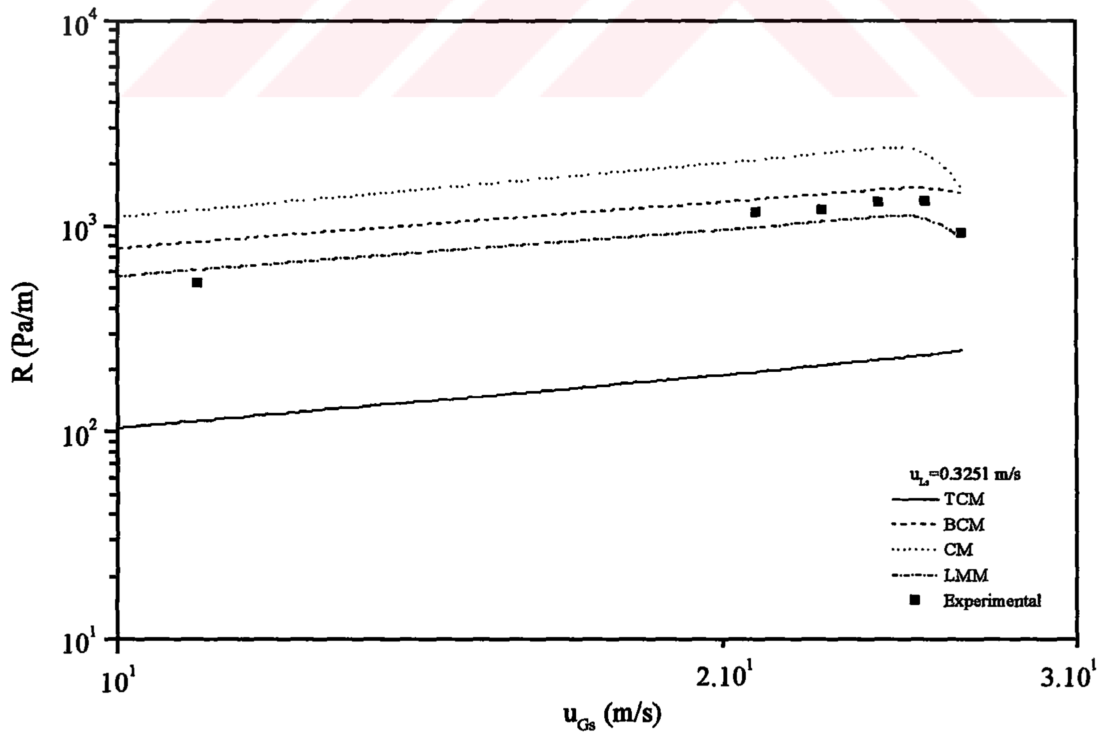

Figure 5.44. Comparison of the experimentally obtained pressure losses with the empirical methods for a constant superficial liquid velocity of 0.3251 m/s.

The comparison of the experimental data with the empirical methods are shown in figure 5.44. for the maximum superficial liquid velocity tested (0.3251 m/s). The experimental pressure measurements are located between the results of LMM and BCM. This is valid for almost all superficial liquid velocities.

The results of BCM get closer to the experimental data as the superficial liquid velocity is increased. It is obviously seen that the results of TCM depart from the measurements as the superficial liquid velocity is increased.

The pressure losses obtained from the horizontal tube experiments can be predicted approximately by the empirical method of Lockhart-Martinelli. The results of the pressure measurements are also compared with the experimental study of Spedding et al. (1998). The authors presented the experimental pressure drop data obtained using horizontal pipe with 0.058 m inner diameter. The pipe diameter of their study is very close to that of this investigation (0.059 m). However, they used different constant superficial liquid velocities than those of this study. Figure 5.45. shows the comparison of experimental pressure losses with the Spedding's results.

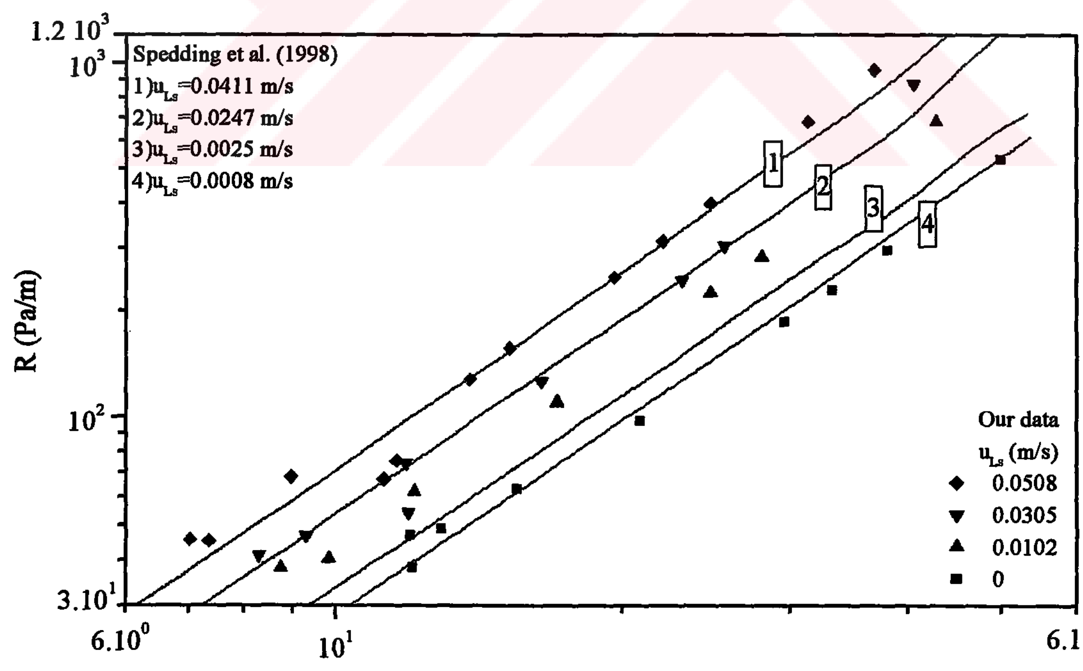

Figure 5.45. Comparison of experimental pressure losses with the results of Spedding et al. (1998).

The selected data points in horizontal flow of this investigation are close to the constant superficial liquid velocities of Spedding's investigation. The pressure drops of single phase gas flow are lower than the pressure drops for $u_{Ls} = 0.0008$ m/s of Spedding's investigation (line 4). Because of very low superficial liquid velocities, it can be assumed that the differences between the results of this investigation and Spedding et al. (1998) are negligible. The slopes of the experimental results of this work are approximately similar to those of Spedding et al. (1998).

The experimentally obtained pressure losses of horizontal gas liquid flow are also compared with the experimental results of Kokal and Stanislav (1989). The authors conducted gas liquid flow experiments in pipes having different inner diameters. The diameters of test pipes were 0.0258 m, 0.0512 m, and 0.0763 m, respectively. The pressure losses obtained in this thesis are shown in the same figure (figure 5.46.) with the 0.0512 m i.d. results of Kokal and Stanislav (1989).

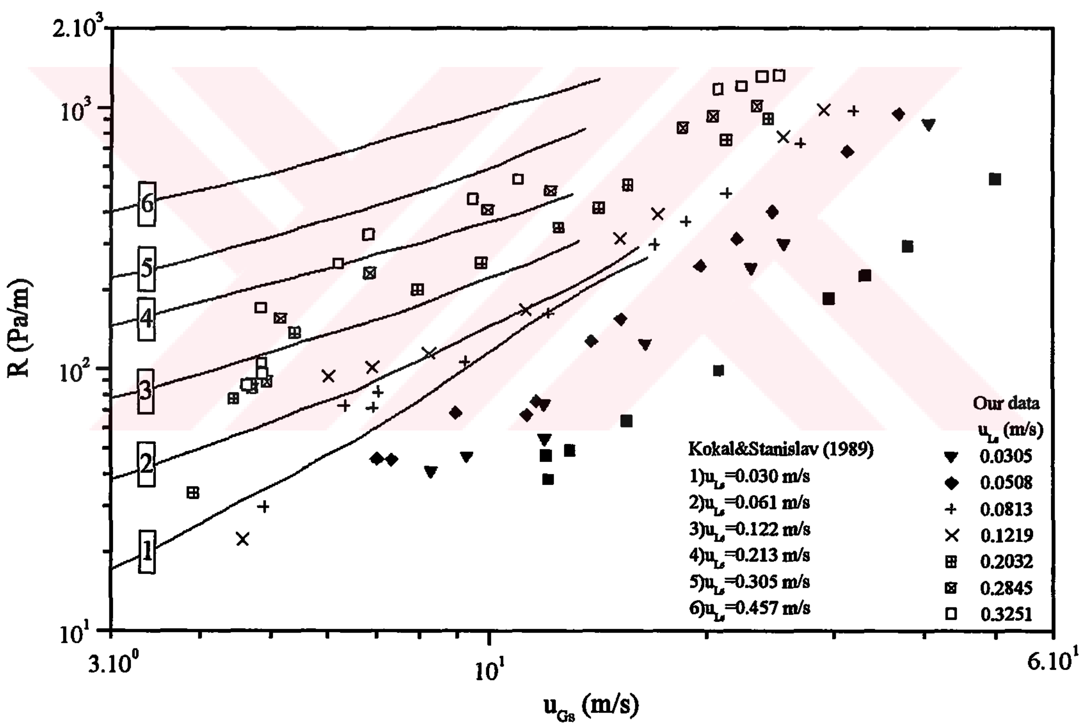

Figure 5.46. Comparison of experimental pressure losses with the results of Kokal and Stanislav (1989).

The experimentally obtained pressure losses of horizontal gas liquid flow are lower than those of Kokal and Stanislav (1989). For example, the pressure losses for $u_{Ls} = 0.3251$ m/s could be expected to sit between the lines of 5 and 6. Additionally, the pressure losses for $u_{Ls} = 0.1219$ m/s could be nearly equal to those of the line 3, but experimentally obtained results of this study are lower than the results of Kokal and Stanislav (1989). This difference is due to the inner diameter of the test pipe.

Kokal and Stanislav (1989) used a test pipe with 0.0512 m inner diameter, but the experiments of this work were carried out in a pipe with 0.059 m inner diameter. Kokal and Stanislav (1989)'s experimental results show that, for the constant superficial liquid velocity, pressure losses decrease gradually, as the inner diameter of pipe is increased. This is shown in figure 5.47.

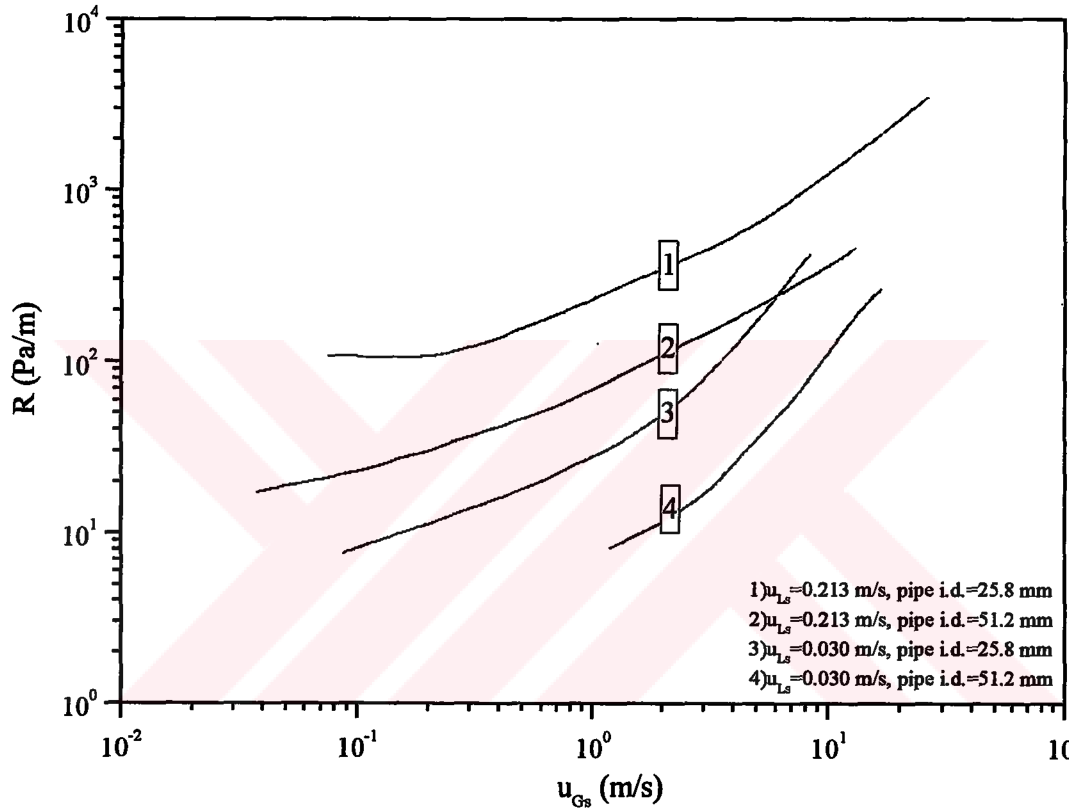

Figure 5.47. Comparison of pressure drops for different pipe diameters (Kokal and Stanislav, 1989).

Line 1 and 2 indicate the variation of pressure drop with superficial gas velocity for a constant superficial liquid velocity of 0.213 m/s. The difference between these curves is due to the different pipe diameters. The lower pressure drops were obtained from the experiments with 0.0512 m inner diameter tube. Lines 3 and 4 which are obtained with a different superficial liquid velocity show the same trend. Thus, the pressure losses of this study can be considered accurate according to the comparisons with other results of empirical methods and of experimental studies.

Figure 5.48. and 5.49. show the pressure drop values for horizontal flow experiments. The selected superficial liquid velocities are given in the legends of the figures. These two figures show the variation of pressure drop with superficial gas

velocity for different superficial liquid velocities. The pressure gradient increases as the superficial gas velocity is increased. Pressure drop also increases with the increase of superficial liquid velocity.

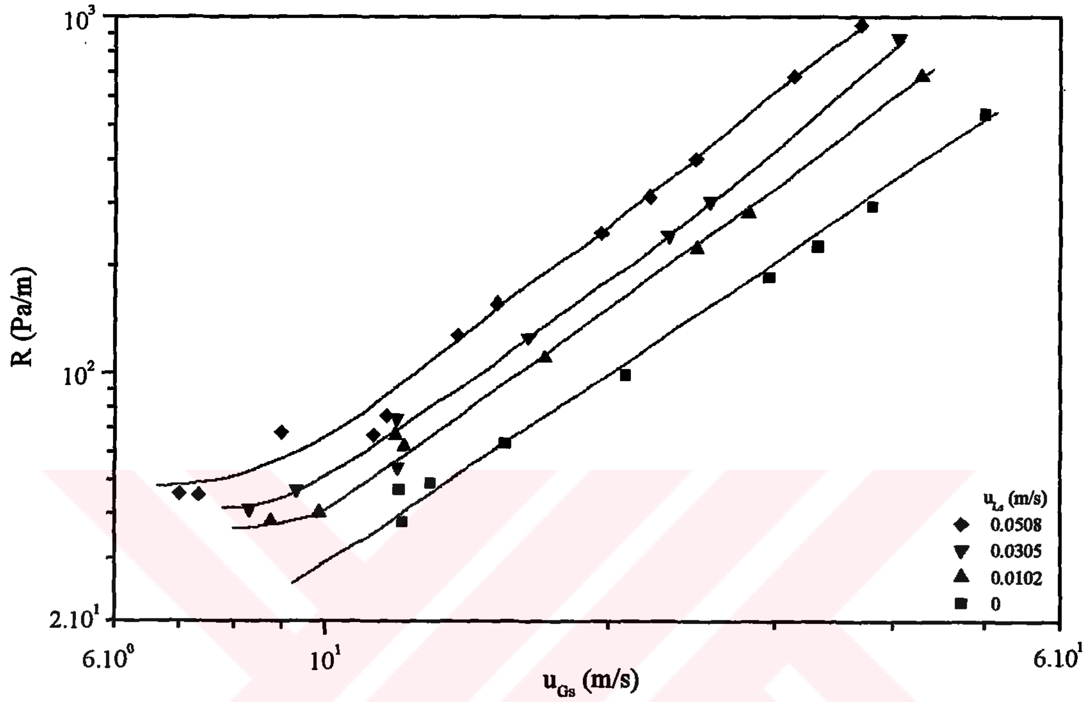

Figure 5.48. Pressure drop values for horizontal flow experiments.

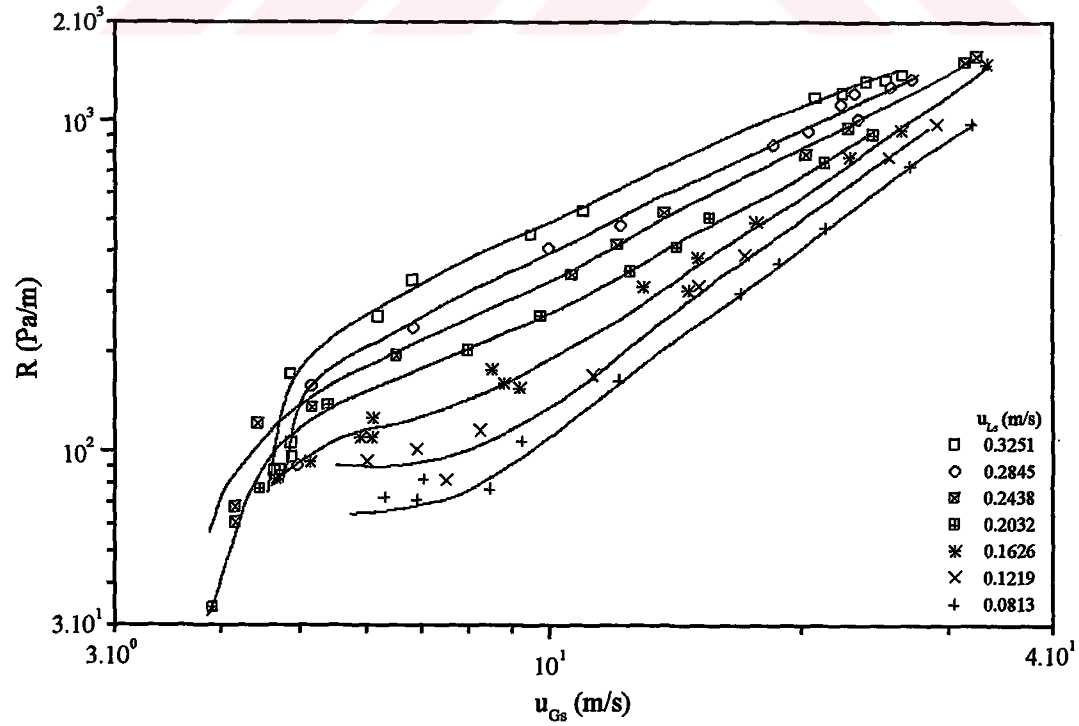

Figure 5.49. Pressure drop values for horizontal flow experiments.

The pressure losses obtained from +5° inclination experiments are shown in figures 5.50. and 5.51. The variations of pressure drops with superficial gas and liquid velocities represent a similar trend to those of horizontal flow. However, the slopes of pressure drop lines decrease as the pipe inclination is increased when they are compared with the data obtained in the horizontal tube. It can be seen from figures 5.50. and 5.51. that, there is a tendency of pressure drops to converge towards a constant pressure drop for the low superficial gas velocities.

The variations of pressure losses for +10° inclination experiments are shown in figures 5.52. and 5.53. The pressure losses obtained in the constant superficial liquid velocities of 0.0305 m/s and 0.0508 m/s are taken a minimum value near the superficial gas velocity of 15 m/s.

According to figure 5.53., it can be estimated approximately that, this minimum superficial gas velocity value decreases as the superficial liquid velocity is increased.

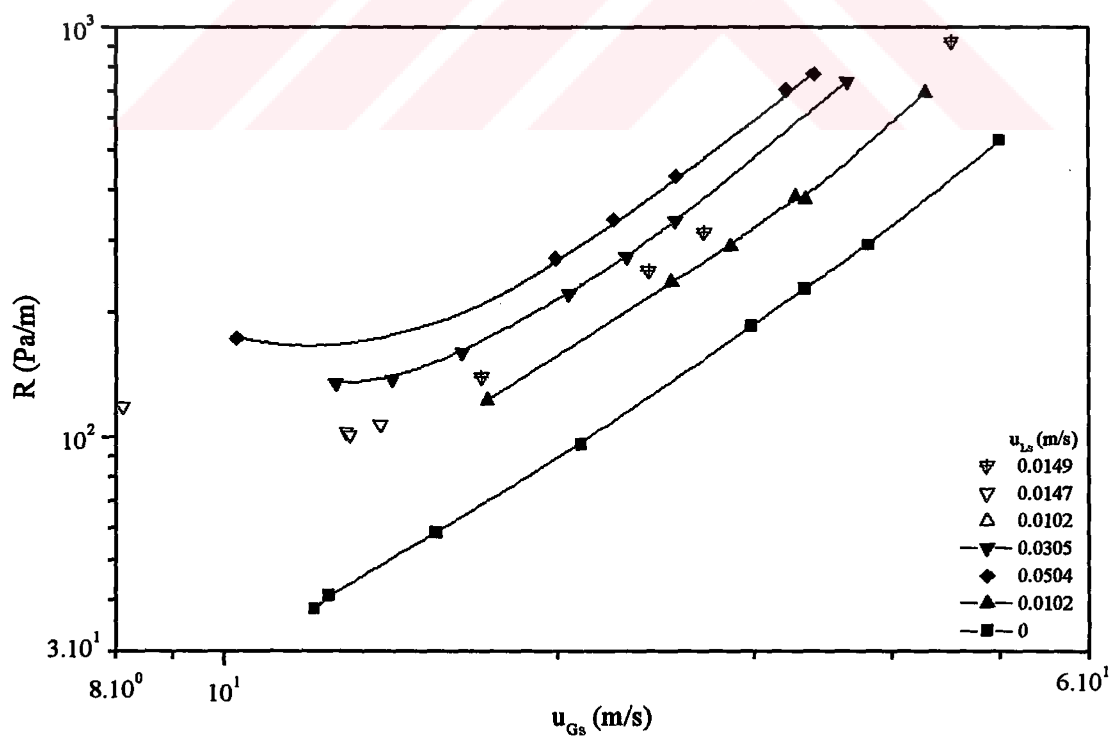

Figure 5.50. Pressure drop values for +5° inclination experiments.

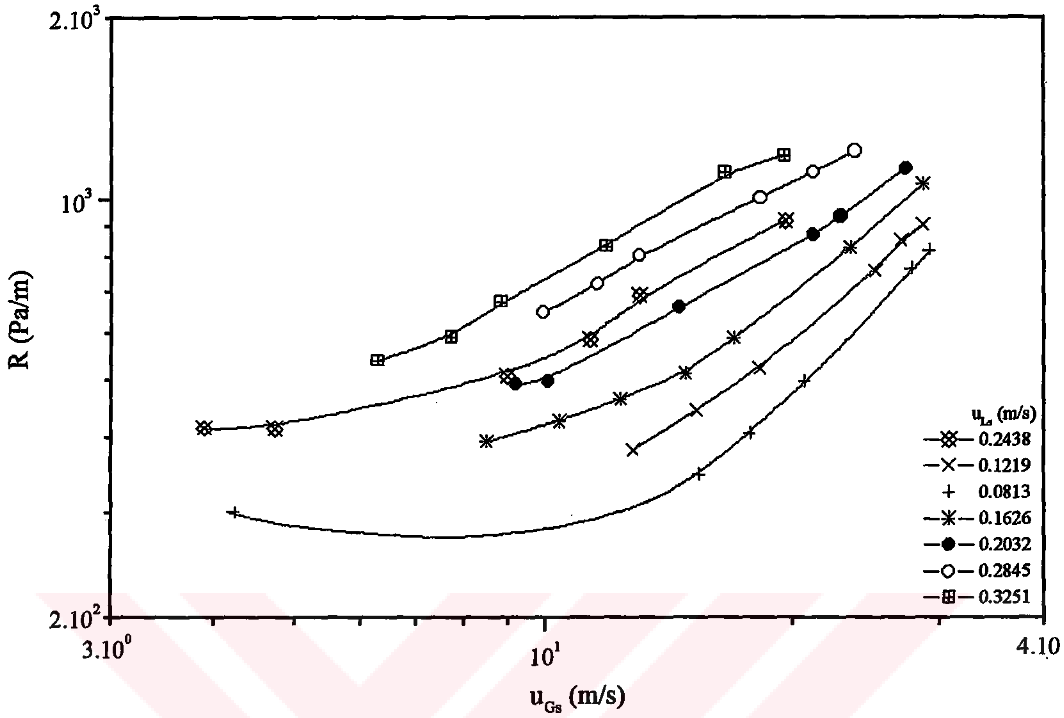

Figure 5.51. Pressure drop values for +5° inclination experiments.

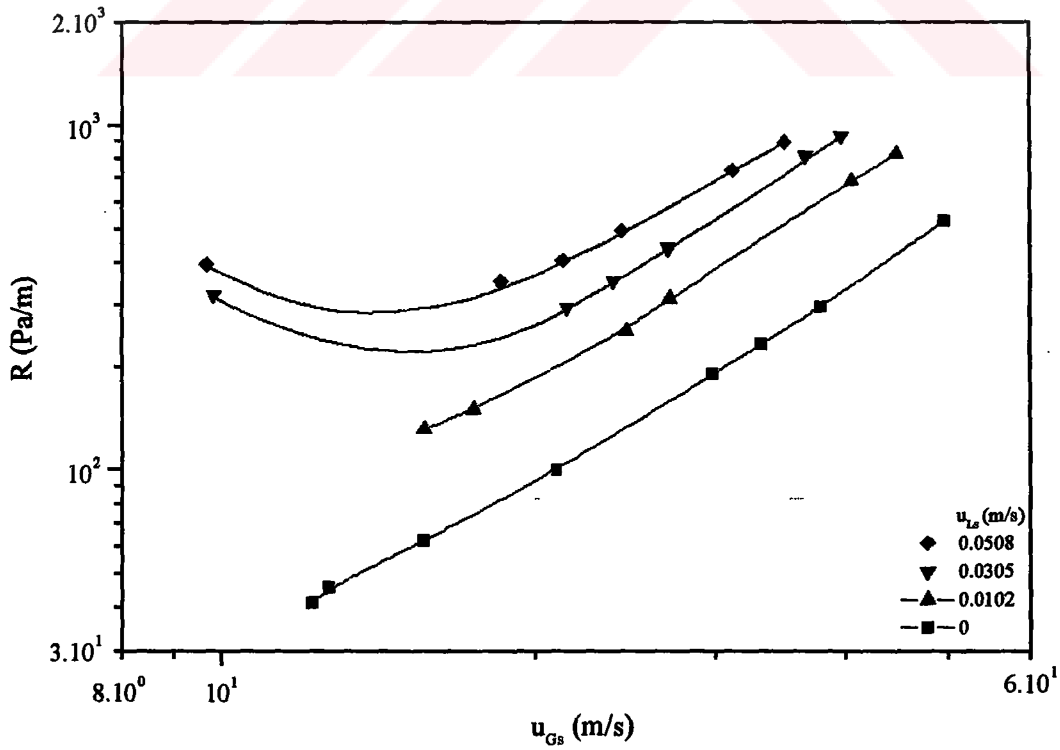

Figure 5.52. Pressure drop values for +10° inclination experiments.

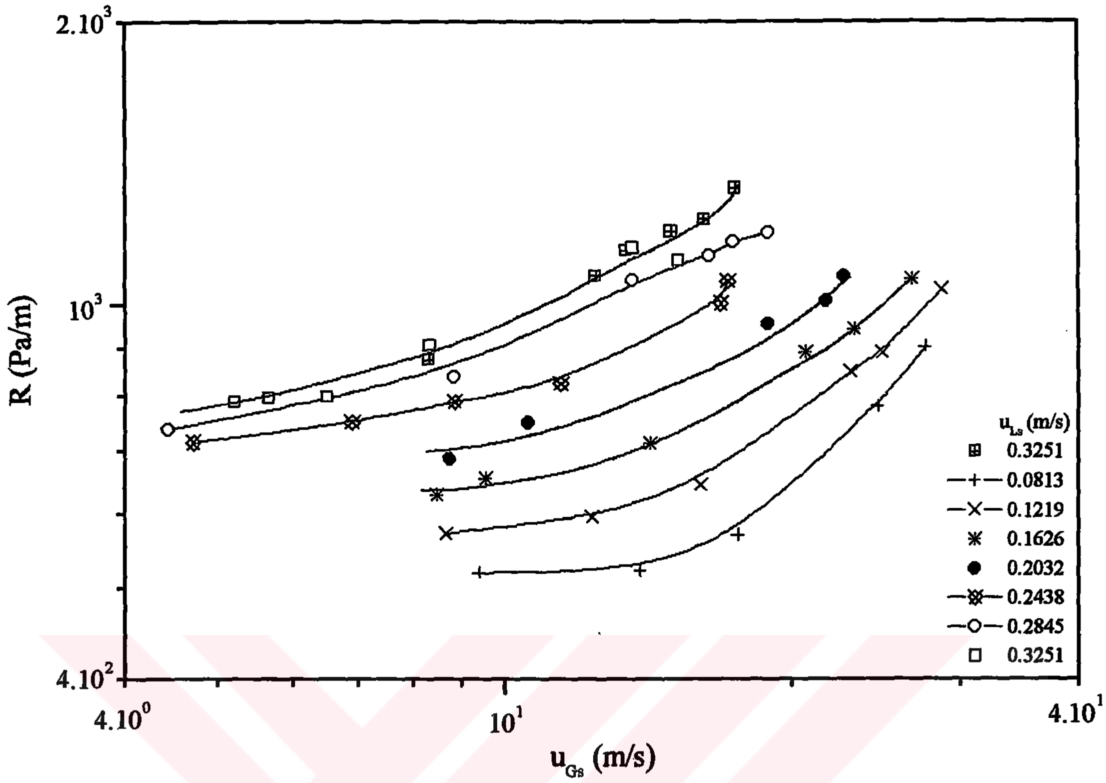

Figure 5.53. Pressure drop values for +10° inclination experiments.

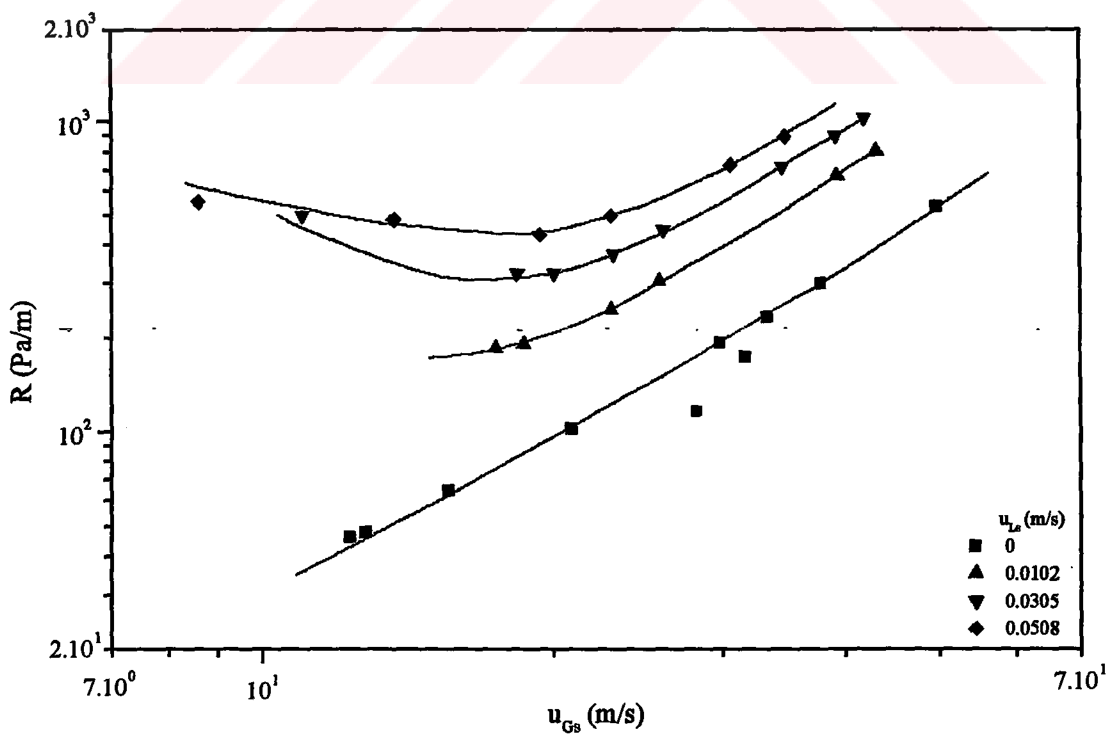

Figure 5.54. Pressure drop values for +15° inclination experiments.

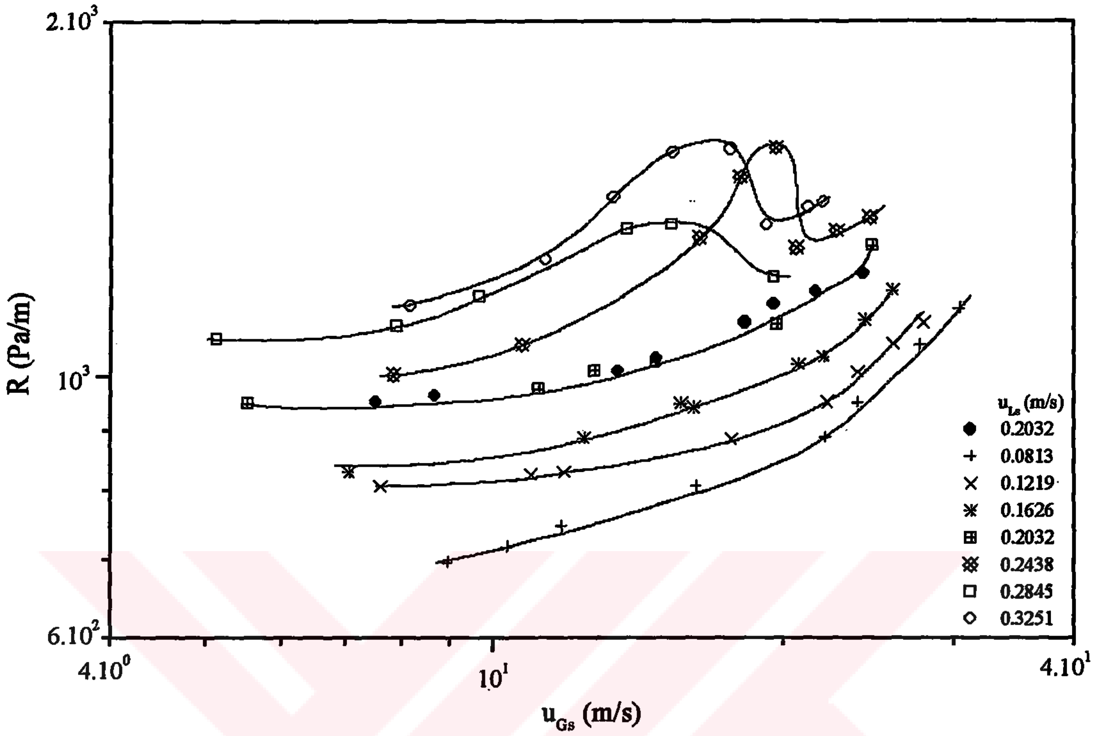

Figure 5.55. Pressure drop values for +15° inclination experiments.

The pressure losses obtained from +15° inclination experiments are shown in figure 5.54. and 5.55. The variations of pressure drops with superficial gas and liquid velocities show a similar trend to those of previous experiments. However, a peculiarity has been systematically observed in the pressure drops of higher superficial liquid velocities. The pressure losses obtained from the constant superficial liquid velocities of 0.2438 m/s, 0.2845 m/s, and 0.3251 m/s pulsate about the superficial gas velocities of 19.5 m/s, 15 m/s, and 17 m/s, respectively. There is no any estimation about the reason of these irregularities.

The pressure losses obtained from the horizontal, +5°, +10°, and +15° inclined tubes are compared with each other. This comparison is carried out for each constant superficial liquid velocity selected. Figure 5.56. shows the variation of the pressure drop with the superficial gas velocity for single phase gas flow in the test pipe with different inclinations. One can conclude that, there are no considerable differences between the measurements.

The pressure losses obtained from the horizontal, +5°, +10°, and +15° inclined tubes for single phase gas flow are approximately equal to each other. Two data point of +15° inclination experiments are located slightly far about the superficial gas velocity of 30 m/s. This is possible due to the measurement errors, and they can be neglected when interpreting the results.

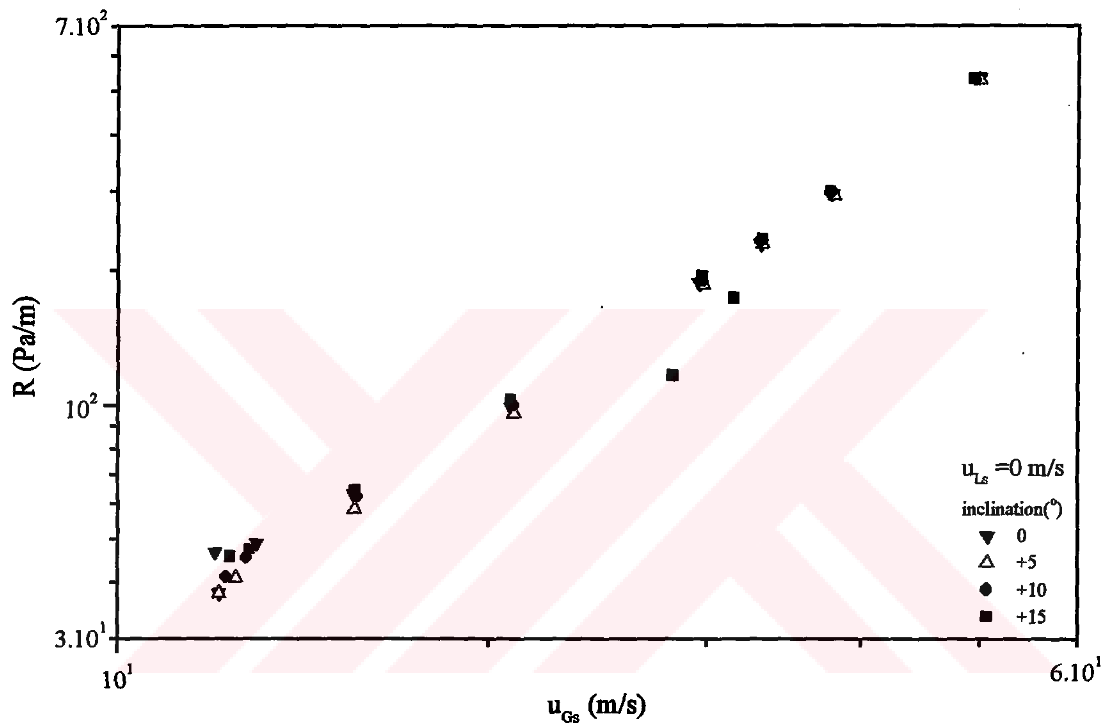

Figure 5.56. Pressure drop values obtained from the horizontal, +5°, +10°, and +15° inclined tubes for a superficial liquid velocity of 0 m/s.

The minimum value of superficial liquid velocity for the comparison of the pressure losses in the test pipe with different inclinations was 0.0102 m/s. Even for the conditions of minimum superficial liquid velocity, the pressure drops data of the inclined tube experiments are different than those of horizontal tube experiments. Figure 5.57. shows the variations of pressure losses with superficial gas velocity for the constant superficial liquid velocity of 0.0102 m/s. Lines between the measured data points were drawn because to indicate the trend of the data. Figure 5.57. depicts that there are significant differences in the pressure losses obtained from the different inclinations for low superficial gas velocities, even for the constant superficial liquid velocity of 0.0102 m/s. However, the differences decrease as the superficial gas velocity is increased. The flow patterns observed in all experiments are mixed and annular droplets as the superficial gas velocity is increased for constant superficial liquid velocity.

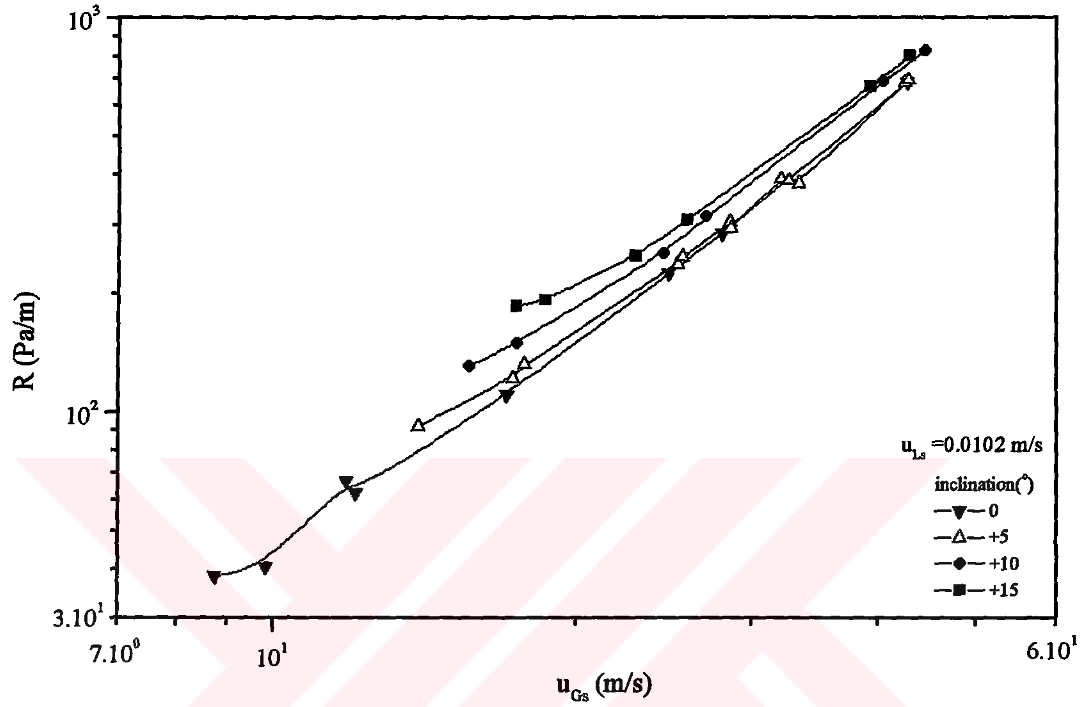

Figure 5.57. Pressure drop values obtained from horizontal, +5°, +10°, and +15° inclined tube experiments for a superficial liquid velocity of 0.0102 m/s.

Figure 5.58. shows a similar variation for a different constant superficial liquid velocity. However, the trends of +5°, +10°, and +15° inclined tube experiments for low superficial gas velocities are more obvious than before. The convergence of pressure losses of different inclination experiments are very important. This can be explained with the help of momentum equation which consist of the terms of frictional, accelerational, and potential pressure gradients. The effect of potential pressure gradient decreases compared with the frictional, and accelerational pressure gradients as the velocity is increased. Therefore, the inclination of the test pipe loses its effect on the pressure loss with the increasing of superficial gas velocity.

Figures from 5.59. to 5.66. show the variations of pressure losses with superficial gas velocity for different constant superficial liquid velocities.

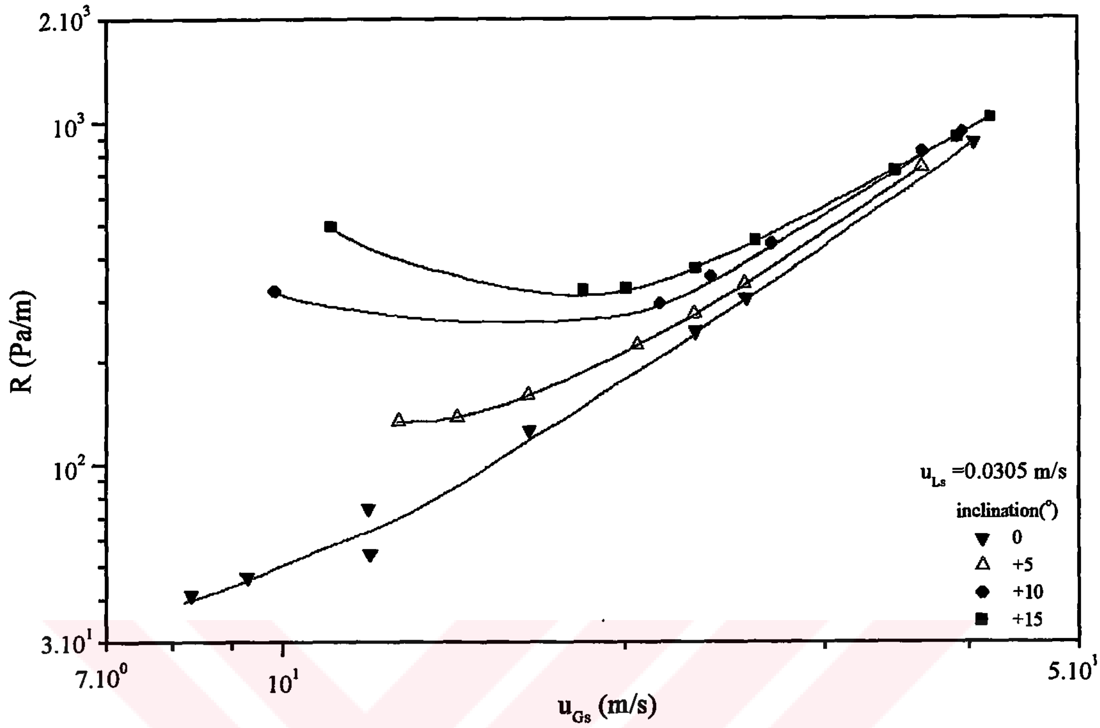

Figure 5.58. Pressure drop values obtained from horizontal, +5°, +10°, and +15° inclined tube experiments for a superficial liquid velocity of 0.0305 m/s.

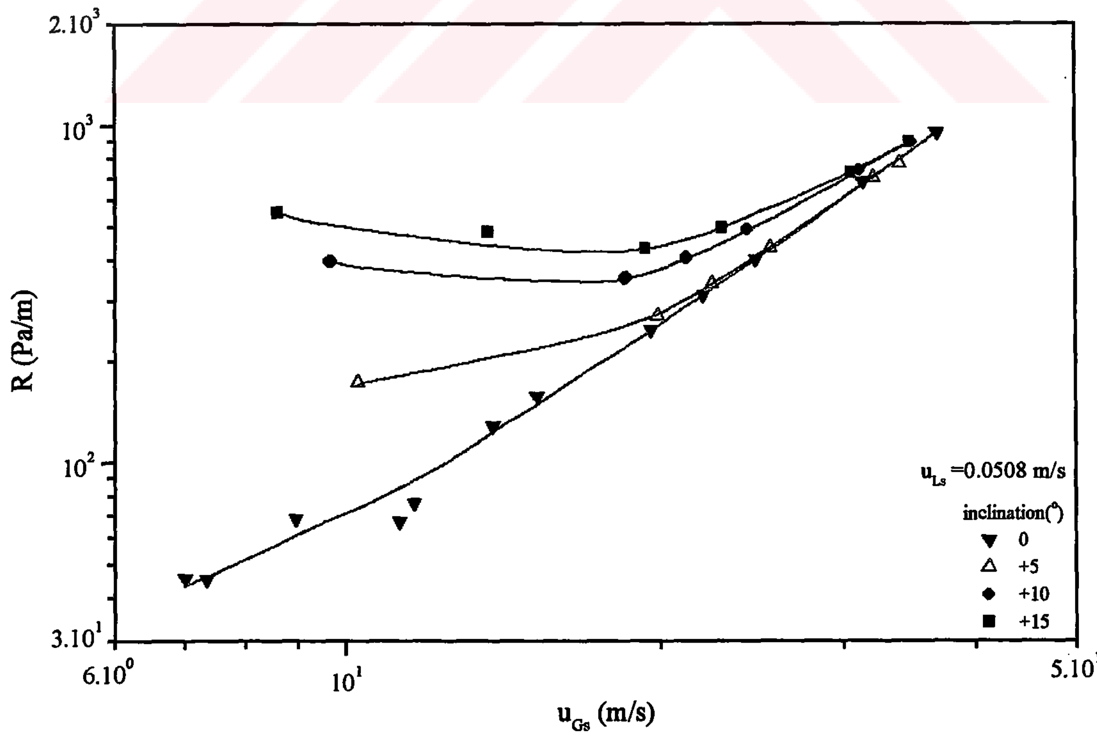

Figure 5.59. Pressure drop values obtained from horizontal, +5°, +10°, and +15° inclined tube experiments for a superficial liquid velocity of 0.0508 m/s.

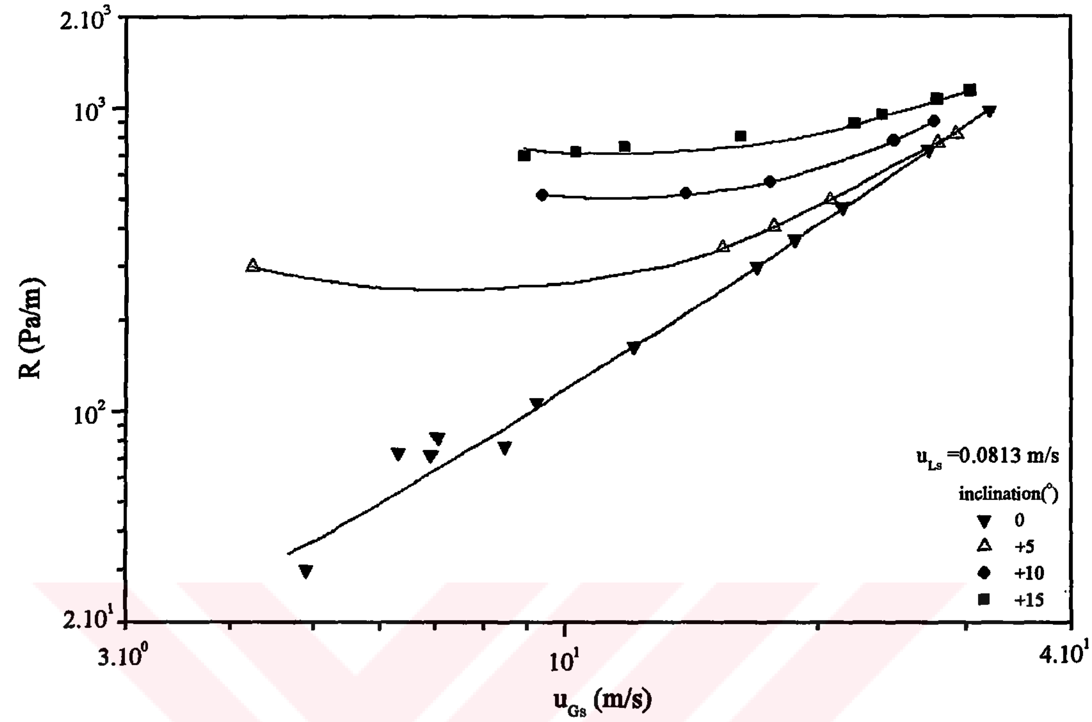

Figure 5.60. Pressure drop values obtained from horizontal, +5°, +10°, and +15° inclined tube experiments for a superficial liquid velocity of 0.0813 m/s.

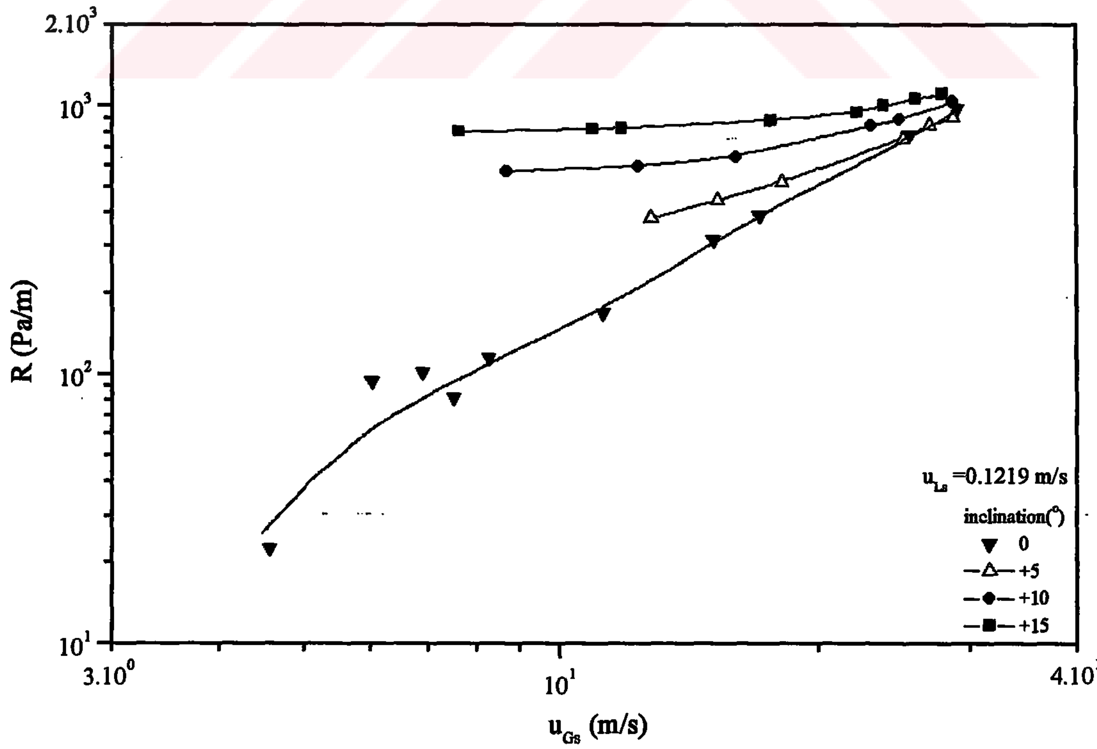

Figure 5.61. Pressure drop values obtained from horizontal, +5°, +10°, and +15° inclined tube experiments for a superficial liquid velocity of 0.1219 m/s.

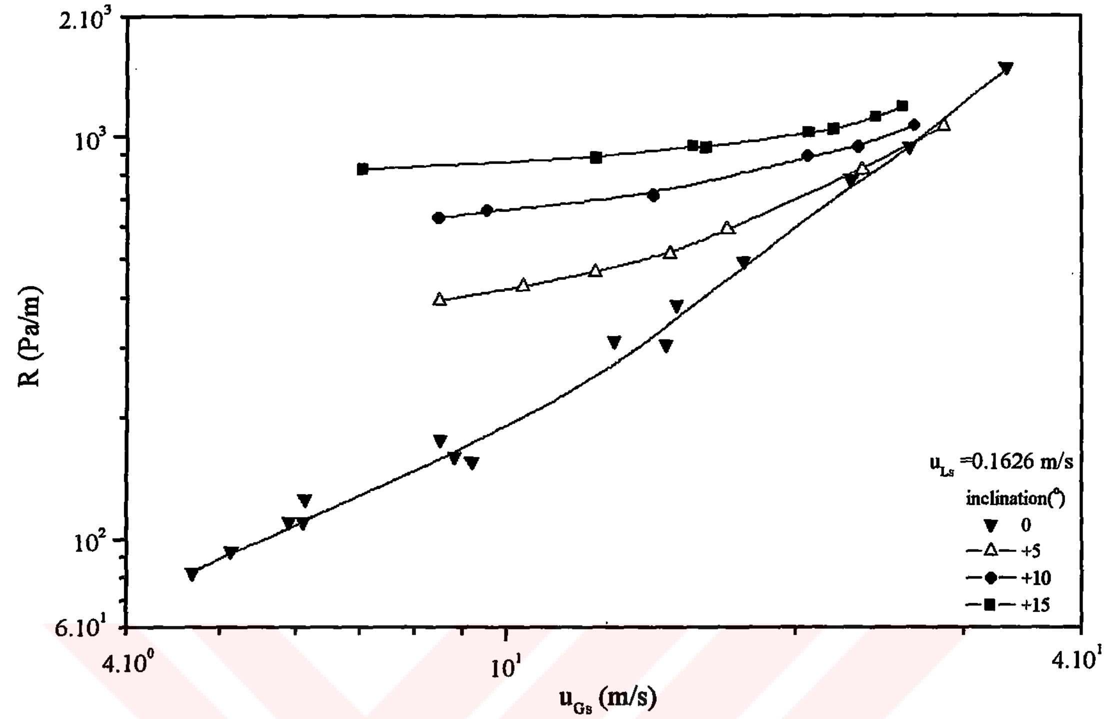

Figure 5.62. Pressure drop values obtained from horizontal, +5°, +10°, and +15° inclined tube experiments for a superficial liquid velocity of 0.1626 m/s.

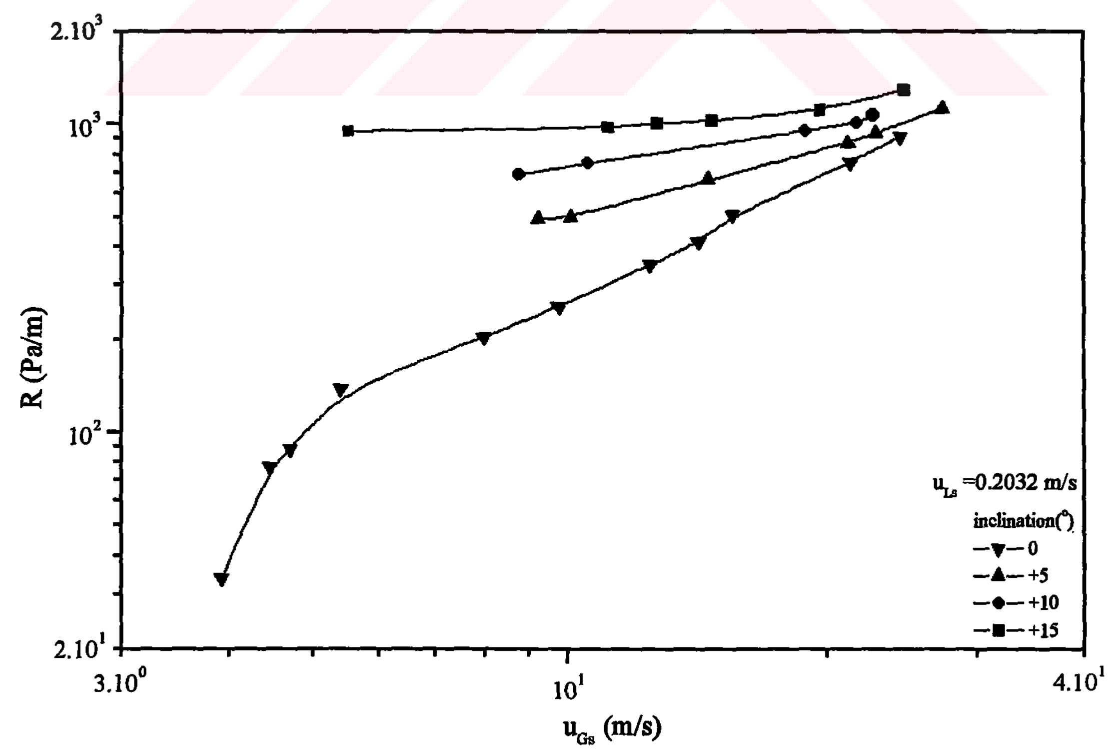

Figure 5.63. Pressure drop values obtained from horizontal, +5°, +10°, and +15° inclined tube experiments for a superficial liquid velocity of 0.2032 m/s.

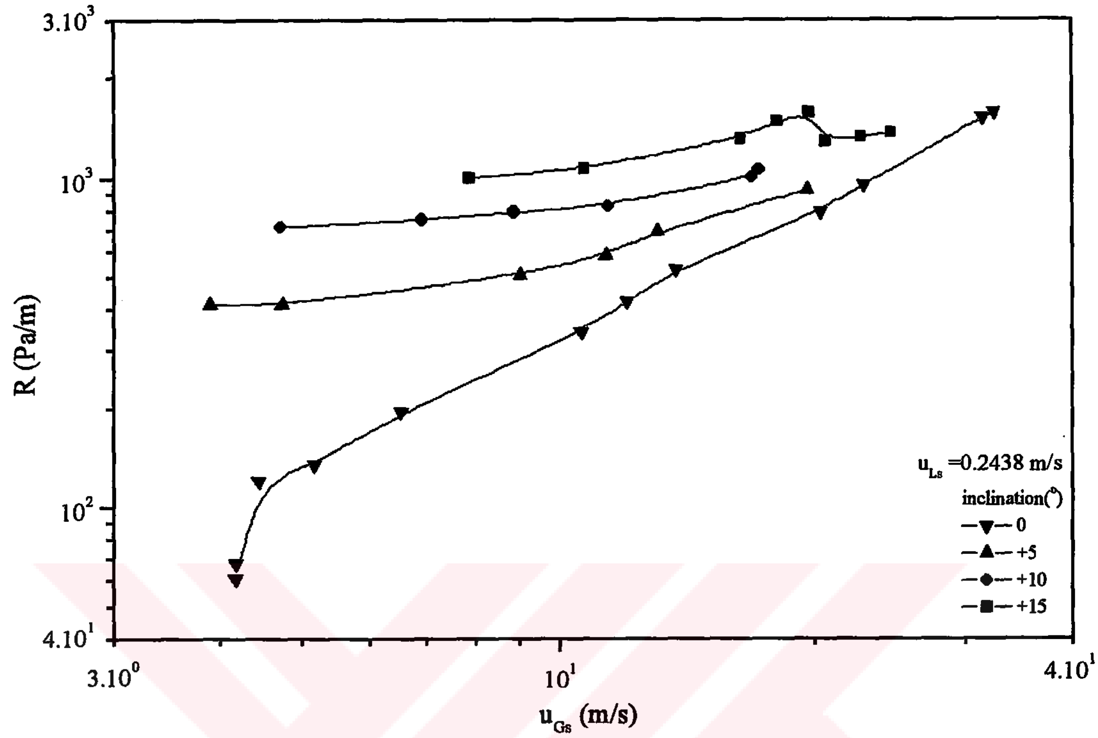

Figure 5.64. Pressure drop values obtained from horizontal tube, +5°, +10°, and +15° inclined tube experiments for a superficial liquid velocity of 0.2438 m/s.

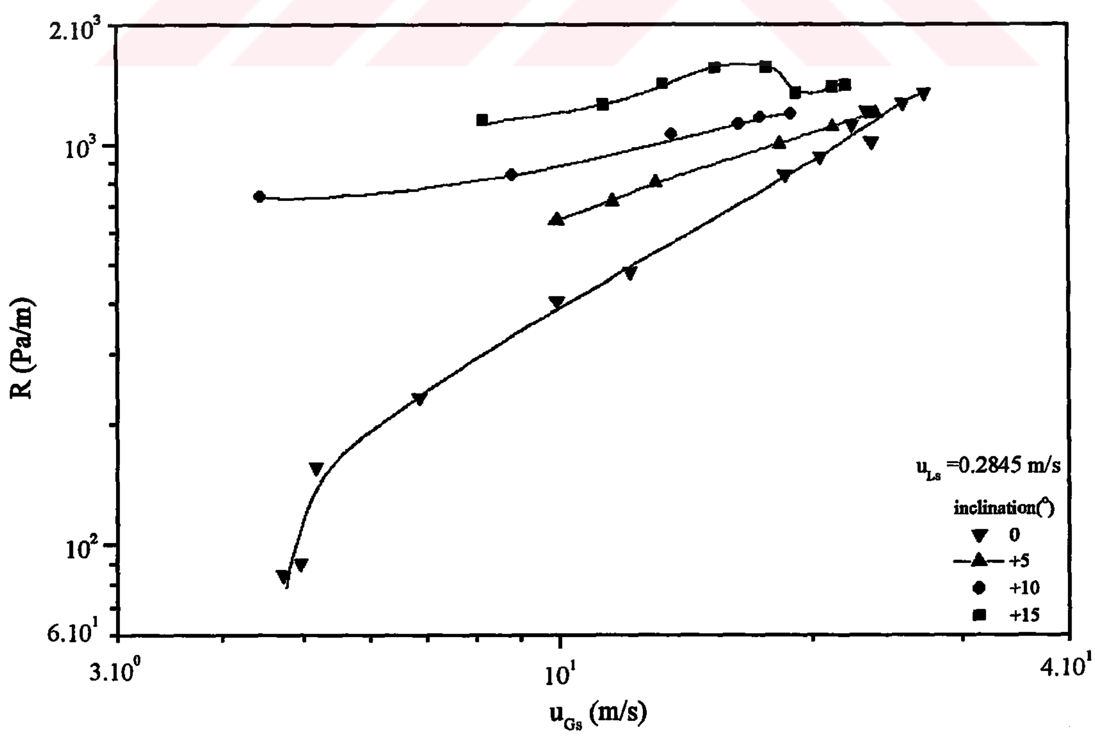

Figure 5.65. Pressure drop values obtained from horizontal tube, +5°, +10°, and +15° inclined tube experiments for a superficial liquid velocity of 0.2845 m/s.

Figure 5.66. show the same variations for the maximum superficial liquid velocity of 0.3251 m/s. One can express that the pressure losses of +15° inclination experiments change less than those of the horizontal flow experiments.

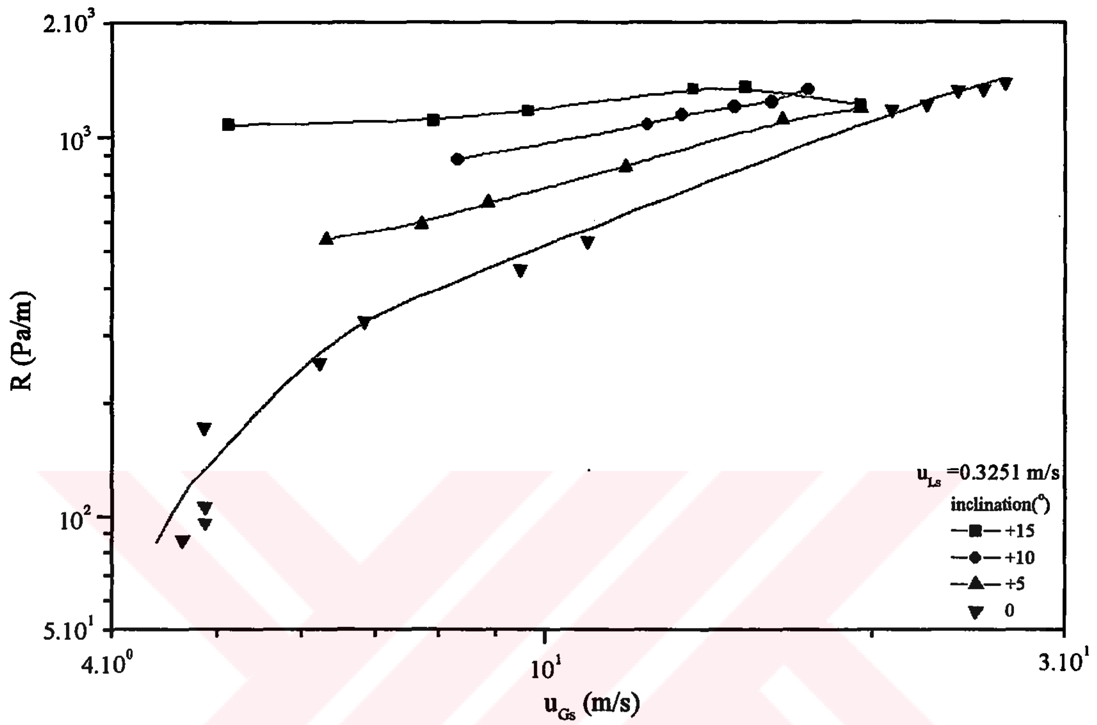

Figure 5.66. Pressure drop values obtained from horizontal tube, +5°, +10°, and +15° inclined tube experiments for a superficial liquid velocity of 0.3251 m/s.

The amplitudes of pressure losses measured in the experiments are very important because of the safety of industrial equipments. This can be simply defined as the difference between the maximum and minimum values of mean pressure loss. High values of amplitudes cause vibrations and an influence similar to fatigue test. The swinging forces shorten the life of material, namely, of devices.

Figures 5.67. and 5.68. show the variations of the pressure amplitudes with the superficial gas velocity for the horizontal tube experiments for constant superficial liquid velocities. The differences of amplitudes for single phase and two phase flow are shown in figure 5.67. for low constant superficial liquid velocities. The amplitudes of pressure loss increase as the superficial liquid velocity is increased.

The amplitudes of pressure loss in horizontal tube experiments are shown in figure 5.68. for high superficial liquid velocities. The amplitudes of pressure loss in horizontal tube experiments increase gradually with the increasing of superficial liquid velocity. The highest amplitudes of pressure loss in horizontal tube experiments were measured in the experiments with the superficial liquid velocity of 0.3251 m/s. This can be seen in figure 5.68.

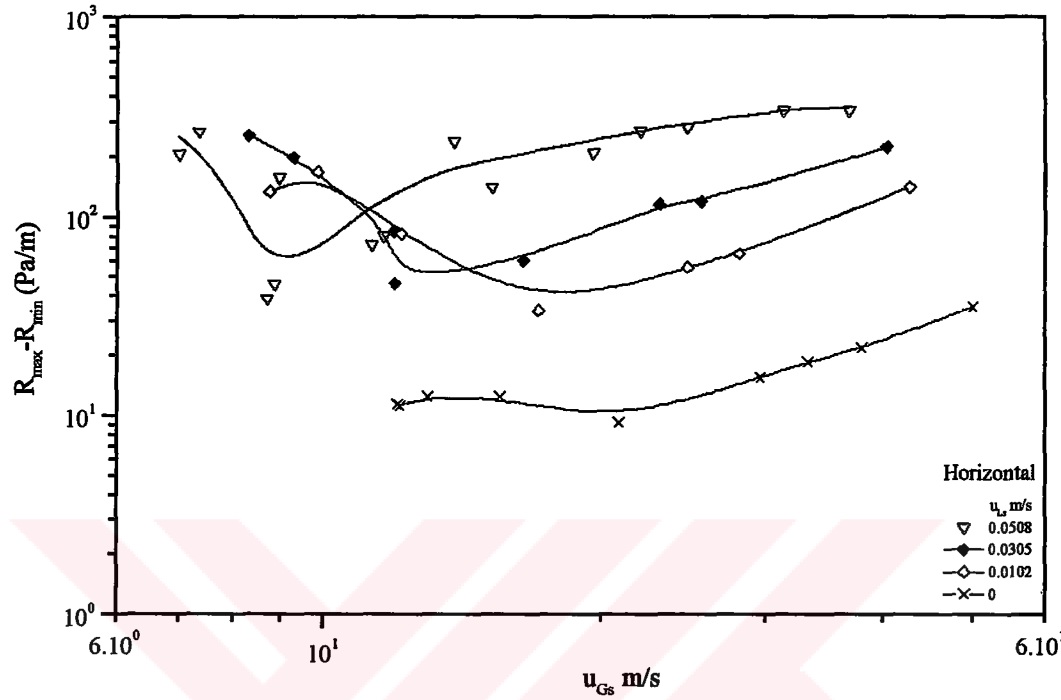

Figure 5.67. Pressure amplitude values obtained from horizontal tube experiments for low superficial liquid velocities.

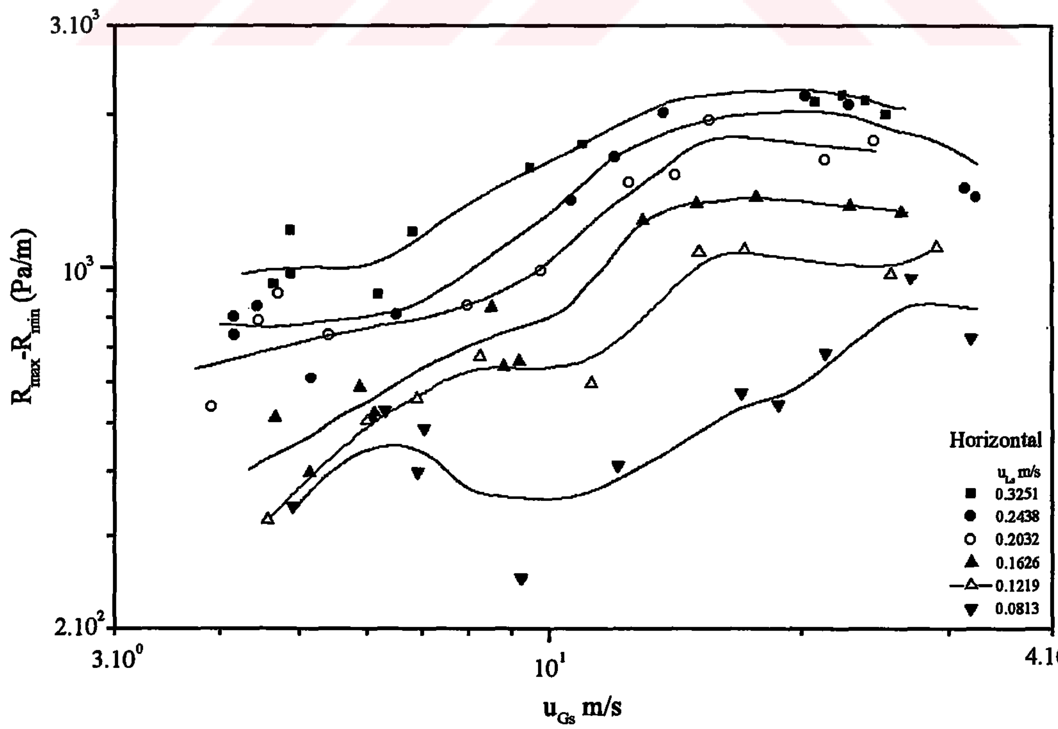

Figure 5.68. Pressure amplitude values obtained from horizontal tube experiments for high superficial liquid velocities.

Similar variations of the amplitudes of pressure loss are shown in the figures 5.69. and 5.70. for +15° inclination experiments. A similar trend has been observed in the +15° inclination experiments. The amplitudes of pressure loss in +15° inclination experiments increase gradually with the increasing of superficial liquid velocity. The amplitudes of pressure loss for low constant superficial liquid velocities change approximately parallel with the superficial gas velocity. This variation is a little different for high constant superficial liquid velocities because they are mixed. Despite this mixed variations, each of them follows a systematic trend. The amplitudes of pressure loss for high constant superficial liquid velocities increase as the superficial liquid velocity is increased. They all decrease systematically as the superficial gas velocity is increased.

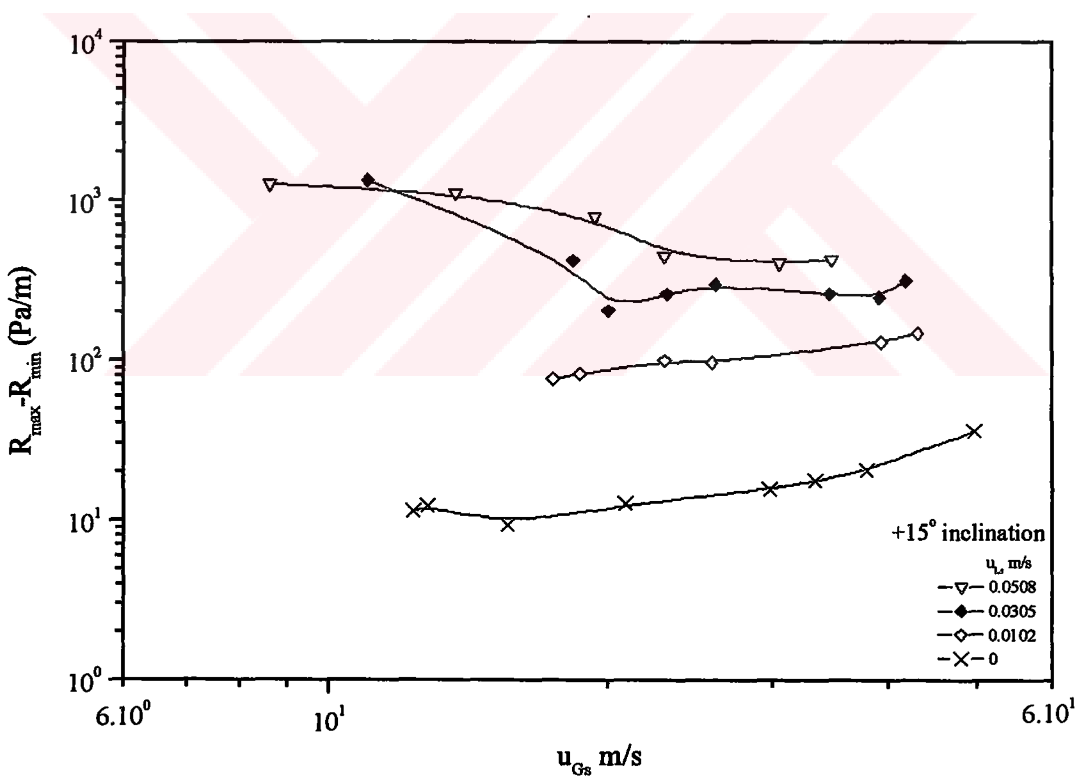

Figure 5.69. Pressure amplitude values obtained from +15° inclination experiments for low superficial liquid velocities.

Figure 5.71. shows the variations of pressure amplitudes with the superficial gas velocity for single phase gas flow. The values of pressure amplitudes of all inclination experiments are very low, and they are approximately equal to each other. The pressure amplitudes increase with the increasing of the superficial gas velocity.

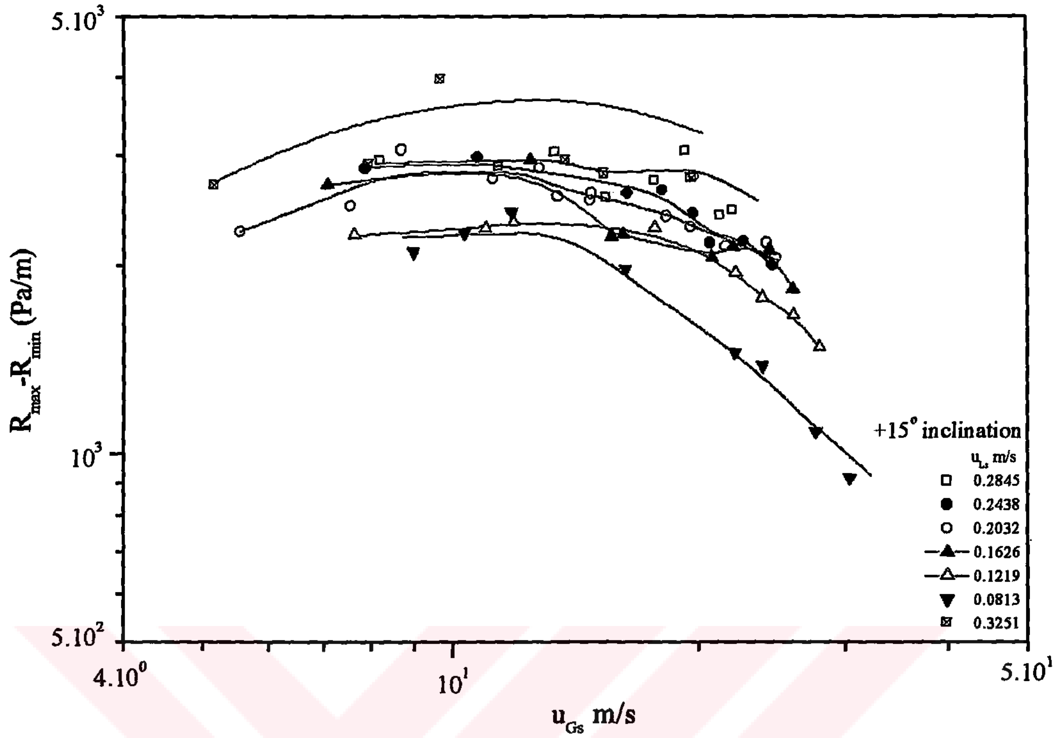

Figure 5.70. Pressure amplitude values obtained from +15° inclination experiments for high superficial liquid velocities.

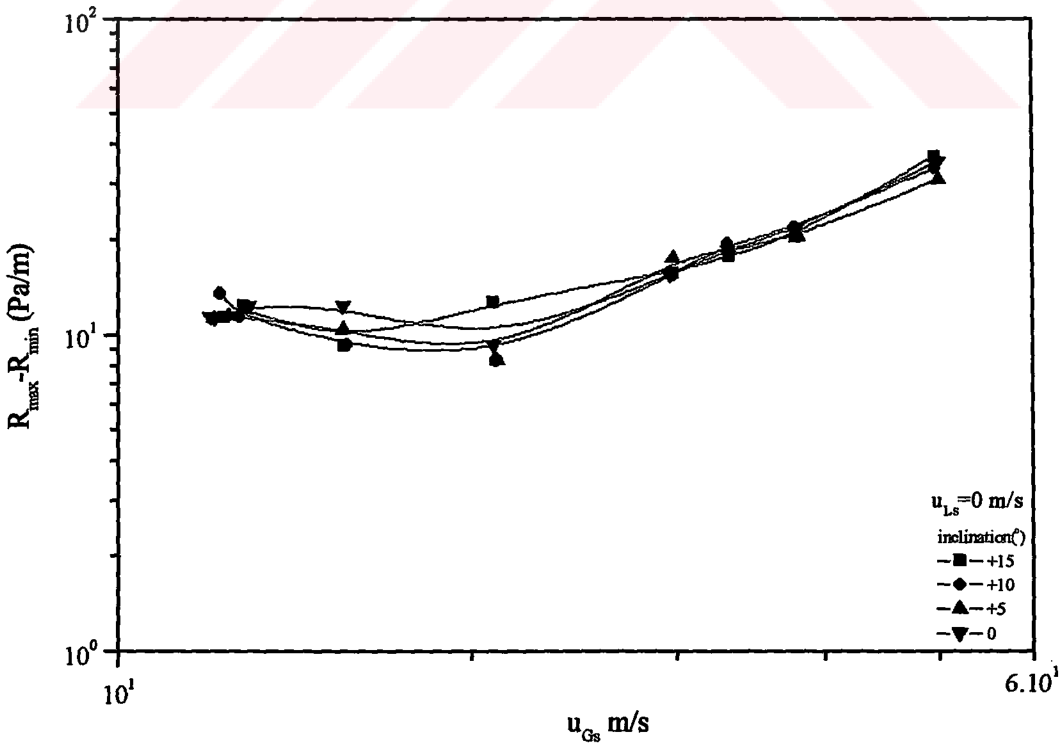

Figure 5.71. Pressure amplitude values obtained from horizontal tube, +5°, +10°, and +15° inclination experiments for a superficial liquid velocity of 0 m/s.

The same comparisons of the pressure amplitudes for gas liquid flows are given for three different constant superficial liquid velocities. They represent the results of low, intermediate, and high constant superficial liquid velocities, respectively. Figure 5.72. shows the comparison of pressure amplitudes with superficial gas velocity for all inclination experiments and for a constant superficial liquid velocity of 0.0813 m/s. The values of amplitudes are greater than those of the single phase flow. Therefore, one can express that the pressures begin to pulsate when the two phase flow is entered. Additionally, it is concluded from figure 5.72. that the pressure amplitudes increase as the inclination is increased.

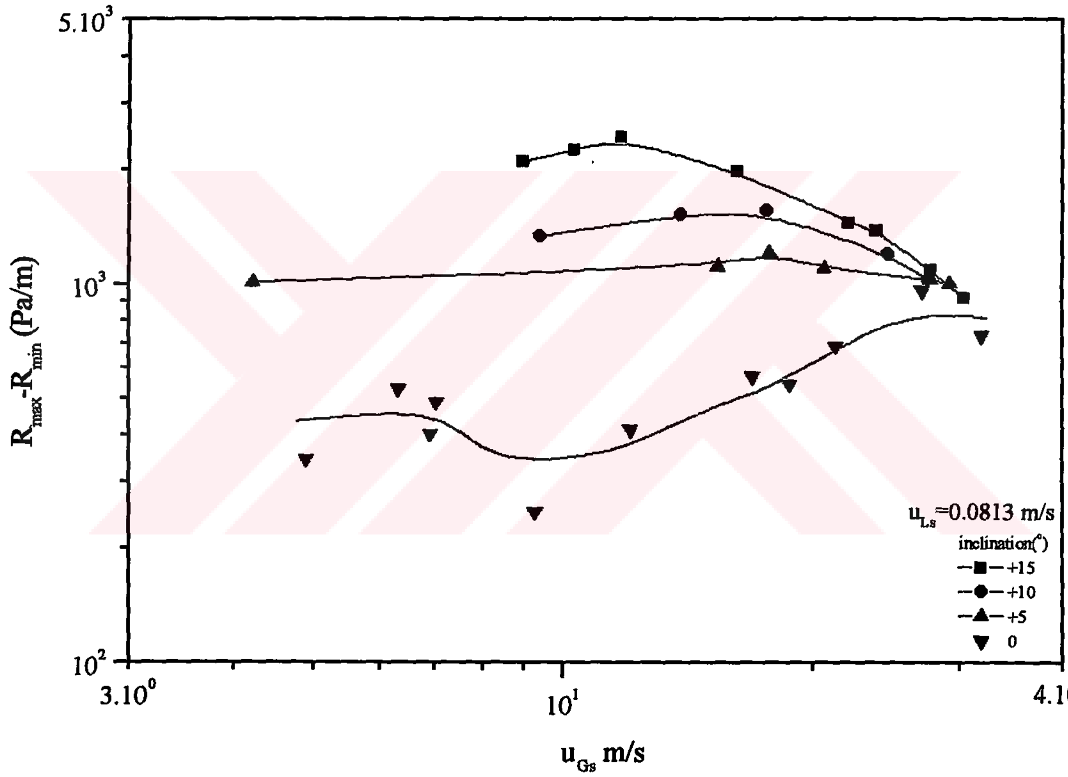

Figure 5.72. Pressure amplitude values obtained from horizontal tube, +5°, +10°, and +15° inclination experiments for a superficial liquid velocity of 0.0813 m/s.

The same trend of the amplitudes of pressure for a intermediate superficial liquid velocity of 0.2032 m/s can be seen in figure 5.73. The values of amplitudes are greater than those of 0.0813 m/s. The measured data of the amplitudes of pressure for different inclinations close to each other for high superficial gas velocities.

The variations of the amplitudes of pressure for a superficial liquid velocity of 0.3251 m/s are shown in figure 5.74. These are the highest values of the pressure amplitudes. They increase with the increasing of the inclination of the test pipe like those of 0.0813 m/s and 0.2032 m/s. The trend of the data show that they will get closer to each other for the higher superficial gas velocities.

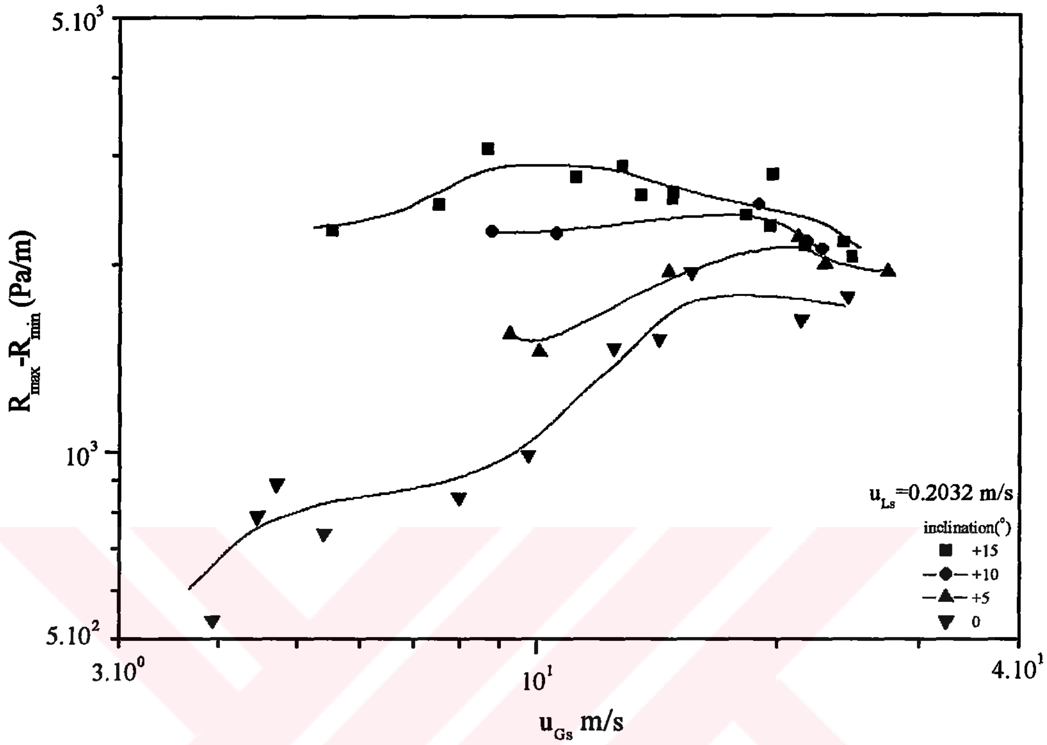

Figure 5.73. Pressure amplitude values obtained from horizontal, +5°, +10°, and +15° inclination experiments for a superficial liquid velocity of 0.2032 m/s.

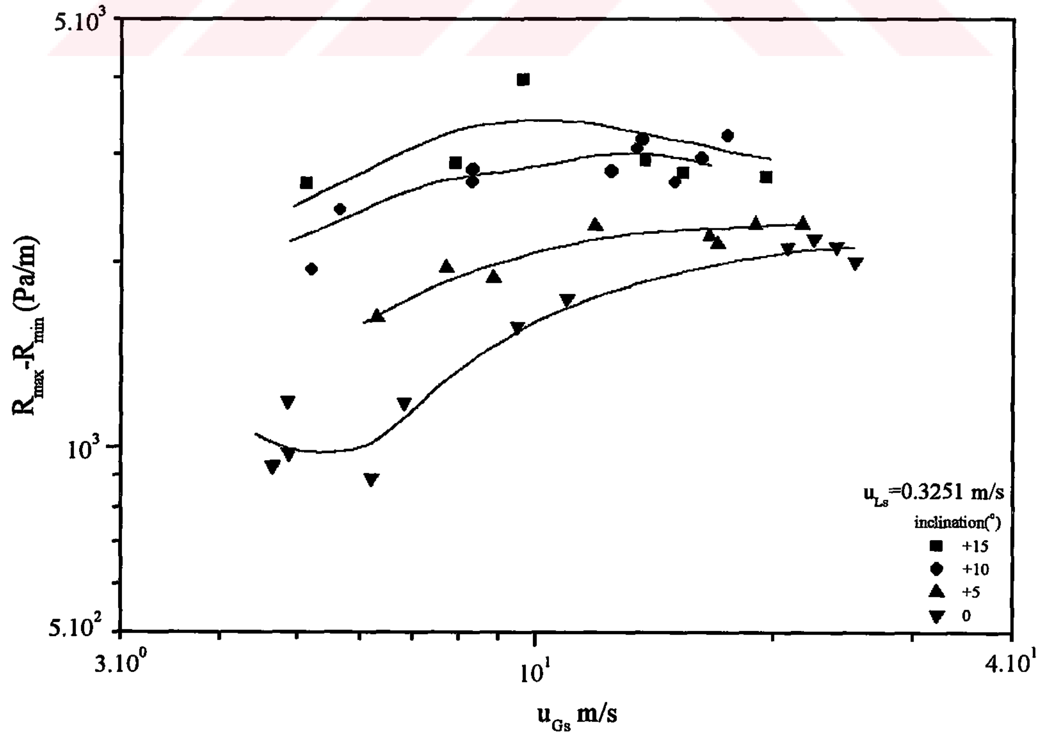

Figure 5.74. Pressure amplitude values obtained from horizontal, +5°, +10°, and +15° inclination experiments for a superficial liquid velocity of 0.3251 m/s.

5.1.6. Void Fractions of Horizontal, +5°, +10°, and +15° Inclination Experiments

Prediction and measurement of void fraction in gas liquid flows are essential for many industrial processes. For instance, the prediction of void fraction occurring during two phase gas liquid flow in pipes is of particular interest to the petroleum, chemical, and nuclear industries. In the nuclear industry, two-phase flow occurs in reactor cooling equipment, and liquid holdup (1-void fraction) greatly affects heat transfer. Two phase flow occurs frequently in chemical processing, and the design of processing equipment and piping systems requires the knowledge of liquid holdup as well, besides the pressure drop, and flow pattern. Instant variations of void fraction are very important for the determinations of flow patterns. The time dependent variation of void fraction in slug flow regime is a good example, particularly. One can at the same time see how the flowrates of a pipe operated in the slug flow regime are affected from the instantaneous variation of void fraction. Large fluctuations in the amount of liquid holdup in the pipes change the flowrate, thus, this results in overloading of processing equipment.

Void fractions in gas liquid pipe flow with different inclinations are investigated to determine the effect of pipe inclination angle on void fraction. Several good correlations exist for predicting pressure drop and liquid holdup in either horizontal or vertical flow, but these correlations have not been successful when applied to inclined pipe flow. Many gathering lines and long-distance pipelines pass through areas of hilly terrain. This presents no problem in single-phase flow because the potential energy lost going uphill is regained in the downhill section. This is not the case for two-phase flow, because the liquid holdup, and thus the mixture density, are usually much lower in downhill flow. For this reason, pressure recovery in the downhill sections is usually neglected in the design of two-phase pipelines (Beggs and Brill, 1973).

Beggs and Brill (1973) developed correlations for liquid holdup and friction factor for predicting pressure gradients for two phase flow in pipes at all angles for many flow conditions. Their results are shown in figure 5.75. Figure 5.75. shows the variation of liquid holdup with angle of pipe from horizontal.

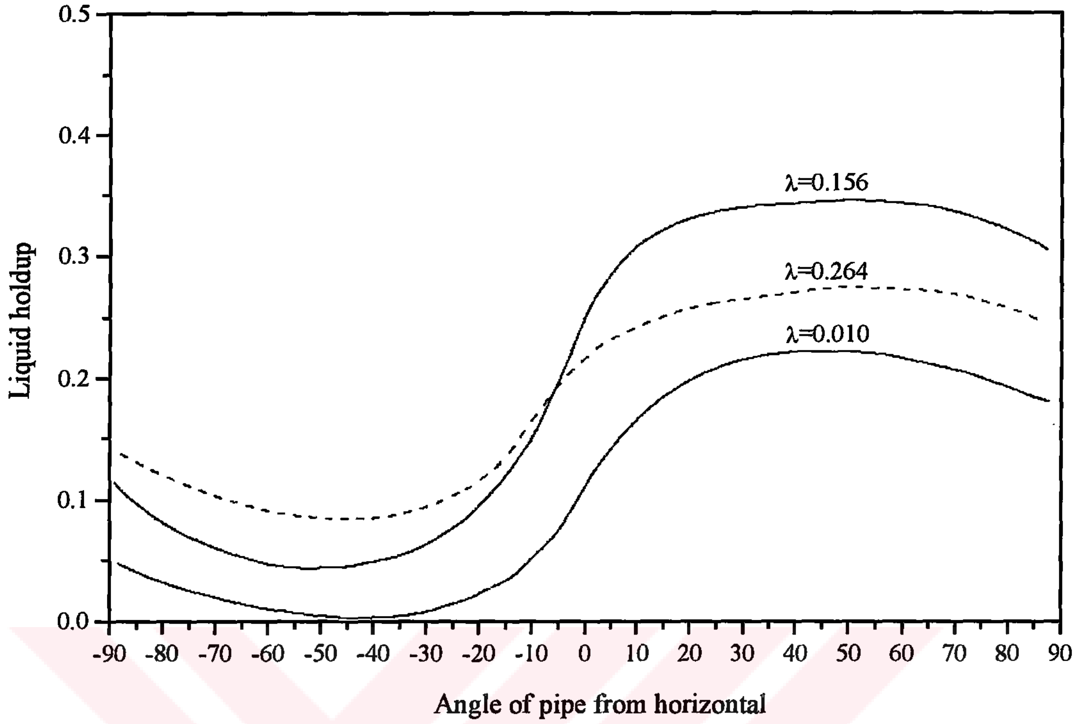

Figure 5.75. Variation of liquid holdup with angle of pipe from horizontal (+:upwards, Beggs and Brill, 1973)

λ is defined as the input liquid content which is equal to $V_L/(V_L+V_G)$. Especially, the input liquid content of 0.010 is close to some of our experimental data. Those experimental data are compared with the results of Beggs and Brill (1973) for the input liquid content of 0.010. Figure 5.76. shows the comparison of our experimental data with those of Beggs and Brill (1973). The results of Beggs and Brill were converted to the void fraction in figure 5.76. Most of the input liquid contents of our experimental data were not exactly equal to 0.010. These data were selected with a margin of ±5 and low values of input liquid content located in the upper region of the graph. The high values of input liquid content of our experimental data located in the lower region of the line. This is an expected result because the void fraction increases as the input liquid content is decreased. Additionally, void fractions measured in our experiments are lower than those of Beggs and Brill (1973) for the exactly same input liquid content values. This is probably due to the difference between the pipe diameters. Void fractions decrease as the pipe diameter is increased for the same superficial velocities and inclination angles (Kokal and Stanislav, 1989).

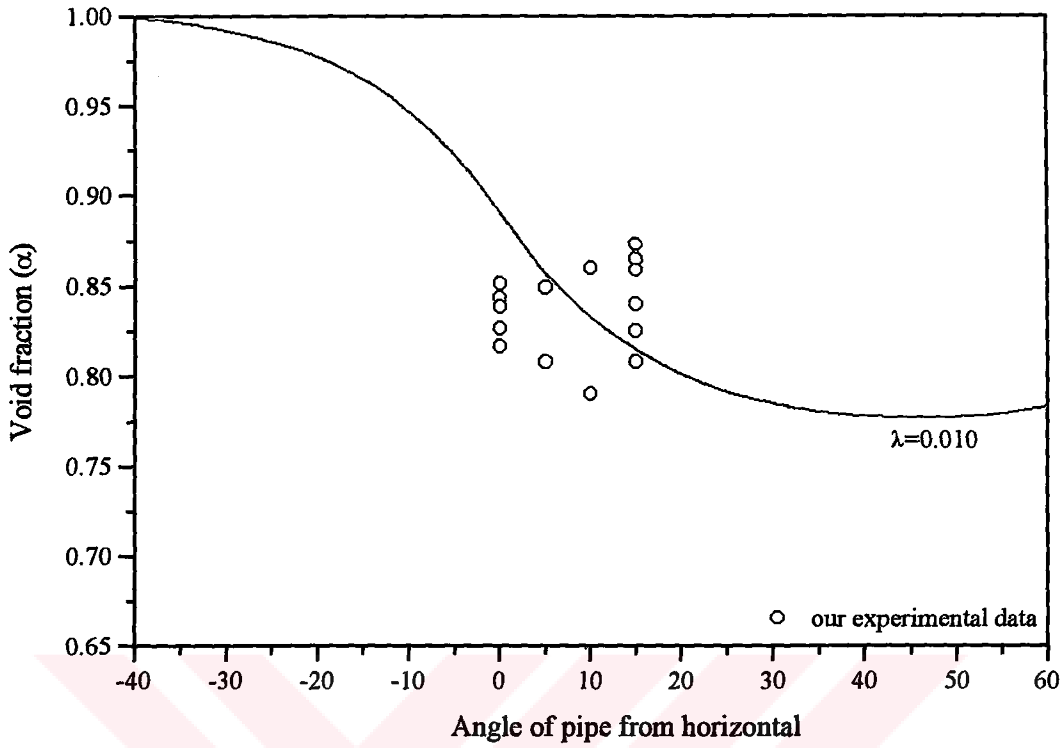

Figure 5.76. Comparison of our experimental data with those of Beggs and Brill (1973).

Kokal and Stanislav (1989) investigated the effect of pipe diameter on void fraction. They used three test pipes with different diameters and their results showed that pipe diameter has an effect on the void fraction. Figure 5.77. shows the variation of void fraction with superficial gas velocity for two different pipe diameters and for the constant superficial liquid velocity and inclination. Figure 5.77. shows that void fractions of the large pipe are lower than those of the small pipe for the same superficial velocities and inclination angles.

The diameter of the first test pipe (51.2 mm) of Kokal and Stanislav (1989) is close to that of our test pipe (59 mm). The void fractions measured by Kokal and Stanislav (1989) in 51.2 mm pipe are compared with some of our measurements. Figure 5.78. shows this comparison. The inclination of the test pipe is +5°. The void fractions obtained in this study are lower than those of Kokal and Stanislav (1989). It should be firstly expressed that the results of other investigators don't reach a fully agreement with each others, as well. However, our results were measured for a little bit higher superficial liquid velocities. This certainly causes a decrease in void fraction in the pipe. Another parameter is the pipe diameter whose effect on the void fraction is explained before. The diameter of our test pipe is larger than that of the

Kokal and Stanislav (1989). Thus, one can conclude that the results of our experiments agree with those of Kokal and Stanislav (1989).

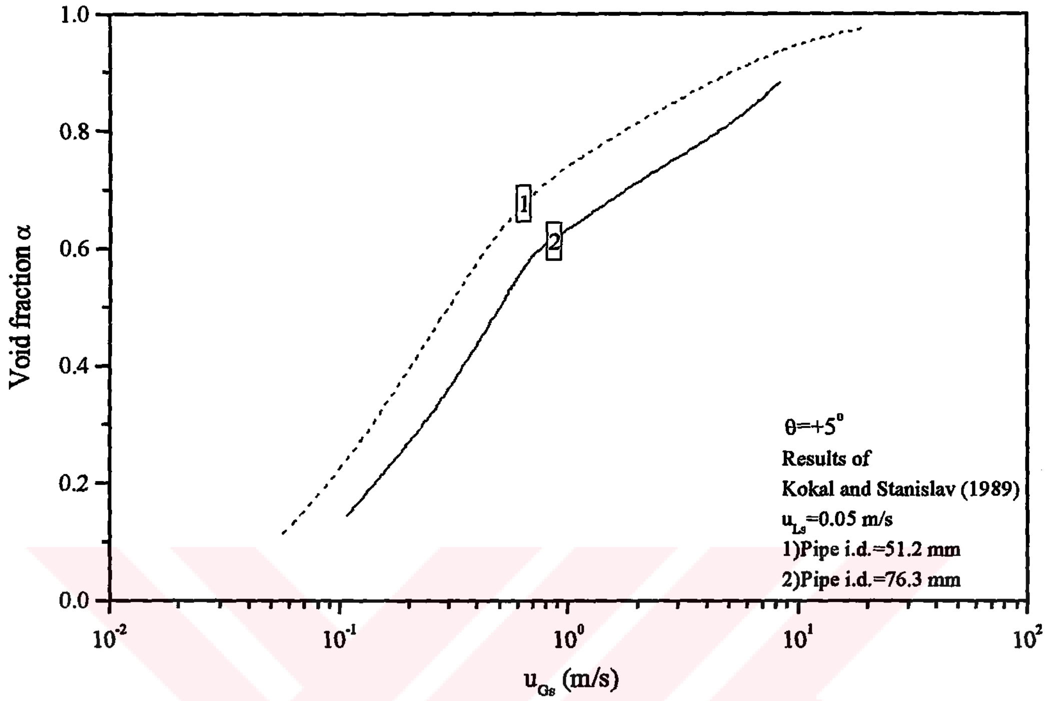

Figure 5.77. Variation of void fraction with superficial gas velocity for two different pipe diameters and for a constant superficial liquid velocity and inclination (Kokal and Stanislav, 1989).

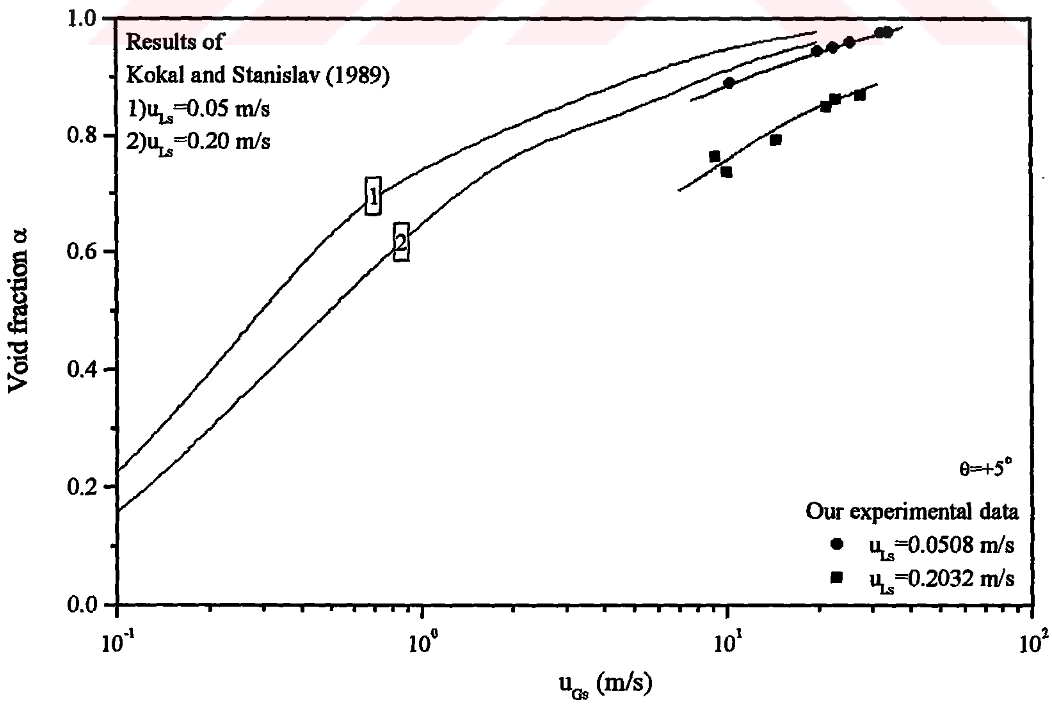

Figure 5.78. Comparison of our experimental data with the results of Kokal and Stanislav (1989).

Figure 5.79. shows the variation of liquid holdup with superficial gas velocity for horizontal flow. These results have been measured by Spedding et al. (1998). The liquid holdup values measured by Spedding et al. (1998) are converted to the void fractions. These values are compared with the void fractions measured in the horizontal flow experiments. Figure 5.80. shows the comparison of our horizontal flow experiments with those of the Spedding et al. (1998).

The nearest constant superficial liquid velocities of this study to those of Spedding et al. (1998) are selected for the comparison of void fractions. For example; line 5 in figure 5.80. shows the variation of void fraction with superficial gas velocity for a constant superficial liquid velocity of 0.0411 m/s. The experimental void fraction measurements for a constant superficial liquid velocity of 0.0508 m/s are located lower than those of 0.0411 m/s. This is physically meaningful, because void fraction decreases as the superficial liquid velocity is increased.

The void fractions given by Spedding et al. (1998) were measured in a test pipe with an inner diameter of 50.8 mm. The inner diameter of our test pipe is greater than that of Spedding et al. (1998). Thus, void fractions measured in our experiments should be lower than those of Spedding et al. (1998) according to results of Kokal and Stanislav (1989).

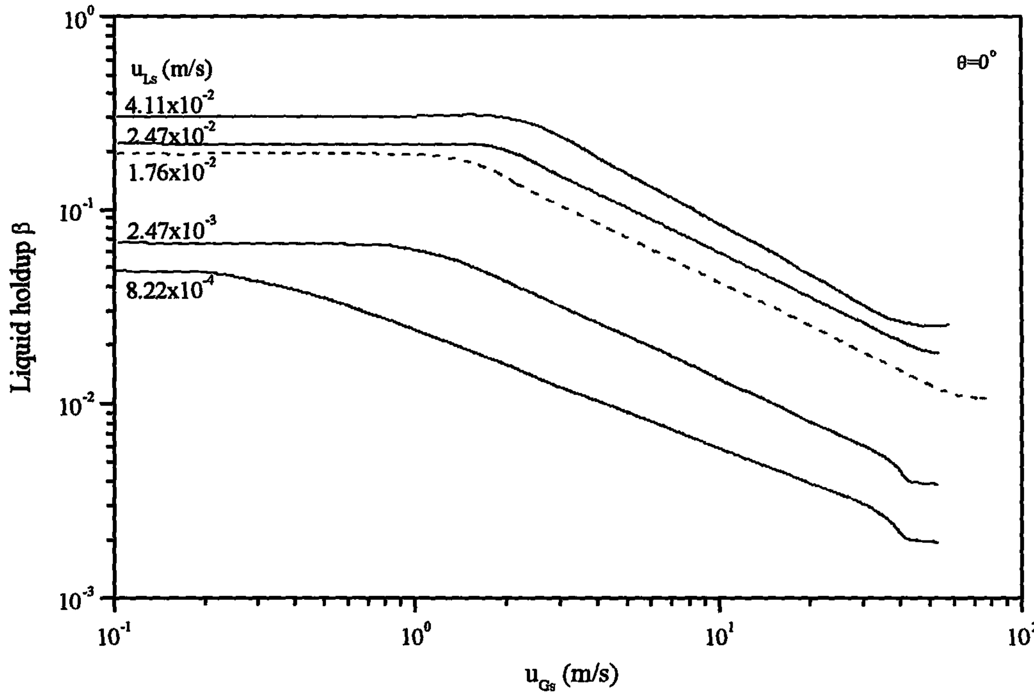

Figure 5.79. Variation of liquid holdup with superficial gas velocity for horizontal flow (Spedding et al. (1998)).

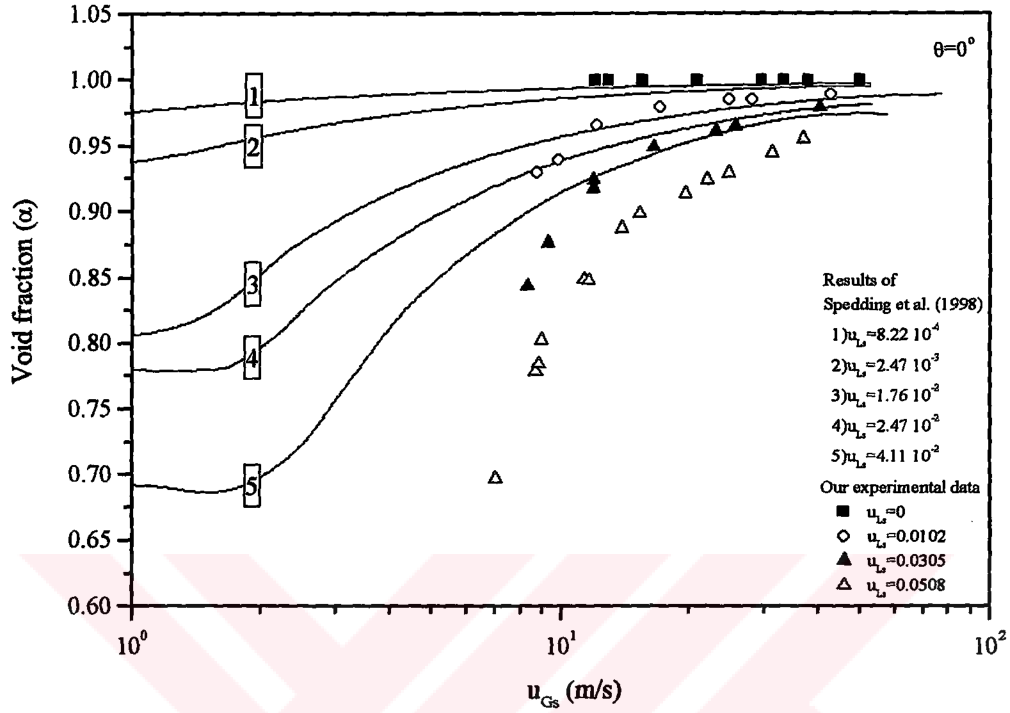

Figure 5.80. Comparison of our experimental data with the results of Spedding et al. (1998).

The void fractions measured in experiments are compared with the void fractions calculated using two different methods. First one of these methods are proposed by Lochart-Martinelli (LMM). Second method is the theoretical calculation method (TCM). Calculation of void fraction according to these methods have been explained in detail by Yılmaz (2001). Void fractions of horizontal flow experiments are used for the comparison with these methods. Figure 5.81. shows the comparison of measured void fractions with those calculated according to LMM and TCM.

Figure 5.81. shows that the measured void fractions is well predicted by TCM for low superficial gas velocities. The predictions of LMM are better than those of TCM for high superficial liquid velocities. This comparison is carried out for a constant superficial liquid velocity of 0.0102 m/s. Another comparison is given below for a constant superficial liquid velocity of 0.0508 m/s (Figure 5.82.).

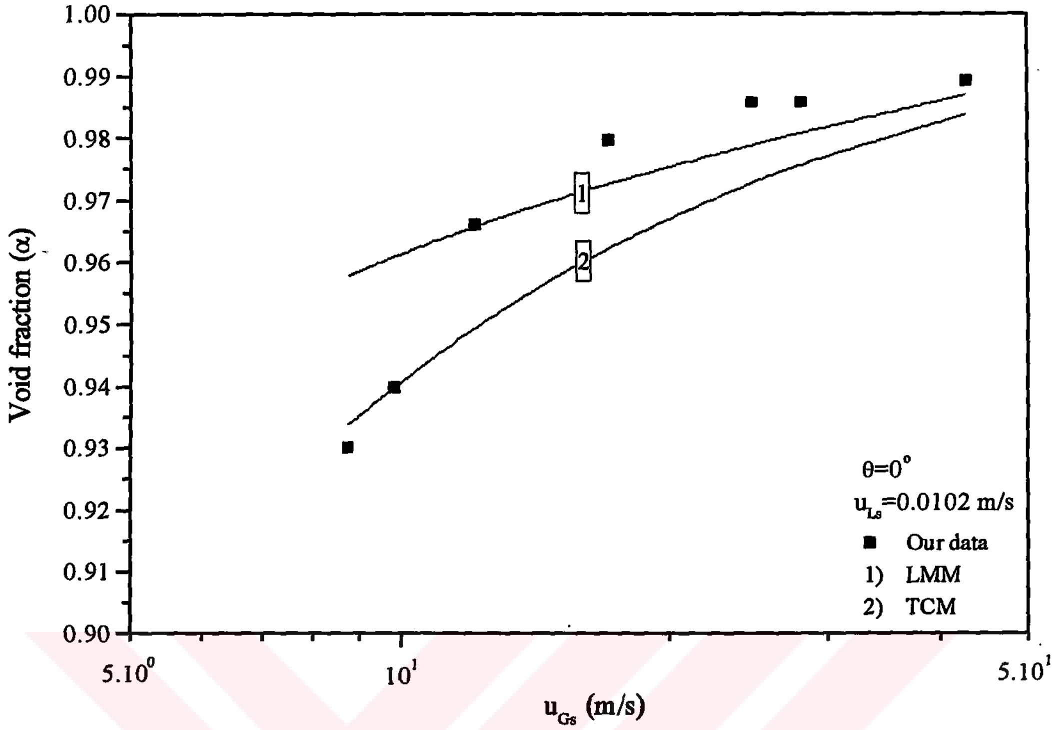

Figure 5.81. Comparison of measured void fractions with those calculated according to LMM and TCM.

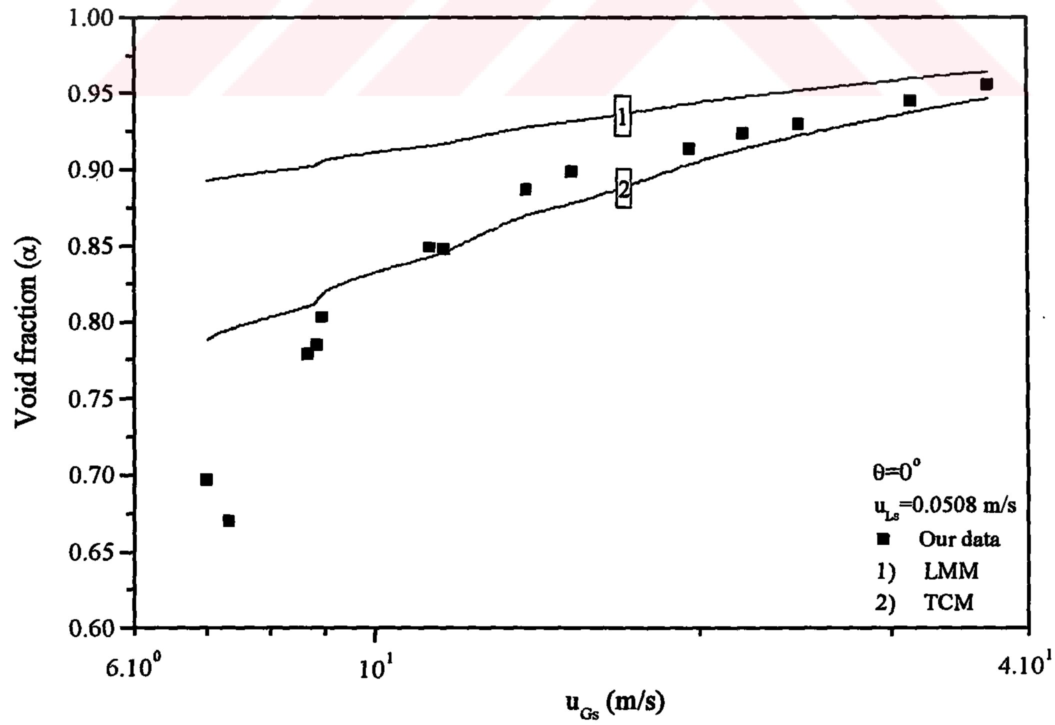

Figure 5.82. Comparison of measured void fractions with those calculated according to LMM and TCM.

The measured void fractions in the horizontal flow experiments are lower than those of TCM for the superficial gas velocities below 10 m/s. Rest of the measured values are located between the results of LMM and TCM.

A similar trend is observed for a constant superficial liquid velocity of 0.2032 m/s (Figure 5.83.). The LMM predicts higher void fractions than our data, but the TCM predicts lower void fractions than ours, for the superficial gas velocities between 5 and 20 m/s.

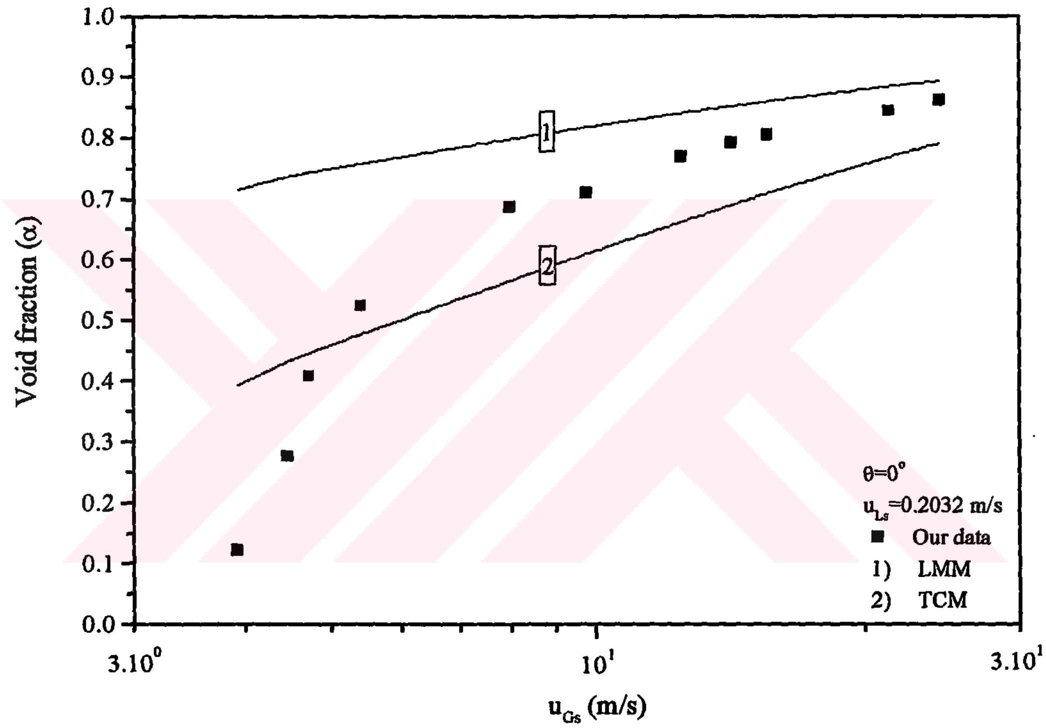

Figure 5.83. Comparison of measured void fractions with those calculated according to LMM and TCM.

The highest constant superficial liquid velocity of our experiments is 0.3251 m/s. The comparison of the measured void fractions with those calculated according to LMM and TCM is shown in figure 5.84. The measured void fractions are mostly located between LMM and TCM. Three of the void fractions measured are lower than those of TCM below the superficial gas velocity of 5 m/s.

Comparisons of the void fractions measured with the LMM and TCM for all superficial gas and liquid velocities have shown that the measured void fractions are in agreement with the LMM and TCM. The void fractions measured in our experiments locate between those of the LMM and TCM in the majority of measurement range. The variations of the measured void fractions with the superficial gas velocity for all the constant superficial liquid velocities are nearly similar to each other. The trend of variation of the measured void fraction are different than those of the LMM and TCM. The measured void fraction increases steeply for low superficial gas velocities, and then follows the same trend like those of LMM and TCM.

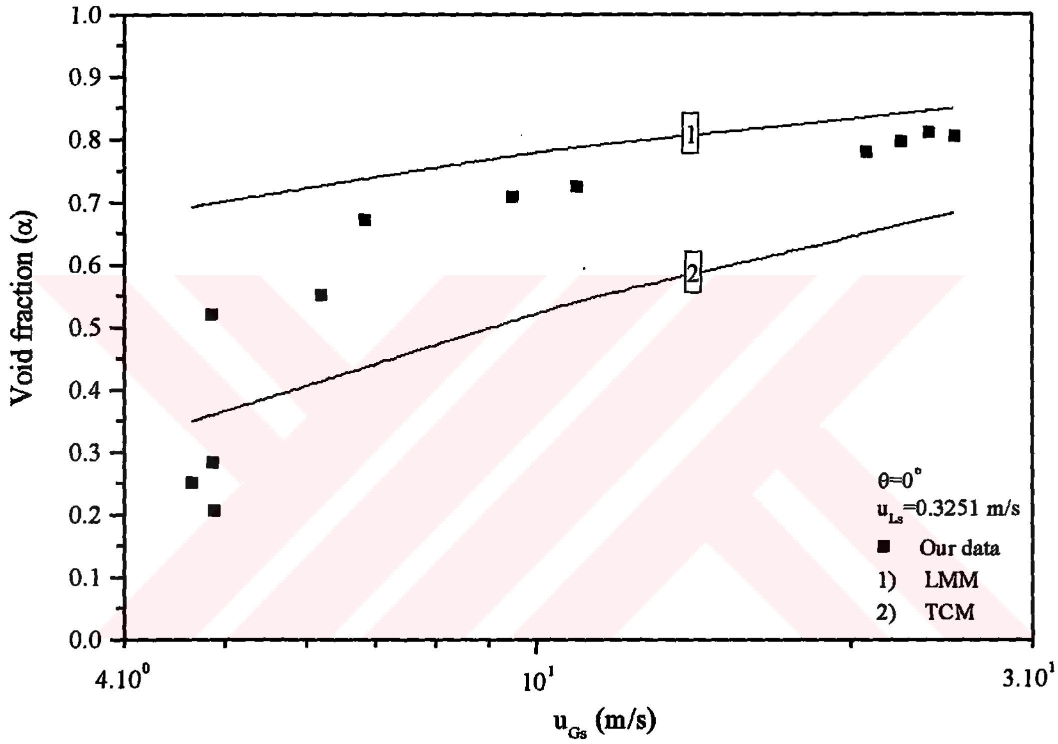

Figure 5.84. Comparison of measured void fractions with those calculated according to LMM and TCM.

The reason of the steep increase of void fraction for low superficial gas velocities is probably due to the measurement process of the void fraction. The flow pattern in that region is mostly slug or blow through slug flow. The void fractions of these flow patterns greatly change with time. Thus, the mean void fractions which are used for this comparison are dependent on slug frequency, slug length, and slug velocity. The measurement process of the void fraction takes at most 2 or 3 seconds, and two or three slugs can be catched during this period of time. Thus, the mean void fraction measured can be lower than that of sufficiently long time period depending on the frequency and velocity of liquid bulks.

After comparisons of the void fractions measured with the results of other investigations and methods, the void fractions measured in the experiments with different inclinations have been compared with each other. Figure 5.85. shows the variation of void fraction with superficial gas velocity for different inclinations of experimental setup for a constant superficial liquid velocity of 0.0102 m/s. This is the minimum value of superficial liquid velocity used in experiments of two phase flow. The measured void fractions of +10° inclination experiments are absent for this constant superficial liquid velocity because of a misreading of the void fraction sensor. The measured void fractions of +15° inclination experiments are lower than those of the horizontal flow and +5° inclination experiments. However, the measured void fractions of +15° inclination experiments are higher than that of the horizontal flow experiments.

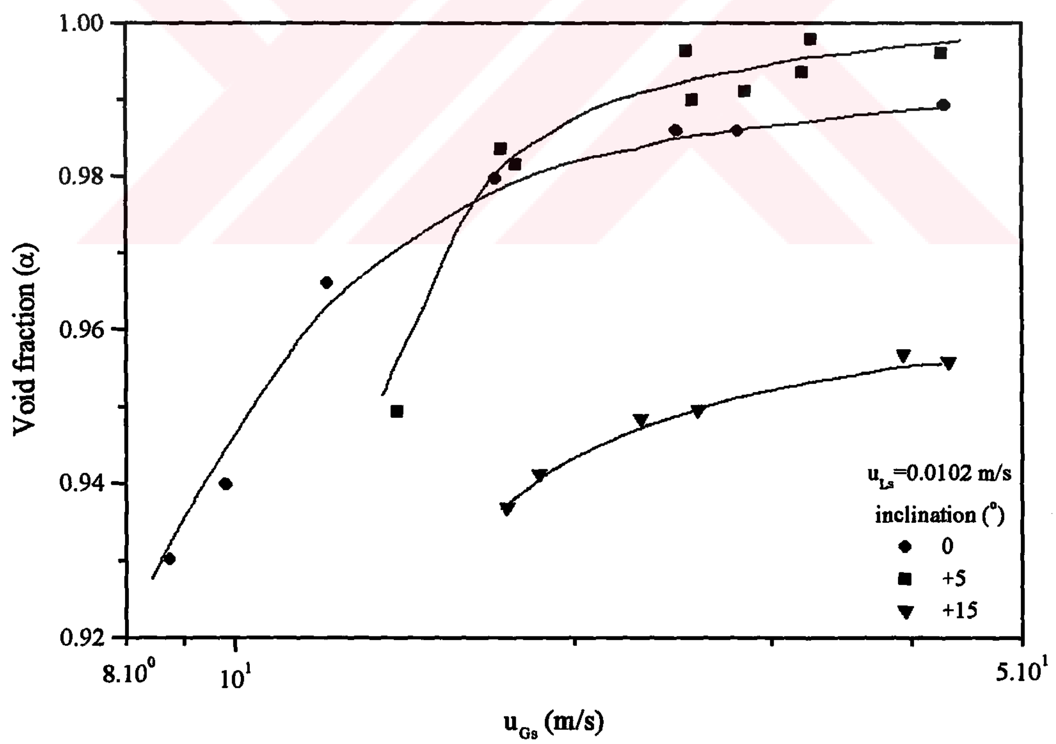

Figure 5.85. Variation of void fraction with superficial gas velocity for different inclinations of experimental setup for a constant superficial liquid velocity of 0.0102 m/s.

Figure 5.86. shows the variation of void fraction with superficial gas velocity for horizontal flow, +5°, +10°, and +15° inclinations of experimental setup for a constant superficial liquid velocity of 0.0508 m/s. The results of +5° inclination

experiments are higher than those of others. However, the void fractions measured in +15° inclination experiments are not the minimum values in the graph. The void fractions of +10°, and +15° inclination experiments are lower than those of horizontal flow experiments below the superficial gas velocity of 15 m/s, but they locate between those of horizontal flow and +5° inclination experiments above the superficial gas velocity of 15 m/s.

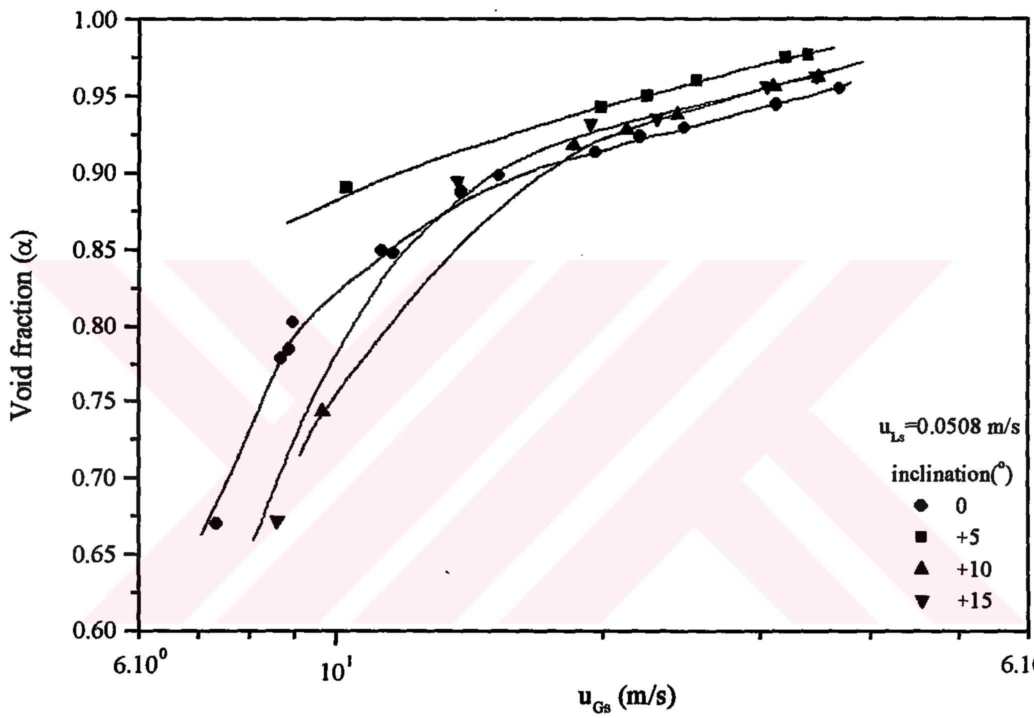

Figure 5.86. Variation of void fraction with superficial gas velocity for different inclinations of experimental setup for a constant superficial liquid velocity of 0.0508 m/s.

Similar variation of void fractions with superficial gas velocity, especially for those of +10° and +15° inclination experiments, are shown in figure 5.87. for the constant superficial liquid velocity of 0.0813 m/s. The void fractions measured of +5° inclination experiments are still higher than the others. The void fraction values of +10°, and +15° inclination experiments are lower than those of horizontal flow experiments below the superficial gas velocity of 10 m/s, but they sit between those of horizontal flow and +5° inclination experiments above the superficial gas velocity of 10 m/s. However, the void fractions of +10°, and +15° inclination experiments approach to those of horizontal flow experiments.

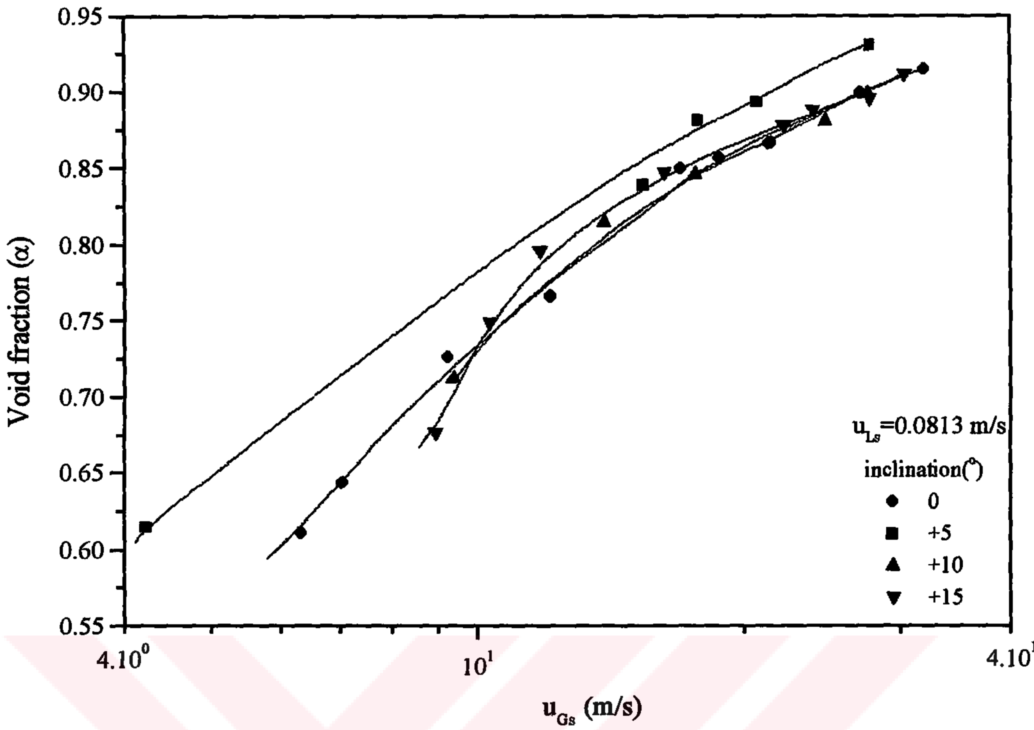

Figure 5.87. Variation of void fraction with superficial gas velocity for different inclinations of experimental setup for a constant superficial liquid velocity of 0.0813 m/s.

Similar variations of void fractions for different inclination experiments are shown in figure 5.88. below for a constant superficial liquid velocity of 0.1219 m/s. The results of +5° inclination experiments are higher than the others, and the void fractions measured in horizontal flow experiments are approximately minimum. The void fractions measured of +10°, and +15° inclination experiments are completely located between those of horizontal flow and +5° inclination experiments. There is a similarity between the void fractions of +10°, and +15° inclination experiments for the constant superficial liquid velocities of 0.0813 and 0.1219 m/s. They get closer to the void fractions of horizontal flow experiments as the superficial gas velocity is increased.

The comparison of void fractions for different inclinations for a constant superficial liquid velocity of 0.1626 m/s are shown in figure 5.89. The void fractions measured in +5° inclination experiments are the minimum values in this superficial liquid velocity. They are lower than those of horizontal flow, +10°, and +15° inclination experiments. The results of +10° and +15° inclination experiments are very close to each other. They are higher than those of horizontal flow experiments. There are no big differences between the void fractions of +10°, and +15° inclination experiments. Additionally, the similar trend of the void fractions for horizontal flow, +5°, +10°, and +15° inclination experiments attract the attention. They come closer to each other as the superficial liquid velocity is increased.

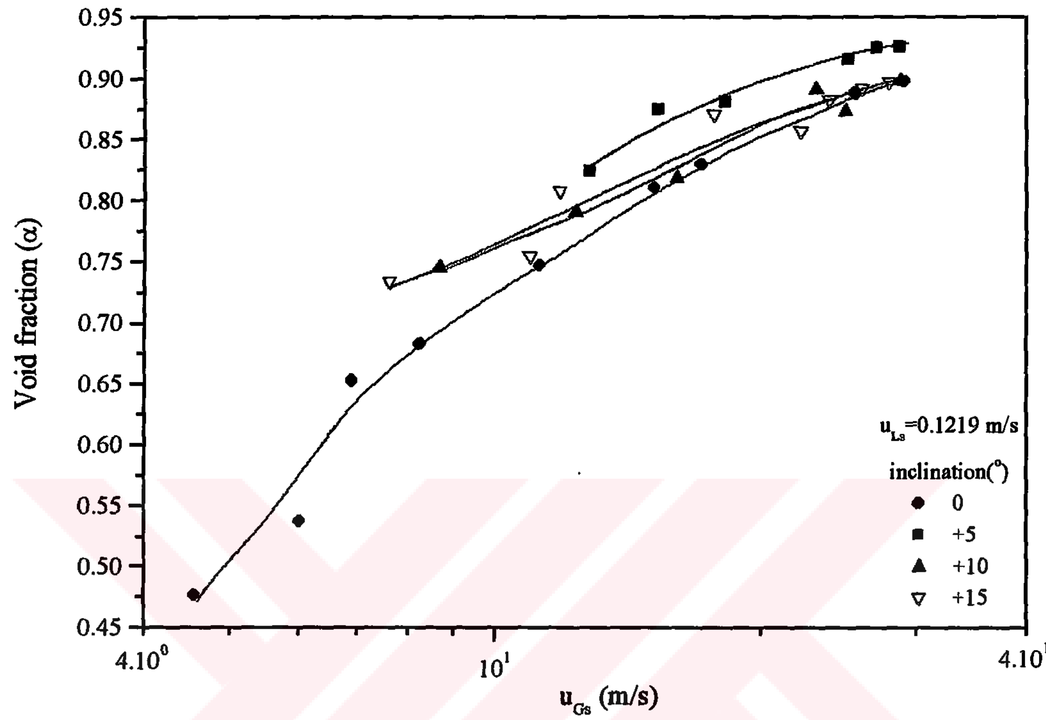

Figure 5.88. Variation of void fraction with superficial gas velocity for different inclinations of experimental setup for a constant superficial liquid velocity of 0.1219 m/s.

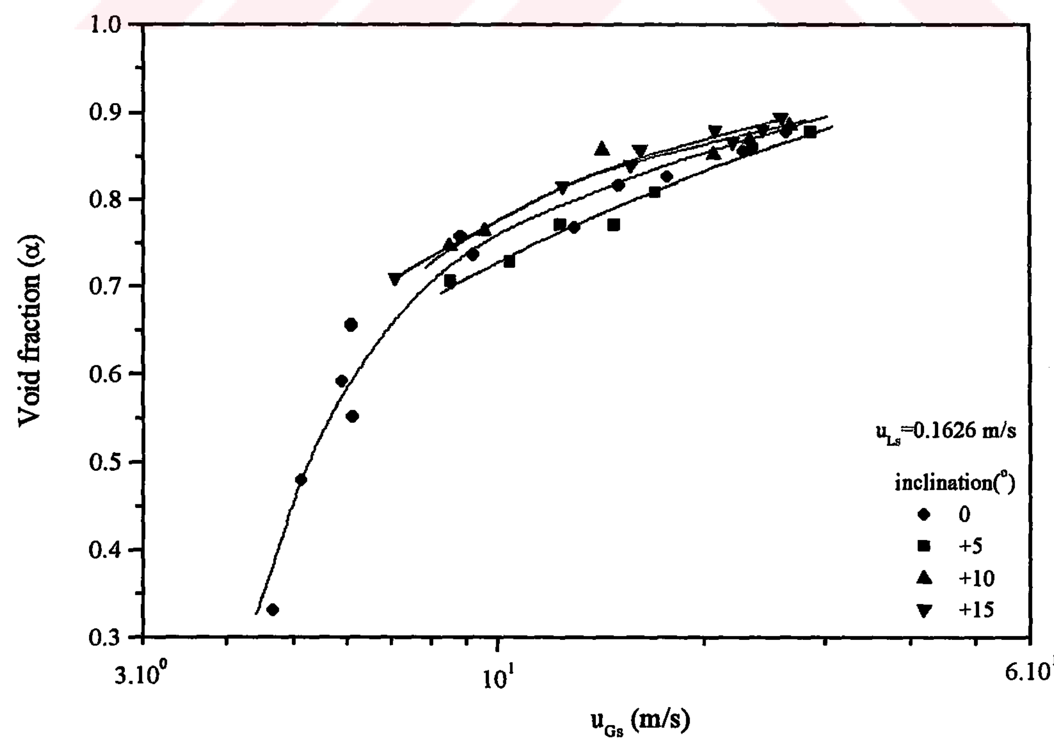

Figure 5.89. Variation of void fraction with superficial gas velocity for different inclinations of experimental setup for a constant superficial liquid velocity of 0.1626 m/s.

The variations of the measured void fractions for a constant superficial liquid velocity of 0.2032 m/s are similar to those of a constant superficial liquid velocity of 0.1626 m/s. This is shown in figure 5.90. The void fractions of all inclination experiments are spread out as mixed regardless of the difference of inclination. The approximately mean lines of the measured void fractions are very close to each other above the superficial gas velocity of 10 m/s. One can express that there are no big differences as the inclination of the experimental setup is increased.

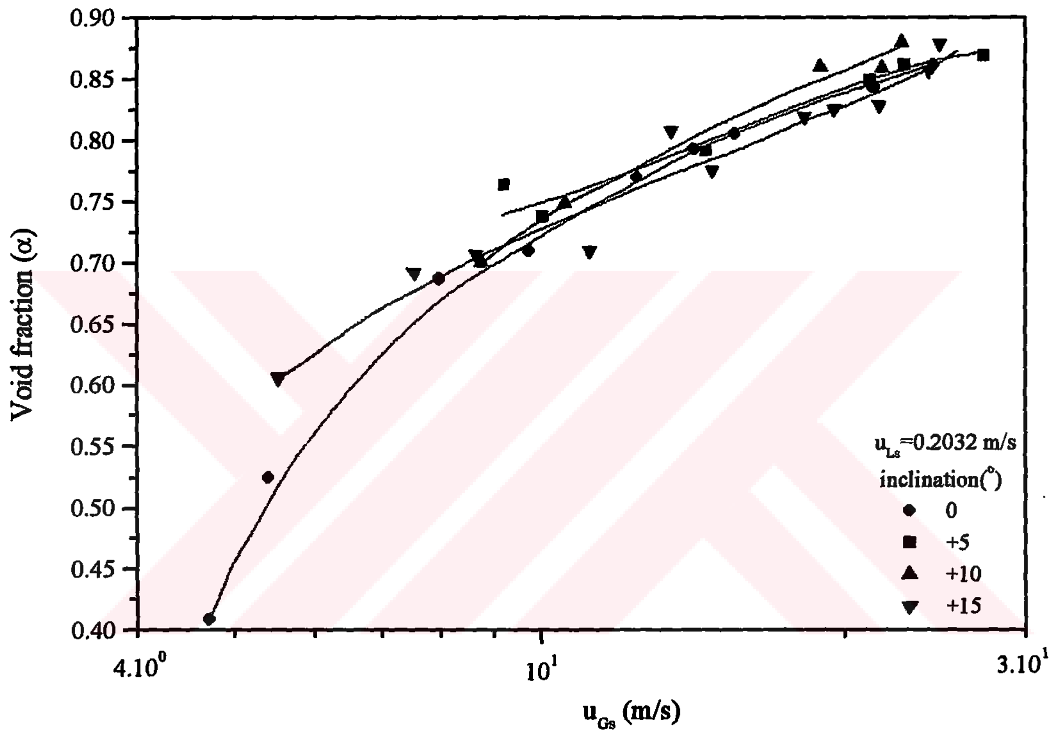

Figure 5.90. Variation of void fraction with superficial gas velocity for different inclinations of experimental setup for a constant superficial liquid velocity of 0.2032 m/s.

Similar variations of void fractions for different inclination experiments are shown in figure 5.91. for a constant superficial liquid velocity of 0.2438 m/s. The approximation of measured data are seen between the superficial gas velocities of 10 and 20 m/s. There is a separation of data out of this region.

Similar variation to the previous figure is shown in figure 5.92. for a constant superficial liquid velocity of 0.3251 m/s. There is an approximation of measured data between the superficial gas velocities of 7 and 10 m/s. One can conclude from the variations of void fractions with superficial gas velocity for all constant superficial liquid velocities that there is a region in which void fractions of different inclination experiments get closer to each other. In addition, this region is withdrawn as the constant superficial liquid velocity is increased.

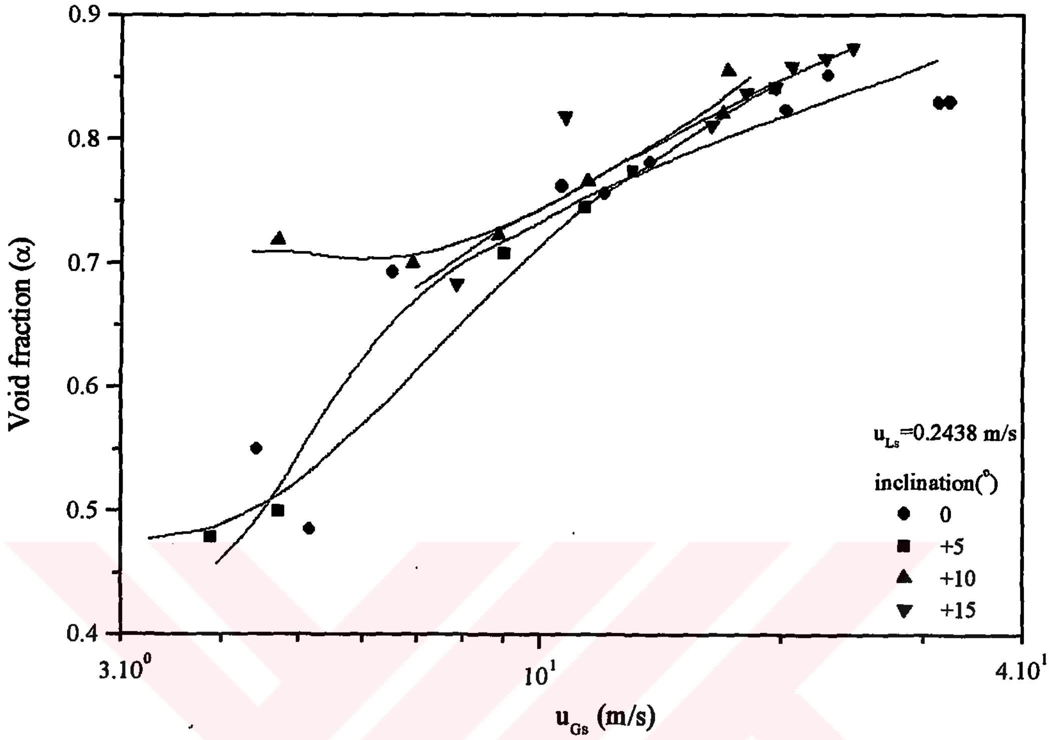

Figure 5.91. Variation of void fraction with superficial gas velocity for different inclinations of experimental setup for a constant superficial liquid velocity of 0.2438 m/s.

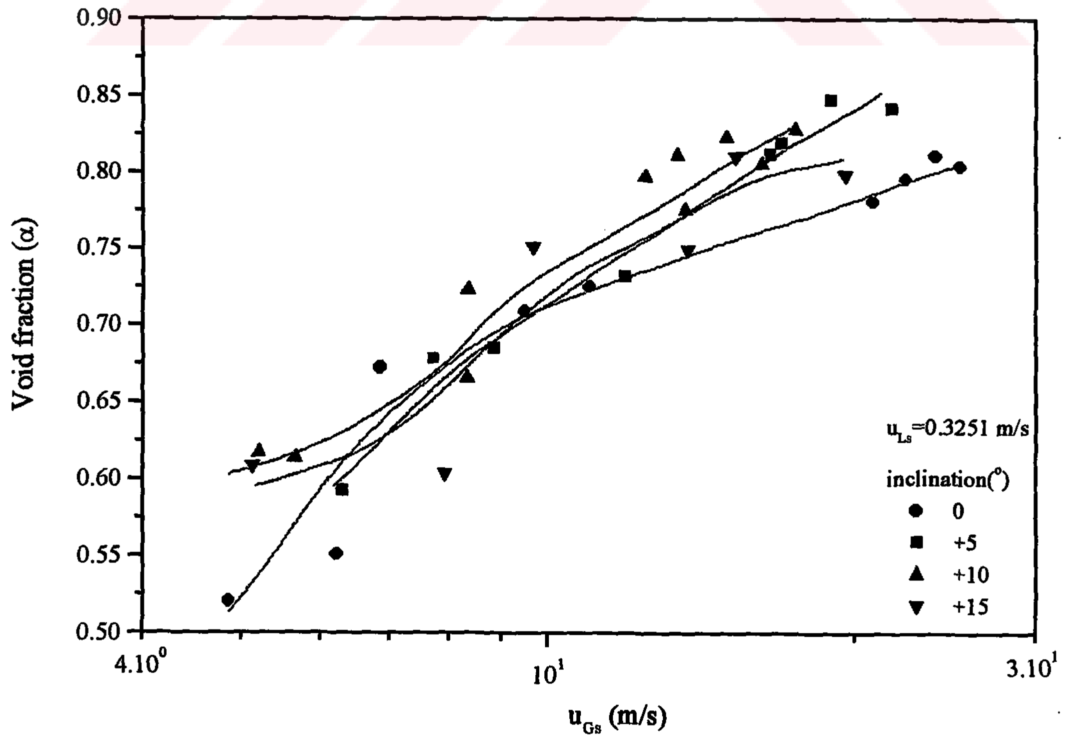

Figure 5.92. Variation of void fraction with superficial gas velocity for different inclinations of experimental setup for a constant superficial liquid velocity of 0.3251 m/s.

Figure 5.93 shows the variation of slopes of void fraction curves with the constant superficial liquid velocity. The slopes of the void fractions curves are measured in the region where the curves get closer to each other.

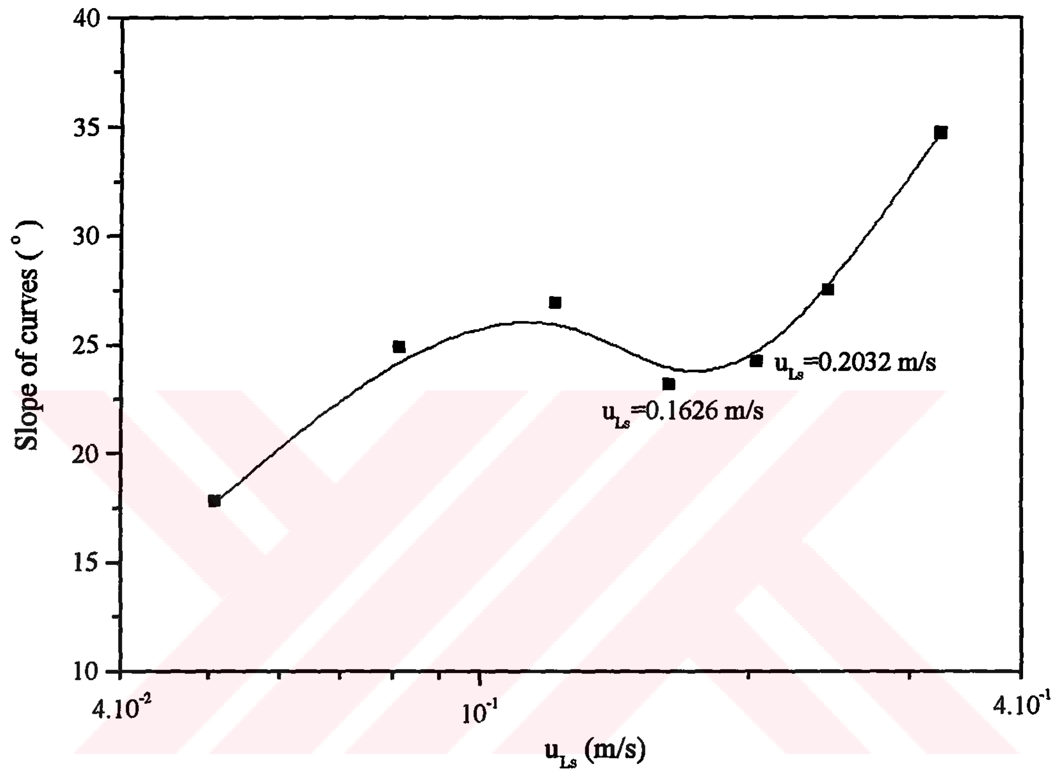

Figure 5.93. Variation of slopes of void fraction curves with the constant superficial liquid velocity.

The slope of curves increase as the superficial liquid velocity is increased except two points which are shown in the figure 5.93. The slopes of curves decrease for two constant superficial liquid velocities of 0.1626 and 0.2032 m/s. This is interesting because the most closeness between the void fractions of different inclination experiments are seen in these experiments. The other experiments show a tendency of dispersed variation of different inclination experiments.

As a result of discussions on void fractions; it can be expressed that inclination of the experimental setup has an effect on the void fraction. This effect is clearly shown in figures, but it is not possible to conclude from these figures how the void fraction is affected from the changing of the inclination. More data are needed to express a concrete conclusions.

5.1.7. Slug Velocities of Horizontal, +5°, +10°, and +15° Inclination Experiments

The primary characteristic of slug flow is its inherent intermittence. The slug flow is unsteady, even when the flow rates of gas and liquid are kept constant at the pipe inlet. The elementary part of slug flow is a cell, involving the region of a long bubble plus the region of the following liquid slug (Figure 5.94.).

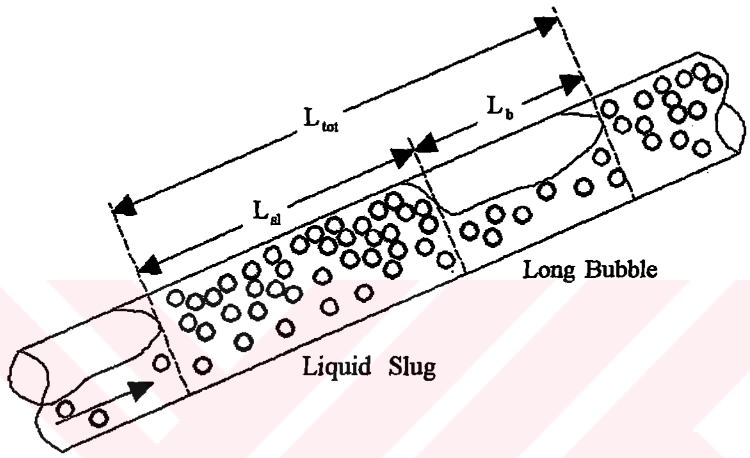

Figure 5.94. A unit cell of a slug flow.

The slug of liquid of length L_{sl} carrying dispersed bubbles, travels at a velocity V_{sl}. It overruns a slower moving liquid in the separated film. During stable slug flow, liquid is shed from the back of the slug at the same rate liquid is picked up at the front. As a result, the slug length stays constant as it travels along the tube.

For horizontal or near horizontal tubes, the liquid shed at the back decelerates under the influence of wall shear and forms a stratified layer. For vertical or near vertical tubes the liquid forms a falling annular film and accelerates as it moves downward. The separated section containing a large gas bubble has a length, L_b. Most of the gas is transported in these large gas bubbles.

As this kind of flow occurs over a wide range of intermediate flow rates of gas and liquid, it is interesting for many industrial processes such as the production of oil and gas, the geothermal production of steam, the boiling and condensation processes, the handling and transport of cryogenic fluids and the emergency cooling of nuclear reactors. The existence of slug flow can create problems for the designer or operator. The high momentum of the liquid slugs can create considerable force as they change direction passing through elbows, tees, etc. Furthermore, the low frequencies of slug flow can be in resonance with large piping structures and severe damage can take place. In addition, the intermittent nature of the flow makes it necessary to design liquid separators to accommodate the largest slug length. In contrast, there are numerous practical benefits which can result from operating in the slug flow pattern. Because of the very high liquid velocities, it is usually possible to move larger amounts of liquids in smaller lines than would otherwise be possible in two phase flow. In addition, the high liquid velocities cause very high convective heat and mass transfers resulting in very efficient transport operations (Hewitt et al.(1996)).

Nicklin et al.(1962) proposed a model for the prediction of slug velocity. In the past forty years, the model of unit cell has been perfected by several investigators so that it appears as the ultimate 1D approach. The concept bases on the two following assumptions. Firstly, there exists a frame of a given velocity V_{sl} in which the flow is almost steady. Secondly, in this frame the flow of long bubbles and liquid slugs is fully developed. Nicklin et al.(1962) formulated the slug velocity, V_{sl}, as a function of the mixture velocity. According to the results of several investigators, the $V_{sl}(u_{mix})$ relation is linear over certain ranges of mixture velocity, $u_{mix} = u_{Gs} + u_{Ls}$, supporting the assumption of Nicklin et al. (Hewitt et al.(1996)). The velocity of single bubble motion is expressed by Nicklin et al.(1962) as follows;

$$V_{sl} = C_0 u_{mix} + C_{\infty}\sqrt{gD} \tag{5.2}$$

where C_0 and C_{∞} are two coefficients which remains constant for some range of mixture velocity and fluid properties. However, secondary effects due to viscosity, surface tension and pipe inclination complicate this law. Nicklin et al.(1962) proposed two different values for the coefficients of C_0 and C_{∞}. These are;

a) $C_0 = 1.2$ and $C_{\infty} = 0$. (5.3)

b) $C_0 = 1$ and $C_{\infty} = 0.54$. (5.4)

The value of the constant C_0 is based upon the assumption that the propagation velocity of the bubbles equals the maximum local velocity in front of the nose tip (Nicklin et al.(1962)). Therefore, $C_0 = 1.2$ which is the ratio $u_{\max} / u_{mean}$ for turbulent flow can be used as a good engineering approximation. The calculated slug velocities of this investigation have been compared with the expression of Nicklin et al.(1962) using the coefficients given in eqs.(5.3) and (5.4).

Kouba and Jepson (1990) studied experimentally the flow characteristics in horizontal slug flow in a 150-mm-diameter pipeline. For several of the tests, high-speed video together with flash photography were used to study the flow characteristics detail at the front of the slug and in the slug body. The authors expressed that the ratio of the translational velocity of the slug to the mixture velocity decreases continuously up to 2.0 at low-mixture velocities and 1.25 above the mixture velocity of approximately 3 m/s. After this point, the ratio of the translational velocity of the slug to the mixture velocity remains constant at 1.25. This shows that there is a drift velocity, u_d, required in the calculation of V_{sl} below 3 m/s. This has also been reported by Jepson (1988) to be true in a 300-mm-diameter pipeline. Most of the mixture velocities measured in this investigation are greater than 3 m/s, therefore, the equation below have been used for the comparison of the calculated slug velocities of this investigation.

$$V_{sl} = 1.25 u_{mix} \tag{5.5}$$

The variation of slug velocity with the mixture velocity is shown in figure 5.95. The calculated slug velocities in horizontal flow experiments are also given for different constant superficial liquid velocities. The predictions of Nicklin et al.(1962) and Kouba and Jepson (1990) are given in the same figure. The trend of the data is predicted well by the equations of the authors mentioned above. The slug velocities of horizontal experiments are higher predicted by these expressions, however, one should remember that Kouba and Jepson (1990) have talked about an uncertainty below the mixture velocity of 3 m/s.

The slug velocities calculated in the +5° inclination experiments are mostly in agreement with the others. The slug velocities below the mixture velocity of 3 m/s are higher than those of the others. Nicklin et al. (1962) (b) predict the experimental results more precisely above the mixture velocity of 3 m/s. The variation of slug velocity with the mixture velocity is shown in figure 5.96. for different constant superficial liquid velocities. According to figure 5.96., there is a feeling that slug velocity increases as the constant superficial liquid velocity is increased. However, more data is needed for the concrete conclusion.

The slug velocities calculated in the +10° inclination experiments are mostly in disagreement with the others. The slug velocities below the mixture velocity of 3 m/s are higher than those of the others. Nicklin et al. (1962) (a) and Kouba and Jepson (1990) predict the experimental results more precisely above the mixture velocity of 3 m/s. The variation of slug velocity with the mixture velocity is shown in figure 5.97. for different constant superficial liquid velocities..

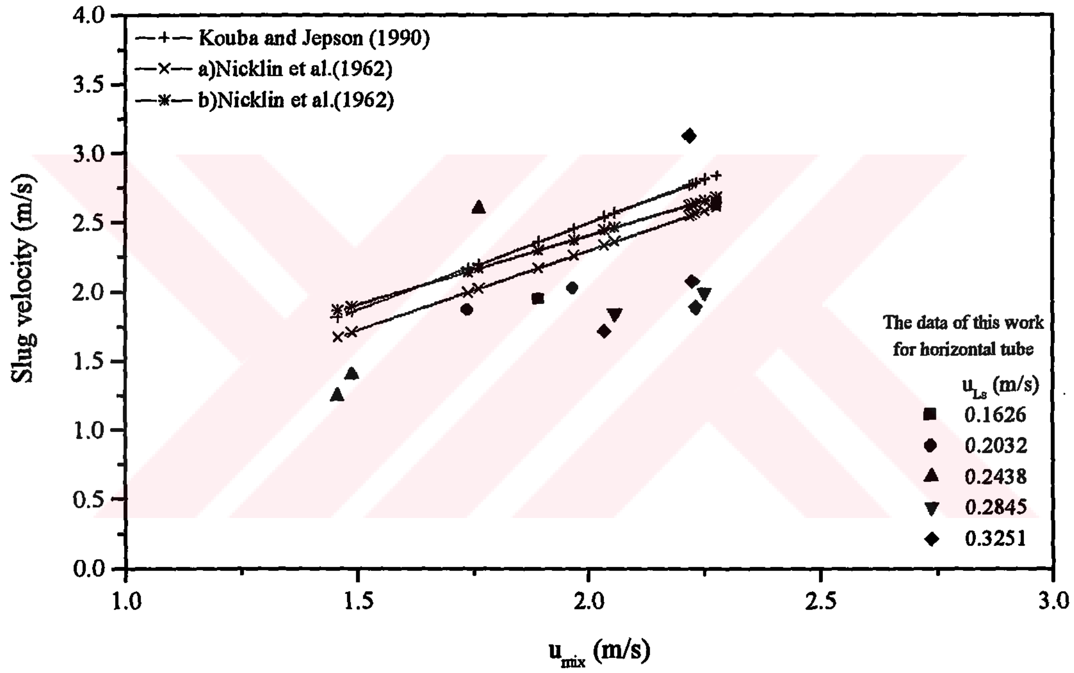

Figure 5.95. Variation of slug velocity with the mixture velocity for horizontal tube.

According to figure 5.97., there is the same feeling expressed in previous graph that slug velocity increases as the constant superficial liquid velocity is increased. However, more data is needed for the concrete conclusion.

The variation of slug velocity with the mixture velocity is been shown in figure 5.98. for different constant superficial liquid velocities. The slug velocities calculated in the +15° inclination experiments are mostly in agreement with the others. According to the figure 5.98., it is more clear than previous figures that the slug velocity increases as the constant superficial liquid velocity is increased. However, more data is needed for the concrete conclusion.

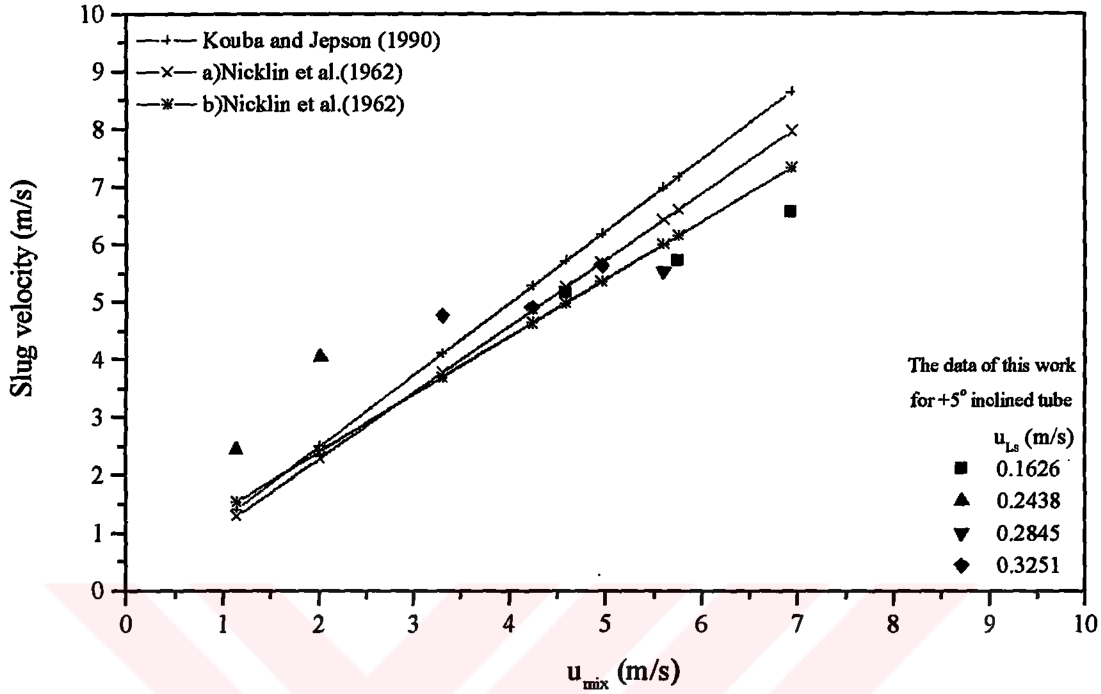

Figure 5.96. Variation of slug velocity with the mixture velocity for +5° inclined tube.

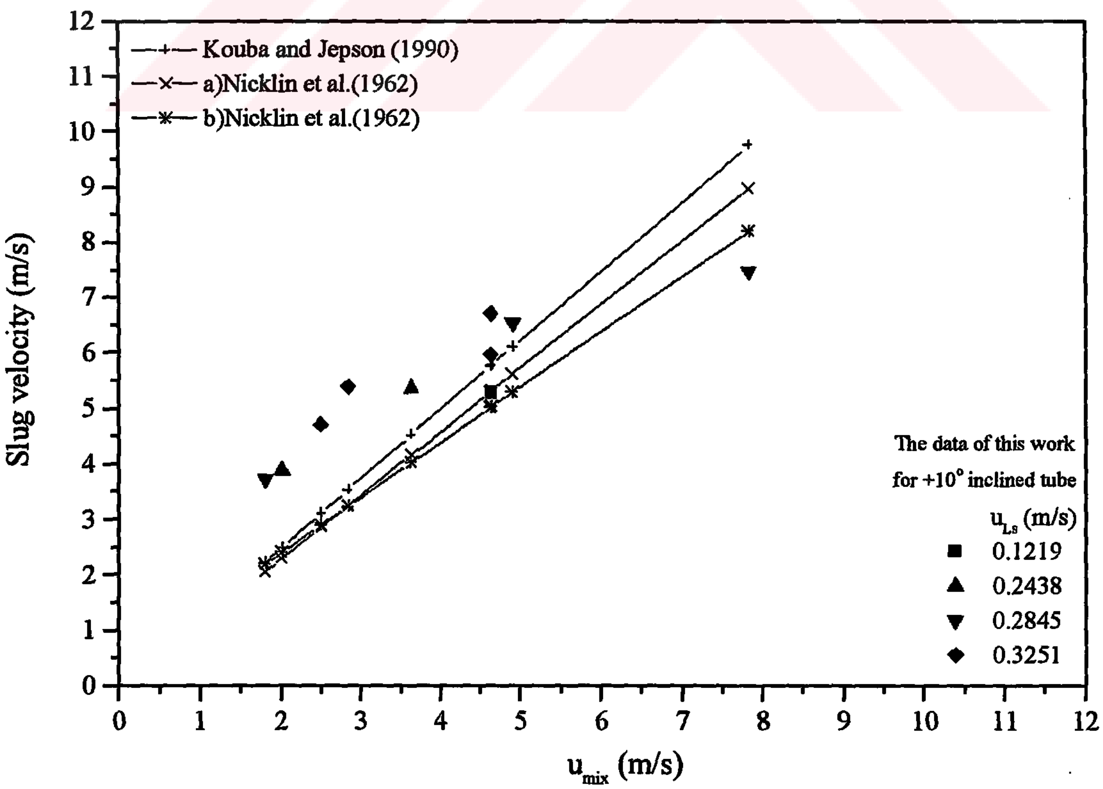

Figure 5.97. Variation of slug velocity with the mixture velocity for +10° inclined tube.

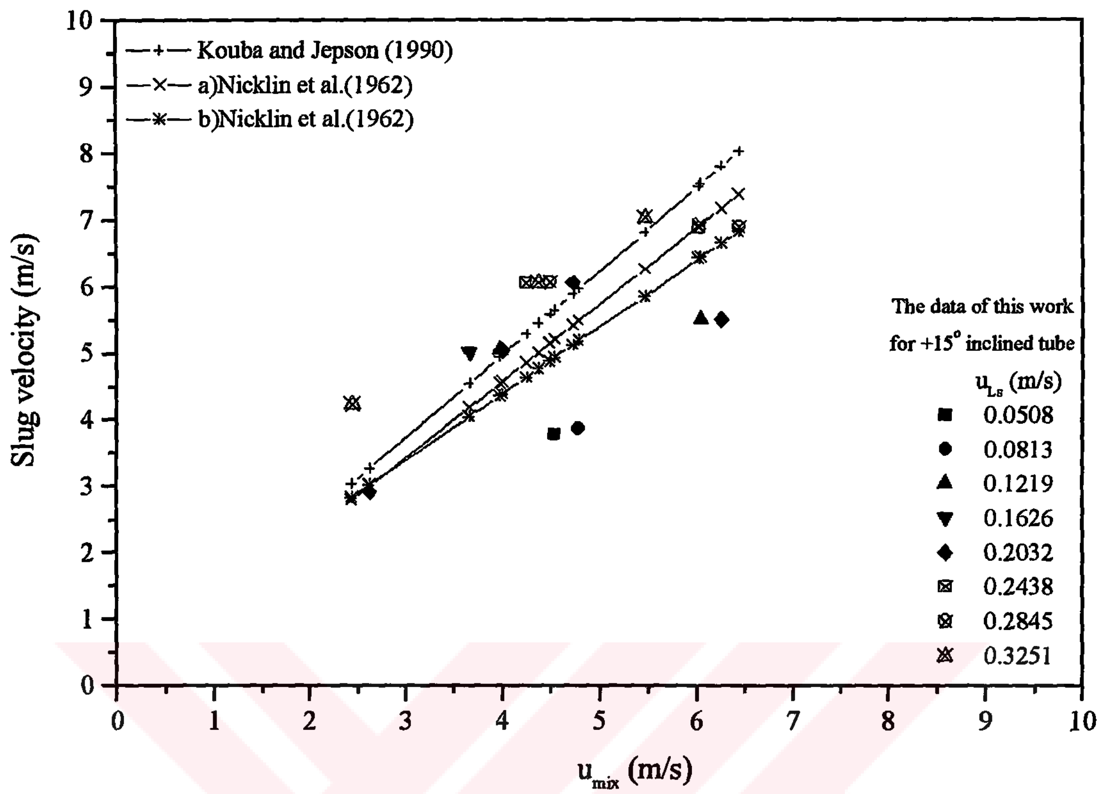

Figure 5.98. Variation of slug velocity with the mixture velocity for +15° inclined tube

Figures 5.99. to 5.104. show the variation of slug velocity with mixture velocity for different inclinations. The superficial liquid velocity is constant for each graph. However, the results of some inclinations are absent below a constant superficial liquid velocity of 0.2032 m/s, because of measurement errors. Figure 5.99. shows the variation of slug velocity with mixture velocity for a constant superficial liquid velocity of 0.1219 m/s. There are only the results of +10° and +15° inclination experiments for a constant superficial liquid velocity of 0.1219 m/s. Only one data for +10° and two data for +15° inclination experiments are seen in the figure. Naturally, they are not enough for a concrete conclusion, but, it is seen that there is a tendency to increase as the mixture velocity is increased. The calculated slug velocities of +10° and +15° inclination experiments are very close to each other for this constant superficial liquid velocity.

There are more data for a constant superficial liquid velocity of 0.1626 m/s. Only, the results of +10° inclination experiments are absent in figure 5.100. The calculated slug velocities of horizontal tube, +5°, and +10° inclination experiments are in agreement with the predictions of Nicklin et al. (1962) and Kouba and Jepson

(1990). Additionally, it is more clear from this figure that slug velocity increases as the inclination is increased.

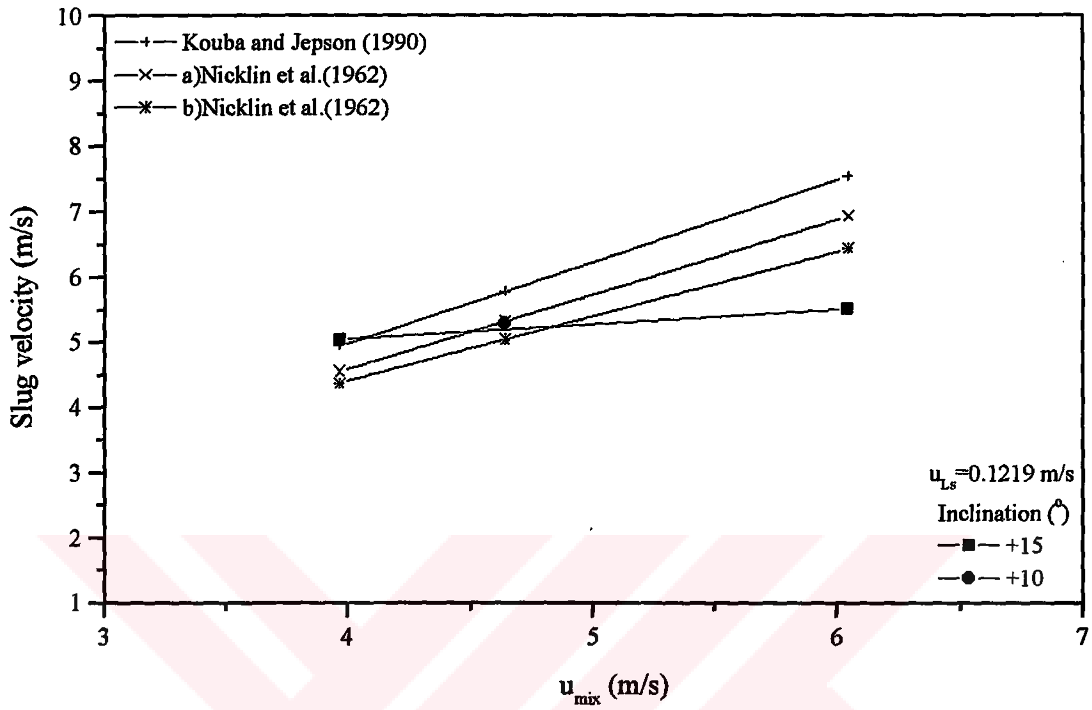

Figure 5.99. Variation of slug velocity with mixture velocity for a constant superficial liquid velocity of 0.1219 m/s.

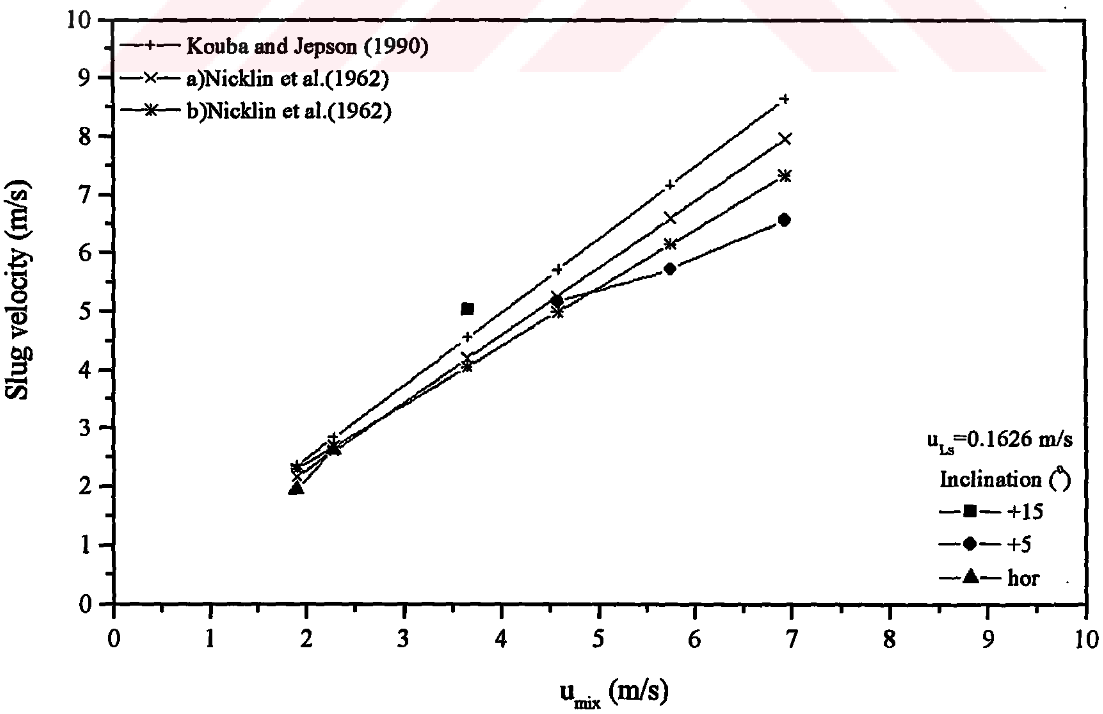

Figure 5.100. Variation of slug velocity with mixture velocity for a constant superficial liquid velocity of 0.1626 m/s.

Figure 5.101. shows the variation of slug velocity with mixture velocity for a constant superficial liquid velocity of 0.2032 m/s. There are only the results of horizontal and +15° inclination experiments for a constant superficial liquid velocity of 0.2032 m/s. Two data for horizontal and four data for +15° inclination experiments are seen in the figure. They are wholly in agreement with the others. The results of horizontal experiments are predicted higher by the Nicklin et al. (1962) and Kouba and Jepson (1990). It can be again expressed that slug velocity increases as the inclination is increased.

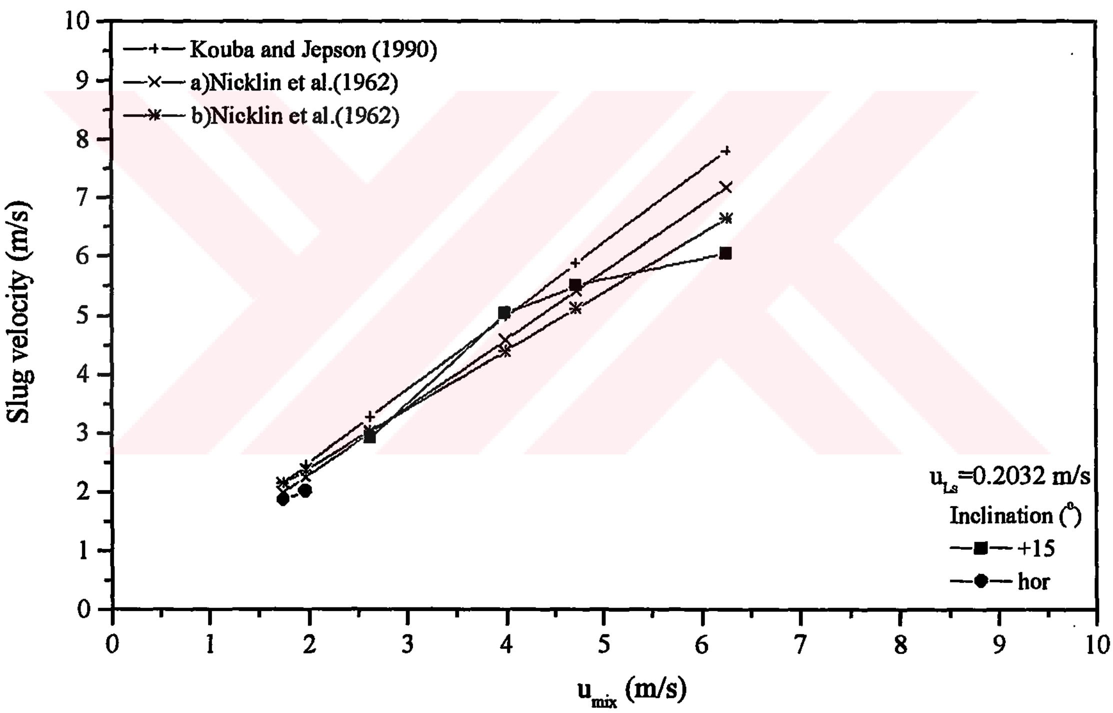

Figure 5.101. Variation of slug velocity with mixture velocity for a constant superficial liquid velocity of 0.2032 m/s.

There are more data for a constant superficial liquid velocity of 0.2438 m/s. The results of horizontal, +5°, +10°, and +15° inclination experiments are present in figure 5.102. The calculated slug velocities of horizontal flow experiments are in agreement with the predictions of Nicklin et al. (1962) and Kouba and Jepson (1990), but, those of the +5°, +10°, and +15° inclination experiments are predicted lower. Although the calculated slug velocities of the +5°, +10°, and +15° inclination experiments are very close to each other, there is a tiny feeling as if slug velocity increases as the inclination is increased.

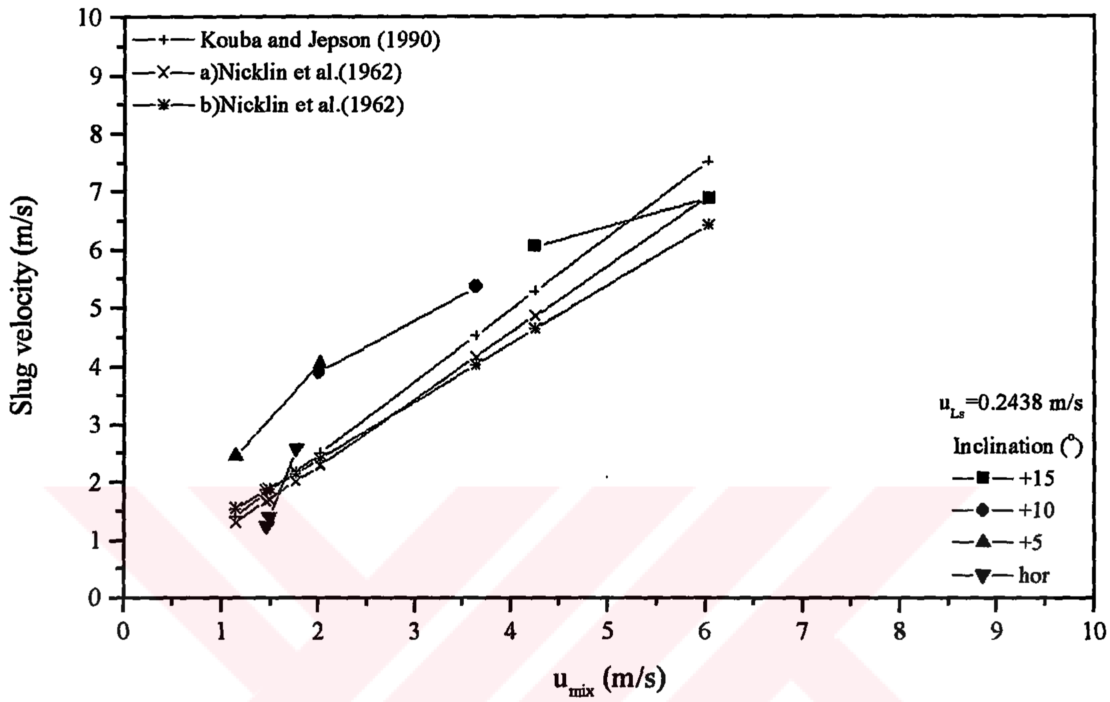

Figure 5.102. Variation of slug velocity with mixture velocity for a constant superficial liquid velocity of 0.2438 m/s.

The variations of the calculated slug velocities with mixture velocity are shown in figures 5.103. and 5.104. for different inclinations and for the constant superficial liquid velocities of 0.2845 m/s and 0.3251 m/s. The two figures are very similar to each other. The results of +10° inclination experiments are the highest in both of them.

The calculated slug velocities of +5° inclination experiments are located between those of horizontal and +15° inclination experiments. One can finally conclude that the inclination of the test pipe has an effect on the slug velocity. However, more data are needed for the precise and concrete conclusion.

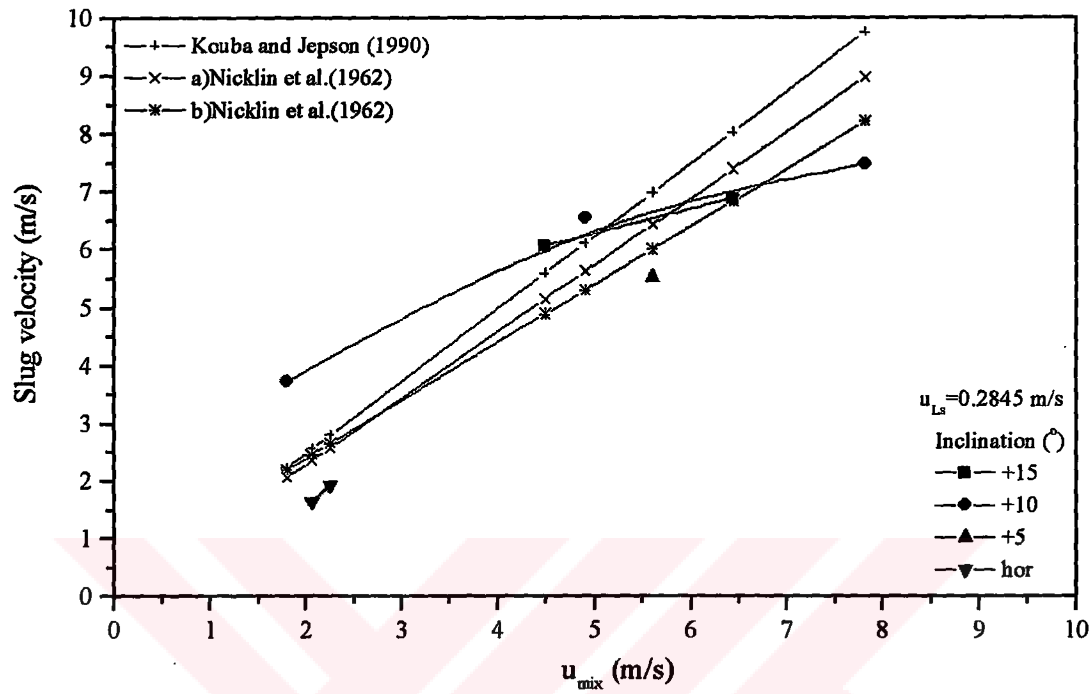

Figure 5.103. Variation of slug velocity with mixture velocity for a constant superficial liquid velocity of 0.2845 m/s.

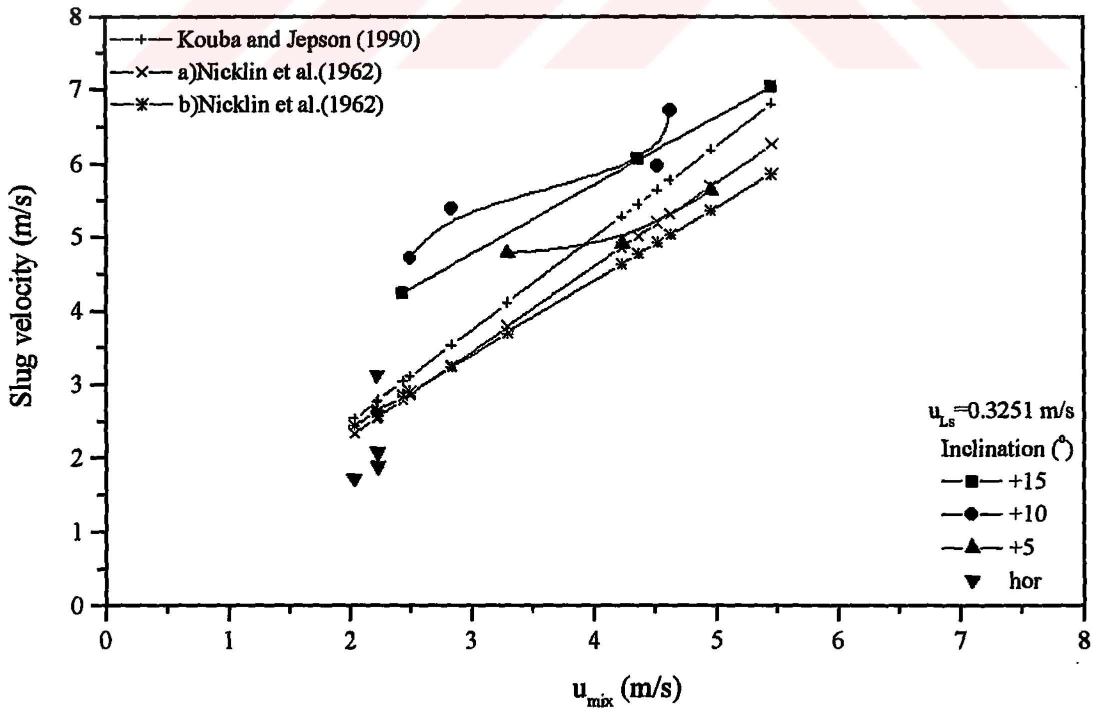

Figure 5.104. Variation of slug velocity with mixture velocity for a constant superficial liquid velocity of 0.3251 m/s.

5.1.8. Slug Lengths of Horizontal, +5°, +10°, and +15° Inclination Experiments

The slug length is here defined as the length of liquid slug flow, and it is determined from the residence time of a slug at the trigger LEDs and the slug velocity. The accurate determination of the length of a slug is highly dependent on the discrimination level of the LED and data acquisition system. The potential problem is the small fluctuations resulted from the presence of electrical noise. It should be noticed that it is necessary to eliminate this small fluctuations and the disturbances shorter than the distance between the LEDs should not be considered in the analysis.

Slug flow has been the focus of research for many years. However, most of the research has been carried out in developed slug flow. In order to determine the region where slug flow can be considered as fully developed, efforts have been made to determine the minimum stable slug length. The minimum stable slug length is defined as the length required for the re-establishment of a fully developed velocity profile at the rear of the liquid slug so that the trailing bubble is unaffected by the wake of the leading one. The development of the slug length distribution and the establishment of a stable developed distribution can be seen as follows. The propagation velocity of a trailing bubble is related to the maximum instantaneous velocity ahead of it (Moissis and Griffith (1962), Shemer and Barnea (1987)). Bubbles behind short slugs travel much faster than bubbles behind long slugs. Therefore, trailing bubbles that are faster than the leading ones will overtake the leading bubbles. During the merging process the liquid slug length as well as the bubble length increase. The process of overtaking is terminated once all the slugs are long enough so that the velocity profile at the back of the slugs is fully developed and all the bubbles propagate at the same velocity.

Different models concerning the liquid slug length have been focused on determining the minimum stable slug length. Theoretical work has been carried out by Dukler et al. (1985) who developed a physical model in which they state that the minimum stable slug length is determined by the re-establishment length of the wall boundary layer in the liquid slug. They assumed that the liquid at the front of the slug is well mixed, the wall boundary layer is distorted and a uniform velocity profile is obtained at a certain distance from the bubble. From this point, a boundary layer is developed on the pipe wall until a fully developed velocity profile is achieved. The maximum velocity is located at the centerline but its value increases with the distance from the gas bubble in contrast to experimental observations. They determined the variation of the dimensionless minimum stable slug length L_{stab} /D with Reynolds number. Experimental mean liquid slug lengths are found to be higher than the minimum stable slug length as predicted by the theory. This fact can be explained by assuming that the most probable slug length may differ from the minimum stable slug length, probably being two times the minimum length (resulting from the merger of two slugs slightly shorter than L_{stab}). They state that the specific geometry of the test installation i.e. the liquid and gas feeding devices, probably affects the distance required for the stabilization process, the entry region length and the distribution of the observed slug lengths.

Taitel et al. (1980) considered for the vertical case, the liquid film falling along the Taylor bubble as a two-dimensional jet which enters a stagnant pool of liquid (the slug). Therefore, a stable slug is one which is long enough so that the jet has been absorbed by the fluid and the velocities have slowed down to that of the surroundings. In this approach the time averaged velocity profiles behind the bubble are considered and the maximum velocity is always at the centerline of the pipe decaying gradually with the distance from the bubble as was observed by the authors experimentally. The minimum stable slug length was found to equal L_{stab} = 16D. The same concept was applied to horizontal slug flow by Barnea and Brauner (1985). They found a minimum stable slug length of L_{stab} = 32D. They stated that the minimum stable slug length is independent upon the gas and liquid flow rates and is constant for a given pipe diameter. The approach of both Dukler et al. (1985) and Taitel et al. (1980) yield the same prediction of the minimum stable slug length L_{stab} = 16D for vertical slug flow.

Experimental work with respect to the determination of the minimum stable slug length has been done by Shemer and Barnea (1987) who used hydrogen bubble technique to visualize the instantaneous velocity profiles in slug flow. They assume that the translational velocity of the Taylor bubble equals the maximum instantaneous velocity ahead of it, thereby reducing the prediction of the minimum stable slug length to an estimate of the extent of the wake region behind the Taylor bubble. For vertical flow a minimum stable slug length of 20D is found and for horizontal flow L_{stab} = 25D.

In developed slug flow most of the experimental research concerning the liquid slug length has been focused on determining the mean liquid slug length. Griffith and Wallis (1961) carried out measurements in developed slug flow in vertical pipes of ½", ¾" and 1" diameter. They found that the mean liquid slug length is relatively independent of flowrates and depends solely on the pipe diameter.

Barnea and Shemer (1989) estimated experimentally the mean liquid slug length. The experiments were carried out in a vertical air-water system using a Plexiglas pipe, 10 m long with a 5 cm i.d. and an electrical conductance probe located at 6 m from the entrance. The tip probe output was processed into a binary signal representing the gas or the liquid duration at the tip probe. The liquid slug length was calculated by multiplying the liquid slug duration with the translational velocity as calculated by the Nicklin et al. (1962) correlation for developed slug flow. The mean slug length was found to be practically independent of the gas superficial velocity, and varied in the range of 10D-15D. These values correspond reasonably well with the minimum stable slug length from the models of Taitel et al. (1980) and Dukler et al. (1985). However, as was mentioned before, the models for minimum stable slug underpredict the mean liquid slug length which should lie between the minimum stable slug length and twice this value.

Costigan and Whalley (1997) carried out experiments using two wall conductance probes mounted at approximately 5 and 6 m from the inlet in vertical air-water flows in a 32 mm diameter tube. They used a cross-correlation technique to determine the translational velocity from the signals of the two probes. Using this translational velocity they calculated the slug length distribution which they found to be normally distributed. The maximum slug length observed was 15D whereas the mean liquid slug length was around 12D.

Nydal et al. (1992) carried out an experimental investigation on the statistical properties of slug flow in two horizontal pipes of 52.9 mm i.d. stainless steel and 90 mm i.d. acrylic pipe of 17 m length. They used three conductance probes in order to calculate for each slug unit the slug front velocity, the slug bubble velocity, the slug length and the slug holdup. They differed between developed slugs and developing slugs that are highly aerated and develop into developed slugs. They therefore defined a non-dimensional developing length for slug flow as the distance from the gas inlet where all the developing slugs have disappeared. They found that this length increases with increasing gas velocity and decreases with increasing liquid velocity. The mean slug length in developed slug flow is seen to be fairly insensitive to the flow rates and was found to lie between L_{smean} = 15D to 20D for 5cm i.d. and L_{smean} = 12D to 16D for 9cm i.d. The measured bubble velocities were found to be slightly higher than single bubble velocities in pure liquid flows. The results of Nydal et al. (1992) in the horizontal pipe of 52.9 mm i.d. stainless steel are shown in figure 5.105. This figure shows the experimentally obtained mean slug lengths versus mixture velocity. As mentioned before, the mean slug lengths increase with increasing gas velocity and decreases with increasing liquid velocity.

Felizola and Shoham (1995) investigated the effect of the inclination angle on slug flow phenomena of a mixture of air and kerosene in a 51mm i.d. transparent pipe using three capacitance sensors. The sensors were installed at 9.1 m from the inlet section with a distance between them of 0.472 m. They determined the residence time of the slug body at each capacitance sensor and the matching translational velocity was determined by detecting the time it takes the slug front to pass between a pair of capacitance sensors. Using both the residence time and the translational velocity they found that for horizontal flow the mean liquid slug length equals L_{smean} = 27D and for vertical flow L_{smean} = 22D. For inclined flow, as the inclination angle increases from the horizontal, the mean liquid slug length decreases, reaching its minimum value of 16D at approximately 60 degrees and then increases with further inclination until vertical flow.

Little work has been carried out to determine the development of the slug length distribution in gas-liquid slug flow from unsteady to steady slug flow. Barnea and Taitel (1993) developed a simplified model that calculates the slug length distribution at any desired position along the pipe. The model assumes that randomly distributed short liquid slugs are generated at the entrance of the pipe. Two kinds of entrance distributions were chosen: the first a random number set with a uniform distribution within a prescribed range and the second a normal distribution with a prescribed average and standard deviation. In the model it is assumed that the Taylor bubbles do not deform as they propagate along the pipe thus the velocity of the liquid slug front is assumed to be equal to the velocity of the tail of the liquid slug ahead of it. The translational velocity of a bubble as a function of the length of the liquid slug ahead of it has to be given as an input relation. The relation expressed by Moissis and

Griffith (1962) for vertical flow was adopted. It was found that the evolution of the length distribution along the pipe, the fully developed distribution, the maximal slug length and the standard deviation are not sensitive to the slug length distribution at the pipe entrance. The slug length distribution in the developed region follows approximately the lognormal distribution. For fully developed flow all the slugs were found to be longer than the minimum stable slug length, the mean slug length about 1.5 times the minimum stable slug length and the maximum length about 3 times the minimum stable slug length. The model provides information on the length of the entry region needed to establish fully developed slug flow and yields the distribution at any point in the developing zone.

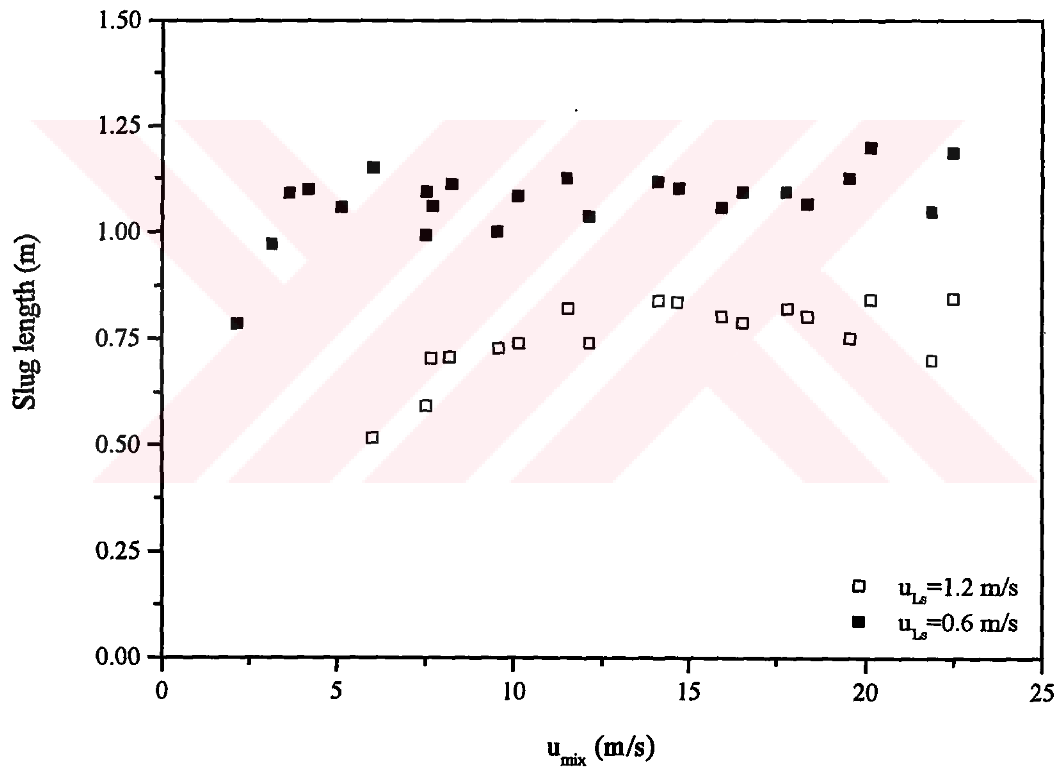

Figure 5.105. Experimentally obtained mean slug lengths versus mixture velocity. (Results of Nydal et al. (1992) in the horizontal pipe of 52.9 mm i.d. stainless steel)

Sæther et al. (1990) performed a fractal statistics analysis of liquid slug lengths in horizontal or developing inclined flows. The analysis enables to predict the liquid slug length distribution at a fixed point along the pipe. Input variables are the mixture velocity, the average liquid slug length and its standard deviation. Comparison with their experimental results shows that liquid slug length distributions for horizontal flow obey fractal statistics.

Figure 5.106. shows the variation of the mean slug length with mixture velocity for different constant superficial liquid velocities. The calculated mean slug lengths decrease with increasing mixture velocity. However, the trends of the lines so change that they will as if increase with increasing mixture velocity after a minimum value. There is no any meaningful explanation about the variation of the mean slug lengths with the increasing of the constant superficial liquid velocity.

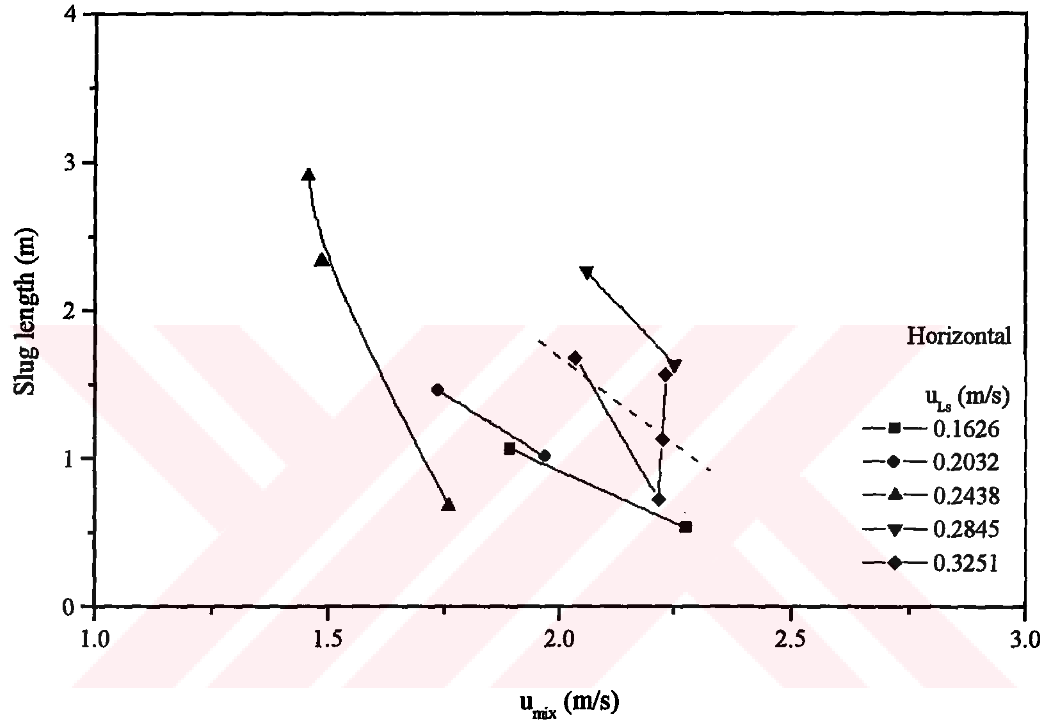

Figure 5.106. Variation of the mean slug length with mixture velocity for different constant superficial liquid velocities in horizontal tube experiments.

The calculated mean slug lengths of horizontal flow experiments are compared with the results of Nydal et al. (1992). This comparison is shown in figure 5.107. Nydal et al. (1992) expressed that the mean slug lengths increase with increasing gas velocity and decreases with increasing liquid velocity. All of the constant superficial liquid velocities of this investigation are less than those of Nydal et al. (1992). Namely, the calculated mean slug lengths of this investigation should be relatively greater than those of Nydal et al. (1992). One can easily see from figure 5.107. that most of the results of this investigation are greater than those of Nydal et al. (1992). Meanwhile, the difference between the test pipe diameters should be considered. Griffith and Wallis (1961) carried out measurements in developed slug flow in vertical pipes of ½", ¾" and 1" diameter. They found that the mean liquid slug length is relatively independent of flowrates and depends solely on the pipe diameter. Although

Griffith and Wallis (1961) carried out measurements in vertical pipes, the calculated mean slug lengths of horizontal flow experiments can be probably effected from the changing of pipe diameter.

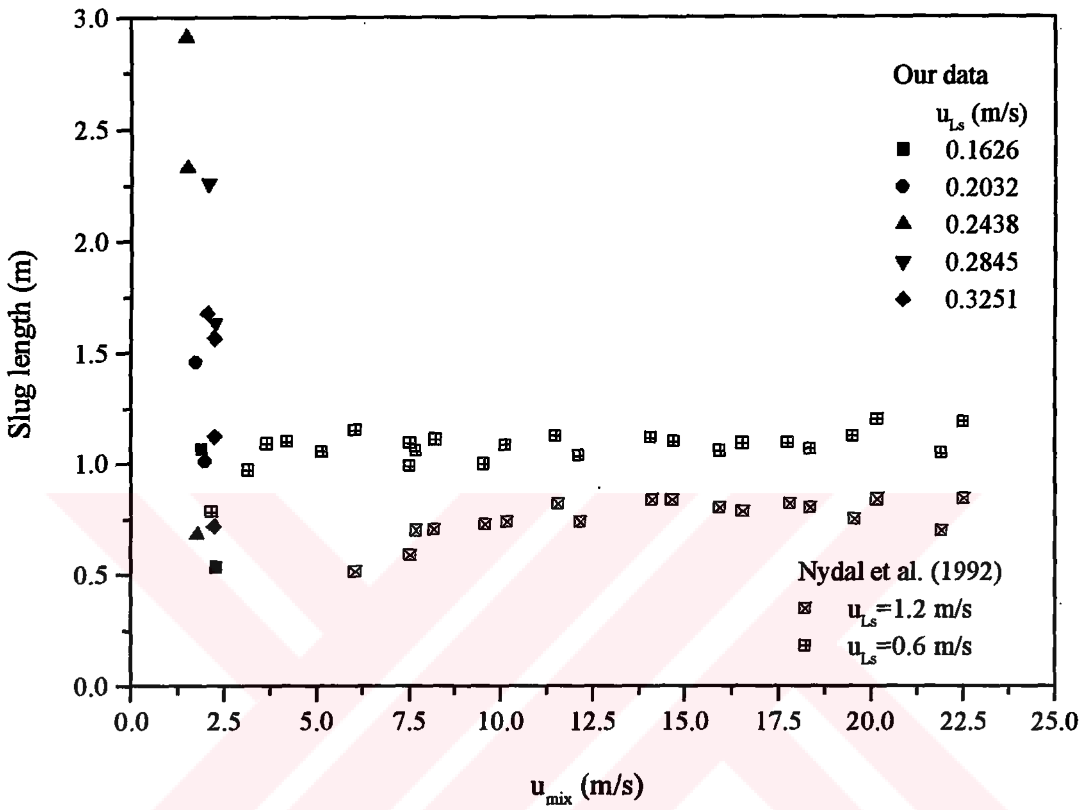

Figure 5.107. Comparison of the calculated mean slug lengths of horizontal flow experiments with the results of Nydal et al. (1992).

Figure 5.108. shows the variations of the calculated mean slug lengths of +5° inclination experiments with mixture velocity. The lengths of slugs increase with the increasing of mixture velocity. Except the results of a constant superficial liquid velocity of 0.3251 m/s, the mean slug lengths increase with increasing gas velocity and decreases with increasing liquid velocity.

Figure 5.109. shows the variations of the calculated mean slug lengths of +10° inclination experiments with mixture velocity. It can be clearly seen from this figure that the lengths of slugs increase with the increasing of mixture velocity and constant superficial liquid velocity. This is not in agreement with the results of Nydal et al. (1992). However, the results of these authors are valid for horizontal flow and the mean slug lengths of +10° inclination experiments can be perhaps different from theirs.

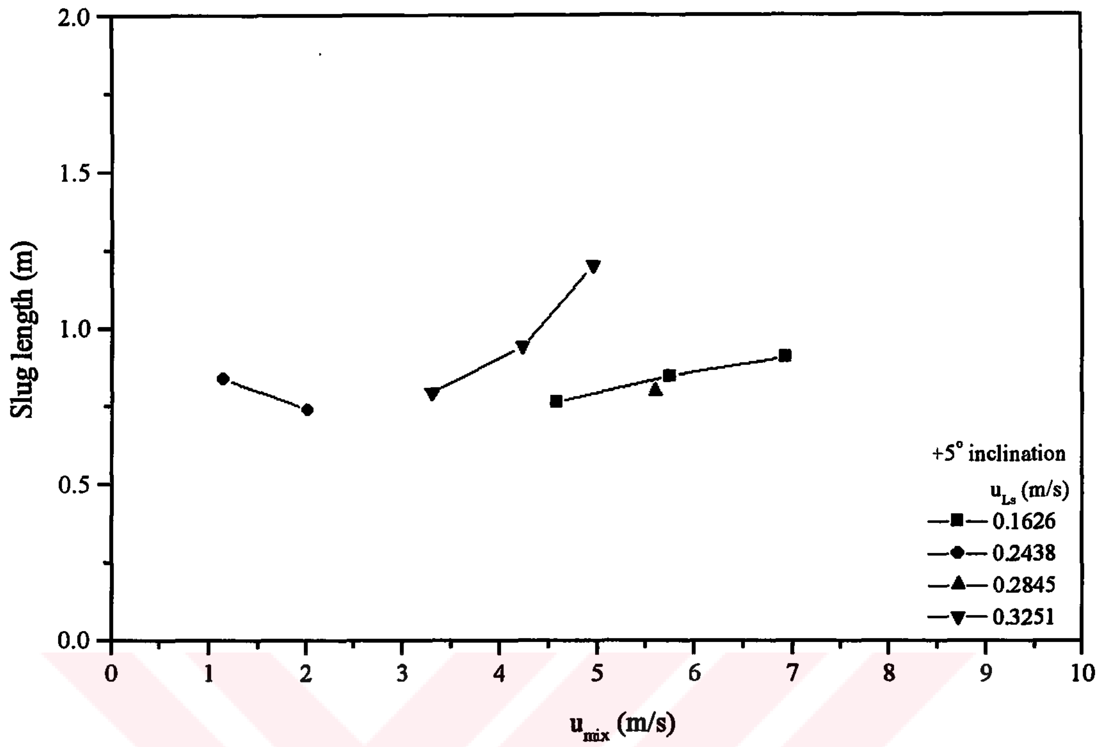

Figure 5.108. Variation of the mean slug length with mixture velocity for different constant superficial liquid velocities in +5° inclination experiments.

Figure 5.110. shows the variations of the calculated mean slug lengths of +15° inclination experiments with mixture velocity. The lengths of slugs increase with the increasing of mixture velocity. It can be seen from this figure without any doubt that the lengths of slugs increase with the increasing of mixture velocity and constant superficial liquid velocity. There is a tendency of the all data as if they will converge to a same value after a mixture velocity. More experimental results are needed for a concrete conclusion.

Another way to compare the experimental calculated mean slug lengths is to match the results of different inclination experiments in a graph. Figure 5.111. shows the variation of mean slug length with mixture velocity for two different inclinations, but for a constant superficial liquid velocity of 0.1219 m/s. One can express with respect to this figure that the calculated mean slug length increases as the inclination is increased.

Figure 5.112. shows the variation of mean slug length with mixture velocity for three different inclinations, and for a constant superficial liquid velocity of 0.1626 m/s. It can be expressed from this figure that the calculated mean slug length increases with the increasing of the inclination.

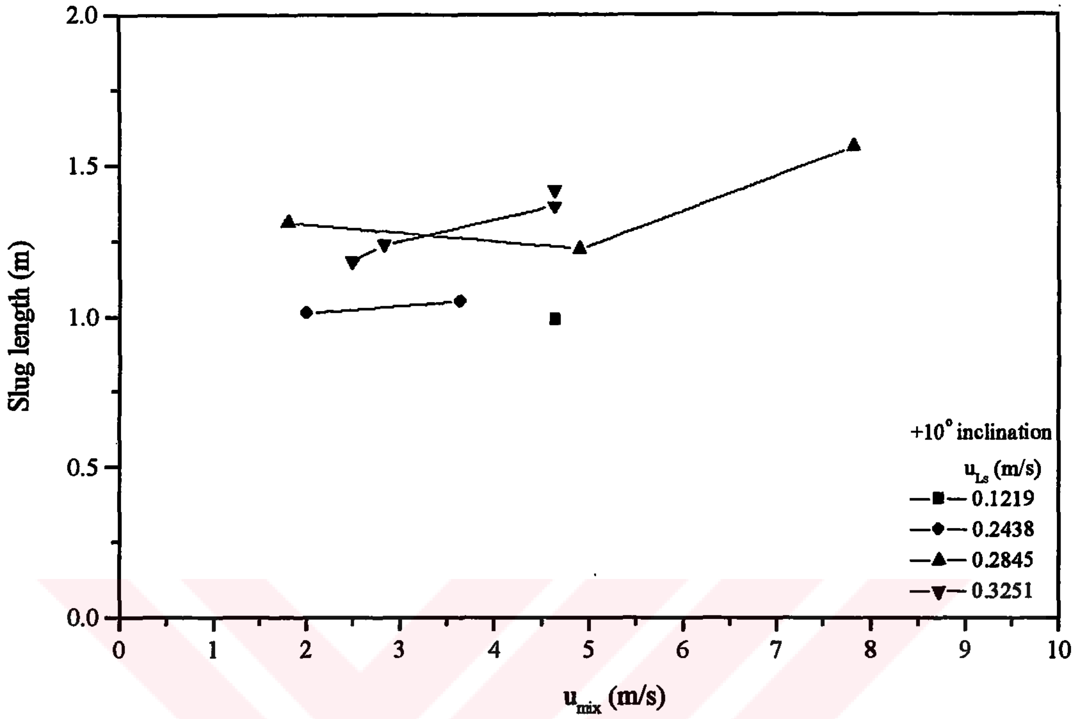

Figure 5.109. Variation of the mean slug length with mixture velocity for different constant superficial liquid velocities in +10° inclination experiments.

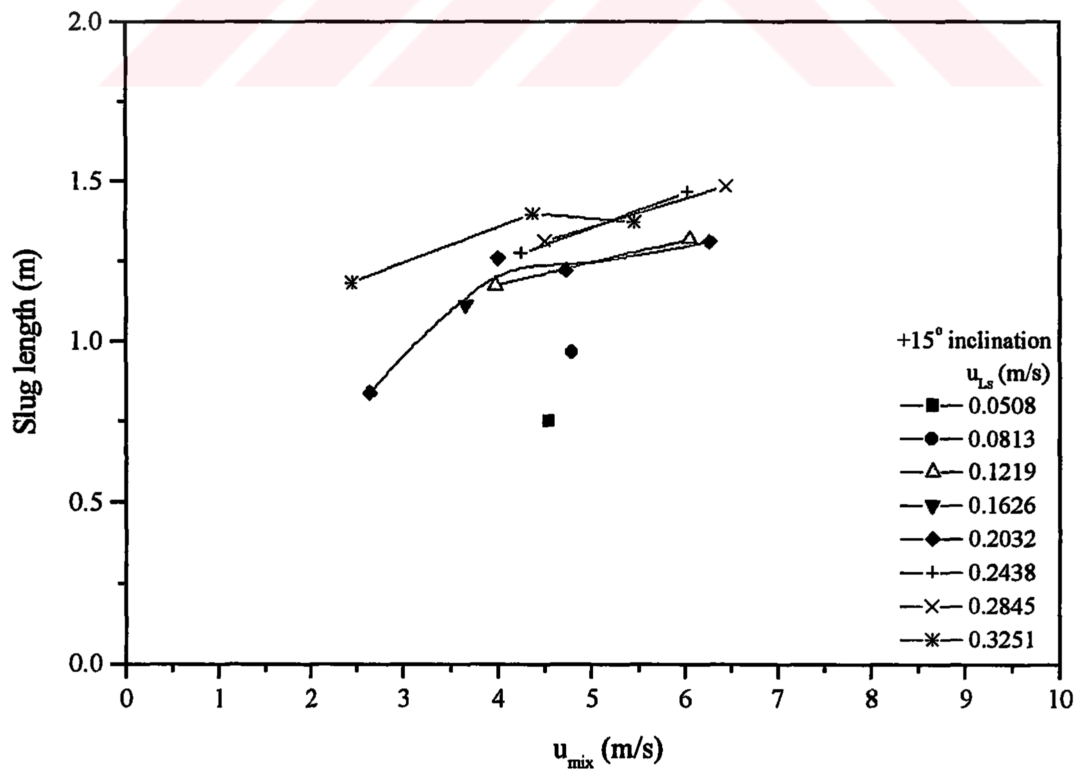

Figure 5.110. Variation of the mean slug length with mixture velocity for different constant superficial liquid velocities in +15° inclination experiments.

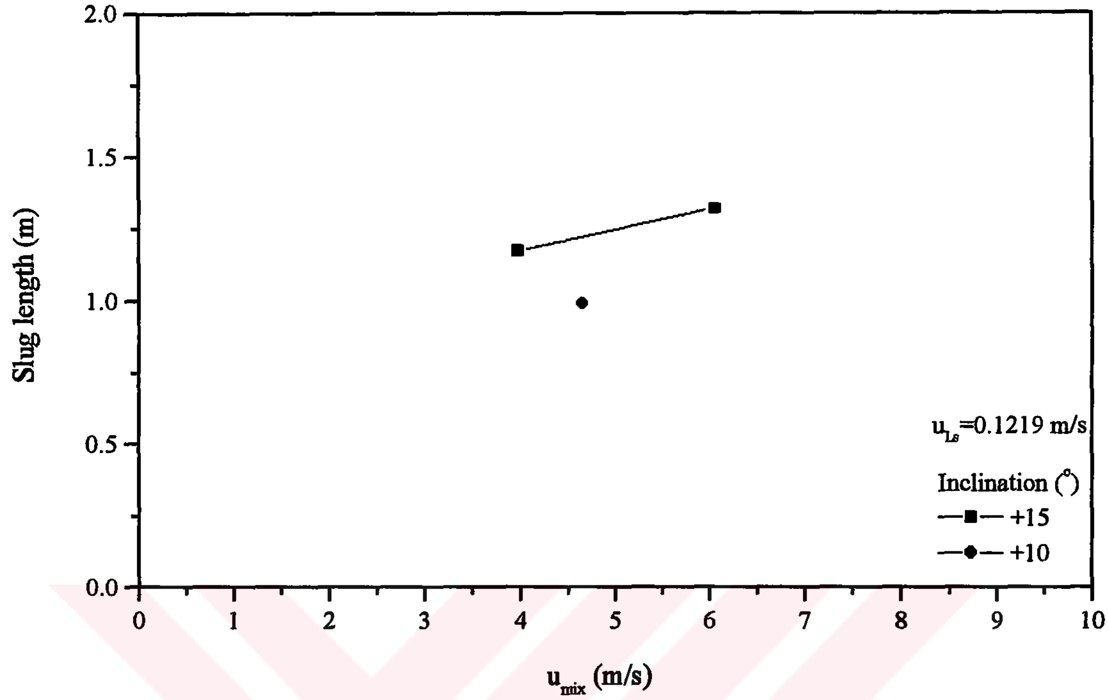

Figure 5.111. Variation of mean slug length with mixture velocity for two different inclinations for a constant superficial liquid velocity of 0.1219 m/s.

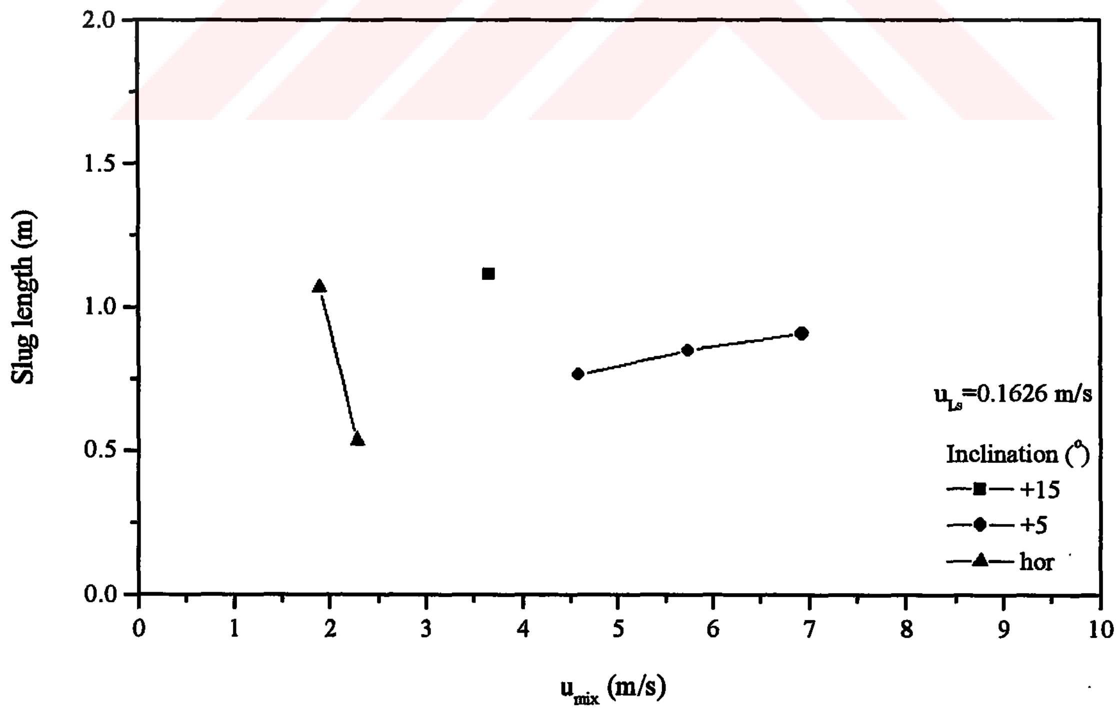

Figure 5.112. Variation of mean slug length with mixture velocity for three different inclinations for a constant superficial liquid velocity of 0.1626 m/s.

Figure 5.113. shows the variation of mean slug length with mixture velocity for two different inclinations, and for a constant superficial liquid velocity of 0.2032 m/s.

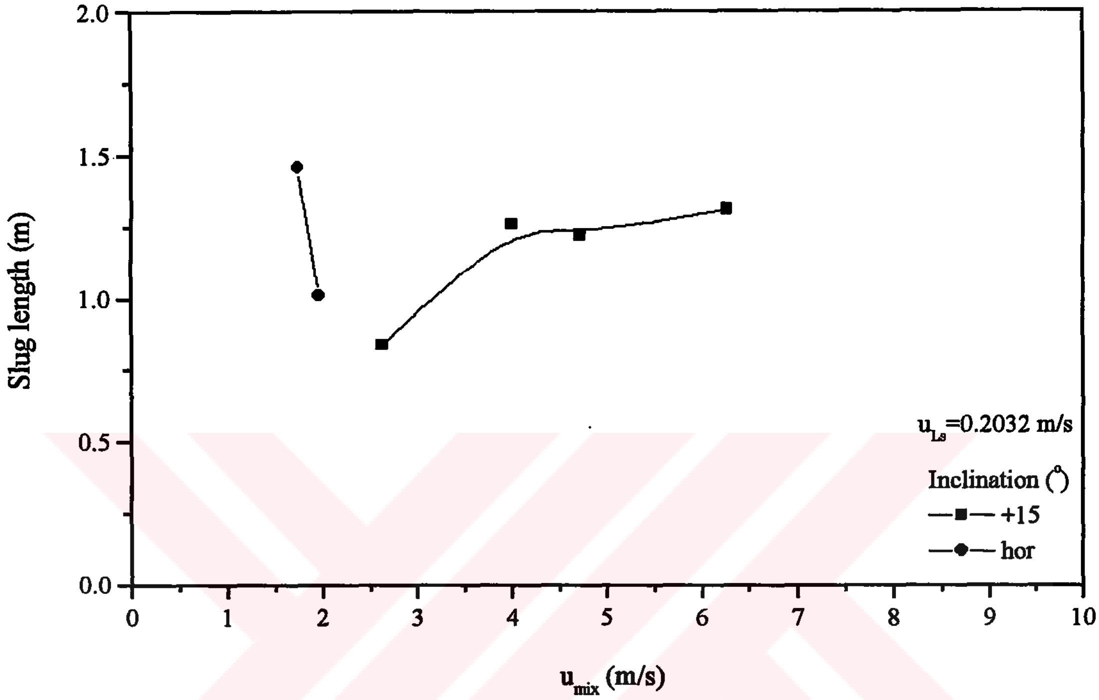

Figure 5.113. Variation of mean slug length with mixture velocity for two different inclinations for a constant superficial liquid velocity of 0.2032 m/s.

Figure 5.114. shows the variation of mean slug length with mixture velocity for four different inclinations, and for a constant superficial liquid velocity of 0.2438 m/s. It is more clear from this figure except the results of horizontal flow that the calculated mean slug length increases with the increasing of the inclination.

Figure 5.115. shows the variation of mean slug length with mixture velocity for four different inclinations, and for a constant superficial liquid velocity of 0.2845 m/s. It is again clear from this figure except the results of horizontal flow that the calculated mean slug length increases with the increasing of the inclination.

Figure 5.116. shows the variation of mean slug length with mixture velocity for four different inclinations, and for a constant superficial liquid velocity of 0.3251 m/s. It is more clear from this figure except the results of horizontal flow that the calculated mean slug length increases with the increasing of the inclination.

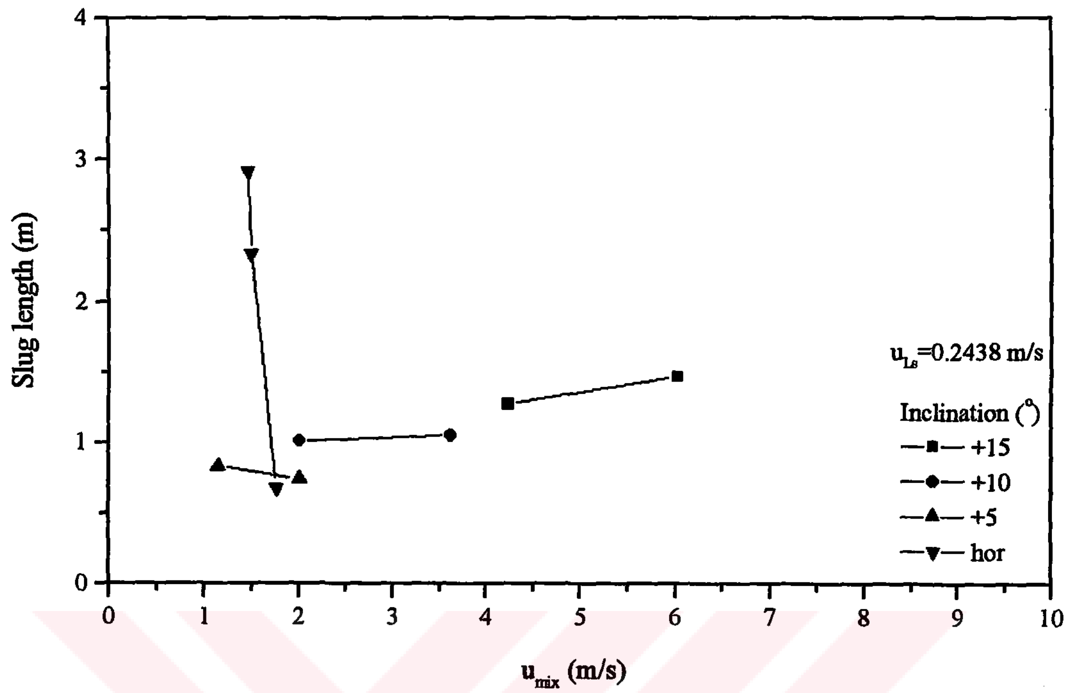

Figure 5.114. Variation of mean slug length with mixture velocity for four different inclinations for a constant superficial liquid velocity of 0.2438 m/s.

As a conclusion of slug lengths, the variations of mean slug lengths in horizontal experiments are unexplainably different from the results of inclined flow experiments. This is perhaps due to a measurement error or merging of two slugs to each other. There are no more data available to see accurately what is going on.

Felizola and Shoham (1995) investigated the effect of the inclination angle on slug flow phenomena of a mixture of air and kerosene in a 51mm i.d. tube. For inclined flow, they concluded that as the inclination angle increases from the horizontal, the mean liquid slug length decreases, reaching its minimum value of 16D at approximately 60 degrees and then increases with further inclination until vertical flow. However, according to the results of this investigation, the calculated mean slug length increases with the increasing of the inclination up to +15°. The two investigations are contradictory with each other. There is not any further work which has been carried out to determine the effects of inclination on mean slug length. Felizola and Shoham (1995) used a mixture of air and kerosene in a 51mm i.d. tube. Air-water mixture have been used in a pipe with 59 mm i.d. in this investigation. This section is very important from this viewpoint.

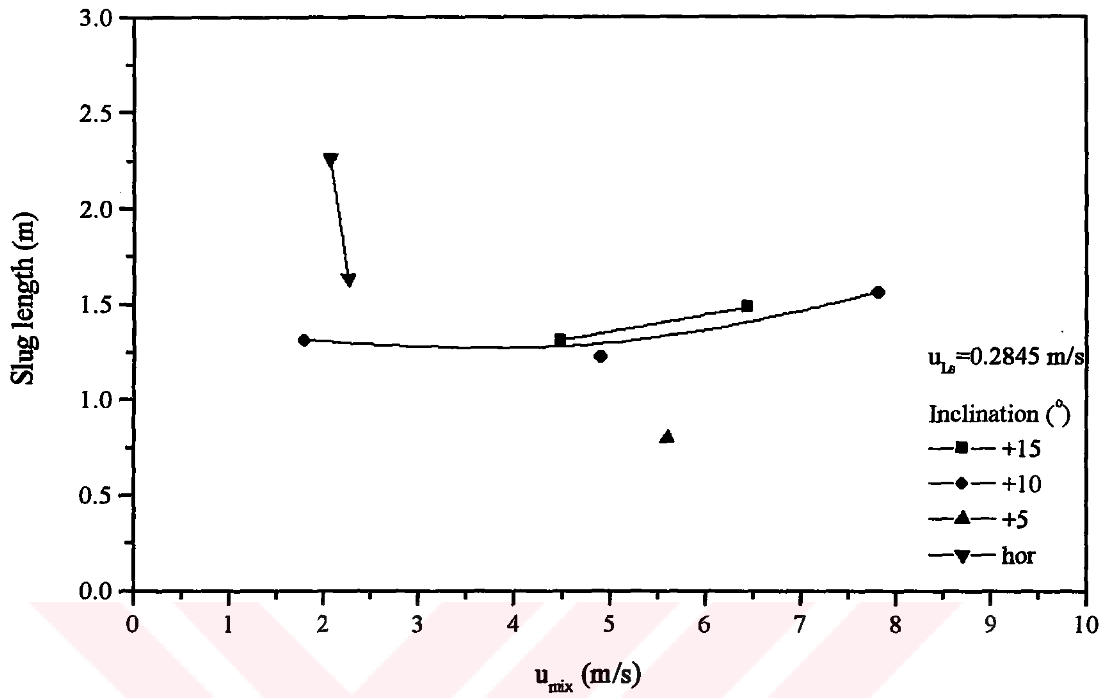

Figure 5.115. Variation of mean slug length with mixture velocity for four different inclinations for a constant superficial liquid velocity of 0.2845 m/s.

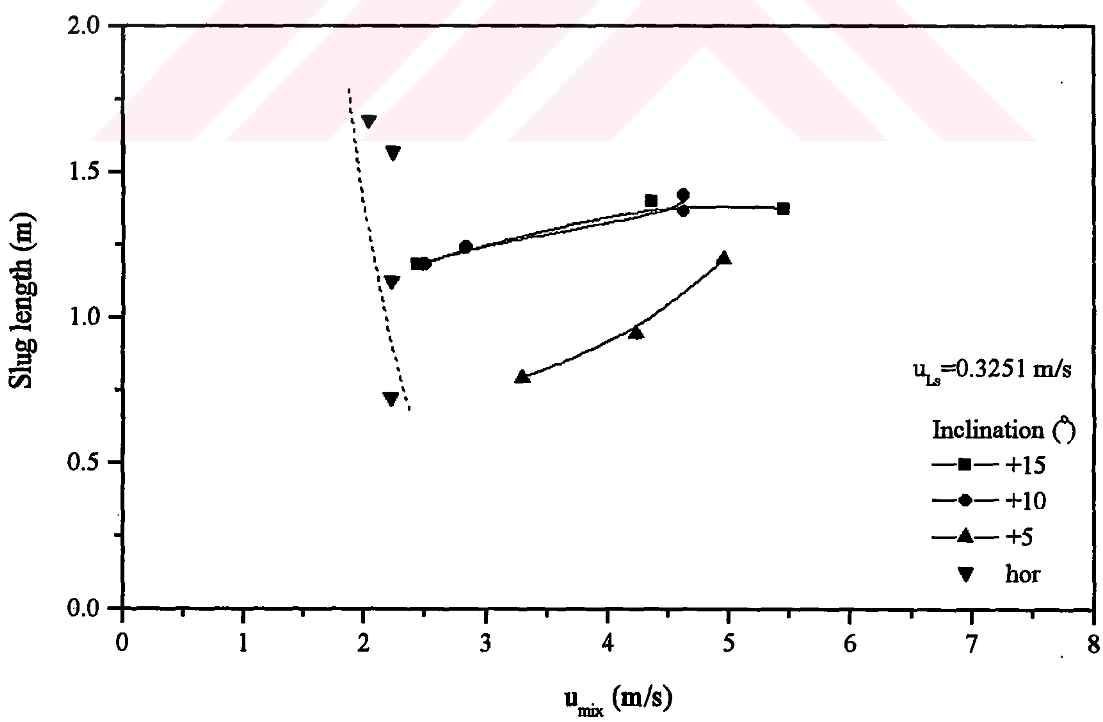

Figure 5.116. Variation of mean slug length with mixture velocity for four different inclinations for a constant superficial liquid velocity of 0.3251 m/s.

5.1.9. Slug Frequencies of Horizontal, +5°, +10°, and +15° Inclination Experiments

Determining the slug frequency requires the analysis and understanding of the mechanism of slug formation. The slug formation is an entry region phenomena (Taitel and Dukler (1977)). Visual observations reveal that the slug is created as a result of unsteady waves formed on a growing stratified film which blocks the air passage.

Taitel and Dukler (1977) modelled the complicated entrance phenomenon using open channel flow equations for the purpose of analytically predicting the slug frequency as well as to improve the understanding of slug initiation phenomenon. The authors studied gas liquid flows in horizontal and near horizontal pipes. They found the agreement of the theory with the experimental results within 25% not satisfactory, but quite acceptable. The results of Taitel and Dukler (1977) for air-water mixture and 38.1 mm pipe diameter have been compared with the horizontal flow slug frequencies of this investigation. Figure 5.117. shows the variation of slug frequency with the superficial gas velocity.

The closest superficial liquid velocity of this investigation to that of the Taitel and Dukler (1977) is 0.3251 m/s. The calculated slug frequencies of this investigation should be lower than those of Taitel and Dukler (1977) because the slug frequency decreases with the decreasing of the superficial liquid velocity. Additionally, the difference between the test pipe diameters is an another reason for the low slug frequencies. The slug frequency decreases as the pipe diameter is increased (Tronconi (1990), Jepson and Taylor (1993)).

Tronconi (1990) investigated the effects of gas and liquid flow rates, pipe diameter, gas density and liquid viscosity on slug frequency. The author expressed that these effects can be explained by modifications of the wave properties due to changes in liquid level of the stratified flow existing in the pipe inlet region prior to the slug formation. The results of Tronconi (1990) for air-water mixture and 40.2 mm pipe diameter have been compared with the horizontal flow slug frequencies of this investigation. Figure 5.118. shows the variation of slug frequency with the superficial gas velocity.

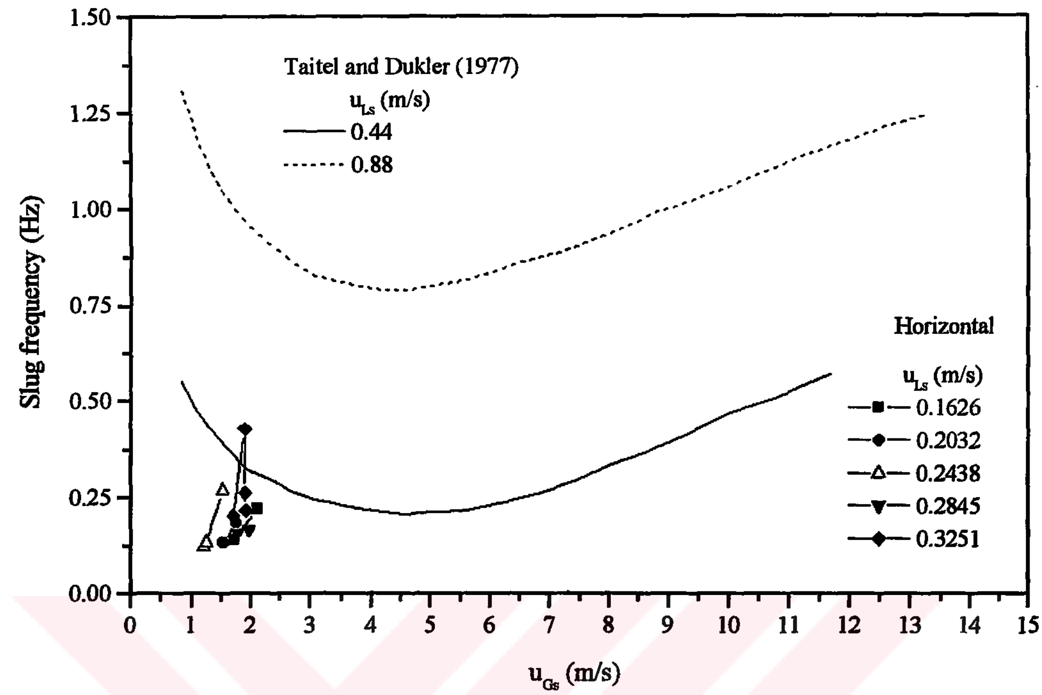

Figure 5.117. Variation of slug frequency with the superficial gas velocity. Comparison of the horizontal tube experiments with the results of Taitel and Dukler (1977)

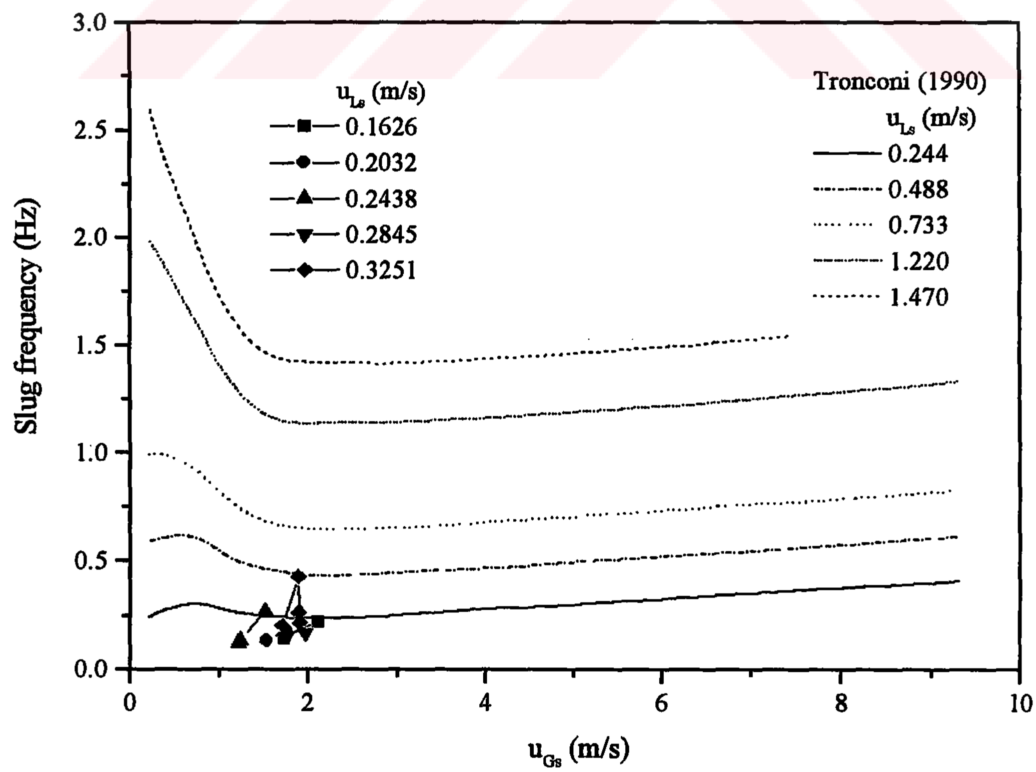

Figure 5.118. Variation of slug frequency with the superficial gas velocity. Comparison of the horizontal tube experiments with the results of Tronconi (1990).

The superficial liquid velocities of the horizontal flow experiments are around the two values of the superficial liquid velocities of figure 5.118. above. These are 0.244 and 0.488 m/s. Moreover, the superficial liquid velocity of 0.2438 m/s of this investigation is very close to the superficial liquid velocity of 0.244 m/s of that of Tronconi (1990). The marker of up triangle of our data shows the calculated slug frequencies of the superficial liquid velocity of 0.2438 m/s. They are mostly lower than those (bottom solid line) of 0.244 m/s of Tronconi (1990). They are probably due to the difference between the pipe diameters. The tests were done in 59 mm diameter pipe in this investigation and it is greater than that of Tronconi (1990). It is expressed before that the slug frequency decreases as the pipe diameter is increased (Tronconi (1990), Jepson and Taylor (1993)).

Jepson and Taylor (1993) investigated the slug flow and its transitions in large-diameter horizontal pipes. They used air-water mixture as a two phase fluid in a 300 mm diameter horizontal pipeline. The authors expressed that the transitions differ substantially from those for small-diameter pipes and are not predicted accurately by any theoretical model. They presented data on slug frequency, length, holdup, translational velocity and pressure gradient comparing them with existing data. Jepson and Taylor (1993)'s results show that the pipe diameter has a large effect on all these properties.

Figure 5.119. shows the comparison of slug frequency for three different pipe diameters and two different superficial liquid velocities. Jepson and Taylor (1993) proposed this comparison, but the data of this investigation were added in the same figure. First of all, the superficial liquid velocities of the horizontal flow experiments are approximately less than the half of those of Jepson and Taylor (1993). Thus, the calculated slug frequencies should be lower than those of Jepson and Taylor (1993) because of the lower superficial liquid velocities. In spite of the lower superficial liquid velocities, the horizontal flow data of this investigation sit between the data of 51.2 and 300 mm diameter data of Jepson and Taylor (1993). If the superficial liquid velocities of this investigation were equal to those of Jepson and Taylor (1993), the calculated slug frequencies of this investigation would be closer to the data of 51.2 mm pipe diameter. According to this figure, the calculated slug frequencies of this study are reasonably predicted and can be regarded to be sufficiently in agreement with the results of Jepson and Taylor (1993).

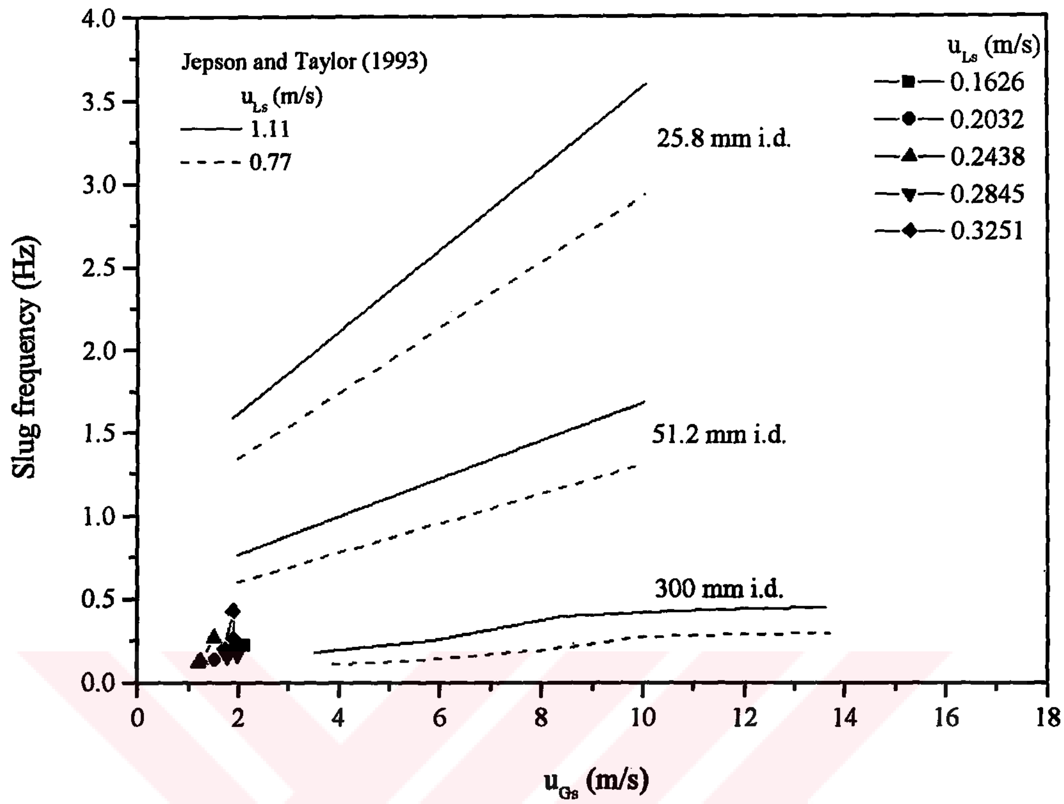

Figure 5.119. Comparison of slug frequency for three different pipe diameters and two different superficial liquid velocities (Jepson and Taylor, 1993). The horizontal tube data of this investigation are added in the same figure.

Andreussi et al. (1993) characterised the air-water slug flow at atmospheric conditions in horizontal pipes of 31 and 53 mm inner diameter with local (optical) and cross-sectional (conductance) probes. Local measurements included the radial void fraction distribution in the slugs, the size of the dispersed bubbles in the slug and the aeration of the liquid layer under the slug bubble. From cross-sectional holdup measurements, slug lengths and frequencies were determined, as well as the length of the highly aerated mixing zone in the front of the slugs. They finally concluded that, at low liquid flow rates, close to the transition to stratified flow, the slug frequency is too closely related to the geometry of the pipe (inlet conditions, pipe length). However, their observations indicated that, at higher liquid flow rates, the slug frequency or slug length are weakly dependent on the pipe geometry. The slug frequencies of the authors in horizontal pipe of 53 mm inner diameter are compared with those of this investigation. Figure 5.120. shows the variation of the slug frequency with mixture velocity in horizontal pipes.

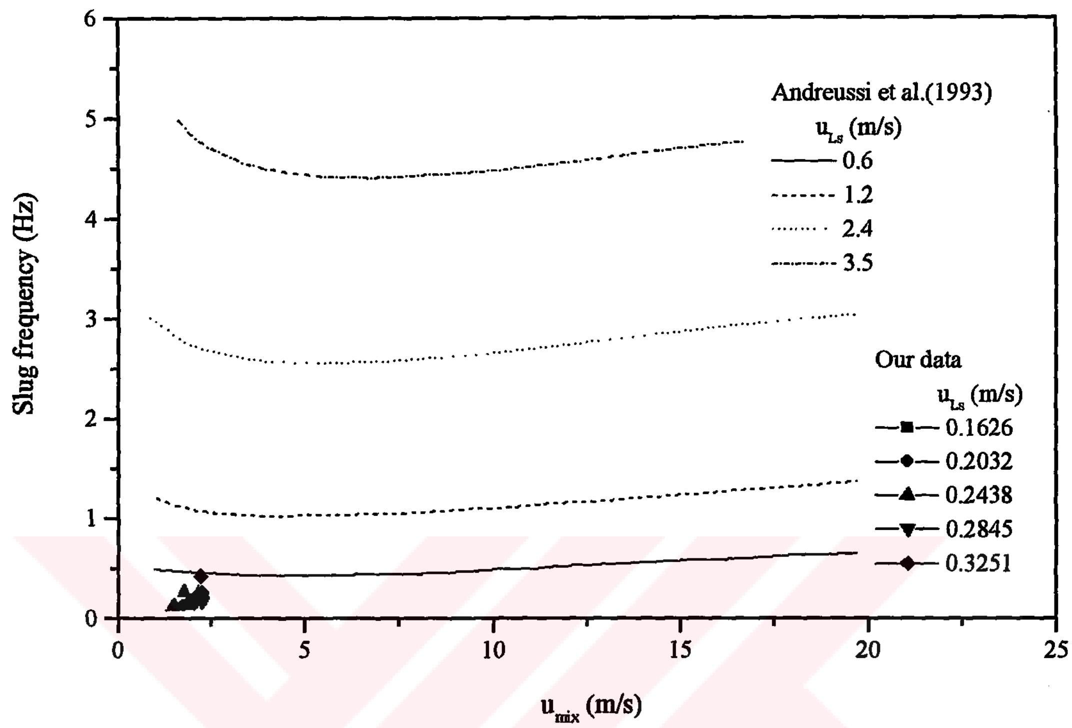

Figure 5.120. Variation of the slug frequency with mixture velocity in horizontal pipes.

The pipe diameter of this investigation is greater than that of Andreussi et al. (1993). Thus, it is explainable that the slug frequencies should be lower than those of Andreussi et al. (1993) because of the higher pipe diameter and lower superficial liquid velocities. As before explained, the slug frequency decreases with the increasing of the pipe diameter, and with the decreasing of the superficial liquid velocity.

All comparisons of slug frequency show that the calculated slug frequencies of horizontal flow experiments are sufficiently in agreement with the others. Henceforth, the slug frequencies of this investigation will be compared with each other, for instance; for different constant superficial liquid velocities and inclinations.

Figure 5.121. shows the variation of slug frequency with mixture velocity for different constant superficial liquid velocities in horizontal pipe. Except the slug frequencies for 0.2845 and 0.3251 m/s, the rest of the data increase as the superficial liquid velocity is increased.

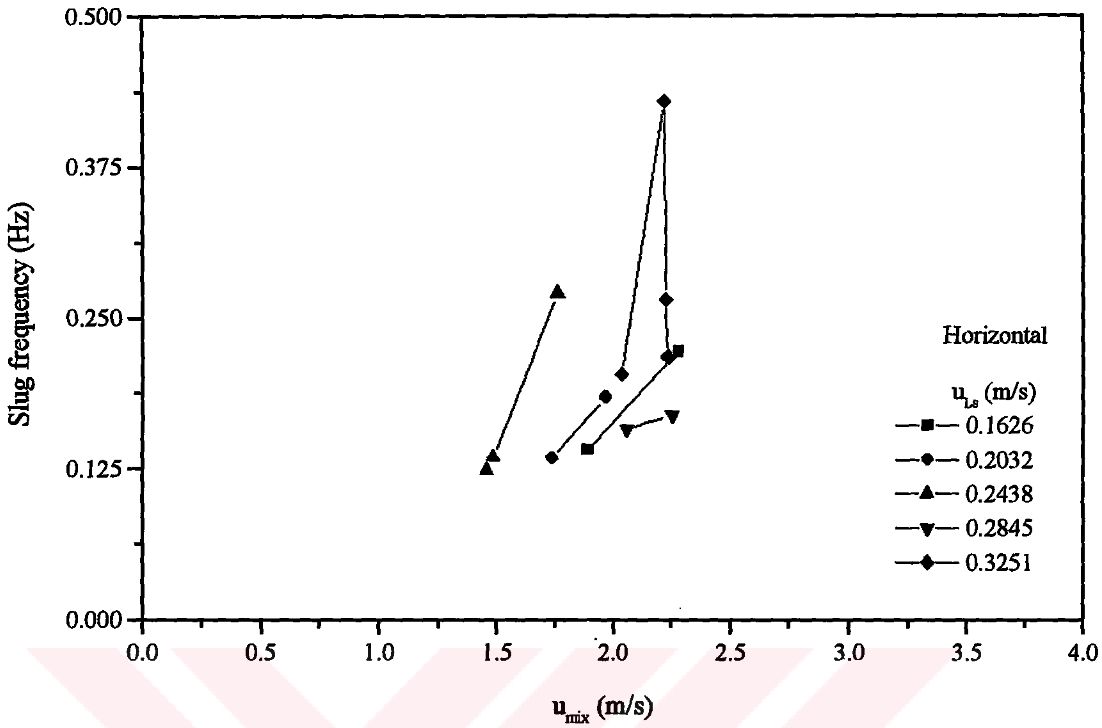

Figure 5.121. Variation of the slug frequency with mixture velocity in horizontal pipes.

Figure 5.122. shows the variation of slug frequency with mixture velocity for different constant superficial liquid velocities in +5° inclination pipe. The dashed lines have been drawn as an estimation of data trends. The slug frequencies increase as the superficial liquid velocity is increased. However, more data are required for the determination of the trends.

Figure 5.123. shows the variation of slug frequency with mixture velocity for different constant superficial liquid velocities in +10° inclination pipe. Except the two slug frequencies for 0.3251 m/s, the rest of the data increase as the superficial liquid velocity is increased.

Figure 5.124. shows the variation of slug frequency with mixture velocity for different constant superficial liquid velocities in +15° inclination pipe. Except the slug frequency for 0.0508 m/s, the rest of the data increase as the superficial liquid velocity is increased.

From here, the slug frequencies of different inclinations are compared for a constant superficial liquid velocity. For example, the variation of slug frequency with mixture velocity for different inclinations is shown in figure 5.125. for a constant superficial liquid velocity of 0.1219 m/s. The results of horizontal and +5° inclination pipe experiments are absent. One can conclude with respect to this figure that the slug frequency increases with the increasing of the pipe inclination.

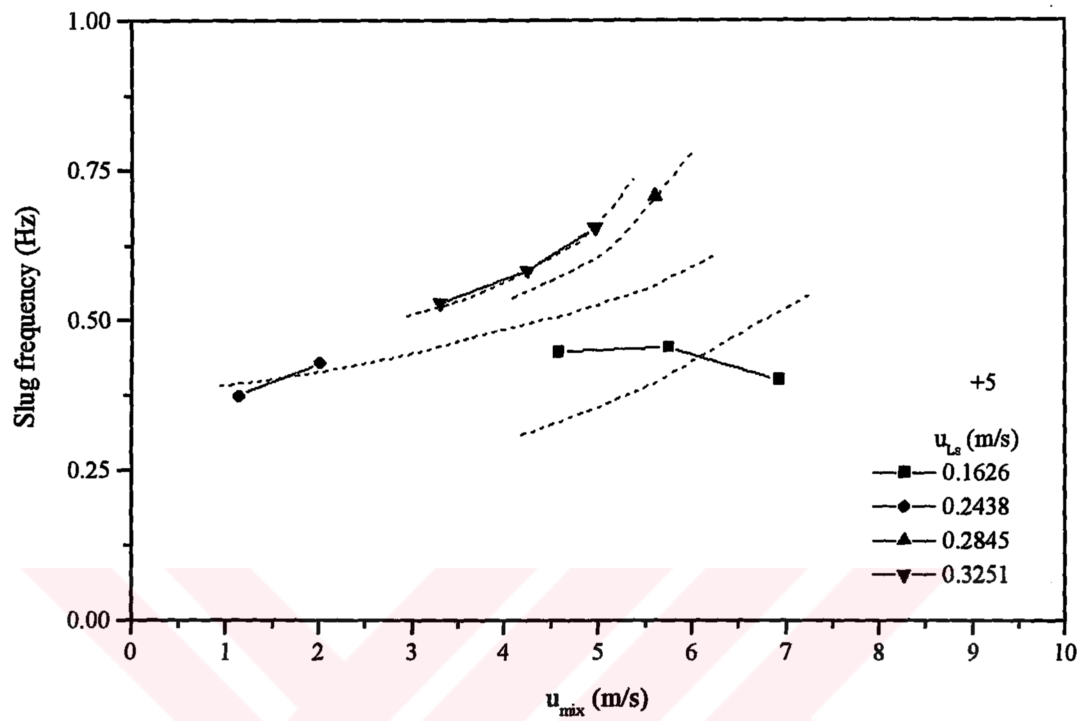

Figure 5.122. Variation of the slug frequency with mixture velocity in +5° inclination pipe.

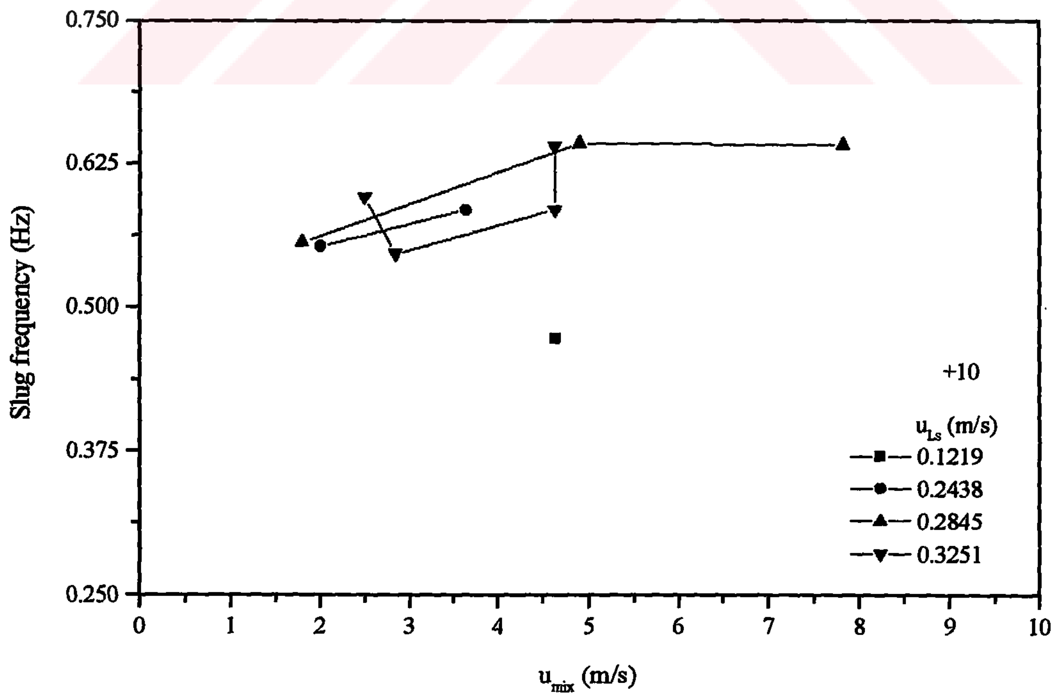

Figure 5.123. Variation of the slug frequency with mixture velocity in +10° inclination pipe.

The variation of slug frequency with mixture velocity for different inclinations is shown in figure 5.126. for a constant superficial liquid velocity of 0.1626 m/s. The results of +10° inclination pipe experiments are absent. It can be expressed with respect to this figure that the slug frequency increases with the increasing of the pipe inclination.

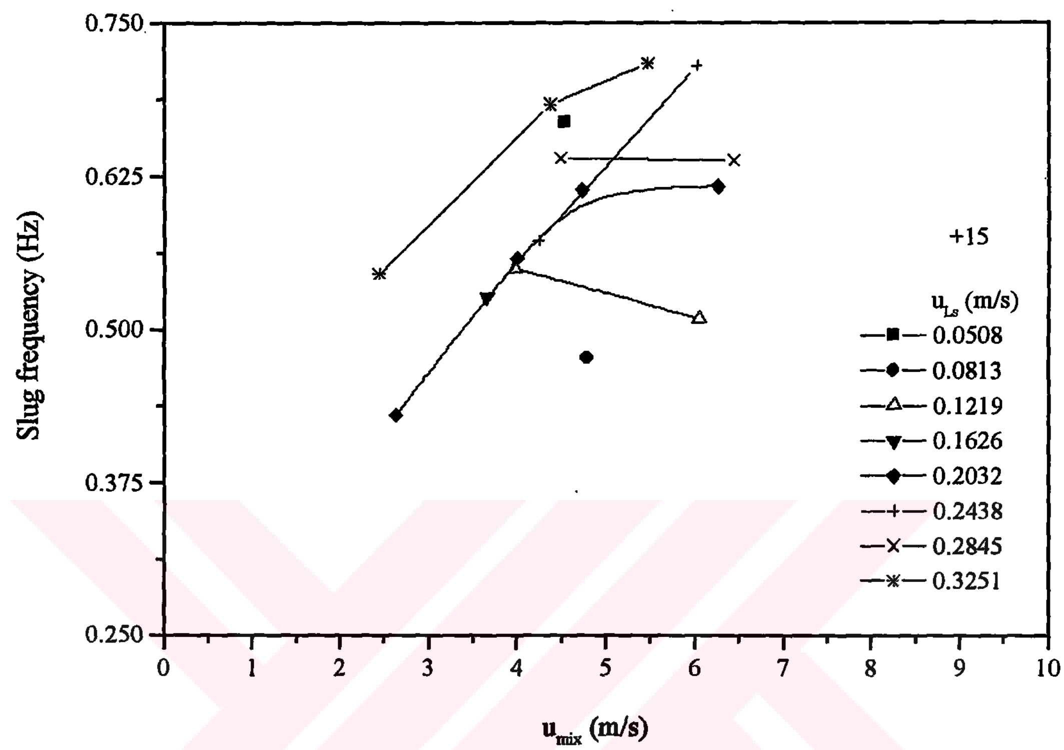

Figure 5.124. Variation of the slug frequency with mixture velocity in +15° inclination pipe.

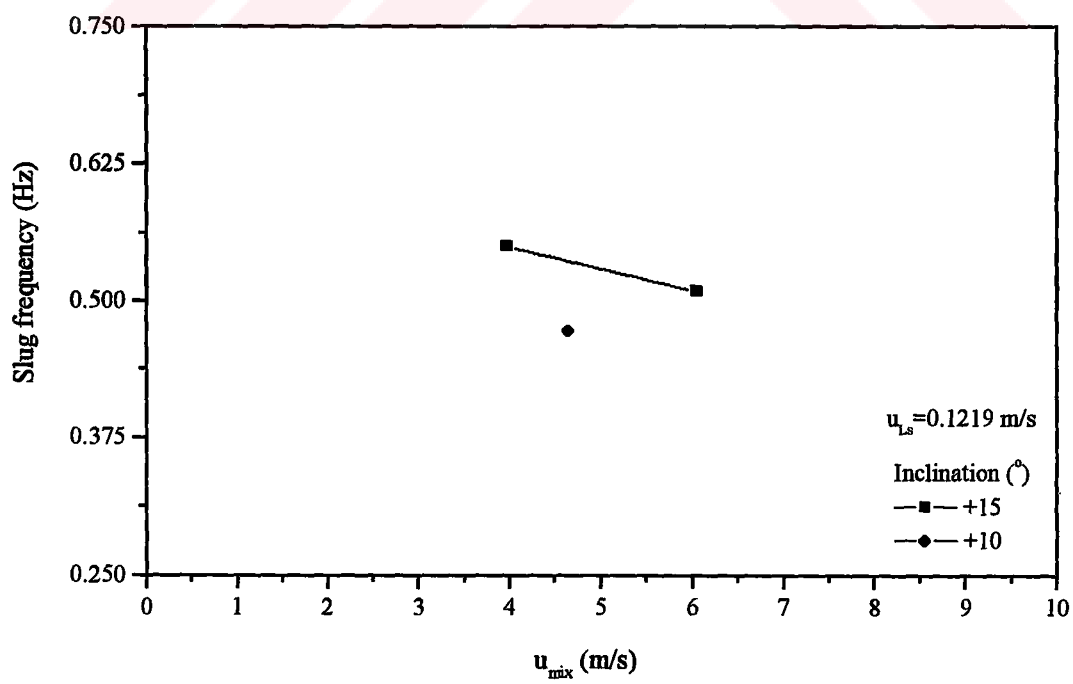

Figure 5.125. Variation of slug frequency with mixture velocity for different inclinations for a constant superficial liquid velocity of 0.1219 m/s.

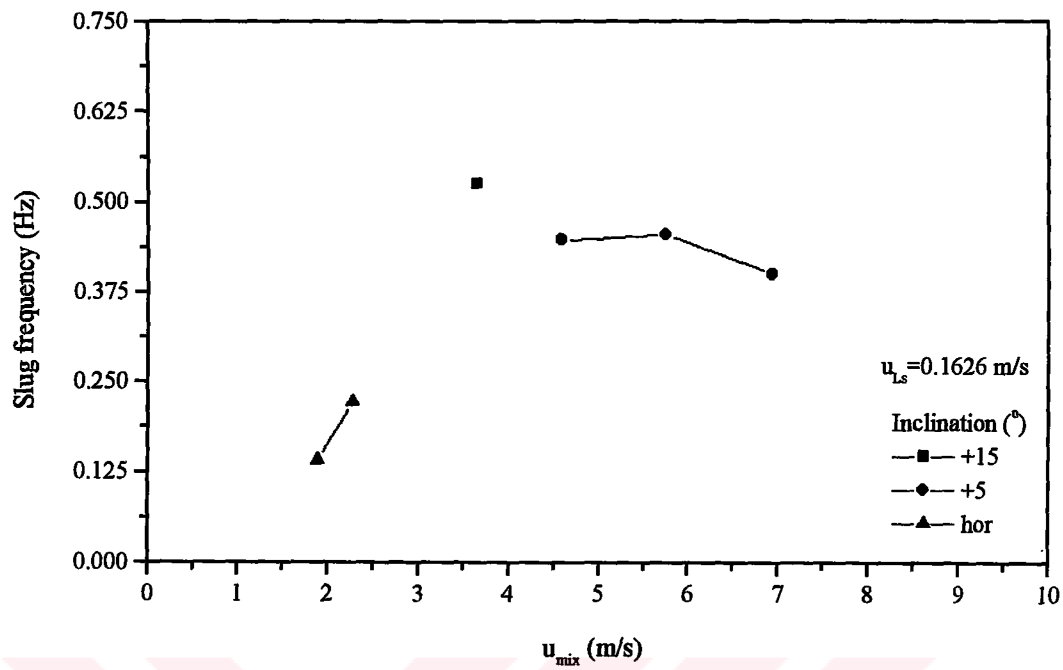

Figure 5.126. Variation of slug frequency with mixture velocity for different inclinations for a constant superficial liquid velocity of 0.1626 m/s.

Figure 5.127. shows the variation of slug frequency with mixture velocity for different inclinations for a constant superficial liquid velocity of 0.2032 m/s. The results of +5° and +10° inclination pipe experiments are absent because of the measurement error. One can conclude with respect to this figure that the slug frequency increases with the increasing of the pipe inclination.

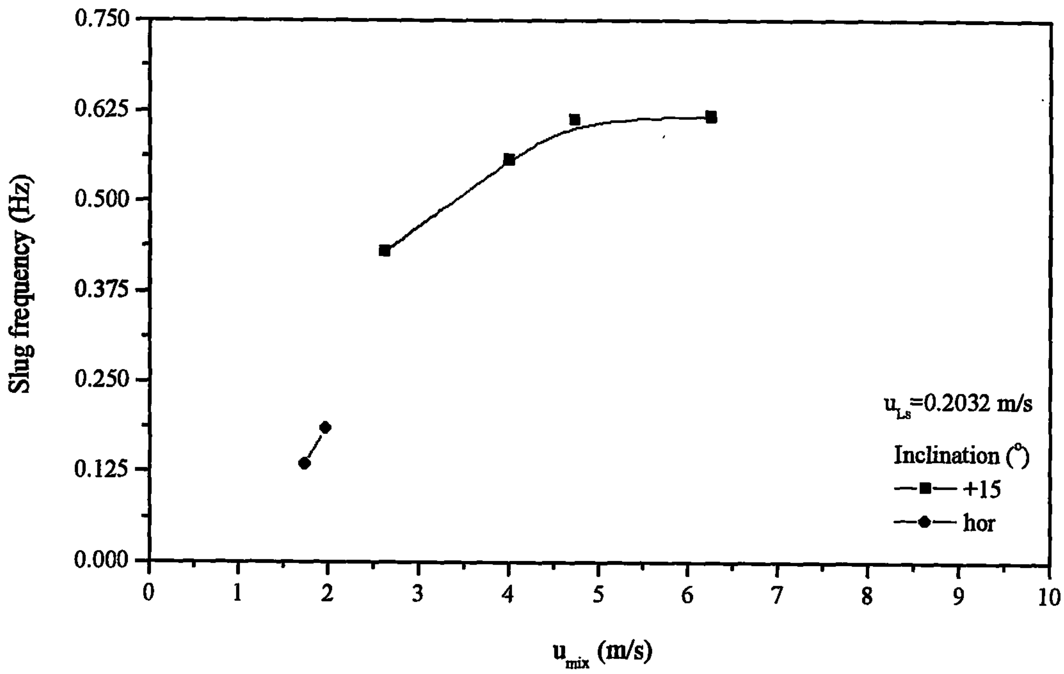

Figure 5.127. Variation of slug frequency with mixture velocity for different inclinations for a constant superficial liquid velocity of 0.2032 m/s.

The variation of slug frequency with mixture velocity for different inclinations is shown in figure 5.128. for a constant superficial liquid velocity of 0.2438 m/s. This is very clear from this figure that the slug frequency increases with the increasing of the pipe inclination. There is a tendency of the data of +5°, +10° and +15° inclination experiments to be closing to each other for higher mixture velocities. Figure 5.129. shows the variation of slug frequency with mixture velocity for different inclinations for a constant superficial liquid velocity of 0.2845 m/s. Except the slug frequency for +5° inclination pipe, the rest of the data increase as the inclination of the pipe is increased. The tendency of the data of +5°, +10° and +15° inclination experiments to be closing to each other for higher mixture velocities is more clear in this figure. One can conclude with respect to this figure that the slug frequency increases with the increasing of the pipe inclination.

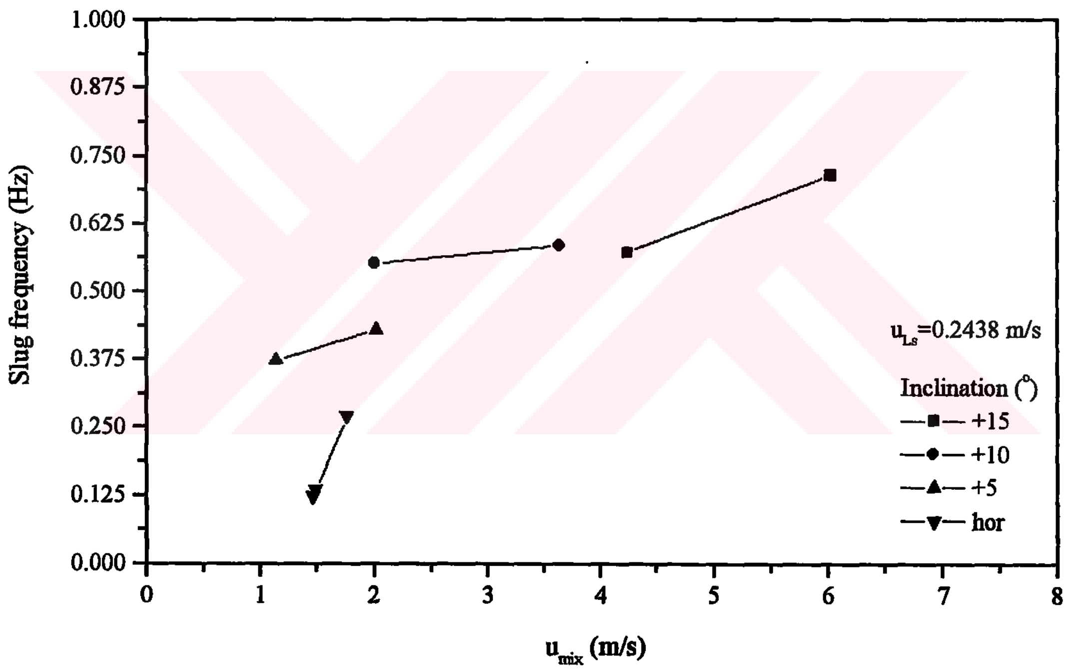

Figure 5.128. Variation of slug frequency with mixture velocity for different inclinations for a constant superficial liquid velocity of 0.2438 m/s.

The variation of slug frequency with mixture velocity for different inclinations is shown in figure 5.130. for a constant superficial liquid velocity of 0.3251 m/s. This superficial liquid velocity is the maximum value of this investigation. This is very clear from this figure that the slug frequency increases with the increasing of the pipe inclination. However, all the different inclination slug frequencies are getting closer to each other as the constant superficial liquid velocity is increased. This situation is especially more clear for the data of +5°, +10° and +15° inclination experiments and for higher mixture velocities.

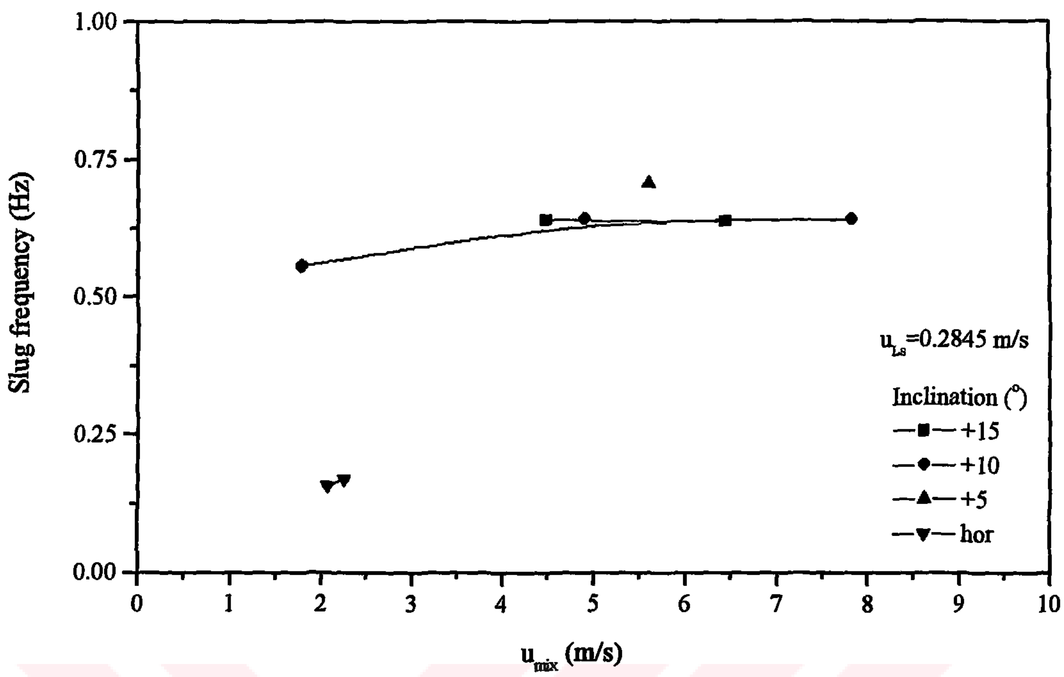

Figure 5.129. Variation of slug frequency with mixture velocity for different inclinations for a constant superficial liquid velocity of 0.2845 m/s.

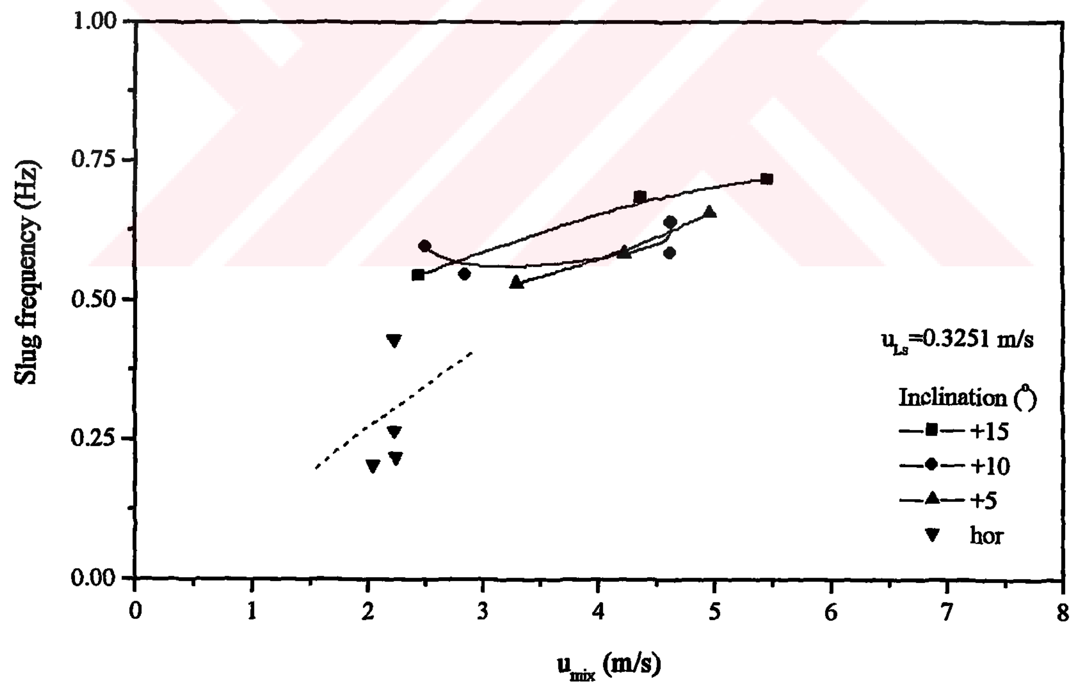

Figure 5.130. Variation of slug frequency with mixture velocity for different inclinations for a constant superficial liquid velocity of 0.3251 m/s.

As a conclusion of the slug frequencies; Slug frequency increases as the pipe diameter is decreased. Slug frequency increases with the increasing of the superficial liquid velocity. Slug frequency increases as the pipe inclination is increased, additionally, gets closer to each other with the increasing of the superficial liquid velocity.

5.2. Experimental System 2

5.2.1. Flow Patterns of Circular Pipe Experiments

The experiments on the experimental system 2 were conducted in the Laboratory of Department of Mechanical Engineering at Çukurova University, Turkey. The technical properties of this experimental setup were previously given including all important points in the section of "Material and Method". In the stages of establishment of the experimental setup 2, many preliminary experiments were carried out. Some of them were omitted because of incorrect measurements and results. Finally, the number of 205 experiments were selected between them which were carried out in horizontal circular pipe of 40 mm inner diameter. In some of these experiments, flow patterns and void fractions were not able to observe and measure, but all of these experiments have the pressure transmitter signals and the traces of the LEDs. Therefore, a few data are compared in the flow pattern maps. Two different flow pattern maps were selected for the comparison of flow pattern observations. The flow pattern maps of Baker (1954) and Weisman (1979) were previously used for the comparison of the flow pattern observations of the experimental system 1.

The flow patterns observed in this experimental setup are called under the name of 8 different types. All of these flow patterns are very close to each other. For instance, "Slug+Plug" means that the observed flow pattern demonstrates the properties of "Slug flow" and "Plug flow" at the same time. There are long slugs in which shorter plugs are accommodated. Other observed flow patterns given in the label of figure 5.131. should be regarded in this manner.

The flow pattern observations of circular horizontal pipe experiments are shown in the flow pattern map of Baker (1954) in figure 5.131. First of all, one can express that all observed flow patterns are located in the appropriate region of the map. For example, there are no annular flow observations in the experiments, and none of the data are sit in the annular region of the flow pattern map. It attracts the attention that the markers of slug flow (open squares) are mostly in the right place of the map. Additionally, the markers of undeveloped slug flow (solid down triangles) are mostly located in the intersection region of stratified, plug, and slug flows. It is concluded that these data are in agreement with the flow pattern map of Baker (1954).

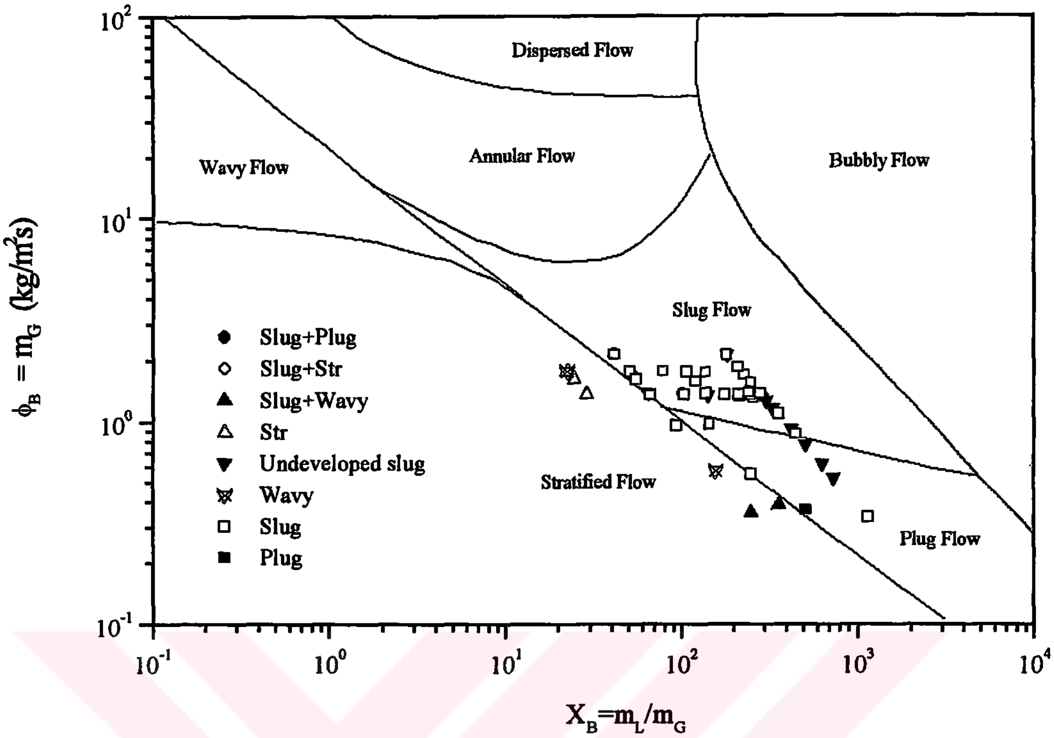

Figure 5.131. The flow pattern observations of circular horizontal pipe experiments in the flow pattern map of Baker (1954).

The same flow pattern observation data are shown in the flow pattern map of Weisman (1979) in figure 5.132.

Henceforth, the observed flow patterns are individually compared with the flow pattern map of Baker (1954) and Weisman (1979). Figure 5.133. shows the slug flow observations in the flow pattern map of Baker (1954). They mostly coincide with the slug flow predictions of Baker (1954).

Figure 5.134. shows the slug flow observations in the flow pattern map of Weisman (1979). The slug flow predictions of Baker (1954) is better that those of Weisman (1979).

The undeveloped slug flow observations of this investigation are compared with the flow pattern maps of Baker (1954) and Weisman (1979). The undeveloped slug flow means that the slug is developing throughout the test pipe. Especially, the lengths of the slugs, which become shorter or longer, change along the test pipe. Figure 5.135. shows the undeveloped slug flow observations in the flow pattern map of Baker (1954). These observations have mostly taken place in the intersection region of slug and plug flow.

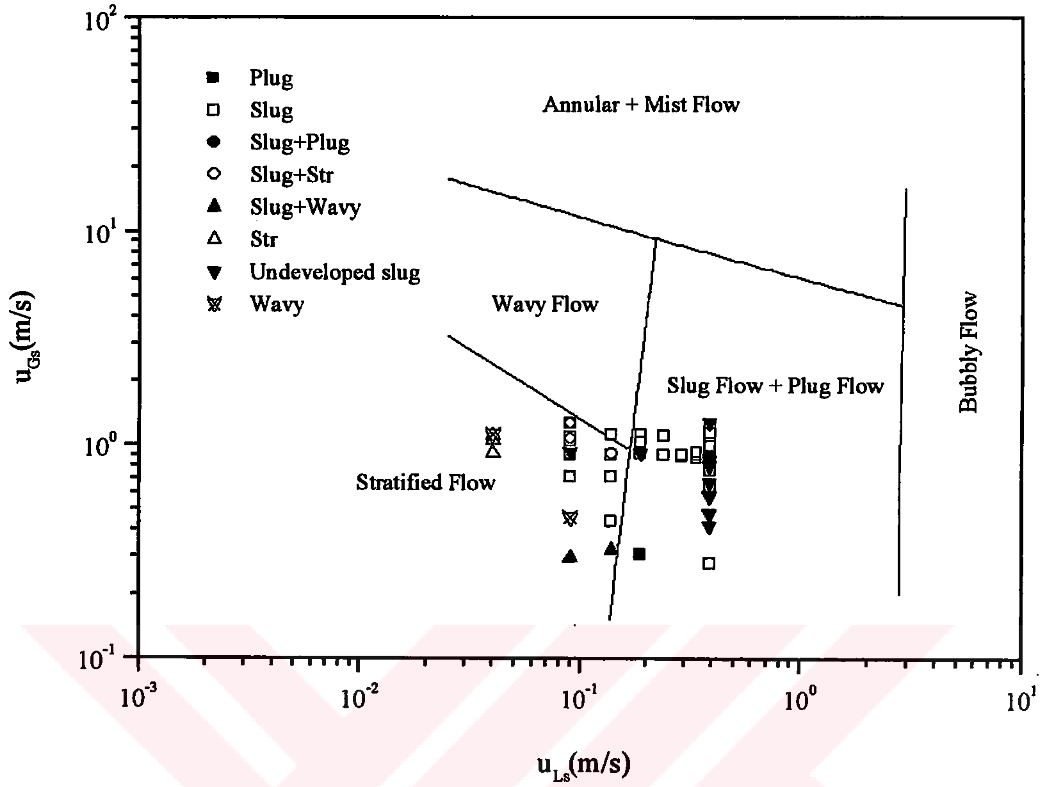

Figure 5.132. The flow pattern observations of circular horizontal pipe experiments in the flow pattern map of Weisman (1979).

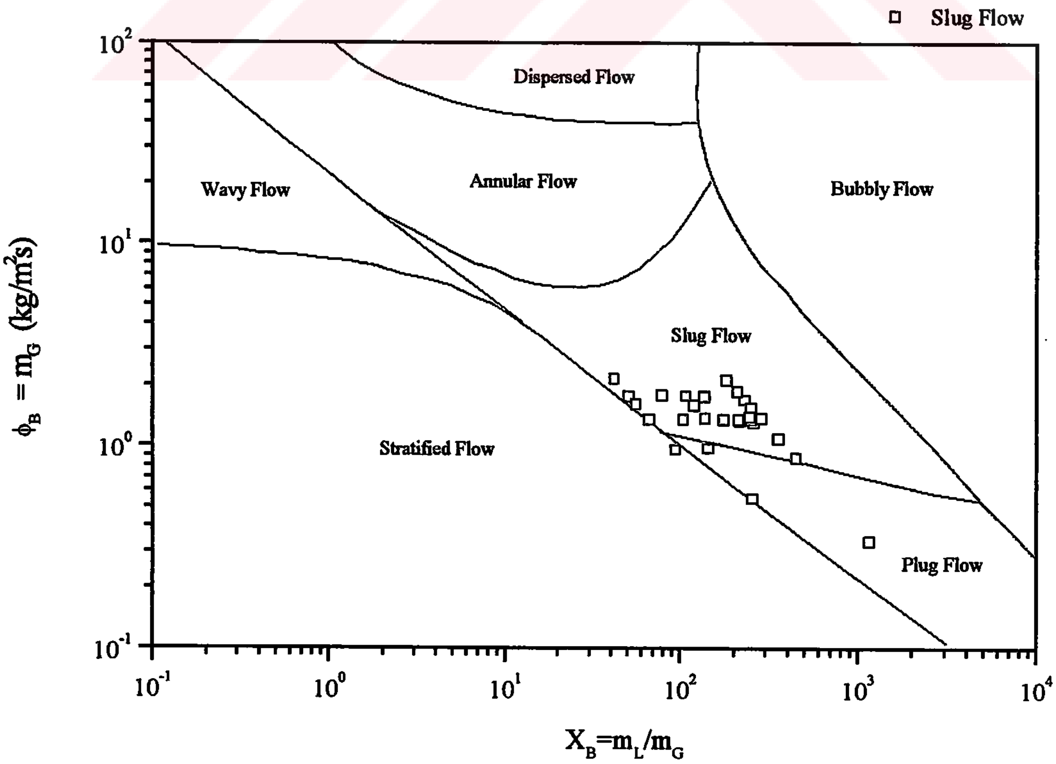

Figure 5.133. Slug flow observations in the flow pattern map of Baker (1954).

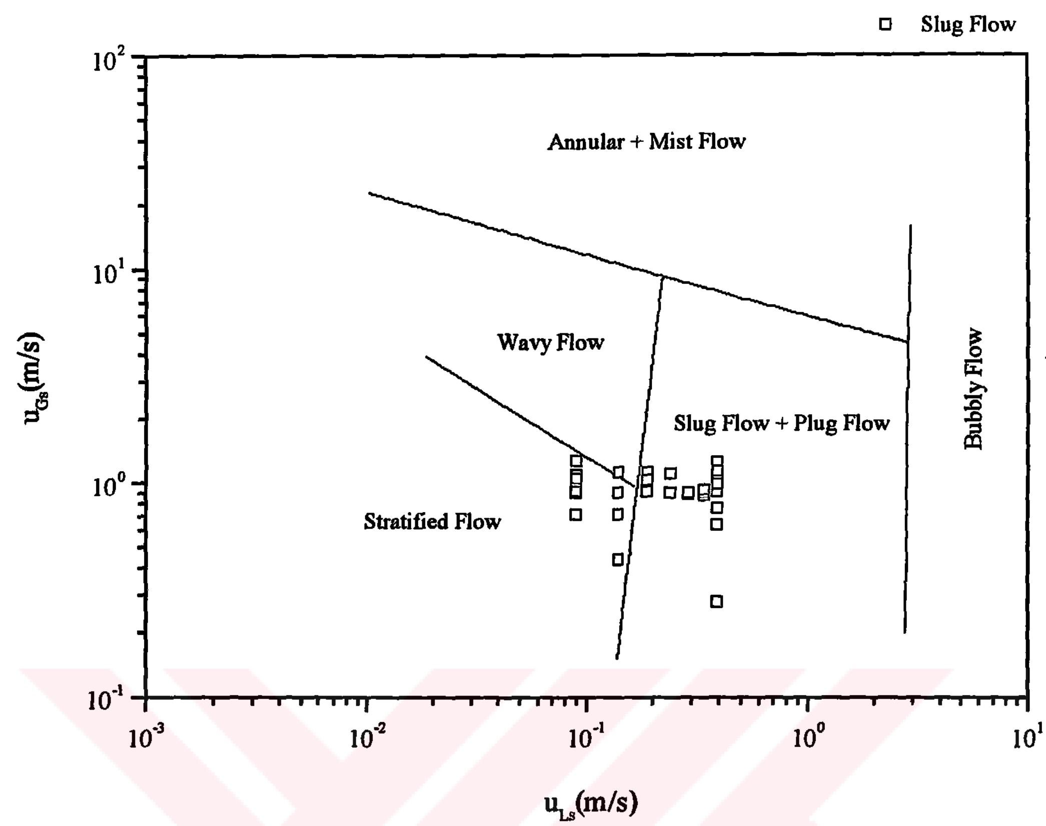

Figure 5.134. Slug flow observations in the flow pattern map of Weisman (1979).

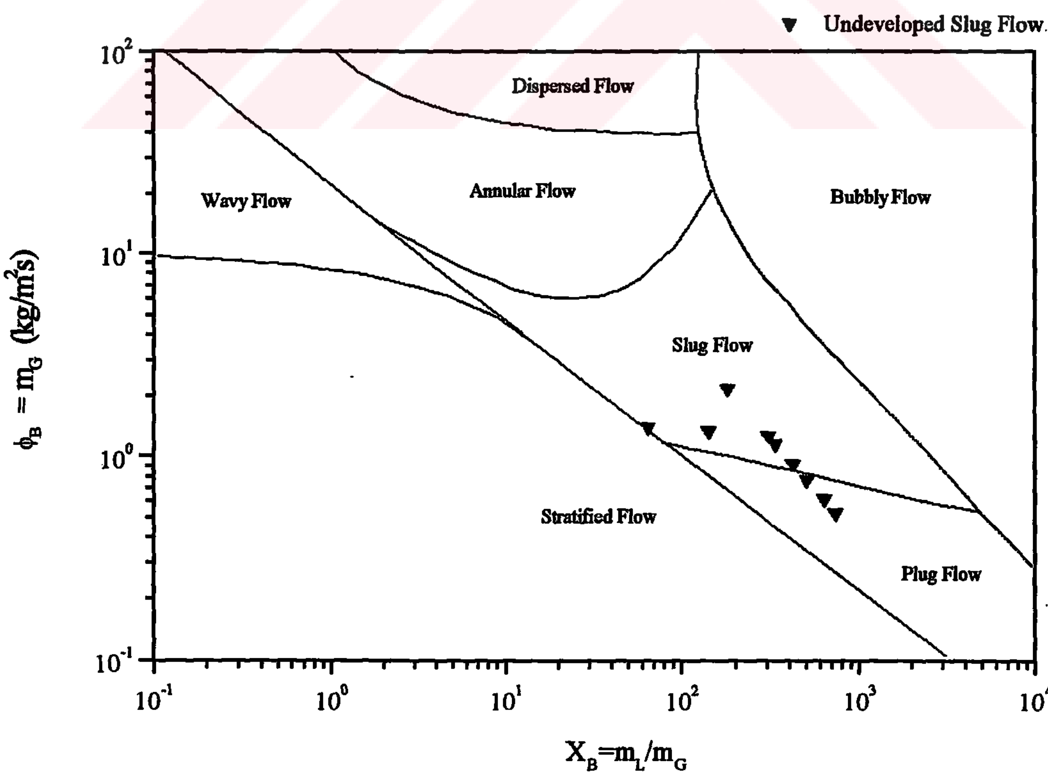

Figure 5.135. Undeveloped slug flow observations in the flow pattern map of Baker (1954).

Figure 5.136. shows the undeveloped slug flow observations in the flow pattern map of Weisman (1979). These observations are mostly located in the region of slug+plug flow. Thus, it can be expressed that the undeveloped slug flows take place in the region of slug+plug flow. However, the name of undeveloped slug flow consists of not only the slug+plug flow, but also only slugs with the changing lengths. Namely, there are slugs in which have no plugs, but the lengths of them change along the test pipe. The map of Baker (1954) predicts the undeveloped slug flow better than that of Weisman (1979).

The slug+wavy flow observations are sit in the unexpected region of both flow pattern map. They are expected to be closer to the wavy flow region of the flow pattern maps. However, there are only two observations, and they are not enough to reach a concrete conclusion.

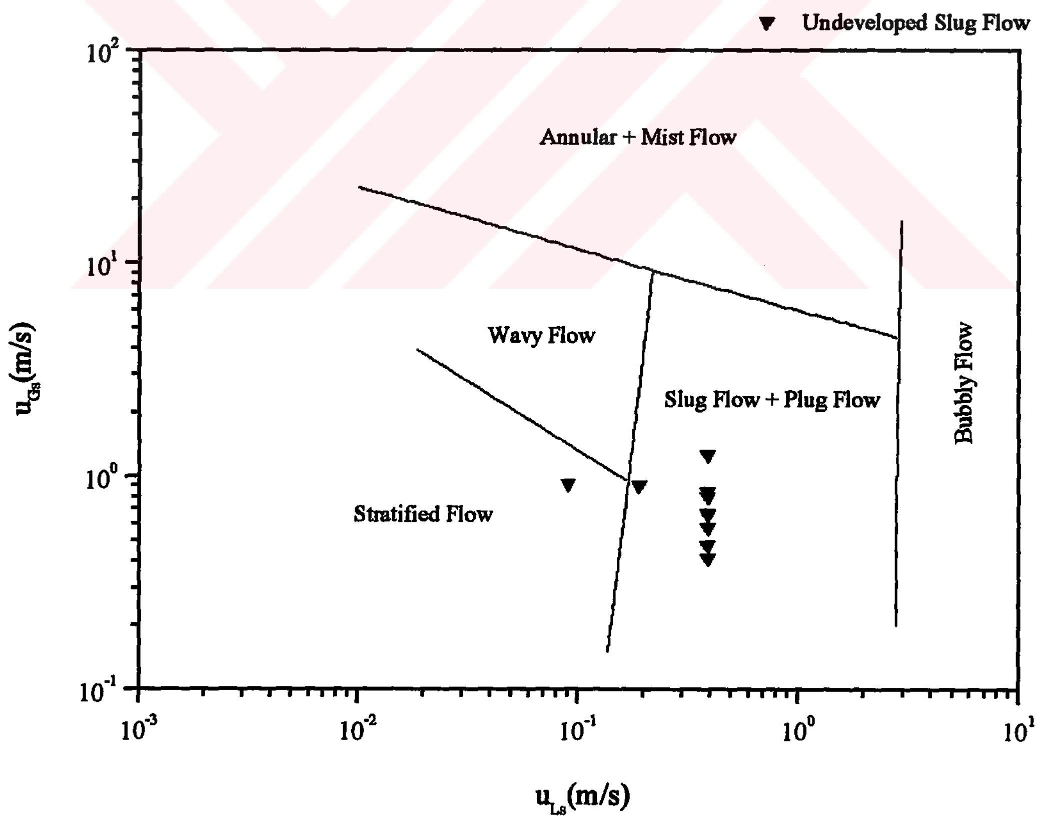

Figure 5.136. Undeveloped slug flow observations in the flow pattern map of Weisman (1979).

Figures 5.137. and 5.138. show these observations in the flow pattern maps of Baker (1954) and Weisman (1979).

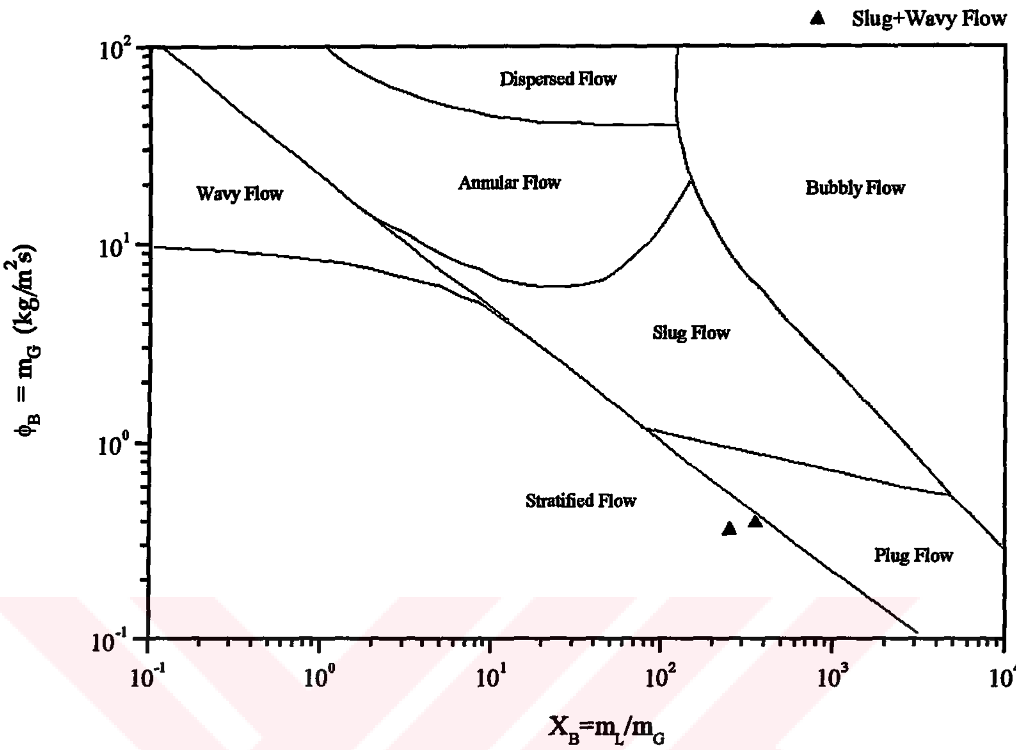

Figure 5.137. Slug+wavy flow observations in the flow pattern map of Baker (1954).

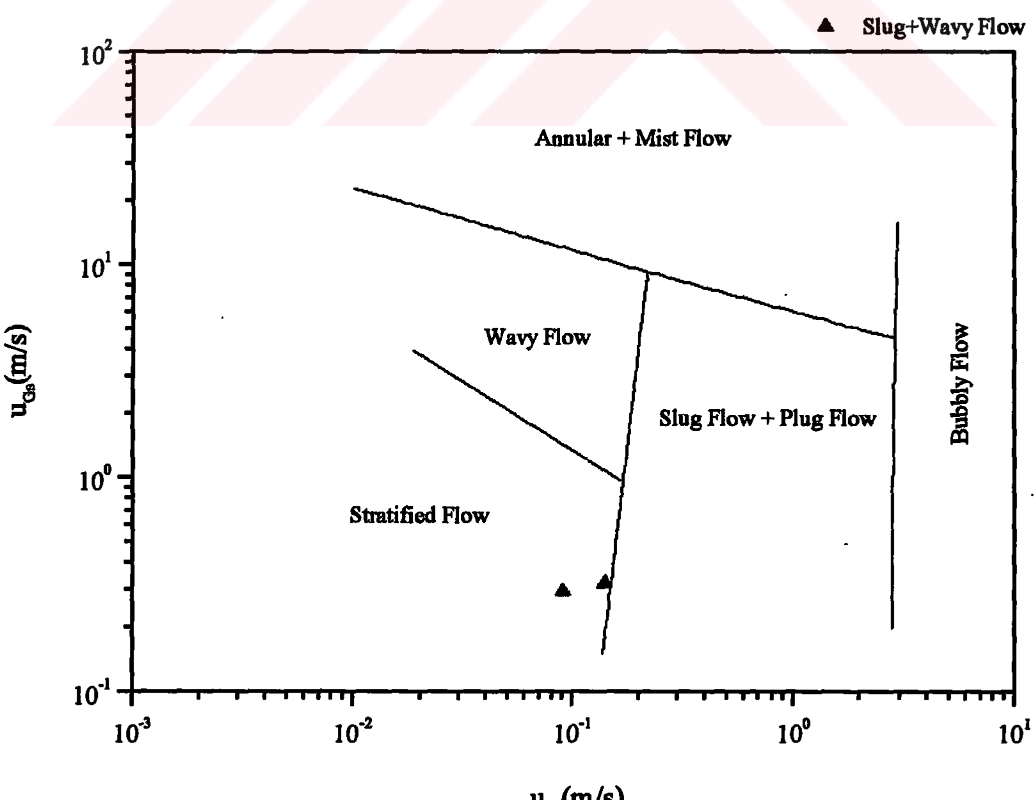

Figure 5.138. Slug+wavy flow observations in the flow pattern map of Weisman (1979).

The slug+stratified flow observations are shown in figures 5.139. and 5.140. in the flow pattern maps of Baker (1954) and Weisman (1979). The predictions of Baker (1954) are in the expected region of the map. They sit just near to the transition regions of two flow patterns. Baker (1954)'s map predicts the slug+stratified flow observations better than that of Weisman (1979).

The slug+plug flow observation is shown in figures 5.141. and 5.142. in the flow pattern maps of Baker (1954) and Weisman (1979). The predictions of Baker (1954) and Weisman (1979) are in the expected region of the maps. The prediction of Baker (1954) is close to the transition region of two flow patterns. However, Weisman (1979)'s map predicts the slug+plug flow observation better than that of Baker (1954).

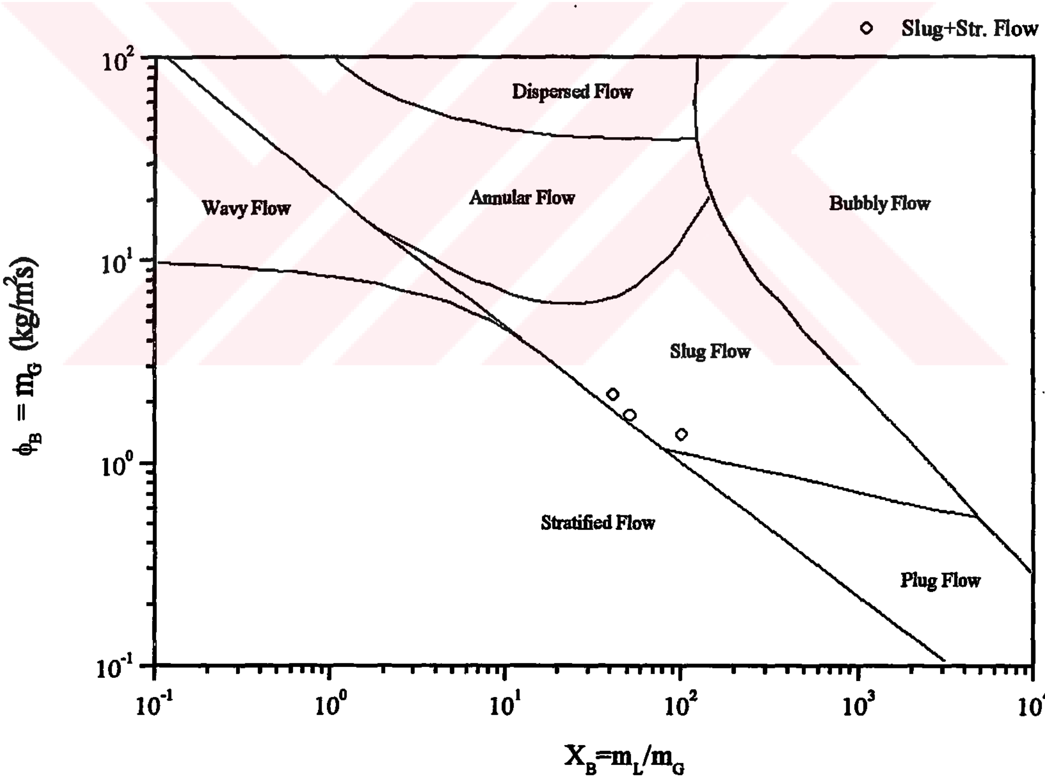

Figure 5.139. Slug+str. flow observations in the flow pattern map of Baker (1954).

The plug flow observation has been shown in figures 5.143. and 5.144. in the flow pattern maps of Baker (1954) and Weisman (1979). The predictions of Baker (1954) and Weisman (1979) are in the expected region of the maps. The predictions of Baker (1954) and Weisman (1979) are close to the transition region of plug and stratified flow patterns. Both maps predict the plug flow observation sufficiently.

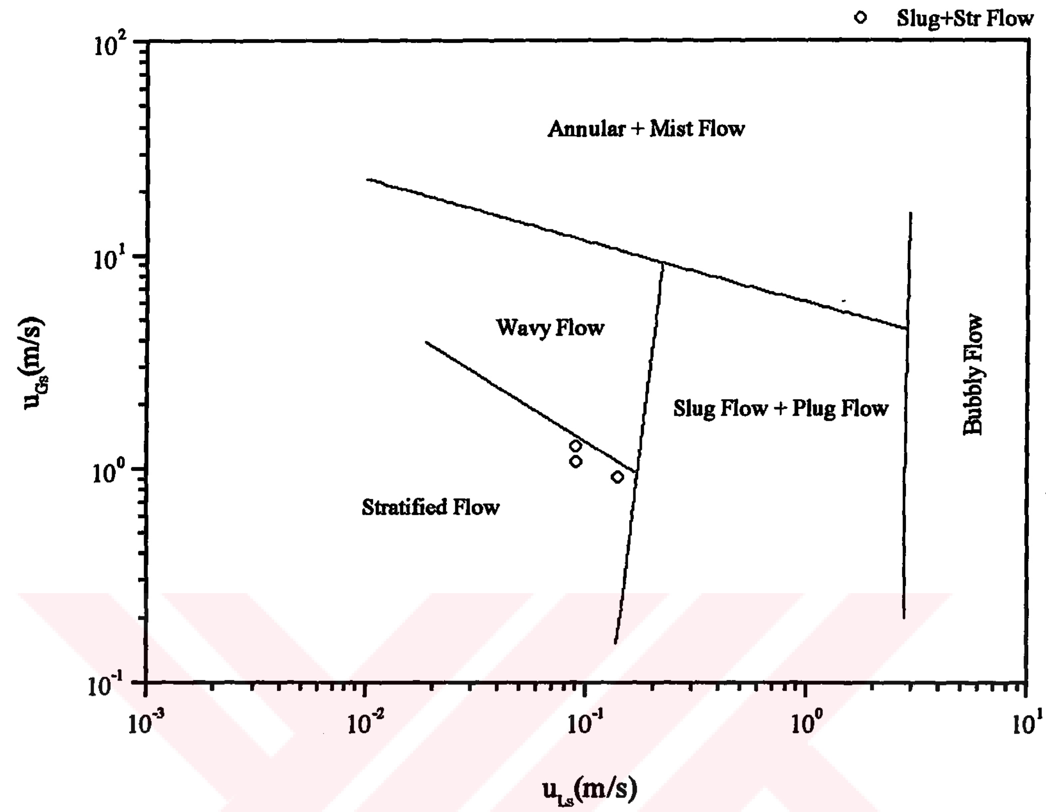

Figure 5.140. Slug+str. flow observations in the flow pattern map of Weisman (1979).

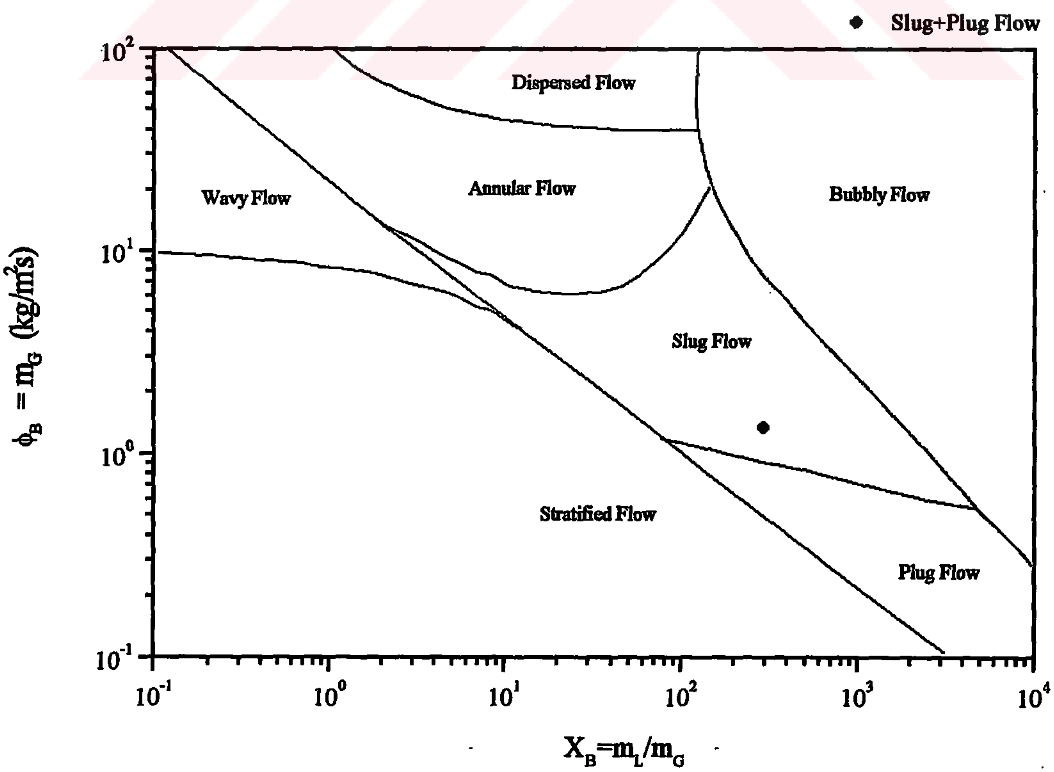

Figure 5.141. Slug+plug flow observations in the flow pattern map of Baker (1954).

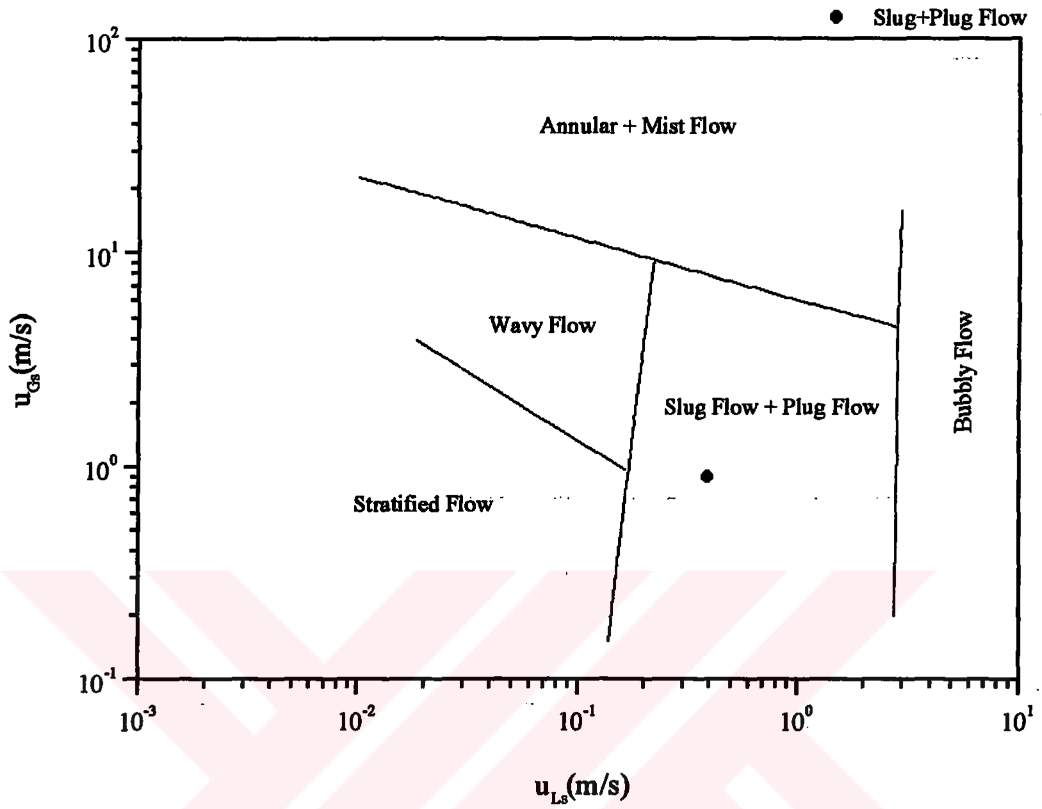

Figure 5.142. Slug+plug flow observations in the flow pattern map of Weisman (1979).

The wavy flow observations are shown in figures 5.145. and 5.146. in the flow pattern maps of Baker (1954) and Weisman (1979). The predictions of Baker (1954) and Weisman (1979) are in the unexpected region of the maps. The predictions of Baker (1954) and Weisman (1979) are close to the transition region of plug, slug and stratified flow patterns. Both maps predict the wavy flow observation insufficiently. However, there are only two observations, and they are not enough to reach a concrete conclusion.

Figures 5.147. and 5.148. show the stratified flow observations in the flow pattern maps of Baker (1954) and Weisman (1979). These observations are all located in the expected region of the maps. Thus, it can be expressed that the stratified flow observations are sufficiently predicted by both of the maps.

As a conclusion of the flow pattern observations, they are mostly in agreement with the others. This is important from the view point of the reliability of the measurement system.

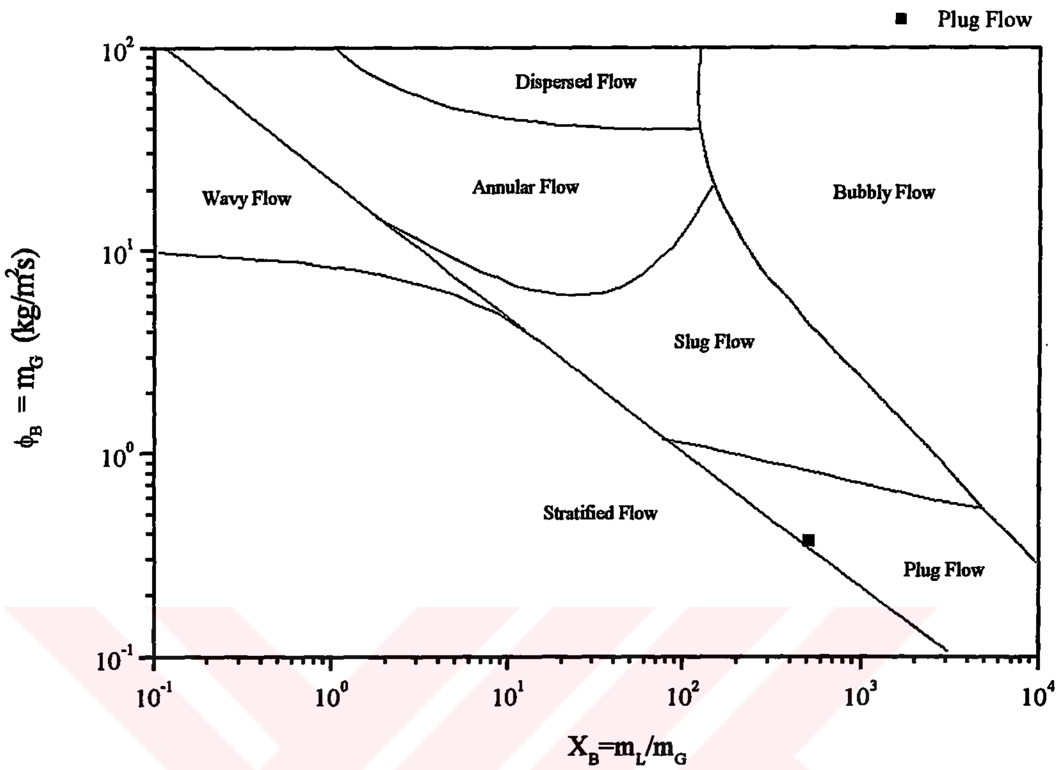

Figure 5.143. Plug flow observations in the flow pattern map of Baker (1954).

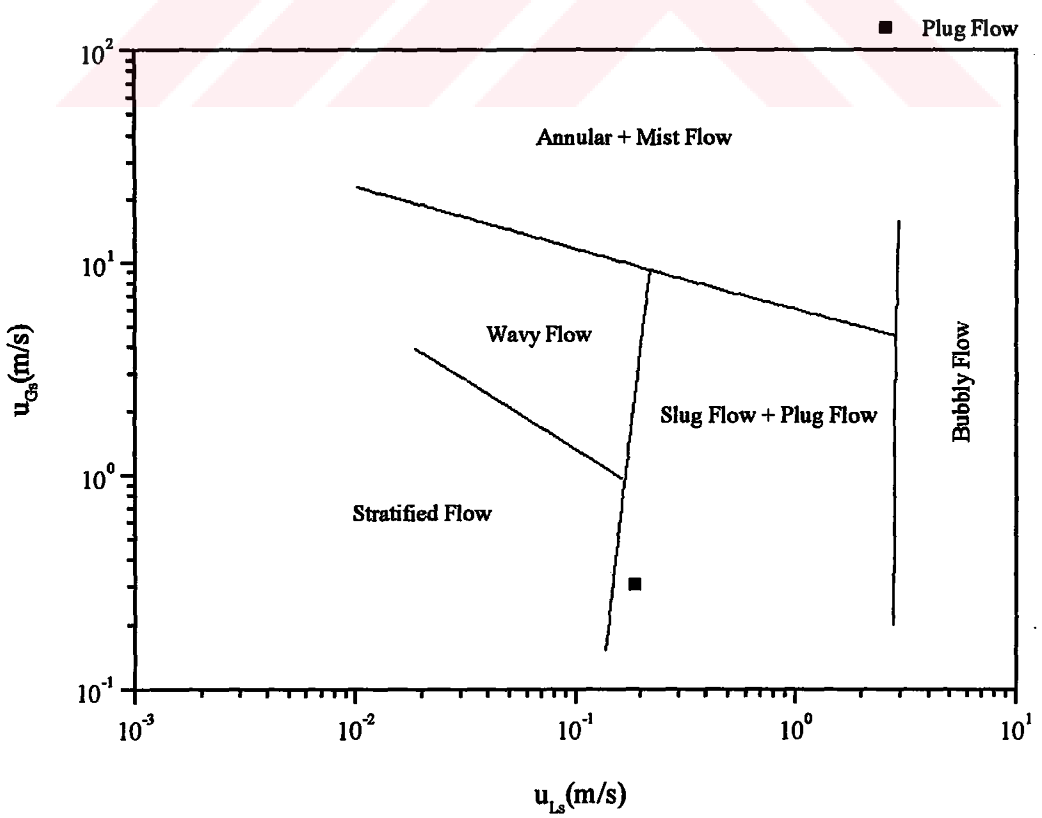

Figure 5.144. Plug flow observations in the flow pattern map of Weisman (1979).

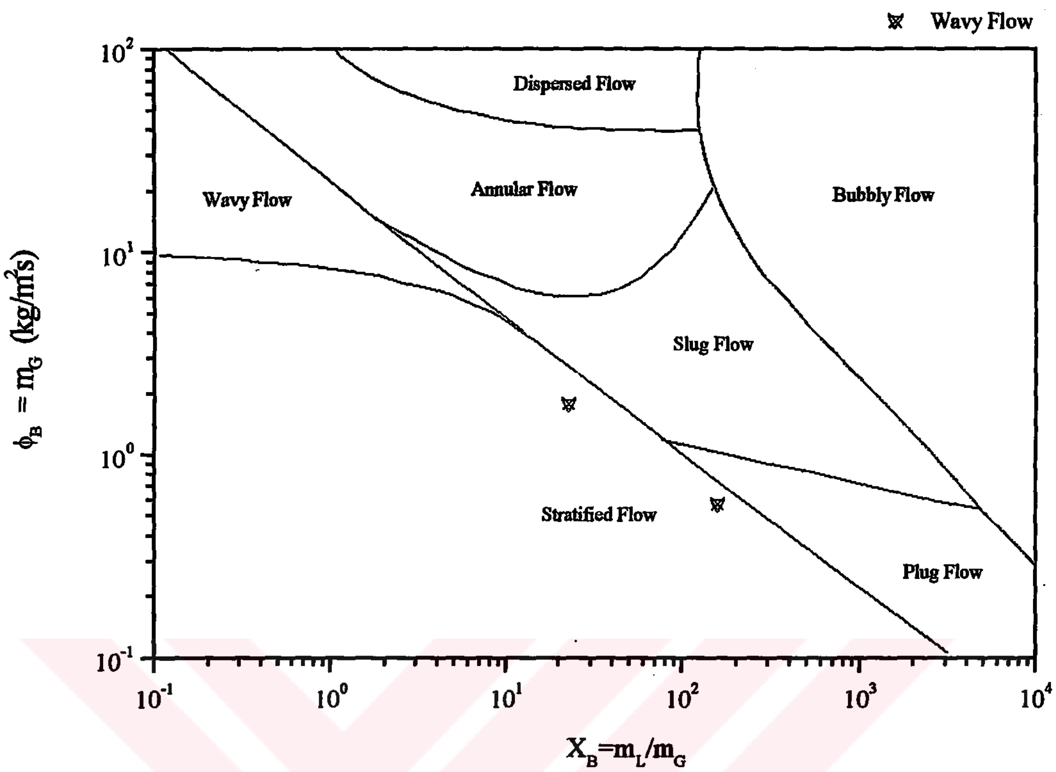

Figure 5.145. Wavy flow observations in the flow pattern map of Baker (1954).

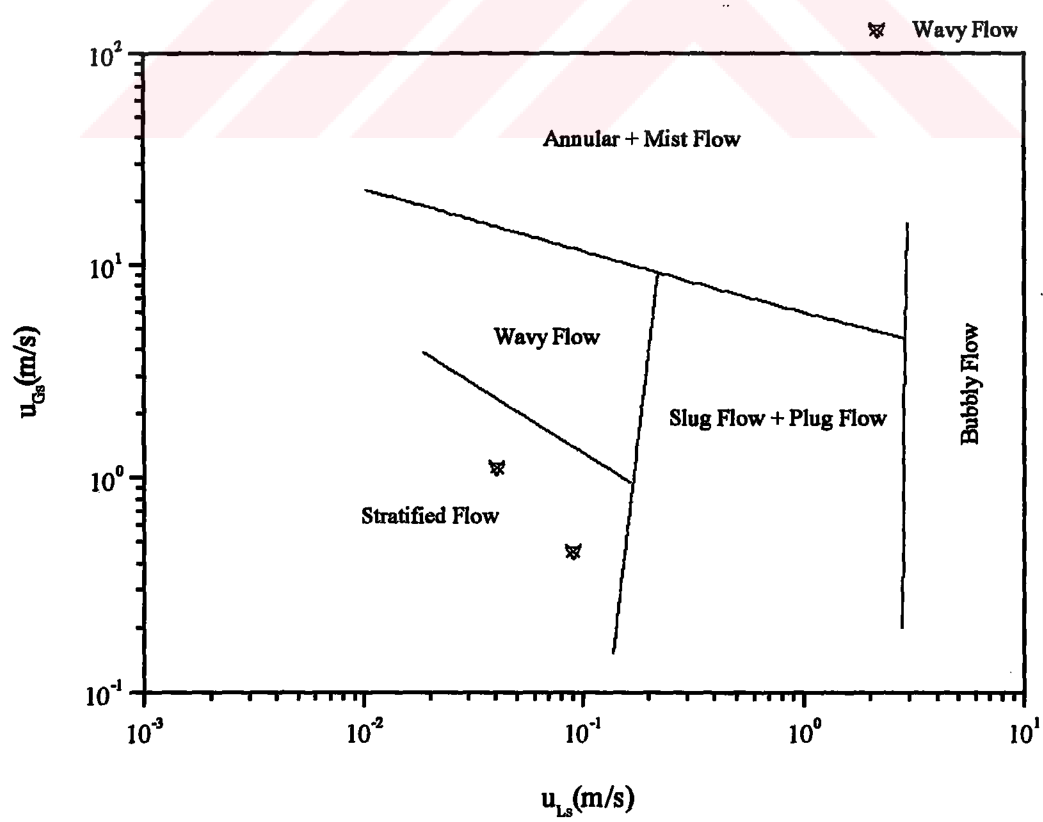

Figure 5.146. Wavy flow observations in the flow pattern map of Weisman (1979).

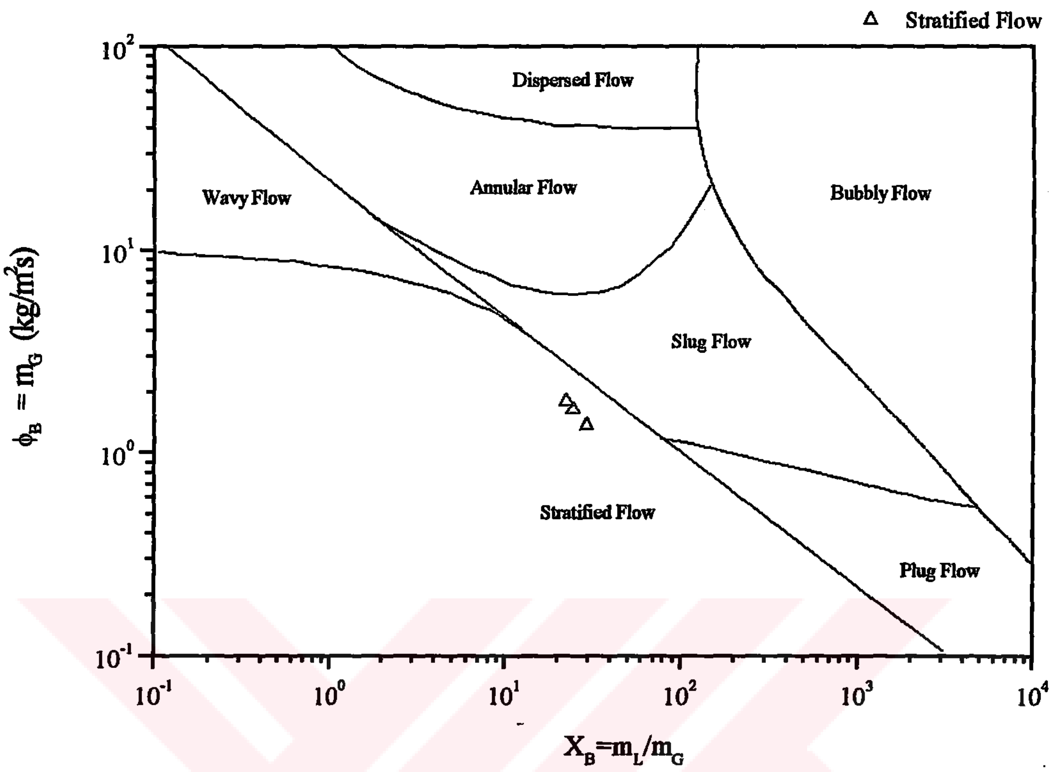

Figure 5.147. Stratified flow observations in the flow pattern map of Baker (1954).

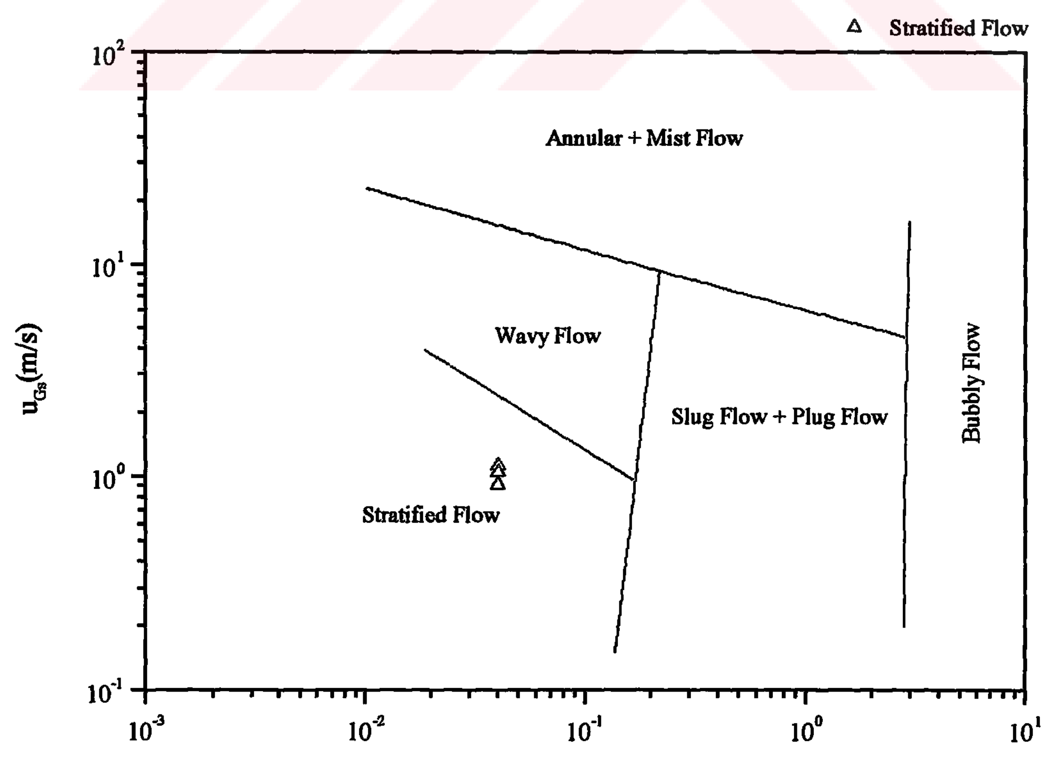

Figure 5.148. Stratified flow observations in the flow pattern map of Weisman (1979).

5.2.2. Pressure Losses of Circular Pipe Experiments

The pressure losses measured in the horizontal circular pipe experiments are shown in figure 5.149. These pressure values were calculated using the arithmetic means of the results of the pressure transducers 1 and 2. The pressure losses at the superficial gas velocity of 0 m/s are the results of the single phase liquid flow. This figure clearly demonstrates that the resistance (R) increases with the increasing of the superficial gas velocity for a constant superficial liquid velocity. However, the resistance (R) also increases with the increasing of the superficial liquid velocity for a constant superficial gas velocity.

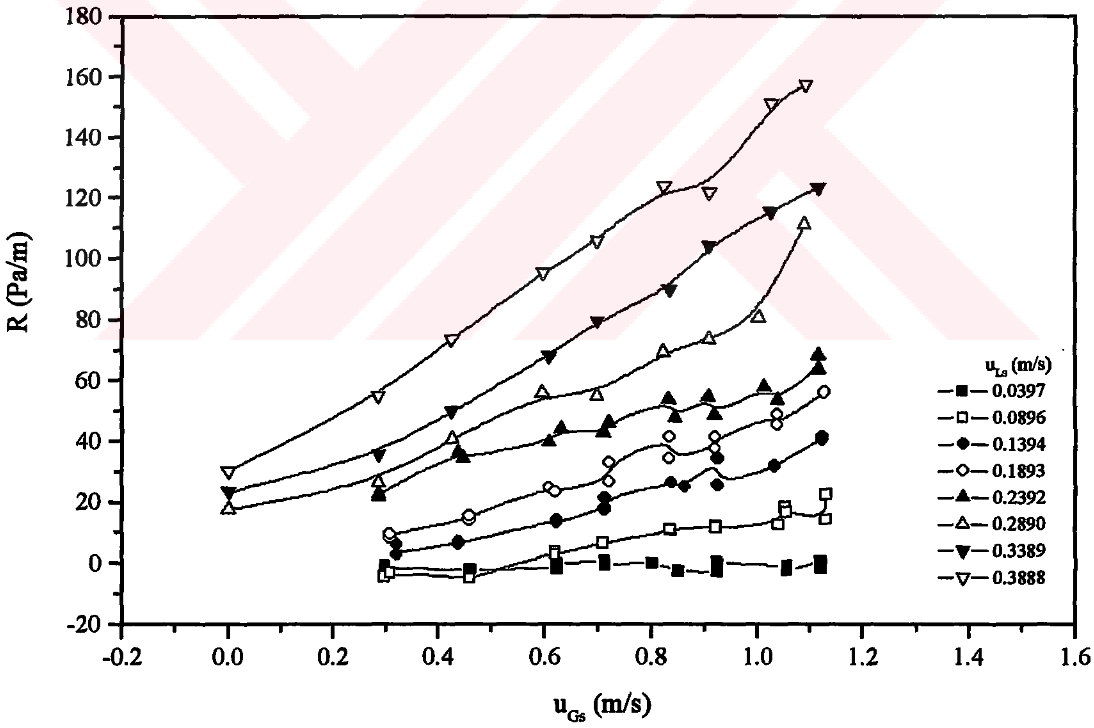

Figure 5.149. The pressure losses measured in the horizontal circular pipe experiments.

The measured pressure losses in the horizontal circular pipe experiments are compared with the empirical methods of Lockhart-Martinelli (LMM), Chisholm (CM), and Boroczy-Chisholm (BCM). The detailed calculation procedures of these methods can be found in Yılmaz (2001). The resistances measured in each constant superficial liquid velocity are compared with the results of LMM, CM, and BCM.

These comparisons are shown from figure 5.150. to 5.157. The most reliable predictions are obtained using the LMM.

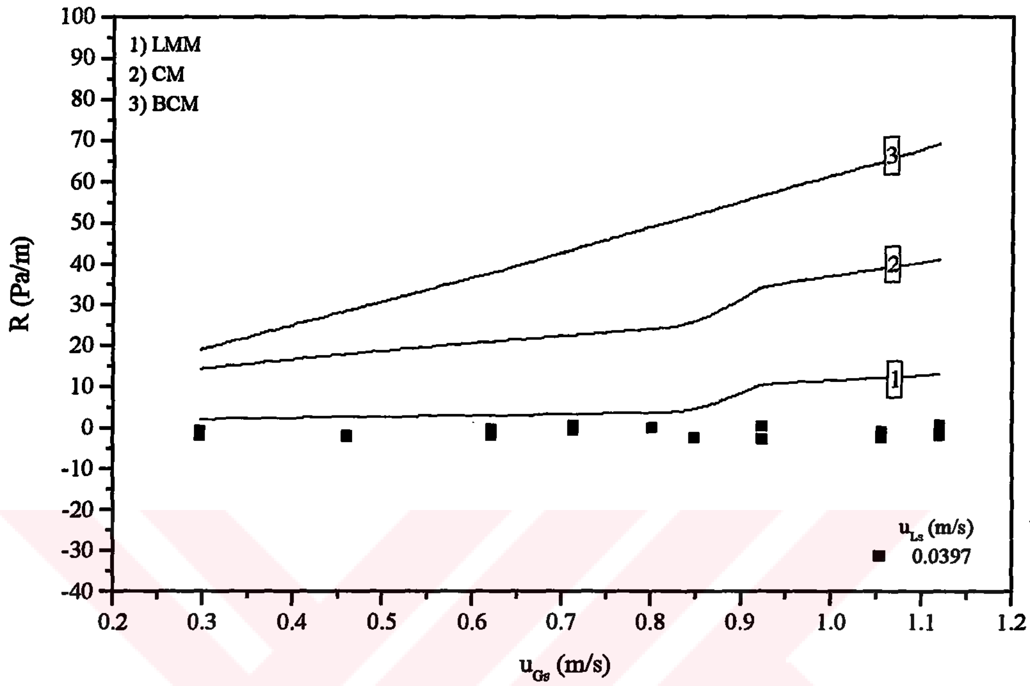

Figure 5.150. Comparison of the measured resistances with the results of LMM, CM, and BCM for a constant superficial liquid velocity of 0.0397 m/s.

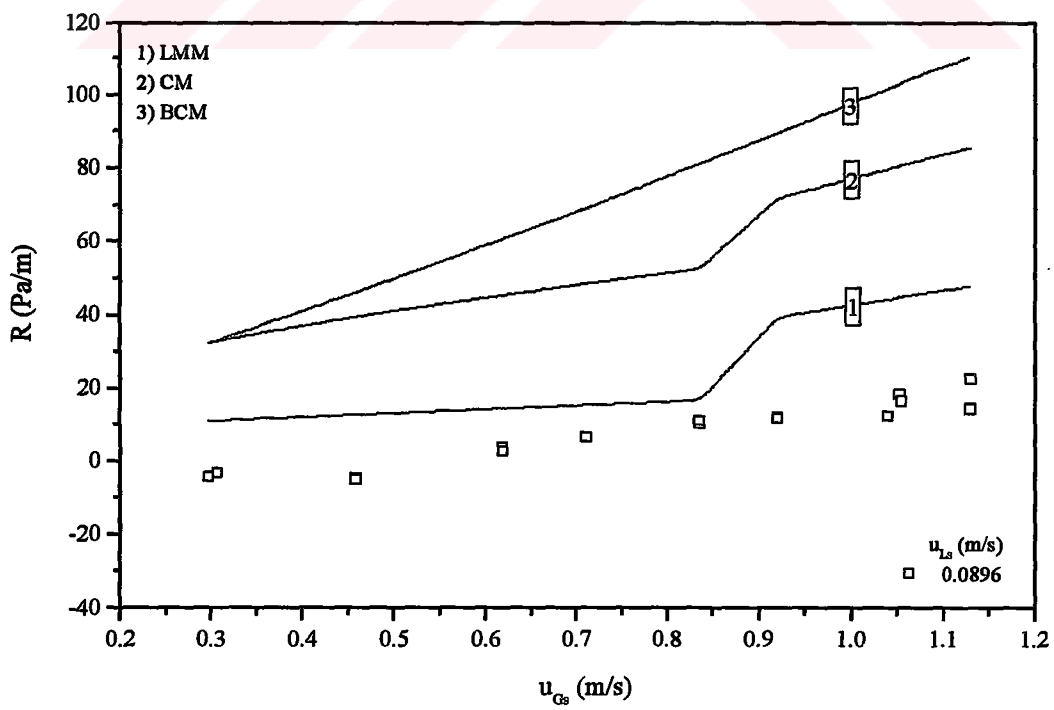

Figure 5.151. Comparison of the measured resistances with the results of LMM, CM, and BCM for a constant superficial liquid velocity of 0.0896 m/s.

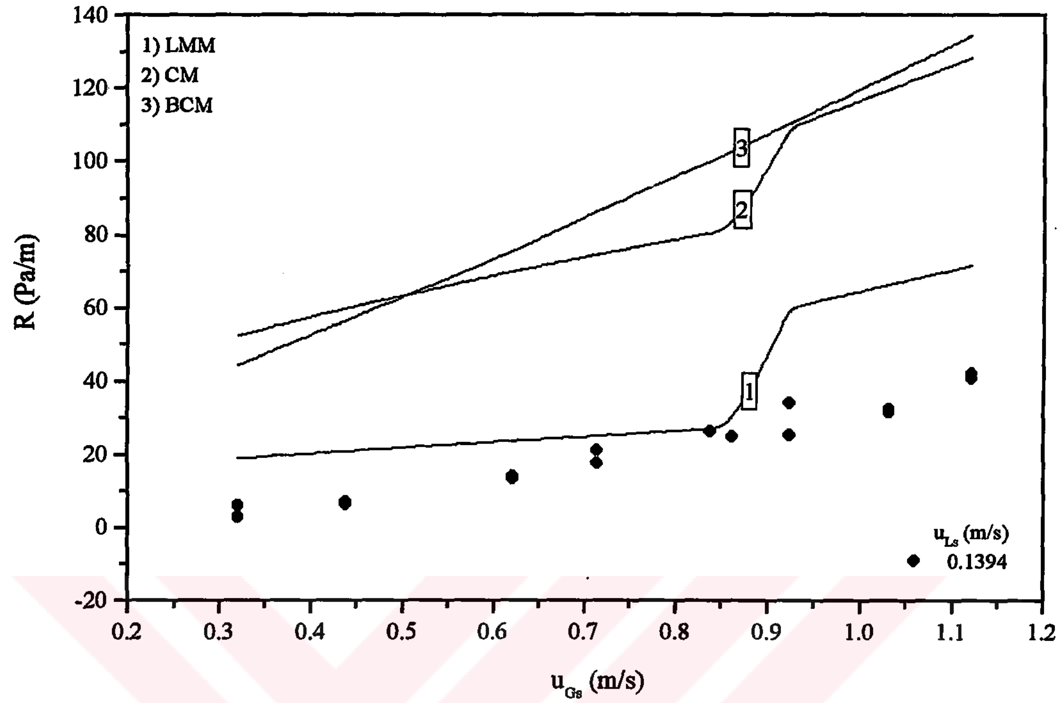

Figure 5.152. Comparison of the measured resistances with the results of LMM, CM, and BCM for a constant superficial liquid velocity of 0.1394 m/s.

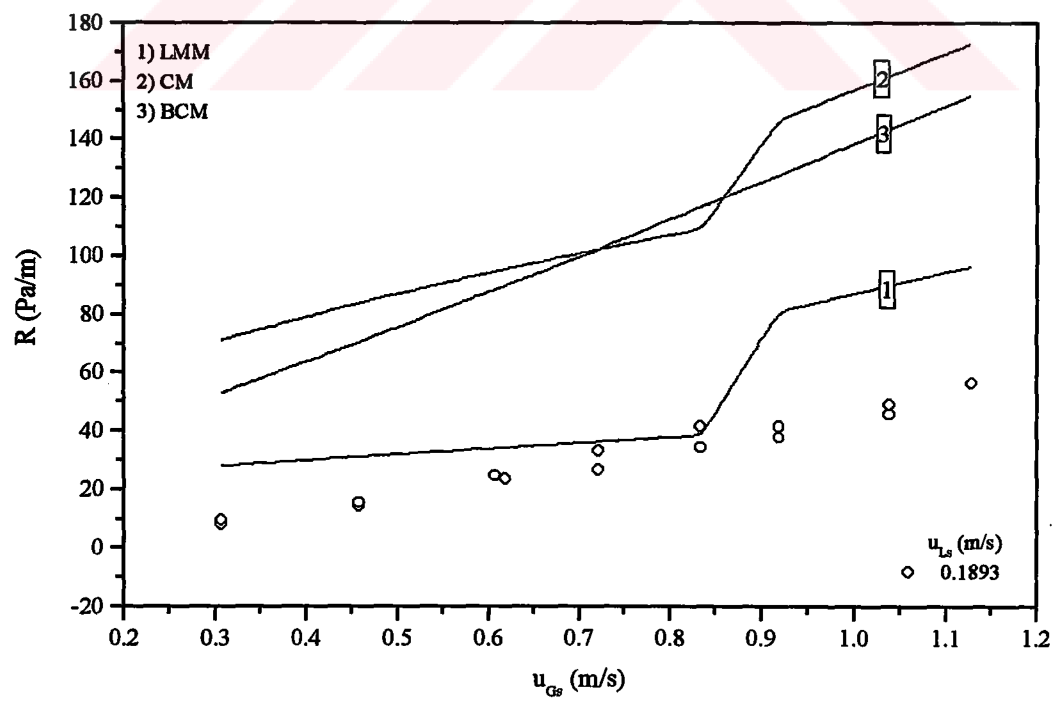

Figure 5.153. Comparison of the measured resistances with the results of LMM, CM, and BCM for a constant superficial liquid velocity of 0.1893 m/s.

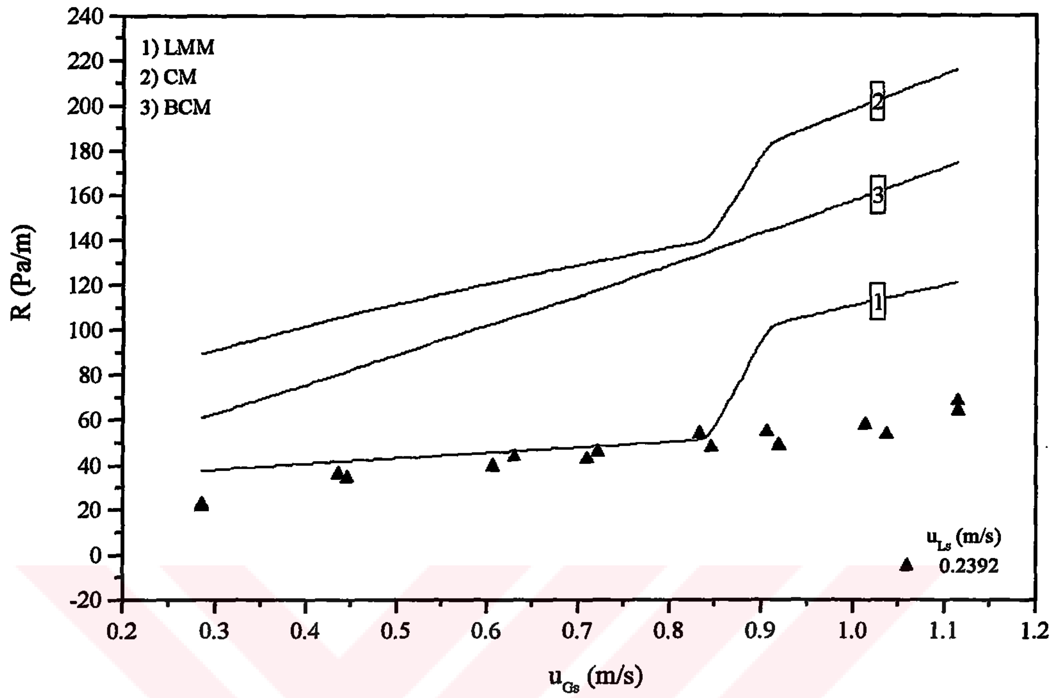

Figure 5.154. Comparison of the measured resistances with the results of LMM, CM, and BCM for a constant superficial liquid velocity of 0.2392 m/s.

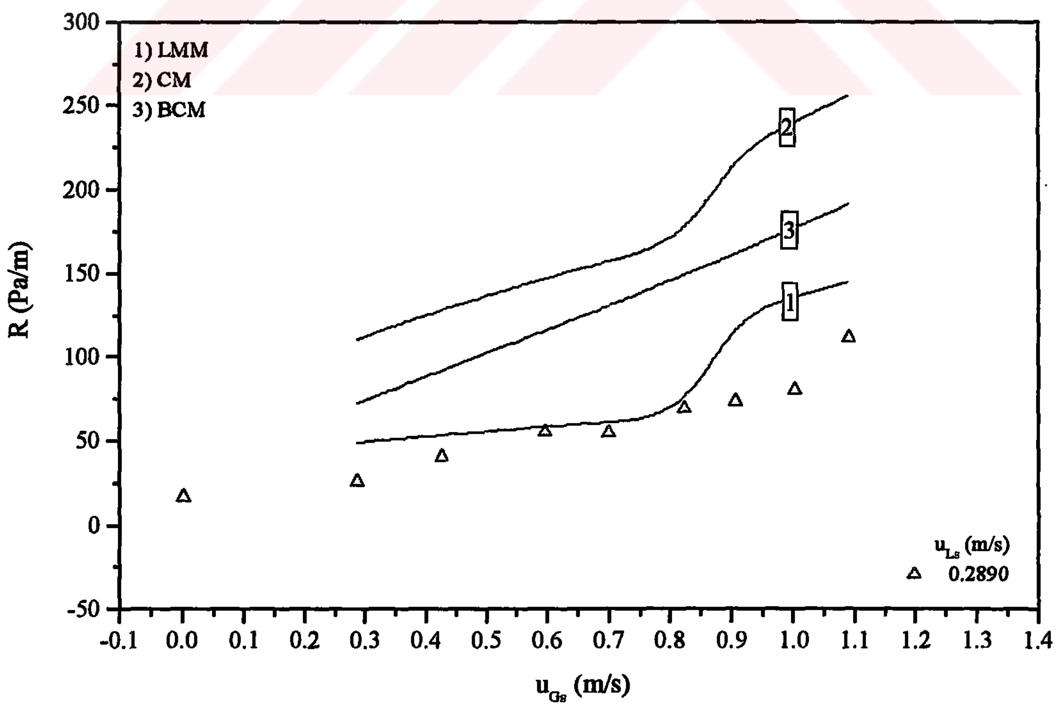

Figure 5.155. Comparison of the measured resistances with the results of LMM, CM, and BCM for a constant superficial liquid velocity of 0.2890 m/s.

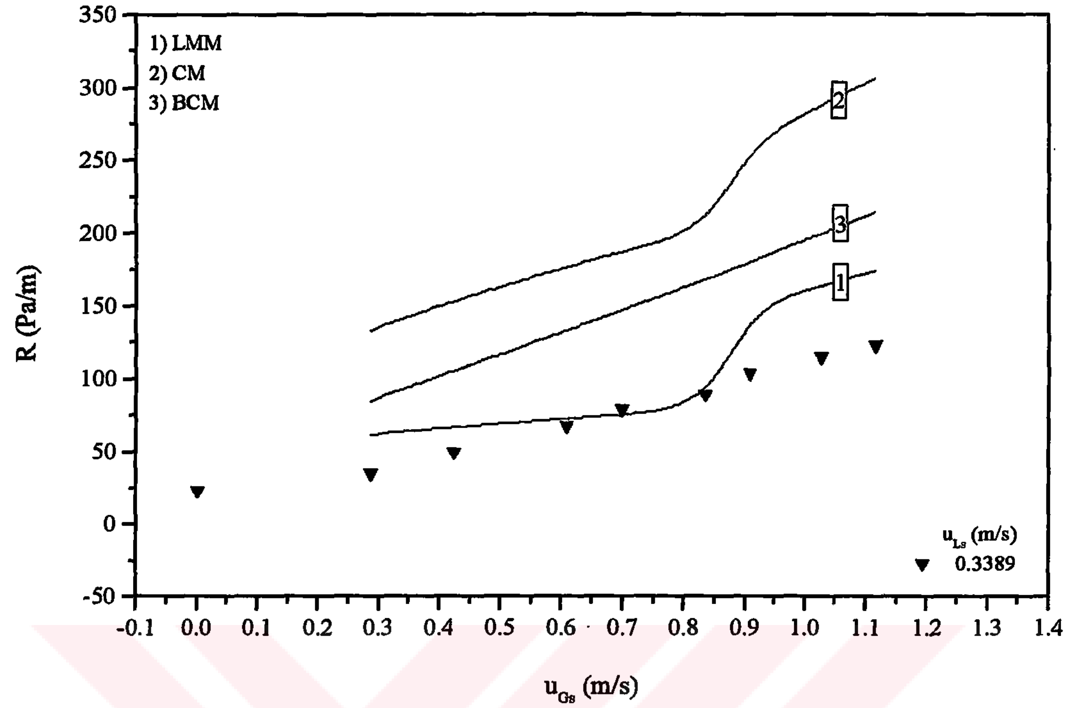

Figure 5.156. Comparison of the measured resistances with the results of LMM, CM, and BCM for a constant superficial liquid velocity of 0.3389 m/s.

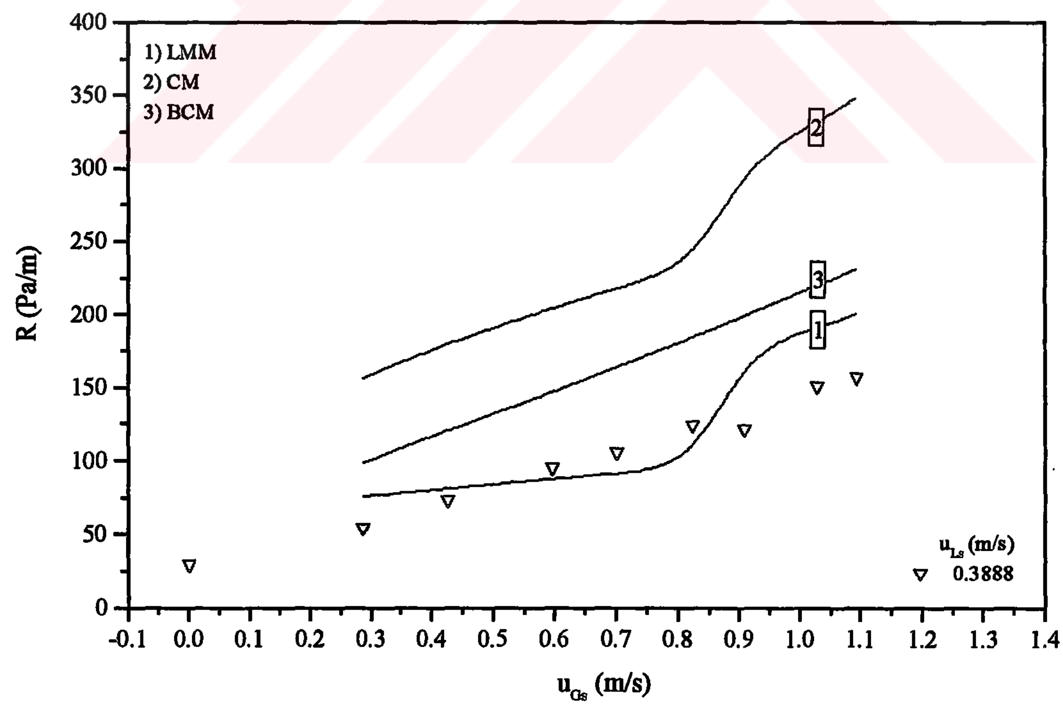

Figure 5.157. Comparison of the measured resistances with the results of LMM, CM, and BCM for a constant superficial liquid velocity of 0.3888 m/s.

The measured pressure losses are also compared with the study of Kokal and Stanislav (1989). These pressure losses measured in a 51.2 mm inner diameter test pipe. It should be remembered from the first section of "Results and Discussion"; Kokal and Stanislav (1989)'s experimental results showed that, for a same constant superficial liquid velocity, pressure losses decrease as the inner diameter of pipe is increased. Namely, because of the smaller inner diameter of our test pipe (40 mm) than that of Kokal and Stanislav (1989) (51.2 mm), our results should be higher than those of Kokal and Stanislav (1989). However, it is concluded from our results that the resistance (R) increases with the increasing of the superficial liquid velocity for a constant superficial gas velocity.

Figure 5.158. shows the variation of resistance with the superficial gas velocity for a constant superficial liquid velocity of 0.0397 m/s. According to the interpretation given in previous paragraph, our results should be greater than those of line 1, because the constant superficial liquid velocity of 0.0397 m/s is greater than 0.030 m/s. Additionally, our results should also be greater than those of line 1, because the inner diameter of test pipe of this investigation is smaller than 51.2 mm. However, our results are less than those of Kokal and Stanislav (1989). This is possibly due to the very low superficial liquid velocity. The pressure transducers are not sufficiently sensitive to measure these pressure losses.

The comparisons of experimental results with those of Kokal and Stanislav (1989) are shown from figures 5.158. to 5.165.

From the pressure losses measured in the horizontal circular pipe with 40 mm inner diameter, the following conclusions can be made: The resistance (R) increases with the increasing of the superficial gas velocity for a constant superficial liquid velocity. The resistance (R) also increases with the increasing of the superficial liquid velocity for a constant superficial gas velocity. The measured pressure losses are predicted best by the empirical method of Lockhart-Martinelli. The other methods of CM and BCM predict higher values than the measured pressure losses. The measured pressure losses are lower than the experimental results of Kokal and Stanislav (1989). However, the differences between the pipe diameters and the superficial liquid velocities disable the comparison of data effectively. The measured pressure losses are approximately in agreement with the measurements of Kokal and Stanislav (1989).

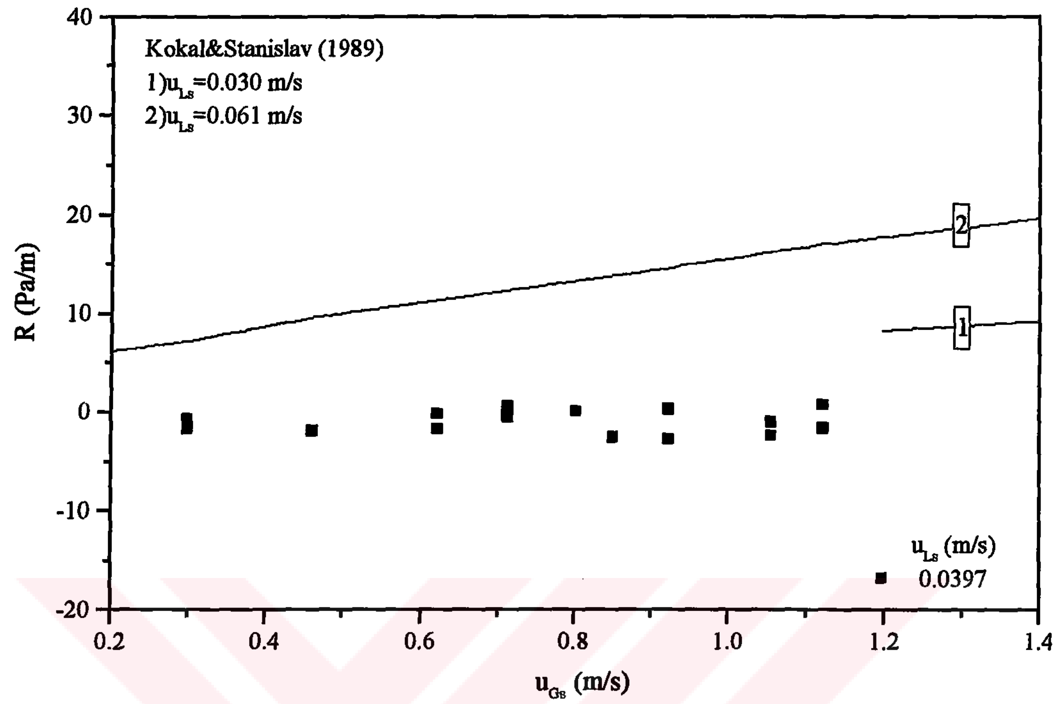

Figure 5.158. Comparison of the measured resistances of this investigation with the study of Kokal and Stanislav (1989).

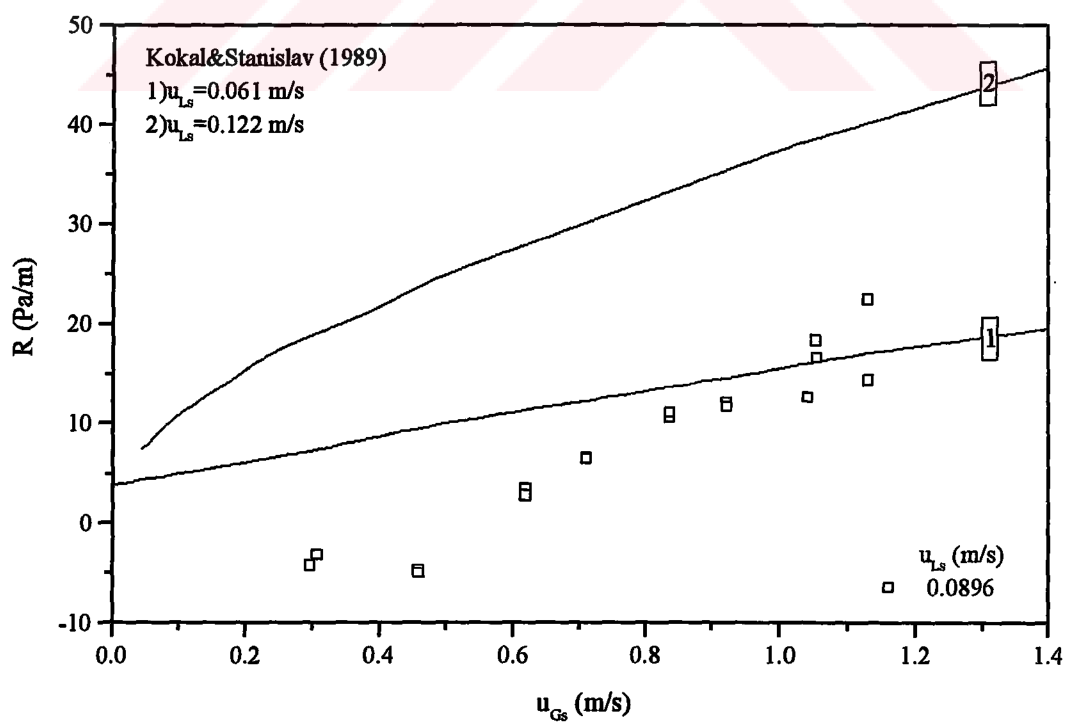

Figure 5.159. Comparison of the measured resistances of this investigation with the study of Kokal and Stanislav (1989).

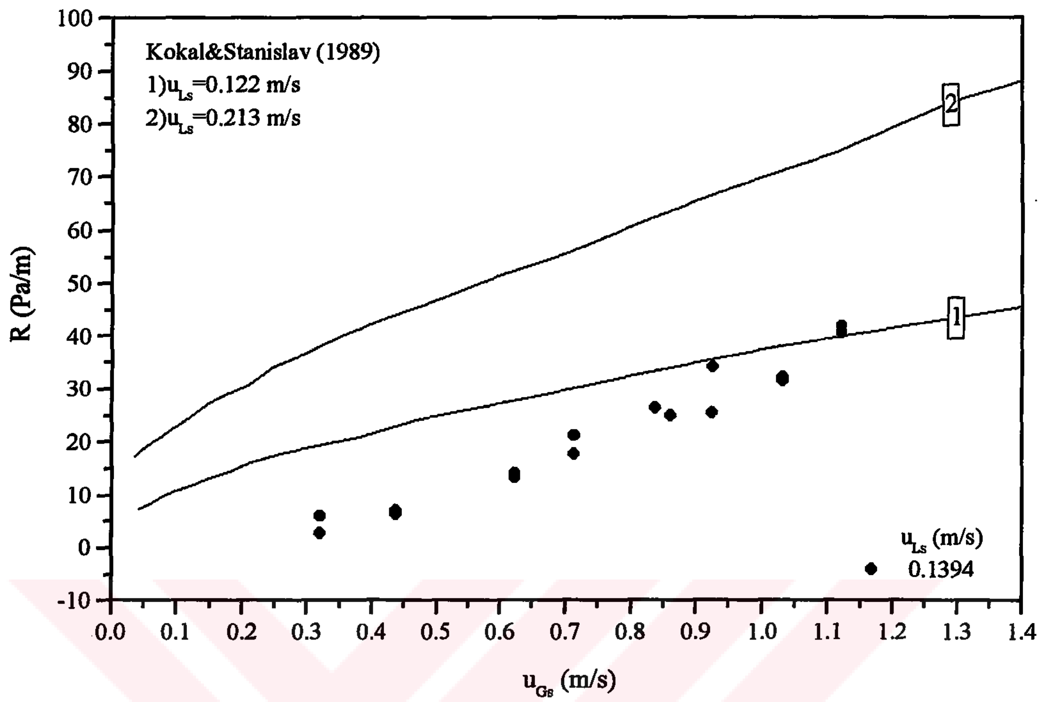

Figure 5.160. Comparison of the measured resistances of this investigation with the study of Kokal and Stanislav (1989).

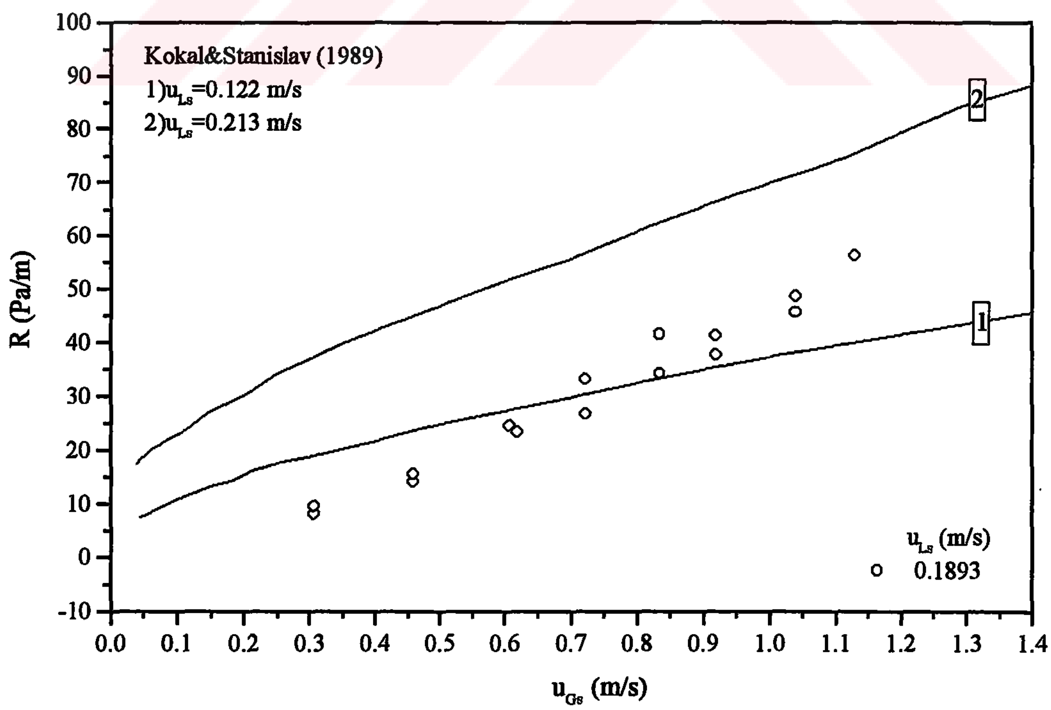

Figure 5.161. Comparison of the measured resistances of this investigation with the study of Kokal and Stanislav (1989).

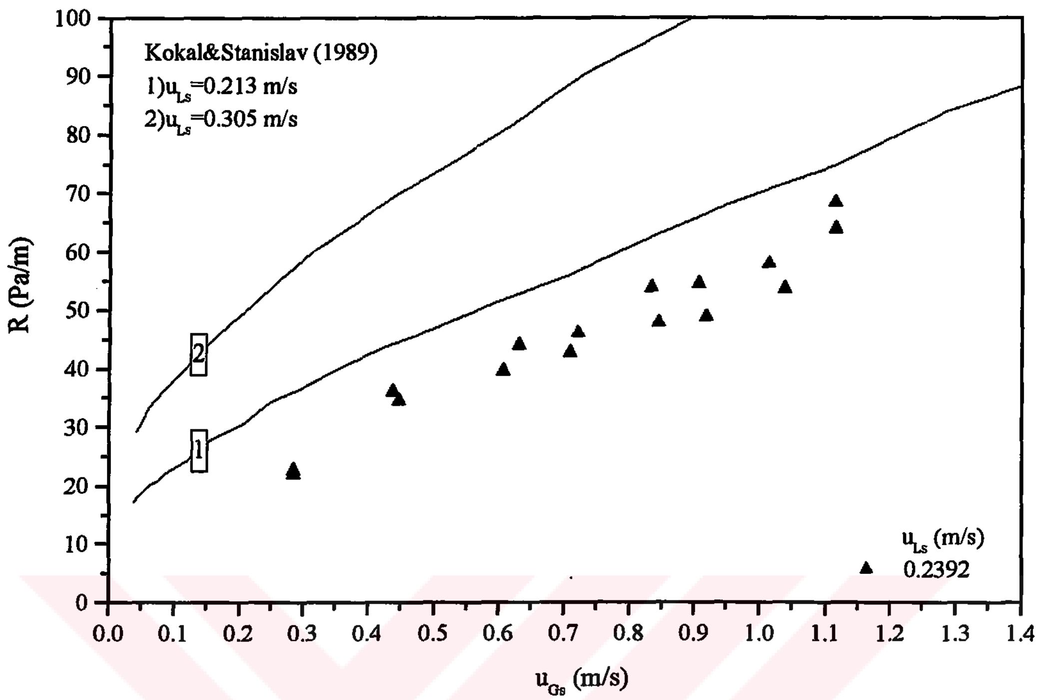

Figure 5.162. Comparison of the measured resistances of this investigation with the study of Kokal and Stanislav (1989).

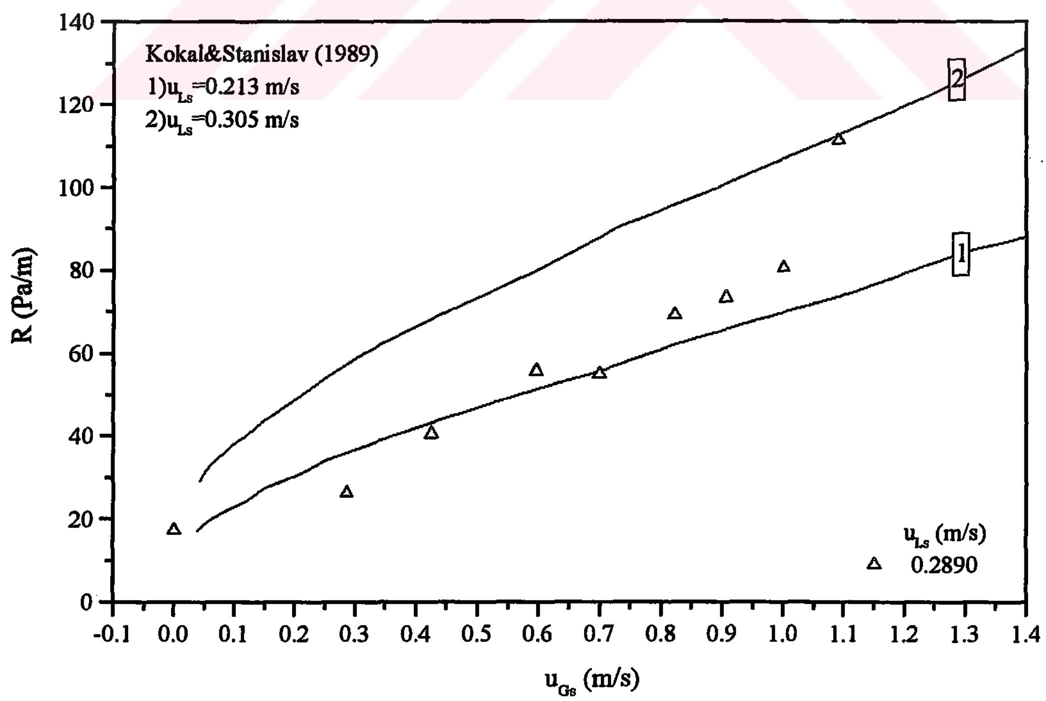

Figure 5.163. Comparison of the measured resistances of this investigation with the study of Kokal and Stanislav (1989).

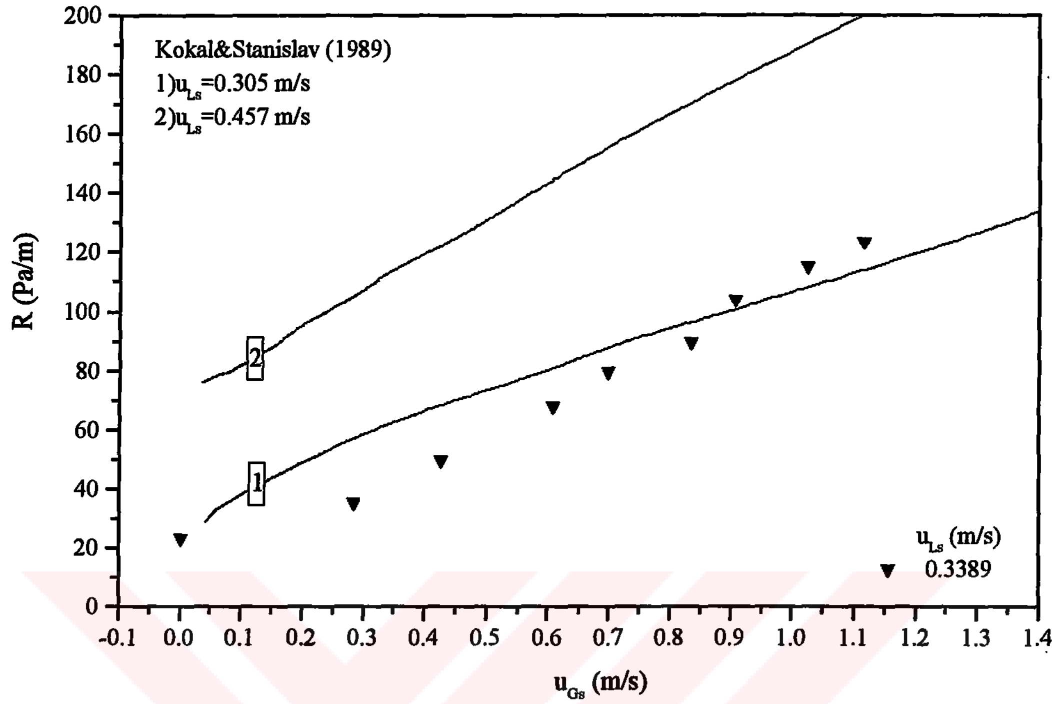

Figure 5.164. Comparison of the measured resistances of this investigation with the study of Kokal and Stanislav (1989).

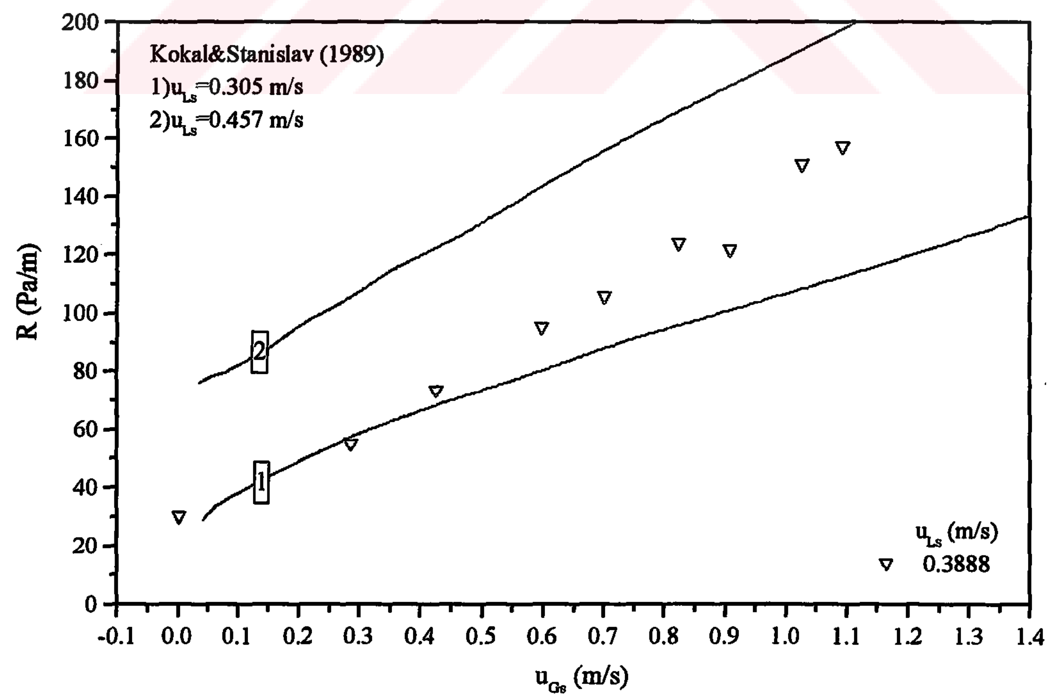

Figure 5.165. Comparison of the measured resistances of this investigation with the study of Kokal and Stanislav (1989).

5.2.3. Void Fractions of Circular Pipe Experiments

The void fractions measured in the horizontal circular pipe experiments are shown in figure 5.166. The measurement and calculation procedure of the void fractions measured in the horizontal-circular, concentric, and eccentric pipe experiments were previously explained in the section of "Void Fraction Calculation". The whole of measurements in the horizontal circular pipe experiments are shown in figure 5.166. to see how they change. However, this figure disables to analyse any one of the data separately.

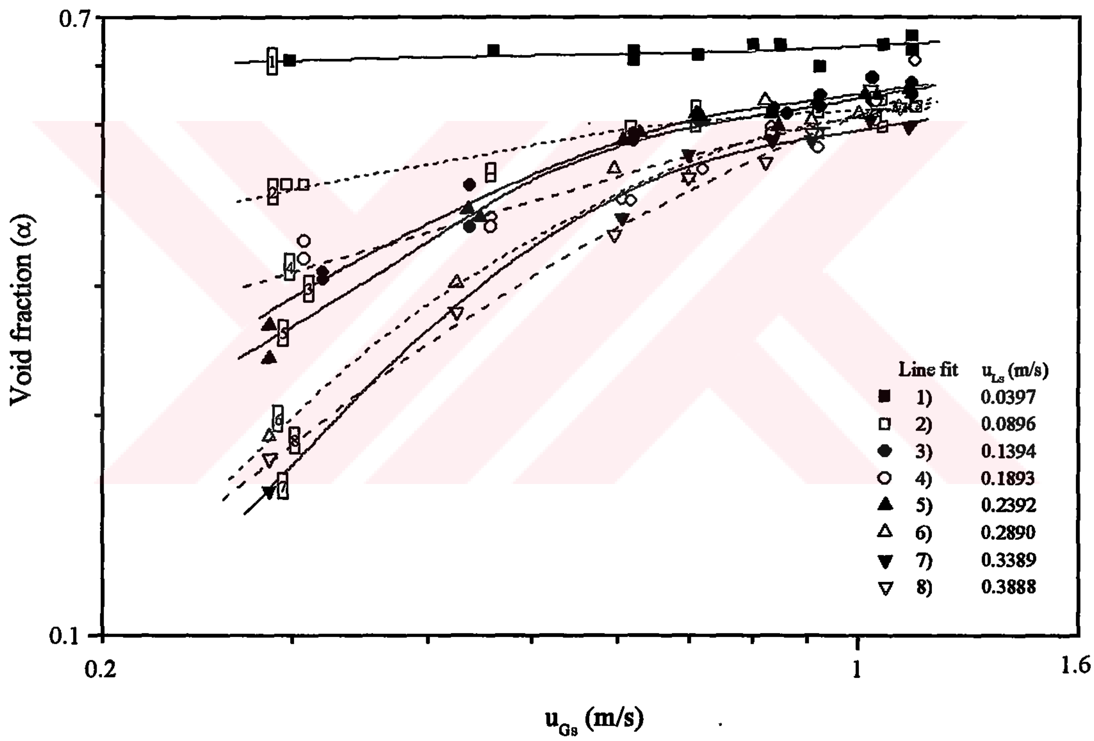

Figure 5.166. The measured void fractions in the horizontal circular pipe experiments.

Therefore, the data of measured void fractions are dealt with in two different groups. The first and second groups of the data have been shown in figures 5.167. and 5.168. It can be expressed from these figures that the measured void fractions increase with the increasing of the superficial gas velocity. However, they decrease as the constant superficial liquid velocity is increased.

Some of the experimental results of this investigation are compared with the results of Spedding et al.(1998). This comparison is shown in figure 5.169. Spedding et al.(1998) produced these results in a 50.8 mm inner diameter pipe. It is previously concluded with respect to the Kokal and Stanislav (1989) that, for a constant superficial liquid velocity, void fractions increase with the decreasing of pipe diameter (40 mm). Additionally, it was expressed in the beginning of this section that the void fractions also increase as the constant superficial liquid velocity is decreased. Thus, it was expected that our results would be greater than those of Spedding et al.(1998). Especially, when we regard the data of 0.0397 m/s of this investigation, these void fractions should be greater than those of line 5, because of small pipe diameter and superficial liquid velocity. It is impossible to give a reliable interpretation for the data of 0.0896 and 0.1394 m/s. They should be less than those of Spedding et al.(1998), because of the higher superficial liquid velocities. However, they should be close to those of Spedding et al.(1998), because of the smaller pipe diameter. In addition to this, it is better to analyse the trends of our experimental data using the fitted lines of 6, 7 and 8. There is a similarity between the trends of 5 and 6. However, the trends of 7 and 8 resemble to the curved regions of 4 and 5.

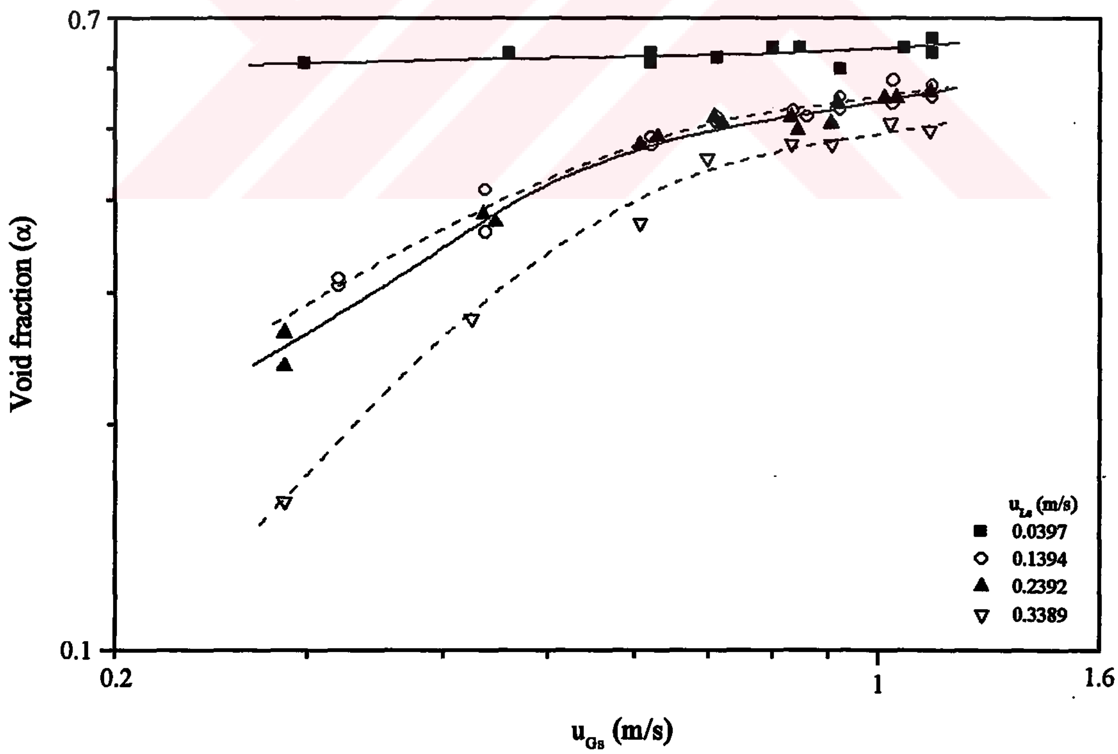

Figure 5.167. The measured void fractions in the horizontal circular pipe experiments.

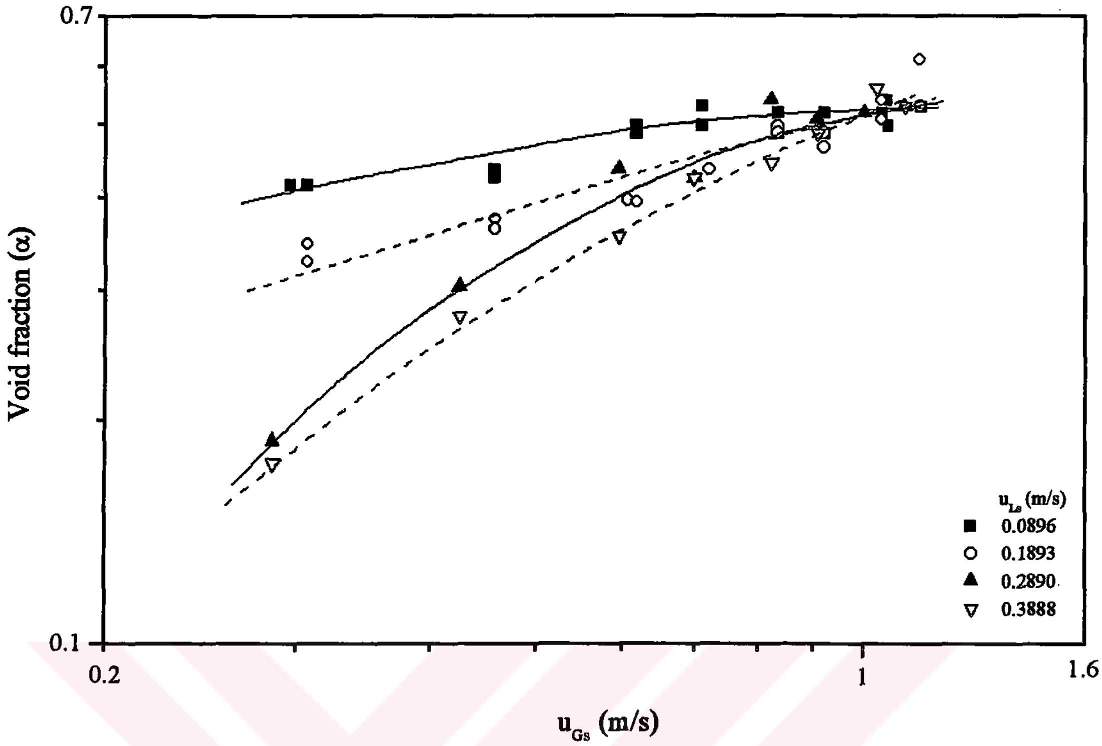

Figure 5.168. The measured void fractions in the horizontal circular pipe experiments.

Some of the experimental results of this investigation are compared with the results of Kokal and Stanislav (1989). This comparison is shown in figure 5.170. Kokal and Stanislav (1989) produced these results in a 25.8 mm inner diameter pipe. For a constant superficial liquid velocity, void fractions decrease with the increasing of pipe diameter (40 mm). Additionally, the void fractions also decrease as the constant superficial liquid velocity is increased. Therefore, as it is expected, all of the data except two of 0.0397 m/s are lower than those of Kokal and Stanislav (1989). For example, when we compare the lines 5 and 9, line 9 should be lower than line 5, because of the higher pipe diameter. However, line 9 should be higher than line 5, because of the lower superficial liquid velocity. It can be concluded that our results are in agreement with those of Kokal and Stanislav (1989).

The void fractions measured in the horizontal circular pipe experiments are compared with the results of two different empirical methods. These are Lockhart-Martinelli Method (LMM) and Rouhani Method (RM). The void fraction equation proposed by LMM is given in eq.(5.6) as follows.

$$\alpha = \frac{1}{\left(1 + X^{0.8}\right)^{0.378}} \tag{5.6}$$

where X is the Lochart-Martinelli parameter (Yılmaz, 2001).

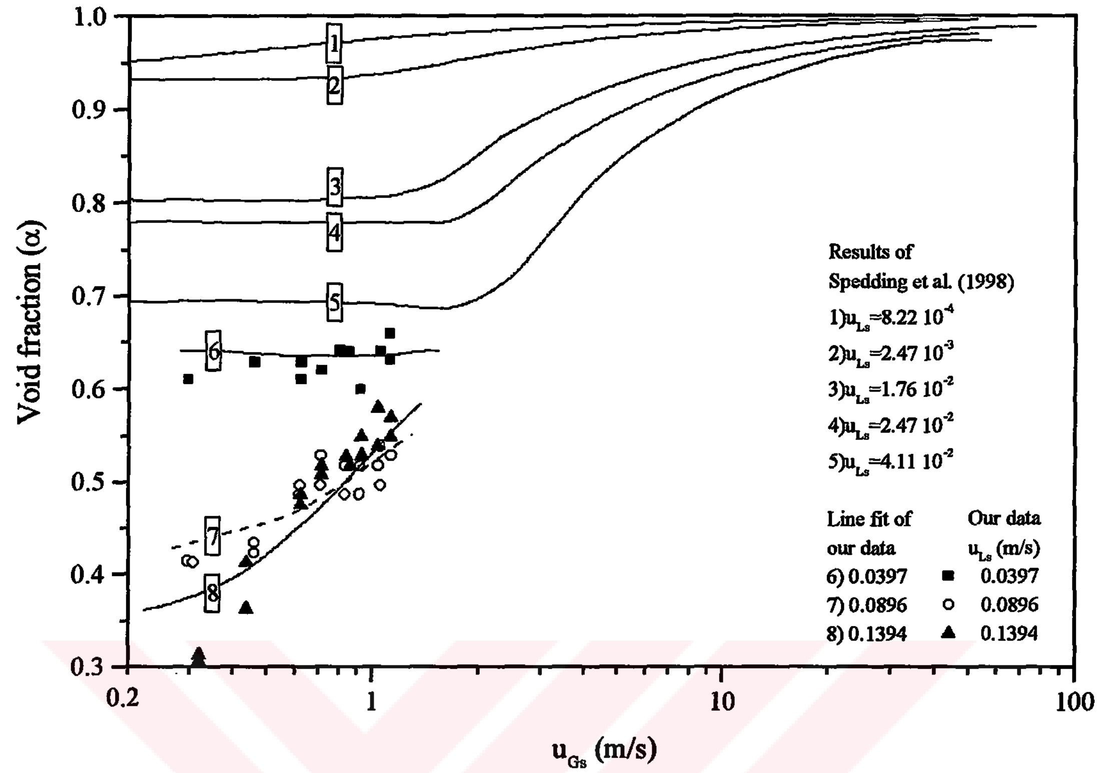

Figure 5.169. Comparison of some of the experimental results of this investigation with the results of Spedding et al.(1998).

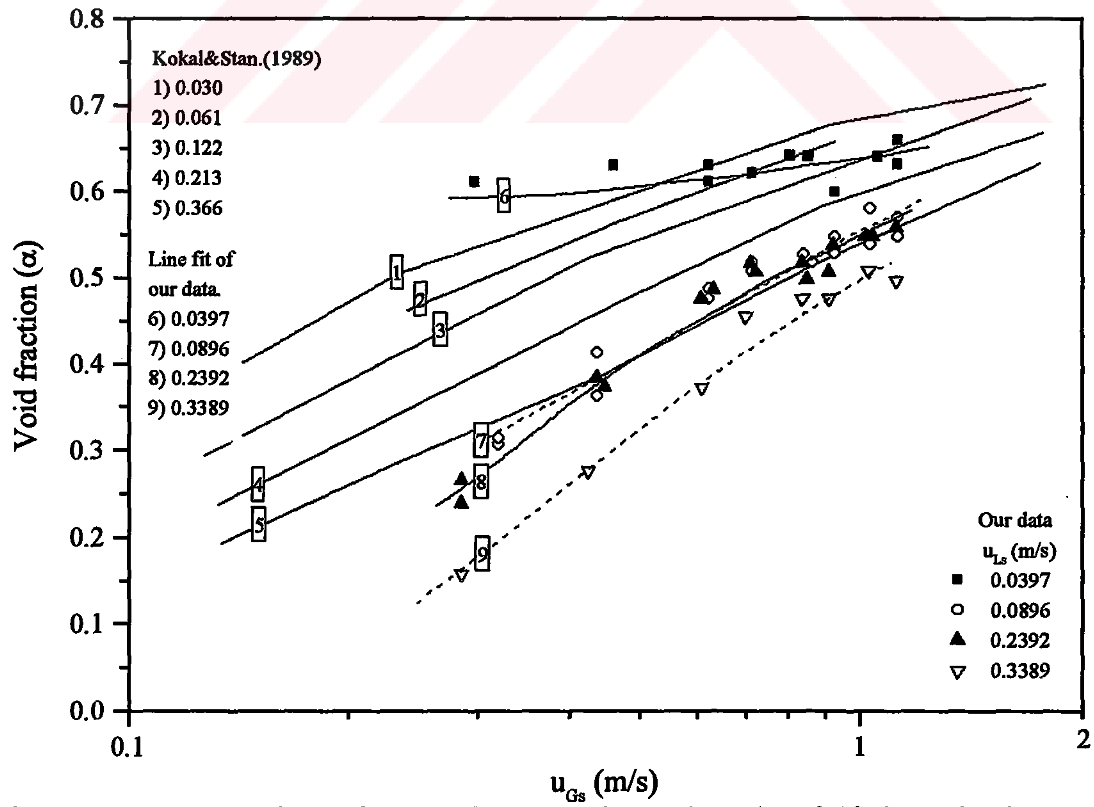

Figure 5.170. Comparison of some of the experimental results of this investigation with the results of Kokal and Stanislav (1989).

The method of Rouhani for void fraction calculation is explained from eqs.(5.7) to (5.9) as below,

$$\alpha = \frac{1}{C\left[1 + \rho_g^*(\frac{1}{\dot{x}} - 1) + \frac{u_{rel}\rho_g}{\dot{m}_g}\right]} \quad (5.7)$$

In this equation, the constant **C** and relative velocity, u_{rel}, are determined as follows,

$$u_{rel} = 1.18\left[\frac{g\,\sigma}{\rho_l}(1 - \frac{\rho_g}{\rho_l})\right]^{1/4} \quad (5.8)$$

$$C = 1 + 0.12\,(1 - \dot{x}) \quad (5.9)$$

Figures from 5.171. to 5.178. show the comparisons of experimental results of this investigation with the void fractions proposed by LMM and RM. The results of LMM and RM are getting closer to those of this study, as the superficial liquid velocity is increased. However, the void fractions proposed by LMM are more harmonious than those of RM with the experimental results. The trend of the results of RM is getting approximately similar to that of our data as the constant superficial liquid velocity is increased.

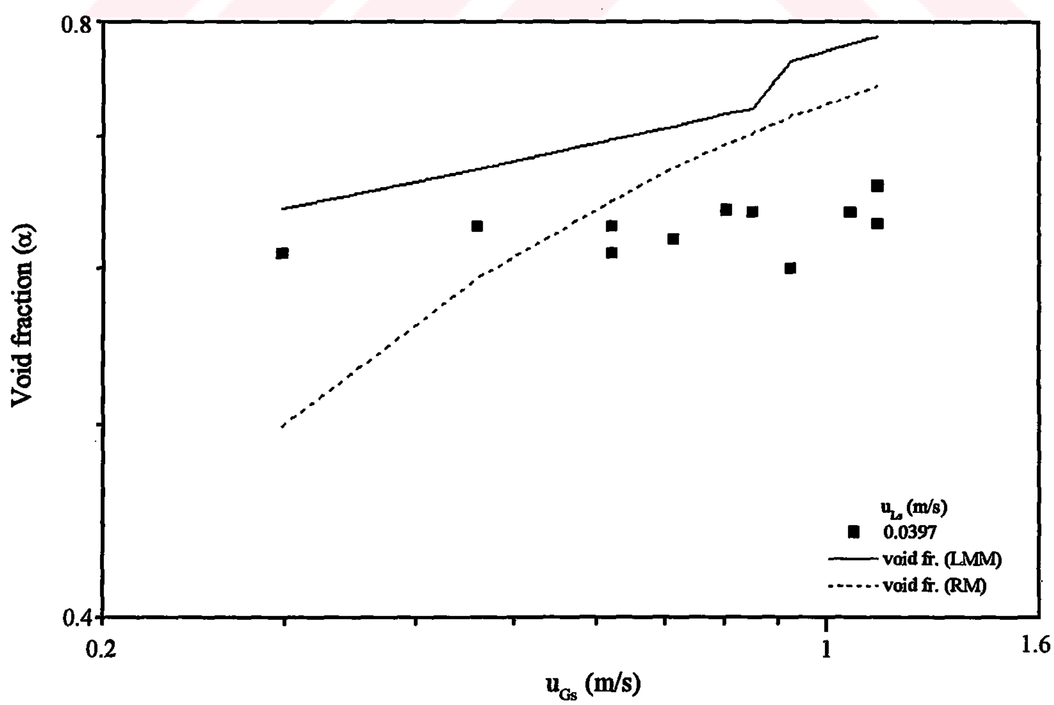

Figure 5.171. Comparisons of experimental results of this investigation with the void fractions proposed by LMM and RM for $u_{Ls} = 0.0397$ m/s.

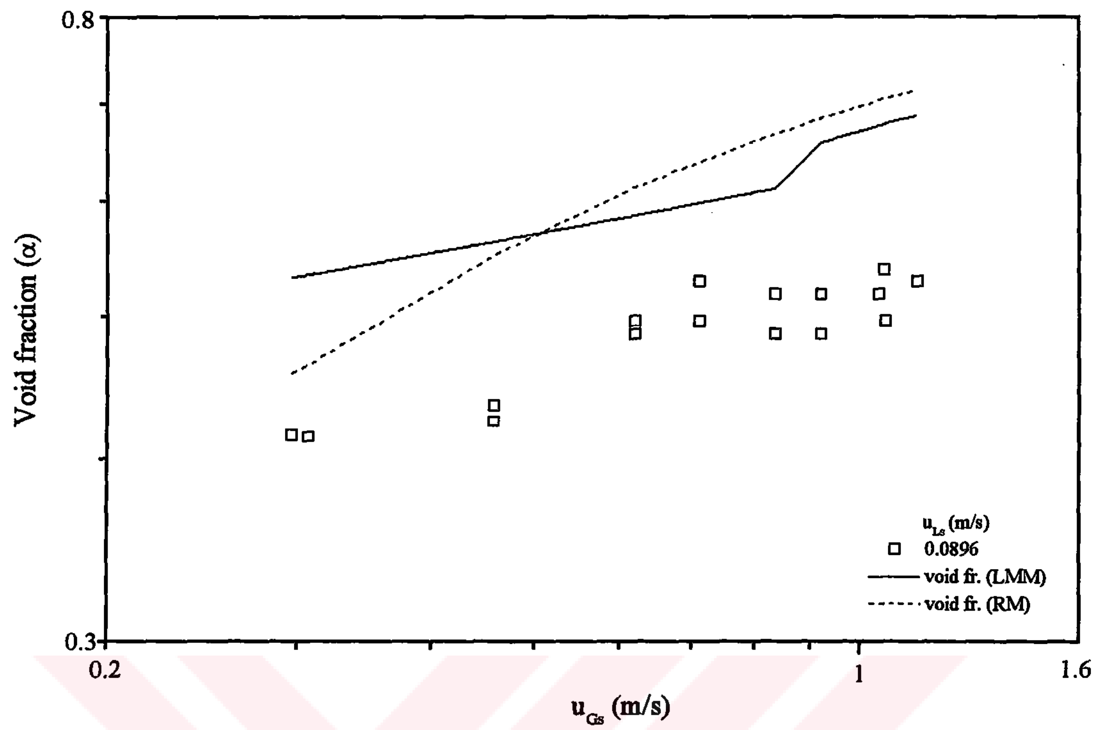

Figure 5.172. Comparisons of experimental results of this investigation with the void fractions proposed by LMM and RM for u_{Ls} =0.0896 m/s.

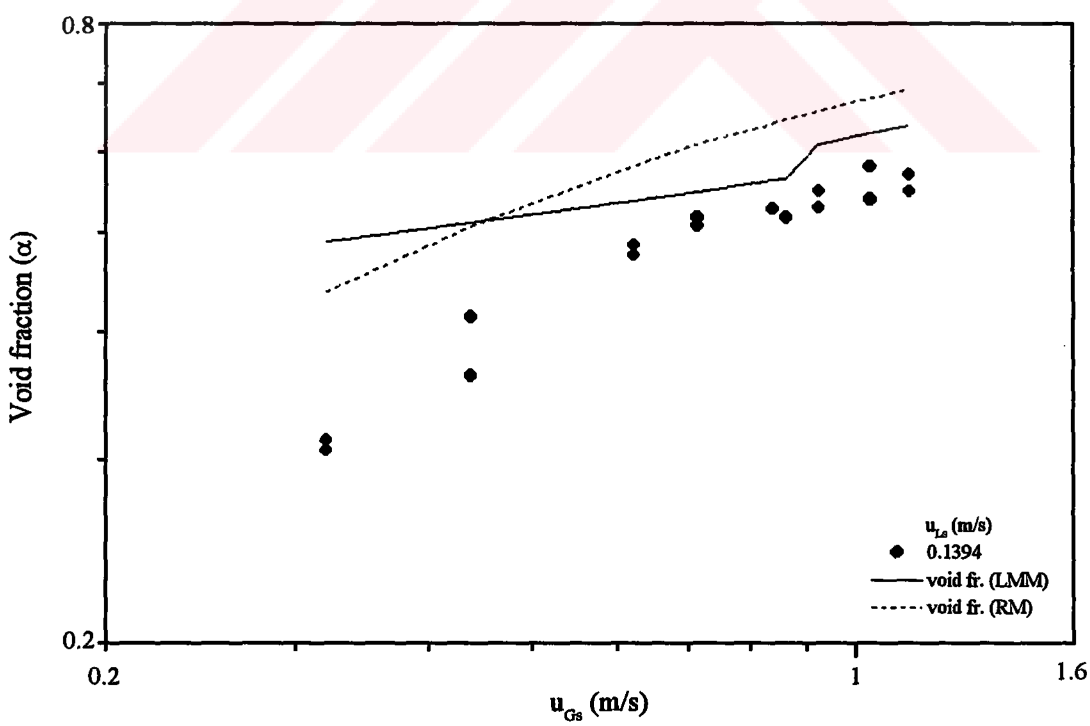

Figure 5.173. Comparisons of experimental results of this investigation with the void fractions proposed by LMM and RM for u_{Ls} =0.1394 m/s.

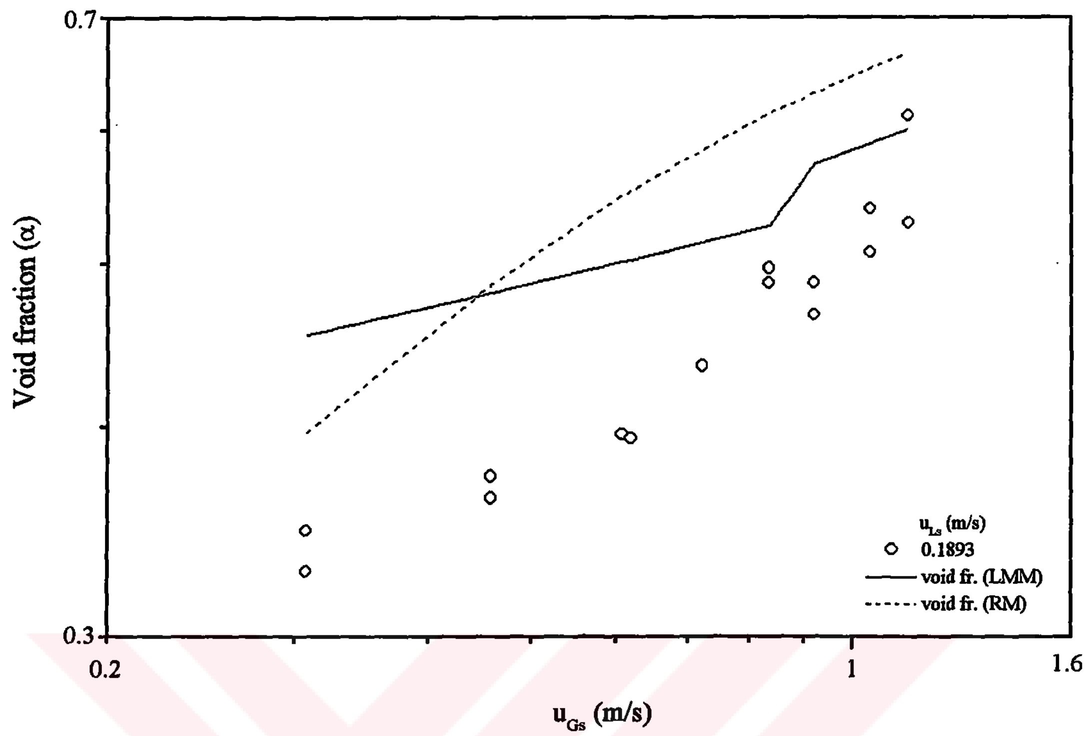

Figure 5.174. Comparisons of experimental results of this investigation with the void fractions proposed by LMM and RM for $u_{Ls} = 0.1893$ m/s.

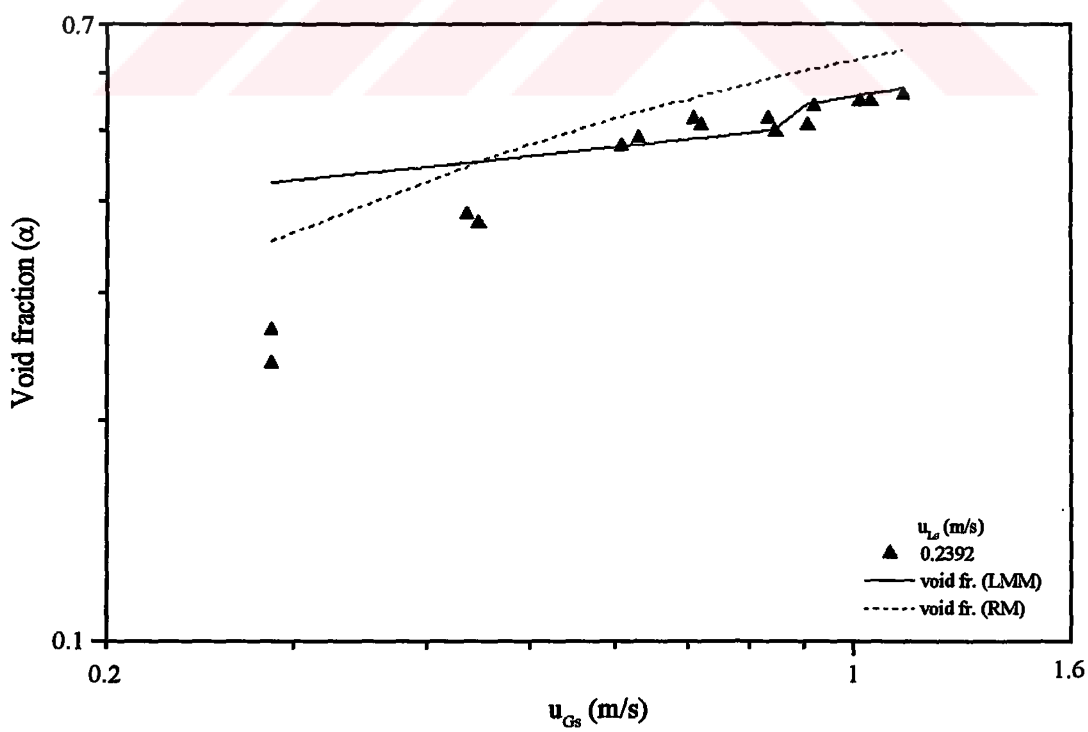

Figure 5.175. Comparisons of experimental results of this investigation with the void fractions proposed by LMM and RM for $u_{Ls} = 0.2392$ m/s.

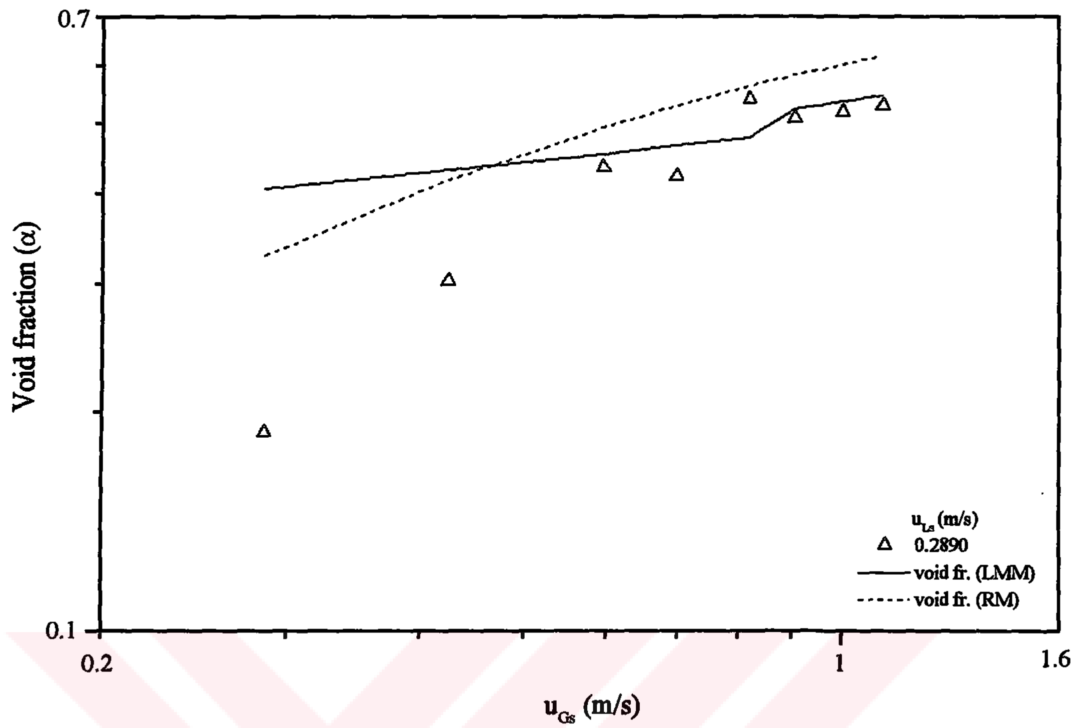

Figure 5.176. Comparisons of experimental results of this investigation with the void fractions proposed by LMM and RM for u_{Ls} =0.2890 m/s.

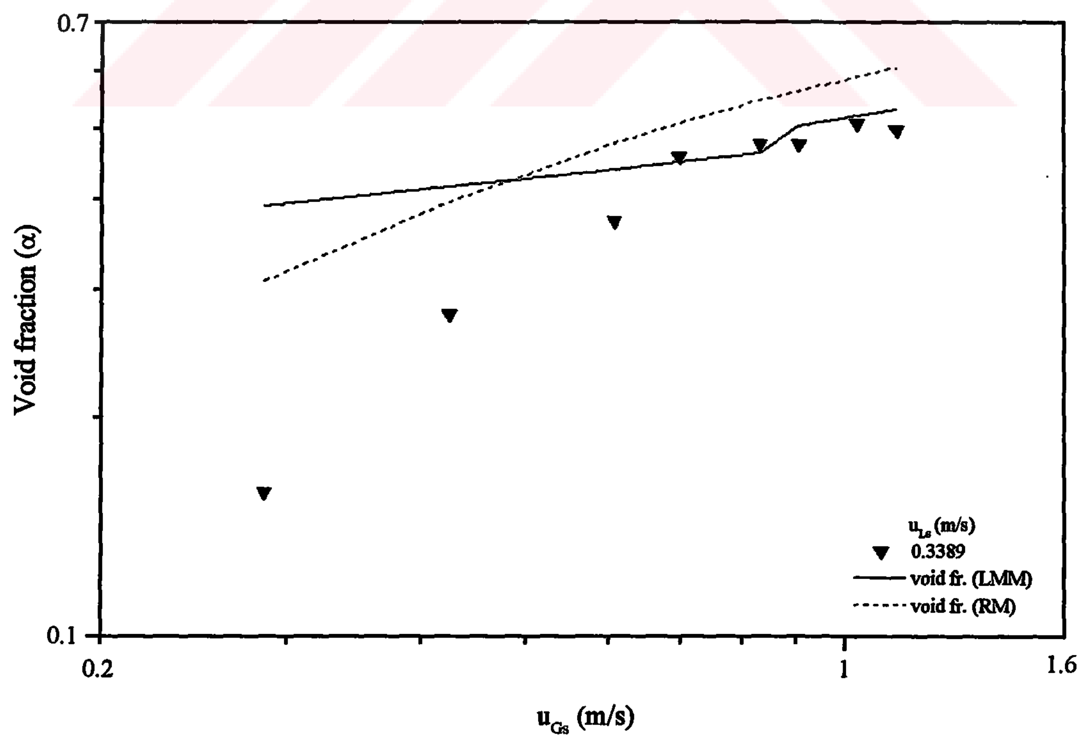

Figure 5.177. Comparisons of experimental results of this investigation with the void fractions proposed by LMM and RM for u_{Ls} =0.3389 m/s.

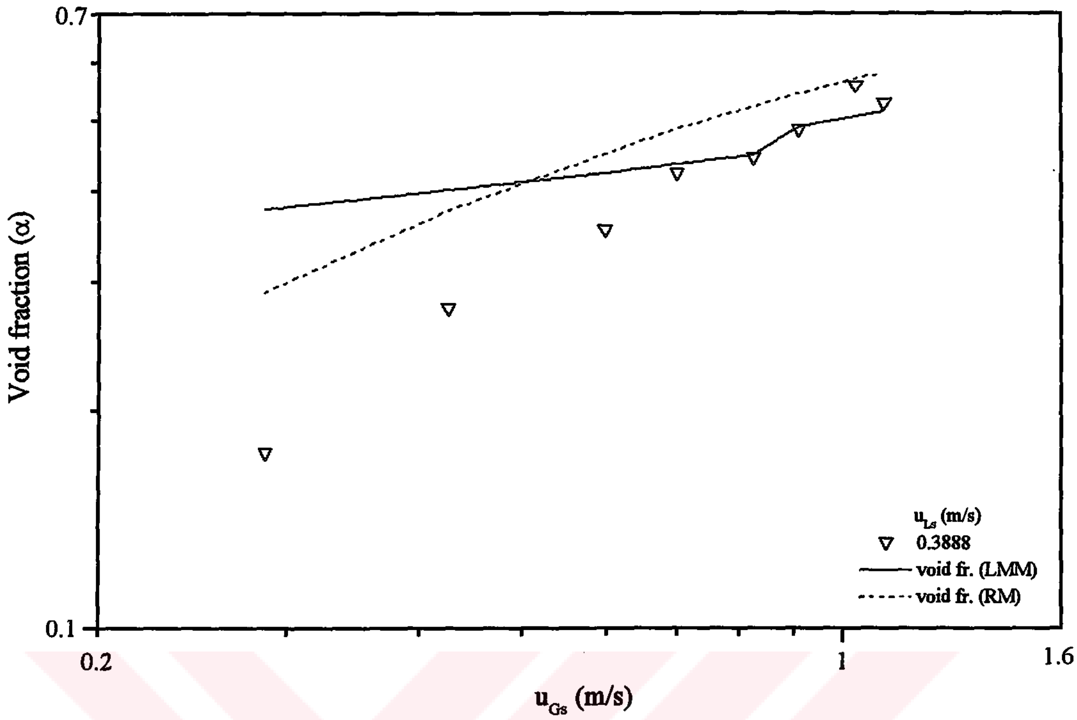

Figure 5.178. Comparisons of experimental results of this investigation with the void fractions proposed by LMM and RM for $u_{Ls} = 0.3888$ m/s.

For the void fractions of circular pipe experiments, the following conclusions can be made: The measured void fractions increase with the increasing of the superficial gas velocity. However, they decrease as the constant superficial liquid velocity is increased.

-The measured void fractions in horizontal circular pipe experiments are relatively in agreement with the results of Spedding et al. (1998).

-However, they agree better with the results of Kokal and Stanislav (1989) than those of Spedding et al. (1998).

-The measured void fractions in horizontal circular pipe experiments are in good agreement with the results of LMM and RM. They are compatible and getting closer to those of this study, as the superficial liquid velocity is increased. However, the void fractions proposed by LMM are more harmonious than those of RM with the experimental results. The trend of the results of RM is getting approximately similar to that of our data as the constant superficial liquid velocity is increased.

-According to the statements above, the measurement and calculation of the mean void fractions are reliable to compare the further results of concentric and eccentric pipe experiments.

5.2.4. Comparisons of Circular Pipe Experiments with Concentrically (CONC) and Eccentrically (ECC) Inserted Rod

The final experiments were carried out in annular and crescent-shaped horizontal gaps. These geometries were obtained with the help of the transparent plexiglas pipe of 40 mm inner diameter and a circular rod of 25 mm outer diameter. Initially, the circular rod of 25 mm outer diameter and 6 m length was concentrically inserted into the plexiglas pipe of 40 mm inner diameter. Thus, an annular gap was obtained in the test pipe. After carrying out of all gas-liquid two phase flow experiments, the same inserted rod was eccentrically located at the bottom in the test pipe. The further information about this geometry are given in the section of "Void Fraction Calculation". The eccentricity between the test pipe and inserted rod was equal to 1. Henceforth, the abbreviations of "CONC" and "ECC" are used to call the test geometries of annular and crescent-shaped horizontal gaps, respectively. The flow patterns, pressure losses, void fractions, and slug velocities-lengths-frequencies are compared to clarify the differences between the CONC and ECC experiments.

5.2.4.1. Flow Patterns

The flow patterns observed in the CONC and ECC experiments were different than those of the circular pipe experiments, especially for slug and plug flow. The liquid slugs mostly consisted of dispersed small bubbles in its body. The flowing of slugs were very interesting that small liquid bulks in front of the liquid slugs rushed helically forward on the surface of the inserted rod. The definitions of the flow patterns observed in the CONC and ECC experiments are given as follows,

slug: liquid slugs without bubbles and have approximately the same lengths throughout the test section.

bubbly slug: liquid slugs with less or many bubbles and have approximately the same lengths throughout the test section.

undeveloped bubbly slug: liquid slugs with less or many bubbles and have the increasing or decreasing lengths throughout the test section.

BTS+slug: Blow through slugs in front of liquid slugs which are

	without bubbles and have approximately the same lengths throughout the test section.
BTS+ bubbly slug:	Blow through slugs in front of liquid slugs which have less or many bubbles and have approximately the same lengths throughout the test section.
plug:	plug flow without bubbles and have approximately the same lengths throughout the test section.
slug+plug:	slug and plug flow
bubbly slug+plug:	bubbly slug and plug flow
BTS+slug+plug:	BTS+slug and plug flow
BTS+ bubbly slug+plug:	BTS+ bubbly slug and plug flow
undeveloped bubbly slug+plug:	undeveloped bubbly slug and plug flow

The flow patterns observed in the CONC and ECC experiments are explained in the flow pattern map of Weisman (1979). Even if this map is proposed for a circular test pipe, it is thought that this map would give an opinion about the observed flow patterns.

Figure 5.179. shows the observed flow patterns of the CONC experiments in the Weisman (1979)'s map. All observations are located in the regions of wavy, stratified, and slug+plug flow. However, most of the observed flow patterns consist of small dispersed bubbles. Figure 5.180. closely shows the same flow pattern map and observations. According to the observations, the transition lines of slug+plug flow and bubbly flow move to the left as indicated by dashed lines. This means that the transition to the slug+plug flow and bubbly flow start in the lower superficial liquid velocities than those of circular pipes.

Figure 5.181. shows the observed flow patterns of the ECC experiments in the Weisman (1979)'s map. All observations are sit in the regions of wavy, stratified, and slug+plug flow. However, most of the observed flow patterns consist of blow through slugs (BTS) and small dispersed bubbles.

Figure 5.182. closely shows the same flow pattern map and observations. According to the observations, the transition lines of slug+plug flow and bubbly flow move to the left as indicated by dashed lines. Additionally, the blow thorough slugs start in the upper region of observed data. The observed flow patterns of the ECC experiments show that the transition to the slug+plug flow and bubbly flow start in the lower superficial liquid velocities than those of circular pipes. In addition to this, one can

express that there is a tendency to the annular flow in the lower superficial gas velocities. The observation of BTS confirms this opinion.

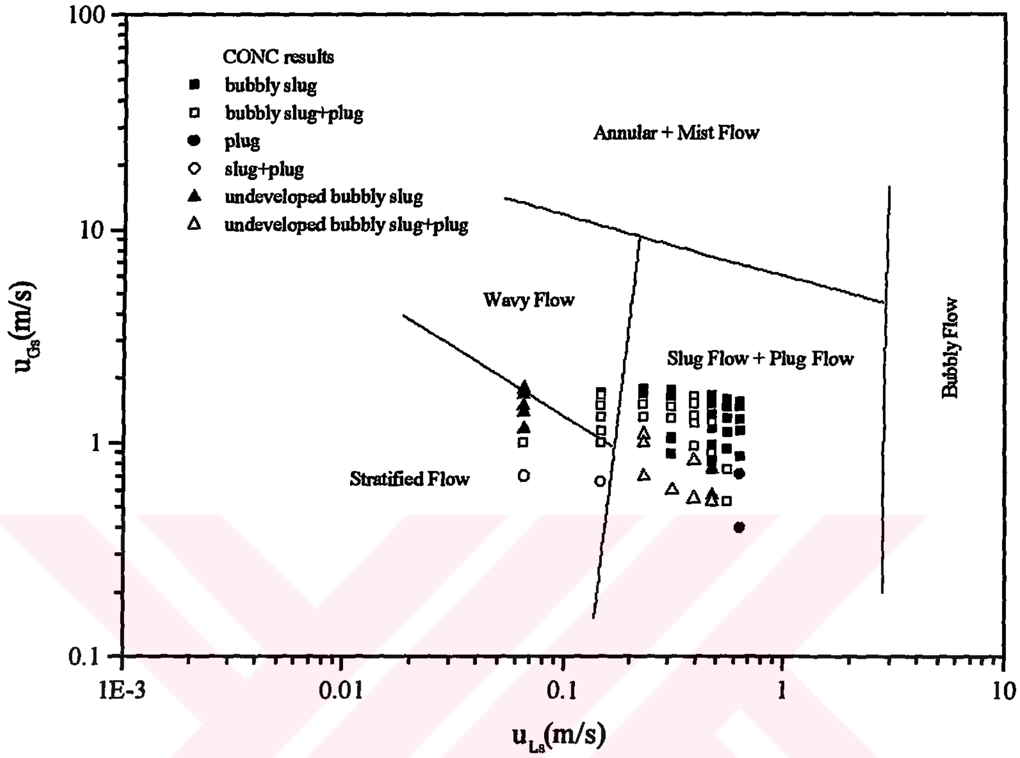

Figure 5.179. The observed flow patterns of the CONC experiments in the Weisman's map.

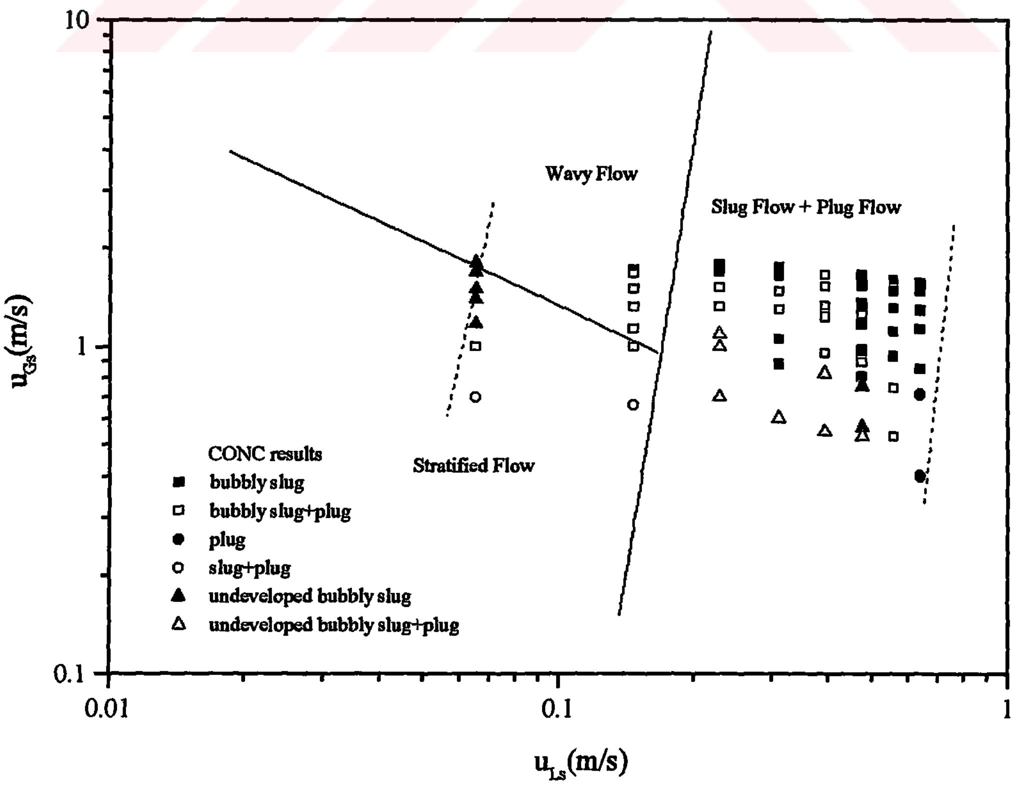

Figure 5.180. The observed flow patterns of the CONC experiments in the Weisman's map.

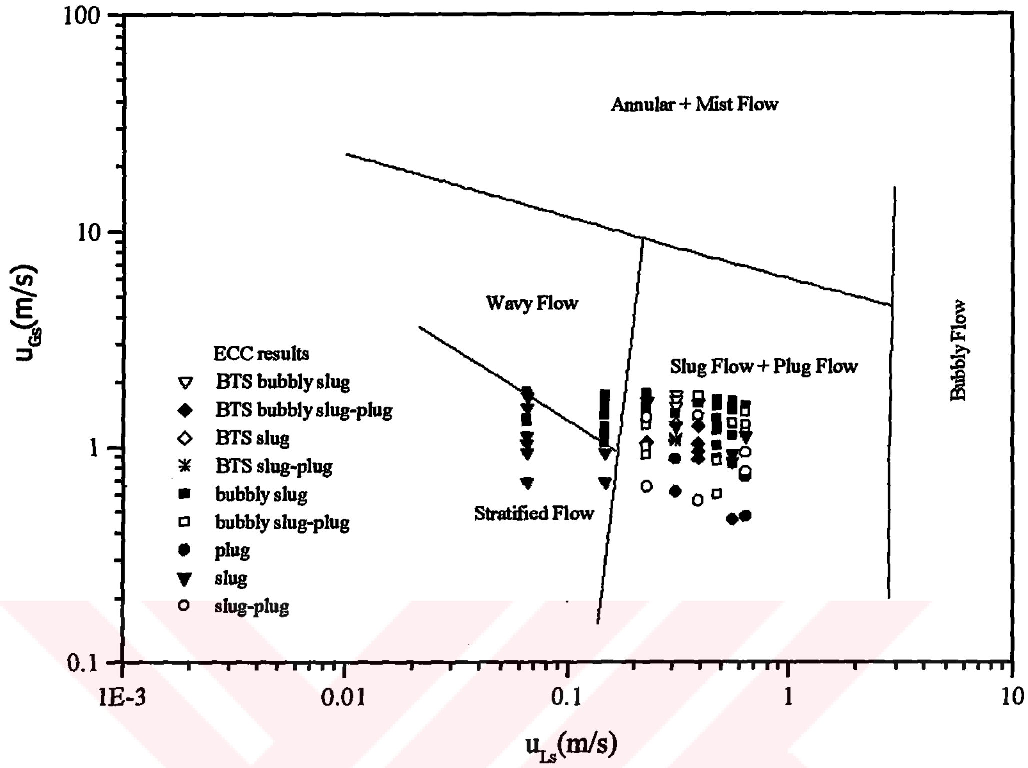

Figure 5.181. The observed flow patterns of the ECC experiments in the Weisman's map.

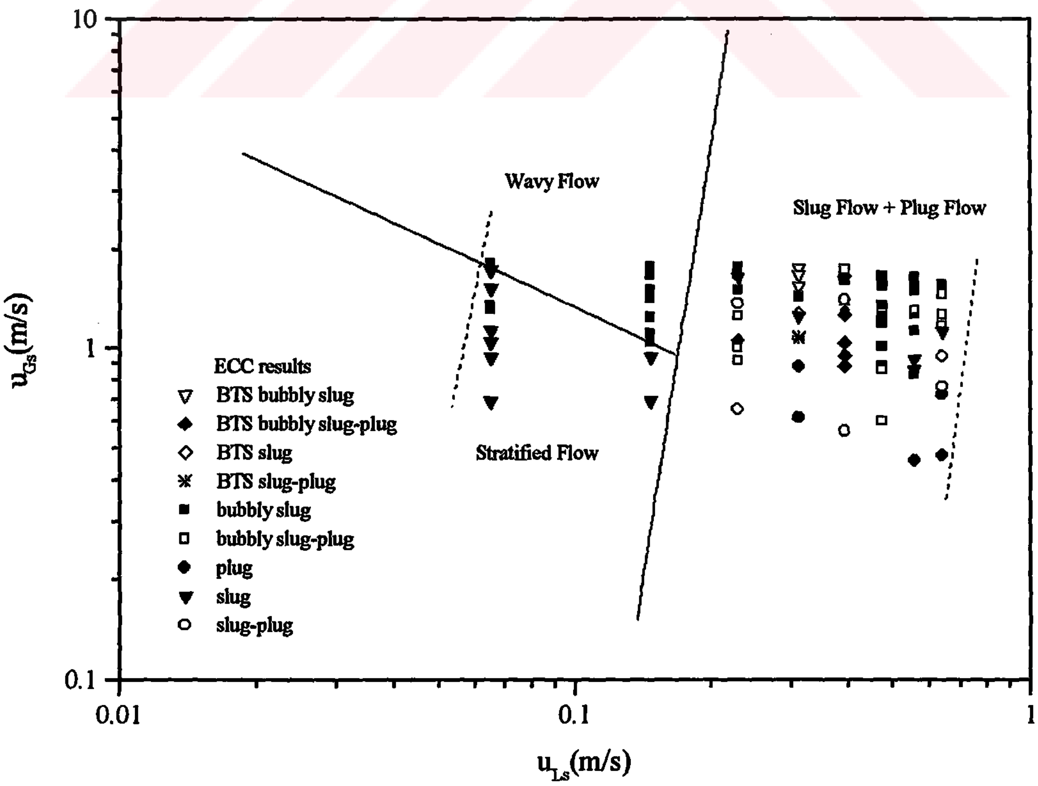

Figure 5.182. The observed flow patterns of the ECC experiments in the Weisman's map.

There are four different flow patterns which have the same definition in the CONC and ECC experiments. These are bubbly slug, bubbly slug+plug, plug, and slug+plug. These same observations of the CONC and ECC experiments are compared to reveal the differences between these geometries. Figure 5.183. shows the comparisons of bubbly slug flow observed in the CONC and ECC experiments. In spite of both of geometries are tested in the same measurement area, bubbly slug flow observed in ECC experiments start in the lower superficial liquid velocities than those of observed in CONC experiments.

Figure 5.184. shows the comparisons of bubbly slug+plug flow observed in the CONC and ECC experiments. In spite of both of geometries are tested in the same measurement area, bubbly slug+plug flow observed in CONC experiments start in the lower superficial liquid velocities than those of observed in ECC experiments.

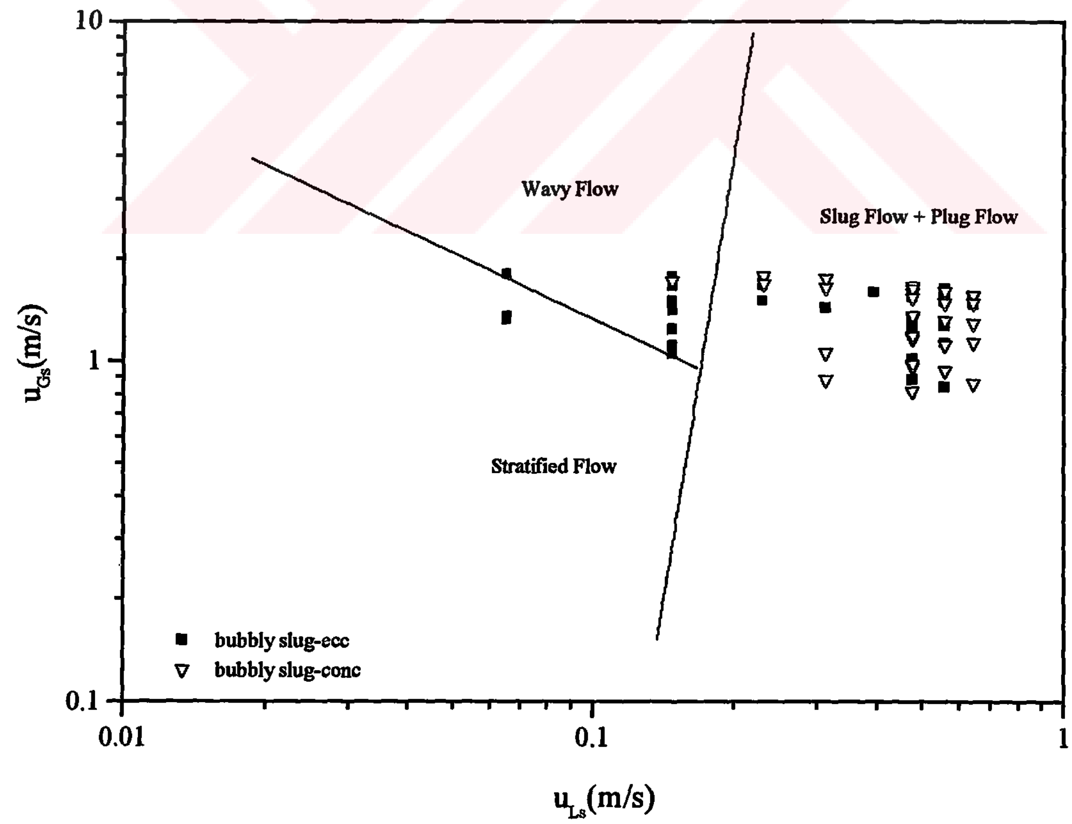

Figure 5.183. Comparison of bubbly slug flow observed in the CONC and ECC experiments.

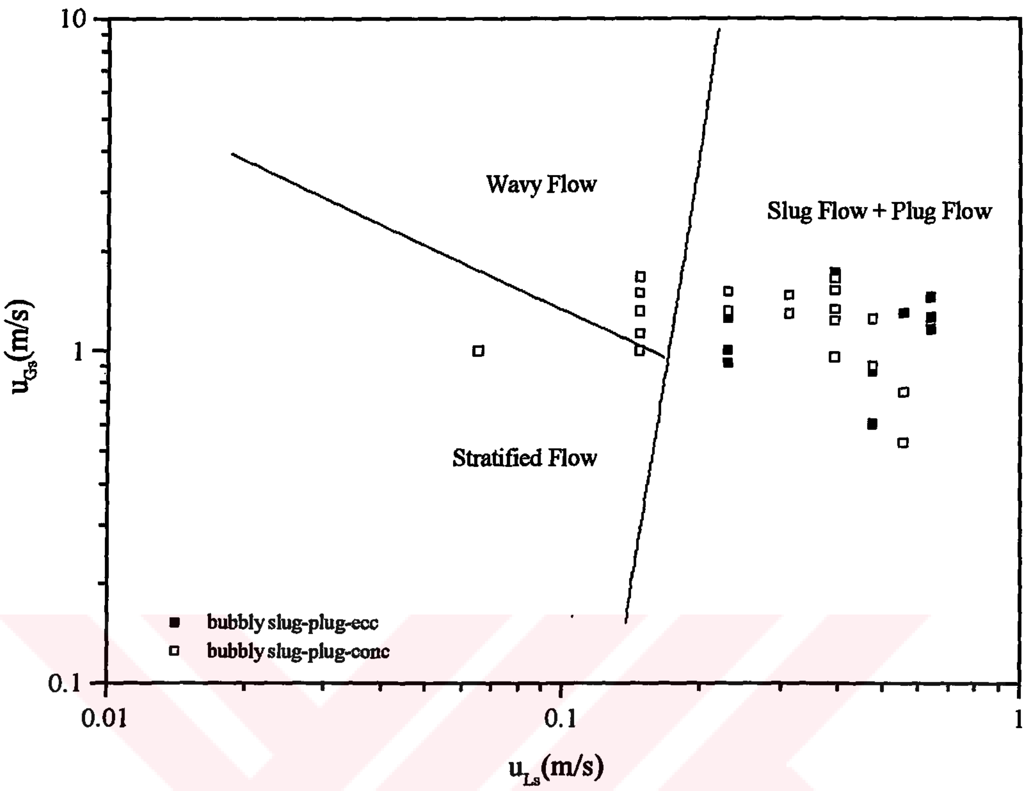

Figure 5.184. Comparison of bubbly slug+plug flow observed in the CONC and ECC experiments.

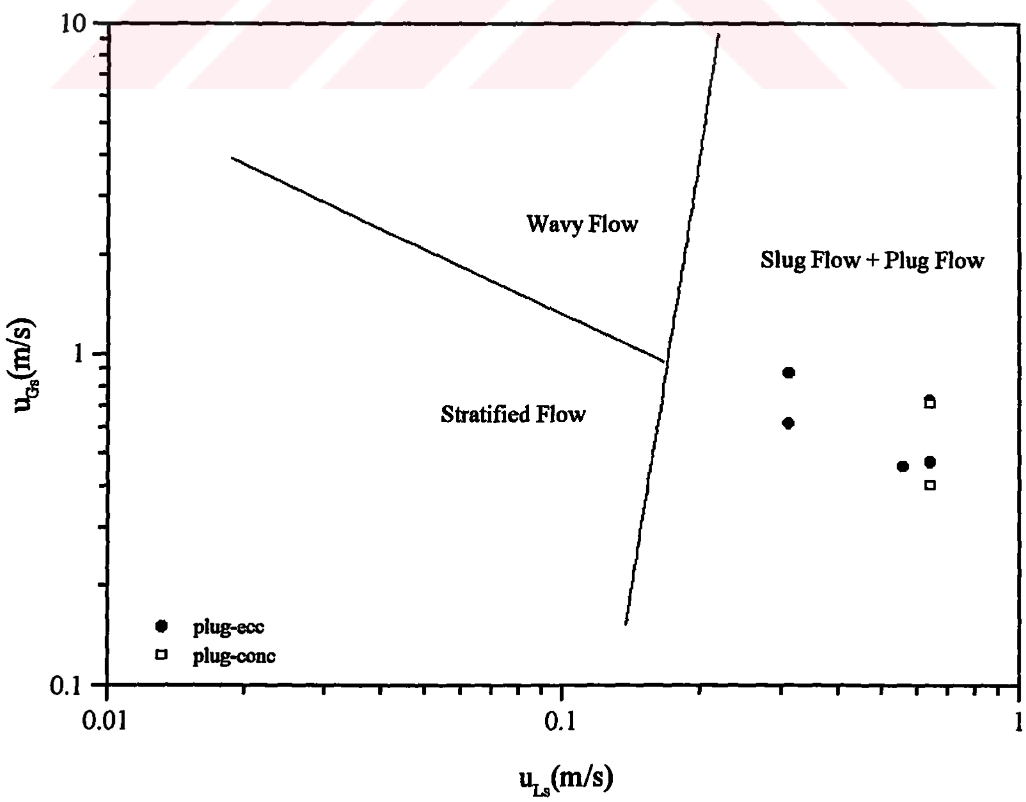

Figure 5.185. Comparison of plug flow observed in the CONC and ECC experiments.

Figure 5.185. shows the comparisons of plug flow observed in the CONC and ECC experiments. In spite of both of geometries are tested in the same measurement area, plug flow observed in ECC experiments start in the lower superficial liquid velocities than those of observed in CONC experiments.

Figure 5.186. shows the comparisons of slug+plug flow observed in the CONC and ECC experiments. In spite of both of geometries are tested in the same measurement area, slug+plug flow observed in CONC experiments start in the lower superficial liquid velocities than those of observed in ECC experiments. Additionally, the slug+plug flow observed in the ECC experiments coincide with the predictions of Weisman (1979).

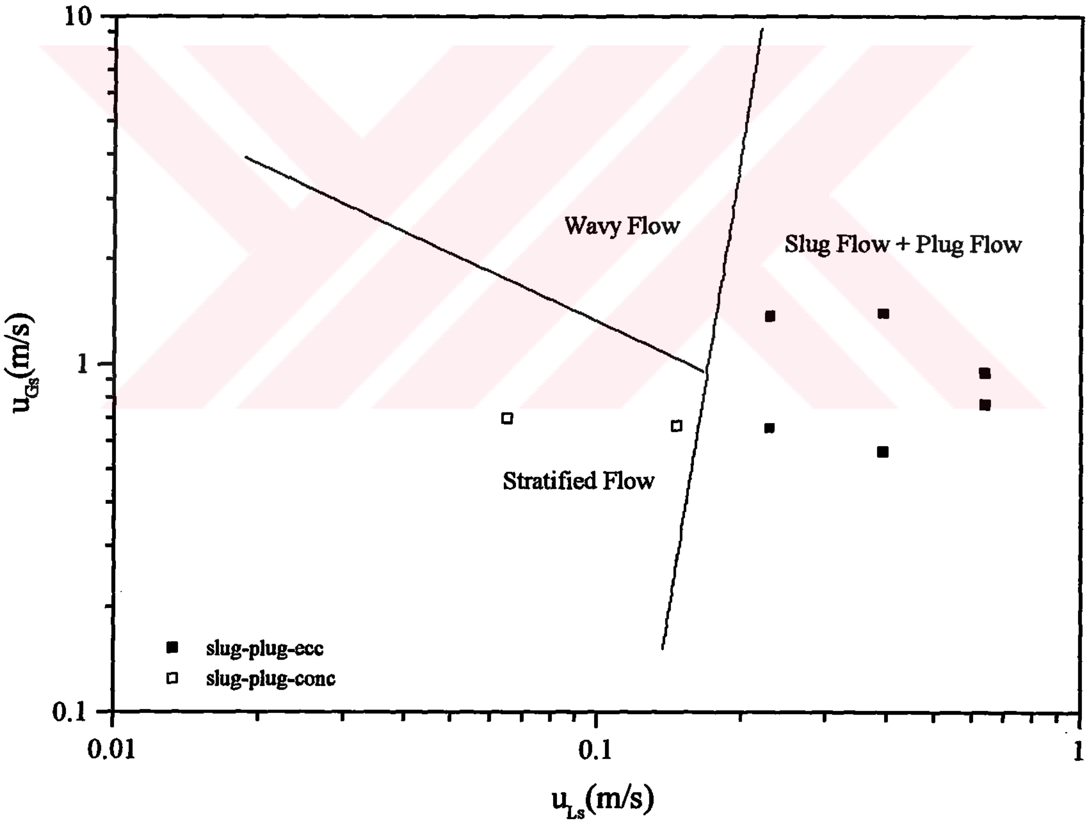

Figure 5.186. Comparison of slug+plug flow observed in the CONC and ECC experiments.

These effectively comparisons of flow patterns observed in the CONC and ECC experiments show that the flow patterns are affected from the eccentricity of the inserted rod. BTS flow is special to the ECC experiments, because there was no any BTS observation in the CONC experiments.

5.2.4.2. Pressure Losses

The pressure losses measured in the CONC and ECC experiments are compared with the results of empirical methods and each others. Figure 5.187. shows the measured pressure losses in the CONC experiments. Lines (linear fitting) are fitted to the data of each constant superficial liquid velocity to see the trend of the data easily. These experiments are approximately repeatable. It is proofed with the experiments at a constant superficial liquid velocity of 0.474 m/s. These two experiments were carried out in different days. The pressure losses measured in both experiments are very close to each other.

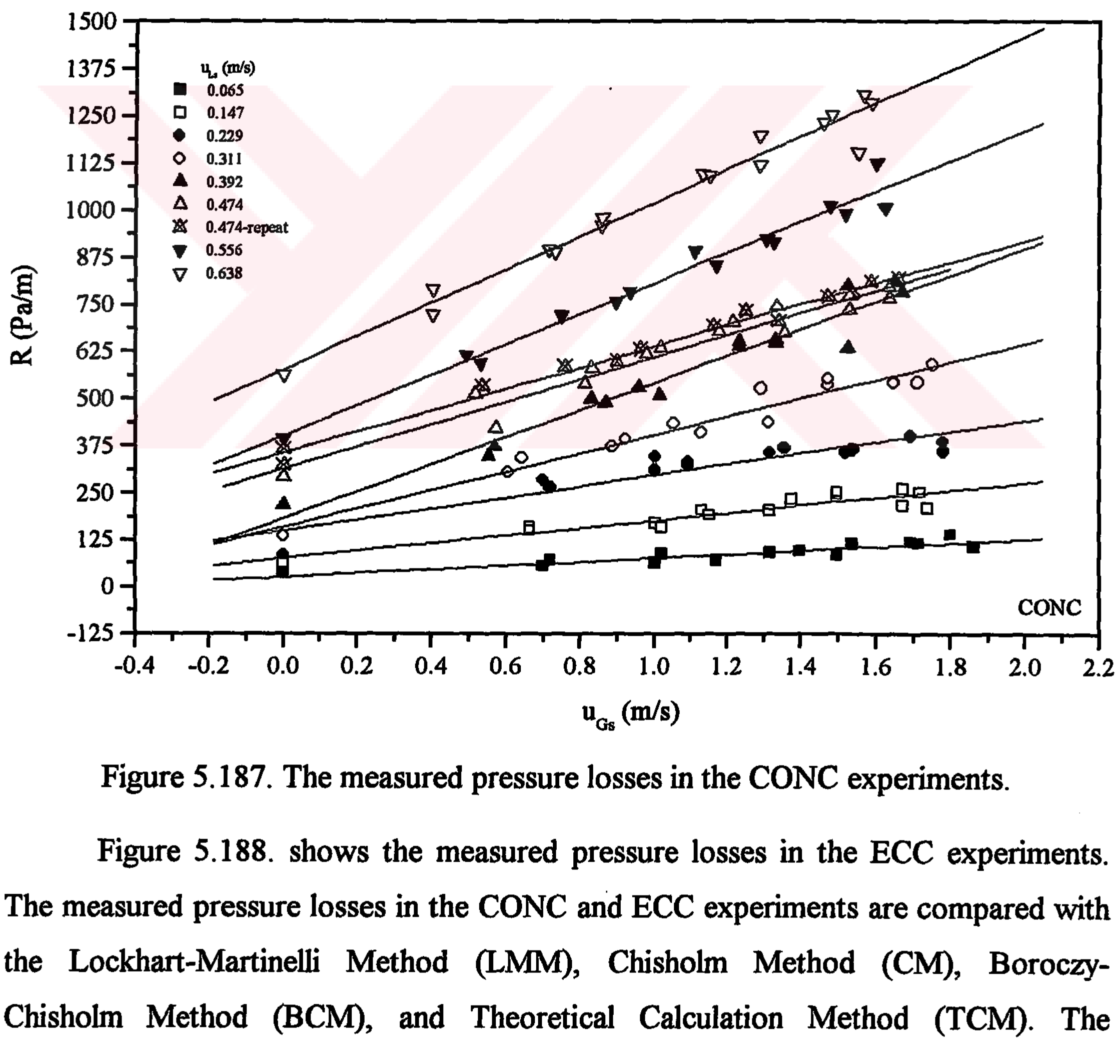

Figure 5.187. The measured pressure losses in the CONC experiments.

Figure 5.188. shows the measured pressure losses in the ECC experiments. The measured pressure losses in the CONC and ECC experiments are compared with the Lockhart-Martinelli Method (LMM), Chisholm Method (CM), Boroczy-Chisholm Method (BCM), and Theoretical Calculation Method (TCM). The comparisons are shown for three different constant superficial liquid velocities which are 0.065, 0.392, and 0.638 m/s.

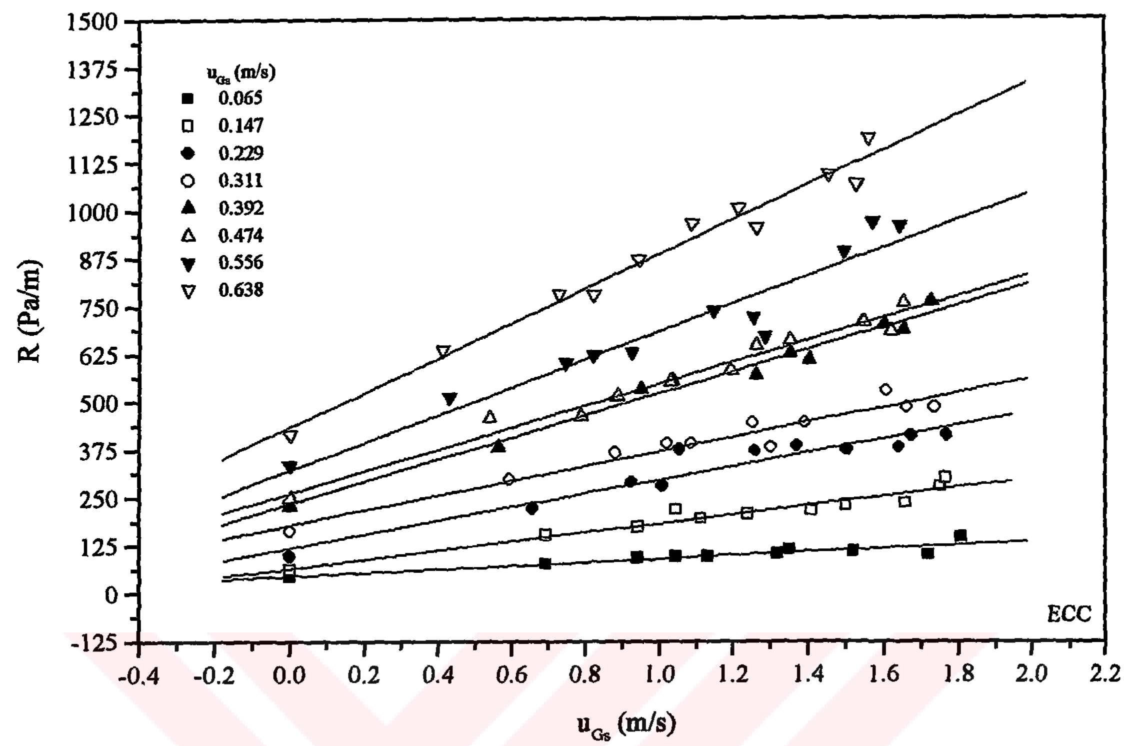

Figure 5.188. The measured pressure losses in the ECC experiments.

Figures 5.189. and 5.190. show the comparisons of the pressure losses measured in the CONC and ECC experiments with the empirical methods for 0.065 m/s. The experimental data are located between the results of LMM and CM. However, LMM predicts the experimental data better than CM.

Figures 5.191. and 5.192. show the comparisons of the pressure losses measured in the CONC and ECC experiments with the empirical methods for 0.392 m/s. The experimental data are sit between the results of LMM and BCM. However, LMM predicts the ECC results better than BCM.

Figures 5.193. and 5.194. show the comparisons of the pressure losses measured in the CONC and ECC experiments with the empirical methods for 0.638 m/s. The experimental data are located between the results of LMM and BCM. However, BCM predicts the CONC results better than LMM.

It is shown that the pressure losses measured in both experiments are approximately predicted by empirical methods. Additionally, the approximately prediction of the pressure losses by the empirical methods increase the reliability of the measurement system and calculation procedures. Henceforth, the pressure losses of CONC and ECC experiments are compared with each other for constant superficial liquid velocities.

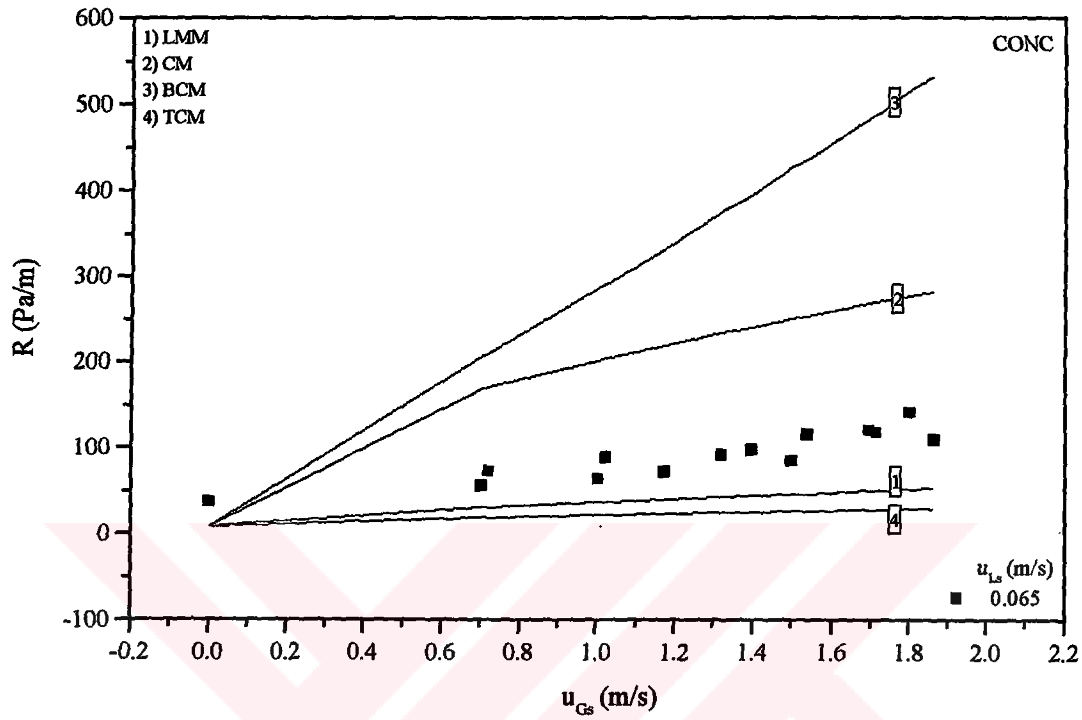

Figure 5.189. Comparison of the pressure losses measured in the CONC with the empirical methods for u_{Ls} =0.065 m/s.

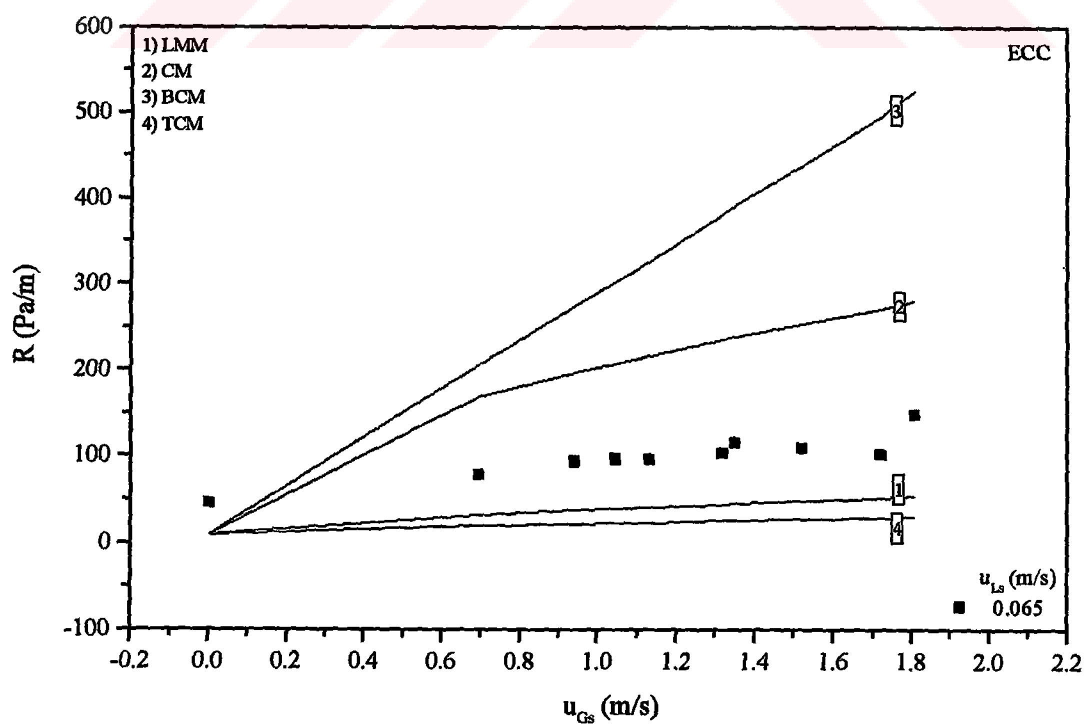

Figure 5.190. Comparison of the pressure losses measured in the ECC with the empirical methods for u_{Ls} =0.065 m/s.

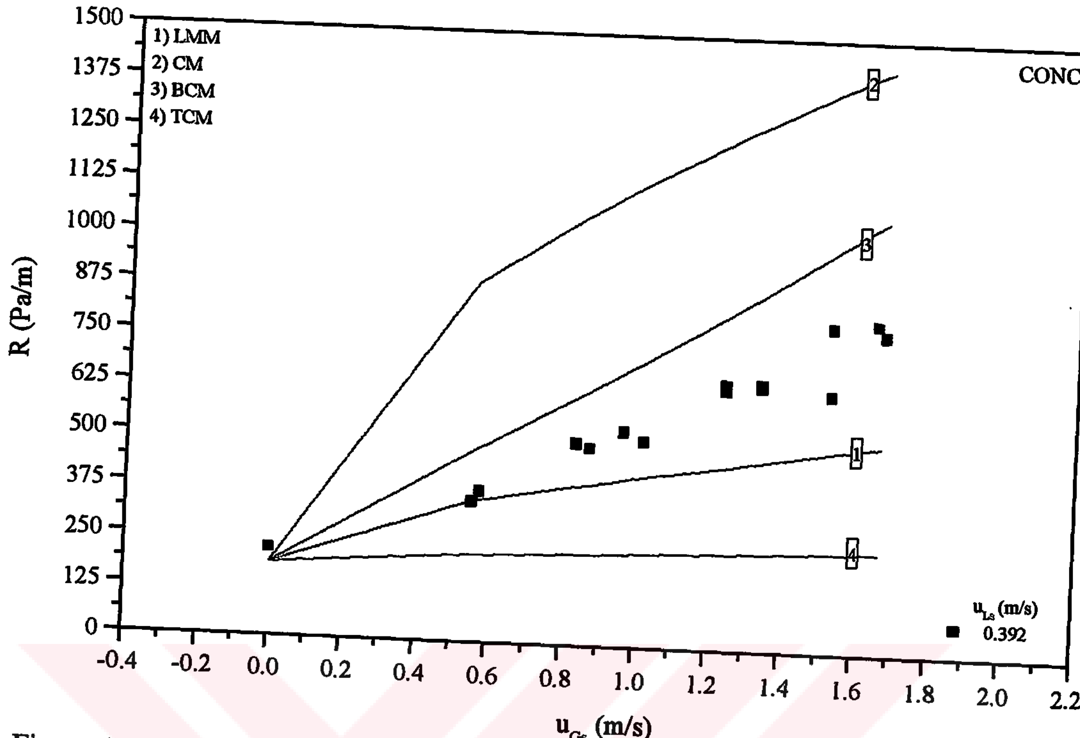

Figure 5.191. Comparison of the pressure losses measured in the CONC with the empirical methods for $u_{Ls} = 0.392$ m/s.

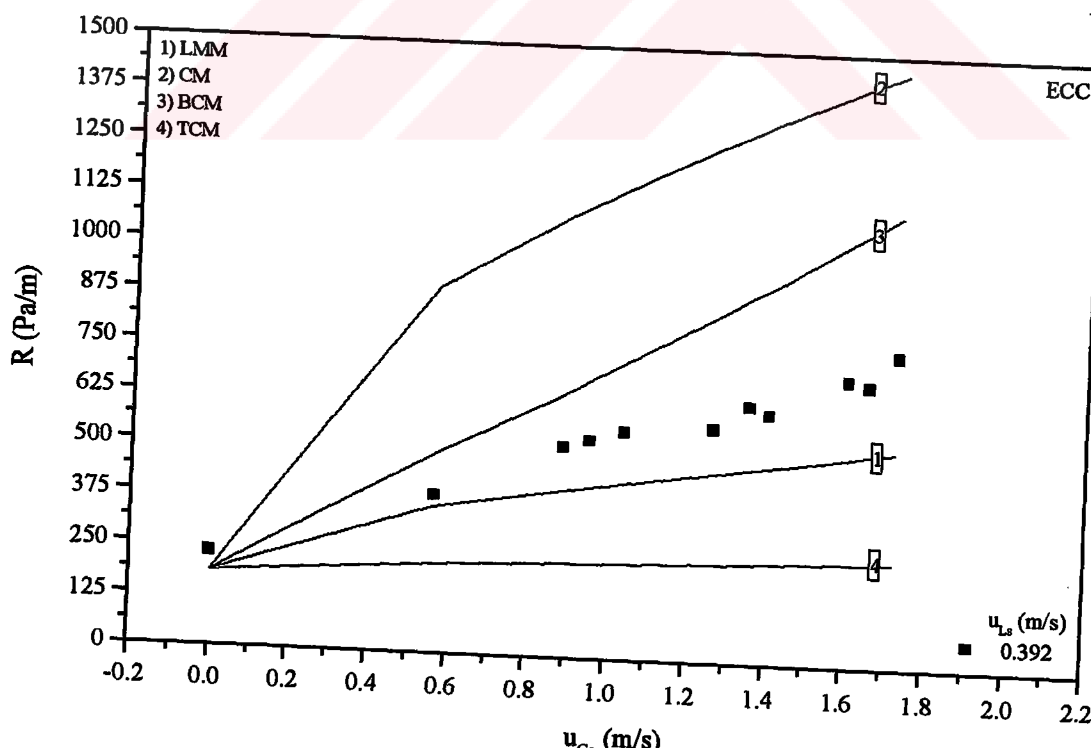

Figure 5.192. Comparison of the pressure losses measured in the ECC with the empirical methods for $u_{Ls} = 0.392$ m/s.

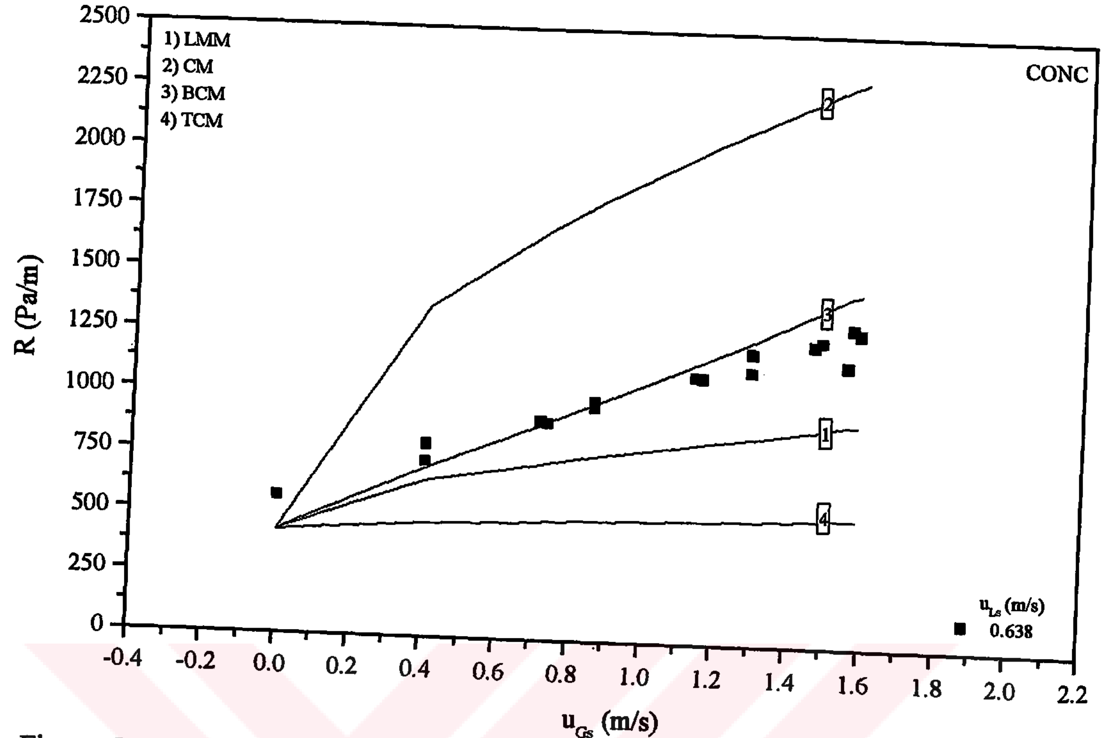

Figure 5.193. Comparison of the pressure losses measured in the CONC with the empirical methods for u_{Ls} =0.638 m/s.

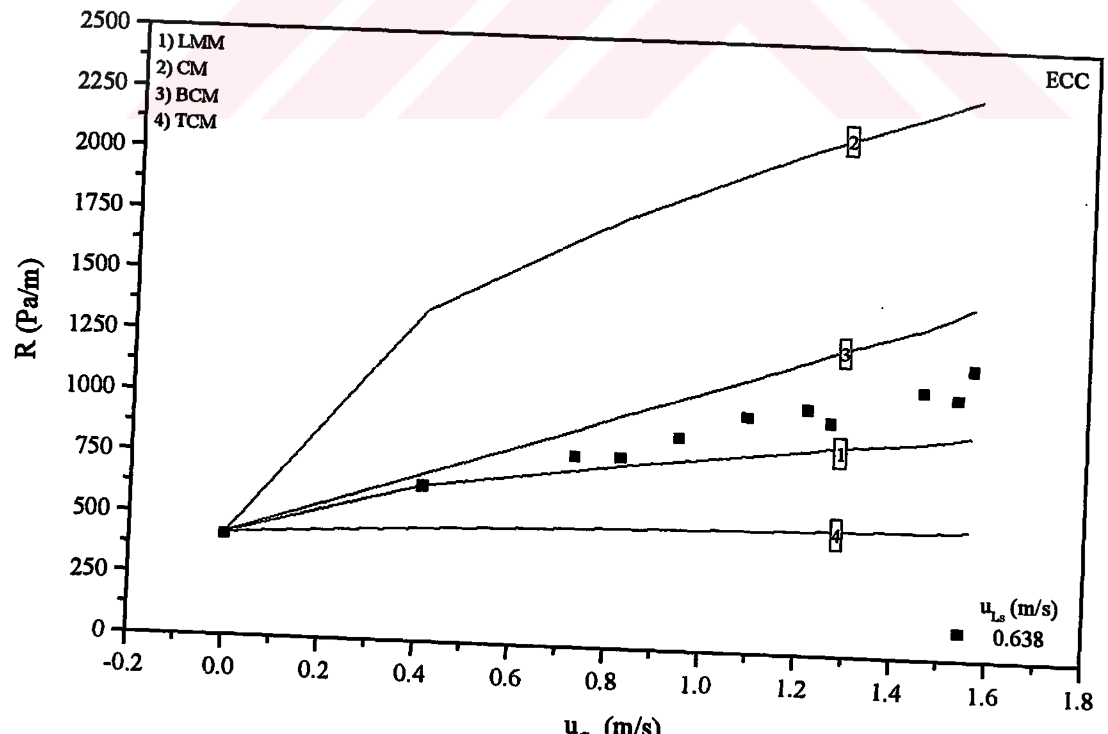

Figure 5.194. Comparison of the pressure losses measured in the ECC with the empirical methods for u_{Ls} =0.638 m/s.

Figure 5.195. shows the comparison of the CONC and ECC results with each others for the superficial liquid velocity of 0.065 m/s. The **solid line** shows the line fitted to the CONC data. The ECC results are greater than those of CONC results. However, the absolute differences between the values are very small.

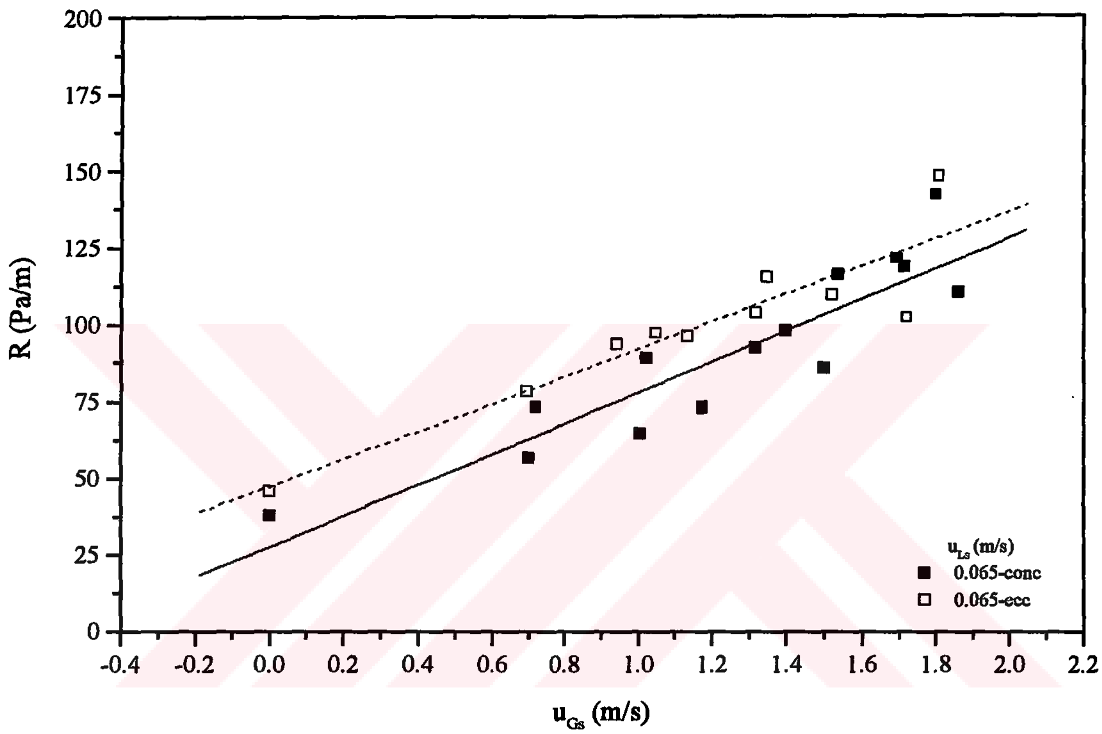

Figure 5.195. Comparison of the CONC and ECC results with each others for u_{Ls} =0.065 m/s.

Figure 5.196. shows the comparison of the CONC and ECC results with each others for a superficial liquid velocity of 0.147 m/s. The ECC results are greater than those of CONC results above the superficial gas velocity of 0.7 m/s. However, the ECC results are lower than those of CONC results below the superficial gas velocity of 0.7 m/s. The absolute differences between the values are very small.

Figure 5.197. shows the comparison of the CONC and ECC results with each others for a superficial liquid velocity of 0.229 m/s. The ECC results are greater than those of CONC results above the superficial gas velocity of 1.1 m/s. However, the ECC results are lower than those of CONC results below the superficial gas velocity of 1.1 m/s.

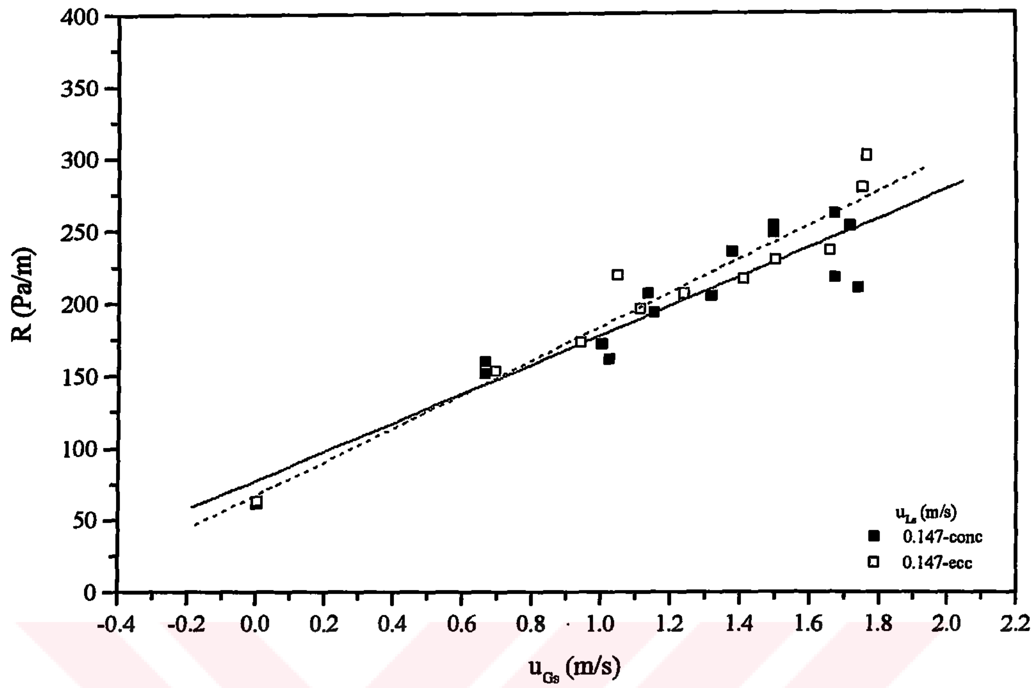

Figure 5.196. Comparison of the CONC and ECC results with each others for u_{Ls} =0.147 m/s.

Figure 5.198. shows the comparison of the CONC and ECC results with each others for a superficial liquid velocity of 0.311 m/s. The CONC results are greater than those of ECC results above the superficial gas velocity of 0.4 m/s. However, the CONC results are lower than those of ECC results below the superficial gas velocity of 0.4 m/s.

Figure 5.199. shows the comparison of the CONC and ECC results with each others for a superficial liquid velocity of 0.392 m/s. The CONC results are greater than those of ECC results above the superficial gas velocity of 0.8 m/s. However, the CONC results are lower than those of ECC results below the superficial gas velocity of 0.8 m/s.

Figure 5.200. shows the comparison of the CONC and ECC results with each others for a superficial liquid velocity of 0.474 m/s. The CONC results are greater than those of ECC throughout the all superficial gas velocities.

Figure 5.201. shows the comparison of the CONC and ECC results with each others for a superficial liquid velocity of 0.556 m/s. The CONC results are greater than those of ECC as those of 0.474 m/s throughout the all superficial gas velocities. The absolute differences between the data increase with the increasing of superficial gas velocity.

Figure 5.202. finally shows the comparison of the CONC and ECC results with each others for a superficial liquid velocity of 0.638 m/s. The CONC results are greater

than those of ECC as those of 0.474 and 0.556 m/s throughout the all superficial gas velocities. The absolute differences between the data remain approximately constant with the increasing of superficial gas velocity.

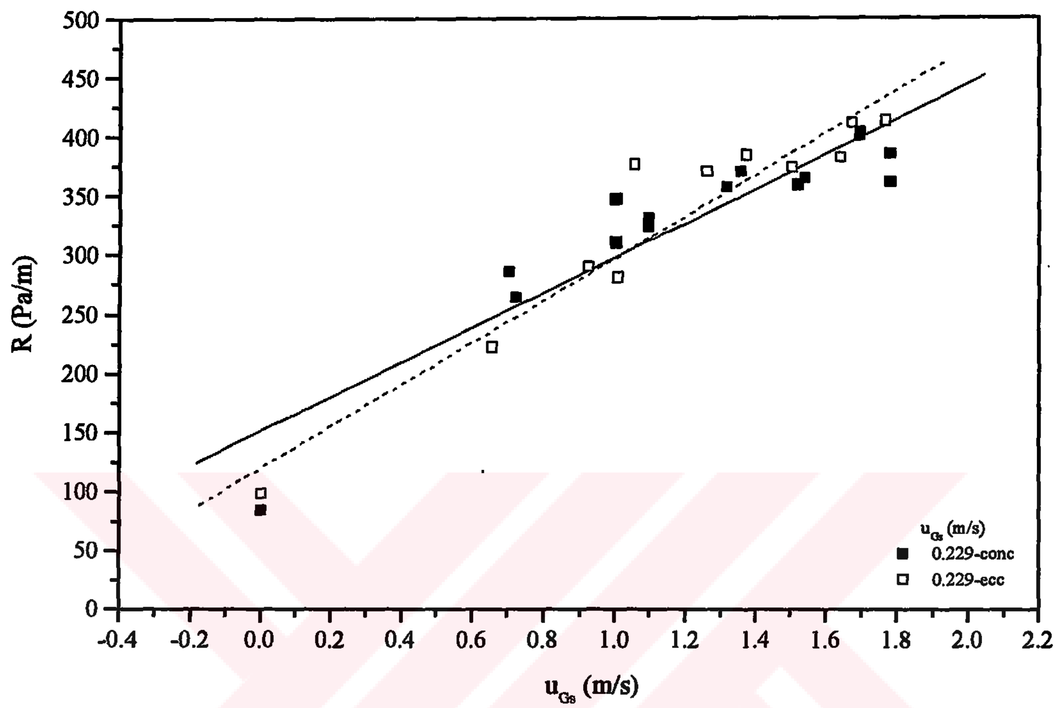

Figure 5.197. Comparison of the CONC and ECC results with each others for u_{Ls} = 0.229 m/s.

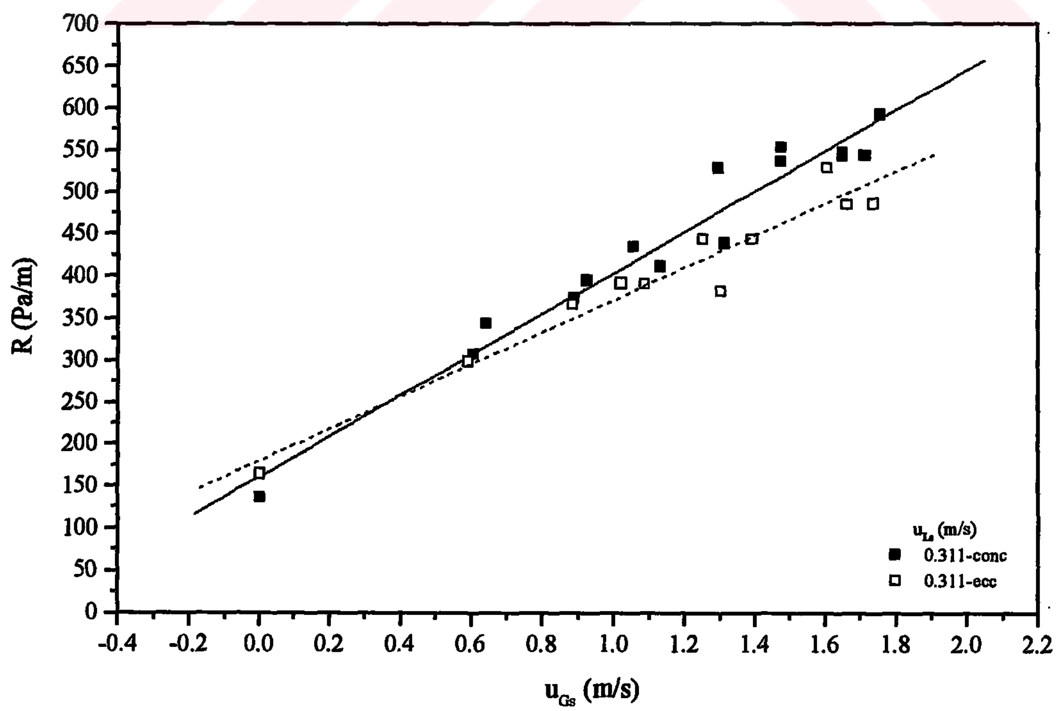

Figure 5.198. Comparison of the CONC and ECC results with each others for u_{Ls} = 0.311 m/s.

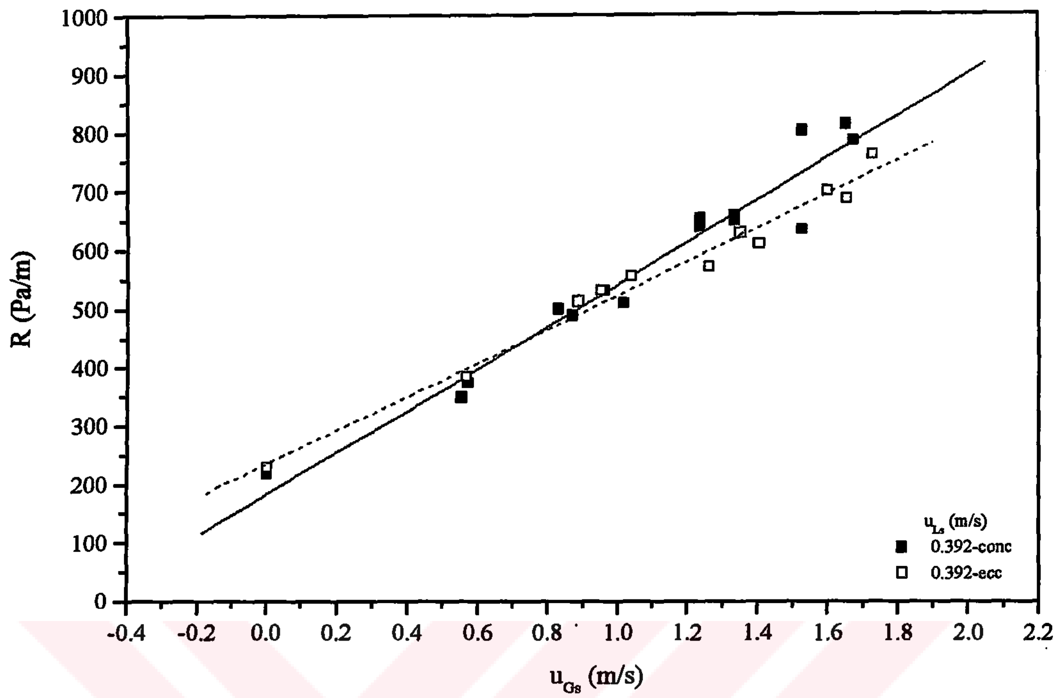

Figure 5.199. Comparison of the CONC and ECC results with each others for u_{Ls} =0.392 m/s.

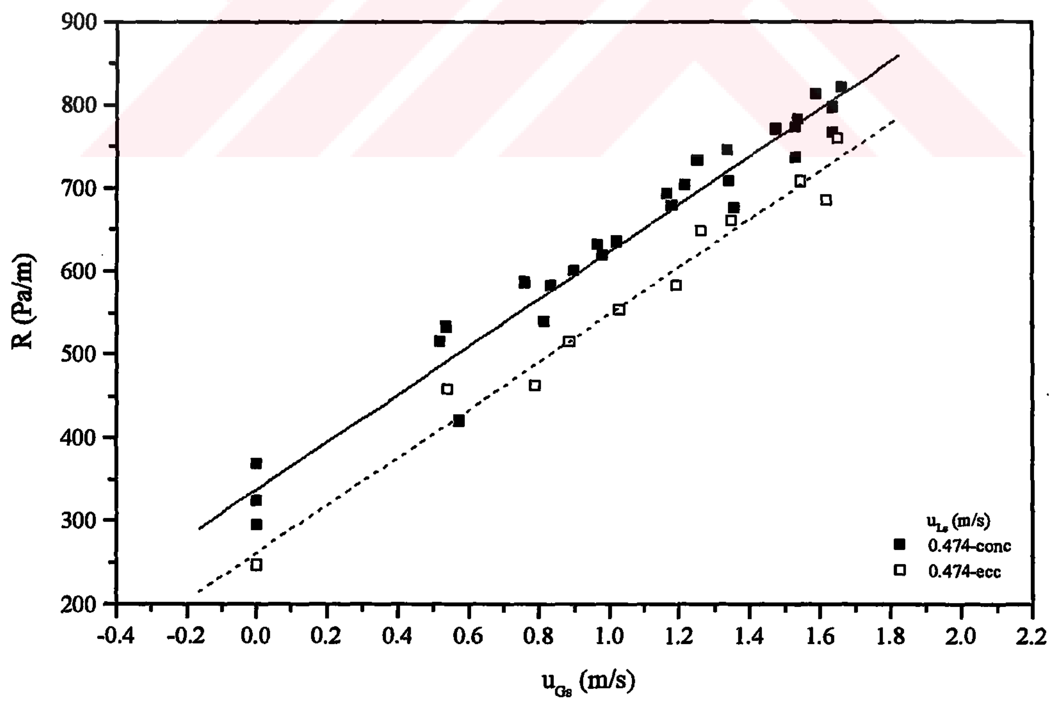

Figure 5.200. Comparison of the CONC and ECC results with each others for u_{Ls} =0.474 m/s.

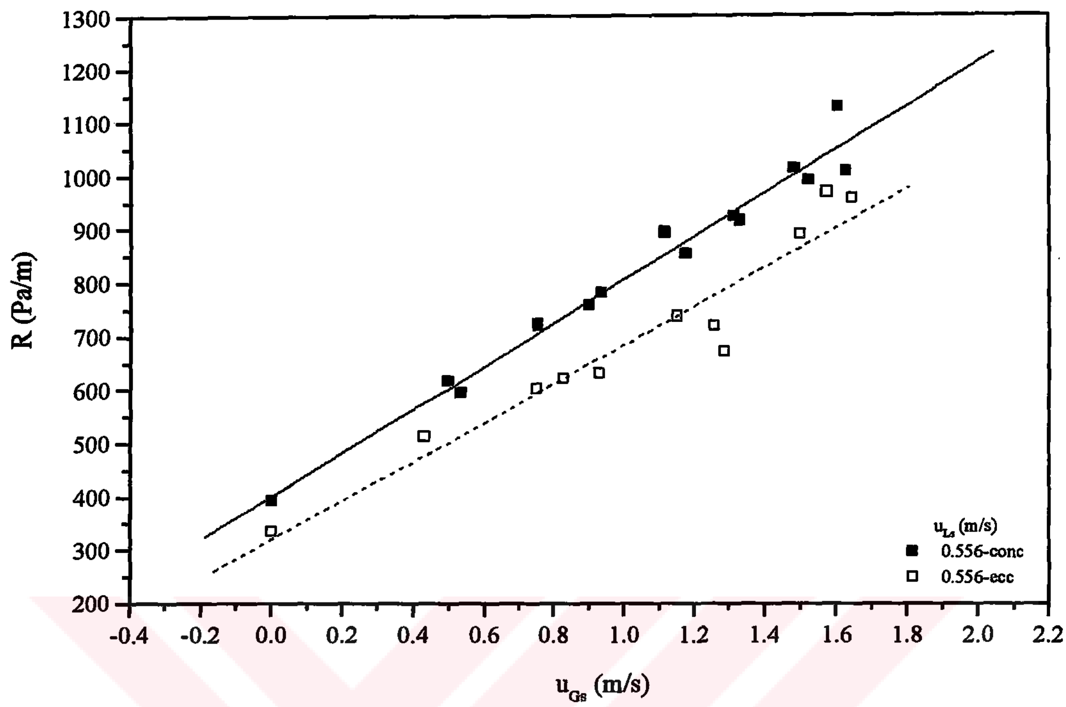

Figure 5.201. Comparison of the CONC and ECC results with each others for $u_{Ls}=0.556$ m/s.

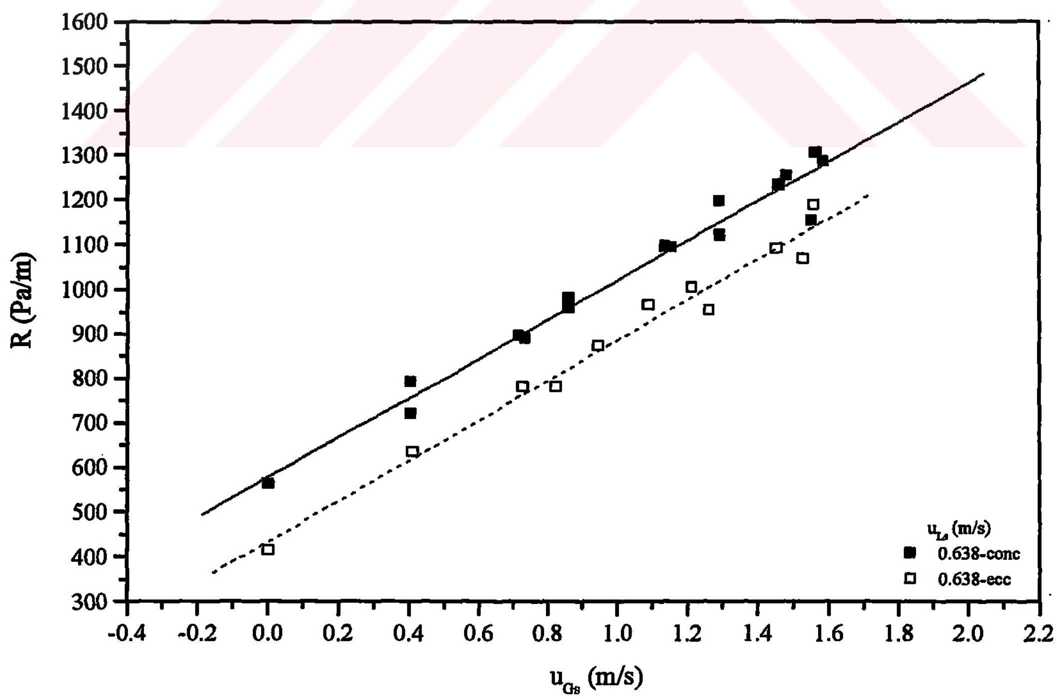

Figure 5.202. Comparison of the CONC and ECC results with each others for $u_{Ls}=0.638$ m/s.

From the comparisons of the CONC and ECC pressure losses, the following conclusions can be made: Pressure losses increase with the increasing of the superficial gas velocity. Pressure losses also increase with the increasing of the superficial liquid velocity. There is a transition region about the superficial liquid velocity of 0.474 m/s. In spite of the repeated experiments of 0.474 m/s (0.474-repeat) of the CONC experiments, the same trend is obtained approximately as those of 0.474 m/s (figure 5.187.). However, there is also a transition region in 0.474 m/s of the ECC experiments (figure 5.188.).

The experimental data are located between the results of LMM and BCM. The predictions get better as the superficial liquid velocity is increased. The results of the ECC experiments get smaller than those of the CONC experiments as the superficial liquid velocity is increased. The differences between the pressure losses of the CONC and ECC experiments are absolutely small in the low superficial liquid velocities. The pressure losses of the CONC and ECC experiments are approximately equal to each others between the superficial gas velocities of 0.4 m/s and 0.8 m/s for the superficial liquid velocities of 0.147 m/s, 0.229 m/s, 0.311 m/s, and 0.392 m/s. One can conclude that the pressure losses in the circular gaps are effected from the eccentricity of the inserted rod.

5.2.4.3. Void Fractions

The void fractions measured in the CONC experiments are shown in figures 5.203. and 5.204. The numbered lines were fitted to see easily the trends of the experimental results.

Figure 5.203. shows the variation of void fractions of the CONC experiments with the superficial gas velocity for the constant superficial liquid velocities of 0.065, 0.229, 0.392, and 0.556 m/s. These data indicate that the void fractions measured in the CONC experiments increase with the increasing of the superficial gas velocity. Additionally, the void fraction also increases as the constant superficial liquid velocity is decreased. However, the void fractions of the different constant superficial liquid velocities converge to each other as the superficial gas velocity is increased.

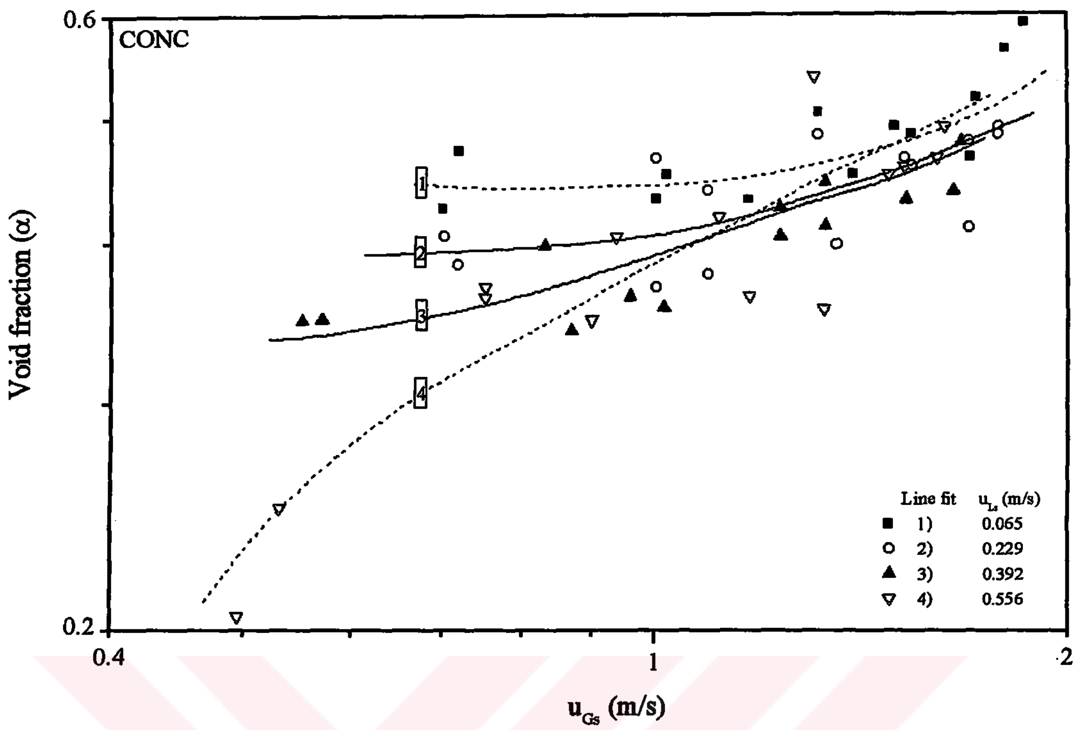

Figure 5.203. The void fractions measured in the CONC experiments.

The second group of the measured void fractions in the CONC experiments are shown in figure 5.204. The data of these constant superficial liquid velocities show the same tendency as the data given in figure 5.203.

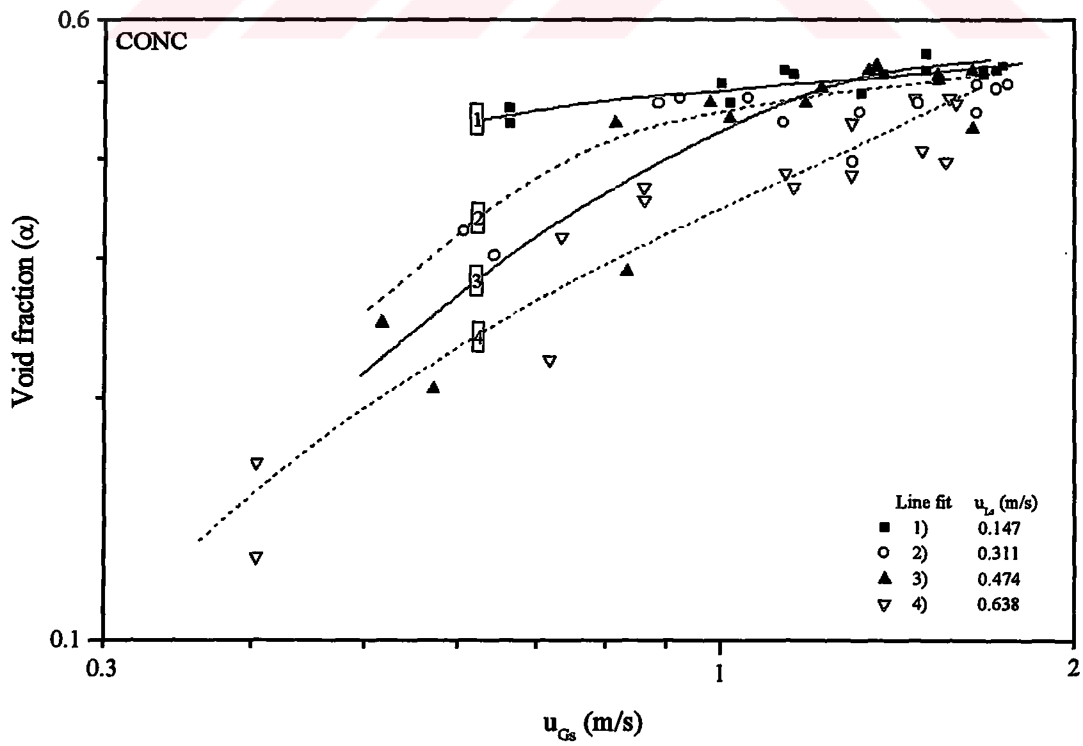

Figure 5.204. The void fractions measured in the CONC experiments.

For the comparison of the void fractions measured in the CONC and ECC experiments, the void fraction data of the ECC experiments are necessary. Figures 5.205. and 5.206. show the void fractions measured in the ECC experiments. The numbered lines were fitted to see easily the trends of the experimental results.

Figure 5.205. shows the variation of void fractions of the ECC experiments with the superficial gas velocity for the constant superficial liquid velocities of 0.065, 0.229, 0.392, and 0.556 m/s. These data indicate that the void fraction measured in the ECC experiments increases with the increasing of the superficial gas velocity. However, there is no any concrete conclusion about the variation of the void fractions with the constant superficial liquid velocity. However, there is a feeling, excepting the constant superficial liquid velocity of 0.065 m/s, that the void fractions of the different constant superficial liquid velocities increase as the superficial liquid velocity is increased. Additionally, the void fractions of the different constant superficial liquid velocities diverge to each other as the superficial gas velocity is increased. This is also valid for the data of 0.638 m/s shown in figure 5.206.

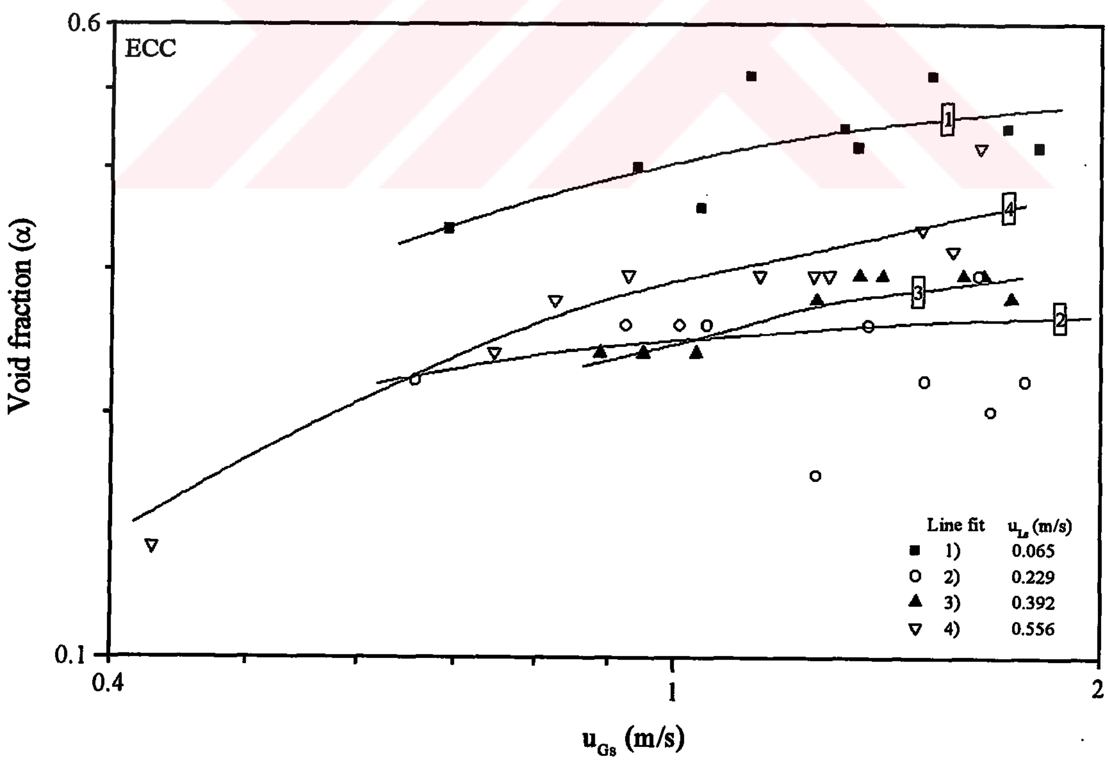

Figure 5.205. The void fractions measured in the ECC experiments.

The comparisons of the results of the CONC and ECC experiments are carried out for each superficial liquid velocity. Figures 5.207. to 5.214. show the variations of the void fractions measured in the CONC and ECC experiments for the constant superficial liquid velocities of 0.065, 0.147, 0.229, 0.311, 0.392, 0.474, 0.556, and 0.638 m/s. The results of the ECC experiments are always lower than those of the CONC experiments. The solid and dashed lines show the fitted lines to the data of the CONC and ECC experiments, respectively.

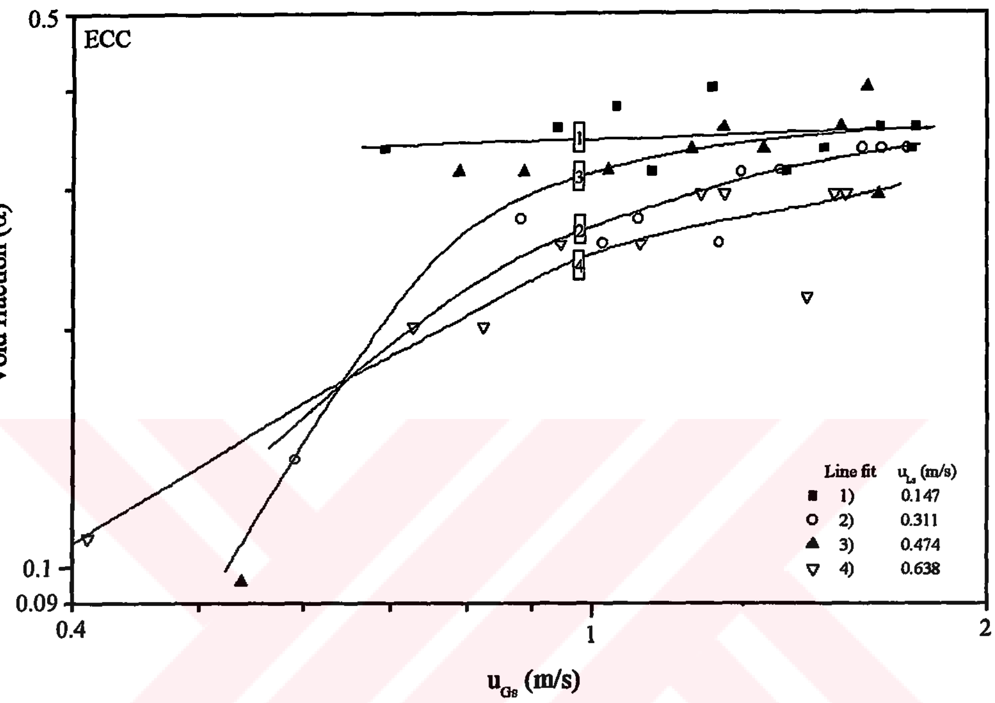

Figure 5.206. The void fractions measured in the ECC experiments.

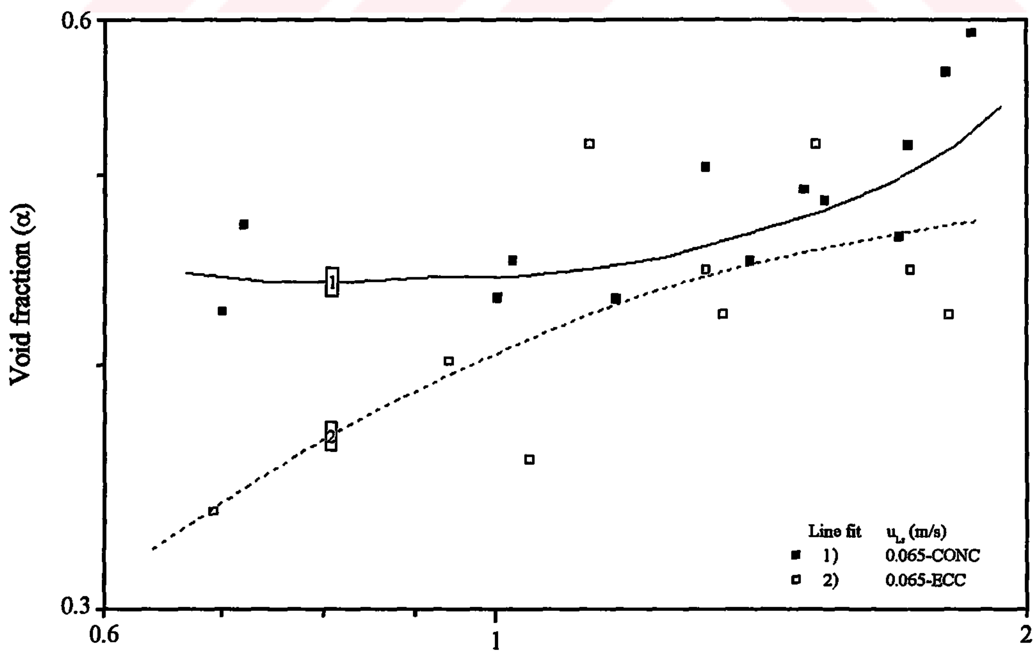

Figure 5.207. Comparison of the void fractions measured in the CONC and ECC experiments for a constant superficial liquid velocity of 0.065 m/s.

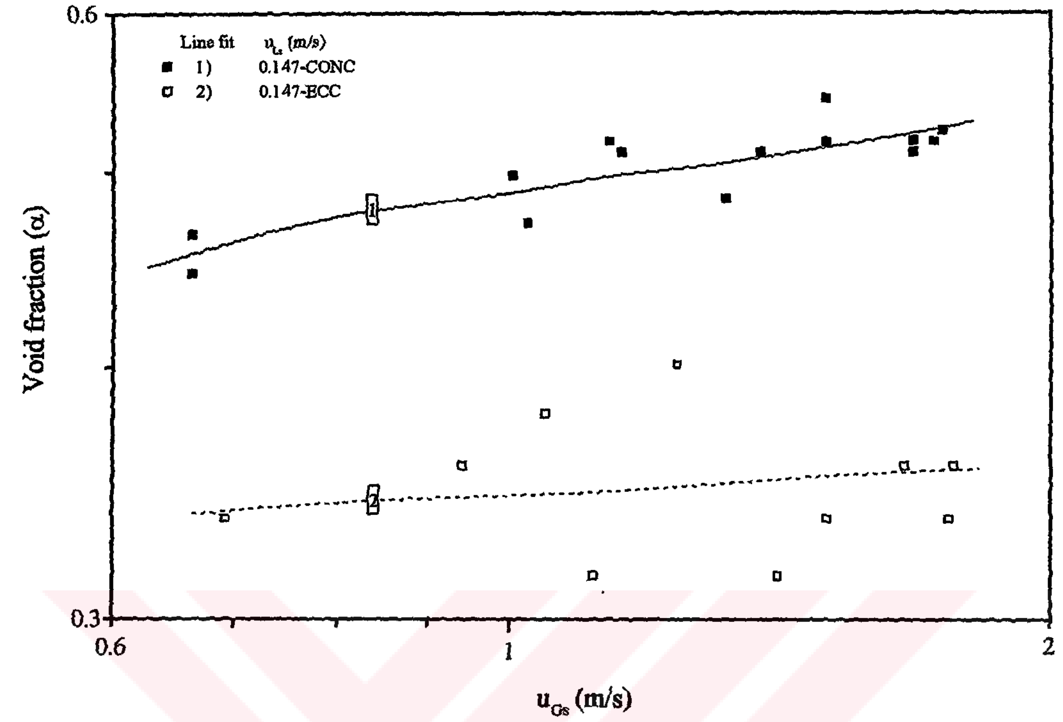

Figure 5.208. Comparison of the void fractions measured in the CONC and ECC experiments for a constant superficial liquid velocity of 0.147 m/s.

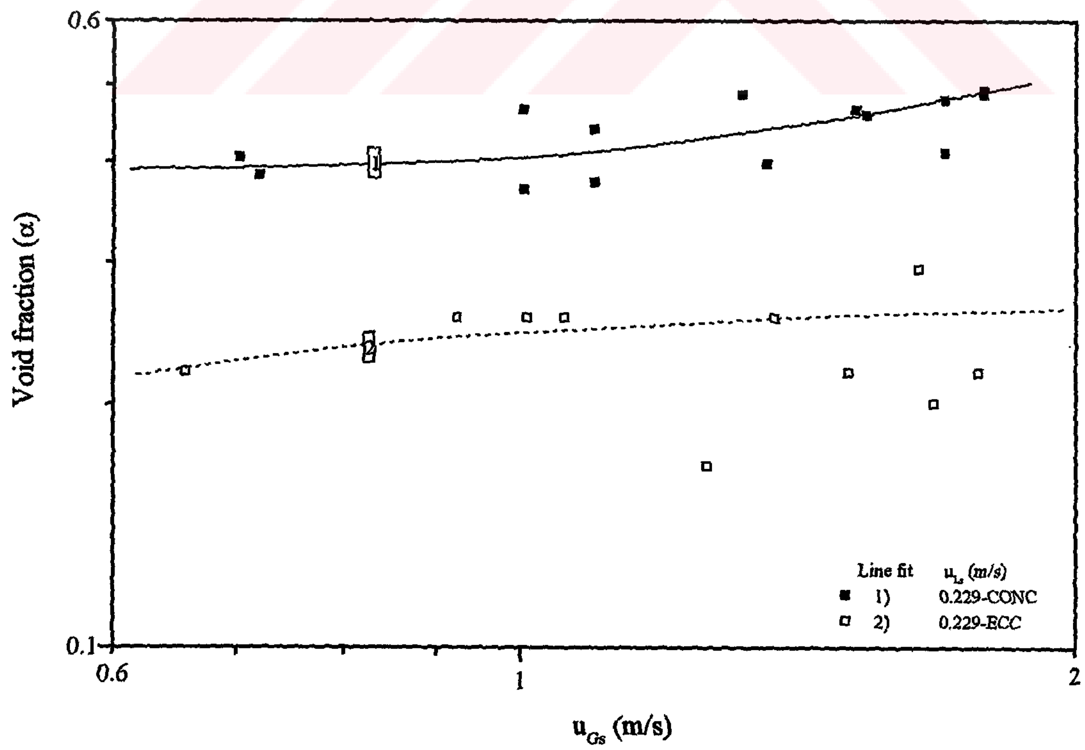

Figure 5.209. Comparison of the void fractions measured in the CONC and ECC experiments for a constant superficial liquid velocity of 0.229 m/s.

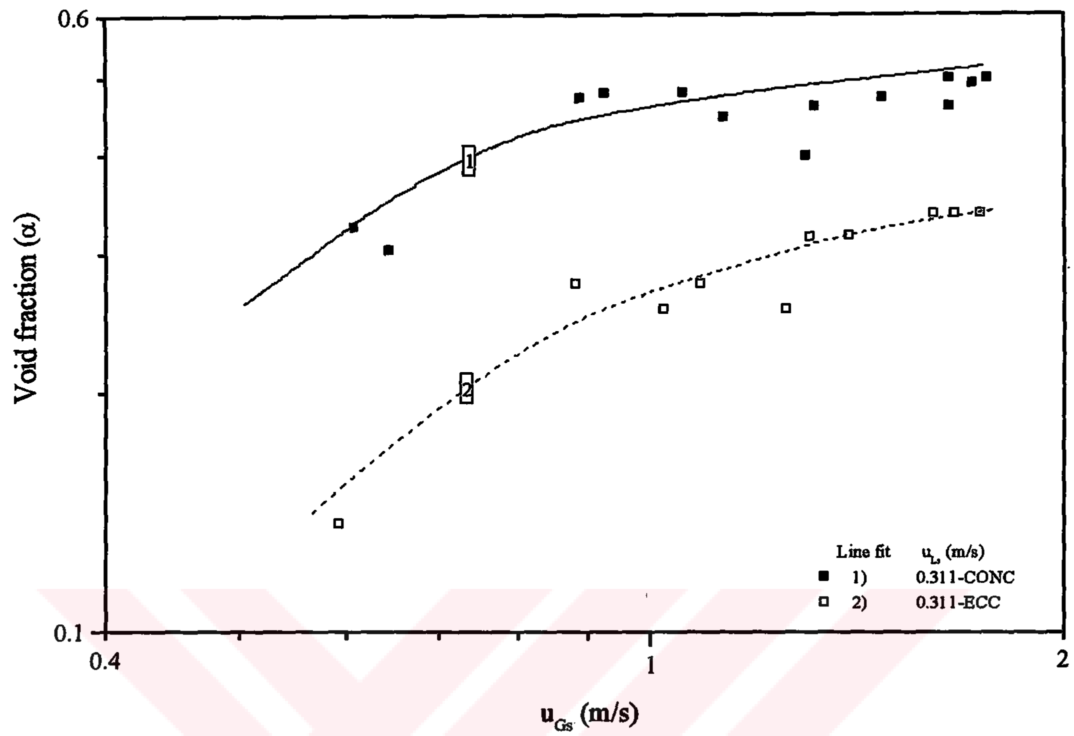

Figure 5.210. Comparison of the void fractions measured in the CONC and ECC experiments for a constant superficial liquid velocity of 0.311 m/s.

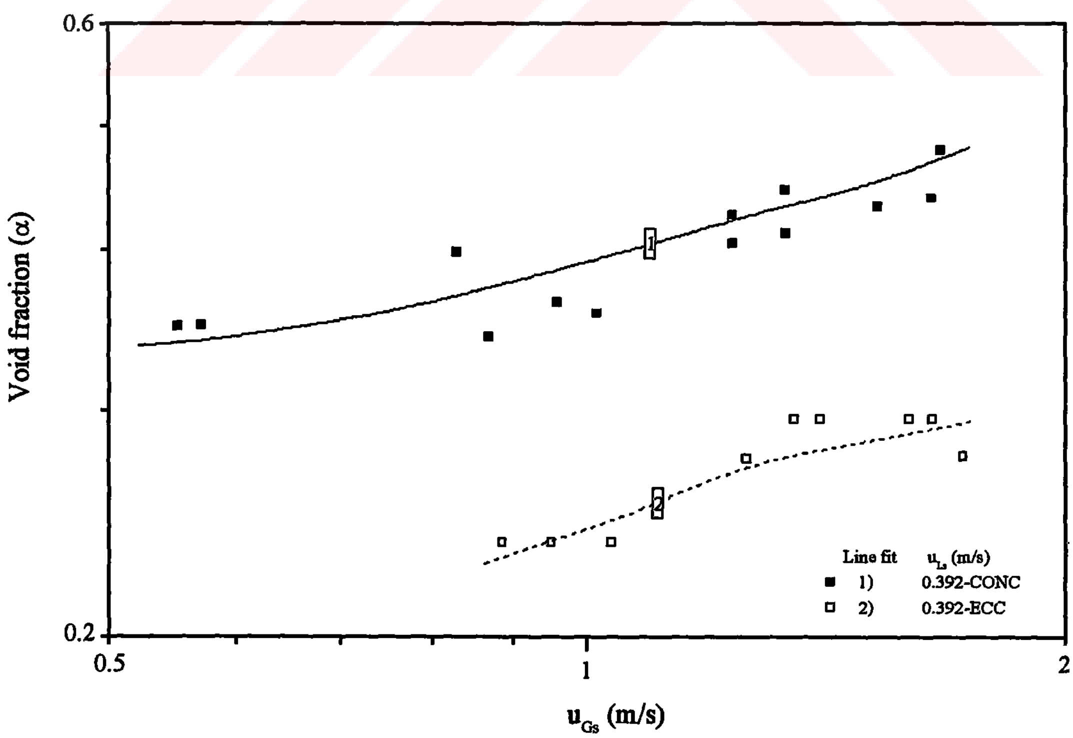

Figure 5.211. Comparison of the void fractions measured in the CONC and ECC experiments for a constant superficial liquid velocity of 0.392 m/s.

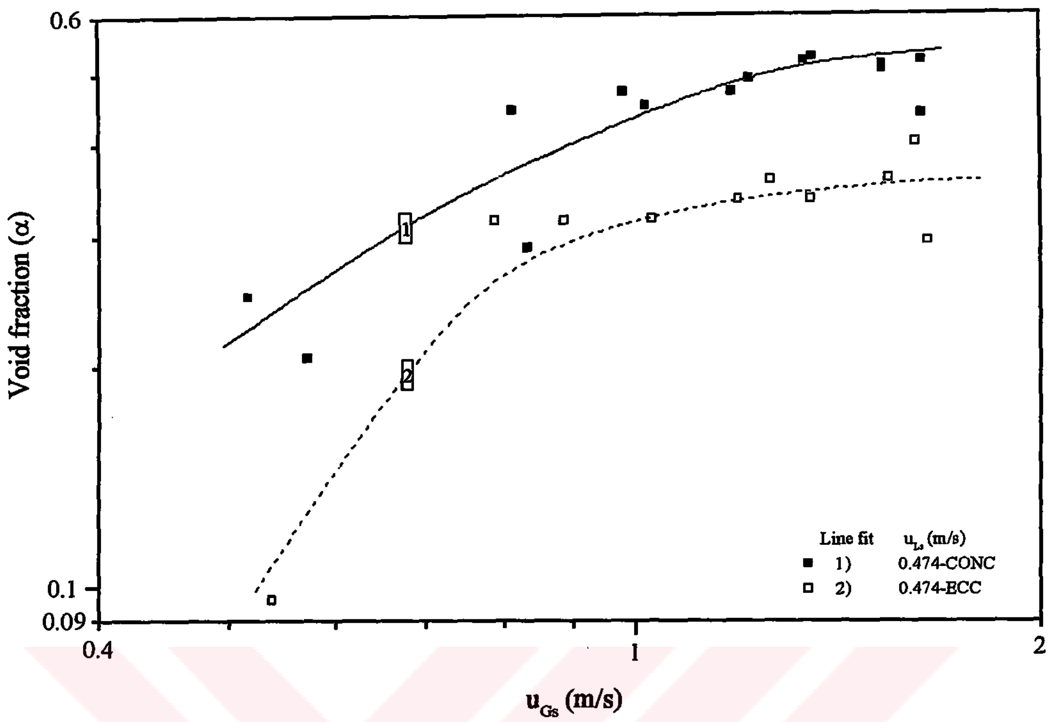

Figure 5.212. Comparison of the void fractions measured in the CONC and ECC experiments for a constant superficial liquid velocity of 0.474 m/s.

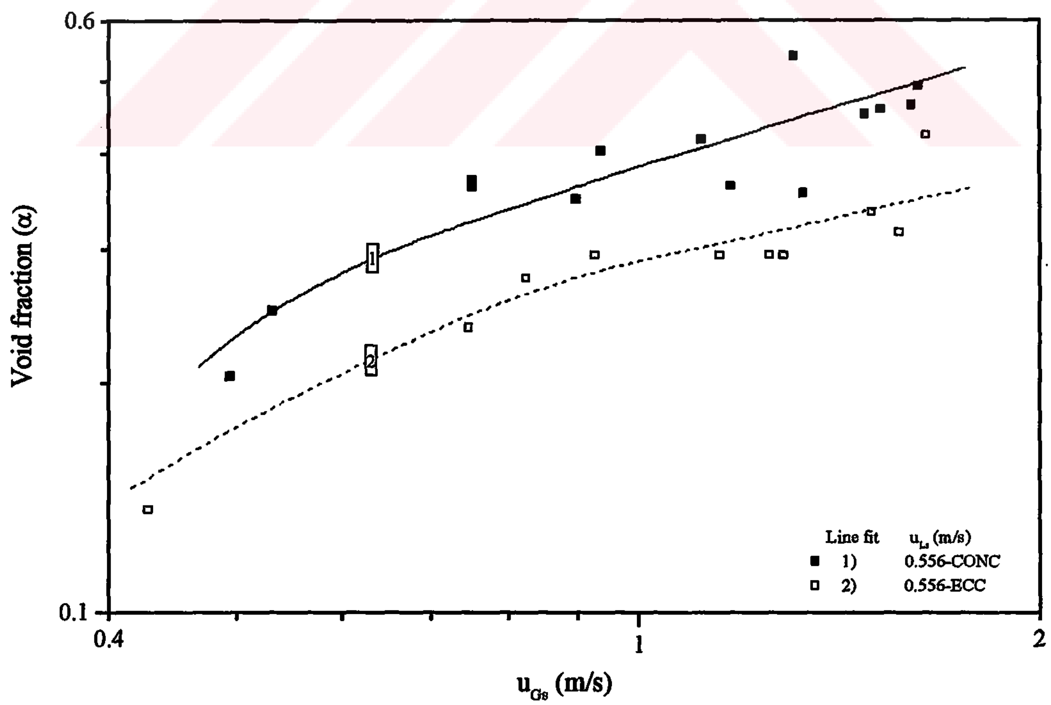

Figure 5.213. Comparison of the void fractions measured in the CONC and ECC experiments for a constant superficial liquid velocity of 0.556 m/s.

From the void fraction comparisons of the CONC and ECC experiments, the following conclusions can be made:

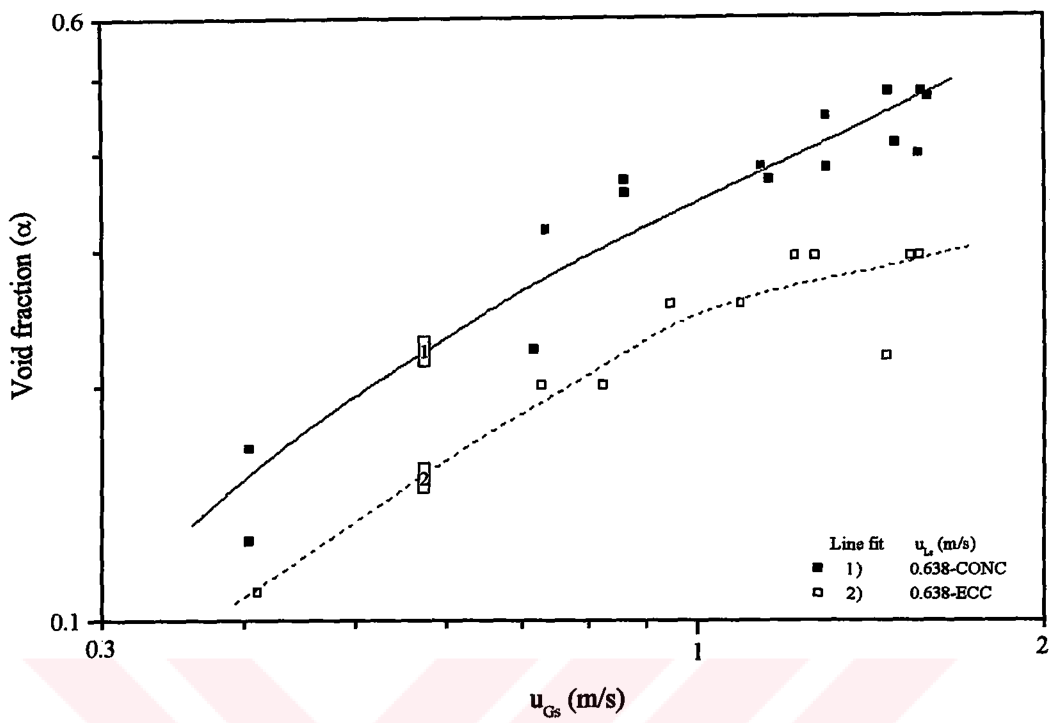

Figure 5.214. Comparison of the void fractions measured in the CONC and ECC experiments for a constant superficial liquid velocity of 0.638 m/s.

Void fractions measured in the CONC experiments increase with the increasing of the superficial gas velocity. The void fractions measured in the CONC experiments also increase as the constant superficial liquid velocity is decreased. The void fractions of the different constant superficial liquid velocities in the CONC experiments converge to each other as the superficial gas velocity is increased. The void fractions measured in the ECC experiments increase with the increasing of the superficial gas velocity. However, there is no any concrete conclusion about the variation of the void fractions with the constant superficial liquid velocity. There is a feeling, excepting the constant superficial liquid velocity of 0.065 m/s, that the void fractions of the different constant superficial liquid velocities in the ECC experiments increase as the superficial liquid velocity is increased. Additionally, the void fractions of the different constant superficial liquid velocities in the ECC experiments diverge to each other as the superficial gas velocity is increased. This is also valid for the data of 0.638 m/s shown in figure 5.206. The void fractions of the ECC experiments are always lower than those of the CONC experiments. One can finally conclude that, the void fractions in the ECC experiments are different than those of the CONC experiments. Namely, void fractions are effected from the eccentricity of the inserted rod.

5.2.4.4. Slug Velocities, Lengths, and Frequencies

The slug velocities, lengths, and frequencies measured in the CONC and ECC experiments are discussed in this section. The calculation of the slug velocities, lengths, and frequencies using the traces of the LEDs are extensively explained in the section of "Cross Correlation Technique". The calculated slug lengths of the CONC and ECC experiments are compared with the observations of the same experiments. The slug lengths are approximately estimated and taken notes on the observation sheet at the same time with the experiments. Certainly, the sensitive estimation of a slug length is directly depended on the ability of the observer. The length estimation capability of the observer were inspected for many different materials which have different lengths. An approximately calibration curve were proposed for the correction of the observed slug lengths in the CONC and ECC experiments. This is explained in the section of "Prediction of Slug Length".

The slug velocities are compared with the results of Nicklin et al.(1962). Additionally, the calculated time (from LED1 to LED2) with the cross correlation technique are compared with the results of a simultaneously real velocity measurement with the help of a chronometer. In this experiment, the velocities of many slugs were tried to measure between the stations of LED1 and LED2 (1m). The velocities of different slugs which have measured with the help of the chronometer are 4.00, 3.23, and 3.03 m/s. In addition to these, a slug velocity, 3.31 m/s, for this experiment is calculated with the help of the cross correlation technique using the traces of LEDs. Although we calculated only one slug velocity value for many different slugs, it is impossible to be only one constant slug velocity of many different slugs. Thus, this calculated slug velocity is a mean value of whole slugs in the experiments. Namely, the calculated slug velocity is greatly in agreement with the real measurements.

Figures from 5.215. to 5.217. show the comparisons of the CONC and ECC results with the Nicklin's predictions. Nicklin et al. (1962) predicts higher than those of this investigation. However, they are approximately in agreement with each others.

Figure 5.218. shows the comparison of slug velocities calculated from the CONC and ECC experiments for a constant superficial liquid velocity of 0.392 m/s. The ECC results are lower than those of CONC below the $u_{Gs} = 1.55$ m/s.

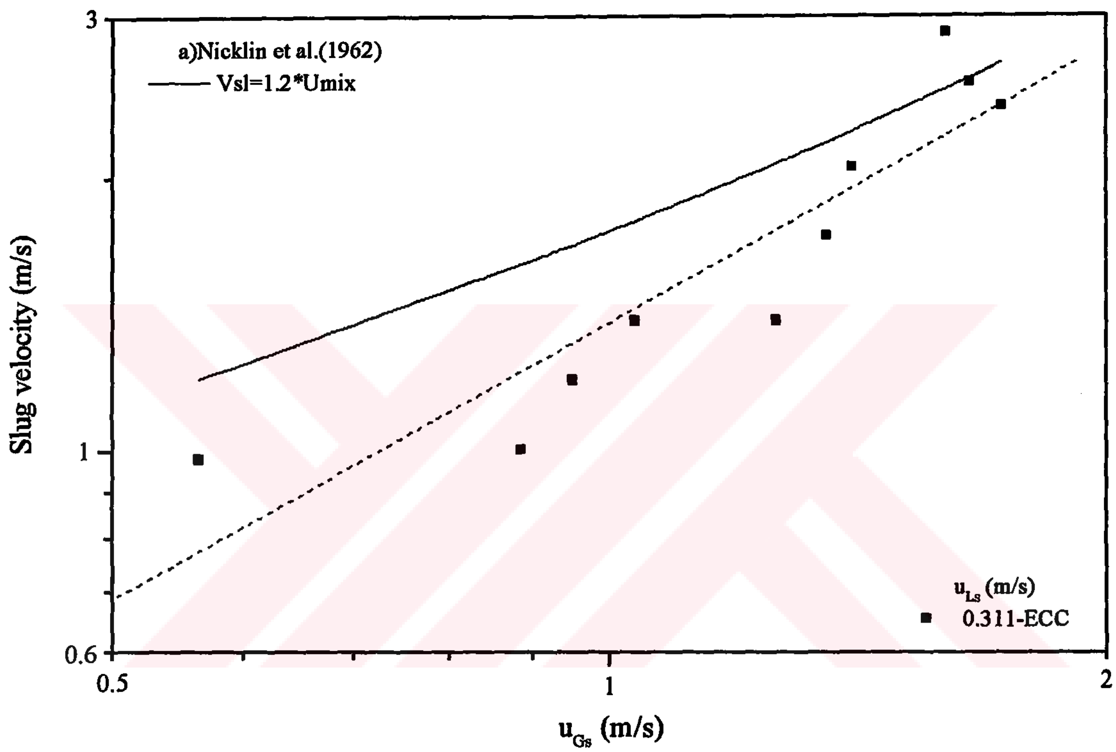

Figure 5.215. Comparisons of the ECC results with the Nicklin et al. (1962)'s predictions.

Figures from 5.219. to 5.211. show the comparison of slug length with the observed lengths. The "observation" means that is raw observed slug length, however the "calibrated observation" means this values are obtained using the equation (3.47) (in the section of "Visual Prediction of Slug Length").

Figure 5.222. shows the results of the $u_{Ls} = 0.311$ and $u_{Ls} = 0.392$ m/s of the ECC experiments. The slug length increases as the superficial liquid velocity is increased below the $u_{Gs} = 1.75$ m/s. Additionally, the slug lengths tend to be constant with the increasing of the superficial liquid velocity.

Figure 5.223. shows the variation of slug length with the superficial gas velocity for the constant superficial liquid velocity. The CONC results increase with the increasing of the superficial gas velocity. However, the slug lengths of the ECC experiments tend to be constant with the increasing of the superficial gas velocity. It can be expressed that the eccentricity of the inserted rod effects the slug lengths. This situation is also evident from the flow pattern maps of the CONC and ECC experiments. There are the flow patterns of "undeveloped bubbly slug" and "undeveloped bubbly slug+plug" in the flow pattern maps of the CONC experiments. These flow patterns have been described to express the different lengths of the observed slugs. However, there are no the term of "undeveloped" in the descriptions of the ECC flow patterns.

The slug frequencies measured in the CONC and ECC experiments are compared with the results of Taitel and Dukler (1977) (figure 5.224.). Although the results of Taitel and Dukler (1977) are valid for the circular pipes, our data are located in the reasonable region of the figure.

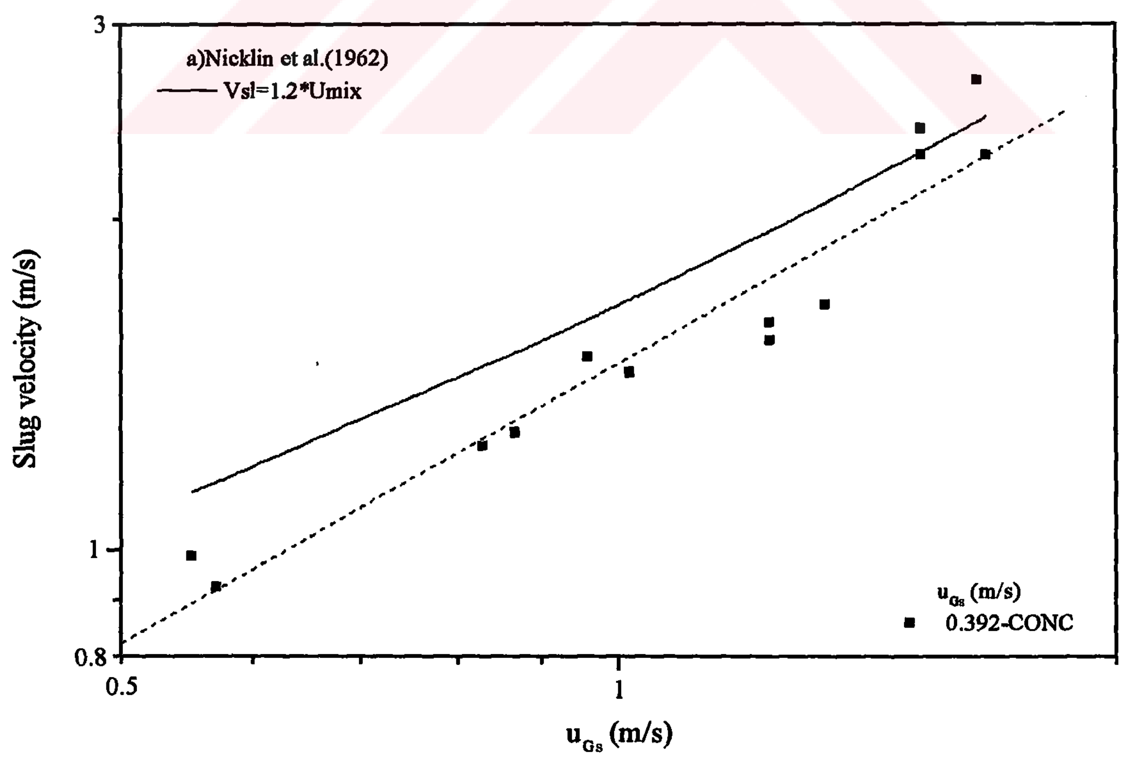

Figure 5.216. Comparisons of the CONC results with the Nicklin et al. (1962)'s predictions.

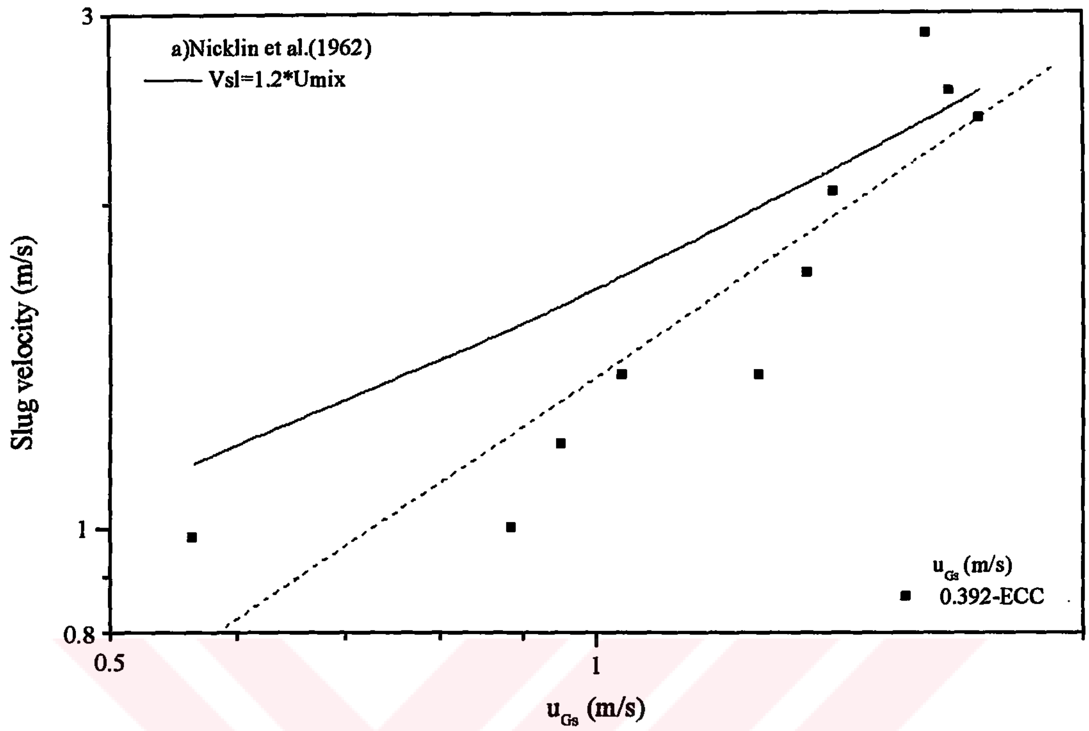

Figure 5.217. Comparisons of the ECC results with the Nicklin et al. (1962)'s predictions.

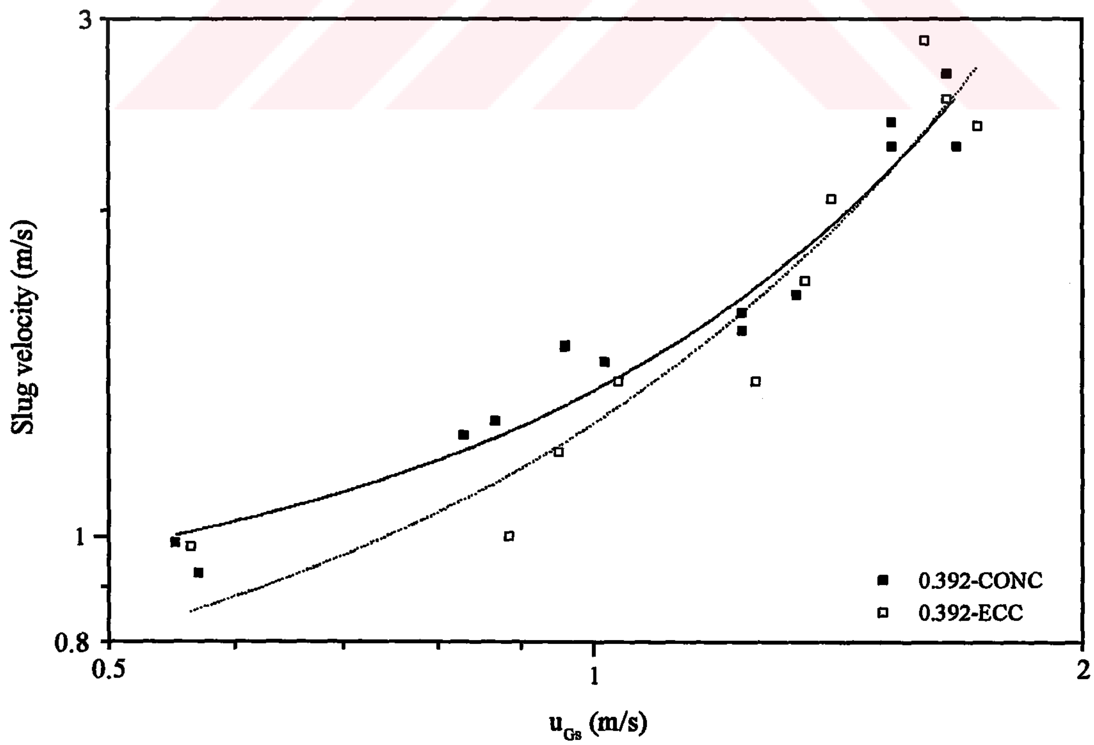

Figure 5.218. Comparison of slug velocities calculated from the CONC and ECC experiments for $u_{Ls}=0.392$ m/s.

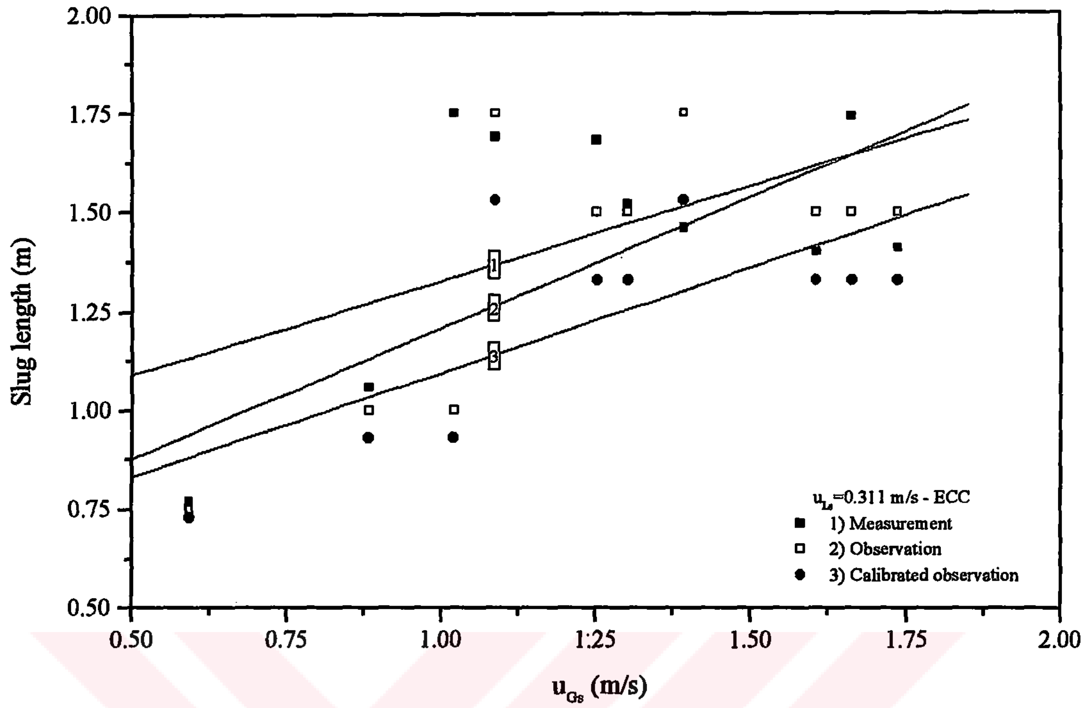

Figure 5.219. Comparison of slug length with the observed lengths in the ECC experiments for u_{Ls} =0.311 m/s.

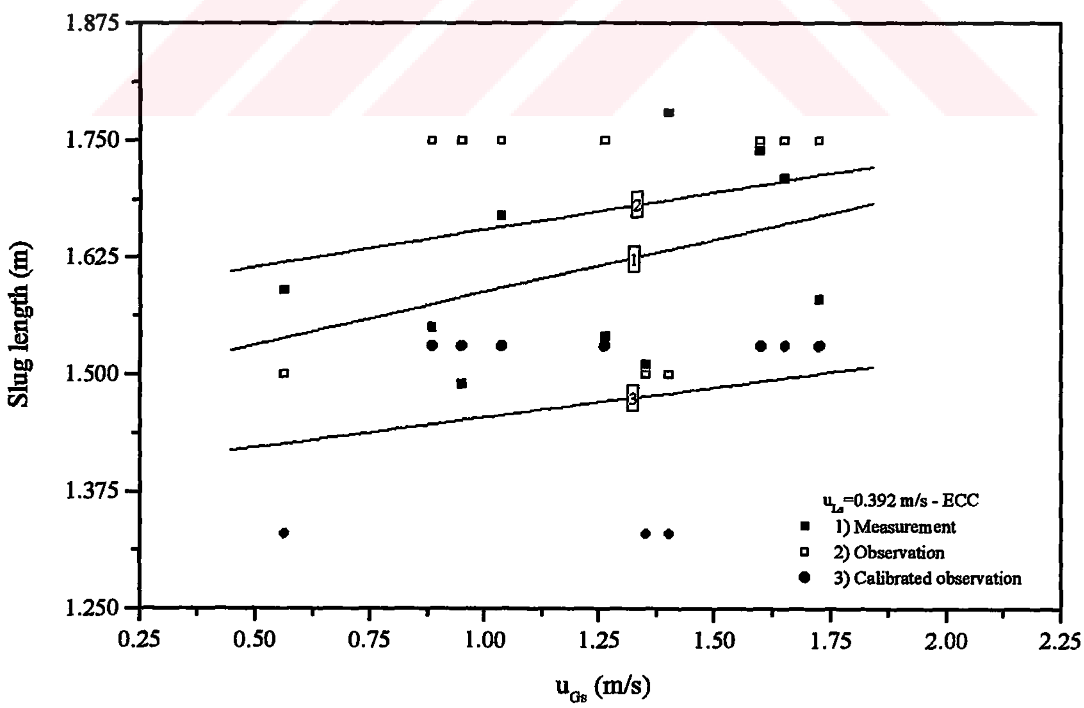

Figure 5.220. Comparison of slug length with the observed lengths in the ECC experiments for u_{Ls} =0.392 m/s.

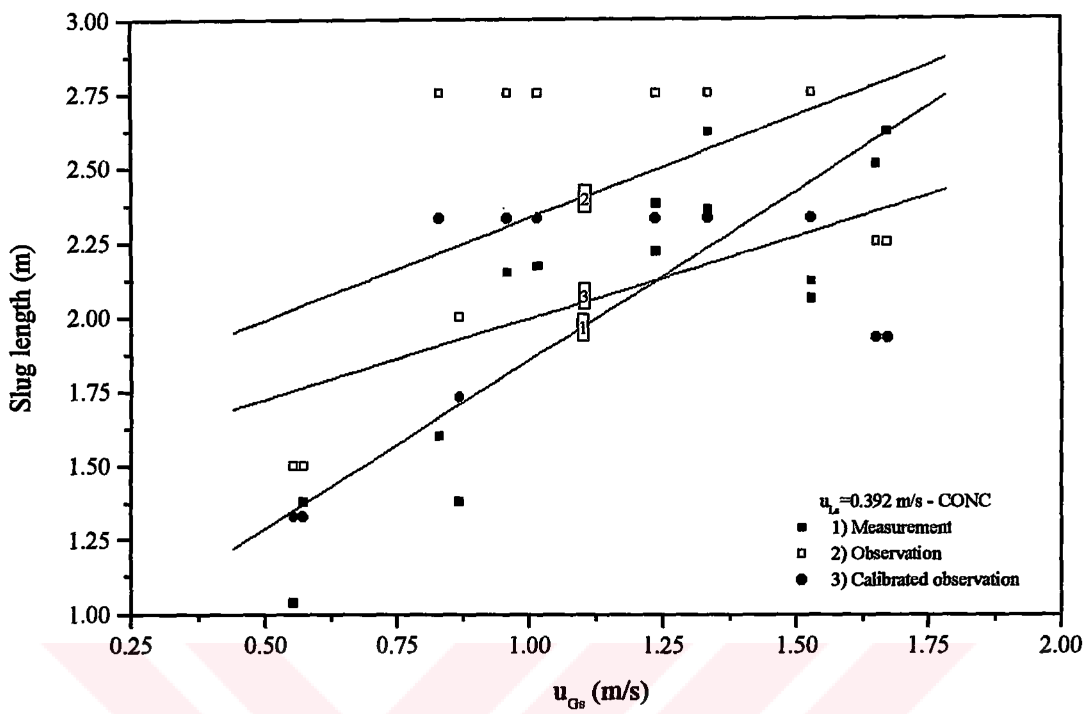

Figure 5.221. Comparison of slug length with the observed lengths in the CONC experiments for $u_{Ls} = 0.392$ m/s.

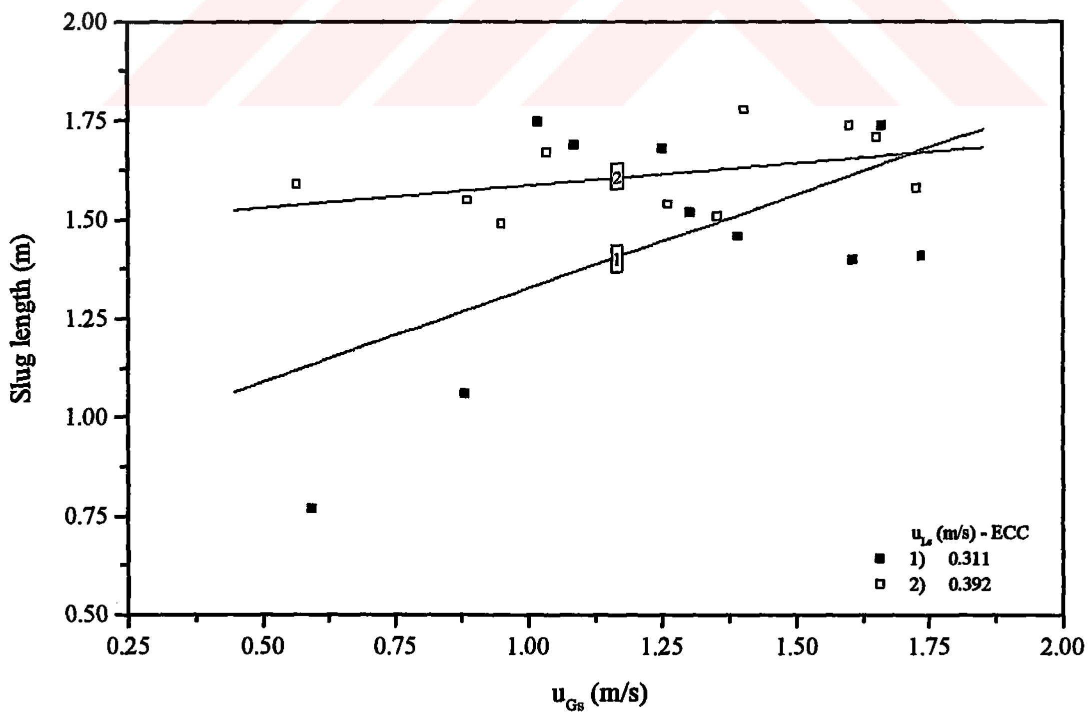

Figure 5.222. Comparison of slug length with the superficial gas velocity in the ECC experiments for $u_{Ls} = 0.311$ m/s, and $u_{Ls} = 0.392$ m/s.

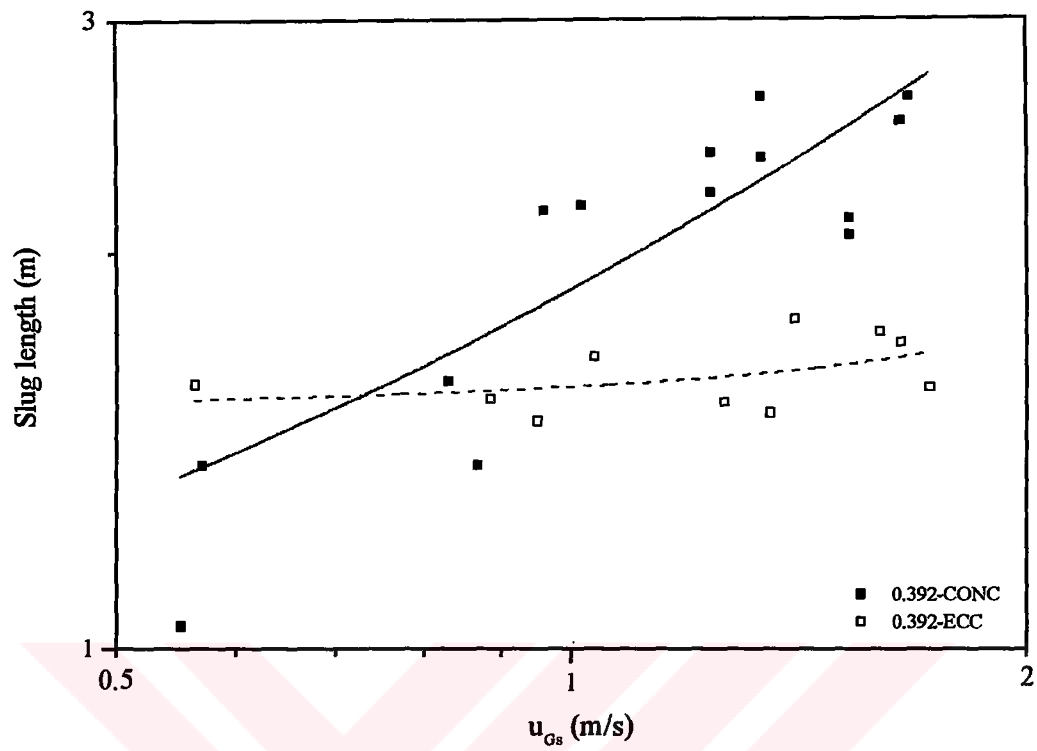

Figure 5.223. Comparison of slug length with the superficial gas velocity in the CONC and ECC experiments for u_{Ls} =0.392 m/s.

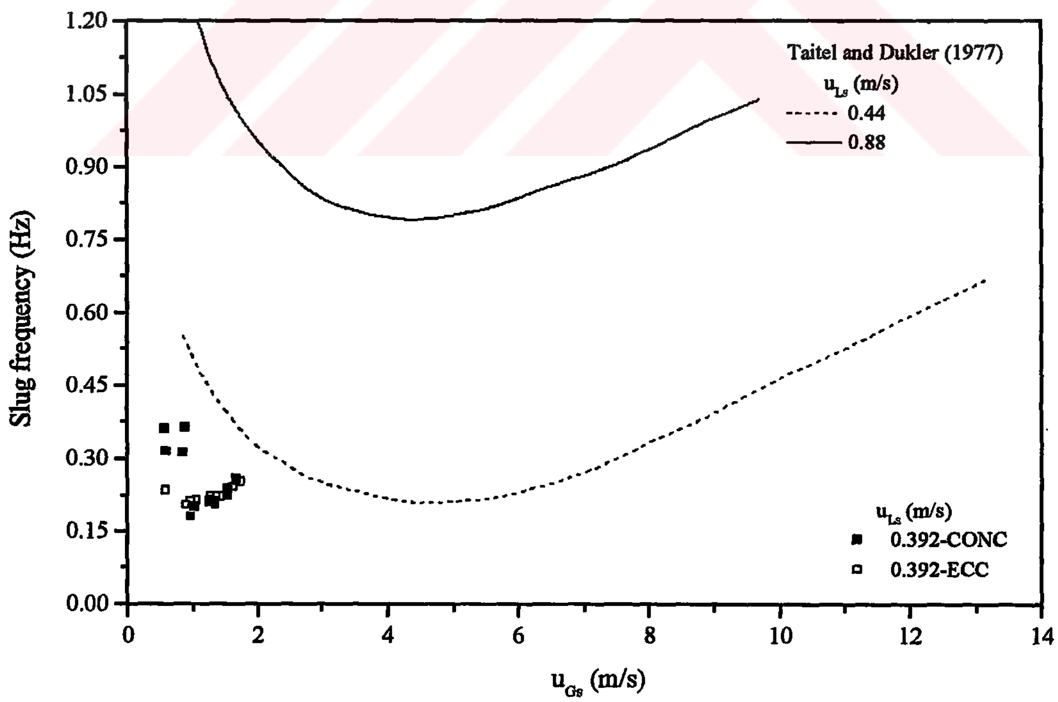

Figure 5.224. Comparison of the slug frequencies measured in the CONC and ECC experiments with the results of Taitel and Dukler (1977).

According to the results of the ECC experiments shown in figure 5.225., the slug frequency increases with the increasing of the constant superficial liquid velocity. Additionally, despite the scattered data of the $u_{Ls} = 0.311$, the data of the $u_{Ls} = 0.392$ m/s are rather ordered.

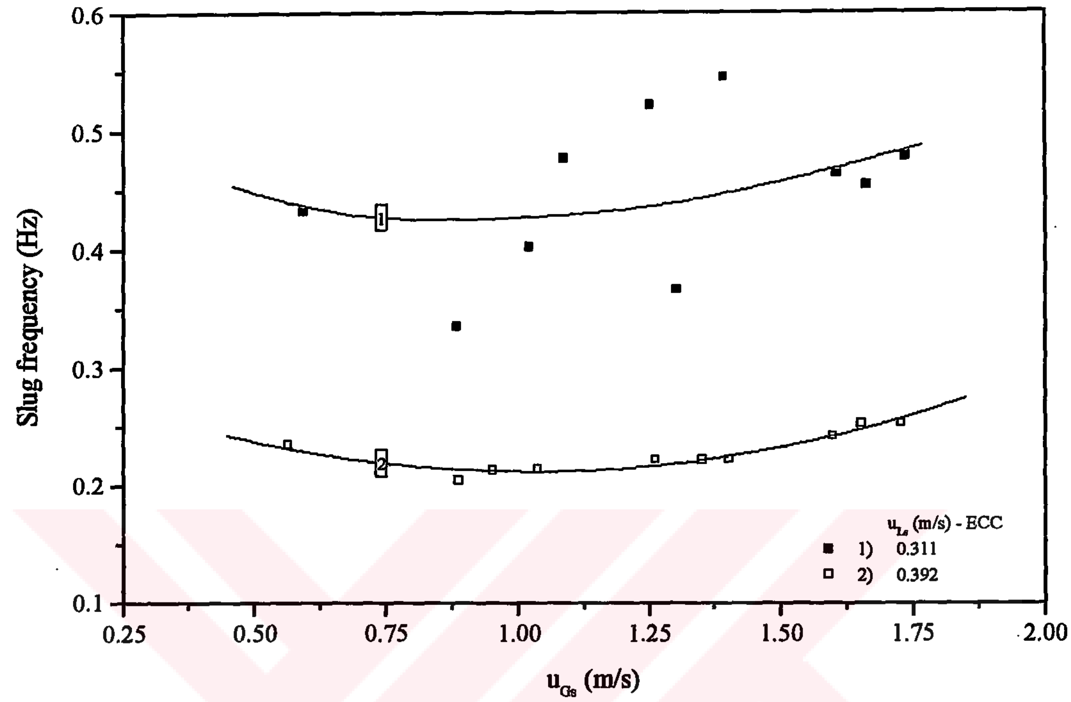

Figure 5.225. Comparison of slug frequency with the superficial gas velocity in the ECC experiments for u_{Ls} =0.311 m/s, and u_{Ls} =0.392 m/s.

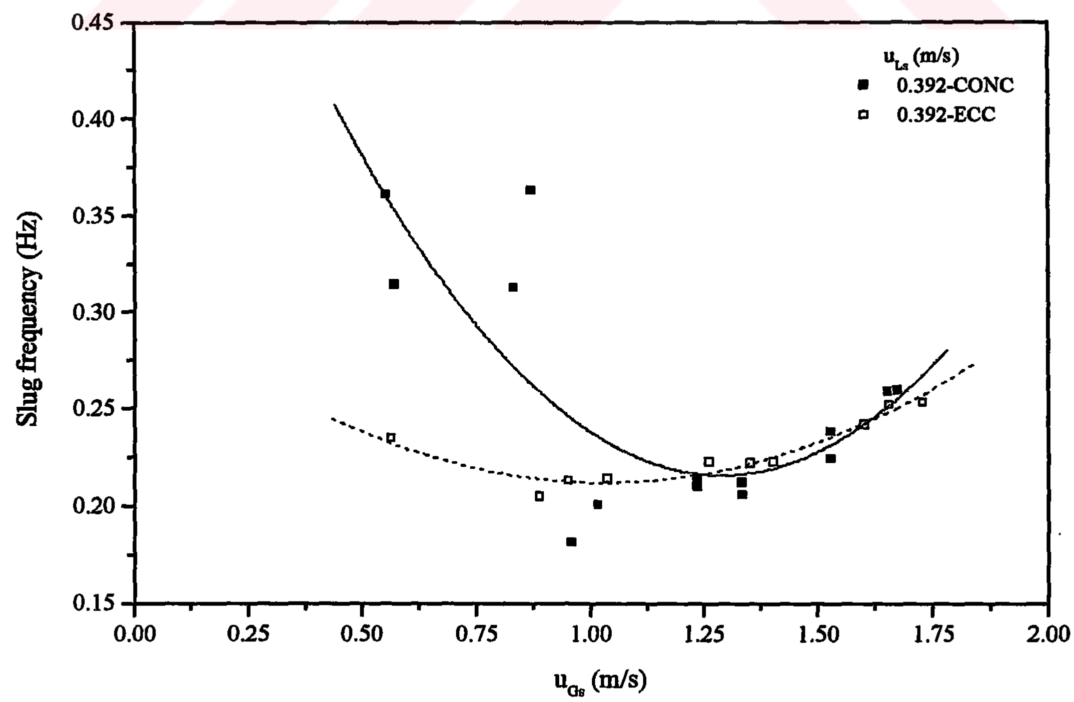

Figure 5.226. Comparison of slug frequency with the superficial gas velocity in the CONC and ECC experiments for u_{Ls} =0.392 m/s.

Figure 5.226. shows the comparison of the slug frequencies of the CONC and ECC experiments. It is very clear from this figure that the slug frequency is effected from the eccentricity of the inserted rod. In addition to this, despite the scattered data of the CONC experiments, the slug frequencies of the ECC experiments are rather ordered.

For the slug velocities, lengths, and frequencies, the following conclusions can be made:

Slug velocities can be approximately determined with the help of LED traces using the cross correlation technique. The calculated slug velocity is sufficiently in agreement with the real velocity measurements with the help of a chronometer. The slug velocities can be predicted by Nicklin et al.(1962) (*eqs.(5.2) and (5.3)*). However, the predicted values are always higher than those calculated using the CONC and ECC experiments. The calculated slug velocities of the CONC experiments are higher than those of the ECC experiments below the superficial gas velocity of 1.55 m/s. The calculated, observed, and calibrated observed slug lengths are in agreement with each others.

The slug lengths of the CONC experiments increase with the increasing of the superficial gas velocity. However, the slug lengths of the ECC experiments tend to be constant with the increasing of the superficial gas velocity. One can conclude that the eccentricity of the inserted rod effects the slug lengths. The slug frequencies measured in the CONC and ECC experiments have been compared with the results of Taitel and Dukler (1977). Although the results of Taitel and Dukler (1977) are valid for the circular pipes, our data have taken place in the reasonable region of the figure (5.224.). The slug frequency increases with the increasing of the constant superficial liquid velocity. The slug frequency is effected from the eccentricity of the inserted rod. In addition to this, despite the scattered data of the CONC experiments, the slug frequencies of the ECC experiments are rather ordered. It can be finally expressed that the slug velocities, lengths, and frequencies are effected from the eccentricity of the inserted rod. In spite of the scattered data of the CONC experiments, the results of the ECC experiments are rather ordered.

6. CONCLUSIONS AND RECOMMENDATIONS

In this study, gas liquid two phase flows in the horizontal and upwardly inclined pipes have been investigated. The first section of the experiments were carried out in Germany with the supporting of the Institute of Process Engineering at Hanover University and German Academic Exchange Service (DAAD). Gas liquid flows in the plexiglas test pipe with 59 mm inner diameter were investigated for the positions of horizontal, +5°(upwards), +10°, and +15° inclination.

1)The observed flow patterns have been compared with the flow pattern maps of Baker (1954), Weisman (1979), and Mandhane (1974). The observations are mostly in agreement with the flow pattern maps of Baker (1954) and Weisman (1979).

2)Pressure losses measured in these experiments have been compared with the empirical methods and those of other investigators. They are rather in agreement with them. The variations of pressure losses with respect to the superficial gas and liquid velocities and inclinations have been examined.

3)The tomographic measurements techniques have been used to measure the void fraction. The measured void fractions are mostly in agreement with the empirical methods and others. However, in annular and annular+mist flow, this sensor is insufficient to determine the void fraction.

4)Slug velocities, lengths, and frequencies have been calculated and compared with the results of other investigators.

The second part of this experimental study was conducted in the Laboratory of Department of Mechanical Engineering at Çukurova University, Adana, Turkey. Gas liquid flows in the horizontal plexiglas test pipe with 40 mm inner diameter were investigated. Afterwards, a circular rod with 25 mm outer diameter were concentrically inserted in the horizontal plexiglas test pipe with 40 mm inner diameter. Thus, an annular gap was obtained between the inserted rod and test pipe. Following the observations of flow patterns and measurements of pressure losses, void fractions and slug velocities-lengths-frequencies (slug VLF), the inserted rod was eccentrically replaced in the test pipe. It is concluded from the comparisons of the flow patterns, pressure losses, void fractions and slug VLFs that the eccentricity of the inserted rod has an effect on them. The details of these effects are given in the "Results and Discussion".

For future studies, it is recommended that different eccentricities of the inserted rod should be tested. The adjustment of the eccentricity of the inserted rod can be carried out with the help of a mechanism. Thus, the whole experiments can be carried on without any interruption. Additionally, different geometries should be tested, for example; a rectangular rod can be inserted in the test pipe and all measurements can be repeated.

The spherical valves which are used to measure the void fraction should be replaced with the quick-closing valves. Thus, more void fraction measurements can be carried out in less time.

The design of more sensitive electrical circuits is possible with the help of an experienced electrician. The used circuits are not very sensitive because of the low quality soldering and lack of knowledge about electronic circuits. They can be redesigned and improved including more complicated circuits by an experienced electrician. Thus, the simultaneously measurement of the void fractions and slug velocities can be possible.

REFERENCES

BAKER, O., 1954. Simultaneous flow of oil and gas. Oil Gas Journal, Vol.53, pp.185.

BARNEA, D., and BRAUNER, N., 1985. Holdup of the liquid slug in Two Phase Intermittent Flow. Int. J. Multiphase Flow 11, pp.43-49.

BARNEA, D., and TAITEL, Y., 1993. A model for slug length distribution in gas-liquid slug flow. Int. J. Multiphase Flow 19, pp.829-838.

BEGGS, H.D., and BRILL, J.P., 1973. A Study of Two-Phase Flow in Inclined Pipes. Journal Petroleum Technology 25, May, pp.607-617.

AGRAWAL, S.S., GREGORY, G.A., and GOVIER, G.W., 1973. An Analysis of Horizontal Stratified Two Phase Flow in Pipes. The Canadian Journal of Chemical Engineering, Vol.51, pp.280-286.

JAGOTA, A.K., RHODES, E., and SCOTT, D.S., 1973. Measurement of Residence Times, and Film and Drop Velocities in Two Phase Annular Flow. The Canadian Journal of Chemical Eng., Vl.51, pp.393-400.

HOOGENDOORN, C.J., 1959. Chemical Engineering Science, 9, pp.205.

MANDHANE, J.M., GREGORY, G.A., and AZIZ, K., 1974. A Flow Pattern Map for Gas-Liquid Flow in Horizontal Pipes. Int. J. Multiphase Flow, Vol.1, pp. 537-553.

RUSSELL, T.W.F., ETCHELLS, A.W., JENSEN, R.H. and ARRUDA, P.J., 1974. Pressure Drop and Holdup in Stratified Gas Liquid Flow. AIChE Journal, Vol.20, No.4, pp.664-669.

TAITEL, Y. and DUKLER, A.E., 1976. A Model for Predicting Flow Regime Transitions in Horizontal and Near Horizontal Gas-Liquid Flow. AIChE Journal, Vol.22, No.1, January, pp.47-55.

LOCKHART, R.W. and MARTINELLI, R.C., 1949. Proposed Correlation of

Data for Isothermal Two Phase, Two Component Flow in Pipes. Chem. Eng. Prog., 45, pp.39-48.

TAITEL, Y. and DUKLER, A.E., 1976. A Theoretical Approach to the Lockhart-Martinelli Correlation for Stratified Flow. Int. J. Multiphase Flow, Vol.2, pp.591-595.

OWEN, C., JONES, JR., and DELHAYE, J.M., 1976. Transient and Statistical Measurement Techniques for Two-Phase Flows: A Critical Review. Int. J. Multiphase Flow, Vol.3, pp. 89-116.

TAITEL, Y. and DUKLER, A.E., 1977. A Model for Slug Frequency during Gas-Liquid Flow in Horizontal and Near Horizontal Pipes. Int. J. Multiphase Flow, Vol.3, pp.585-596.

GREGORY, G.A., NICHOLSON, M.K., and AZIZ, K., 1978. Correlation of the Liquid Volume Fraction in the Slug for Horizontal Gas-Liquid Slug Flow. Int. J. Multiphase Flow, Vol.4, pp.33-39.

TAITEL, Y., LEE, N., and DUKLER, A.E., 1978. Transient Gas-Liquid Flow in Horizontal Pipes: Modelling the Flow Pattern Transitions. AIChE Journal, Vol.24, No.5, pp.920-934.

WEISMAN, J., DUNCAN, D., GIBSON, J., and CRAWFORD, T., 1979. Effects of Fluid Properties and Pipe Diameter on Two-Phase Flow Patterns in Horizontal Lines. Int. J. Multiphase Flow, Vol.5, pp.437-462.

BARNEA, D., SHOHAM, O., TAITEL, Y., and DUKLER, A.E., 1980. Flow Pattern Transition for Gas-Liquid Flow in Horizontal and Inclined Pipes: Comparison of Experimental Data with Theory. Int. J. Multiphase Flow, Vol.6, pp.217-225.

TAITEL, Y., BARNEA, D., and DUKLER, A.E., 1980. Modelling Flow Pattern Transitions for Steady Upward Gas-Liquid Flow in Vertical Tubes. AIChE Journal, Vol.26, No.3, pp.345-354.

IIDA, Y., 1980. Prediction Method of Flow Patterns in Gas-Liquid Two-Phase

Flow. Bulletin of the JSME, Vol.23, No.178, pp.247-254.

SPEDDING, P.L., and NGUYEN, V.T., 1980. Regime Maps for Air Water Two Phase Flow. Chem. Eng. Science, 35, pp.779-793.

SPEDDING, P.L., CHEN, J.J.J., and NGUYEN, V.T., 1982. Pressure Drop in Two Phase Gas-Liquid Flow in Inclined Pipes. Int. J. Multiphase Flow, Vol.8, No.4, pp.407-431.

HIHARA, E., and SAITO, T., 1984. Slug Flow Transition in Horizontal Gas-Liquid Flow. Bulletin of the JSME, Vol.27, No.234, pp.2771-2778.

MCQUILLAN, K.W., and WHALLEY, P.B., 1985. Flow Patterns in Vertical Two-Phase Flow. Int. J. Multiphase Flow, Vol.11, No.2, pp.161-175.

MUKHERJEE, H., and BRILL, J.P., 1985. Empirical Equations to Predict Flow Patterns in Two-Phase Inclined Flow. Int. J. Multiphase Flow, Vol.11, No.3, pp.299-315.

LIN, P.Y., and HANRATTY, T.J., 1987. Detection of Slug Flow from Pressure Measurements. Int. J. Multiphase Flow, Vol.13, No.1, pp.13-21.

LIN, P.Y., and HANRATTY, T.J., 1987. Effect of Pipe Diameter on Flow Patterns for Air-Water Flow in Horizontal Pipes. Int. J. Multiphase Flow, Vol.13, No.4, pp.549-563.

NICKLIN, D.J., WILKES, J.C., and DAVIDSON, J.F., 1962. Two-Phase Flow in Vertical Tubes. Trans. Inst. Chem. Eng., Vol.40, pp.61-68.

SPEDDING, P.L., and SPENCE, D.R., 1987. Predicting Holdup in Vertical Two-Phase Gas-Liquid Flow. Handbook of Heat and Mass Transfer Vol.4, Advances in Reactor Design and Combustion Science, Chapter 2, ISBN: 0-87201-449-5, pp.57-92.

CHEREMISINOFF, N.P., and CHEREMISINOFF, P.N., 1988. Techniques for Two-Phase Flow Investigations. Flow Measurement for Engineers and Scientists, Marcel Decler Inc. New York, ISBN: 0-8247-7931-6, pp.114-175

KELESSIDIS, V.C., and DUKLER, A.E., 1989. Modelling Flow Pattern Transitions for Upward Gas-Liquid Flow in Vertical Concentric and Eccentric Annuli. Int. J. Multiphase Flow, Vol.14, No.2, pp.777-785.

BARNEA, D., and SHEMER, L., 1989. Void Fraction Measurements in Vertical Slug Flow: Applications to Slug Characteristics and Transition. Int. J. Multiphase Flow, Vol.15, No.4, pp.495-504.

ISSA, R.I., and TANG, Z.F., 1990. Modelling of Vertical Gas-Liquid Slug Flow in Pipes. ASME Advances in Gas-Liquid Flows, FED-Vol.99, HTD-Vol.155, pp.65-71.

TRONCONI, E., 1990. Prediction of Slug Frequency in Horizontal Two-Phase Slug Flow. AIChE Journal, Vol.36, No.5, May, pp.701-709.

MA, Y.P., CHUNG, N.N., PEI, B.S., LIN, W.K., and HSU, Y.Y., 1991. Two Simplified Methods to Determine Void Fractions for Two-Phase Flow. Nuclear Tech., Vol.94, April, pp.124-133.

JEPSON, W.P., and TAYLOR, R.E., 1993. Slug Flow and its Transitions in Large Diameter Horizontal Pipes. Int. J. Multiphase Flow, Vol.19, No.3, pp.411-420.

BACHALO, W.D., 1994. Experimental Methods in Multiphase Flows. Int. J. Multiphase Flow, Vol.20, Suppl., pp.261-295.

FELIZOLA, H., and SHOHAM, O., 1995. A Unified Model for Slug Flow in Upward Inclined Pipes. Journal of Energy Resources Technology, Vol.117, pp.7-12.

SPEDDING, P.L., WATTERSON, J.K., RAGHUNATHAN, S.R., and FERGUSON, M.E.G., 1998. Two-phase Co-current Flow in Inclined Pipe. Int. J. of Heat and Mass Transfer, Vol.41, pp.4205-4228.

EKBERG, N.P., GHIAASIAAN, S.M., ABDEL-KHALIK, S.I., YODA, M., and JETER, S.M., 1999. Gas Liquid Two Phase Flow in Narrow Horizontal Annuli. Nuclear Engineering and Design, 192, pp.59-80.

BONNECAZE, R.H., ERSKINE, JR., and GRESKOVICH, E.J., 1971. Holdup and Pressure Drop for Two-Phase Slug Flow in Inclined Pipelines. AIChE Journal, Vol.17, No.5, pp.1109-1113.

BÜYÜAKÇALI, B., 1999. Two phase gas liquid flows in horizontal tube with various inserts. MSc. Thesis, Çukurova University Institute of Natural and Applied Sciences, 75.

COSTIGAN, G., and WHALLEY, P.B., 1997. Slug flow regime identification from dynamic void fraction measurements in vertical air-water flows. Int. J. Multiphase Flow 23, No. 2, pp.263-282.

DUKLER, A.E., and TAITEL, Y., 1986. Flow Pattern Transitions in Gas Liquid Systems: Measurement and Modelling. Multiphase Science and Technology, Hemisphere Publ. Corp., Vol.2, Chapter 1, Washington, pp.1-94.

DUKLER, A.E., MOALEM MARON, D., and BRAUNER, N., 1985. A physical model for predicting the minimum stable slug length. Chemical Engineering Science 40, No.8, pp.1379-1385.

GRIFFITH, P., and WALLIS, G.B., 1961. Two-phase flow. Journal of heat Transfer, pp.307-320.

KOKAL, S.L., and STANISLAV, J.F., 1989. An experimental study of two phase flow in slightly inclined pipes I: Flow patterns, II: Liquid holdup and pressure drop. Chem. Eng. Sci. Vol.44, No.3, pp. I:665-679, II:681-693.

MOISSIS, R., and GRIFFITH, P., 1962. Entrance effects in a two phase slug flow. Journal of Heat Transfer.

NYDAL, O.J., PINTUS, S., and ANDREUSSI, P., 1992. Statistical Characterization of Slug Flow in Horizontal Pipes. Int.J. Multiphase Flow Vol. 18, No.3, pp.439-453.

ÖZGÜ, M.R., CHEN, J.C., and EBERHARDT, N., 1973. A Capacitance Method for Measurement of Film Thickness in Two-Phase Flow. Rev. Sci. Instrum, Vol.44, No.12, pp.1714-1716.

SÆTHER, G., BENDIKSEN K., MÜLLER, J., and FRØLAND, E., 1990. The fractal statistics of liquid slug lengths. Int. J. Multiphase Flow 16, No.6, pp.1117-1126.

SHEMER, L., and BARNEA, D., 1987. Visualization of the instantaneous velocity profiles in gas-liquid slug flow. Physico Chemical Hydrodynamics 8, No.3, pp.243-253.

SINGH, G., and GRIFFITH, P., 1970. Determination of the Pressure Drop Optimum Pipe Size for a Two-Phase Slug Flow in an Inclined Pipe. Journal of Engineering for Industry, November, pp.717-726.

VINAGE, I., 1996. Experimentelle untersuchungen an zweiphasigen gas-flüssigkeit ringströmungen in horizontalen und leicht aufwartsgeneigten rohrleitungen. Diplomarbeit, Institut für Verfahrenstechnik Universitat Hannover, 103.

YILMAZ, T., 2001. Gas Liquid Flows and Heat Transfer. Çümvak, Adana, 242.

CURRICULUM VITAE

Hasan DANIŞMAN was born on September 11, 1971 in Korkuteli-ANTALYA. In 1988, he graduated from High School in Antalya and enrolled in the Mechanical Engineering Department of Çukurova University. He graduated with a Bachelor of Science degree in Mechanical Engineering on June 26, 1992. He obtained MSc degree from the same department on September 9, 1995. He started the studies leading to degree of PhD in 1996 at the Department of Mechanical Engineering, Çukurova University. He worked as a Research Assistant in the Department of Mechanical Engineering, at Çukurova University between 1993 and 1998. He took a scholarship from German Academic Exchange Service (DAAD) in 1998. He worked in the Institute of Process Engineering at University of Hanover in Germany between 1998 and 1999. Since the middle of 1999, he has been working as a Lecturer at Çukurova University and has continued to working on experimental studies on two phase flow.

APPENDIX 1

```
C*******THIS PROGRAM DETERMINES THE FLOW PATTERNS
C*******OF EXPERIMENTS CARRIED OUT IN GERMANY.
C*******IT USES THE FLOW PATTERN MAP PROPOSED BY BAKER (1954)
C*******FOR HORIZONTAL TWO PHASE FLOW.

      OPEN(5,FILE='d:\hdtez238\hdPhDtez1\bakerinp2.txt')
      OPEN(6,FILE='d:\hdtez238\hdPhDtez1\bakerout2.out')

      read(5,*)
      write(6,1)'NO','DATE','EXP NO','mL/mG','mG','APAT','FLOW PATTERN'
1     format(a4,1x,a6,1x,a8,1x,a7,1x,a4,1x,a6,1x,a14)
9     read(5,*) ano,date,expno,ugs,uls,aml,gffi,ay

c THE CONSTANTS OF FUNCTIONS OF FLOW PATTERN TRANSITIONS OF BAKERS MAP
c Function 1=(Y1)
      aa11=8.95266
      an11=-0.04079
      aa21=21.53185
      an21=-0.66158
      ann1=-2.52319
c Function 2=(Y2)
      aa12=21.21076
      an12=-0.72354
      aa22=20.176
      an22=-0.65075
      ann2=11.47546
c Function 3=(Y6)
      aa13=2.7088805
      an13=-0.19026
c Function 4=(Y3)
      aa14=19.3787226
      an14=-0.4842
      aa24=0.022443
      an24=1.372508
      ann4=1.051905
c Function 5=(Y4)
      aa15=1.899736e11
      an15=-4.63371
      aa25=1164.774198
      an25=-0.90518
      ann5=1.618326
c Function 6=(Y5)
      aa16=103.988872
      an16=-0.97255
      aa26=39.492536
      an26=0.001437
      ann6=1.597836
c     APAT=Flow pattern key
c     THE FUNCTIONS OF FLOW PATTERN TRANSITIONS OF BAKER'S MAP
c     Bubbly Flow
      ay5=((aa15*gffi**an15)**ann5+(aa25*gffi**an25)**ann5)**(1/ann5)
      if(ay.ge.ay5) then
      if(ay.ge.30) then
```

```
      apat=8
c     write(*,*) 'FROTH'
      else
      apat=7
c     write(*,*) 'BUBBLY'
      endif
      goto 120
      else
      endif
c     Stratified Flow
      ay1=((aa11*gffi**an11)**ann1+(aa21*gffi**an21)**ann1)**(1/ann1)
      if(ay.lt.ay1) then
      apat=1
c     write(*,*) 'STRATIFIED'
      goto 120
      else
      endif
c     Wavy Flow
      ay2=((aa12*gffi**an12)**ann2+(aa22*gffi**an22)**ann2)**(1/ann2)
      if(ay.lt.ay2) then
      apat=2
c     write(*,*) 'WAWY'
      goto 120
      else
      endif
c     Plug, Slug, Annular, Dispersed Flow
      ay3=aa13*gffi**an13
      if(ay.lt.ay3) then
      apat=3
c     write(*,*) 'PLUG'
      goto 120
      else
      endif
      ay4=((aa14*gffi**an14)**ann4+(aa24*gffi**an24)**ann4)**(1/ann4)
      if(ay.lt.ay4) then
      apat=4
c     write(*,*) 'SLUG'
      goto 120
      else
      endif
      ay6=((aa16*gffi**an16)**ann6+(aa26*gffi**an26)**ann6)**(1/ann6)
      if(ay.lt.ay6) then
      apat=5
c     write(*,*) 'ANNULAR'
      goto 120
      else
      apat=6
c     write(*,*)'DISPERSED'
      goto 120
      endif
120     if(apat.eq.1) then
        write(6,5) ano,date,expno,gffi,ay,apat,'Stratified Flow'
        else
        if(apat.eq.2) then
        write(6,5) ano,date,expno,gffi,ay,apat,'Wavy Flow'
        else
          if(apat.eq.3) then
          write(6,5) ano,date,expno,gffi,ay,apat,'Plug Flow'
```

```
          else
          if(apat.eq.4) then
          write(6,5) ano,date,expno,gffi,ay,apat,'Slug Flow'
          else
          if(apat.eq.5) then
          write(6,5) ano,date,expno,gffi,ay,apat,'Annular Flow'
          else
          if(apat.eq.6) then
          write(6,5) ano,date,expno,gffi,ay,apat,'Dispersed Flow'
          else
          if(apat.eq.7) then
          write(6,5) ano,date,expno,gffi,ay,apat,'Bubby Flow'
          else
          if(apat.eq.8) then
          write(6,5) ano,date,expno,gffi,ay,apat,'Froth Flow'
          else
          end if
          end if
          end if
          end if
          end if
          end if
          end if
          end if
       if(ano.eq.227) then
          go to 130
          else
          goto 9
         end if
5         format(f5.0,1x,f8.0,1x,f4.0,1x,f10.7,1x,f10.7,1x,f3.0,1x,a15)
c        write(*,*) 'The end of the Program.'
130      STOP
         end
```

APPENDIX 2

```
C*******THIS PROGRAM DETERMINES THE FLOW PATTERNS
C*******OF EXPERIMENTS CARRIED OUT IN GERMANY.
C*******IT USES THE FLOW PATTERN MAP PROPOSED BY WEISMAN (1979)
C*******FOR HORIZONTAL TWO PHASE FLOW.

    OPEN(5,FILE='d:\hdtez238\hd2PhaseAdana\circSarpinp1.txt')
    OPEN(6,FILE='d:\hdtez238\hd2PhaseAdana\weismanSarpout1.txt')

          read(5,*)
         write(6,1)'INPNO','NO','DATE','mG','mL/mG','APAT','Flow Pattern'
1        format(a4,1x,a4,1x,a6,1x,a8,1x,a7,1x,a4,1x,a6,1x,a14)
9         read(5,*) ainpno,ano,date,uls,amL,ugs,ay,gffi

c THE CONSTANTS OF FUNCTIONS OF FLOW PATTERN TRANSITIONS OF WEISMAN
MAP
c Function 1
     aa11=0.301021
     an11=-0.64514
c Function 2
     aa12=1.72303e-7
     an12=0.11399
```

```
c Function 3
      aa13=6.11456
      an13=-0.28557
c Function 4
      aa14=4.38e-36
      an14=1
c      APAT=Flow pattern key
c      THE FUNCTIONS OF FLOW PATTERN TRANSITIONS OF WEISMAN MAP
c     Bubbly Flow
      uls4=2.853
      if(uls.ge.uls4) then
      weipat=5
c      write(*,*) 'BUBBLY'
      goto 120
      else
      endif
c     Annular-Wisp Flow
      ugs3=aa13*uls**an13
      if(ugs.ge.ugs3) then
      weipat=4
c     write(*,*) 'ANNULAR-WISP FLOW'
      goto 120
      else
      endif
c      Slug-Plug Flow
      uls2=(aa12*ugs)**an12
      if(uls.ge.uls2) then
      weipat=3
c     write(*,*) 'SLUG-PLUG FLOW'
      goto 120
      else
      endif
c      Wavy Flow
      ugs1=aa11*uls**an11
      if(ugs.ge.ugs1) then
      weipat=2
c      write(*,*) 'WAVY FLOW'
      goto 120
c     Stratified Flow
      else
      weipat=1
c     write(*,*) 'STRATIFIED FLOW'
      endif
120   if(weipat.eq.1) then
         write(6,5) ano,date,expno,uls,ugs,weipat,'Stratified Flow'
          else
          if(weipat.eq.2) then
              write(6,5) ano,date,expno,uls,ugs,weipat,'Wavy Flow'
          else
          if(weipat.eq.3) then
              write(6,5) ano,date,expno,uls,ugs,weipat,'Slug-Plug Flow'
          else
          if(weipat.eq.4) then
              write(6,5) ano,date,expno,uls,ugs,weipat,'Annular-Wisp Flow'
          else
          if(weipat.eq.5) then
              write(6,5) ano,date,expno,uls,ugs,weipat,'Bubbly Flow'
          else
```

```
          end if
          end if
          end if
          end if
          end if
if(ano.eq.205) then
          go to 130
          else
          goto 9
     end if
5     format(f5.0,1x,f8.0,1x,f4.0,1x,f10.7,1x,f10.7,1x,f3.0,1x,a15)

c     Write(*,*) 'The end of the Program.'
130   STOP
     end
```

APPENDIX 3

```
C*******THIS PROGRAM DETERMINES THE FLOW PATTERN
C*******IN A HORIZONTAL PIPE
C*******IT USES THE FLOW PATTERN MAP PROPOSED BY MANDHANE(1974)
C*******FOR HORIZONTAL TWO PHASE FLOW.

     OPEN(5,FILE='d:\hdtez238\fortrprogs\inpFile\mandinp1.txt')
     OPEN(6,FILE='d:\hdtez238\fortrprogs\outFile\mandout1.txt')

          read(5,*)
          write(6,1)'NO','DATE','EXP NO','ULs','UGs','MANDPAT','FLOW PATT.'
1         format(a4,2x,a6,2x,a8,2x,a7,2x,a4,2x,a6,2x,a10)
9         read(5,*) uls,ano,date,expno,ugs

c THE CONSTANTS OF FUNCTIONS OF FLOW PATTERN TRANSITIONS OF MANDHANE'S
MAP
c Function 1
     aa11=1.1074
          an11=-0.3911
          aa21=0.2918
          an21=-0.87154
          ann1=-9.5446
c Function 2
     aa12=0.2884
          an12=-0.8785
          aa22=0.698
          an22=0.22064
          ann2=3.7262
c Function 3
     aa13=22.8138
          an13=0.0162
          aa23=3.18253
          an23=-0.55031
          ann3=-4.01947
c Function 4
     aa14=3.2998
          an14=-0.5359
          aa24=37.45575
          an24=0.68666
          ann4=3.55263
```

```
c Function 5
     aa15=37.9525
          an15=0.70104
          aa25=40.5216
          an25=0.37958
          ann5=-8.9862
c    THE FUNCTIONS OF FLOW PATTERN TRANSITIONS
c         The combination of functions 3,4 and 5
          if(uls.lt.0.1025) then
          ugs3=((aa13*uls**an13)**ann3+(aa23*uls**an23)**ann3)**(1/ann3)
          ugs345=ugs3
          goto 25
          else
          if(uls.lt.0.4341) then
          ugs4=((aa14*uls**an14)**ann4+(aa24*uls**an24)**ann4)**(1/ann4)
          ugs345=ugs4
          goto 25
c         uls 0.4341 den büyük eşit ise
          else
          ugs5=((aa15*uls**an15)**ann5+(aa25*uls**an25)**ann5)**(1/ann5)
          ugs345=ugs5
          goto 25
          end if
          end if
c         The combination of functions 1 and 2
25        if(uls.lt.0.3539) then
          ugs1=((aa11*uls**an11)**ann1+(aa21*uls**an21)**ann1)**(1/ann1)
          ugs12=ugs1
          goto 26
c         uls 0.3539 dan büyük ise
          else
          ugs2=((aa12*uls**an12)**ann2+(aa22*uls**an22)**ann2)**(1/ann2)
          ugs12=ugs2
          goto 26
          end if
c    Dispersed flow
26        uls6=0.09344
          uls7=0.1533
     uls8=4.1205
     if(uls.ge.uls8) then
          if(ugs.lt.ugs345) then
     mandpat=6
c    write(*,*) 'Dispersed Flow'
     goto 120
     else
c    write(*,*) 'Annular-Mist Flow'
     endif
          else
     endif
c    Annular-Mist Flow
          if(ugs.ge.ugs345) then
c    write(*,*) 'Annular-Mist Flow'
          mandpat=5
          goto 120
          else
          end if
c    Slug Flow
          if(uls.lt.uls8) then
```

```
          if(uls.ge.uls6) then
          if(ugs.ge.ugs12) then
          if(ugs.lt.ugs345) then
c    write(*,*) 'SLUG FLOW'
          mandpat=4
     goto 120
          else
          end if
          else
          end if
          else
          end if
          else
          end if
c         Bubble elongated bubble flow
          if(uls.lt.uls8) then
          if(uls.ge.uls7) then
          if(ugs.lt.ugs12) then
c    write(*,*) 'Elongated bubble flow'
          mandpat=3
     goto 120
          else
          end if
          else
          end if
          else
          end if
c    wavy flow
          if(uls.lt.uls6) then
          if(ugs.lt.ugs345) then
          if(ugs.ge.ugs12) then
c    write(*,*) 'Wavy Flow'
          mandpat=2
     goto 120
          else
          end if
          else
          end if
          else
          end if
c         Stratified flow
          if(uls.lt.uls7) then
          if(ugs.lt.ugs12) then
c    write(*,*) 'Stratified flow'
          mandpat=1
     goto 120
          else
          end if
          else
          end if
120  if(mandpat.eq.1) then
     write(6,5) ano,date,expno,uls,ugs,ugs12,ugs345,mandpat,'Str.Flow'
          else
          if(mandpat.eq.2) then
          write(6,5) ano,date,expno,uls,ugs,ugs12,ugs345,mandpat,'Wavy Flow'
          else
          if(mandpat.eq.3) then
          write(6,5) ano,date,expno,uls,ugs,ugs12,ugs345,mandpat,'Bubb.Elon'
```

```
        else
        if(mandpat.eq.4) then
        write(6,5) ano,date,expno,uls,ugs,ugs12,ugs345,mandpat,'Slug Flow'
        else
        if(mandpat.eq.5) then
        write(6,5) ano,date,expno,uls,ugs,ugs12,ugs345,mandpat,'Ann.Mist'
        else
        if(mandpat.eq.6) then
        write(6,5) ano,date,expno,uls,ugs,ugs12,ugs345,mandpat,'Disp.Flow'
        else
        end if
        end if
        end if
        end if
        end if
        end if
    if(ano.eq.103) then
         go to 130
         else
         goto 9
     end if
5       format(f5.0,1x,f8.0,1x,f4.0,1x,4(f10.5,1x),i3,1x,a15)
c    Write(*,*) 'The end of the Program.'
130  STOP
     end
```

APPENDIX 4

```
! This program calculates the cross-correlation values of leds.
!
    double precision row1,anf1,anf2,anf12,anf22
        dimension row1(7550),anf1(7550),anf2(7550),ar(7550)

        open(4,FILE='d:\tez238\2PhaseAdana\inp-out\02817trinp.txt')
        open(5,FILE='d:\tez238\2PhaseAdana\inp-out\02817trout.txt')

        n=2972
        anf12=0
        anf22=0
!       delay=0

        do i=1,n
        read(4,*) row1(i),anf1(i),anf2(i)
        end do

        do j=1,n
        anf12=anf1(j)+anf12
        anf22=anf2(j)+anf22
        end do

        anf1m=anf12/row1(n)
        anf2m=anf22/row1(n)

!       write(5,*) anf1m,anf2m
        do delay=0,n-1
```

```
      bpay=0
      bdx2=0
      bdy2=0

      do i=1,n-delay
      adx=anf1(i)-anf1m
      adx2=adx**2

      ady=anf2(i+delay)-anf2m
      ady2=ady**2

      apay=adx*ady
      bpay=apay+bpay

      bdx2=adx2+bdx2
      bdy2=ady2+bdy2
      end do

      ar(delay)=bpay/(sqrt(bdx2)*sqrt(bdy2))
      write(5,*) delay,ar(delay)
      end do
      close(4)
      close(5)
c
      stop
      end
```

APPENDIX 5

```
C*******THIS PROGRAM CALCULATES THE VOID FRACTION
C*******IN A HORIZONTAL CONCENTRIC AND ECCENTRIC ANNULI
       OPEN(UNIT=5,FILE='d:\tez238\fortrprogs\inpFile\voideccinp1.txt')
      OPEN(UNIT=6,FILE='d:\tez238\fortrprogs\OutFile\voideccout1.txt')

      pi=3.141593
c     inner diameter of outer pipe
      di=40
c     outside diameter of outer pipe
      dout=50.4
c     inner radius
      ri=di/2
c     outer radius
      rout=dout/2
c     1/4 periphery of outer pipe
      alcey=pi*dout/4
c     insert diameter
      dins=25
      rins=dins/2
      areaic=pi*(di**2-dins**2)/4
      rfark=ri-rins
c     eccentricity=decc/(ri-rins)
c   decc=rfark-hecc
c     CONC=ecc=0
c     ECC=ecc=1
```

```
      ecc=1
      decc=ecc*rfark
      hecc=rfark-decc
      hust=hecc+dins

55    read(5,*) ano,date,al

      if(al.le.alcey) then
      alfa=al*(360/(pi*dout))
      ax=rout*COS(alfa*pi/180)
      ah=ri-ax
      area=ri**2*(pi-ACOS(ah/ri-1)+(ah/ri-1)*sqrt(1-(ah/ri-1)**2))

      else
      al2=al-alcey
      alfa=al2*(360/(pi*dout))
      ax=rout*sin(alfa*pi/180)
      ah=ri+ax
      area=ri**2*(pi-ACOS(ah/ri-1)+(ah/ri-1)*sqrt(1-(ah/ri-1)**2))
      end if

      if(ah.ge.hecc) then
      if(ah.le.hust) then
      ahins=ah-hecc
      aa1=ahins/rins-1
      ab1=acos(ahins/rins-1)
      Ains=rins**2*(pi-ab1+(aa1)*sqrt(1-(aa1)**2))
      else
      Ains=pi*(dins)**2/4
      end if
      else
      Ains=0
      end if

      area2=area-Ains
      aliqh=area2/areaic
      voidfr=1-aliqh

      write(6,5) ano,date,al,aliqh,voidfr

      if (ano.eq.158) then
      goto 50
      else
      goto 55
      end if

5   format(f4.0,1x,4(f9.4,1x))

50    stop
      end
```